

**Metabolomic Analysis of the Allelopathic
Interactions between Marine Planktonic Microalgae**

DISSERTATION

zur Erlangung des akademischen Grades
doctor rerum naturalium (Dr. rer. nat.)

vorgelegt dem Rat der Chemisch-Geowissenschaftlichen Fakultät der
Friedrich-Schiller-Universität Jena

von

Katharina Christine Eick

geboren am 10.06.1987 in Stuttgart

Gutachter

1. Prof. Dr. Georg Pohnert, Friedrich-Schiller-Universität Jena
2. Prof. Dr. Severin Sasso, Friedrich-Schiller-Universität Jena

Tag der Verteidigung: Mittwoch, 13.12.2017

Für meine Familie

Acknowledgements

My PhD journey was quite an adventure, considering that the worlds of analytical chemistry and science were comparably new to me when I started. Coming from a teaching background in biology and chemistry, I was excited to dive into a new challenge and combine my university background with my intrinsic passion for the marine environment. In retrospective, the past years were demanding, thrilling and extremely valuable for my personal and professional development. However, this journey would not have been possible without a lot of people, which I would like to sincerely thank at this point (hopefully without forgetting anyone).

First and foremost, I want to thank my supervisor Dr. Georg Pohnert, who accepted me in his group and gave me both freedom and guidance to find my way. I cannot thank him enough for his constant support and trust. I highly valued our discussions, his mindful inputs into my project and his sharp advice during the creation of this thesis. Secondly, I want to thank Prof. Severin Sasso, who agreed to be my second supervisor, for his support and proficient advice.

I am especially thankful to Dr. Jens Schumacher for his statistical guidance. He really helped me to improve the quality of my statistical evaluation and to understand underlying principles of multivariate statistics. Furthermore, he supported me with a custom-made R-script for the endometabolomic CAP analysis, which exactly fitted the needs of my experimental design.

Endless thanks to my office mate Karen Bondoc, who inspired me both scientifically and personally. I not only found her to be a critical and sharp-minded scientist but also a dear friend. She supported me in the context of R-based modeling with insightful discussions about the methodology, R-script support and general R-knowledge.

Special thanks goes to all former and current members of the Pohnert group, which I had the pleasure to work with during my PhD. Particularly, I appreciated any kind advice and support that helped me finding my way in the laboratory and made me a better chemist, biologist and scientist. Thanks to Dr. Tino Jaschinski and Dr. Michaela Mausz, for introducing me to the GC-EI/TOF/MS instrument and handing on their technical knowledge. Beyond that, Dr. Michaela Mausz and Julia Althammer introduced me into the metabolomic work-flow and the realization of metabolomic best-practices. When learning how to work with flow cytometry, Dr. Michaela Mausz kindly shared her experienced advice and measurement protocols with me. The work of Dr. Carsten Paul formed the basis of my project. Therefore, I highly appreciated the time he took in the very beginning of my project to introduce me into his thought process and previous experiments. Although we never met in person, Dr. Charles Vidoudez was very present in my

work, as he provided the methodological basics used in my metabolomic analysis. Thanks to Dr. Thomas Wichard for inspiring discussions on statistical procedures and metabolomics, as well as to Mathias Hirth, Constanze Kuhlisch, Dr. Nico Überschaar and Tim Baumeister. Thanks to Dr. Michaela Mausz, Dr. Carsten Paul and Matthias Hirth for placing their metabolite-standard measurements at my disposal. Thanks to Kathleen Thume, for synthesizing and providing me with DMSO that I used in my experiments and to Raphael Seidel and Marcel Ritter for bringing the fun in workday life, I highly enjoyed sharing a common office with you. I want to thank Hannes Richter for the support in the laboratory and nutrient measurements, Madlen Kühn and Sarah Tippner for the support in the office and all other group members likewise for fruitful discussions, support and a good time.

In the process of creating this thesis, several people contributed to improving the manuscript by reading and commenting on parts of my PhD thesis. Thanks to Stefanie Allert, Karen Bondoc, Verena Jeschke, Sofia Koller, Tycho Stange and Dr. Thomas Wichard. Furthermore, thanks to Prof. Ulrich Schubert for granting me access to the flow cytometer of his work group and to Dr. Alexandra Rinkenauer and Tanja Bus for their help with the instrument. I am grateful to Frank Malien from the GEOMAR in Kiel for nutrient measurements and to my student assistants Pia Ponnath and Anna Zimmermann for counting diatom cells.

I want to deeply acknowledge my funding by the Foundation of German Business, as well as the numerous opportunities offered by their personal development program. Similarly, I want to thank the JSMC for giving me access to a highly motivated scientific network and multiple opportunities to actively engage in scientific projects and workshops.

Last but not least, I want to thank all the special people that accompanied me during my PhD journey and kept my spirit high. Endless thanks to my family for their unconditional support and love. Especially, to my grandmother and mother for their inspiration, for being strong women and always believing in me. Also, I am deeply grateful for the friendship of Sofia Koller, who never fails to build me up and inspires me to strive even more. Although we are usually miles and miles apart, I can always count on her support. Thanks to Tycho Stange for his unbreakable belief in me, his love and unconditional support in all matters. He made the seemingly endless all-nighters towards the end bearable and kept me going by providing me with an endless supply of energy drinks and encouragements. Furthermore, thanks to Martina Wagner, Andreas Bergmann and Thomas Kächele for being my virtual office mates and for going every step of the way with me. Great thanks to Isabell Götz, Katalin Vollmann, Maja Rischert, René Benndorf, Verena Jeschke, Elisa Nössler-Hofmann, Sindy Park, Martin Dietz, Stefanie Allert and many others for creating the best Jena-memories.

Table of Content

Table of Content	I
List of Figures	IV
List of Tables	VII
Abbreviations	IX
1 Introduction	1
1.1 Ecological relevance of marine phytoplankton	1
1.2 The nature of chemically-mediated interactions	5
1.3 Allelopathy in phytoplankton communities	7
1.4 Prominent methods in allelopathy research	12
1.5 The stimulatory interaction between <i>S. costatum</i> and <i>T. weissflogii</i>	18
1.6 Objective	19
2 Interaction of <i>T. weissflogii</i> with <i>S. costatum</i>	21
2.1 Study design	21
2.1.1 General approach	22
2.1.2 Design: Interaction experiment	24
2.1.3 Design: Medium experiments	30
2.1.4 Design: Evaluation of DMSP as growth mediator	32
2.2 Interaction experiment with <i>T. weissflogii</i> and <i>S. costatum</i>	34
2.2.1 Diatom growth in mono- and co-cultivation	34
2.2.2 Metadata	39
2.2.3 Exometabolomic investigation	39
2.2.4 Endometabolomic investigation	69
2.3 Medium experiments	97
2.3.1 <i>T. weissflogii</i> medium experiment	97
2.3.2 <i>S. costatum</i> medium experiment	99
2.3.3 Metadata	102
2.4 Evaluation of DMSP as growth mediator	108
2.4.1 Influence of DMSP pulses on diatom growth	108
2.4.2 Influence of continuously available DMSP on diatom growth	109
2.5 Discussion of the metabolomic strategy	111
2.5.1 Metabolomic sampling and extraction protocol	112
2.5.2 Chemical analysis via GC-TOF/EI/MS	112
2.5.3 Metabolomic data processing and statistics	117
2.6 Interim conclusion	123
3 Interaction of <i>T. weissflogii</i> with <i>S. marinoi</i>	131
3.1 Experimental design	131
3.2 Results	132

3.2.1	Diatom growth.....	132
3.2.2	Metadata	135
3.2.3	Exometabolomic investigation	138
3.2.4	Endometabolomic investigation	161
3.3	Interim Conclusion	187
4	Interaction of <i>T. weissflogii</i> with <i>S. dohrnii</i>.....	191
4.1	Experimental design	191
4.2	Interim conclusion	191
5	Concluding Discussion	193
	Summary and outlook.....	205
	Zusammenfassung und Ausblick.....	210
6	Material and methods	215
6.1	Algae.....	215
6.1.1	Strains.....	215
6.1.2	Medium.....	215
6.1.3	Cultivation Parameters of Algal Stock	215
6.2	Co-cultivation	216
6.2.1	Chamber parts.....	216
6.2.2	Chamber preparation and maintenance	216
6.2.3	Culture preparation	217
6.2.4	Co-cultivation parameters.....	218
6.2.5	Sampling procedure	218
6.2.6	Biological replication in co-cultivation	218
6.2.7	Experimental specifics.....	219
6.3	Evaluation of DMSP as growth mediator.....	221
6.3.1	Cultivation parameters.....	221
6.3.2	Chemicals	221
6.3.3	DMSP addition to <i>T. weissflogii</i> culture.....	221
6.3.4	Experimental specifics.....	222
6.4	Sampling.....	222
6.5	Metadata acquisition.....	223
6.5.1	Chlorophyll a fluorescence.....	223
6.5.2	Photosystem II activity measurements	223
6.5.3	Cell counts	224
6.5.4	pH	224
6.5.5	Flow cytometry measurements.....	224
6.5.6	Nutritional analysis.....	227
6.6	Metabolomic analysis	228
6.6.1	Chemicals and consumables.....	228
6.6.2	Protocol for metabolomic sample preparation and storage	230
6.6.3	Derivatization	232
6.6.4	GC-MS measurements.....	233
6.7	Data analysis.....	236
6.7.1	Metadata analysis	236

6.7.2	Metabolomic data processing	238
6.7.3	Metabolomic data analysis	240
6.7.4	Metabolite identification	243
References	247
Curriculum Vitae	263
Selbstständigkeitserklärung	267
7 Digital Appendix	269
7.1	Appendix: Interaction of <i>T. weissflogii</i> with <i>S. costatum</i>	269
7.1.1	Diatom growth.....	269
7.1.2	Exometabolomic investigation	273
7.1.3	Endometabolomic investigation	282
7.1.4	Metadata	284
7.1.5	Influence of the initial environment of the interaction partner on diatom growth parameters.....	287
7.2	Appendix: Interaction of <i>T. weissflogii</i> with <i>S. marinoi</i>	291
7.2.1	Diatom growth.....	291
7.2.2	Exometabolomic investigation	295
7.2.3	Endometabolomic investigation	319
7.3	Appendix: Interaction of <i>T. weissflogii</i> with <i>S. dohrnii</i>	331
7.3.1	Diatom growth.....	331
7.3.2	Metadata	334
7.3.3	Exometabolomic investigation	337
7.3.4	Endometabolomic investigation	353
7.3.5	Supplements: Diatom growth.....	376
7.3.6	Supplements: Exometabolomic investigation	380
7.3.7	Supplements: Endometabolomic investigation	397
7.4	Appendix: Modified CAP function for R.....	411

List of Figures

Figure 1: Co-cultivation chamber before (a) and after (b) assembly. Scale bar represents 10 cm. Source: (Paul et al., 2013) with permission of Springer.....	14
Figure 2: Experimental design to investigate the interaction between <i>T. weissflogii</i> and <i>S. costatum</i> in a small-scale co-cultivating set-up.....	23
Figure 3: Experimental design to investigate the influence of the initial environment in the interaction between <i>T. weissflogii</i> and <i>S. costatum</i>	31
Figure 4: Diatom growth in the interaction experiment of <i>T. weissflogii</i> with <i>S. costatum</i>	35
Figure 5: Constrained score and loading plots of exometabolomic samples from the overall analysis of the interaction between <i>T. weissflogii</i> and <i>S. costatum</i>	47
Figure 6: Constrained score and loading plots of exometabolomic samples from the daywise subset analysis of the interaction between <i>T. weissflogii</i> and <i>S. costatum</i>	54
Figure 7: Exemplary MST #109 with interaction-induced release mechanism on day 16 in the interaction between <i>T. weissflogii</i> and <i>S. costatum</i> (intensity pattern I).....	60
Figure 8: Exemplary metabolites #48 and #133 with interaction-induced release mechanism on day 16 and subsequent temporal regulation in the interaction between <i>T. weissflogii</i> and <i>S. costatum</i> (intensity pattern I).....	61
Figure 9: Exemplary MST #44 with interaction-induced release-uptake mechanism in the interaction between <i>T. weissflogii</i> and <i>S. costatum</i> (intensity pattern I on day 16).....	62
Figure 10: Exemplary metabolites #49 and #50 with interaction-induced release mechanism on day 16 in the interaction between <i>T. weissflogii</i> and <i>S. costatum</i> (intensity pattern I).....	63
Figure 11: Exemplary MSTs #62 and #77 with interaction-induced release mechanism on day 26 as well as on day 26 and 32 in the interaction between <i>T. weissflogii</i> and <i>S. costatum</i> (intensity pattern I).....	63
Figure 12: Intensity dynamic of exemplary exometabolites, enhanced in co-cultivation on day 32 (interaction between <i>T. weissflogii</i> and <i>S. costatum</i>).....	64
Figure 13: Exemplary metabolites #135 and #41 with interaction-induced uptake, transformation or reduced release mechanisms on day 16 in the interaction between <i>T. weissflogii</i> and <i>S. costatum</i> (intensity pattern II).....	65
Figure 14: Exemplary metabolites #1 and #104 with interaction-induced uptake, transformation or reduced release mechanisms on day 26 as well as day 26 and 32 in the interaction between <i>T. weissflogii</i> and <i>S. costatum</i> (intensity pattern II).....	66
Figure 15: Potential infochemicals with interaction-induced uptake, transformation or reduced release mechanisms on day 32 in the interaction between <i>T. weissflogii</i> and <i>S. costatum</i> (intensity pattern II).....	67
Figure 16: Constrained score and loading plots of endometabolomic samples from <i>T. weissflogii</i> in a species-specific subset analysis of the interaction between <i>T. weissflogii</i> and <i>S. costatum</i>	75
Figure 17: Constrained score and loading plots of endometabolomic samples from <i>T. weissflogii</i> in a daywise subset analysis of the interaction between <i>T. weissflogii</i> and <i>S. costatum</i>	76
Figure 18: Constrained score and loading plots of endometabolomic samples from <i>S. costatum</i> in a species-specific subset analysis of the interaction between <i>T. weissflogii</i> and <i>S. costatum</i>	86
Figure 19: Constrained score and loading plots of endometabolomic samples from <i>S. costatum</i> in a daywise subset analysis of the interaction between <i>T. weissflogii</i> and <i>S. costatum</i>	87
Figure 20: Diatom growth in the medium experiment of <i>T. weissflogii</i>	98
Figure 21: Diatom growth in the medium experiment of <i>S. costatum</i>	100
Figure 22: PSII efficiency of the diatom cultures in the medium experiment of <i>T. weissflogii</i> and <i>S. costatum</i>	103
Figure 23: pH of the diatom cultures in the medium experiment of <i>T. weissflogii</i>	104
Figure 24: Bacterial abundance in the medium experiment of <i>T. weissflogii</i> with <i>S. costatum</i>	105

Figure 25: Influence of multiple DMSP pulses (100 nM, 1 μ M, 2.5 μ M) on the growth of <i>T. weissflogii</i> (RCC76).....	109
Figure 26: Influence of continuous DMSP addition on the growth of <i>T. weissflogii</i> (RCC76).....	110
Figure 27: Diatom growth in the interaction experiment of <i>T. weissflogii</i> and <i>S. marinoi</i>	132
Figure 28: PSII efficiency of the diatoms in the interaction experiment of <i>T. weissflogii</i> with <i>S. marinoi</i>	135
Figure 29: Bacterial abundance in the medium experiment of <i>T. weissflogii</i> with <i>S. marinoi</i>	136
Figure 30: Nutrient levels in the medium experiment of <i>T. weissflogii</i> with <i>S. marinoi</i>	137
Figure 31: Constrained score and loading plots of exometabolomic samples from the overall analysis of the interaction between <i>T. weissflogii</i> and <i>S. marinoi</i>	142
Figure 32: Constrained score and loading plots of exometabolomic samples from the daywise subset analysis of the interaction between <i>T. weissflogii</i> and <i>S. marinoi</i>	149
Figure 33: Exemplary metabolite #132 with interaction-induced release mechanism on day 18 and distinct temporal regulation, in the interaction between <i>T. weissflogii</i> and <i>S. marinoi</i> (intensity pattern I).....	153
Figure 34: Exemplary MST #180 with interaction-induced release mechanism on day 18 but predominance on day 42 in the interaction between <i>T. weissflogii</i> and <i>S. marinoi</i> (intensity pattern I).....	153
Figure 35: Exemplary MST #205 with interaction-induced release mechanism on day 18 and potential origin from <i>S. marinoi</i> in the interaction between <i>T. weissflogii</i> and <i>S. marinoi</i> (intensity pattern I).....	154
Figure 36: Exemplary MST #260 with interaction-induced release on day 30 and distinct temporal regulation mechanism, in the interaction between <i>T. weissflogii</i> and <i>S. marinoi</i> (intensity pattern I).....	155
Figure 37: Exemplary MST #53 with interaction-induced release mechanism on day 30 in the interaction between <i>T. weissflogii</i> and <i>S. marinoi</i> (intensity pattern I).....	155
Figure 38: Exemplary MST #27 with interaction-induced release mechanism on day 42 and predominance on this day in the interaction between <i>T. weissflogii</i> and <i>S. marinoi</i> (intensity pattern I).....	156
Figure 39: Exemplary MST #206 and #179 with interaction-induced release mechanism on day 42 and distinct temporal regulation in the interaction between <i>T. weissflogii</i> and <i>S. marinoi</i> (intensity pattern I).....	157
Figure 40: Exemplary MST #81 with interaction-induced release mechanism on day 42 in the interaction between <i>T. weissflogii</i> and <i>S. marinoi</i> (intensity pattern I).....	157
Figure 41: Potential infochemical with interaction-induced uptake, transformation or reduced release mechanisms on day 18 in the interaction between <i>T. weissflogii</i> and <i>S. marinoi</i> (intensity pattern II).....	158
Figure 42: Exemplary metabolites #193 and #306 with interaction-induced uptake, transformation or reduced release mechanisms on day 18 in the interaction between <i>T. weissflogii</i> and <i>S. marinoi</i> (intensity pattern III).....	159
Figure 43: Exemplary MST #66 and #251 with interaction-induced uptake, transformation or reduced release mechanisms on day 30 and 42 in the interaction between <i>T. weissflogii</i> and <i>S. marinoi</i> (intensity pattern II / III).....	160
Figure 44: Constrained score and loading plot of endometabolomic samples from <i>T. weissflogii</i> in a species-specific subset analysis of the interaction between <i>T. weissflogii</i> and <i>S. marinoi</i>	165
Figure 45: Constrained score and loading plots of endometabolomic samples from <i>T. weissflogii</i> in a daywise subset analysis on day 30 of the interaction between <i>T. weissflogii</i> and <i>S. marinoi</i>	166
Figure 46: Constrained score and loading plots of endometabolomic samples from <i>S. marinoi</i> in a species-specific subset analysis of the interaction between <i>T. weissflogii</i> and <i>S. marinoi</i>	177

Figure 47: Constrained score and loading plots of endometabolomic samples from <i>S. marinoi</i> in a daywise subset analysis of the interaction between <i>T. weissflogii</i> and <i>S. marinoi</i>	178
---	-----

List of Tables

Table 1: Relationship between MST intensity patterns and heatmap groups.	41
Table 2: Permutation and cross-validation test results for the CAP analysis of different a-priori groups in the exometabolome analysis of the interaction between <i>S. costatum</i> and <i>T. weissflogii</i>	43
Table 3: Heatmap of relative exometabolite intensities for the overall analysis of the interaction between <i>T. weissflogii</i> and <i>S. costatum</i>	50
Table 4: Heatmap of relative exometabolite intensities for the subset analysis of the interaction between <i>T. weissflogii</i> and <i>S. costatum</i> on day 16.	55
Table 5: Heatmap of exometabolite intensities for the subset analysis of the interaction between <i>T. weissflogii</i> and <i>S. costatum</i> on day 26.	58
Table 6: Permutation and cross-validation test results for the overall analysis of different a-priori groups in the endometabolome analysis of the interaction between <i>S. costatum</i> and <i>T. weissflogii</i>	71
Table 7: Permutation and cross-validation test results for the species-specific subset analysis of different a-priori groups in the endometabolome analysis of the interaction between <i>S. costatum</i> and <i>T. weissflogii</i>	72
Table 8: Permutation and cross-validation test results for the species-specific and daywise subset analysis of different a-priori groups in the endometabolome analysis of the interaction between <i>S. costatum</i> and <i>T. weissflogii</i>	73
Table 9: Heatmap of endometabolite intensities for the species-specific and daywise analysis of <i>T. weissflogii</i> in the interaction with <i>S. costatum</i>	81
Table 10: Heatmap of endometabolite intensities for the species-specific and daywise analysis of <i>S. costatum</i> in the interaction with <i>T. weissflogii</i>	92
Table 11: Permutation and cross-validation test results for the CAP analysis of different a-priori groups in the exometabolome analysis of the interaction between <i>S. marinoi</i> and <i>T. weissflogii</i>	140
Table 12: Heatmap (part I) of exometabolite intensities for the overall analysis of the interaction between <i>T. weissflogii</i> and <i>S. marinoi</i>	144
Table 13: Partial Heatmap of relative exometabolite intensities for the daywise subset analysis of the interaction between <i>T. weissflogii</i> and <i>S. marinoi</i>	151
Table 14: Permutation and cross-validation test results for the overall analysis of different a-priori groups in the endometabolome analysis of the interaction between <i>S. marinoi</i> and <i>T. weissflogii</i>	162
Table 15: Permutation and cross-validation test results for the species-specific subset analysis of different a-priori groups in the endometabolome analysis of the interaction between <i>S. marinoi</i> and <i>T. weissflogii</i>	164
Table 16: Permutation and cross-validation test results for the species-specific and daywise subset analysis of different a-priori groups in the endometabolome analysis of the interaction between <i>S. marinoi</i> and <i>T. weissflogii</i>	164
Table 17: Heatmap of endometabolite intensities categorized by MST classes for the species-specific and daywise analysis of <i>T. weissflogii</i> in the interaction with <i>S. marinoi</i>	171
Table 18: Heatmap of endometabolite intensities categorized by MST classes for the species-specific and daywise analysis of <i>S. marinoi</i> in the interaction with <i>T. weissflogii</i>	182
Table 19: Sampling strategy per chamber-half for co-cultivation experiments	223
Table 20: Detector settings for flow cytometry sample measurements (parameters modified from protocols of Michaela Mausz)	226
Table 21: Chemical compounds of the RI-mix	229
Table 22: Overview over cell counts used for the endometabolomic normalization of <i>T. weissflogii</i> and <i>Skeletonema</i> sp. in the interaction experiments.	231

Table 23: General GCT settings	233
Table 24: GCT Tuning settings	234
Table 25: Analysis settings of AMDIS.....	239
Table 26: Analysis settings of MET-IDEA	240
Table 27: Analysis parameters for CAP12.exe	241
Table 28: MS libraries	244

Abbreviations

A	Amine
A Acid	Sugar acid
Alc	Alcohol
Alk	Alkaloid
AMDIS	Automated Mass Spectral Deconvolution and Identification System
amu	Atomic mass unit
ANOVA	Analysis of Variance
ASW	Artificial seawater
CA	Carboxylic acid
CAP	Canonical Analysis of Principal Coordinates
CDA	Canonical Discriminant Analysis
Chla	Chlorophyll a fluorescence
CS	Complex sugar
Da	Dalton
denDF	Degrees of freedom in the denominator
DMS	Dimethylsulfide
DSMP	Dimethylsulphoniopropionate
DT	A-priori grouping by treatment per day
dv.	Derivative
GC	Gas chromatography
GC-EI/TOF/MS	Gas chromatography coupled with electron ionization time-of-flight mass spectroscopy
GC-TOF/MS	Gas chromatography coupled with time-of-flight mass spectroscopy
LC	Liquid chromatography
MET-IDEA	Metabolomics Ion-based Data Extraction Algorithm
MS	Mass spectrometry
MSI	Metabolomics Standards Initiative
MST	Mass spectral tag
NMR	Nuclear magnetic resonance
numDF	Degrees of freedom in the numerator
O	Others
PCoA	Principal Coordinate Analysis
PSII efficiency	Photosystem II efficiency
PUA	Polyunsaturated aldehyde
PVDF	Polyvinylidene fluoride
RFU	Relative fluorescence units
RI	Retention index
RMS	Mean residual value
RT	Retention time
S	Sugar
S Alc	Sugar alcohol
SD	Standard deviation

SOP	Standard operating procedure
St	Sterol
T (<i>compound class</i>)	Terpene
T (<i>CAP context</i>)	A-priori grouping by treatment
TIC	Total ion current
U	Unknown
UPLC-ESI/MS	Ultra-fast liquid chromatography coupled with electrospray ionization mass spectroscopy
v/v_{sw}	Inoculated culture volume per volume of ASW medium
δ_1^2	First squared canonical correlation

1 Introduction

1.1 Ecological relevance of marine phytoplankton

All photosynthetic, pelagic organisms that live in the aquatic environment and are mainly moved by the water currents, are defined as phytoplankton. Phytoplankton comprises organisms of a multitude of phyla showing all forms and sizes. It can generally be confined from bacterioplankton and zooplankton. While the former consists of all prokaryotic organisms like bacteria and archaea, the latter is composed of autotrophic and heterotrophic microorganisms. The global impact of phytoplankton first became evident during the oxygenation of the Earth's atmosphere, which took place approximately 2.4 billion years ago (Bekker et al., 2004). By emitting oxygen as a photosynthetic byproduct, these organisms created the opportunity for the evolution of life resulting in the flora and fauna we know today.

Although marine unicellular algae make up only 0.2 % of global primary producer biomass (Field et al., 1998) they have tremendous impact on marine and terrestrial ecosystems: Via fixation of atmospheric CO₂ and synthesis of organic compounds they are responsible for approximately 50 % of global primary production (Field et al., 1998) and drive the global carbon cycle (Keeling and Shertz, 1992). As they provide the organic matter that fuels higher trophic levels, they form the basis of the marine food web. Furthermore, they impact global climate not only via fixation of CO₂, but also indirectly via the emission of compounds that act as cloud condensation nuclei that influence the Earth's albedo (Bates, Charlson and Gammon, 1987; Charlson et al., 1987).

The characteristics of the ocean are closely linked to phytoplankton physiology. Interestingly, it has been found that the proportion of the major elements C:N:P in the marine system is constrained to the ratio 106:16:1 (Redfield, 1958). This stoichiometry, called Redfield ratio, characterizes the elemental composition of nutrients in the ocean and the one of phytoplankton biomass¹. As it is not clear, whether this ratio in phytoplankton biomass results from the elemental composition of the ocean or vice versa, a reciprocal interaction between organisms and environment is strongly suggested (Falkowski, 1994, 2012).

¹ (Redfield, 1958) referring to (Fleming, 1940)

Another aspect of this close interaction between chemical and biological environment is the ‘biological pump’². Dead phytoplankton cells and other fine particle matter slowly sink into deep layers of the ocean. Over time *inter alia* these deep layers are enriched with organic carbon³ and nutrients (Falkowski, Barber and Smetacek, 1998). This dynamic is called the biological pump. During upwelling events in spring or summer, when insolation increases and more nutrients enter the euphotic zone, this deep sea storage can again be exploited by phytoplankton (Falkowski, 1994). Thus, phytoplankton dynamics create biogeochemical cycles, regulate atmospheric CO₂ levels via deep sea storage and ultimately lead to fossil fuels via sedimentation (Falkowski et al., 1998; Falkowski, 2012).

When conditions for growth become better, mass occurrences of certain phytoplanktonic species occur, which are called phytoplankton blooms. Especially well known and studied are harmful algal blooms (HABs), or ‘red tides’ (Shilo, 1967; Smayda, 1997a). They can be formed by various phytoplanktonic species⁴, which all share the trait of producing toxic compounds (Smayda, 1997b). One prominent example is Paralytic Shellfish Poisoning, which is caused by saxitoxins that are excreted by several dinoflagellates, *e.g.* *Alexandrium* sp. (Anderson et al., 1990). These toxins are accumulated in bivalve mollusks, like mussels, and consumed either directly or indirectly by humans with potentially lethal effects (Grattan, Holobaugh and Morris, 2016).

These HABs are preferentially produced by flagellates, mostly dinoflagellates. Together with coccolithophores and diatoms, they represent the three dominant groups of marine eukaryotic phytoplankton that largely dominate modern oceans (Falkowski et al., 2004).

Diatoms

Diatoms (phylum Bacillariophyta) are dominant, eukaryotic key players in the marine phytoplankton and comprise approximately 30 % of all phytoplankton species⁵. Contrary to dinoflagellates, most diatoms are non-toxic, with the exception of several *Pseudo-nitzschia* species, which produce the neurotoxin Domoic acid (Zabaglo et al., 2016). Diatoms are characterized by their rigorous silicified cell wall, called a frustule, which is made up of hydrated silicon dioxide and organic material (Armbrust et al., 2004). It is hypothesized that frustules evolved to provide diatoms

² Term used by (Falkowski, 1994, 2012; Falkowski et al., 1998)

³ (Falkowski et al., 1998) referring to (Volk and Hoffert, 1985)

⁴ (Smayda, 1997a) referring to (Sourmia, 1995)

⁵ (Allen, Vardi and Bowler, 2006) referring to (Falkowski et al., 2004)

with an effective mechanical protection against their predators (Hamm et al., 2003). As the frustule is rather heavy and diatom cells therefore sink during and after death, diatoms are a vital part of the biological pump (Bowler, Vardi and Allen, 2010).

Diatoms are traditionally divided into centric and pennate diatoms (Kooistra et al., 2007). While pennate diatoms exhibit bilateral symmetry, centric diatoms are characterized by radial symmetry. It is hypothesized that pennate diatoms form the younger group, which developed from centric diatom ancestors (Kooistra et al., 2007). Generally, diatoms are considered the most species-rich group of algae with over 200 000 different species (Mann and Droop, 1996).

Within the phytoplankton, diatoms contribute massively to the primary production. They are thought to be responsible for 20 % of the global primary production⁶ and are globally distributed (Guillard and Kilham, 1977). As diatoms prefer nutrient-rich conditions they favorably occur in well-mixed coastal and upwelling regions as well as the photic zone in the open ocean (Bowler et al., 2010). Interestingly, the open ocean resembles a biological desert most of the time as conditions are rather oligotrophic (Ryther, 1969). However, during certain times of the year nutrient-rich conditions can be found in the open oceans as well (as summarized in (Ragueneau et al., 2000)).

The role of diatoms in phytoplankton blooms can be exemplified by the well-studied North Atlantic spring bloom. It is generated and dominated by diatoms and initiated by changing abiotic conditions (Lochte et al., 1993; Sieracki, Verity and Stoecker, 1993). For example due to mesoscale eddies, circular moving water masses that episodically re-enrich the euphotic zone with new nutrients. It has been suggested that these eddies trigger diatom productivity and are closely linked to diatom maxima found in the open-ocean Northeast Atlantic (Romero et al., 2016).

Due to the fact that diatoms are superior competitors for nutrients (e.g. nitrate⁷), they dominate the onset of the bloom (Bowler et al., 2010). However, as soon as silicate becomes limited, diatom abundance declines and other phytoplanktonic groups, like small dinoflagellates, become abundant. Thus, a characteristic species succession is created during the course of the bloom, representing biological diversity within phytoplankton. However, biological diversity is not only constituted by different species. Just recently it has been found that genetically distinct populations of the diatom *Thalassiosira gravida* co-exist during the North Atlantic spring bloom (Chen and Rynearson, 2016). The biological diversity, represented by multiple, genetically distinct populations within single

⁶ (Bromke et al., 2013) referring to (Falkowski et al., 1998; Field et al., 1998)

⁷ (Allen et al., 2006) referring to (Sarhou et al., 2005)

species, might present a crucial evolutionary advantage of the diatom genus and might be one reason for their global success (Chen and Rynearson, 2016).

Skeletonema sp. and Thalassiosira sp.

Among centric diatoms, the genera *Skeletonema* and *Thalassiosira* represent well-researched and globally distributed taxonomic groups. Both genera comprise dominant bloom formers in the group of non-toxic phytoplankton species⁸ and have been reported to co-occur in the marine environment (Paul et al., 2009). Interestingly, both genera are well studied in the context of chemically-mediated interactions (see chapter 1.3 and 1.5 for more details).

The genus *Thalassiosira* comprises about 100 species in the freshwater and marine environment⁹. The species *T. pseudonana* became especially popular, as it was the first diatom whose genome was fully sequenced (Armbrust et al., 2004). It is considered an important model organism, as the genetic information provides a valuable tools in the investigation of diatom biochemistry. However, by now whole-genome sequencing has been reported for a number of phytoplankton species (see (Ianora et al., 2011) and included references). Interestingly, *T. pseudonana* is a highly conserved species, as it exhibits low genetical diversity among available strains (Rad-Menéndez et al., 2015). Another representative of the genus *Thalassiosira* is *T. weissflogii*, a diatom well known for its interaction with *Skeletonema costatum* (Paul et al., 2009).

Within the genus *Skeletonema*, *S. costatum sensu lato* (s.l.) represents a diatom key player that can be globally found with exception of the Antarctic Ocean (Kooistra et al., 2008). In 1973, Hasle¹⁰ described a huge morphological diversity within *S. costatum* (s.l.) and recently, the species concept of *S. costatum* (s.l.) has been revoked (Kooistra et al., 2008). Based on molecular data and diatom morphology, *S. costatum* (s.l.) has been separated into multiple species (Medlin et al., 1991; Zingone et al., 2005; Sarno et al., 2005, 2007), *inter alia*: *S. pseudocostatum*, *S. costatum sensu stricto* (s.s.), *S. grevillea*, *S. ardens*, *S. dohrnii*, *S. grethae*, *S. japonicum* and *S. marinoi*. As a consequence, the identity of previously as *S. costatum* reported species is questionable (Zingone et al., 2005). Therefore, it is very important to refer to strain numbers and if applicable consider re-identification of commonly used strains, as performed by Kooistra et al. (Kooistra et al., 2008). For the scope of

⁸ *Skeletonema* blooms: see (Kooistra et al., 2008) and references / *Thalassiosira* blooms: see (Dreux Chappell et al., 2013) and references

⁹ (Dreux Chappell et al., 2013) referring to (Round, Crawford and Mann, 1990)

¹⁰ As referred to by (Kooistra et al., 2008)

this thesis, the chemically-mediated interaction between *S. costatum* and *T. weissflogii* as reported by (Paul et al., 2009) will be of high interest.

1.2 The nature of chemically-mediated interactions

In recent years, chemically-mediated interactions came to the fore, as their widespread nature in the marine environment became evident. Not only are they important for phytoplanktonic blooms, but they can also impact ecosystem structure and function on a very basic level (Borowitzka, 2016). Interestingly, physiochemical properties (like nutrients, temperature, light etc.) set the upper limit for biomass formation in bloom situations, but are neither sufficient to explain species succession and abundance in bloom situations (Smetacek and Cloern, 2008), nor species diversity. Besides abiotic factors as nutrient depletion dynamics, biotic factors like grazer or pathogen abundance and chemically-mediated interactions need to be taken into account (Ianora et al., 2006; Pohnert, Steinke and Tollrian, 2007; Smetacek and Cloern, 2008; Strom, 2008).

The discipline investigating these chemically-mediated mechanisms is called ‘chemical ecology’. It matured from a strong chemical focus on natural product discovery into an integrative science that combines chemical and biological aspects to unravel ecological relationships (Hay, 1996). Due to increasingly elaborate experimental designs, high-resolution analytical techniques and up-to-date data analysis tools, chemical ecology is a rapidly evolving and fast growing discipline (Kubanek et al., 2005; Ianora et al., 2006, 2011; Poulson, Sieg and Kubanek, 2009; Sieg, Poulson-Ellestad and Kubanek, 2011; Roy et al., 2013; Schwartz et al., 2016).

As summarized in a number of comprehensive reviews on chemical ecology¹¹, several key life processes have been found to be chemically-mediated in the marine environment: *inter alia* sexual mate recognition and location (Gillard et al., 2013), population synchronization (Vardi et al., 2006, 2007; Vidoudez and Pohnert, 2008; Bidle, 2016), chemical defense in predator-prey interactions (Selander et al., 2006), host-pathogen interactions (Amin, Parker and Armbrust, 2012) and allelopathic interactions among phytoplankton (Gross, 2003). In the context of this thesis, the focus was set on the latter.

Substances involved in chemically-mediated interactions are generally called semiochemicals (Nordlund and Lewis, 1976; Dicke and Sabelis, 1988). However, further terminology is

¹¹Inter alia: (Hay, 1996, 2009; Cembella, 2003; Ianora et al., 2006, 2011; Pohnert et al., 2007; Poulson et al., 2009; Pohnert, 2009; Sieg et al., 2011; Roy et al., 2013; Borowitzka, 2016; Schwartz et al., 2016)

heterogeneous and depends on the proposed context, as reviewed by (Dicke and Sabelis, 1988). Subsequently, a terminology based on the one suggested by (Nordlund and Lewis, 1976) and refined by Dicke and Sabelis (Dicke and Sabelis, 1988) will be used¹²: Semiochemicals are toxins and nutrients on the one hand, which have a direct beneficial or detrimental effect on the interaction partner and infochemicals on the other hand, which carry a message to the partner to elicit response.

Among infochemicals, allelochemicals comprise substances that take part in interspecific interactions, while pheromones mediate sexual processes or social responses within the same species. Furthermore, allelochemicals can be classified according to cost-benefit criteria: Kairomones benefit the receiver, but not the emitter, allomones benefit the emitter and synomones benefit both receiver and emitter (Dicke and Sabelis, 1988). In general, the origin criterion of (Nordlund and Lewis, 1976) has been abandoned, because it neglects the possible importance of 3rd party organisms, *e.g.* via modification or co-production of infochemicals, in chemically-mediated interaction (Dicke and Sabelis, 1988).

When talking about chemically-mediated interactions in the marine environment, it is not only important to recognize the terminology, but also the structural conditions in the aqueous medium. An enormous challenge in chemically-mediated interactions is its scaling ((Zimmer and Zimmer, 2008) and references herein). While emitting organisms might be sized in the μm -range, communication can occur on a scale of kilometers, like in the example of dimethylsulfide (DMS), which originates from phytoplankton and influences various trophic levels up to seabirds (Hay and Kubanek, 2002; Pohnert et al., 2007; Nevitt, 2008). Also on a small scale level, pulses of dimethylsulphoniopropionate (DMSP) have been documented to attract motile phytoplankton species, bacteria and microzooplankton (Seymour et al., 2010). In both cases, the success of communication is determined by chemical, physical and biological properties, as reviewed by Zimmer and Zimmer (Zimmer and Zimmer, 2008).

Every emitting organisms needs a receiving organisms that ‘speaks the same language’, meaning is able to decipher a signal coded by an infochemical (Pohnert, 2009). Thus, among biological properties, the existence of an excretion system in the emitter, suitable biochemical receptors in the perceiver and the supply of a biologically active concentration are crucial (Willis, 1985; Borowitzka, 2016). In the marine environment, infochemicals are transferred via an aqueous medium. In a chemical sense, infochemicals must have characteristics that enable transfer and provide sufficient

¹² Further references in (Dicke and Sabelis, 1988)

stability until the message reaches the receiver (Zimmer and Zimmer, 2008). These substances would be expected to be hydrophilic and rather stable (Zimmer and Zimmer, 2008). However, even infochemicals with hydrophobic character and low solubility have been documented, as they can be suspended and transported by water motion.

This leads to the third aspect: physical properties (Zimmer and Zimmer, 2008). Due to wind, convection or other turbulences, the marine environment is in constant motion. The availability of an infochemical thus greatly depends on fluid flow dynamics, as dispersal rates are crucial for both motile and non-motile organisms. Recreating these structural conditions in laboratory experiments and creating realistic experimental designs is a tremendous challenge in chemical ecology (Zimmer and Zimmer, 2008).

1.3 Allelopathy in phytoplankton communities

Among chemically-mediated interactions in the phytoplankton, allelopathy is the most studied type (Borowitzka, 2016). It has been reported to be closely associated with competition for resources (Reigosa, Sánchez-Moreiras and González, 1999; Legrand et al., 2003) and to play an important role in maintaining biodiversity and ecosystem functioning¹³. As previously described, bottom-up approaches are not sufficient in explaining species succession and species dominance in the sea, for example, the dominance of diatoms in bloom situations (Strom, 2008). In fact, interactions between planktonic organisms, like allelopathy need to be considered (Keating, 1977; Gross, 2003; Legrand et al., 2003; Fistarol et al., 2004; Prince et al., 2008b; Qiu et al., 2014).

The term allelopathy was introduced by Molisch (Molisch, 1937) and evolved in the subsequent years, with the research field broadening. In 1996, the International Allelopathy Society¹⁴ standardized the definition of allelopathy by stating that allelopathy is either a stimulatory or inhibitory interaction between plants and / or plants and their associated micro- and macrofauna. This definition applies to both terrestrial and aquatic ecosystem and compounds involved in the regulation of the interaction are called allelochemicals.

A demonstrative example of the impact and importance of allelopathy in phytoplankton ecology is given by Keating (Keating, 1977, 1978). Keating's study connected observations of phytoplankton species succession in Linsely Pond with allelopathic effects and documented that excreted

¹³ (Borowitzka, 2016) referring to the review of (Gross, 2003)

¹⁴ (Legrand et al., 2003) referring to <http://allelopathy-society.osupytheas.fr/about/> (January 2017)

allelochemicals of one species affect the succeeding species in a potentially stimulatory way. Interestingly, for species that preceded the excreting organisms in species succession, the effect was neutral to negative. Thus, allelochemicals strongly regulate species succession.

In accordance with Keating, Smayda suggested five types of allelopathic interactions in phytoplankton: (1) mutually stimulatory, (2) mutually inhibitory, (3) selectively inhibitory, (4) selectively stimulatory and (5) neutral interactions (Smayda, 1997a). However, in chemical ecology allelopathy often only refers to inhibitory effects between phytoplanktonic organisms (Inderjit and Duke, 2003; Legrand et al., 2003; Granéli and Pavia, 2006). Only recently, the whole spectrum of allelopathic effects is discussed and brought to attention when allelopathy is reviewed (see (Sieg et al., 2011; Roy et al., 2013; Schwartz et al., 2016) in contrast to (Poulson et al., 2009)).

The outcome of allelopathic interactions is influenced by various factors (Legrand et al., 2003). Abiotic factors like light, pH, temperatures, and nutrient status affect allelopathy (Granéli and Johansson, 2003; Granéli and Hansen, 2006; Granéli and Salomon, 2010), as well as biotic factors like cell physiological state or age (Arzul et al., 1999; Kubanek et al., 2005; Yamasaki et al., 2011), associated bacteria (Gross, 2003)¹⁵, receiver and emitter population density (Sharp, Underhill and Hughes, 1979; Jonsson, Pavia and Toth, 2009; Qiu et al., 2011; Yamasaki et al., 2011), species (Keating, 1977, 1978; Fistarol et al., 2004; Kubanek et al., 2005; Yamasaki et al., 2011; Qiu et al., 2014) and intrastain variability in allelopathic potency (Alpermann et al., 2009, 2010). Hereby, not only the release of the emitting organism is impacted, but also the sensitivity of the receiver, which is similarly influenced by biotic and abiotic stress (Fistarol, Legrand and Granéli, 2005).

To get a better grip on the character of allelopathic interactions and to exemplify the introduced principles, subsequently the allelopathic interactions of one toxic dinoflagellates *Karenia brevis* and one non-toxic diatom *S. costatum* will be presented. Both examples illustrate the complexity of chemically-mediated interactions and further demonstrate that allelopathy can have community-wide consequences.

Exemplifying allelopathy in the context of K. brevis

Initially, the interest in allelopathy research was driven by the phenomenon of HABs. As these blooms are hazardous for vertebrates, including humans, it was of key interest to understand underlying dynamics. One prominent and well-studied example is the red tide dinoflagellate *Karenia*

¹⁵ With reference to (Gross, Wolk and Jüttner, 1991; Gross, Meyer and Schilling, 1996)

*brevis*¹⁶. The toxin produced by *K. brevis* is a polyketide phycotoxin that causes lethal effects in vertebrates and is responsible for neurotoxic shellfish poisoning in humans (Flewelling et al., 2005; Watkins, 2008; Landsberg, Flewelling and Naar, 2009). Therefore, its toxicology, physiology and bloom formation have been intensely studied (Prince et al., 2008b; Vargo, 2009; Brand, Campbell and Bresnan, 2012).

However, in addition to its phycotoxin production, *K. brevis* was also reported to influence the growth of co-occurring phytoplanktonic species via excretion of multiple allelochemicals (Kubanek et al., 2005; Prince et al., 2008b, 2010). The impact of these allelochemicals is both species- and cell-density dependent and can result in inhibitory and stimulatory growth effects on co-occurring phytoplankton species (Kubanek et al., 2005).

Negative allelopathy on co-occurring species ranges from mild to strong inhibition and has been partly reported to be reciprocal (Kubanek et al., 2005; Poulson-Ellestad et al., 2014b). For example, the diatoms *Asterionellopsis glacialis* and *S. costatum* both experience mild inhibition by *K. brevis* (Kubanek et al., 2005). However, compared to other species, the negative effect on both diatoms was less pronounced and only mild inhibition was documented. Interestingly, the sensitivity of co-occurring species to *K. brevis* allelopathic shows high variability in some studies (Poulson-Ellestad et al., 2014b). Nevertheless it is suggested that resistance to negative allelopathy is connected to the evolutionary exposure of co-occurring species to *K. brevis* (Kubanek et al., 2005; Schwartz et al., 2016).

Besides negative allelopathic effects, the cryptophyte *Rhodomonas lens* has been reported to be stimulated by the presence of *K. brevis* (Kubanek et al., 2005). As this interaction is caused by allelochemicals (Kubanek et al., 2005), it is categorized as positive allelopathy. Interestingly, some species are completely unaffected by the presence of *K. brevis* as well (Kubanek et al., 2005).

The observation of different allelopathic effects all caused by one species illustrates nicely, how such species can influence bloom succession in the marine environment. Furthermore, in addition to direct allelopathic effects, the response of co-occurring species also impacts species diversity. For example, the two diatoms *A. glacialis* and *S. costatum* are able to undermine negative allelopathy of *K. brevis* (Prince et al., 2008b). Besides the ability to resist *K. brevis* allelopathy by themselves as

¹⁶ Subsequent summary based on the research and reviews by (Kubanek et al., 2005; Prince et al., 2008b)

reported above, these organisms reduce negative allelopathic effects of *K. brevis* bloom exudates on other species as well (Prince et al., 2008b).

Exemplifying allelopathy in the context of S. costatum

Considering non-toxic phytoplankton species, allelopathy of the diatom *S. costatum* has been well studied¹⁷. Yamasaki et al. demonstrated that allelopathic effects of *S. costatum* are both species-specific and cell density dependent (Yamasaki et al., 2011). Furthermore, the allelopathic effect is suggested to be time-dependent, as filtrates from cultures in the late stationary phase exhibited strongest inhibitory effects. Multiple allelochemicals with both positive and negative effects on the growth of co-occurring phytoplankton species were produced (Yamasaki et al., 2011). They investigated the allelopathic effect of *S. costatum* on three diatoms (*Asterionellopsis glacialis*, *Thalassiosira* sp. and *Chaetoceros* sp.) and four dinoflagellates (*Heterosigma akashiwo*, *Prorocentrum dentatum*, *Prorocentrum triestinum* and *Prorocentrum minimum*), all co-occurring with *S. costatum* in the fishing port of Hakozaki (Hakata, Bay, Fukuoka, Japan).

S. costatum can suppress the growth of *H. akashiwo* and vice versa (Yamasaki et al., 2007). The outcome of the observed reciprocal interaction is determined by the fact, which species reaches high cell densities first, as it limits the growth of the less abundant partner. Furthermore, Pratt (Pratt, 1966) documented that while high cell densities of *H. akashiwo*¹⁸ inhibited *S. costatum*, low cell densities had a stimulatory effect on the growth of *S. costatum*. These effects were suggested to explain alternating blooms of *S. costatum* and *H. akashiwo* in the field (Pratt, 1966; Shikata et al., 2008)¹⁹ and the observation that inferior species seem to vanish during blooms of the dominant species¹⁹.

In 2012, Yamasaki described two chemically stable, low-molecular weight allelochemicals, with characteristic ESI-MS fragments of m/z (ratio of mass to charge) 268 and 514, to be involved in negative allelopathic effects of *S. costatum* (Yamasaki et al., 2012). As the negative allelopathic effect on *H. akashiwo* becomes manifested in morphological and lytic effects, the allelochemicals were hypothesized to attack cell membranes (Yamasaki et al., 2011).

¹⁷ Subsequent summary based on the research and reviews of (Yamasaki et al., 2007)

¹⁸ (Yamasaki et al., 2011) stated that the species *Olisthodiscus luteus* as specified by (Pratt, 1966) equaled the species designation *H. akashiwo* in their study

¹⁹ (Honjo, Shimouse and Hanaoka, 1978) as referred to by (Yamasaki et al., 2007)

On the other hand, stimulatory effects of *S. costatum* filtrates have been observed as well. Interestingly, at certain filtrate concentrations and / or cell density ratios, every investigated species also exhibited higher cell yields, compared to their respective control. For example, *P. minimum* and *A. glacialis* had higher maximum growth rates, cell yields and a shorter lag period before the onset of the regular growth phase. The diatom *T. rotula* experienced a stimulatory growth effect, as seen in elevated cell yields. It was hypothesized that these results are closely linked to the observation of bloom succession around *S. costatum* (Yamasaki et al., 2011).

In 2014, Qiu et al. took it a step further and pointed out that via allelopathy *S. costatum* has the potential to shape interspecific competition. It was documented that *S. costatum* exhibits inhibitory effects on the growth of three flagellate species (*Akashiwo sanguinea*, *Chattonella spp.*, *H. akashiwo*), when grown under non-contact culturing conditions, while *Skeletonema* itself remained unaffected by its partners (Qiu et al., 2014). In tri-algal cultures, it was furthermore observed that *S. costatum* changed the relative proportion of the three flagellates to each other (Qiu et al., 2014). Due to the fact that the degree of inhibition was species-specific, each flagellate was inhibited to different intensities. The most susceptible species, *A. sanguinea* and *H. akashiwo*, were reduced in abundance and as a result, the proportion of the least susceptible species *C. antiqua* increased. Thus, it was postulated that negative allelopathy is not only beneficial for the releasing organism but potentially also for any species that shows reduced susceptibility (Fistarol et al., 2004; Qiu et al., 2014).

Similar conclusions were drawn by Yamasaki: Among the three *Prorocentrum* species investigated, *P. minimum* was most tolerant towards negative allelopathic effects of *S. costatum* (Yamasaki et al., 2011). This has the potential to explain the partial occurrence of mixed blooms of *S. costatum* and *P. minimum* species in the field and the observation that first *P. minimum* and after that *P. dentatum* and *P. triestinum* followed *S. costatum* in the bloom succession.

To sum it up, both model organisms clearly depict the complexity, extent, interdependence and impact of chemically-mediated interactions in the context of allelopathy.

Identification of allelochemicals

The unambiguous identification of allelochemicals is still missing and represents one of the current challenges in chemical ecology. However, some studies were able to partially characterize the compounds mediating phytoplankton interactions. The subsequent summary is based on the review of (Sieg et al., 2011; Borowitzka, 2016). The results suggest a variety of compounds and compound

classes to be involved, which can generally be classified as low-molecular weight and high-molecular weight substances, as proposed by (Tameishi et al., 2009).

Prince et al. reported multiple, rather polar, low-molecular weight allelochemicals (500 – 1000 Da) with aromatic functional groups to mediate the negative allelopathic effect of *K. brevis* on the diatom *A. glacialis* (Prince et al., 2010). Yamasaki et al. described both inhibitory and stimulatory effects of the diatom *S. costatum* on the raphidophyte *H. akashiwo* and suggested at least two low-molecular weight allelochemicals (m/z 268 and 514) to be involved in the inhibitory effect (Yamasaki et al., 2012).

Among high-molecular weight substances, it has been shown that *H. akashiwo* releases polysaccharide protein complexes of >3500 Da with allelopathic effect on the diatoms *T. rotula* and *S. costatum* (Yamasaki et al., 2009). Furthermore, *Alexandrium* dinoflagellates exude several stable allelochemicals in the range of 5,000-500,000 Da with negative allelopathic effect on *Rhodomonas salina*, which are hypothesized to have amphipathic chemical characteristics (Ma et al., 2009). And the interaction between the dinoflagellate *Prorocentrum minimum* and the diatom *S. costatum* was caused by one or several high molecular weight (> 3,000 Da), polysaccharide-like allelochemicals, emitted by *P. minimum* (Tameishi et al., 2009).

In summary, the exudation of multiple allelochemicals by an organism seems to be a common strategy. Due to the fact that the effect of allelochemicals is strongly species-specific and dependent on various biotic and abiotic factors, the release of multiple compounds with potentially synergistic effects might be of advantage (Sieg et al., 2011).

1.4 Prominent methods in allelopathy research

The fact that only a few allelochemicals have been identified yet proves that the investigation of chemically-mediated interactions presents considerable challenges. Firstly, realistic ecological assays are needed to reproduce the effects observed in the field and to gain new hypotheses. Secondly, adequate and sensitive chemical methods need to be coupled with elaborate data analysis tools to identify involved allelochemicals. And thirdly, results and hypotheses obtained in laboratory experiments must be validated under natural conditions, *e.g.* via field experiments.

Recreating chemically-mediated interactions

Several methodologies have been used to investigate allelopathy. In a first step, the allelopathic effect needs to be recreated. This can be done in various ways, the most static way is to take either medium extracts of a putatively allelopathic active species²⁰ or the medium itself²¹ and add it to the culture of another species to then observe resulting consequences. Medium extract hereby means that potential allelochemicals present in the medium of a culture are chemically extracted and thus concentrated. However, this approach offers a very punctual and simplified insight in allelopathic interactions. By adding the culture medium / extract of one organism to another organism at a certain time point in their respective life phases, the static approach simulates only one specific time point in an allelopathic interaction. Continuous monitoring of the interaction is difficult due to the simulation design.

In this context, some studies used cell extracts of allelopathic species for the investigation and simulation of allelopathy²². However, this method doesn't appear reasonable for investigating chemically-mediated actions, as allelochemicals need to be present in the environment, not the cell itself, to be noted by a receiving organism. Thus, simulating allelopathy by adding intracellular extracts of an organism to the culture of another organism is a very counterintuitive approach.

A more elaborate and dynamic way to recreate chemically-mediated interactions is to bring both interaction partners into contact with each other and observe the interaction. Several researchers used mixed cultures for this purpose, meaning that one organism is directly inoculated into the culture of its interaction partner²³. (Paul et al., 2009) used a dialysis tube approach, which separated both interaction partners in 'mixed cultures'. In principle, one organism is inoculated into a culture vessel and the second organism is inoculated into a dialysis tube. Subsequently, the dialysis tube is submerged into the culture similar to a tea bag being introduced into a cup of water. In contrast to mixed cultures (*sensu stricto*), this method reduces any interaction to non-contact chemical communication between the organism in the culture vessel and its partner in the dialysis tube. However, due to the design of the set-up, this approach enabled sampling of only one of the interaction partners, as the dialysis tube was not accessible to sampling.

²⁰ Compare (Prince, Myers and Kubanek, 2008a; Tameishi et al., 2009; Yamasaki et al., 2010)

²¹ Compare (Fistarol et al., 2004; Tameishi et al., 2009)

²² Compare (Freeberg, Marshall and Heyl, 1979) as referred to by (Kubanek et al., 2005)

²³ E.g. (Schmidt and Hansen, 2001; Tillmann, John and Cembella, 2007)

Yamasaki and Qiu and further improved this technique by using well-plates and filter membranes, which separated interaction partners (Yamasaki et al., 2007; Qiu et al., 2014). Unfortunately, only small volumes of cultures can be investigated with this method, which might not be sufficient to obtain effectual allelochemicals amounts.

Therefore in 2013, Paul introduced a further developed co-cultivation approach, as depicted in **Figure 1** (Paul, 2012; Paul, Mausz and Pohnert, 2013). Opposite to their early dialysis tube set-up, this approach is based on co-cultivation chambers: Glass vessels that each consist of two chamber halves, which are separated by a semi-permeable hydrophilic membrane filter with a pore size of 0.22 μm (see 6.2.1 for details). The membrane filter allows free diffusion of potential infochemicals and nutrients (as shown by Pau et al. (Paul et al., 2013)), but prevents interspecific contact of diatom cells and mixing of bacterial communities associated with the diatoms species.

Thus, with this cell-contact free approach, it is possible to simplify the complexity of chemically-mediated interactions, focusing on the interaction between two partners in their respective bacterial environment. Another major advantage of the co-cultivation set-up is the accessibility of both chamber halves via individual openings, allowing continuous sampling under sterile conditions. The volume of each co-cultivation set-up allows sample sizes that are big enough to guarantee a sufficient yield of allelochemicals for subsequent investigation. Furthermore, the state of the cultures can be monitored at all times during the interaction. This is due to the fact that opposite to static simulations, dynamic simulations depict the interaction process as a whole as both interaction partners are in constant presence with each other. It might be said, that static simulations are snapshots of the interactions, while dynamic simulations represent a movie of the interaction.

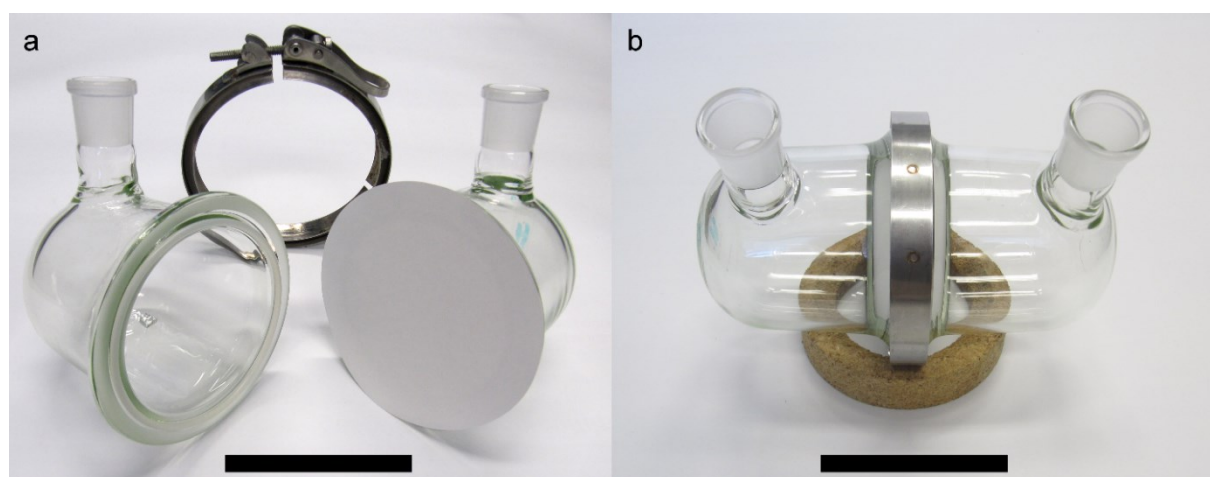


Figure 1: Co-cultivation chamber before (a) and after (b) assembly. Scale bar represents 10 cm. Source: (Paul et al., 2013) with permission of Springer.

Investigation of allelochemicals

In a second step, it is of interest to unravel the underlying mechanisms of chemically-mediated interactions, for example by identifying involved allelochemicals.

A very basic and traditional approach to identify allelochemicals is bioassay-guided fractionation (Prince and Pohnert, 2010): In a first step, an active crude extract from the medium of an allelopathic organism is obtained and tested for allelopathic activity with the help of a bioassay. Hereby, the extract is added to the culture of a competitor, which is then monitored for alterations indicating allelopathic effects. In a next step, the extract is further fractionated and each fraction is again tested for allelopathic activity. This process is repeated until the crude extract is narrowed down to fractions optimally containing pure compounds with allelopathic activity, which then can be identified via standard analytical techniques. An example of a bioassay-guided fractionation approach can be found in Yamasaki et al. (Yamasaki et al., 2010, 2012).

This approach has several drawbacks, as reviewed by Prince and Pohnert (Prince and Pohnert, 2010): on the one hand, the workflow is immensely time-consuming and due to repeated losses during fractionation it yields very small quantities of allelochemicals. On the other hand, multiple extractions and fractionation steps bear immense risks of losing chemical compounds due to residues or degradation. Furthermore, synergistic effects between allelochemicals cannot be displayed by the bioassay guided fractionation approach, as concurring allelochemicals might be separated in the process and not present in the same fraction during the bioassays. Most importantly, the traditional approach doesn't account for induced mechanisms of allelochemicals excretion, because it is focused on the investigation of the medium of one species rather than the interaction process.

Metabolomic techniques

A powerful alternative is offered by metabolomic techniques. The metabolome of an organism represents the link between genotypes and phenotypes (Fiehn, 2002). Compared to genome, transcriptome and proteome, the metabolome offers a uniquely specific description of biochemical functions and roles of an organism (Oliver, 1996; Fiehn, 2002). The metabolome of a cell consists of various metabolites, which themselves are intermediate products of the cell's biochemical pathways.

In chemical ecology, metabolomic techniques are commonly used to unravel underlying mechanisms of chemically-mediated interactions (Prince and Pohnert, 2010; Sardans, Penuelas and

Rivas-Ubach, 2011; Kuhlisch and Pohnert, 2015). Various techniques are applied in the metabolomics field (Fiehn, 2002; Shulaev, 2006; Prince and Pohnert, 2010): ‘Targeted metabolomics analysis’, ‘metabolite profiling’, ‘metabolic fingerprinting’ and ‘metabolomics’²⁴. The choice of technique determines the scope of the investigation and varies with the research question.

While a targeted metabolomics analysis is focused on a small subset of metabolites, *e.g.* fatty acids (Vidoudez and Pohnert, 2011), the general metabolomics approach tries to quantify and identify all existing metabolites of a system. Metabolomic fingerprinting is similarly global as it is not targeted (Huseby et al., 2012). It doesn’t identify the individual metabolites, but is focused on abstract pattern recognition on the basis of unidentified mass spectral tags (MSTs)²⁵. This technique is often used in disease research to characterize and recognize diseases via biomarkers and specific metabolomic fingerprints (Ellis and Goodacre, 2006; Ellis et al., 2007).

As defined by Kopka, an MST is unambiguously characterized by molecular mass to charge (m/z) ratio, retention index and a full a GC-EI/MS mass spectrum (Kopka, 2006). Depending on the context, one might rather refer to ‘MSTs’ than to compounds or metabolites, as one compound might be represented by multiple MSTs in a metabolomic investigation. For example, different MSTs can result due to varying degrees of derivatization efficiency of compounds with multiple functional groups (Gehrke, Nakamoto and Zumwalt, 1969; Kanani and Klapa, 2007).

Metabolomic profiling offers a compromise of the previously described strategies. It counts as a global approach, as it tries to identify as many metabolites as possible (Vidoudez and Pohnert, 2011; Matusz, 2014). However, it can be restricted to a selected number of pre-defined metabolites, *e.g.* certain compound classes or metabolites of certain biochemical pathways. Furthermore, metabolomic profiling is considered to be semi-quantitative, as it works with relative MST quantities rather than with absolute quantities. In most studies, the majority of MSTs remain unidentified.

Especially popular in marine chemical ecology are targeted metabolomics analysis and metabolomic profiling. Vidoudez et al. used a profiling approach in the metabolomic investigation of the diatom *S. marinoi* (Vidoudez and Pohnert, 2011) with the aim to connect metabolomic patterns to different growth phases. Furthermore, they performed a targeted metabolomics analysis of

²⁴ Subsequent explanation based on the reviews of (Fiehn, 2002; Shulaev, 2006)

²⁵ In the following, MS-based techniques are discussed exclusively. Alternative NMR approaches are not yet established in the marine, metabolomic-based investigation of interactions.

polyunsaturated aldehydes (PUAs) and fatty acids, as these MST classes are hypothesized to be involved in intraspecific signaling and programmed cell death (Vardi, 2008), anti-grazing defenses (Miralto et al., 1999), allelopathy (Hansen and Eilertsen, 2007; Ribalet et al., 2007) and bacteria-phytoplankton interactions²⁶ (Ribalet et al., 2008)²⁷ (as reviewed by Poulson et al. (Poulson et al., 2009).

The metabolomic profiling protocol of (Vidoudez and Pohnert, 2011), consisting of extraction, derivatization and GC/MS analytics, is optimally suited for the investigation of planktonic organisms and was used in the scope of this thesis (see chapter 2.5.1 and 6.6 for more details).

Metabolomic strategies in environmental science

If metabolomic techniques are used to investigate organism's interactions with the environment, the term environmental metabolomics should be used, as suggested by (Miller, 2007). A major challenge in environmental metabolomics is setting a metabolomic baseline to identify metabolomic changes connected to certain environmental stimuli (Viant, 2007). Biological variability of metabolomic samples demands an appropriate experimental strategy to set the focus on 'relevant' changes. For example, (Vidoudez and Pohnert, 2011) used a comparative approach in the previously described investigation of *S. marinoi*. This was achieved by comparing samples from different growth phases of *S. costatum* cultures under closely monitored conditions with each other.

In the context of chemically-mediated interactions, (Paul et al., 2009) used a comparative metabolomic approach to investigate the stimulatory effect of the diatom *S. costatum* and the diatom *T. weissflogii*. By comparing each diatom's metabolome in an interaction situation with the metabolome in a non-interaction situation, the focus was set on interaction-induced metabolomic alterations. Again, the cultures were closely monitored and experimental specifics were standardized among cultures and samples. In the context of this thesis, the interaction between *S. costatum* and *T. weissflogii* has a special relevance and will thus be described shortly.

²⁶ Controversially discussed by (Paul et al., 2012)

²⁷ Summary based on the review of (Poulson et al., 2009). See (Caldwell, 2009; Leflaive and Ten-Hage, 2009; Ianora and Miralto, 2010; Borowitzka, 2016) for further reviews.

1.5 The stimulatory interaction between *S. costatum* and *T. weissflogii*²⁸

Paul investigated the stimulatory effect of *S. costatum* on *T. weissflogii* cultures (Paul et al., 2009): Both diatoms are well-known to researchers of the marine environment, have previously been studied and been reported to co-occur. When both diatoms are grown together under non-contact conditions, the significantly enhanced growth of *T. weissflogii* and unaltered growth of *S. costatum* has been documented. These observations have been hypothesized to be caused by positive allelopathic interactions between the diatom species. However, underlying mechanisms of the observed growth effect were unknown at that time.

The recreation of the interaction was conducted with the simplified dialysis tube co-cultivation set-up previously described. The investigation of underlying mechanisms was performed with a comparative metabolomic profiling technique. Opposite to traditional approaches, which only investigate selected parameters of an interaction, this powerful tool-set allows a global investigation of chemically-mediated interactions. The metabolomic approach sets the focus on physiological responses of both partners in the interaction.

The study results confirmed chemical cross-talk between *S. costatum* and *T. weissflogii*. It was documented that several metabolites were only found in the medium of *S. costatum* and several only in the medium of *T. weissflogii*. As these metabolites were neither present in the medium of the respective partner, nor during the interaction of both organisms with each other it was hypothesized that either inhibition of synthesis / excretion, transformation or active uptake by the interaction partner occurred. Communication via exuded compounds was strongly suggested. The endometabolomic investigations confirmed significant changes in cell physiology due to the interaction. Both interaction partners seem to be able to sense the presence of each other.

The identification of involved compounds remained open. Via UPLC-ESI/MS, compounds were only characterized by *m/z* retention time pairs. However, it was suggested that neither amino acids nor extracellular carbohydrates were involved in communication. Several hypotheses for underlying mechanisms were presented: allelopathic interactions, heterotrophic interactions, release and

²⁸ Chapter is based on the investigation of Paul et al. (Paul et al., 2009)

subsequent uptake of nutrients and involvement of associated bacteria. To get more insight into this interaction, further investigations are necessary.

1.6 Objective

Astonishingly, the global response of diatoms to their environment is a comparably under investigated topic. As previously described, diatoms are of essential importance for marine and terrestrial ecosystems, especially in bloom events. It is thus of high interest to unravel underlying mechanisms of allelopathic phytoplankton dynamics, particularly in bloom situations. So far, research focused on negative allelopathic effects and, if at all, allelochemicals involved in negative allelopathic effects were described. However, some positive growth effects were documented and discussed in the context of positive allelopathy, for example, the stimulatory interaction between *S. costatum* and *T. weissflogii* (Paul et al., 2009).

By choosing an untargeted, comparative GC/TOF-MS -based metabolomic approach with continuous monitoring of diatom cultures, this thesis aims at further characterizing diatom interactions in the context of allelopathy. The focus is set on the interaction of *Skeletonema* sp. with the co-occurring species *T. weissflogii*. Compared to previous studies, the identification of significant interaction-induced metabolomic responses was advanced by combining elaborate co-cultivation set-ups with GC/TOF-MS metabolomic profiling techniques. In this context, available MS libraries facilitated the identification of significant metabolites.

Chapter 2 presents the investigation of the interaction between *T. weissflogii* (RCC76) and *S. costatum* (RCC75), chapter 3 the interaction between *T. weissflogii* (CCMP1336) and *S. marinoi* (CCMP1332) and chapter 4 the interaction between *T. weissflogii* (CCMP1336) and *S. dohrnii* (CCMP3373).

In my thesis, I used both the hypothesis- and the discovery-driven nature of metabolomic techniques (Miller, 2007) to:

- describe cellular responses of each diatom to the presence of a partner (endometabolome)
- describe interaction-induced alterations in the chemical environment (exometabolome)
- gain hypotheses about potential infochemicals and release / uptake mechanisms (exometabolome)
- unravel interaction and communication principles.

Furthermore, I tested the hypothesis of involvement of associated bacteria via a medium exchange experiment (chapter 2.3), and the potential stimulatory effect of the prominent semiochemical DMSP on diatom growth (chapter 2.4).

2 Interaction of *T. weissflogii* with *S. costatum*

This chapter aims at further unravelling the stimulatory interaction between the diatoms *T. weissflogii* and *S. costatum*, as documented by Paul et al. and previously introduced in chapter 1.5 (Paul et al., 2009).

Before presenting and discussing the results of the individual experiments, I describe and discuss the general approach and individual experimental strategies in chapter 2.1. Subsequently, the experimental specifics for the individual investigations are given. Hereby, the principles described for the interaction experiment in chapter 2.2 form the basis of the “medium experiment” in chapter 2.3 and the interaction experiments in chapter 3 and 4 as well.

Chapter 2.2 investigates the interaction between *S. costatum* and *T. weissflogii*. The observed growth effect is documented and the focus is set on the metabolomic investigation of the chemical-interaction. Here, an intracellular and extracellular perspective on metabolomic changes in both diatoms is presented, using gas chromatography coupled with time-of-flight mass spectroscopy (GC-TOF/MS) based metabolomic profiling. Subsequently, the metabolomic alterations are connected to the observed growth effects.

Chapter 2.3 supplements these results by testing the possible influence of the diatom partners' bacterial communities and chemical environments on diatom growth at the onset of the investigation. Furthermore, chapter 2.4 tests the hypothesis of dimethylsulphoniopropionate (DMSP) being responsible for the stimulatory growth observed in *T. weissflogii*.

In chapter 2.5, an interim conclusion on the interaction between *T. weissflogii* and *S. costatum* is given, merging the insights of the individual experiments. An overall conclusion on all interaction-investigations and a discussion of metabolite flux between the partners is presented in chapter 5.

2.1 Study design

The value of metabolomic investigations is strongly influenced by the way metabolomic data is reported. The Metabolomic Standards Initiative (MSI) developed minimal reporting standards to guarantee proper sharing, use and re-use of metabolomic data (Fiehn et al., 2007; Fernie et al., 2011). Only with an adequate description of *inter alia* the biological context, chemical analysis and data processing, metabolomic data can be sustainably used, correctly interpreted and maximum value can

be extracted (Fiehn et al., 2007). This chapter addresses these aspects with additional specifics documented in the material and methods part (chapter 6.1 -6.7).

2.1.1 General approach

Small scale co-cultivation set-up

I used an elaborate small scale co-cultivation set-up, introduced by Paul to recreate the interaction between *S. costatum* and *T. weissflogii* ((Paul et al., 2013), **Figure 1**). This co-cultivation set-up has been previously introduced in chapter 1.4. Specifics about parts, assembly and handling are documented in chapter 6.2.

The eligibility of this set-up for the investigation of chemically-mediated interactions has been tested by Paul (Paul et al., 2013): Firstly, the installation of a biocompatible 0.22 μm polyvinylidene fluoride (PVDF) filter guarantees the separation of algae and associated bacteria in both chamber halves (tested by (Paul et al., 2013), data not shown). Secondly, in investigations of chemically-mediated interactions the free flux of infochemicals between the partners is essential. Therefore, various diffusion assays have been evaluated by Paul, confirming free flux of compounds between both chamber halves within the first hours after addition. Hereby, the diffusion of macronutrients was investigated via nitrate diffusion, and the diffusion of potential infochemicals via DMSP – a highly polar, low molecular weight metabolite – and the less polar heptadienal. The results confirm that the set-up is ideally suited for the investigation of chemical mediated interactions and nutrient effects.

However, it must be noted that some compounds (*e.g.* heptadienal) have been found to be potentially adsorbed by the glass or the membrane, resulting in reduced concentrations (Paul et al., 2013). Furthermore, highly lipophilic substances have not been evaluated (Paul et al., 2013). Although it has been shown that high molecular weight substances like Microcystin can diffuse through the membrane (Dunker et al., 2017), they are not in the range of the GC-analysis. Thus, in the interpretation of experimental results it must be taken into consideration that these substances are possibly excluded / reduced in abundance due to experimental design.

Comparative investigation principles

The interaction was investigated in a comparative manner: I compared each species in interaction with itself in a non-interaction control, not only in the metabolomic analysis (chapter 2.2.3 and

2.2.4), but also concerning growth parameters (chapter 2.2.1) and metadata (chapter 2.2.2). Thus, I created an adequate baseline, as called for by Viant (Viant, 2007).

To do so, I introduced a primary set of treatment groups that formed the basis of all co-cultivation experiments. The interaction was explored via the co-cultivation group (**Figure 2B**): Each chamber housed both diatom species, one in each chamber half. To provide the non-interaction context, two control groups were established: The mono-cultivation group of *T. weissflogii* (**Figure 2A**), containing *T. weissflogii* culture in both chamber halves of one chamber set-up, and the mono-cultivation group of *S. costatum* (**Figure 2C**), containing *S. costatum* culture in both halves. However, depending on the experimental design of the individual experiments, I introduced additional treatment groups (see chapter 2.1.3 for more information).

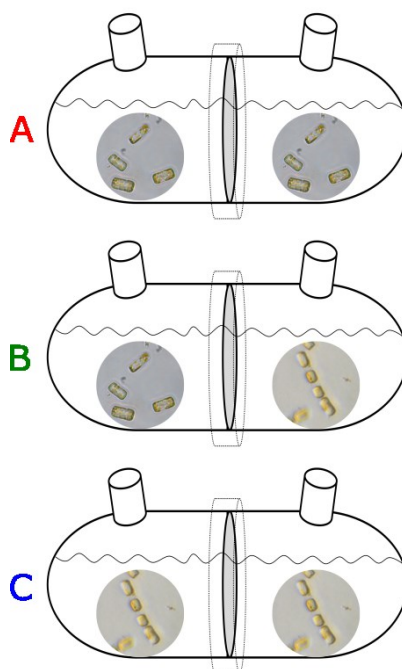


Figure 2: Experimental design to investigate the interaction between *T. weissflogii* and *S. costatum* in a small-scale co-cultivating set-up.

Each chamber consisted of two chamber halves which were filled with cultures of the same diatom species (**A**, **C**) or with cultures of two different species (**B**) to recreate a chemically-mediated interaction. **A:** Mono-cultivation group with *T. weissflogii* (control; $n^{29} = 3$), **B:** Co-cultivation group, *T. weissflogii* with *S. costatum* (investigated interaction; $n = 3$), **C:** Mono-cultivation group with *S. costatum* (control; $n = 3$).

To ensure maximally possible comparability and to focus on interaction-based effects rather than artificially introduced differences in measured parameters, I took the following measures: each experiment was based on one stock culture of *S. costatum* and of *T. weissflogii* respectively, with

²⁹ “n” refers to the number of replicates (see chapter 6.2.6 for more details)

identical pretreatment. All treatment groups were cultured and sampled identically and in a randomized manner. Sample treatment, storage and analysis was standardized and randomized at least within each sampling day. Data analysis and work-up has been standardized (more details in chapter 6). Thus, I precluded the introduction of serial errors and artifacts and minimized biological variability among cultures.

2.1.2 Design: Interaction experiment

The interaction experiment aims at further elucidating the impact of the chemical interaction between *S. costatum* (RCC75) and *T. weissflogii* (RCC76) on both partners (Paul et al., 2009). While Paul et al. used a rather simple, dialysis-tube based co-cultivation set-up and ultra-performance liquid chromatography electrospray mass spectrometry (UPLC-ESI/MS) analysis, I built this experiment on the elaborate co-cultivation chamber set-up previously described (**Figure 2**) and a gas chromatography electron ionization time-of-flight mass spectrometry (GC-EI/TOF/MS) analysis to gain complementary and more specific insights. Advantages of this approach are discussed in chapter 1.4 (discussion of co-cultivation set up) and chapter 2.5 (discussion of metabolomic strategy).

The experiment was conducted over 32 days, starting with stock cultures in exponential growth phase, which were diluted with fresh artificial seawater medium (ASW) (v/v_{sw} 1/3) at the onset of the experiment. Each of the primary treatment groups contained three chambers, which replicated the respective set-up in triplicates (**Figure 2**). Diatom growth was monitored via chlorophyll a fluorescence (chl a) and the physiological state of the cultures via photosystem II efficiency (PSII efficiency), a parameter reflecting nutrient stress. Both parameters were measured every 2nd to 4th day. On three distinct points of the growth curve (day 16, 26 and 32) I took samples for cell counts and metabolomic analysis. I chose the first time point (day 16) to represent the onset of the documented growth effect (Paul et al., 2009), the latter points in time to represent early (day 26) and late stages of the growth effect (day 32).

I chose a batch culture approach to recreate the growth dynamics in bloom situations. The three growth phases observed in batch cultures – the regular, stationary and declining phase (see chapter 2.2.1) – recreate the phases observed in blooms. In blooms, the regular growth phase is followed by a decline in growth due to nutrient limitation and a final senescence phase ((Gran, 1931; Fogg and Thake, 1987) as referred to by (Diekmann et al., 2009)).

The number of biological replicates depends on the character of the measured parameter. It was mainly determined by the fact, if a measured parameter was specific for the chamber half, or the whole chamber (more details in chapter 6.2.6). Generally, I set the focus on biological replication with at least three replicates, which was rated most significant by Fernie et al. (Fernie et al., 2011). Furthermore, I repeated the interaction experiment of *T. weissflogii* and *S. costatum* to confirm the robustness of results (results not shown here).

Chl a fluorescence and PSII efficiency as estimators of biomass and nutrient stress

As previously described, I conducted continuous monitoring of diatom growth via chl a fluorescence, as this parameter is a very easy and – compared to cell counts – a much faster way to estimate biomass. Chl a fluorescence parameters have been widely used to monitor phytoplankton biomass and status. However, data must be interpreted with care and at distinct time points of interest, cell counts were taken as reliable and unambiguous representation of biomass.

Considering chl a fluorescence, a correlation between biomass and *in vivo* fluorescence has been reported and the comprehension that chl a fluorescence ‘equals’ biomass is wide spread (Kruskopf and Flynn, 2006). However, chl a fluorescence has been found to be highly variable, for example due to species differences, diel changes or nutrient limitation (Kruskopf and Flynn, 2006). Therefore, depending on the experimental context, Kruskopf and Flynn strongly challenged the eligibility of chl a fluorescence – and PSII efficiency – as robust and reliable indicators of biomass and nutrient status (Kruskopf and Flynn, 2006).

In the course of this thesis, these limitations were considered and no inter-species comparisons were made (Kruskopf and Flynn, 2006). By using a comparative approach, I set the focus on interaction-induced alterations. I used the correlation between chl a fluorescence and biomass to estimate diatom biomass and draw hypotheses about diatom growth phases, based on chl a development over time. Meaning that fast increase of chl a fluorescence indicates the regular growth phase, stable chl a fluorescence indicates the stationary growth phase and decline in chl a fluorescence indicates the declining phase. However, in consideration of the highly variable nature of chl a fluorescence, I took cell counts into account to substantiate any biomass related statement, *e.g.* hypotheses about growth phases. If at all, parameters were expressed on cell count basis (*e.g.* endometabolomic alterations).

Considering PSII efficiency, Yentsch et al. (Yentsch et al., 2004) strongly advocated the validity of interpreting PSII efficiency in batch cultures as an indicator of nutrient stress (Yentsch et al., 2004). However, this opinion is challenged by Kruskopf and others (Kruskopf and Flynn, 2006). These authors reported high species-specific variability in PSII efficiency, as well as uncertainty in the interpretation of PSII efficiency due to the influence of environmental factors, like irradiation or time of day.

Nevertheless, Kruskopf et al. suggested the utility of PSII efficiency in single species investigations, while strongly advising against using it in mixed communities. Furthermore, Parkhill et al. proclaimed PSII efficiency to be a sensitive indicator of nutrient stress during unbalanced growth (Parkhill, Maillet and Cullen, 2001). Based on these assessments, I used PSII efficiency as a tool in the estimation of nutrient stress. Especially considering that my focus is set on intraspecific investigations of PSII efficiency differences – thus fulfilling the single species criterion and considering that the investigation was based on batch cultures – fulfilling the criterion of unbalanced growth.

Decreasing values of PSII efficiency indicate nutrient stress conditions and reduced photosynthetic rate (Roy and Legendre, 1979; Parkhill et al., 2001). When nutrient storages in the cell are exploited and nutrient availability is limited, the synthesis of essential cellular compounds is blocked and as a result the cells experience adverse physiological effects ((Parkhill et al., 2001) and references herein) – the PSII efficiency declines. However, any interpretation must be made with care, as the correlation between PSII efficiency and nutrient stress has been documented to break down if phytoplankton becomes acclimated to nutrient stress (Parkhill et al., 2001). In consideration of the rather short termed nature of my batch culture experiments, this constraint was considered not applicable.

Apart from the monitoring character of chl_a fluorescence and PSII efficiency, I used both parameters to screen for interaction-induced alterations / effects in each diatom partner. Based on the assumption that all environmental parameters are kept stable (all cultures originated from one stock culture, were treated alike and were handled, sampled and stored under equal conditions), differences in fluorescence parameters (chl_a fluorescence and PSII efficiency) within each species and sampling point have the power to indicate interaction-induced differences in physiology.

Metabolomic analysis

Analogous to the approach of Paul, I chose a comparative metabolomic profiling analysis, focusing on both, the endometabolome and the exometabolome of the interacting organisms (Paul et al., 2009). The metabolomic strategy is discussed in chapter 2.5.

Exometabolome

The exometabolome represents the chemical environment of the diatoms. It comprises all stable metabolic substances that were exuded from the organisms and thus present in the culture medium at the specific sampling time. The exometabolome was characteristic for the whole chamber (n = 3 per treatment group)³⁰. It is important to note that a fixed volume of medium was investigated per chamber at all three sampling points. The exometabolome was therefore not normalized to cell counts, but reflected the chemical environment, as it was shaped by all interaction-induced alterations (including altered growth characteristics). Therefore, it was of interest to identify metabolites causing differences between mono- and co-cultivation, rather than to create a metabolomic inventory of the chemical environments. By defining distinct MST intensity patterns among the treatment groups, I identified potential interaction-induced infochemicals and gained hypotheses about induced release and / or uptake mechanisms in the course of the interaction.

Endometabolome

The endometabolome reflects all metabolites that are present within the cells at a certain time. Opposite to the exometabolome, the endometabolome characterized each chamber half by itself. This is due to the fact that the filter membrane between the chamber halves separated each chamber in two realms. As a consequence, each chamber of the mono-cultivation groups resulted in two endometabolomic samples per species (n = 6 for each species in mono-cultivation)³¹, while the chamber of the co-cultivation group resulted in one endometabolomic sample per species (n = 3 for each species in co-cultivation)³². I chose this approach, resulting in twice the amount of replicates in the mono-cultivation groups, to standardize procedures between the mono- and co-cultivation groups, and to maximize the power of the metabolomic investigation. The interdependency between

³⁰ n = 2 on day 26 (see chapter 6.4 for specification)

³¹ n = 4 within mono-cultivated *T. weissflogii* on day 16, n = 5 within mono-cultivated *S. costatum* on day 16 and 32 (see chapter 6.4 for details)

³² See chapter 6.2.6 for more details

samples of the mono-cultivation groups was accounted for in the statistical analysis (as discussed in chapter 2.5.3).

Within each experiment, I obtained the endometabolome on the basis of a fixed cell count, as suggested by (Vidoudez, 2010). In the interaction experiment between *T. weissflogii* and *S. costatum* I normalized the endometabolome to a count of 18.7×10^6 cells. The normalization by cell count enables the comparability between samples and the interpretation of endometabolomic alterations on single cell level. However, inter species comparison is not advised, as *Skeletonema* sp. and *Thalassiosira* sp. are quite different in cell sizes and thus in biomass per cell count. *Thalassiosira* sp. have been reported to range in size from 2-186 μm (mostly $< 80 \mu\text{m}$) and *S. costatum* ranges from 2-61 μm ³³. However, this was not a restriction as I set the focus on interaction-induced endometabolomic alterations within each species.

It must be noted that sample handling during the workflow of the endometabolomic analysis was not optimal, as documented in chapter 6.6.3. Nevertheless, the investigation of interaction-induced endometabolomic alterations within each sampling day was thought to be meaningful.

Endometabolomic data can unambiguously be used to draw conclusions about altered physiology of an organism, as the metabolome directly represents the phenotype of an organism (Fiehn, 2002). Via metabolomic profiling, several snapshot of the metabolism of an organism under different conditions are taken and subsequently analyzed for differences ((Poulson-Ellestad et al., 2014a) and references herein).

Data pre-processing

Data pre-processing was an important step in the metabolomic analysis workflow. After performing background noise correction on the raw spectra, I carried out chromatographic peak detection and deconvolution. Before quantification of MSTs, all detected peaks were aligned and characterized by ion / retention-time pairs. I manually checked the automatic quantification via peak integration and corrected if necessary. Furthermore, I tested adjacent peaks for redundancy and eliminated them if they turned out to be deconvolution artifacts.

³³ Source: „Phyto’pedia – The Phytoplankton Encyclopedia Project“

https://www.eoas.ubc.ca/research/phytoplankton/diatoms/centric/skeletonema/s_costatum.html (02.2017)

https://www.eoas.ubc.ca/research/phytoplankton/diatoms/centric/thalassiosira/thalassiosira_genus.html (02.2017)

To get rid of potential contaminations, I performed a trifold blank subtraction on the integrated data. Subsequently, I excluded all MSTs that were present in less than three samples, as well as all artificially added substances like ribitol and the RI-mix compounds from the data set.

Statistical analysis

I performed the statistical analysis of the metabolomic data on the basis of $\log_{10}(x+1)$ transformed data and the Bray-Curtis dissimilarity distance measure, using a “Canonical Analysis of Principal Coordinates” (CAP), as introduced by (Anderson and Robinson, 2003; Anderson and Willis, 2003a). This approach combined a principal coordinate analysis (PCoA) with a canonical discriminant analysis (CDA). The strength of this method was the unconstrained exploration of individual and group differences between samples based on MST intensities. Furthermore, it allowed for testing of specific hypotheses of sample similarities via CDA and revealed potentially masked, but ecologically important patterns in unconstrained ordination with the help of a canonical ordination.

In the latter context, I used the CDA to test different a-priori groups of samples for significant differences (as indicated by a p-value ≤ 0.05 in the trace statistics). To evaluate the goodness of fit of the defined groups, I considered the misclassification error and the leave-one-out cross validation results. A-priori grouping was performed *inter alia* among treatment groups, sampling days, and treatment groups per sampling day, with the aim to explore the influence of various grouping factors.

After an evaluation of the results subsets of the data (*e.g.* per species or per day) were analyzed to reduce the influence of dominant grouping factors on the analysis, which were not of primary interest for the research question. Finally, only significantly different a-priori groups, including treatment as a grouping factor, were considered to identify correlating MSTs that caused group differences. Depending on the particular analysis, a critical value for the correlation coefficient of the MSTs, correlating with group differences (as represented by the canonical axes) was calculated and set to guarantee significance. (See chapter 6.7.3 for more details).

With this strategy, I guaranteed a comprehensive approach to reduce metabolomic complexity and focus on a set of relevant MSTs. Furthermore, I used tools like score plots, vector plots, heatmaps and boxplots to evaluate the findings visually.

Metadata

In all conducted studies, I collected metadata. Metadata hereby not only comprise ‘data about the data’, as defined by Snyder et al. (Snyder et al., 2014), but also parameter describing the state of the cultures, as defined by Vidoudez and Matusz (Vidoudez, 2010; Matusz, 2014). While the first are documented in the material and method part (chapter 6), the latter will be presented as result of the respective study, including chl a fluorescence and PSII efficiency, cell counts, nutrient levels, pH and bacterial abundance data.

As stated by Fiehn et al., metadata, which describe the system before and after sampling are essential for the correct interpretation of metabolomic data and transfer of findings and knowledge (Fiehn et al., 2007). Chl a fluorescence and cell counts were used to connect the metabolomic alterations observed in the endo- and exometabolome to alterations in growth. Considering further metadata, the first interaction experiment (interaction of *T. weissflogii* and *S. costatum*, chapter 2) reported PSII efficiency and it was known that diatom cultures were non-axenic. In later experiments (chapter 2.3, 3 and 4), the experimental design evolved and included the monitoring of nutrient levels (silicate, phosphate, nitrate and nitrite concentrations), bacterial abundance and pH.

2.1.3 Design: Medium experiments

The cultures of *S. costatum* (RCC75) and *T. weissflogii* (RCC76) used in all investigations involving these species were non-axenic. In general, the utilization of axenic diatom cultures has the advantage of reducing the investigated interaction system to two distinct parties. However, the axenic state poses an artificial stress factor, as bacteria and diatoms naturally co-occur interdependently in the ecosystem (Amin et al., 2012). For this reason and due to the fact that non-axenic cultures were used by Paul for the initial investigation of this particular interaction (Paul et al., 2009), I decided to continue the work on this interaction with non-axenic cultures.

Various interactions ranging from stimulatory to inhibitory are known to exist between bacteria and phytoplankton (Cole, 1982; Amin et al., 2012, 2015). And there is evidence for species-specific interactions with the potential to influence growth (Grossart and Simon, 2007; Amin et al., 2015; Limardo and Worden, 2015). This might be based on a simple non-specific resource swap, where bacteria use organic carbon sources exuded by phytoplankton and vice versa supply them with remineralized nutrients. Or it might be caused by chemically-mediated interactions.

It was also further documented that marine diatoms harbor distinct bacterial communities in their natural environment (Schäfer and Abbas, 2002; Grossart et al., 2005). By introducing the bacterial communities, which were associated with the diatom partners in the stock cultures, into the co-cultivation set-up, a third interaction party with the potential to influence diatom growth might have been added to the diatom system.

Therefore, I designed two medium experiments, one for each diatom species respectively, to investigate the influence of the initial environment of each partner on the respective other diatom partner. More specifically the initial environment comprised (1) the bacterial community of the partner, (2) its nutrient depletion status and (3) the non-induced exometabolome of the diatom partner at the onset of the experiment. Both experiments were independent and conducted to supplement the findings of the interaction experiment.

Experimental strategy

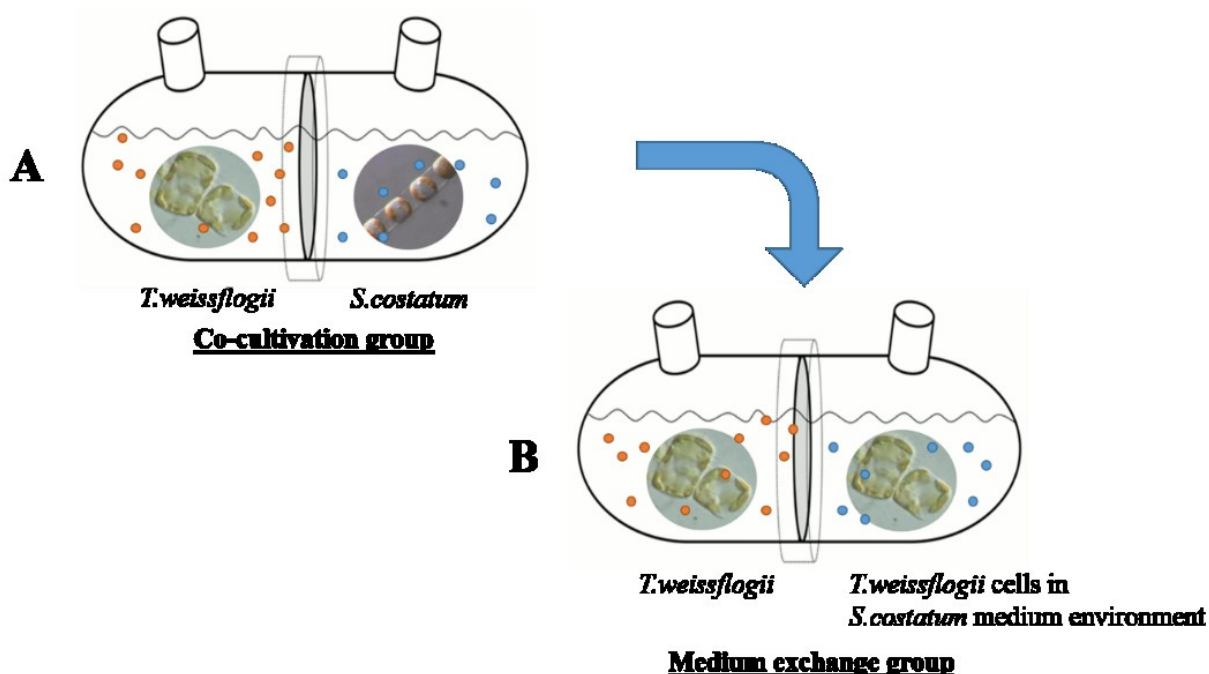


Figure 3: Experimental design to investigate the influence of the initial environment in the interaction between *T. weissflogii* and *S. costatum*.

Co-cultivation group (A) and medium exchange group (B) are visualized schematically. The bacterial communities are represented by colored dots. **Red** characterizing the bacterial community of *T. weissflogii*, **blue** the one of *S. costatum*.

The principle idea of the experimental strategy will be exemplarily explained for the investigation of *S. costatum* environment on *T. weissflogii*. In general, I used the co-cultivation and mono-cultivation group (see primary treatment groups in chapter 2.1.1 (Figure 2A, C) as positive and

negative control. Additionally, I introduced a new experimental group: the medium exchange group (**Figure 3**). In the medium exchange group, one chamber half contained the unmodified *T. weissflogii* culture and the other chamber half contained *T. weissflogii* cells in the spent medium of *S. costatum* culture (see chapter 6.2.3 for details). To maximize comparability and explanatory power of the medium exchange group, I designed it to highly resemble the co-cultivation group. The only difference was that the interaction partner itself was removed and substituted with diatom cells of the same species. Thus, any change in growth of the investigated species (*T. weissflogii* in this example) would be caused by the partner's initial environment, not by the presence of the partner itself.

By comparing the diatom growth parameters of the medium exchange group with diatom growth parameters in the negative and positive control, it was my aim to evaluate the impact of the initial environment of the respective partner on both diatom species. See chapter 6.2.7 for experimental specifics.

To recreate the sampling strategy of the co-cultivation group and to guarantee maximally possible comparability between all treatment groups, I sampled the unmodified chamber half in the medium exchange group. This measure was taken to minimize the impact of variability introduced due to the modification process, *e.g.* via additional stress imposed on the modified cultures or loss of biomass during the process. Variability was reflected in slightly altered parameters between the modified and unmodified chamber half of the medium exchange group (*e.g.* chl_a fluorescence, data not shown). However, the sampling strategy counteracted this problem and the variability in growth parameters did not alter the main conclusions drawn from the medium experiments.

2.1.4 Design: Evaluation of DMSP as growth mediator

To test the hypothesis of DMSP involvement in the interaction effect between *T. weissflogii* and *S. costatum*, I investigated the influence of DMSP on the growth of both diatom partners.

DMSP is a phytoplankton-derived metabolite that plays a key role in the marine environment: it bears the potential to influence biogeochemistry, the global climate and marine ecology, both directly and indirectly, via its degradation products. DMSP and dimethyl sulfide (DMS), as its enzymatic cleavage product, play a major role in the global sulphur cycle (Andreae, 1990). By diffusing into the atmosphere and forming sulphur aerosols that impact cloud formation, dimethylsulfide (DMS) can have an impact on global climate (Bates et al., 1987; Charlson et al.,

1987). Furthermore, both DMSP and DMS have been found to act as foraging cues between several trophic levels (Steinke, Stefels and Stamhuis, 2006; Seymour et al., 2010). The main producers of DMSP are phytoplankton species, including some members of diatoms (Stefels, 2000).

In algae, DMSP acts as osmolyte (Karsten, Wiencke and Kirst, 1991), cryoprotectant (Kirst et al., 1991), antioxidant (Sunda et al., 2002) and it plays a role in overflow mechanisms, protecting the cell of compound and energy excess (Stefels, 2000). For autotrophs, which are not able to produce DMSP, taking up and assimilating DMSP constitutes a source of carbon and reduced sulphur (Kiene, Linn and Bruton, 2000; Vila-Costa et al., 2006).

In the context of the interaction between *S. costatum* and *T. weissflogii*, only *S. costatum* is able to de-novo synthesize DMSP, while *T. weissflogii* seems to completely rely on the active uptake of externally available DMSP (Spielmeyer, Gebser and Pohnert, 2011; Spielmeyer and Pohnert, 2012). The DMSP uptake of *T. weissflogii* is not only substantial, but also fast. Studies show that *T. weissflogii* is able to take up 60% of externally available DMSP within the first minutes (Spielmeyer et al., 2011). Furthermore, DMSP enhances bacterial growth in otherwise unfavorable osmotic environments (Chambers et al., 1987; Cosquer et al., 1999).

In consideration of the DMSP characteristics and the DMSP dynamics in different organisms, I designed experiments to test the influence of DMSP on diatom growth. The aim of this investigation was to elucidate if DMSP release and uptake between the interaction partners *T. weissflogii* and *S. costatum* was the underlying principle causing enhanced growth of *T. weissflogii* in interaction.

Experimental strategy

The concentration of dissolved DMSP in seawater is smaller than 2.8 nM over a broad range of ocean water types (Kiene and Slezak, 2006). However, in diatom blooms, DMSP concentrations up to one order of magnitude higher have been documented (Matrai and Keller, 1993). To investigate DMSP influence on the growth of *T. weissflogii*, I conducted two experiments: One to recreate the constant availability of DMSP (100 nM) and one to investigating the influence of timely distinct DMSP pulses of different concentrations (100 nM, 1 μ M, 2.5 μ M) on diatom growth. The DMSP concentrations used, resembled relatively high natural concentrations, as they would occur in bloom situations or due to spatially higher concentrated DMSP patches. See chapter 6.2.7 for experimental specifics.

2.2 Interaction experiment with *T. weissflogii* and *S. costatum*

2.2.1 Diatom growth in mono- and co-cultivation

Compared to mono-cultivation, *T. weissflogii* showed significantly enhanced growth in co-cultivation with *S. costatum* (**Figure 4**). Cell counts were elevated by up to 81 % (day 26) and chl a up to 1.4 - fold (day 23) due to the interaction. However, the effects on the growth of *S. costatum* were ambiguous. But I could repeatedly show that the presence of *T. weissflogii* had significant impact on the chl a fluorescence of *S. costatum* and caused an increase of up to 1.5 - fold (**Figure 4**). I was able to reproduce these observed growth effects in the interaction of *T. weissflogii* and *S. costatum* (data not shown).

I used a linear mixed modeling approach to investigate if there were time-dependent differences between co-cultivated and mono-cultivated diatoms of the same species, regarding chl a and cell counts. A one-way repeated measures ANOVA was not a suitable approach, because the assumption of homoscedasticity on the data was violated due to the inherent characteristic of the experimental design. However, this can be dealt with by incorporation into a mixed linear model (Zuur et al., 2009).

I proposed four linear mixed models (characteristics described in chapter 6.7.1) and evaluated their goodness of fit for each metadata response variable individually. I selected models with the help of the Akaike Information Criterion (AIC) on the basis of the restricted maximum likelihood estimation. The AIC measures both the fit of the model and the complexity of the model (Zuur et al., 2009). The lowest AIC indicated the best fitted model. AIC of succeeding models were compared via ANOVA, i.e. if the model with lowest AIC is significantly better than the one with second lowest AIC. Only if the improvement was significant, the lower AIC model was chosen as best fitting.

I validated models visually with the help of standard model validation graphs (as named in (Zuur et al., 2009) and documented in **Appendix 1 - Appendix 6**): (a) residuals versus fitted values to verify homogeneity, (b) a histogram of the residuals for normality and (c) residuals versus each explanatory variable to check independence.

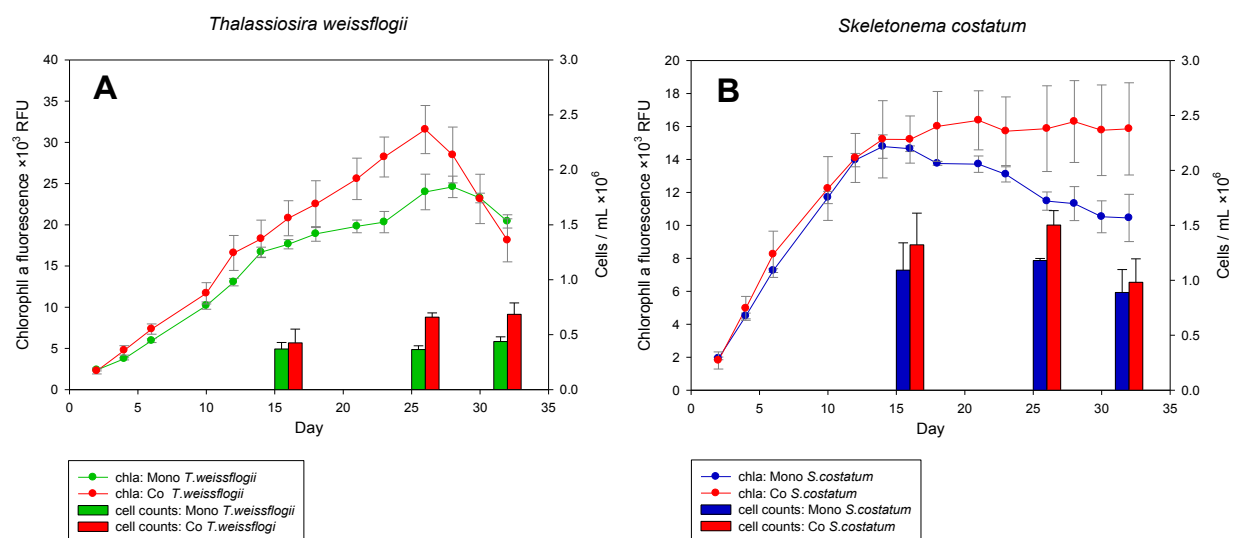


Figure 4: Diatom growth in the interaction experiment of *T. weissflogii* with *S. costatum*.

The line plot shows means of chl a (RFU: relative fluorescence units), bar charts represent average diatom cell counts (cells / mL) of *T. weissflogii* (graph A) and *S. costatum* (graph B). The treatment groups are indicated by color: mono-cultivation of *S. costatum* (blue, control), mono-cultivation of *T. weissflogii* (green, control) and the co-cultivation of each species (red, interaction). Values show as means + SD (n = 3 biological replicates). Notice different scaling of y-axis.

Growth of T. weissflogii

Both, chl a fluorescence ($F(13,52)^{34} = 20.740$, $P \leq 0.0001$) and cell counts ($F(2,8) = 8.731$, $P = 0.0097$) developed significantly different over time in co-cultivation, compared to mono-cultivation (Figure 4A).

Typically, diatom growth in batch cultures with a limited amount of nutrients present passes through several phases. In resemblance to the seven growth phases of bacterial batch cultures (Buchanan, 1918), diatom growth was divided into three phases to simplify the matter: regular growth phase, stationary phase and declining phase. In theory, the regular growth phase corresponded to a growth period comprising four growth phases as described by (Buchanan, 1918): initial stationary phase, regular growth phase, logarithmic growth phase and phase of negative growth acceleration. For convenience I summarized these phases and categorized them as regular growth. Subsequently, the stationary phase was indicated by more or less constant biomass and the declining phase by decreasing cell numbers. These growth phases were indicated by chl a fluorescence dynamics and substantiated via cell counts.

³⁴ F(numDF, denDF)

Chl a fluorescence of mono-cultivated *T. weissflogii* cultures indicated regular growth until day 14 and stationary growth until day 28 (indicated by a phase of minor chl a increase). Subsequently, the chl a fluorescence rapidly decreased (potentially the declining phase of growth). I hypothesized co-cultivated *T. weissflogii* to show regular growth until day 26, followed by a more pronounced decline of fluorescence (potentially the declining phase).

Although only very few data points were available, I used cell counts to substantiate the growth phase estimation made by chl a fluorescence. Cell counts of *T. weissflogii* mono-cultures did not substantially increase throughout all three sampling points (**Figure 4A**). Mean values were around $3.9 \times 10^5 \pm 4 \times 10^4$ cells / mL throughout all three days with an increase of 18% between day 16 and 32. These findings supported the hypothesis of a stationary growth phase between day 14 and 28 via chl a fluorescence. Cell counts in co-cultivated *T. weissflogii* cultures increased by approximately 55% between day 16 and 26, thus indicating that the culture was still in a state of increased growth. Again, these findings substantiated the indications from chl a fluorescence, which increased until day 26 as well. However, while chl a fluorescence rapidly declined from day 26 on, cell counts stayed almost stable between day 26 and 32 with an increase of only 4 %. In both cultivation types, maximum cell numbers were reached on day 32, with $6.9 \times 10^5 \pm 1.0 \times 10^5$ cells / mL in co-cultivation and $4.4 \times 10^5 \pm 0.4 \times 10^5$ cells / mL in mono-cultivation (**Figure 4A**).

In the chl a fluorescence growth curves, the regular growth phase lacks the initial stationary phase, which would be characterized by slow or even no growth. The dilution of the cultures at the onset of the experiments was deliberately chosen in a way to minimize this phase. For the investigation of the stimulatory growth effect between *T. weissflogii* and *S. costatum*, late regular and stationary growth phase were most relevant. Furthermore, sampling points at the onset of each experiment were rather scarce, as this period was not the focus of the investigation.

It seems that biomass was correlating well with chl a fluorescence in the regular and stationary growth phase. However, in late stationary phase, chl a fluorescence decline was not coupled to immediate decrease in biomass. As previously discussed, chl a fluorescence is also impacted by other factors than biomass, e.g. nutrient limitation and extreme alterations in physiological state that impact photosynthetic activity (Kruskopf and Flynn, 2006). Thus, the strong decrease in chl a fluorescence might reflect severe nutrient limitation and / or the preparation of cell death with delayed visibility in cell counts. This interpretation is stressed by the simultaneous drop in PSII efficiency (**Appendix 21A**), indicating reduced photosynthetic performance of *T. weissflogii* and

impairment of cell physiology (Maxwell and Johnson, 2000). At this point the restriction of Kruskopf et al. becomes relevant, limiting the explanatory power of chl a fluorescence as biomass indicator (Kruskopf and Flynn, 2006).

The comparison of interaction and non-interaction context revealed the following: Compared to mono-cultivation, chl a fluorescence was heightened in co-cultivation between day four and 28, with up to 1.4 - fold higher fluorescence on day 23. From day 26 on, the decline of chl a fluorescence of *T. weissflogii* in co-cultivation was steeper than in mono-cultivated cultures. Here, cells in co-cultivation might have experienced more severe consequences from nutrient limitation due to enhanced growth and cell division, resulting in more pronounced decrease in chl a fluorescence and ultimately cell death. Cell counts in co-cultivation were higher on all three sampling days. Starting with a slight increase on the first day of sampling (15% compared to mono-cultivation), a clear increase in cell counts compared to mono-cultivation was visible on the latter two sampling points of up to 81% on day 26.

In summary, co-cultivated *T. weissflogii* not only reached higher absolute cell counts, but also remained in the regular growth phase longer than mono-cultivated cultures. These findings were statistically significant and coherent in both chl a fluorescence and cell counts.

Growth of S. costatum

Similar to *T. weissflogii*, chl a fluorescence in co-cultivated *S. costatum* developed significantly different compared to mono-cultivation over time ($F(13,52)=31.695$, $P \leq 0.0001$). However, in cell counts there was no statistically significant interaction between day and treatment and no significant treatment dependent effect. Neither the mean cell counts between treatments nor the development between the treatments over time showed statistically significant differences for *S. costatum*.

Both mono- and co-cultivated cultures started from almost the same fluorescence values on day three (**Figure 4B**). Until day 12 the increase of chl a was similar in both groups, representing the regular growth phase of the culture. However, further developments in fluorescence were group dependent: *S. costatum* in mono-cultivation reached maximum fluorescence on day 14, with a subsequent decrease until day 32. On the other hand, co-cultivated *S. costatum* showed rather stable values of 15638 ± 665 RFU between day 12 and 32 and reached maximum fluorescence on day 21. The difference between chl a in mono- and co-cultivation was highest on day 32, with 52 % higher values in co-cultivation, compared to mono-cultivation. It seemed that in the time frame of this

experiment (until day 32) *S. costatum* did not enter the declining phase, characterized by sudden and strong decrease of chl a fluorescence (**Figure 4B**).

Cell numbers of mono- and co-cultivated *S. costatum* showed a tendency of increase-decline-dynamic with maximum values on day 26 (**Figure 4B**). As the increase of cell numbers between day 16 and 26 was only 8% in mono- and 14% in co-cultivation, the observation that cultures were in stationary phase of growth at these points in time was confirmed. In both mono- and co-cultivation, a decrease in cell numbers between day 26 and 32 could be observed (25% in mono- and 35% in co-cultivation). This might indicate the beginning of a declining phase, which however was not visible in chl a fluorescence dynamics.

Compared to mono-cultivation, co-cultivation of *S. costatum* showed increased cell-counts on all days, with up to 27% higher cell numbers on day 26. However, statistically these findings were not significant. With exception of the first sampling point, these findings were correlating with higher chl a fluorescence in co-cultivation compared to mono-cultivation.

Again, I observed differences in chl a fluorescence and cell count dynamics. For example on day 16, where cell counts differed by 21 %, but chl a fluorescence was more or less the same. Again, it needs to be stressed that chl a fluorescence is influenced by various parameters beyond biomass (see chapter 2.1.2). A fact that substantially complicates its unambiguous interpretation. In the context of this study, I mainly used it as an estimator for biomass and indicator for interaction-induced alterations in diatoms.

In summary, while *S. costatum* showed a significantly higher chl a fluorescence in co-cultivation compared to mono-cultivation, differences in cell counts couldn't be confirmed statistically. Nevertheless, these results strongly suggest an interaction-induced response of *S. costatum*. Further interpretation of the interaction-induced alterations are conducted on the basis of metabolomic analyses.

2.2.2 Metadata

The metadata were used to monitor the state of the cultures in the interaction experiments (appendix, chapter 7.1.4). They were screened for relevant interaction-induced differences. For the interaction experiment, only PSII efficiency was measured, which developed differently, depending on the diatom species, but was not relevantly influenced by the interaction. No further statistical analyses were conducted. The diatom cultures RCC75 and RCC76 were non - axenic.

2.2.3 Exometabolomic investigation

The CAP showed significant differences in the exometabolomes due to time, treatment and treatment per time. In total, 68 MSTs³⁵ were highly correlating with those significant differences. In consideration of the influence of treatment on diatom exometabolomes, significant differences were found on day 16 and 26. On both days, the exometabolome in co-cultivation and the exometabolomes in both mono-cultivations were distinctly different. For the evaluation of potential release / uptake dynamics, induced by the interaction, I classified 51 MSTs as relevant.

I identified 39 MSTs to be potentially involved in interaction-induced release mechanisms. I found most of them to be correlating with day 16, bearing the capability to mediate the succeeding growth effect observed in the interaction between *T. weissflogii* and *S. costatum* as infochemicals. Interestingly, some of these candidate MSTs exhibited growth phase dependent regulation and indicated a release-uptake mechanism between day 16 and 26. While the chemical identity of most MSTs remained unclear, five fatty acids, three carboxylic acids, one carboxylic acid derivative and one alkaloid were putatively identified among the candidate MSTs.

Furthermore, I proposed 12 candidate molecules to be involved in interaction-induced uptake mechanisms, transformation or reduced release mechanisms. Among the identified MSTs, one carboxylic acid and a terpenoid were correlating with day 16 and an amine and two alkaloids with later stages of the interaction.

The discussion of metabolite flux between the diatom partners is given in chapter 2.6 and 5. Subsequently, the focus is set on showing results.

³⁵ Excluding three potential contaminations (#112, #118, #140) and metabolites that exhibited a median of “0” in all treatments (#8)

Analysis strategy

In the exometabolomic analysis I chose a dual strategy to investigate sample similarities and to identify potential biomarkers. On the one hand, I used an overall CAP analysis (comprising PCoA and CDA) throughout all three sampling points to show global effects and dependencies between the samples. I used a-priori grouping by day (not used for the identification of highly correlated MSTs), treatment and treatment over day in the CDA. On the other hand, I conducted subset analyses of each sampling point. By splitting the overall data-set into three subsets, containing the exometabolomic data of day 16 (subset I), day 26 (subset II) and day 32 (subset III), I set the focus on investigating differences between the treatments, excluding time as factor. Thus, I guaranteed a comprehensive screening for relevant biomarkers.

In order to answer the research questions about interaction specific release and/or uptake of potential infochemicals and about potential chemical communication mechanisms between the diatom partners, I categorized all identified exometabolomic biomarkers and screened for the following abundance patterns:

- (1) Pattern I: MSTs most abundant in the exometabolome in co-cultivation, compared to both mono-cultivations
- (2) Pattern II: MSTs least abundant in co-cultivation, but abundant in both mono-cultivations
- (3) Pattern III: MSTs absent in co-cultivation

In principal, I evaluated the MST intensity in co-cultivation relative to both mono-cultivations (representing the negative controls). If an MST was more abundant in co-cultivation than in the negative controls (pattern I), this might suggest an interaction-induced release. If an MST was less abundant in co-cultivation, compared to both negative controls (pattern II), or if an MST was absent in co-cultivations (pattern III), this might suggest an interaction-induced uptake, transformation or reduced release. In such a way, prominent intensity patterns were defined on the basis of median MST intensities, with the power to answer the research questions.

This approach was based on the assumption that a reference MST intensity in co-cultivation can be calculated as average of the MST intensities found in both mono-cultivations. This reference value represents an MST abundance in co-cultivation obtained by mere mixing of exometabolomes of *S. costatum* and *T. weissflogii*. Accordingly, deviations of an actual MST intensity from this reference value, reflected interaction-induced alterations.

The reference value can be calculated according to **Equation 1**. In general, the exometabolome refers to a certain unit of volume (*e.g.* one co-cultivation chamber set-up). As each chamber consists of two chamber halves, contributing equal volume parts to the total chamber volume, each half shapes 50 % of the exometabolome per chamber. Hence, by taking half of the MST intensity measured in each mono-cultivation group, a reference value for the co-cultivation context can be calculated.

$$\text{Equation 1: } I_{Ref,Co} = \frac{I_{Mono TW} + I_{Mono SC}}{2}$$

Reference intensity in co-cultivation ($I_{Ref,Co}$), MST intensity in mono-cultivation of *T. weissflogii* ($I_{Mono TW}$) and mono-cultivation of *S. costatum* ($I_{Mono SC}$).

The benchmark intensity was only used to define expectations and to deduce the three clear-cut intensity patterns (pattern I-III), described above. An overview over the categorization in the heatmaps and the screening process is given in **Table 1**: It connects the MST groups in the heatmaps with the predefined intensity patterns and indicates potential relevance of these groups.

Table 1: Relationship between MST intensity patterns and heatmap groups.

Heatmap group	Intensity pattern	Potential relevance
A	Pattern I	Interaction-induced release mechanisms
B	Pattern II	Interaction-induced uptake mechanisms,
	Pattern III	reduced-release mechanism or transformation
C	-	Other
Sc	-	Potential biomarkers for <i>S. costatum</i>
Tw	-	Potential biomarkers for <i>T. weissflogii</i>

Data exploration via CAP

Overall analysis

In the exometabolomic analysis of the interaction between *T. weissflogii* and *S. costatum*, I obtained 142 MSTs after data pre-processing of 26 samples. The first explorative data analysis via PCoA shows three distinct groups of samples in the PCoA score plot (**Appendix 7**). One group was solely characterized by samples on day 16, whereas the other two groups represented mixtures of samples on day 26 and 32. This suggested strong influence of time on diatom exometabolomes. The plot did not show distinct sample grouping by treatment. However, it is known that ecologically relevant patterns might be masked in the unconstrained score plot (Anderson and Willis, 2003a). Thus, a CDA was performed, using a-priori grouping by day, treatment and treatment per day, to test different a-priori group hypotheses. The statistical diagnostics for the overall analysis, evaluating both the ordination and classification, are given in **Table 2**.

In general, the trace statistic confirmed significant differences between the tested a-priori groups. The squared canonical correlation (δ_1^2) and its corresponding p-value verified a significant correlation of observed differences and correlating MSTs with the first canonical axis. The misclassification error evaluated the classification success. The lower the error, the more distinct were the groups. In case of high misclassification errors, but significant differences between the groups, the cross-validation results were considered to identify similarities and dissimilarities between single a-priori groups. In general, I considered classification and ordination success in combination to evaluate the separation of a-priori groups (more details in chapter 2.5.3 and 6.7.3).

The CDA of the overall dataset confirmed significant differences in diatom exometabolomes due to time (trace statistic: $P \leq 0.0001$), as tested via a-priori grouping by day. Furthermore, significant differences in exometabolomes were caused by treatments (trace statistic: $P \leq 0.001$, **Table 2**). A-priori grouping by treatment investigated the influence of treatments on diatom exometabolomes independent of time, while a-priori grouping by treatment per day included both time and treatment as grouping factors, thus investigating differences between treatments in a time-dependent manner.

The classification success of the samples in the overall analysis was rather low, as the misclassification errors ranged between 11.55 - 42.31 %. In comparison, a-priori grouping by day yielded in the lowest misclassification error (11.54 %, **Table 2**), further confirming that time was a

strong grouping factor, forming distinct sample groups. The misclassification errors of a-priori grouping by treatment and treatment per day were 42.31 %.

Table 2: Permutation and cross-validation test results for the CAP analysis of different a-priori groups in the exometabolome analysis of the interaction between *S. costatum* and *T. weissflogii*

A-priori grouping by	m	Groups	Trace statistic	δ_1^2	Misclassification error (%)
Day	3	3	1.609 ($P \leq 0.0001$)	0.980 ($P \leq 0.0001$)	11.54
Treatment	6	3	1.046 ($P = 0.001$)	0.805 ($P = 0.0002$)	42.31
Day & treatment	6	9	3.365 ($P \leq 0.0001$)	0.989 ($P \leq 0.0001$)	42.31
<u>Subset I: day 16</u> treatment	2	3	1.214 ($P = 0.0014$)	0.652 ($P = 0.1534$)	33.33
<u>Subset II: day 26</u> treatment	5	3	1.940 ($P = 0.0234$)	1.000 ($P = 0.003$)	25.00
<u>Subset III: day 32</u> treatment	2	3	0.458 ($P = 0.5185$)	0.458 ($P = 0.397$)	88.89

δ_1^2 being the first squared canonical correlation. m represents the number of PCoA axes included in the CAP.

To get more information about the origin of the high misclassification errors in the overall analysis, I interpreted the cross validation results in detail. By checking the reallocation success for every single a-priori group in the leave-one-out cross validation procedure, it was my aim to differ between well classified sample groups and rather error prone sample groups within each CDA.

The cross-validation results of a-priori grouping by day proved that day 16 was distinctly different from day 26 and 32, as all samples could be 100 % correctly reallocated in the cross validation (**Appendix 8**). Samples from day 26 and 32 showed similarities, as they were misclassified to the respective other day with a probability between 12.50 and 22.22 %.

The a-priori grouping of the exometabolomic dataset by treatment only, without regarding the temporal factor, was showing a misclassification error of 42.31 % (**Table 2**). The cross-validation results indicated that the exometabolomes of *T. weissflogii* and *S. costatum* were distinctly different as they were never wrongly reallocated to the respective other (**Appendix 9**). However, two out of nine exometabolomic samples of mono-cultivated *S. costatum* were wrongly classified as co-cultivated samples and four out of nine samples (making up 44 %) of mono-cultivated *T. weissflogii* samples were wrongly identified as co-cultivation samples in the reallocation process. Exometabolomic samples of co-cultivation only showed a correct reallocation percentage of 37.5 %. Thus, classification by treatment only was rather error prone, as the exometabolome in co-cultivation

seemed to share traits with exometabolomes in both mono-cultivations. A clear separation without regarding time as a factor was difficult.

Subsequently, the combination of both time and treatment as classification factors was investigated, yielding in a misclassification error of 42.31 % (**Table 2**). Again, I deduced the nature of misclassification and the determination of involved groups by looking closer at the results of the cross validation (**Appendix 10**). As shown before, the exometabolome on day 16 was distinctly different from the ones on day 26 and 32. All exometabolomic samples from day 16 could be correctly reallocated to this day. These findings were supported by the PCoA score plot (**Appendix 7**), showing a clear separation of day 16 from day 26 and 32 by principal coordinate axis 1 in multivariate space and by the cross-validation results previously described. Cross-validation furthermore showed that samples could be well classified by treatment within day 16. All samples of mono-cultivation and two out of three samples from co-cultivation were correctly classified in the cross-validation. Samples from co-cultivation showed proximity to samples from mono-cultivated *S. costatum* in multivariate space, indicating similarities between the groups. These similarities were supported by the fact that the wrongly reallocated co-cultivation sample on day 16, as mentioned above, was misclassified as mono-cultivated *S. costatum* (**Appendix 10**).

Furthermore, comprehensive similarities between co-cultivation and *S. costatum* mono-cultivation samples within each day became apparent, as respectively three of eight co-cultivation samples were wrongly classified as such in the cross-validation (**Appendix 10**). Vice versa, one out of nine samples from mono-cultivated *S. costatum* were wrongly reallocated to co-cultivation. The exometabolome of *T. weissflogii* did not form a clear class within day 26 and 32, as the misclassification error was 100 %. These samples were either wrongly allocated to the co-cultivation group (4 out of 6), and / or to the respective other day (3 out of 6).

Subset analysis per day

In a second step, I split the overall dataset into three subsets, containing the exometabolomic data of day 16 (subset I), day 26 (subset II) and day 32 (subset III) to investigate differences between the treatments, removing the influence of time.

The statistical diagnostics confirmed that there were significant differences between the treatments on day 16 ($P = 0.0014$, misclassification error 33.33 %) and day 26 ($P = 0.0234$, misclassification error 25 %), as the trace statistic was significant ($P \leq 0.05$, **Table 2**). However, on day 32, no

significant differences between the treatments were found. The PCoA score plots (**Appendix 11**) of the daywise analysis support the findings on day 16, showing a separation of treatments by a combination of principal coordinate axis 1 and 2. Samples from co-cultivation were located on the upper left, samples from *S. costatum* in mono-cultivation on the upper right and samples from *T. weissflogii* in mono-cultivation at the bottom of the PCoA score plot. On day 26, the PCoA score plot did not show distinct sample grouping, although the trace statistic suggested significant differences.

Using CDA, the results of the statistical diagnostics were confirmed and very distinct sample groups on both day 16 and 26 are visualized in the constrained score plots (**Figure 6A, C**).

The classification of samples by treatment on day 16 showed a misclassification error of 33.33 % (for $m = 3$). Looking at the details of the leave-one-chamber-out cross-validation, in average one out of three samples was wrongly reallocated due to similarities of the co-cultivation group to both mono-cultivation groups (**Appendix 12**). The CAP on day 26 yielded a misclassification error of 25 % (for $m = 3$)³⁶, resulting solely from wrong reallocations of co-cultivation samples to the group of mono-cultivated *S. costatum* (**Appendix 13**). All mono-cultivation samples were reallocated correctly during cross-validation.

In summary, data exploration via CAP showed that time was a dominant factor influencing sample similarities. Nevertheless, the overall analysis indicated significant differences between treatments. Subset analyses for each sampling day confirmed significant differences between the treatments on day 16 and day 26, but not on day 32. Therefore I concluded that on day 16 and 26 the exometabolome in co-cultivation and the exometabolomes in both mono-cultivations were distinctly different.

Identification of exometabolites correlating with relevant a-priori groups

Subsequently, I identified MSTs whose abundance was significantly correlating with the separation of treatments and treatments per day. Thus, I set the focus on interaction-induced exometabolomic alterations. I further investigated a-priori grouping by treatment and treatment per day in the overall analysis, as well as the daywise analysis of subset I (day 16) and subset II (day 26). I didn't consider

³⁶ Only two out of three replicates in the co-cultivation group were available for analysis on day 26.

a-priori grouping by day in the overall analysis, as it was not in the primary scope of the investigation to unravel mere temporal changes in the exometabolomes.

The CDA resulted in a constrained score plot and a corresponding loading plot for each analysis. The score plot visualizes differences between the a-priori sample groups, while the corresponding loading plot visualizes significantly correlating metabolites. For interpretation, the loading plot needs to be superimposed on the constrained score plot. Each vector in the loading plot represents an MST, which was characterized by the MST ID in red (**Figure 5**). In general, only significantly correlated MSTs with the canonical axis and thus with the separation of a-priori groups were plotted. The significance level was adjusted and set for each analysis separately. The direction of an MST vector towards a distinct a-priori group indicated a correlation with the respective group. To distinctly allocate the MSTs to the sample groups, I created heatmaps to visualize median MST intensities over time and treatments.

Each heatmap was created on the basis of auto scaled medians of each treatment group. Scaling adjusts for intensity differences between different MSTs (Van Den Berg et al., 2006). MST intensities are given relative to a scaling factor, in the case of auto scaling this is the standard deviation of an MST among samples (Van Den Berg et al., 2006). A color code ranging from yellow (high intensity) to blue (low intensity) visualizes MST intensities. Due to scaling, conclusions about relative MST intensities may only be drawn within one MST, not between different MSTs.

Additionally I calculated a fold-change and visualized it with a second color code, positive values (black) representing x - fold higher abundance of co-cultivation to the respective mono-cultivation, negative values (grey) representing x - fold higher abundance of the respective mono-cultivation compared to co-cultivation. Within the heatmap, I sorted the MSTs by characteristic abundance patterns, to facilitate the evaluation of potential biomarkers and MSTs of interest. For each analysis I created and discussed an individual heatmap.

Overall analysis

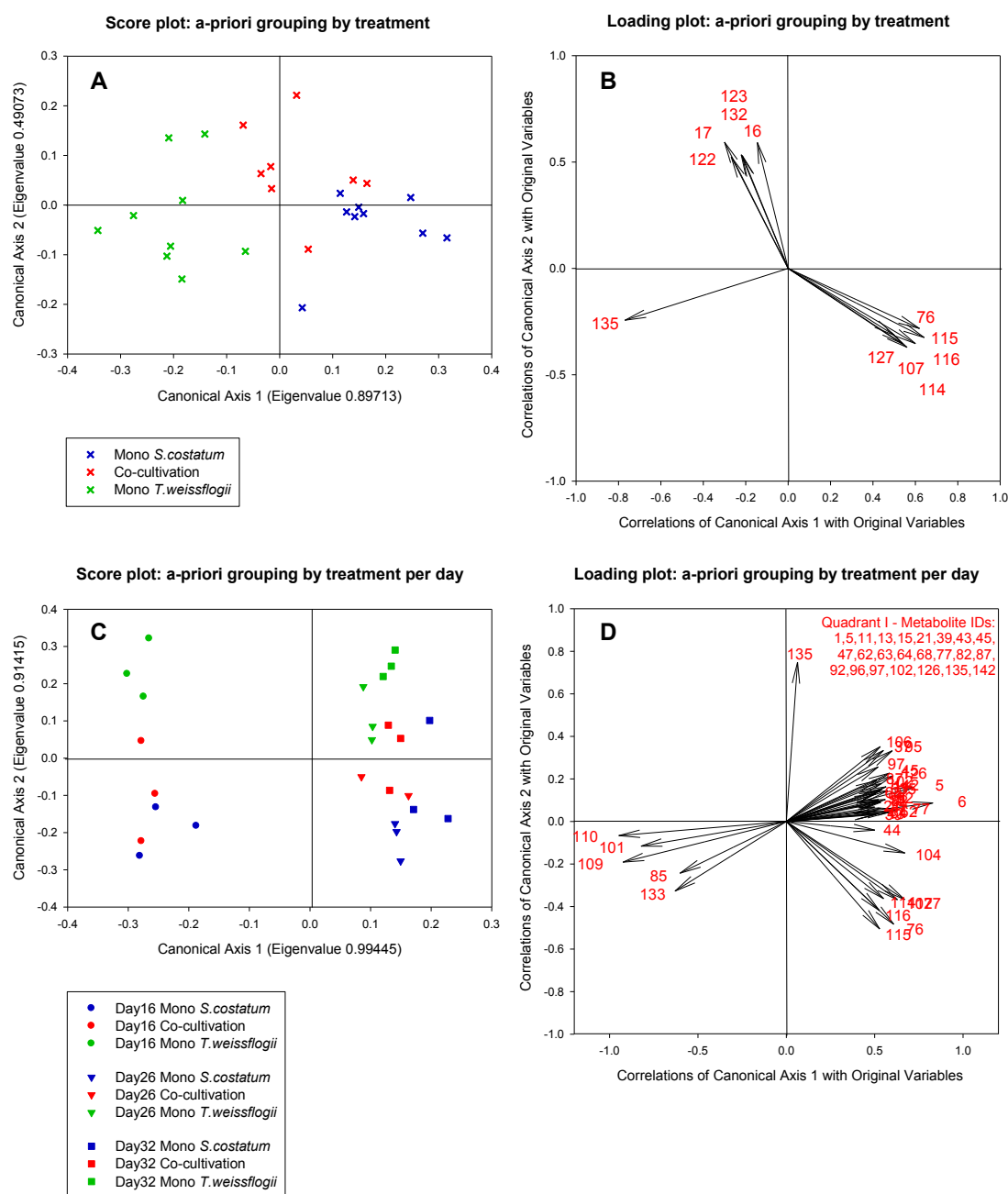


Figure 5: Constrained score and loading plots of exometabolomic samples from the overall analysis of the interaction between *T. weissflogii* and *S. costatum*.

The constrained score plots (graph **A**, **C**) visualize significant differences between the sample groups as found via CDA with a-priori groups by treatment (trace statistic $P = 0.001$, misclassification error of 42.31 % for $m = 6$, graph **A**) and a-priori groups by treatment per day (trace statistic $P = 0.0001$, misclassification error of 42.31 % for $m = 6$, graph **C**). Vectors in the CAP loading plots (graph **B**, **D**) represent MSTs, characterized by their ID (red numbers). Only vectors with a significant correlation coefficient above the critical value of $|r| \geq 0.4958$ ($P \leq 0.01$) are plotted. The direction of the vectors in 2-dimensional space correlates with exometabolomic sample groupings shown in the score plots of the respective analysis.

The constrained score plot of the overall analysis with a-priori grouping by treatment in **Figure 5A** shows a gradual separation of treatments via canonical axis 1. Exometabolomic samples from co-cultivation shared traits of both mono-cultivation exometabolomes, as samples were located between samples of *T. weissflogii* (on the left) and samples of *S. costatum* in mono-cultivation (on the right), as defined by canonical axis 1. Samples from mono-cultivation were furthest apart in multivariate space (**Figure 5A**) and there was no wrong reallocation in the cross-validation process (**Appendix 9**) as well.

The corresponding loading plot (**Figure 5B**) visualizes MSTs with a Pearson's correlation coefficient $|r| \geq 0.4958$ and a highly significant correlation with canonical axis 1 and / or 2 ($P \leq 0.01$). Considering the direction of MST vectors, it became apparent that dehydroabietic acid (#135) was correlating with mono-cultivated *T. weissflogii*, while 2-ethylhexanoic acid (#16), putative 2-octanol (#17), palmitoleic acid (#122, #123) and oleic acid (#132) were correlating with co-cultivation and the remaining MSTs with mono-cultivated *S. costatum*. Metabolites were considered putatively identified, if their R-Match value was ≤ 800 .

In the context of the overall analysis with a-priori grouping by treatment per day (**Figure 5C**), the constrained score plot depicts two distinct sample groups separated by canonical axis 1, representing samples on day 16 (left of the origin) and samples on day 26 and 32 (right of the origin). Within these two groups, treatments were gradually separated by canonical axis 2. Samples from mono-cultivated *T. weissflogii* were located in quadrant I and IV (above the origin) and samples from mono-cultivated *S. costatum* in quadrant II and III (below the origin, with exception of one sample on day 32). Co-cultivation samples were located between the mono-cultivation groups, sharing metabolomic traits with both of them, as visualized by proximity of the groups in multivariate space.

The corresponding loading plot (**Figure 5C**: $|r| \geq 0.4958$, $P \leq 0.01$) indicates that the majority of MSTs was correlating with samples from day 26 and 32, as they were located in quadrant I and II. A clear allocation of metabolites to a-priori groups was difficult, due to the overlap between sample groups in the constrained score plot. However, dehydroabietic acid (#135) was characteristic for mono-cultivated *T. weissflogii*, as it was pointing straight upwards. Furthermore, metabolites #85, #101, #109, #110, #133 were correlating with mono-cultivation of *S. costatum* and / or co-cultivation on day 16, as they were located in quadrant III.

The overall analysis with a-priori grouping by treatment and treatment per day identified 46 highly correlated metabolites (as shown in **Figure 5B** and **D**) and gave a rough idea about their correlation

with sample groups. To draw more specific conclusions, all metabolites are summarized in a heatmap (**Table 3**) and grouped on the basis of characteristic abundance patterns.

The first groups comprise metabolites that were highest abundant in co-cultivation on day 16 (group A16), day 26 (A26) and day 32 (A32). Group B16 - 32 summarize metabolites that were least abundant in co-cultivation compared to both mono-cultivations on day 16 (B16), day 26 (B26) and day 32 (B32). Group Sc comprises potential biomarkers for *S. costatum*, as these metabolites were merely abundant in co-cultivation and mono-cultivation Group C1 represents metabolites that were time-dependent. The majority of metabolites in this group were only present on day 26 and / or day 32 and all other metabolites are listed in group C2.

Table 3: Heatmap of relative exometabolite intensities for the overall analysis of the interaction between *T. weissflogii* and *S. costatum*.

Medians of MST intensities, normalized to the external standard ribitol (per sample) and subsequently metabolite-wise auto scaled, are represented by a color code ranging from high (yellow) to low intensities (blue). White indicates the absence of the respective MST after data pre-processing. Metabolites are sorted according to abundance patterns (separated by black lines), class and RI. Only metabolites significantly correlating with the separation of treatments and treatment per day are shown. The fold change of MST abundance in co-cultivation relative to mono-cultivations is given and coded with a second color code. Black indicates a higher abundance in co-cultivation, grey a higher abundance in mono-cultivation.

ID	Model ion	RT	RI	Name	Class	Ident	Analysis	Metabolite intensity									Fold change		Group				
								Median (n=2/3)									Fold (Co relative to:)						
								Day 16			Day 26			Day 32			Day 16			Day 26		Day 32	
								SC Mono	Co	TW Mono	SC Mono	Co	TW Mono	SC Mono	Co	TW Mono	SC Mono	TW Mono		SC Mono	TW Mono	SC Mono	TW Mono
122	117	14.41	2041	9-Hexadecenoic acid (Palmitoleic acid)	FA	T	-	Yellow	Green	Dark Green	-	-	Green	Dark Green	Green	-	1.8	-	-	-5.3	-5.5	A 16	
123	311.2	14.44	2046	9-Hexadecenoic acid (Palmitoleic acid)	FA	T	Dark Green	Green	Green	-	-	Green	Dark Green	Green	66.5	1.6	-	-	-8.5	-10.3			
132	129	15.63	2255	9-Octadecenoic acid (Oleic acid)	FA	T	-	Yellow	Green	Dark Green	-	-	Green	Dark Green	Green	-	2.0	-	-	-4.4	-5.7		
44	180	9.06	1294	Unknown	U	-	DT	Blue	Green	Green	Yellow	Green	Green	Green	Green	18.6	1.6	-1.7	-1.5	1.6	-1.8		
85	143.1	11.42	1608	Unknown	U	-	DT	Green	Yellow	-	-	-	Green	-	-	9.6	-	-	-	-	-		
101	103.1	12.31	1727	Unknown	U	-	DT	Green	Green	Green	-	-	-	-	-	1.3	1.5	-	-	-	-		
109	143.1	13.02	1822	Unknown	U	-	DT	Green	Green	Green	Dark Green	Dark Green	Dark Green	Dark Green	Dark Green	1.7	3.0	1.9	-13.6	1.7	-1.2		
110	143.1	13.09	1831	Unknown	U	-	DT	Green	Green	Green	-	Dark Green	Dark Green	Dark Green	Dark Green	1.8	1.8	-	-25.5	1.3	1.7		
133	194.1	16.45	2400	Unknown	U	-	DT	Green	Green	Green	Dark Green	Dark Green	Dark Green	Dark Green	Dark Green	1.1	1.5	-1.2	-1.2	1.0	-1.2		
62	168.1	9.86	1401	Unknown	U	-	DT	-	-	-	Green	Green	Green	Green	Green	-	-	2.0	2.0	-1.4	1.1	A 26	
63	123.1	10.02	1423	Unknown	U	-	DT	-	-	-	Green	Green	Green	Green	Green	-	-	3.8	1.9	-1.2	1.2		
77	237.1	10.78	1523	Unknown	U	-	DT	Blue	Green	Green	Yellow	Green	Green	Green	Green	-1.6	-3.4	1.6	1.5	7.4	1.5		
92	143.1	11.73	1650	Unknown	U	-	DT	-	-	-	-	Green	Green	Green	Green	-	-	-	2.6	1.5	1.9		
96	143.1	11.88	1670	Unknown	U	-	DT	-	-	-	-	Green	Green	Green	Green	-	-	-	13.7	1.6	2.8		
47	117.1	9.18	1311	2-Methylpropanoic anhydride	CA dv.	-	DT	-	-	-	Green	Green	Green	Green	Green	-	-	1.7	-1.9	1.4	1.0	A 32	
6	142.1	6.88	1004	Unknown	U	-	DT	-	-	-	Green	Green	Green	Green	Green	-	-	1.3	-1.8	1.2	1.1		
13	116.1	7.33	1064	Unknown	U	-	DT	-	-	-	Dark Green	Green	Green	Green	Green	-	-	2.0	-12.1	1.9	2.2		
21	151.1	7.69	1112	Unknown	U	-	DT	-	-	-	Dark Green	Green	Green	Green	Green	-	-	-1.5	-16.1	2.5	1.7		

ID	Model ion	RT	RI	Name	Class	Ident	Analysis	Median (n=2/3)									Fold (Co relative to:)						Group
								Day 16			Day 26			Day 32			Day 16		Day 26		Day 32		
								SC Mono	Co	TW Mono	SC Mono	Co	TW Mono	SC Mono	Co	TW Mono	SC Mono	TW Mono	SC Mono	TW Mono	SC Mono	TW Mono	
16	201.1	7.46	1081	2-Ethylhexanoic acid	CA	-	T										-1.1	1.8			2.8	-1.4	
106	295.1	12.83	1796	Terephthalic acid	CA		DT														1.0	-1.6	
97	116.1	11.92	1675	Unknown	U	-	DT														-1.3	1.0	
102	159.1	12.43	1743	Unknown	U	-	DT														-1.1	1.8	
142	103.1	18.64	2785	Unknown	U	-	DT														1.8	1.2	
17	187.1	7.51	1088	2-Octanol	Alc	?	T										-1.2	1.1	1.3	-9.2	1.7	-1.7	C 2

In case derivatized molecules are detected, the table entry lists their putative parent compounds. Each MST is characterized by **ID**, **model ion**, retention time (**RT**), retention index (**RI**) and its underlying CAP **analysis**. CAP analyses comprised the overall analysis with a-priori grouping by treatment and day (**DT**) and with a-priori grouping by treatment (**T**). Metabolites were identified via libraries. “?” indicates a reversed match between 700 and 800, “??” a reversed match between 600 and 700 and “???” indicates cases where the reversed match was ≤ 600 . “1” tags metabolites with a match smaller than 600. Class abbreviations: Amine (**A**), alcohol (**Alc**), alkaloid (**Alk**), carboxylic acid (**CA**), complex sugar (**CS**), derivatives of a certain class (**dv.**), sugar (**S**), sugar alcohol (**S Alc**), sugar acid (**S Acid**), sterol (**St**), terpene (**T**), others (**O**), unknown (**U**). **Vidoudez** refers to an MST code given by the in-house library, **GOLM** refers to an MST code given by distinct libraries of the Golm Metabolome Database.

Subset analysis per day

The significant differences between treatments on day 16 and day 26 (**Table 2**) are visualized in the constrained score plots of both days (**Figure 6A, C**).

On day 16, the constrained score plot shows a distinct separation of treatments (**Figure 6A**). Canonical axis 1 separated mono-cultivated *S. costatum* and mono-cultivated *T. weissflogii*. Canonical axis 2 separated samples from co-cultivation from those of mono-cultivation. In general, 38 metabolites were significantly correlating with the first two canonical axes ($|r| > 0.6664$, $P \leq 0.05$). Those metabolites are depicted in a corresponding loading plot (**Figure 6B**). The majority of vectors pointed to the right, presumably characterizing *S. costatum* in mono-cultivation, and to the bottom, presumably characterizing co-cultivation. The vector of MST #38 seemed to be important for the characterization of both mono-cultivations.

Note that the first squared canonical correlation was not significant, indicating that the first component (represented by canonical axis 1) alone was not sufficient to significantly differentiate the data subset. The inclusion of further discriminating components was needed. Thus, the visualization of group differences in the CAP score and loading plot might have been impaired.

To investigate the role of highly correlated metabolites as potential biomarkers, I visualized the intensity patterns of all correlated metabolites³⁷ from the subset analysis of day 16 in a heatmap (**Table 4**). Only metabolites showing median MST intensities unequal to zero in at least one treatment are shown (33 of 38 metabolites, excluding #8, #37, #38, #67 and #124). I classified the metabolites according to abundance pattern, class and retention index.

Group A represents metabolites, which were higher abundant in co-cultivation, compared to mono-cultivation of both diatoms. Group A(1) is furthermore characterized by absence of the metabolites in both mono-cultivations, group A(2) by absence in mono-cultivated *S. costatum*, and metabolites in group A(3) by absence in mono-cultivated *T. weissflogii*. Group B summarizes metabolites that are present only in the mono-cultivation of *S. costatum*, but absent in co-cultivation. Group Sc comprises metabolites that were potential biomarkers for *S. costatum*.

³⁷ Excluding two potential contaminations (diisobutyl phthalate #112 and 3,4-dibutylphthalate #118)

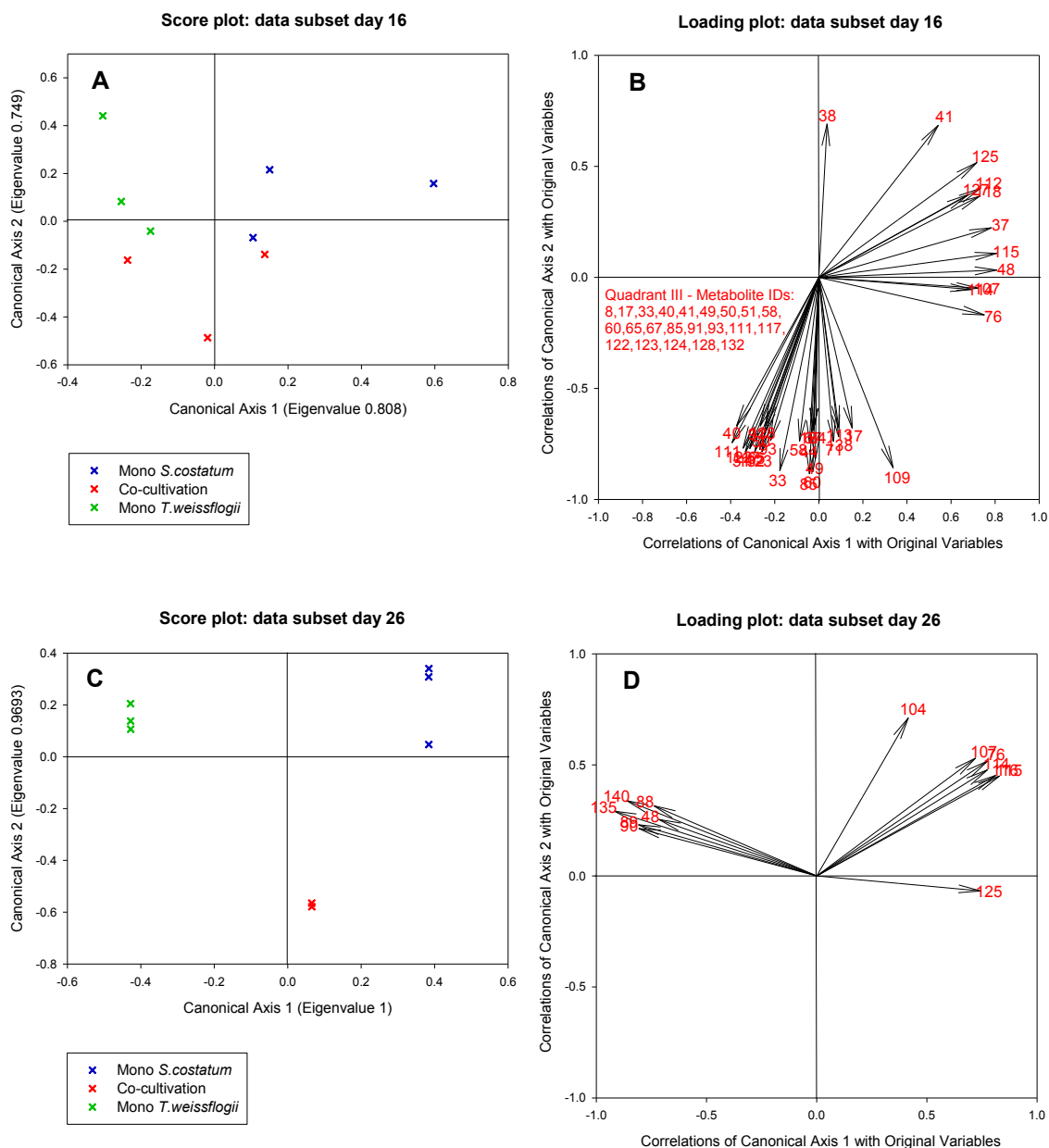



Figure 6: Constrained score and loading plots of exometabolomic samples from the daywise subset analysis of the interaction between *T. weissflogii* and *S. costatum*.

The constrained score plots (graph **A**, **C**) visualize significant differences between the treatments, as confirmed via CDA for the subset analysis on day 16 (graph **A**, **B**) and day 26 (graph **C**, **D**). These differences between treatments are highly significant (day 16: trace statistic $P = 0.0014$, misclassification error of 33.33 % for $m = 2$, day 26: trace statistic $P = 0.0234$, misclassification error of 25 % for $m = 5$). Vectors in the CAP loading plots (graph **B**, **D**) represent metabolites, characterized by their ID (red numbers, pooled per group). Only vectors with a significant correlation coefficient above the critical value of $|r| \geq 0.6664$ ($P \leq 0.05$) for day 16 and $|r| \geq 0.7067$ ($P \leq 0.05$) for day 32 are plotted. The direction of the vectors in 2-dimensional space correlates with exometabolomic sample groupings shown in the score plots of the respective analysis.

Table 4: Heatmap of relative exometabolite intensities for the subset analysis of the interaction between *T. weissflogii* and *S. costatum* on day 16. Medians of MST intensities, normalized to the external standard ribitol (per sample) and subsequently metabolite-wise auto scaled, are represented by a color code ranging from high (yellow) to low intensities (blue). White indicates the absence of the respective MST after data pre-processing. Metabolites are sorted according to abundance patterns (separated by black lines), class and RI. Only metabolites significantly correlating with the separation of treatments and treatment per day are shown. The fold change of MST abundance in co-cultivation relative to mono-cultivations is given and coded with a second color code. Black indicates a higher abundance in co-cultivation, grey a higher abundance in mono-cultivation.

ID	Model ion	RT	RI	Name	Class	Ident	Median MST intensity			Fold change		Group
							low  high			UP	DOWN	
							Median (n=3)			Fold (Co relative to:)		
SC Mono	Co	TW Mono	SC Mono	TW Mono								
50	149.1	9.45	1347	2-Methylbenzoic acid	CA	?	-	high	-	-	A(1)	
58	113.1	9.68	1377	Unknown	U	-	high	-	-			
60	103.1	9.82	1395	Unknown	U	-	high	-	-			
71	145.1	10.50	1486	Unknown	U	-	high	-	-			
91	143.1	11.66	1640	Unknown	U	-	high	-	-			
93	117	11.78	1656	Unknown	U	-	high	-	-			
128	130.1	15.09	2160	Unknown	U	-	high	-	-			
138	112	17.19	2530	Unknown	U	-	high	-	-			
51	120.1	9.49	1352	2-Hexylpyridine	Alk	?	-	high	grey	2.5	A(2)	
111	117	13.22	1848	Myristic acid	FA	*	-	high	grey	1.6		
117	117	13.89	1949	Pentadecanoic acid	FA	*	-	high	grey	1.9		
122	117	14.41	2041	9-Hexadecenoic acid (Palmitoleic acid)	FA		-	high	grey	1.8		
132	129	15.63	2255	9-Octadecenoic acid (Oleic acid)	FA		-	high	grey	2.0		
65	194.1	10.10	1433	Unknown	U	-	-	high	grey	3.3		
48	117	9.34	1332	Nonanoic acid	FA		grey	high	-	1.9	A(3)	
85	143.1	11.42	1608	Unknown	U	-	grey	high	-	9.6		
33	228.1	8.17	1176	4-Hydroxybutanoic acid	CA		blue	high	grey	26.9	A(4)	
40	145.1	8.79	1259	2-Hydroxypentanoic acid	CA	?	blue	high	grey	24.6		
113	117.1	13.66	1908	Pentadecanoic acid	FA	?	grey	high	blue	1.6		

ID	Model ion	RT	RI	Name	Class	Ident	Median (n=3)			Fold (Co relative to:)		Group
							SC Mono	Co	TW Mono	SC Mono	TW Mono	
123	311.2	14.44	2046	9-Hexadecenoic acid (Palmitoleic acid)	FA	-						
44	180	9.06	1294	Unknown	U	-						
49	151.1	9.42	1343	Unknown	U	-						
109	143.1	13.02	1822	Unknown	U	-						
41	148.1	8.88	1271	Succinic acid	CA	-						B
114	110.1	13.71	1918	Unknown	U	-						
115	382.2	13.79	1932	Unknown	U	-						
17	187.1	7.51	1088	2-Octanol	Alc	?						
125	335.2	14.56	2066	Skel_MEDIA_C254_FA? (Vidoudez)	FA	??						Sc
76	184.1	10.76	1521	Skel_MEDIA_C141 (Vidoudez)	U	?						
107	212.1	12.92	1808	Skel_MEDIA_C205 (Vidoudez)	U	-						
127	173.1	14.96	2137	Unknown	U	-						

In case derivatized molecules are detected, the table entry lists their putative parent compounds. Each MST is characterized by **ID**, **model ion**, retention time (**RT**) and retention index (**RI**). Metabolites were identified via libraries. If metabolites were verified with a standard, they are marked with *. “?” indicates a reversed match between 700 and 800, “??” a reversed match between 600 and 700 and “???” indicates cases where the reversed match was ≤ 600 . “1” tags metabolites with a match smaller than 600. Class abbreviations: Amine (**A**), alcohol (**Alc**), alkaloid (**Alk**), carboxylic acid (**CA**), complex sugar (**CS**), derivatives of a certain class (**dv.**), sugar (**S**), sugar alcohol (**S Alc**), sugar acid (**S Acid**), sterol (**St**), terpene (**T**), others (**O**), unknown (**U**). **Vidoudez** refers to an MST code given by the in-house library, **GOLM** refers to an MST code given by distinct libraries of the Golm Metabolome Database.

Although in the PCoA score plot (**Appendix 11**) no distinct grouping is visible on day 26, the CAP score plot (**Figure 6C**) shows very distinct sample groups. Canonical axis 1 alone was sufficient to separate all three treatment groups. Canonical axis 2 furthermore separated co-cultivation samples from mono-cultivation samples. All samples of mono-cultivated *S. costatum* were located in quadrant I, all co-cultivated samples in quadrant II and all samples from mono-cultivated *T. weissflogii* in quadrant IV. Both the trace statistic (1.940, $P = 0.0234$) and the first squared canonical correlation (1.00, $P = 0.003$) were significant.

The CAP loading plot of highly correlated MSTs ($|r| > 0.7067$, $P \leq 0.05$) indicated that nonanoic acid (#48), MSTs #88, #89, #90, and #135 (Group Tw³⁸) were correlating with mono-cultivated *T. weissflogii*, as they were located in quadrant IV (**Figure 6D**). All MST vectors located in quadrant I were characteristic for mono-cultivation of *S. costatum* (#76, #104, #107, #114, #115, 4-pyridoxate (#116), groups B & Sc). And as MST #125 was pointing between the groups of mono-cultivated *S. costatum* and co-cultivation, it was characterizing both groups.


Regarding the heatmap³⁹ (**Figure 5**), group B represents metabolites that were least abundant in co-cultivation compared to both mono-cultivations, indicating possible uptake, transformation or downregulation. Group Sc summarizes metabolites that characterize *S. costatum* mono-cultivation, group Tw metabolites that characterize *T. weissflogii* mono-cultivation. Other metabolites are shown in group C.

³⁸ Octyl pentyl phthalate (#140) was not listed, as it probably is a plasticizer and thus a contamination.

³⁹ Not containing octyl pentyl phthalate (#140)

Table 5: Heatmap of exometabolite intensities for the subset analysis of the interaction between *T. weissflogii* and *S. costatum* on day 26.

Medians of MST intensities, normalized to the external standard ribitol (per sample) and subsequently metabolite-wise auto scaled, are represented by a color code ranging from high (yellow) to low intensities (blue). White indicates the absence of the respective MST after data pre-processing. Metabolites are sorted according to abundance patterns (separated by black lines), class and RI. Only metabolites significantly correlating with the separation of treatments and treatment per day are shown. The fold change of MST abundance in co-cultivation relative to mono-cultivations is given and coded with a second color code. Black indicates a higher abundance in co-cultivation, grey a higher abundance in mono-cultivation.

Median MST intensity
low  high
Fold change
UP **DOWN**

ID	Model ion	RT	RI	Name	Class	Ident	Median (n=2/3)			Fold (Co relative to:)		Group
							SC Mono	Co	TW Mono	SC Mono	TW Mono	
104	221.1	12.51	1754	Skel_MEDIA_C196 (Vidoudez)	U	?				-4.4	-2.6	B
107	212.1	12.92	1808	Skel_MEDIA_C205 (Vidoudez)	U					-3.4	-1.1	
116	309.1	13.84	1940	3-Hydroxy-5-(hydroxymethyl)-2-methylisonicotinic acid (4-Pyridoxate)	CA					-6.5	-	Sc
76	184.1	10.76	1521	Skel_MEDIA_C141 (Vidoudez)	U	?				-2.9	1.1	
114	110.1	13.71	1918	Unknown	U	-				-4.2	1.5	
115	382.2	13.79	1932	Unknown	U	-				-4.2	1.5	
48	117	9.34	1332	Nonanoic acid	FA					2.4	-4.6	Tw
135	239.2	16.69	2442	Abieta-8(14),9(11),12-trien-18-oic acid (Dehydroabietic acid)	T					37.0	-19.0	
88	117.1	11.54	1624	Unknown	U	-				1.2	-5.1	
89	117.1	11.59	1631	Unknown	U	-				2.0	-3.1	
90	117.1	11.63	1637	Unknown	U	-				3.7	-3.5	
125	335.2	14.56	2066	Skel_MEDIA_C254_FA? (Vidoudez)	FA	??				-1.1	3.8	C

In case derivatized molecules are detected, the table entry lists their putative parent compounds. Each MST is characterized by **ID**, **model ion**, retention time (**RT**) and retention index (**RI**). Metabolites were identified via libraries. If metabolites were verified with a standard, they are marked with *. “?” indicates a reversed match between 700 and 800, “??” a reversed match between 600 and 700 and “???” indicates cases where the reversed match was ≤ 600 . “!” tags metabolites with a match smaller than 600. Class abbreviations: Amine (**A**), alcohol (**Alc**), alkaloid (**Alk**), carboxylic acid (**CA**), complex sugar (**CS**), derivatives of a certain class (**dv.**), sugar (**S**), sugar alcohol (**S Alc**), sugar acid (**S Acid**), sterol (**St**), terpene (**T**), others (**O**), unknown (**U**). **Vidoudez** refers to an MST code given by the in-house library, **GOLM** refers to an MST code given by distinct libraries of the Golm Metabolome Database.

Screening for interaction specific release and / or uptake of potential infochemicals

On the basis of observed exometabolomic differences between the treatments and the highly correlated metabolites (as presented in the previous subchapters), I drew hypotheses about interaction specific release and/or uptake of potential infochemicals.

In a first step, I screened all heatmaps (**Table 3**, **Table 4** and **Table 5**) for the defined MST intensity patterns, classified as groups A and B⁴⁰. In a second step, I further evaluated the intensity dynamic of each candidate molecule. As the screening process via heatmaps was only based on median values, an evaluation via boxplots across treatments and time was conducted to include information about variance. Unfortunately, the co-cultivation group on day 26 contained only two biological replicates due to sample loss, which weakened the informative value of the boxplots. Nevertheless, trends were clearly observable as the interpretation of pattern dynamics was performed on the basis of medians. The combination of screening and evaluation resulted in a set of candidate molecules, which were further characterized and classified by prominent intensity dynamics over time and treatments, to facilitate interpretation. It is important to note that the categorization of MSTs by day was not only performed on basis of visual intensity dynamics, but mainly on the significance of correlation, as given by the CAP analysis.

Enhanced abundance of exometabolites in co-cultivation - Pattern I:

In total, 39 different MSTs matched intensity pattern I, potentially indicating interaction-induced release mechanisms (**Appendix 14**, **Appendix 15** and **Appendix 16**). They all share the trait of highest median abundance in co-cultivation, compared to both negative controls on at least one of the sampling days. Boxplots visualized the intensity dynamic over time and treatments by depicting the relative MST intensities (ribitol normalized) of the respective model ion.

Day 16

Most of the MSTs (26 of 39) of pattern I were characteristic for day 16, indicating an interaction-induced release at the onset of the observed diatom growth effect. They originate from group A16 in the heatmap of the overall analysis (**Table 3**) and groups A(1) - A(4) in the heatmap of the daywise analysis on day 16 (**Table 4**). Among these metabolites I classified the intensity development over time into three categories:

⁴⁰ See **Table 1** for more details

(1) Metabolites with predominance on day 16

In **Figure 7** the intensity of MST #109 is depicted among the sampling days as an example for metabolites of pattern I with predominance on day 16. Compared to *S. costatum* mono-cultivation, MST #109 was 1.7 - fold more abundant in co-cultivation and 3 - fold more compared to *T. weissflogii* mono-cultivation on day 16. In total, five unidentified metabolites were allocated to this category, as they were all hardly present on day 26 and 32 in comparison to day 16. The intensity dynamics of all five metabolites (#85, #91, #101, #109, and #110) over treatments and days is summarized in **Appendix 14**. The metabolites of this category were characteristic for a time point at the onset of the observed growth effect. They are potential infochemicals, with the capability to mediate the succeeding interaction-induced growth effect.

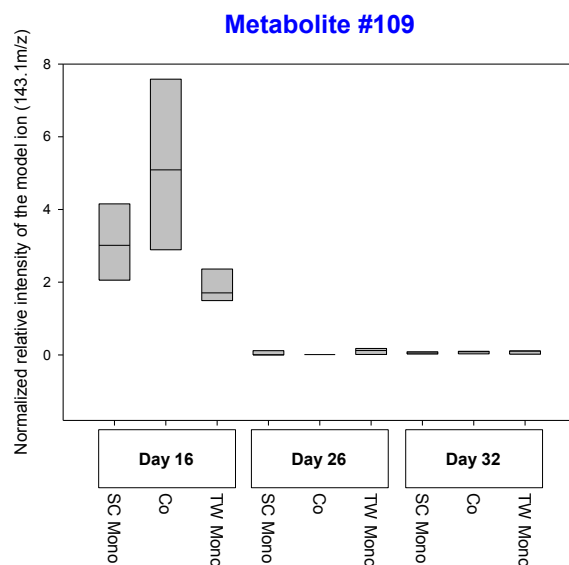


Figure 7: Exemplary MST #109 with interaction-induced release mechanism on day 16 in the interaction between *T. weissflogii* and *S. costatum* (intensity pattern I).

(2) Metabolites with steadily building up or declining intensities

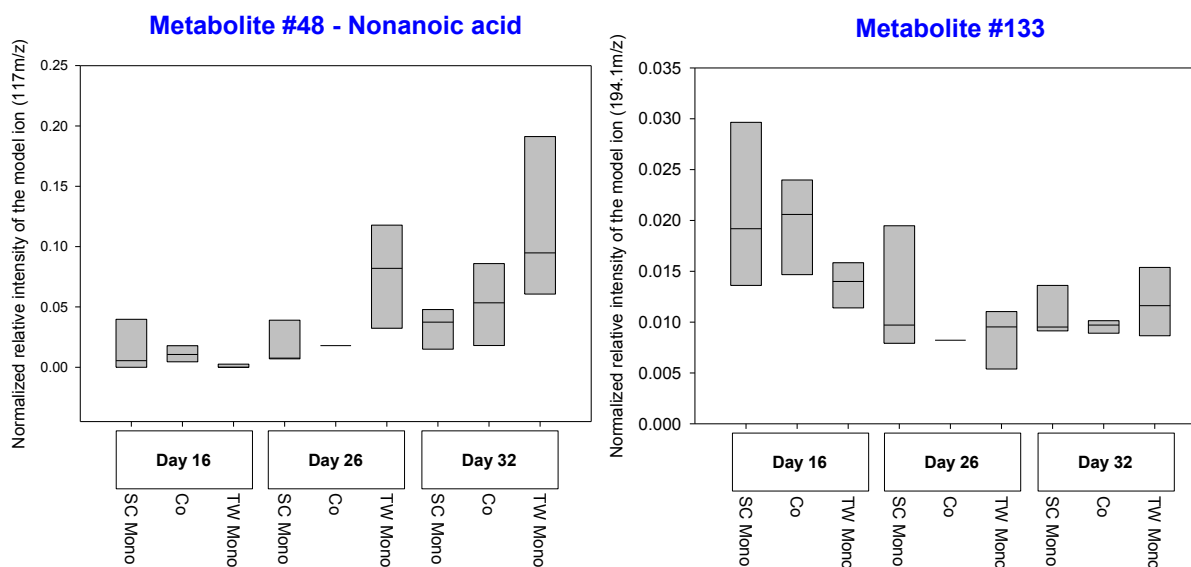


Figure 8: Exemplary metabolites #48 and #133 with interaction-induced release mechanism on day 16 and subsequent temporal regulation in the interaction between *T. weissflogii* and *S. costatum* (intensity pattern I).

Among the metabolites that exhibit pattern I on day 16 in combination with a distinct temporal intensity dynamic, I observed two different trends. The trend of increased MST intensity within each treatment group over time was represented by nonanoic acid (#48) and the trend of decreased intensity by MST #133 (**Figure 8**). In addition to nonanoic acid (#48), I also observed the trend of time dependent increase of MST intensity within each treatment group for metabolites #44 and putative pentadecanoic acid #113 (**Appendix 14**).

On the other hand, MST #133 exhibited an inversed temporal dynamic: It was most abundant on day 16, with 1.1 -to 1.5 - fold higher abundance in co-cultivation, with decreasing intensity towards day 32. A distinct increase / decrease dynamic might indicate growth phase dependent regulation of the respective metabolites.

Furthermore, another striking temporal dynamic, possibly indicating a release-uptake mechanism in the diatom interaction, is introduced with the help of MST #133 (**Figure 8**) and #44 (**Figure 9**).

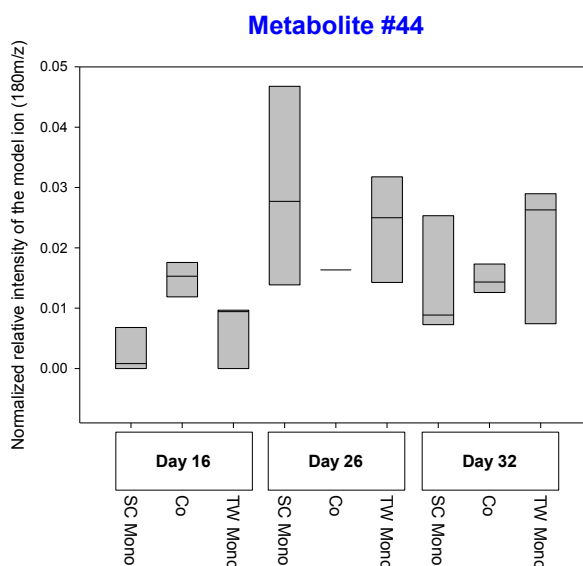


Figure 9: Exemplary MST #44 with interaction-induced release-uptake mechanism in the interaction between *T. weissflogii* and *S. costatum* (intensity pattern I on day 16).

For example: While on day 16 MST #44 was most abundant in co-cultivation compared to both mono-cultivations, on day 26 this ratio inverted. MST #44 was 1.5 - to 1.7 - fold more abundant in both mono-cultivations on day 26 compared to co-cultivation. This trend is also observed for putative 2-hydroxypentanoic acid (#40), putative 2-hexylpyridine (#51), myristic acid (#111), pentadecanoic acid (#117), palmitoleic acid (#122, #123), oleic acid (#132) and seven unknown metabolites (#58, #60, #65, #71, #93, #128, #138), as depicted in **Appendix 14**. Among these metabolites only #44 and #133 exhibit a clear temporal dynamic. All other candidates presented in the appendix show rather unspecific abundance among the sampling days. This might either be caused by a time-independent presence of the respective MST in the exometabolomes, or due to high variance of the data.

- (3) Metabolites with uncategorized abundance pattern throughout all sampling days.

In addition to the already categorized metabolites, 4-hydroxybutanoic acid (#33) and the unknown MST #49 show neither a distinct temporal increase / decrease dynamic, nor a predominance on day 16 (**Appendix 14**). These MSTs are categorized separately and represented by 4-hydroxybutanoic acid (#49) in **Figure 10**. Furthermore, 2-methylbenzoic acid (#50) seems predominant on day 32, although no distinct increase / decrease dynamic is observed (**Figure 10**).

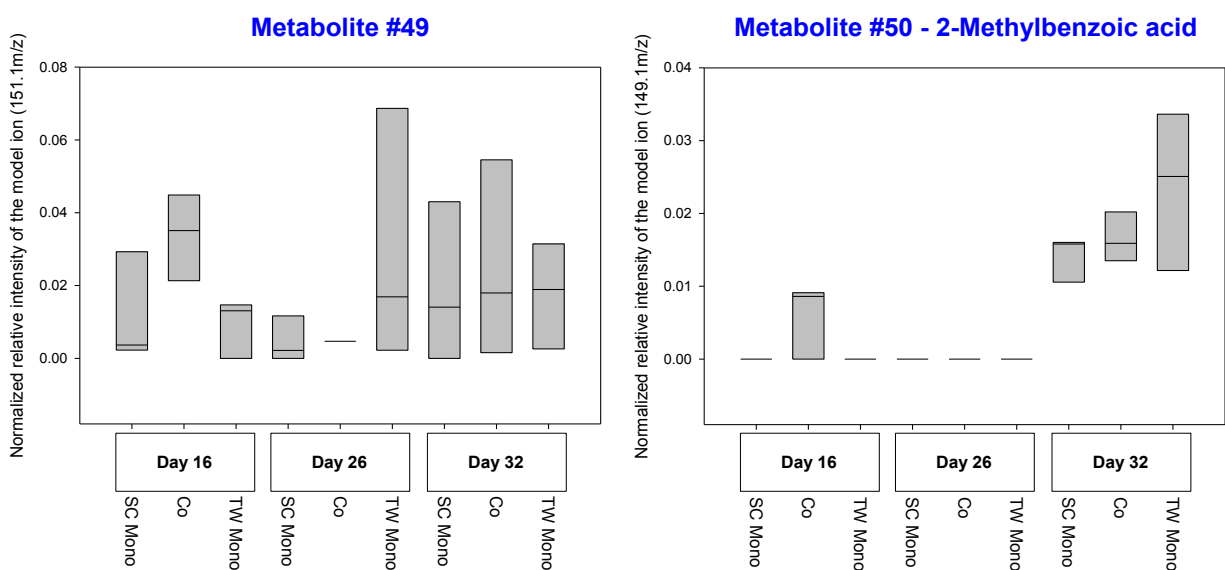


Figure 10: Exemplary metabolites #49 and #50 with interaction-induced release mechanism on day 16 in the interaction between *T. weissflogii* and *S. costatum* (intensity pattern I).

Day 26

Out of the 39 candidate molecules, five unidentified MSTs (#62, #63, #77, #92, #96) were characteristic for day 26 (**Appendix 15**). They belong to group A26 in the heatmap of the overall analysis (**Table 3**). In general, these MSTs were hardly present on day 16, but their intensities increased over time. Thus, they seem characteristic for the stationary phase of growth, as they were most abundant on day 26 and 32 in all groups.

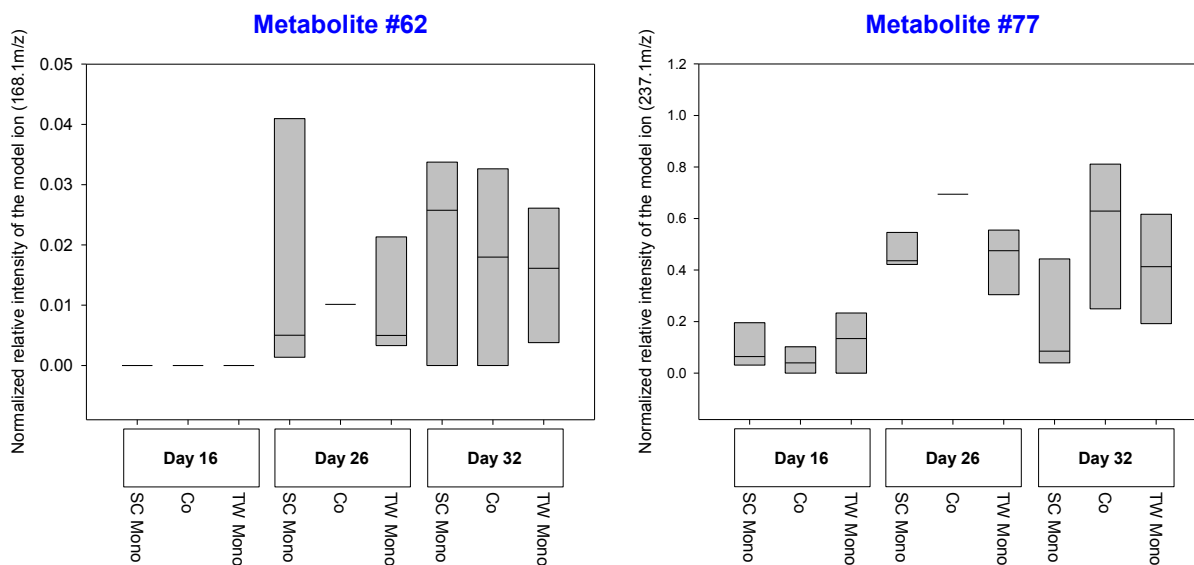


Figure 11: Exemplary MSTs #62 and #77 with interaction-induced release mechanism on day 26 as well as on day 26 and 32 in the interaction between *T. weissflogii* and *S. costatum* (intensity pattern I).

In summary, I observed two different temporal dynamics among these candidate molecules. MSTs #62 and #63 exhibited increased intensity in co-cultivation on day 26, while MSTs #77, #92 and #96 exhibited increased abundance on day 26 and 32. These temporal dynamics are exemplarily visualized in **Figure 11**.

Day 32

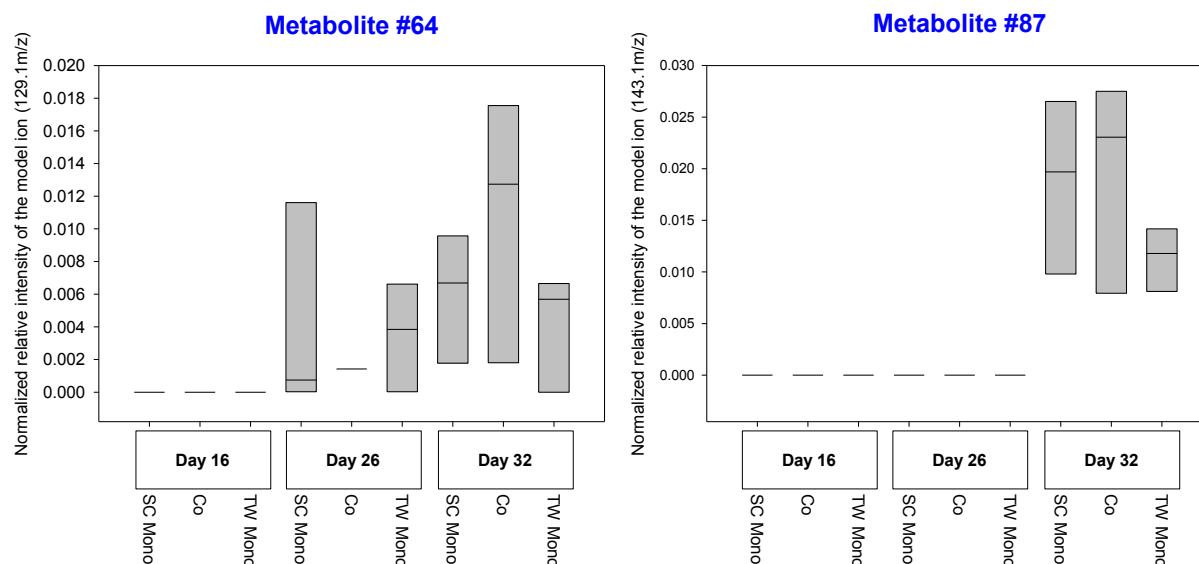


Figure 12: Intensity dynamic of exemplary exometabolites, enhanced in co-cultivation on day 32 (interaction between *T. weissflogii* and *S. costatum*).

Considering day 32, the overall analysis yielded eight characteristic MSTs (#6, #13, #21, #39, #43, 2-methylpropanoic anhydride #47, #64, #87) that were most abundant in co-cultivation, compared to both mono-cultivations (**Appendix 16**). While the majority of MSTs was present on day 26 and 32, MST #87 was only abundant on day 32. These temporal dynamics are represented by MST #64 and #87 in **Figure 12**. Median MST intensities, as visualized in the heatmap (**Table 3**, group A32), were elevated in co-cultivation, but the boxplots of most metabolites on day 32 exhibited high variance in the data.

Reduced abundance of exometabolites in co-cultivation - Pattern II / III:

In total, 12 MSTs matched intensity patterns (II) and (III). These metabolites are classified as groups B16, B26 and B32 in the heatmap of the overall CAP analysis (**Table 3**) and groups B⁴¹ in the heatmap of the subset analysis on day 16 and 26 (**Table 4**, **Table 5**).

⁴¹ Diisobutyl phthalate (#112) was not further discussed, as it was a prominent plasticizer and rated as contaminant.

Day 16

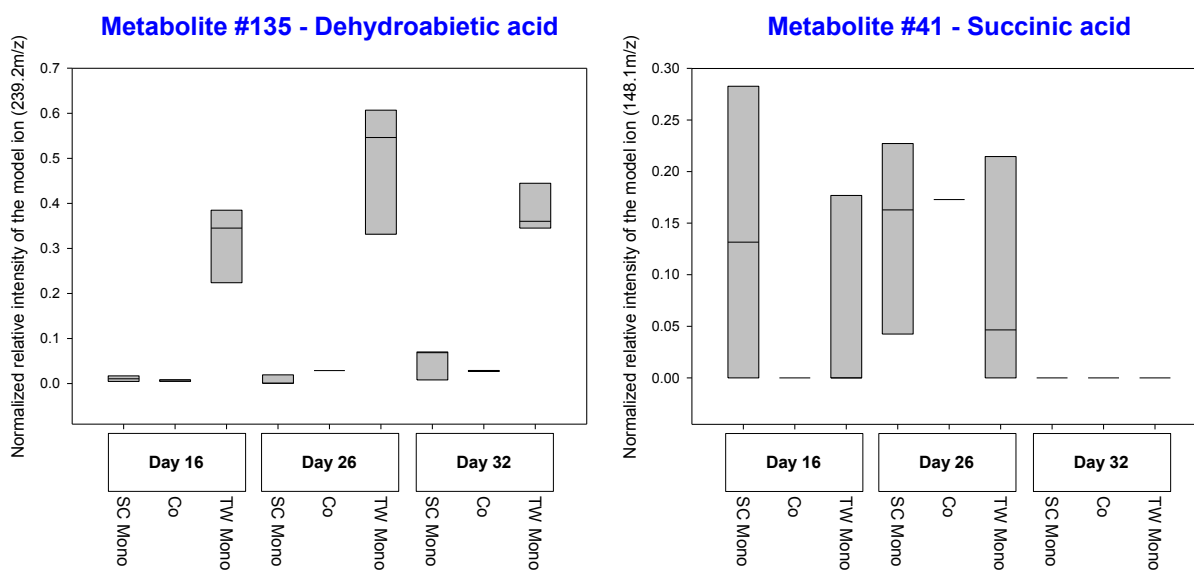


Figure 13: Exemplary metabolites #135 and #41 with interaction-induced uptake, transformation or reduced release mechanisms on day 16 in the interaction between *T. weissflogii* and *S. costatum* (intensity pattern II).

One carboxylic acid and one terpenoid were characteristic for day 16. Succinic acid (#41) seemed to characterize the exometabolomes of both diatom species in mono-cultivation and exhibited reduced abundance in co-cultivation on day 16 (**Figure 13**). Generally, it was present on day 16 and 26 - showing pattern I on the latter- but not on day 32 and seems relevant for the early stages of the interaction.

The terpenoid dehydroabiatic acid (#135) is characteristic for the exometabolome of *T. weissflogii*, as it was most abundant there (**Figure 13**). On day 16, this MST matched pattern II, but furthermore on day 26 and 32 the abundance in co-cultivation was clearly less than expected by the reference value. Thus, it might be hypothesized that dehydroabiatic acid was either taken up by *S. costatum* in co-cultivation, transformed or that the release by *T. weissflogii* was reduced. Considering temporal dynamics, this MST is not only relevant for day 16, but for later stages of the interaction as well.

I identified 4-Pyridoxate (#116) via heatmap screening, but an evaluation of the boxplot indicated that pattern II / III were not matched on day 16 (**Appendix 17**). This metabolite was not further considered.

Day 26

On day 26, I found five MSTs (#1, #95, #104, #107, and #126) to match pattern II / III. MSTs #104 and #107 have been previously documented by Vidoudez, as they were found in the exometabolome of *S. marinoi* (Vidoudez, 2010). However, their chemical identity remained unclear. In the interaction experiment, both metabolites seemed characteristic for the exometabolome of *S. costatum*, as they were most abundant there (**Appendix 17**).

While MSTs #1 and #107 exhibited pattern II only on day 26, MSTs #95, #104 and #126 exhibited pattern II on day 26 and 32. These two different dynamics are visualized exemplarily in **Figure 14**. The metabolites with the former dynamic seemed relevant at the onset of the growth effect on day 26, metabolites of the latter characterized not only the onset of the growth effect, but also the effect during the late stationary phase of growth.

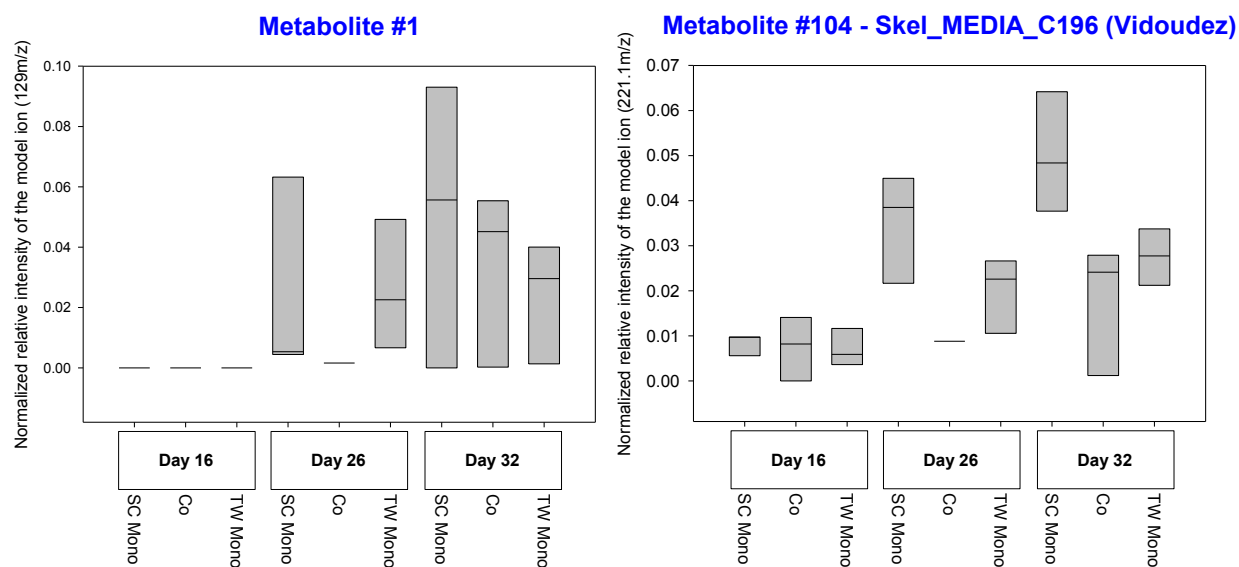


Figure 14: Exemplary metabolites #1 and #104 with interaction-induced uptake, transformation or reduced release mechanisms on day 26 as well as day 26 and 32 in the interaction between *T. weissflogii* and *S. costatum* (intensity pattern II).

Day 32

On day 32, 3-pyridinol (#11), putative 2,2'-iminodiethanol (#37), a metabolite with a pattern similar to lumichrome (#45) and the unidentified MST #114 matched intensity patterns (II) and (III) (**Figure 15**).

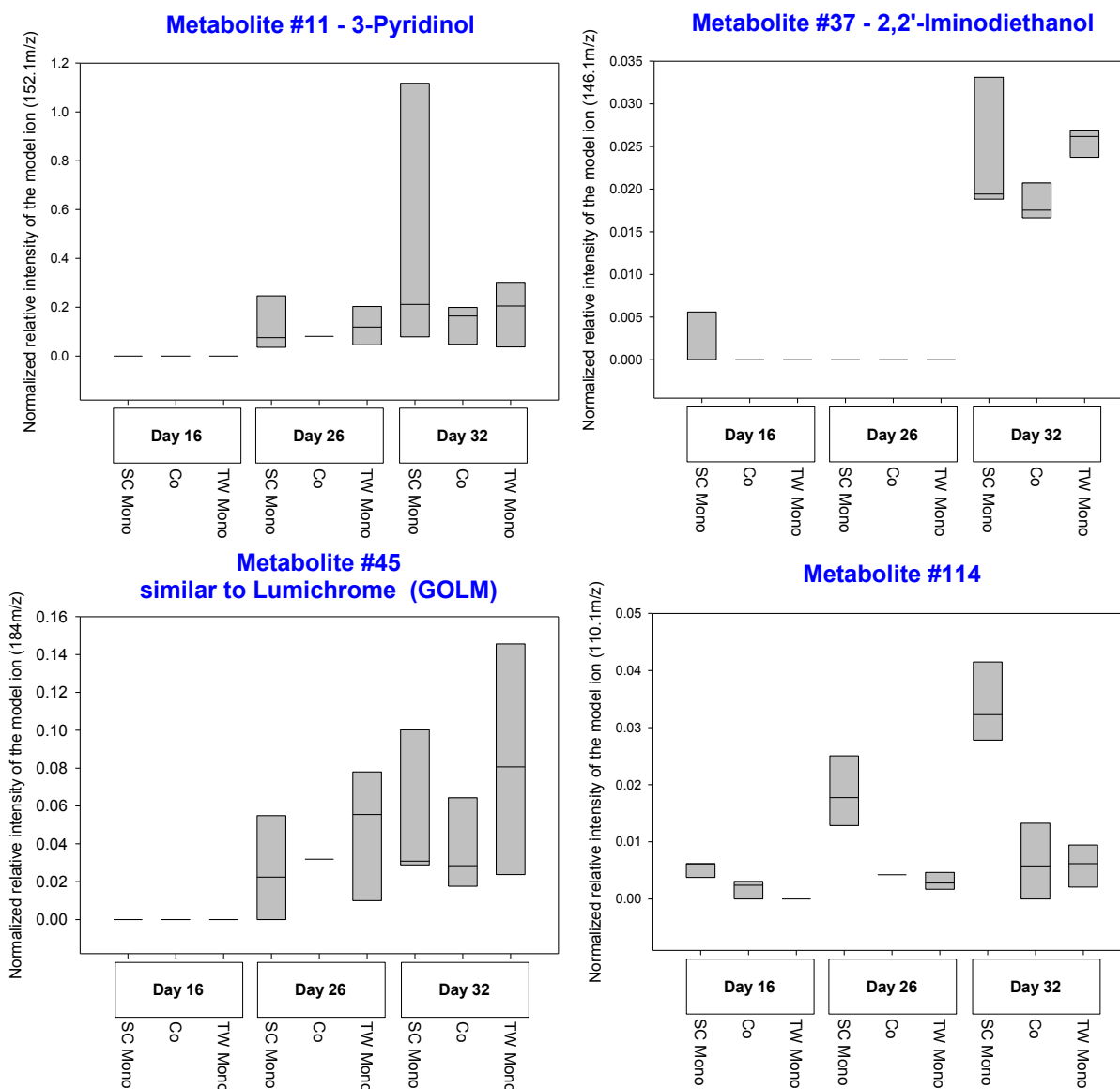


Figure 15: Potential infochemicals with interaction-induced uptake, transformation or reduced release mechanisms on day 32 in the interaction between *T. weissflogii* and *S. costatum* (intensity pattern II).

Putative 2,2'-iminodiethanol (#37) was clearly characteristic for day 32 and least abundant in co-cultivation. It seemed to be highly growth phase dependent and characteristic for the late stationary phase. MST #114 exhibited temporal increase of intensity in all groups. However, on day 26 and 32 the MST intensity in co-cultivation was clearly less than expected by the reference value, which

should be an average value of both mono-cultivation intensities. Throughout all three points in time, this MST was highest abundant in mono-cultivated *S. costatum* and thus characteristic for this species (**Figure 15**).

Furthermore, I found 3-pyridinol (#11) and a metabolite similar to lumichrome (#45) to match pattern II and III. Both were not abundant on day 16, but appeared on the exometabolomes on day 26 and 32 (**Figure 15**).

2.2.4 Endometabolomic investigation

In the interaction between *T. weissflogii* and *S. costatum*, the presence of a partner in co-cultivation significantly changed the endometabolome in the stationary growth phase (day 26 and 32) in both species. In total, 78 MSTs were significantly correlating with these differences in *T. weissflogii* and 87 MSTs in *S. costatum*. To increase clarity, I grouped all relevant metabolites by metabolite classes. Note that only a fraction of all MSTs could be identified and thus classified for evaluation.

Among amino acids, I observed the general trend of upregulation due to the interaction in both species during the stationary phase of growth. Furthermore, in *T. weissflogii* a majority of complex sugars were more abundant in co-cultivation on day 32, compared to mono-cultivation. As were the majority of identified sugars and sugar derivatives. Amines (represented by cadaverine), carbonic acids, fatty acids, alcohols and their respective derivatives, showed the tendency of lower abundance in co-cultivation on day 26 and 32, compared to mono-cultivation.

In *S. costatum* most alcohols, carboxylic acids and a steroid (#276) were upregulated in co-cultivation, compared to mono-cultivation. The trend in alcohols and carboxylic acids was opposite to the one described for *T. weissflogii*. Furthermore, the amine putrescine (#127) was upregulated in co-cultivation in the late stationary phase.

I performed the endometabolomic investigations in the manner of descriptive analyses. Their main purpose was to qualitatively describe metabolomic alterations within the organisms and to potentially support hypotheses drawn from the exometabolomic investigations.

After data pre-processing of 51 samples from three distinct sampling points, I obtained 285 MSTs characterizing the endometabolomes of *T. weissflogii* and *S. costatum* in the interaction experiment (see experimental design in chapter 2.1.2). The number of replicates per treatment group was six for mono-cultivation and three for co-cultivation⁴².

It must be noted that sample handling during the workflow of the endometabolomic analysis was not optimal, as documented in chapter 6.6.3. Suboptimal randomization might have resulted in artificial differences between sampling days. Therefore, the interpretation of time dependent endometabolomic alterations need to be made with care. I still considered data very valuable, as I set the main focus on relative differences between the treatments within each sampling day.

⁴² See chapter 2.1.2 and 6.4 for specification

Furthermore, irregularities in the derivatization process, which concerned subsets of samples from day 26 and 32, might have introduced artificial variability. Freezing and increased exposure to elevated temperature might have affected the derivatization chemistry, the compound degradation and might have impeded the identification of MSTs. Due to the introduced artificial variability, the probability of significant endometabolomic alterations is expected to decrease and existing differences might be masked by the artificial variability. However, as I found significant differences between the treatment groups, this proves the resilience of the data to the described variability. Subsequently, I describe sample similarities and endometabolomic changes.

Analysis strategy

I conducted the endometabolomic characterization of the interaction between *S. costatum* and *T. weissflogii* with a strategy similar to the one used for the exometabolomic analysis. However, the analysis strategy differed slightly, as explained in the following paragraphs, due to the experimental design.

Again, I conducted an overall CAP analysis throughout all three sampling points and both species, to investigate global effects and dependencies between the samples. Furthermore I analyzed species-specific data subsets throughout all three points in time, as well as day-specific data subsets per species. Thus, I set the focus on endometabolomic changes due to treatment, neglecting the influence of species. And on the other hand, I set it on endometabolomic changes within each day, neglecting the influence of time and species. As it was the objective of this study to investigate endometabolomic changes in *S. costatum* and *T. weissflogii* due to the interaction, I always included treatment in a-priori groups in the course of the identification of highly correlated metabolites.

Data exploration via CAP

The unconstrained PCoA score plot of the overall dataset indicated strong grouping of the samples by species affiliation (separation via principal coordinate axis 1) and a gradual separation of samples by time (separation via principal coordinate axis 2, **Appendix 18**). A constrained analysis via CDA confirmed that species and time were dominant factors influencing endometabolomic similarities in the interaction experiment: A-priori grouping of the overall data set by species (*T. weissflogii* and *S. costatum*) and by day (sampling days 16, 26 and 32) yielded very low misclassification errors of 1.96 % (species, **Table 6**) and 5.882 % (day, **Table 6**). A permutation test shows statistically significant differences between these a-priori groups (trace statistic $P \leq 0.001$, **Table 6**).

Table 6: Permutation and cross-validation test results for the overall analysis of different a-priori groups in the endometabolome analysis of the interaction between *S. costatum* and *T. weissflogii*

A-priori grouping by	m	Groups	Trace statistic	δ_1^2	Misclassification error (%)
Species	10	2	0.906 ($P = 0.0003$)	0.906 ($P \leq 0.0001$)	1.96
Day	4	3	0.836 ($P \leq 0.0001$)	0.812 ($P \leq 0.0001$)	5.88
Treatment	11	4	1.640 ($P \leq 0.0001$)	0.936 ($P \leq 0.0001$)	15.69
Day & treatment	12	12	4.916 ($P \leq 0.0001$)	0.970 ($P \leq 0.0001$)	11.77

δ_1^2 being the first squared canonical correlation. m represents the number of PCoA axes included in the CAP.

To investigate endometabolomic alterations induced by the interaction, I introduced treatment (mono-cultivated *S. costatum*, mono -cultivated *T. weissflogii*, co-cultivated *S. costatum* and co-cultivated *T. weissflogii*) and treatment per day as a-priori grouping factors in the CAP. The permutation test results indicated highly significant differences between treatments and treatments per day in the overall analysis (trace statistic $P \leq 0.001$, **Table 6**). Comparing treatment and treatment per day as grouping factors, the latter yielded the lower misclassification error (11.77 %, **Table 6**), compared to a classification by treatment throughout all sampling points (15.69 %, **Table 6**).

The overall analysis provided a first exploration of the endometabolomic data. However, the investigation of interaction-induced alterations of diatom endometabolomes was performed for each species separately. By splitting the overall data set into species-specific subsets, I excluded the strong influence of species on the endometabolome from the analysis. This is especially important, as it cannot be excluded that artificial differences between the species were introduced by using peak sum normalization per sample during data pre-processing (compare discussion in chapter 2.5.3).

Species-specific subset analysis

In the context of the species-specific analysis of *T. weissflogii* and *S. costatum*, the PCoA score plot does not show distinct groups of samples (**Appendix 19**). However, day and treatment seemed to establish a gradual separation: In the case of *T. weissflogii*, principal coordinate axis 2 (**Appendix 19A**) and of *S. costatum*, principal coordinate axis 1 (**Appendix 19B**) spanned a gradient of samples ranging from day 16 to day 32. Time seemed to be the dominant factor influencing sample grouping. Considering treatments, a visible separation was only observed within some days for *T. weissflogii*, but not throughout all points in time. Treatments on day 26 and 32 were separated by principal

coordinate axis 1, while on day 16 treatment groups overlapped. For *S. costatum* no distinct separation of treatments was seen in the PCoA score plot.

These first data explorations were supplemented with a CDA. I tested a-priori grouping by day, treatment and treatment per day, indicating highly significant differences between all a-priori groups ($P \leq 0.01$, **Table 7**). As the misclassification was lowest for a-priori grouping by day (0 %, **Table 7**), I confirmed that time is a dominant grouping factor. Furthermore I tested a-priori grouping by treatment and treatment per day. Although these patterns were mostly hidden in unconstrained ordination, constrained analyses was able to reveal that in both species there were significant differences in the endometabolomes due to treatment. Treatments were significantly different, both independent of time, as shown by a-priori grouping by treatment ($P \leq 0.01$, **Table 7**) and dependent of time, as shown by a-priori grouping by treatment per day ($P \leq 0.001$, **Table 7**). With misclassification errors of 0 % for *S. costatum* and 0 - 8 % for *T. weissflogii*, the sample groups were distinct.

Table 7: Permutation and cross-validation test results for the species-specific subset analysis of different a-priori groups in the endometabolome analysis of the interaction between *S. costatum* and *T. weissflogii*

A-priori grouping by	m	Groups	Trace statistic	δ_1^2	Misclassification error (%)
<i>T. weissflogii</i> : day	6	3	1.736 ($P \leq 0.0001$)	0.893 ($P \leq 0.0001$)	0
<i>T. weissflogii</i> : treatment	7	2	0.772 ($P = 0.0035$)	0.772 ($P = 0.0035$)	8
<i>T. weissflogii</i> : day & treatment	8	6	3.261 ($P \leq 0.0001$)	0.978 ($P = 0.0008$)	4
<i>S. costatum</i> : day	2	3	0.912 ($P \leq 0.0001$)	0.909 ($P \leq 0.0001$)	0
<i>S. costatum</i> : treatment	10	2	0.744 ($P = 0.0079$)	0.744 ($P = 0.0079$)	0
<i>S. costatum</i> : day & treatment	13	6	3.727 ($P = 0.0003$)	0.989 ($P = 0.0007$)	0

δ_1^2 being the first squared canonical correlation. *m* represents the number of PCoA axes included in the CAP.

Daywise subset analysis per species

The analysis of daywise subsets per species indicated that treatments were significantly different on day 26 and day 32 in both *S. costatum* and *T. weissflogii* (trace statistic $P \leq 0.0001$, **Table 8**).

Table 8: Permutation and cross-validation test results for the species-specific and daywise subset analysis of different a-priori groups in the endometabolome analysis of the interaction between *S. costatum* and *T. weissflogii*

A-priori grouping by	m	Groups	Trace statistic	δ_1^2	Misclassification error (%)
<i>T. weissflogii</i> : day 16	5	2	0.994 (P = 0.3011)	0.994 (P ≤ 0.3011)	0
<i>T. weissflogii</i> : day 26	2	2	0.911 (P ≤ 0.0001)	0.911 (P ≤ 0.0001)	0
<i>T. weissflogii</i> : day 32	2	2	0.946 (P ≤ 0.0001)	0.946 (P ≤ 0.0001)	0
<i>S. costatum</i> : day 16	5	2	0.492 (P = 0.902)	0.492 (P = 0.902)	0
<i>S. costatum</i> : day 26	3	2	0.608 (P ≤ 0.0001)	0.608 (P ≤ 0.0001)	0
<i>S. costatum</i> : day 32	1	2	0.901 (P ≤ 0.0001)	0.901 (P ≤ 0.0001)	0

δ_1^2 being the first squared canonical correlation. *m* represents the number of PCoA axes included in the CAP.

These findings were confirmed by the PCoA score plots, which shows distinct sample grouping by treatment. For *T. weissflogii*, these groups were separated by a combination of principal coordinate axis 1 and 2 (**Appendix 20C, E**) and for *S. costatum* by principal coordinate axis 2 on day 26 and axis 1 on day 32 (**Appendix 20D, F**). Misclassification errors of 0 % confirmed distinct groups of samples. Interestingly, on day 16 there was no significant difference between the treatments, as visible in the PCoA score plots (**Appendix 20A, B**) and confirmed by the trace statistic (**Table 8**).

Identification of metabolites correlating with relevant a-priori groups

In analogy with the exometabolomic analysis, I used the CAP to identify metabolites that were correlating with the significant differences between the a-priori groups, described above. By combining a species-specific approach with a daywise subset analysis, I guaranteed a comprehensive analysis of the endometabolome.

In general, I used the constrained score plots and corresponding loading plots to visualize the differences between the a-priori groups and to visualize the correlating metabolites. I considered only metabolites that exceeded a certain significance level of correlation with either canonical axis 1 or canonical axis 2 (P ≤ 0.001 for the species-specific analysis, P ≤ 0.05 for the species-specific daywise analysis). However, I fully based further interpretations and identification of potential biomarkers on heatmaps, visualizing MST intensities among the sampling days and treatments.

T. weissflogii

The score and loading plots in **Figure 16** summarize the results of the species-specific analysis for *T. weissflogii*. I considered both a-priori grouping by treatment (**A, B**) and treatment per day (**C, D**). In the analysis with a-priori grouping by treatment, the constrained score plot (**Figure 16A**) shows a clear time-independent separation of mono- and co-cultivated *T. weissflogii* by canonical axis 1. In total, eight metabolites were significantly correlated ($|r| \geq 0.6178$, $P \leq 0.001$) with the separation of treatments. As visualized in the loading plot, the majority of metabolites characterized *T. weissflogii* in co-cultivation, while only MST #165 was correlating with mono-cultivation (**Figure 16B**).

In the analysis with a-priori grouping by treatment per day, time was taken into account, when considering differences between treatments. The constrained score plot confirmed that the endometabolomes in mono- and co-cultivation were substantially different on day 26 and 32, as treatment groups within these days were separated by canonical axis 2 (**Figure 16C**). Treatment groups on day 16 overlapped and did not indicate significant differences. I statistically confirmed these findings via trace statistics (**Table 7**). In general, samples from day 32 were distinctly different from samples on day 16 and 26, as they were separated by canonical axis 1.

Moreover, 24 of the 29 highly correlated metabolites ($|r| \geq 0.6177$, $P \leq 0.001$, **Figure 16D**) were characteristic for day 32, as their respective MST vectors were located in quadrant III and IV. Of these samples, the majority pointed towards co-cultivation. The remaining five metabolites characterized samples on day 16 and 26. However, a clear affiliation to distinct sample groups was not possible in **Figure 16**.

I summarized the results of the daywise analysis for *T. weissflogii* in **Figure 17**. The constrained score plots show a strong separation of mono- and co-cultivation on day 26 (**Figure 17A**) and day 32 (**Figure 17B**) via canonical axis 1. These findings are in agreement with the results of the species-specific analysis and were confirmed by the permutation test (**Table 8**). Day 16 was not further considered due to lack of significance. All metabolites that were significantly correlating with differences between the treatments on day 26 and 32 ($|r| \geq 0.6664$, $P \leq 0.05$) are visualized in loading plots (**Figure 17B, D**). In total, I identified 42 highly correlated metabolites on day 26 and 30 on day 32. On both days respectively, the majority of metabolites was characteristic for co-cultivation of *T. weissflogii*.

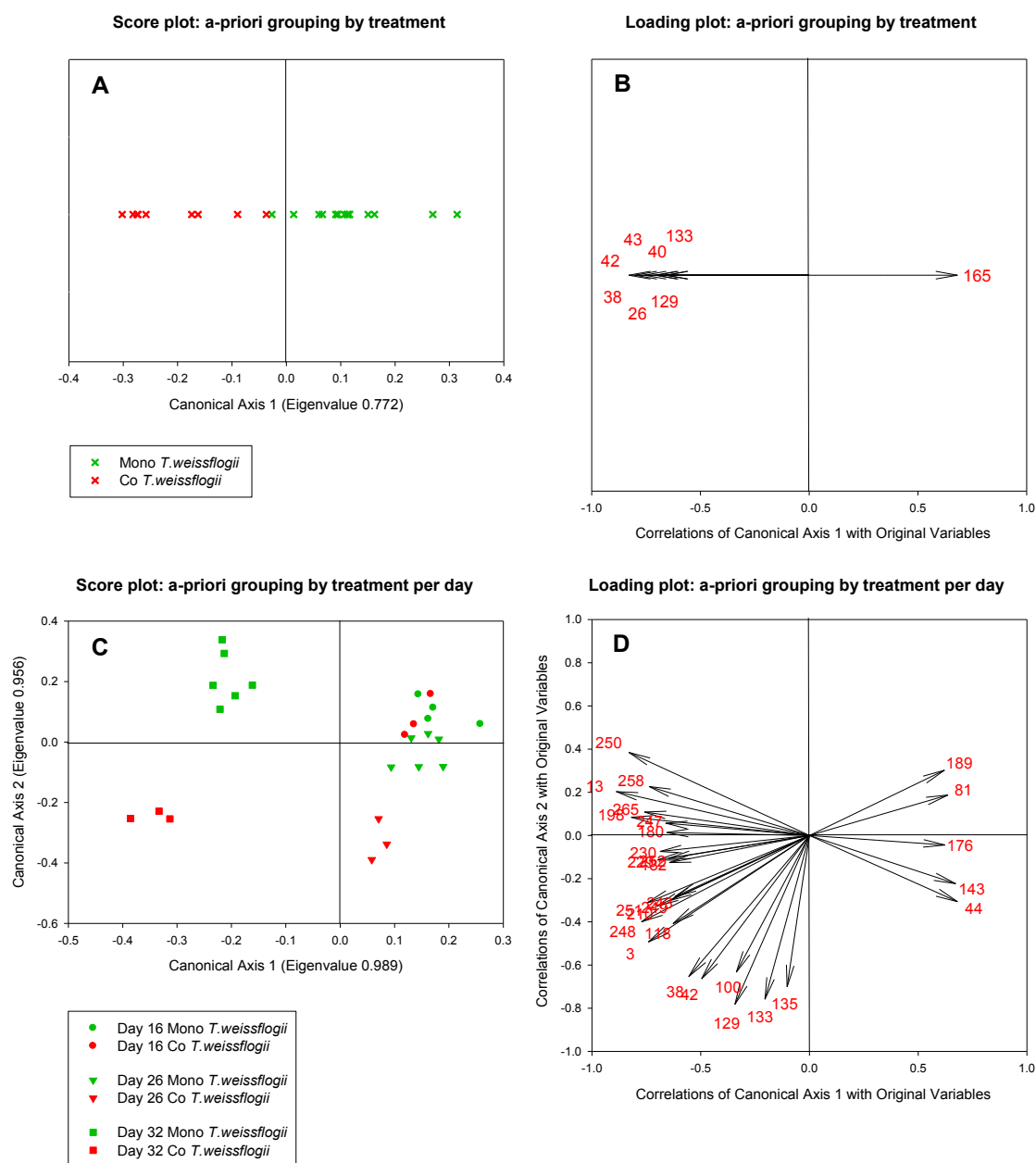


Figure 16: Constrained score and loading plots of endometabolomic samples from *T. weissflogii* in a species-specific subset analysis of the interaction between *T. weissflogii* and *S. costatum*.

The constrained score plots (graph **A**, **C**) visualize significant differences between the sample groups as found via CDA with a-priori groups by treatment (trace statistic $P = 0.0035$, misclassification error of 8 % for $m = 7$, graph **A**) and a-priori groups by treatment per day (trace statistic $P = 0.0008$, misclassification error of 4 % for $m = 8$, graph **C**). Vectors in the CAP loading plots (graph **B**, **D**) represent metabolites, characterized by their ID (red numbers). Only vectors with a significant correlation coefficient above the critical value of $|r| \geq 0.6178$ ($P \leq 0.001$) for a-priori grouping by treatment and $|r| \geq 0.6177$ ($P \leq 0.001$) for a-priori grouping by treatment per day are plotted. The direction of the vectors in 2-dimensional space correlates with endometabolomic sample groupings shown in the score plots of the respective analysis.

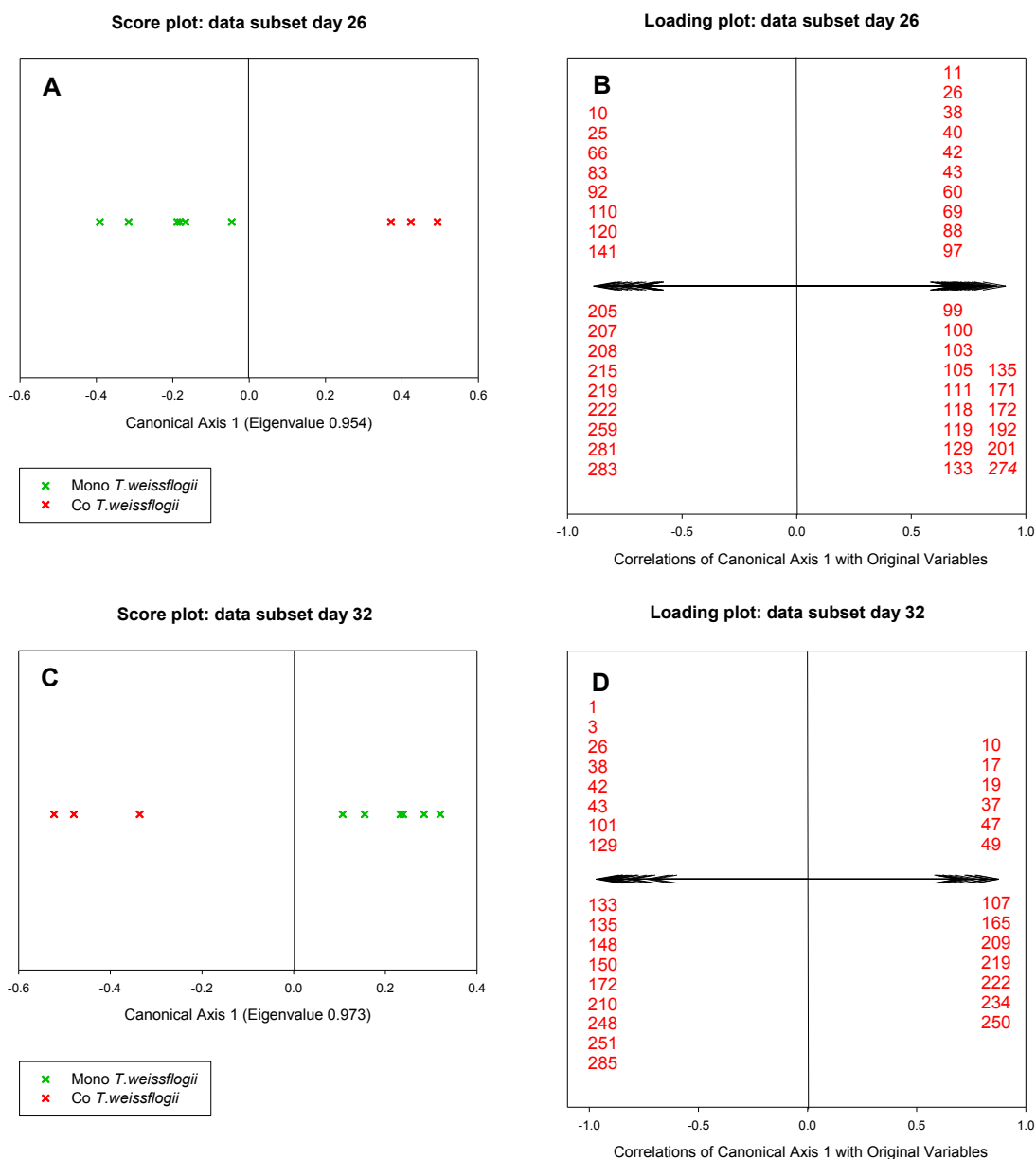


Figure 17: Constrained score and loading plots of endometabolomic samples from *T. weissflogii* in a daywise subset analysis of the interaction between *T. weissflogii* and *S. costatum*.

The constrained score plots (graph **A**, **C**) visualize significant differences between the treatments, as confirmed via CDA for the subset analysis on day 26 (graph **A**, **B**) and day 32 (graph **C**, **D**). These differences between treatments are highly significant (trace statistic $P \leq 0.0001$, misclassification error of 0 % for $m = 2$). Vectors in the CAP loading plots (graph **B**, **D**) represent metabolites, characterized by their ID (red numbers, pooled per group). Only vectors with a significant correlation coefficient above the critical value of $|r| \geq 0.6664$ ($P \leq 0.05$) are plotted. The direction of the vectors in 2-dimensional space correlates with endometabolomic sample groupings shown in the score plots of the respective analysis.

To sum it up, the score plots of the species-specific and daywise analyses clearly visualize the significant differences between the treatments on day 26 and 32. In total 78 MSTs (not counting redundant MSTs found in more than one analysis) were significantly correlating with these differences. Interestingly, within these days, the majority of metabolites was correlating with the co-cultivation group.

All highly correlated MSTs are summarized in a heatmap (**Table 9**). The affiliation of the MSTs to their respective analysis is noted in the heatmap. Metabolites were sorted by class and within class by intensity pattern to facilitate the discussions. To interpret the findings, I considered not only the intensity pattern, but also the underlying analysis. For example, I only considered MSTs identified in the daywise analysis relevant for the separation of treatments within the specific analysis day.

As previously described, most MSTs showed a strong correlation with the co-cultivation group. This was especially true for the group of amino acids. Five amino acids, identified via standards, were highly correlating with the separation of treatments. Alanine (#3), valine (#1, #26), leucine (#38), isoleucine (#42) and threonine (#43) were more abundant in co-cultivation than in mono-cultivation in all investigated points in time of the interaction. Amino acid intensities increased from day 16 to 32, reaching relative maximum intensities that were up to 8.9 - fold (leucine, day 26) higher in co-cultivation, compared to mono-cultivation.

In general, the identification of metabolites in the class of sugars, complex sugars and their respective derivatives via MS libraries was difficult. Although the strategy of MST identification via MS libraries was retained, the sugar identities must be interpreted with caution.

In the class of complex saccharides, the pattern of MST intensities was more complex. I found six different complex sugars and one complex sugar derivative to be highly correlated with the separation of treatments. Sucrose (#243), gentiobiose (#248, #251), putative maltose (#252) and putative lactose (#249) were 1.4 - to 2.2 - fold more abundant in co-cultivation on this day. However, trehalose (#250) and galactinol (#258, #265) were characteristic for mono-cultivation, as they were 1.3 - to 1.8 -fold more abundant on day 32, compared to co-cultivation. In general, the intensities of complex sugars increased over time and showed maximum abundance on day 32, with the exception of a disaccharide (#283), which was characteristic for mono-cultivation and present at early stages of the interaction (day 16 and 26).

Besides complex saccharides, 13 sugars and sugar derivatives were of relevance for the separation of treatments. The majority of them (8 out of 13) were characteristic for co-cultivation on day 26

and 32. Interestingly, these metabolites showed highest abundance on day 26 and / or day 32 and were merely abundant in mono- and co-cultivation on day 16.

The daywise analysis revealed that putative arabinofuranose (#97, #99 and #100), glucopyranose (#192), putative galactofuranoside deriv. (#105), putative glucuronolactone (#119), xylose (#110) and a further unidentified sugar (#281) were significant for the separation of treatments on day 26. With the exception of the latter 2, which were characteristic for mono-cultivation on day 26, all metabolites were 1.4 - to 1.9 - fold more abundant in co-cultivation on this respective day. Putative erythrose (#101), fructose (#148), glucose (#150) and an unknown sugar (#210) were characteristic for co-cultivation on day 32, as they were 1.4 - to 14.5 - fold more abundant compared to mono-cultivation. I identified a sugar acid (#172, putative gluconic acid) to be of relevance for co-cultivation on both day 26 and 32. It was more abundant compared to the negative control on all three sampling points.

It is important to note that sugar acid #172 and #165 were both putatively identified as gluconic acid with the help of metabolite libraries. However, their abundance pattern was opposite, as #165 was characterizing mono- and #172 was characterizing co-cultivation. This opposing trend in abundance might be caused by the fact that either both MSTs origin from the same compound and their intensities need to be interpreted additively, or that both MSTs originate from different metabolites with individual abundance dynamics. The latter might indicate an imprecision in the putative, library based identification.

Generally, the identification of sugars and sugar derivatives via GC-MS is difficult due to the high number of functional groups and the presence of tautomeric forms in solution (Medeiros and Simoneit, 2007; Ruiz-Matute et al., 2011). Therefore, either due to tautomerism, e.g. keto-enol tautomerism, different silylation states or derivatization side reactions of the multiple functional groups compounds can be reflected in various chromatographic peaks and cause a high complexity of the chromatogram (Halket and Zaikin, 2003; Medeiros and Simoneit, 2007; Ruiz-Matute et al., 2011). Due to this high complexity, it is difficult to unambiguously identify sugar and sugar derivative peaks and to clearly differ between compounds. Thus, both MSTs were subsequently only classified on the compound class level. Furthermore, identification of sugars is often only putative.

The remaining two metabolites of the sugar and sugar derivative class were correlating with mono-cultivation of *T. weissflogii*. An unidentified sugar (#143) and a putative inositol isomer (#189)

characterized the mono-cultivation as well. These metabolites shared one trait, they were merely abundant on day 32.

In the remaining classes of metabolites (not considering unknowns), I observed a trend of reduced metabolite abundance in co-cultivation. The amine cadaverin (#66) distinguished the treatments on day 26, as it was 27.4 - fold more abundant in mono-cultivation on this day. The alcohol 2-dodecanol (#83) was found to be relevant on day 26, where it was 6.3 - fold more abundant compared to co-cultivation, whereas the alcohol derivative 3-chloro-1,2-propanediol (#10, #19) was relevant for the separation on day 26 and 32, being more abundant in mono-cultivation both days. Glycerol (#17, #37) was responsible for the separation of treatments on day 32, where it was up to 2.0 - fold more abundant in mono-cultivation compared to co-cultivation.

Among highly correlated carboxylic acids, five metabolites were relevant for the separation of treatments on day 26. Pyroglutamic acid (#88) and oleic acid (#201) were up to 3.8 - fold more abundant in co-cultivation. Putative arachidonic acid (#205, #207), 3-hydroxybutanoic acid (#25) and ethyl palmitate (#171) were up to 4.7 - fold more abundant in mono-cultivation and thus characterizing mono-cultivation on day 26. Propionic acid (#13) intensity increased until reaching maximum values on day 32, with 1.3 - fold higher abundance in mono-cultivation, compared to co-cultivation. 2,3-Dihydroxypropanoic acid (#49) separated the treatments on day 32, also characterizing mono-cultivation due to elevated abundance of 2.3 - fold, compared to co-cultivation.

For fatty acids and fatty acid derivatives the picture was similar. Most class members clearly distinguished mono-cultivation on day 26 and 32, due to higher abundance. Methyl-5,8,11,14,17-icosapentaenoate (#209) and putative 1,3-dihydroxy-2-propanyl myristate (#219, #222) were more abundant in mono-cultivation on day 26 and 32, compared to co-cultivation and their respective abundance on day 16. The intensity dynamics of metabolites #209 and #219 over time differed between mono- and co-cultivation. In co-cultivation there seemed to be a higher availability of these fatty acid derivatives on day 16, with subsequent rapid decline of abundance on day 26 and 32. In mono-cultivation on the other hand, both metabolites were merely present on day 16 and their abundance increased after regular growth phase to reach maximum values on day 26. Furthermore, putative 1,3-dihydroxy-2-propanyl myristate (#180) increased from day 16 and 26 until reaching maximum values on day 32, which were 1.3 - fold higher in mono-cultivation, compared to co-cultivation. I obtained ambiguous results for palmitoleic acid (#176). This metabolite was more

abundant on day 16 and 26, than on day 32, but did not show a clear correlation with one of the treatments throughout all days.

In the class of alkaloids, putative 2-(4-methyl-1-piperazinyl)ethanamine (#47) was found by the daywise CAP to distinguish mono- and co-cultivation on day 32. This metabolite was 1.4 - fold more abundant in mono-cultivation on this day. However, considering the general intensity dynamics, on day 16 and 26, this metabolite was higher abundant in co-cultivation on previous days. Furthermore, the class of others contained two metabolites. The long chained alcohol 9-eicosen-1-ol (#215) characterized day 16 of the interaction, as it was most abundant there. However, it separated treatments on day 26, as it was 4.4 - fold more abundant in mono-cultivation on this day, compared to co-cultivation. Tocopherol (#274) intensity increased during later stages of the interaction. On day 26 and 32 it was 1.8 - to 1.9 - fold more abundant in co-cultivation and thus characteristic for this state.

In total, 24 of the 78 highly correlated MSTs could not be identified and were classified as unknowns. However, six MSTs were documented in the GOLM and in-house library (Vidoudez) and referred to by their respective library-specific code. With exception of one MST (#81), all unknowns were correlating with day 26 and 32, as they were either identified by the daywise analysis, or (if identified in the species-specific analysis) most abundant on day 26 and 32. Considering these two days, the correlation with treatments was approximately equal numbered: 16 metabolites were higher abundant in co-cultivation, eight were higher abundant in mono-cultivation. MST #40, #129 and #133 are potential biomarkers, for co-cultivated *T. weissflogii*, as they were identified in the time-independent analysis (a-priori grouping by treatment) and most abundant in this group.

Table 9: Heatmap of endometabolite intensities for the species-specific and daywise analysis of *T. weissflogii* in the interaction with *S. costatum*. Medians of MST intensities, normalized to peak sum per sample and subsequently metabolite-wise auto scaled, are represented by a color code ranging from high (yellow) to low intensities (blue). White indicates the absence of the respective MST after data pre-processing. Metabolites are sorted according to classes (separated by black lines) and abundance patterns. Only metabolites significantly correlating with the separation of treatments and treatment per day are shown. The fold change of MST abundance in co-cultivation relative to mono-cultivation is given and coded with a second color code. Black indicates a higher abundance in co-cultivation, grey a higher abundance in mono-cultivation.

ID	Model ion	RT	RI	Name	Class	Ident	Analysis	Median MST intensity (Co: n=3, Mono: n=4/6)						Fold change		
								Day 16		Day 26		Day 32		Day 16	Day 26	Day 32
								Mono	Co	Mono	Co	Mono	Co			
66	174.1	9.74	1380	1,5-Pentanediamine (Cadaverine)	A		26						1.6	-27.4	-2.6	
3	116.1	6.80	986	Alanine	AA	*	DT,32						1.5	1.5	3.0	
1	103	6.72	975	Valine	AA	*	32						-	-4.6	3.2	
26	144.1	7.95	1139	Valine	AA	*	T,26,32						2.1	2.6	3.5	
38	158.1	8.48	1211	Leucine	AA	*	DT,T,26,32						4.4	8.9	7.4	
42	158.1	8.69	1239	Isoleucine	AA	*	DT,T,26,32						3.3	6.8	7.0	
43	117.1	8.71	1242	Threonine	AA	*	T,26,32						2.8	1.7	1.7	
44	146.1	8.81	1256	Threonine	AA	*	DT						1.8	-1.2	-	
10	116.1	7.30	1052	3-Chloro-1,2-propanediol	Alc dv.	?	26,32						-2.1	-3.6	-	
83	211.2	10.53	1487	2-Dodecanol	Alc		26						2.1	-6.3	-53.5	
17	117	7.59	1092	Glycerol	Alc	?	32						-1.3	1.1	-1.4	
37	205	8.46	1208	Glycerol	Alc		32						-1.1	-1.9	-2.0	
19	116.1	7.63	1097	3-Chloro-1,2-propanediol	Alc dv.		32						-1.1	-2.6	-1.9	
47	171.1	8.90	1268	2-(4-Methyl-1-piperazinyl)ethanamine	Alk	?	32						1.3	1.1	-1.4	
88	156.1	10.75	1516	5-Oxoproline (pyroglutamic acid)	CA		26						2.5	3.8	2.2	
201	117	15.60	2250	9-Octadecenoic acid (oleic acid)	CA		26						2.0	1.8	1.6	
205	197.1	15.77	2281	5,8,11,14-Icosatetraenoic acid (arachidonic acid)	CA	?	26						-1.5	-2.2	-2.7	
207	197.1	15.84	2293	5,8,11,14-Icosatetraenoic acid (arachidonic acid)	CA	?	26						-1.1	-4.1	-3.0	
25	247.1	7.89	1132	3-Hydroxybutanoic acid	CA		26						1.5	-3.0	1.6	

ID	Model ion	RT	RI	Name	Class	Ident	Analysis	Median (Co: n=3, Mono: n=4/6)								
								Day 16		Day 26		Day 32		Fold		
								Mono	Co	Mono	Co	Mono	Co	Day 16	Day 26	Day 32
171	101.1	14.22	2009	Ethyl palmitate	CA dv.		26							-1.1	-4.7	-2.1
49	189.1	8.99	1280	2,3-Dihydroxypropanoic acid	CA		32							2.4	1.2	-2.3
13	233.1	7.39	1065	Propionic acid	CA		DT							8.9	1.5	-1.3
176	117	14.42	2042	9-Hexadecenoic acid (Palmitoleic acid)	FA		DT							1.2	-1.3	-
180	211.2	14.58	2072	1,3-Dihydroxy-2-propanyl myristate	FA dv.	?	DT							1.8	1.2	-1.3
209	117	15.92	2308	Methyl-5,8,11,14,17-icosapentaenoate	FA dv.		32							1.3	-1.3	-1.4
219	129.1	16.37	2385	1,3-Dihydroxy-2-propanyl myristate	FA dv.		26,32							2.4	-1.5	-10.2
222	343.3	16.55	2418	1,3-Dihydroxy-2-propanyl myristate	FA dv.		26,32							-1.1	-1.8	-1.7
97	217	11.16	1571	Arabinofuranose	S	?	26							-1.6	1.7	1.4
99	217	11.23	1580	Arabinofuranose	S	?	26							-1.2	1.4	1.2
100	217	11.28	1587	Arabinofuranose	S	?	DT,26							-1.2	1.6	1.2
105	217	11.46	1611	Galactofuranoside deriv.	S dv.	?	26							-1.9	1.6	1.4
119	246.1	12.03	1688	Glucuronolactone	S dv.	??	26							1.0	1.7	1.5
172	292.1	14.26	2014	Gluconic acid	S Acid		26,32							1.6	1.9	2.2
192	117	15.14	2170	Glucopyranose	S		26							1.1	1.5	-1.1
110	161.1	11.75	1650	Xylose	S		26							1.3	-3.7	-3.1
281	204.1	25.08	3510	EITMS_N12C_ATHL_3499.7_1135 EC24_ (GOLM)	S		26							-1.7	-2.0	-1.5
101	258.1	11.31	1591	Erythrose	S	?	32							-2.9	7.7	14.5
148	103.1	13.28	1856	Fructose	S		32							1.3	1.0	1.4
150	319.2	13.46	1880	Glucose	S	*	32							-1.0	1.3	2.4
210	204.1	15.98	2317	EITMS_N12C_STUL_2360.7_1135 EC28_G (GOLM)	S		DT,32							4.8	1.9	2.0
143	117	13.04	1824	EITMS_N12C_STUR_1832.7_1135 EC29_ (GOLM)	S		DT							-1.3	-1.1	1.2
165	333	13.98	1965	Gluconic acid	S Acid		T,32							-1.3	-1.1	-1.3
189	319.2	15.00	2144	Skel_Cell_C128_RT14.776 (inositol isomer) (Vidoudez)	S Alc	?	DT							-1.3	-1.4	1.2
283	204.1	25.85	3578	Disaccharide (Vidoudez)	CS		26							-2.3	-1.9	-1.2
243	361.2	17.73	2625	Sucrose	CS	*	DT							1.3	1.6	1.8

ID	Model ion	RT	RI	Name	Class	Ident	Analysis	Median (Co: n=3, Mono: n=4/6)								
								Day 16		Day 26		Day 32		Fold		
								Mono	Co	Mono	Co	Mono	Co	Day 16	Day 26	Day 32
248	204	18.21	2710	Gentiobiose	CS		DT,32						-1.0	1.4	2.0	
251	204.1	18.39	2742	Gentiobiose	CS		DT,32						1.4	1.1	2.2	
252	204.1	18.47	2755	Maltose	CS	?	DT						1.7	1.1	1.4	
249	204.1	18.26	2719	Lactose	CS	?	DT						1.3	1.3	1.7	
250	361.2	18.32	2729	Trehalose	CS	*	DT,32	-					-	1.1	-1.7	
258	204.1	19.05	2846	Galactinol	CS dv.		DT						-1.4	1.1	-1.8	
265	204.1	19.78	2949	Galactinol	CS dv.		DT						1.1	-1.1	-1.3	
215	180.1	16.18	2353	9-Icosen-1-ol	O	??	26						1.1	-4.8	-1.4	
274	237.1	21.05	3131	Tocopherol	O	*	26						-1.2	1.9	1.8	
81	228.1	10.45	1475	Unknown	U	-	DT						-1.4	-1.0	-1.2	
11	117.1	7.31	1054	Unknown	U	-	26	-	-	-	-	-	-	-	-	
40	180.1	8.61	1229	Unknown	U	-	T,26						3.5	2.5	1.5	
60	217.1	9.49	1347	Unknown	U	-	26						3.3	1.8	1.3	
69	201.1	9.89	1401	EITTMS_N12C_ATHR_1442.5_1135 EC44_ (GOLM)	U		26						1.6	2.1	1.2	
103	188.1	11.39	1602	Unknown	U	-	26						1.9	2.8	2.0	
111	117	11.78	1655	Unknown	U	-	26						2.2	2.3	1.4	
118	215.2	11.99	1683	Unknown	U	-	DT,26						3.1	3.2	-1.0	
129	392.2	12.49	1750	Unknown	U	-	DT,T,26,32						-2.5	8.5	7.7	
133	392.2	12.62	1768	Skel_cell_C065 (Vidoudez)	U		DT,T,26,32						-2.1	17.0	8.4	
135	302.1	12.76	1786	Skel_cell_C065 (Vidoudez)	U		DT,26,32						-1.8	11.6	3.8	
92	263.2	10.92	1538	Unknown	U	-	26						1.3	-3.3	-2.0	
120	129	12.06	1692	EITTMS_N12C_ATHR_1704.6_1135 EC44_ (GOLM)	U	?	26						2.4	-2.2	-1.3	
141	386.2	12.97	1814	Unknown	U	-	26	-					-	-3.8	-	
208	120.1	15.86	2297	Unknown	U	-	26						4.0	-1.6	-1.5	
259	211.2	19.22	2870	Unknown	U	-	26						2.0	-3.4	-1.8	
132	204.1	12.60	1764	Unknown	U	-	DT						2.2	-1.1	1.0	
198	117	15.50	2232	Unknown	U	-	DT						1.7	1.5	1.4	

ID	Model ion	RT	RI	Name	Class	Ident	Analysis	Median (Co: n=3, Mono: n=4/6)								
								Day 16		Day 26		Day 32		Day 16	Day 26	Day 32
								Mono	Co	Mono	Co	Mono	Co			
229	217.1	16.97	2492	EITMS_N12C_ATHR_2761.3_1135 EC44_ (GOLM)	U	??	DT						1.6	1.5	1.5	
230	217.1	17.02	2500	Unknown	U	-	DT						4.5	2.9	1.5	
247	204.1	18.02	2676	Unknown	U	-	DT						-1.6	-1.6	1.0	
285	204.1	26.98	3677	Unknown	U	-	32						53.7	1.1	1.5	
107	137.1	11.66	1639	Unknown	U	-	32						2.2	-1.6	-2.9	
234	103.1	17.30	2551	Skel_Cell_C146 (Vidoudez)	U	?	32						1.2	-2.6	-1.6	

In case derivatized molecules are detected, the table entry lists their putative parent compounds. Each MST is characterized by **ID**, **model ion**, retention time (**RT**), retention index (**RI**) and its underlying **CAP analysis**. CAP analyses comprised the overall analysis with a-priori grouping by treatment and day (**DT**), with a-priori grouping by treatment (**T**), as well as daywise subset analysis on day 26 (**26**) and day 32 (**32**). Metabolites were identified via libraries. If metabolites were verified with a standard, they are marked with *. “?” indicates a reversed match between 700 and 800, “??” a reversed match between 600 and 700 and “???” indicates cases where the reversed match was ≤ 600 . “?” tags metabolites with a match smaller than 600. Class abbreviations: Amine (**A**), alcohol (**Alc**), alkaloid (**Alk**), carboxylic acid (**CA**), complex sugar (**CS**), derivatives of a certain class (**dv.**), sugar (**S**), sugar alcohol (**S Alc**), sugar acid (**S Acid**), sterol (**St**), terpene (**T**), others (**O**), unknown (**U**). **Vidoudez** refers to an MST code given by the in-house library, **GOLM** refers to an MST code given by distinct libraries of the Golm Metabolome Database.

S. costatum

The constrained score plots of the species-specific analysis of *S. costatum* visualize the significant differences between a-priori groups. The significance was confirmed via trace statistic, which was calculated by permutation (**Table 7**). Similar to the results found in *T. weissflogii*, a-priori grouping by treatment yielded a clear separation of mono- and co-cultivation of *S. costatum* in the score plot (**Figure 18A**). Seven metabolites were highly correlated ($|r| \geq 0.6074$, $P \leq 0.001$) with the separation of treatments. The corresponding loading plot indicated six out of seven metabolites characterizing co-cultivation, while only MST #282 was correlating with mono-cultivation.

A-priori grouping by treatment per day identified 40 metabolites highly correlating with the separation of groups ($|r| \geq 0.6074$, $P \leq 0.001$). The score plot (**Figure 18C**) visualizes a clear separation of the sampling days by canonical axis 1. Within day 16 and 32, the treatments were distinctly separated from each other by canonical axis 2. On day 26, a separation of treatments was gradually established by canonical axis 1, yet the separation was not as distinct. The corresponding loading plot (**Figure 18D**) shows that 37 out of 40 metabolites were correlating with sampling day 32. Within this day, four metabolites were very distinctly correlating with co-cultivation (#49 (2,3-dihydroxypropanoic acid), #68 (glycerol), #130 (pentonic acid) and #172 (gluconic acid)) and MST #252 (maltose) with mono-cultivation. Furthermore, metabolites #45 (glycine), #143 and #176 (palmitoleic acid) were pointing towards the direction of co-cultivated *S. costatum* on day 16, and were thus characteristic for this group. The affiliation of the other metabolites was evaluated via heatmap.

The permutation test in the daywise analysis confirmed significant differences between treatments on day 26 and 32 (**Table 8**). These differences are visualized in the constrained score plots (**Figure 19A, C**). For both days, canonical axis 1 was distinctly separating mono- from co-cultivation. Day 16 was not further considered, due to lack of significance. In general, 26 metabolites were highly correlating with the separation of treatments on day 26 and 43 metabolites with the separation on day 32. The majority of them was correlating with the co-cultivation group, as they were pointing towards the co-cultivation group in the respective loading plot (**Figure 19B, D**).

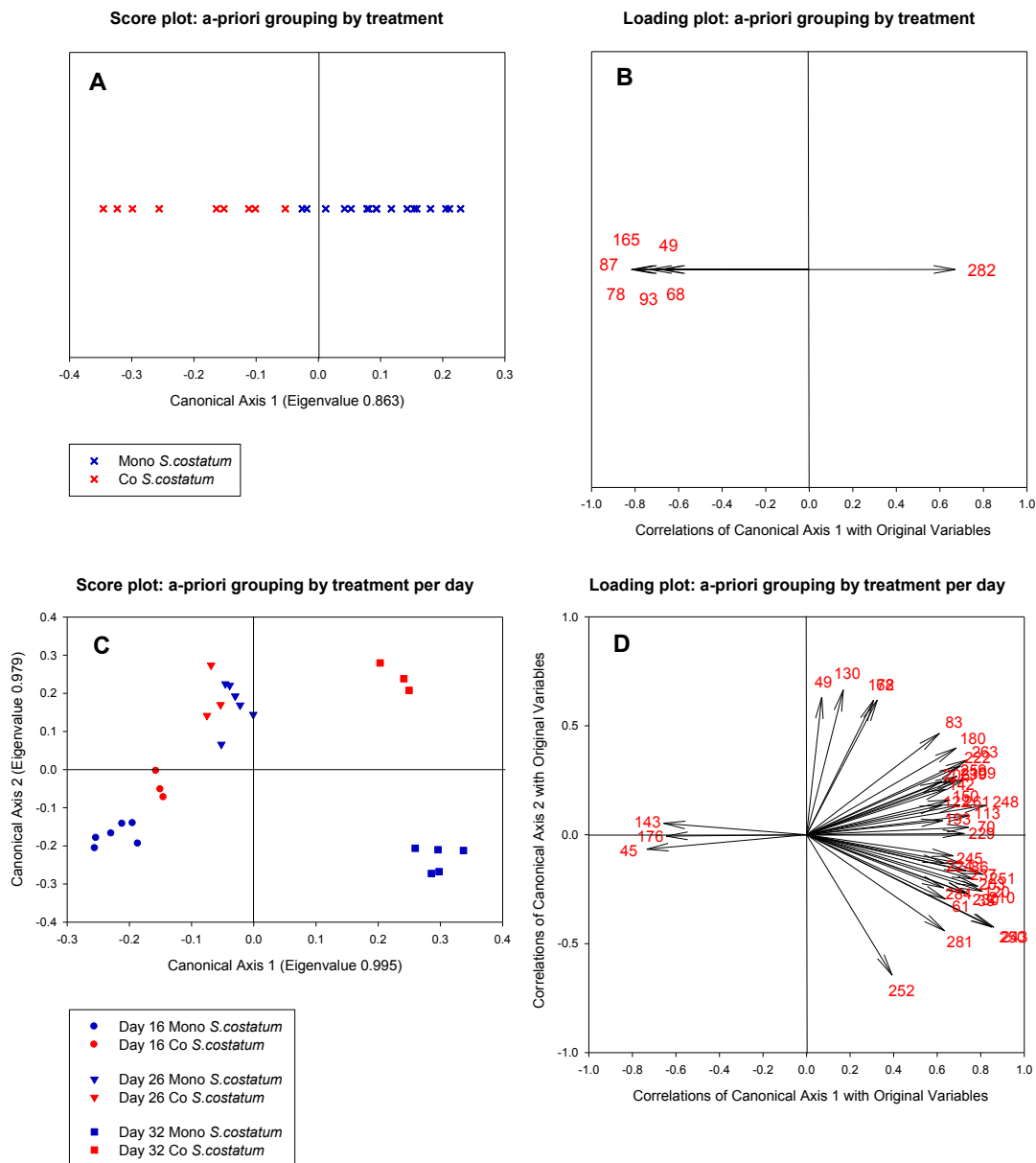


Figure 18: Constrained score and loading plots of endometabolomic samples from *S. costatum* in a species-specific subset analysis of the interaction between *T. weissflogii* and *S. costatum*.

The constrained score plots (graph **A**, **C**) visualize significant differences between the sample groups as found via CDA with a-priori groups by treatment (trace statistic $P = 0.0079$, misclassification error of 0 % for $m = 10$, graph **A**) and a-priori groups by treatment per day (trace statistic $P = 0.0003$, misclassification error of 0 % for $m = 13$, graph **C**). Vectors in the CAP loading plots (graph **B**, **D**) represent metabolites, characterized by their ID (red numbers). Only vectors with a significant correlation coefficient above the critical value of $|r| \geq 0.6074$ ($P \leq 0.001$) for a-priori grouping by treatment and $|r| \geq 0.6074$ ($P \leq 0.001$) for a-priori grouping by treatment per day are plotted. The direction of the vectors in 2-dimensional space correlates with endometabolomic sample groupings shown in the score plots of the respective analysis.

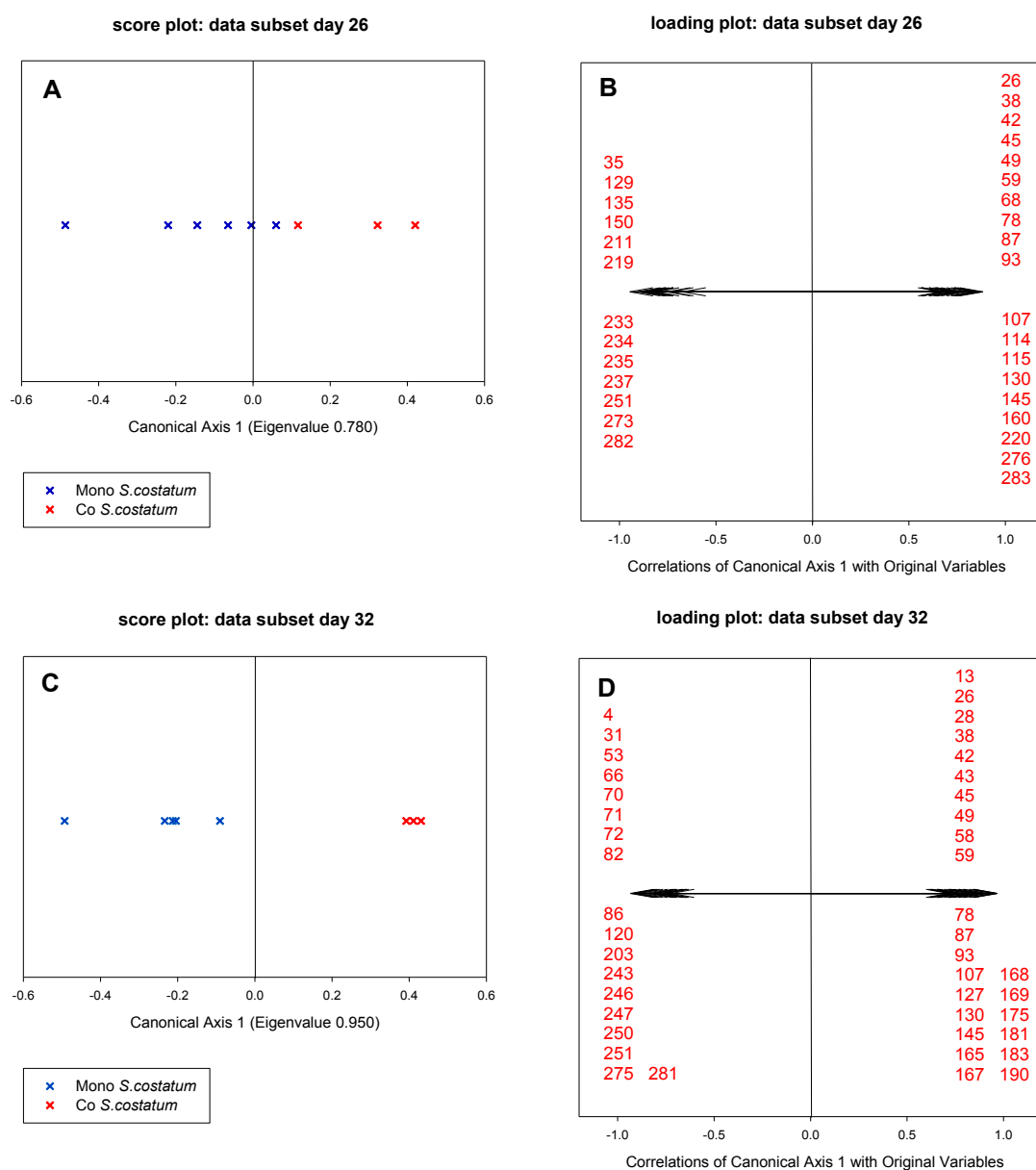


Figure 19: Constrained score and loading plots of endometabolomic samples from *S. costatum* in a daywise subset analysis of the interaction between *T. weissflogii* and *S. costatum*.

The constrained score plots (graph **A**, **C**) visualize significant differences between the treatments, as confirmed via CDA for the subset analysis on day 26 (graph **A**, **B**) and day 32 (graph **C**, **D**). These differences between treatments are highly significant (trace statistic $P \leq 0.0001$, misclassification error of 0 % for $m = 3$ (day 26) and $m = 1$ (day 32)). Vectors in the CAP loading plots (graph **B**, **D**) represent metabolites, characterized by their ID (red numbers, pooled per group). Only vectors with a significant correlation coefficient above the critical value of $|r| \geq 0.6664$ ($P \leq 0.05$) for day 26 and of $|r| \geq 0.7067$ ($P \leq 0.05$) for day 32 are plotted. The direction of the vectors in 2-dimensional space correlates with endometabolomic sample groupings shown in the score plots of the respective analysis.

Considering both analyses together, 87 metabolites were highly correlating with differences in treatments and treatment per day. I summarized and visualized these metabolites in a heatmap (**Table 10**). Subsequently, I evaluated the trends of different metabolite classes and introduced potential biomarkers.

All identified amino acids, with exception of putative alanine (#70), were correlating with co-cultivation of *S. costatum* on day 26 and / or 32. They were up to 2.2 - fold more abundant (isoleucine, day 26) compared to mono-cultivation. Glycine (#45) for example, was identified by the daywise analysis on day 26 and 32, as it was more abundant in co-cultivation. Valine (#26), leucine (#38), isoleucine (#42) and threonine (#43) have also been described in the analysis of *T. weissflogii*. The only difference is that these amino acids showed maximum intensities on day 26 in *S. costatum*, but on day 32 in *T. weissflogii*. On the other hand, putative alanine (#70) was characterizing mono-cultivation, as it was 1.5 - fold higher abundant on day 26 and 1.9 - fold on day 32, compared to co-cultivation.

The trend in alcohols and carboxylic acids was opposite to the one described for *T. weissflogii*, where both classes were correlating with mono-cultivation. In the analysis of *S. costatum*, three carboxylic acids were identified: On the one hand, 2,3-dihydroxypropanoic acid (#49) characterized co-cultivated *S. costatum* on all three sampling days. It was between 1.3 - to 1.8 - fold more abundant, compared to mono-cultivation. On the other hand, propionic acid (#13) and the carboxylic acid derivative threonic acid-1,4-lactone (#59) were relevant for the separation of treatments on day 26 and 32. Both were up to 2.9 - fold higher abundant in co-cultivation during later stages of the interaction. Propionic acid (#13) was also found to be highly correlated in the analysis of *T. weissflogii*. However, although propionic acid (#13) showed the same temporal increase from day 16 to 32, it was correlating with mono-cultivation in *T. weissflogii*.

Another shared metabolite between the analysis of *T. weissflogii* and *S. costatum* with similar correlation trends in both analyses was 2-dodecanol (#83). While for *S. costatum* it was 1.7 - to 1.9 - fold higher correlating with co-cultivation, in *T. weissflogii* it was 6.3 - to 53.5 -fold higher abundant in mono-cultivation. The polyol glycerol (#68, #87) was a potential biomarker for co-cultivation in *S. costatum*, as it was more abundant in co-cultivation on all three sampling days (up to 1.8 - fold on day 32). Putative 1,3,5-pentanetriol (#72) characterized the endometabolome of *S. costatum* in mono-cultivation on day 32, as it was 2.3 - fold more abundant in mono-cultivation on this day.

Three amines were highly correlating with the separation of treatments. Cadaverine (#66) was characterizing mono-cultivation, not only in *S. costatum*, but also in *T. weissflogii*. However, in the analysis of *T. weissflogii*, cadaverin (#66) was affiliated with day 26, while in the analysis of *S. costatum* it was affiliated with day 32. The same correlation trend was visible for 2-[(2-chloroethyl)(ethyl)amino]ethanol (#31), an amine derivative, which was 2 - fold more abundant in mono-cultivation on day 32. Only putrescine (#127) was characteristic for co-cultivation on

day 32. In general the abundance of identified amines increased over time until reaching maximum intensities on day 32.

The temporal dynamic for complex sugars was identical with the one described for *T. weissflogii*. Their respective intensity increased until day 32. In total, eight different complex sugars and derivatives have been identified in the analysis of *S. costatum*. With exception of galactinol (#263) and a disaccharide (#283), which characterized co-cultivation, all members of this class were more abundant in mono-cultivation on day 32. Although sucrose (#243), gentiobiose (#248, #251), trehalose (#250), putative maltose (#252) and galactinol (#263) were relevant in the analysis of both diatoms, five metabolites showed opposite affiliations to treatment. Only trehalose (#250) was characterizing mono-cultivation on day 32 in both species. Considering derivatives of complex saccharides, digalactosylglycerol (#273) and an unidentified disaccharide (#282) were characteristic for mono-cultivation. Interestingly, they were abundant in similar intensities on all three sampling days, not exhibiting an increase as observed for complex saccharides.

The remaining metabolites of the sugar class (including derivatives) show a complex intensity pattern over time and treatments. Within this class, identified metabolites were characterizing both treatments in a balanced way. Thirteen of the 16 sugars (including derivatives) were merely abundant on day 16, but increased in intensity on day 26 and 32. Two unidentified sugars (#210, #281), as well as putative erythritol (#113), galactosylglycerol (#203, #206) and adenosine (#245) were more abundant in mono-cultivation on day 32, compared to co-cultivation. On the other hand, putative pentonic acid (#130), gluconic acid (#165, #172), hexitol (#145), inositol (#175), mannono-(1-4)-lactone (#167), myo-inositol (#183), glucose (#150), hexonic acid (#169), a hexose (#190) and galacturonic acid (#160) were more abundant in co-cultivation on day 32.

Interestingly, gluconic acid was highly correlating with the separation of mono- and co-cultivation independent of time (identified by the CAP with a-priori grouping by treatment). Thus, it was considered a biomarker for co-cultivation. Gluconic acid was between 1.4 - and 2.7 - fold more abundant, compared to mono-cultivation. Putative pentonic acid (#130) and galacturonic acid (#160) were relevant for the separation of treatments on day 26, as they were up to 1.4 - fold more abundant in co-cultivation. Furthermore, an unidentified sugar (#143) was characteristic for mono-cultivation on day 16. I also found sugar #143 in the analysis of *T. weissflogii*, with an identical intensity pattern over time and treatments.

Galactosylglycerol (#211) was most abundant on day 16. However, it was found to only be relevant for the separation of treatments on day 26. Galactosylglycerol was represented by three MSTs (#203, #206 and #211). Their abundance pattern was not homogeneous and no clear overall affiliation of galactosylglycerol to one of the treatments could be visualized. Therefore, I interpreted each MST individually, under consideration of the possibility that different sugarglycerols might be tagged with the name galactosylglycerol, due to difficulties in the library-based identification of sugars.

Among fatty acids, palmitoleic acid (#176) was most abundant on day 16 and 26, at the beginning of diatom growth. It was not abundant on day 32. This observation is in agreement with the results for palmitoleic acid in *T. weissflogii*. However, this metabolite could not clearly be affiliated with one treatment over time. On day 16, palmitoleic acid was more abundant in mono-cultivation and 2.5 - fold more in co-cultivation on day 26. Considering fatty acid derivatives, the picture was not as distinct either. 1,3-Dihydroxy-2-propanyl palmitate was represented by four MSTs (#180, #219, #222 and #235). While #219 and #235 were more abundant in mono-cultivation on day 32, #280 and #222 were more abundant in co-cultivation. Thus, it was not possible to unambiguously affiliate the MST 1,3-dihydroxy-2-propanyl palmitate to one of the treatments. Furthermore, glycerol (#237) was more abundant in mono-cultivation, while 2,3-dihydroxypropyl palmitate (#239) was more abundant in co-cultivation on day 32.

In addition to the already described metabolite classes, I identified one alkaloid and two steroids in the analysis of *S. costatum*. 1H-Pyrrole-2-carboxylic acid (#53) was most abundant on day 16. However, the difference in abundance between treatments was minor (1.1 - fold). Campesterol (#276) was correlating with co-cultivation on day 26 and 32, as it was up to 1.3 - fold more abundant (day 26), compared to mono-cultivation. The previously described sterol #275 (Skel_cell_C178_sterol (Vidoudez, 2010)) characterized mono-cultivated *S. costatum* on day 32, as it was 1.9 - fold more abundant compared to co-cultivation. Generally, this sterol increased in abundance during later stages of the interaction with increasing difference between the treatments. The identification of metabolites in the class of sterols via MS libraries was difficult, as MS spectra can be highly similar. Therefore, the sterol identities must be interpreted with caution.

Among the unknowns, MST #78 and #93 were potential biomarkers for co-cultivated *S. costatum*, as they were identified in the time-independent analysis (a-priori grouping by treatment). In general, the vast majority of metabolites was relevant for the separation of

treatments on day 26 and 32. However, there was no clear quantitative discrimination towards one of the treatments.




To sum it up, most amino acids, alcohols, carboxylic acids and the steroid campesterol (#276) were upregulated in co-cultivation, compared to mono-cultivation. Considering amino acids, these observations were in agreement with the observations in *T. weissflogii*. The trend in alcohols and carboxylic acids was opposite to the one described for *T. weissflogii*. Furthermore, the amine putrescine (#127) was upregulated in co-cultivation in the late stationary phase.

Amines and complex sugars showed the trend of increased abundance in mono-cultivation. The temporal dynamic for complex sugars was identical with the one described for *T. weissflogii*, their respective intensity increased until day 32. The remaining metabolites of the sugar class (including derivatives) and the fatty acids exhibited a complex intensity pattern over time and treatments.

Interestingly, glycerol (#68, #87), 2,3 - dihydroxypropanoic acid (#40), gluconic acid (#165, #172) and the unknown metabolites #78 and #93 were potential biomarkers for co-cultivated *S. costatum*, as they were upregulated in co-cultivation on all three sampling days.

Table 10: Heatmap of endometabolite intensities for the species-specific and daywise analysis of *S. costatum* in the interaction with *T. weissflogii*.

Medians of MST intensities, normalized to peak sum per sample and subsequently metabolite-wise auto scaled, are represented by a color code ranging from high (yellow) to low intensities (blue). White indicates the absence of the respective MST after data pre-processing. Metabolites are sorted according to classes (separated by black lines) and abundance patterns. Only metabolites significantly correlating with the separation of treatments and treatment per day are shown. The fold change of MST abundance in co-cultivation relative to mono-cultivation is given and coded with a second color code. Black indicates a higher abundance in co-cultivation, grey a higher abundance in mono-cultivation.

ID	Model ion	RT	RI	Name	Class	Ident	Analysis	Median MST intensity						Fold change		
								low  high						UP  DOWN 		
								Median (Co: n=3, Mono: n=5/6)						Fold		
								Day 16		Day 26		Day 32		Day 16	Day 26	Day 32
Mono	Co	Mono	Co	Mono	Co											
31	174.1	8.11	1162	2-[(2-Chloroethyl)(ethyl)amino]ethanol	A dv.		32							1.3	-1.1	-2.0
66	174.1	9.74	1380	1,5-Pentanediamine (cadaverine)	A		32							-1.2	-1.3	-1.7
127	174.1	12.43	1742	1,4-Butanediamine (putrescine)	A	*	32							-1.0	1.0	1.7
26	144.1	7.95	1139	Valine	AA	*	26,32							-1.2	1.6	1.6
38	158.1	8.48	1211	Leucine	AA	*	26,32							-1.2	2.1	1.5
42	158.1	8.69	1239	Isoleucine	AA	*	26,32							1.0	2.2	1.5
43	117.1	8.71	1242	Threonine	AA	*	32							-3.9	-1.1	1.5
45	174.1	8.84	1259	Glycine	AA	*	DT,26,32							-1.1	1.1	1.2
70	174.1	9.93	1405	Alanine	AA	?	DT,32	-	-					-	-1.5	-1.9
68	205.1	9.84	1394	Glycerol	Alc		DT,T,26							4.4	1.6	1.9
72	103.1	10.02	1419	1,3,5-Pentanetriol	Alc	?	32							-1.5	1.2	-2.3
83	211.2	10.53	1487	2-Dodecanol	Alc		DT	-	-					-	1.9	1.7
87	248.1	10.69	1509	Glycerol	Alc		T,26,32							1.6	3.0	3.2
53	240.1	9.26	1316	1H-Pyrrole-2-carboxylic acid	Alk	?	32							-1.1	-1.2	-4.0
13	233.1	7.39	1065	Propionic acid	CA		32		-					-	1.2	2.4
49	189.1	8.99	1280	2,3-Dihydroxypropanoic acid	CA		DT,T,26,32							1.3	1.4	1.8

ID	Model ion	RT	RI	Name	Class	Ident	Analysis	Median (Co: n=3, Mono: n=5/6)								
								Day 16		Day 26		Day 32		Day 16	Day 26	Day 32
								Mono	Co	Mono	Co	Mono	Co			
59	247.1	9.47	1344	3,4-Dihydroxydihydro-2(3H)-furanone (Threonic acid-1,4-lactone)	CA dv.		26,32						-1.2	1.8	2.9	
176	117	14.42	2042	9-Hexadecenoic acid (Palmitoleic acid)	FA		DT						-1.3	2.5	-	
219	129.1	16.37	2385	1,3-Dihydroxy-2-propanyl myristate	FA dv.		26						-3.0	-1.2	-1.4	
235	218.1	17.39	2565	1,3-Dihydroxy-2-propanyl palmitate	FA dv.	?	26						-	-1.8	-1.5	
237	147	17.49	2583	C16:1-Glycerol	FA dv.		DT,26						-1.8	-1.5	-1.2	
180	211.2	14.58	2072	1,3-Dihydroxy-2-propanyl myristate	FA dv.	?	DT						-1.1	1.7	1.5	
222	343.3	16.55	2418	1,3-Dihydroxy-2-propanyl myristate	FA dv.		DT						-3.2	1.1	1.3	
239	371.3	17.56	2596	2,3-Dihydroxypropyl palmitate	FA dv.		DT						-	-1.3	1.2	
143	117	13.04	1824	EITMS_N12C_STUR_1832.7_1135EC29_ (GOLM)	S		DT						-2.4	-1.1	-	
211	204	16.01	2324	Galactosylglycerol	S dv.		26						-4.0	-1.8	-1.1	
130	292.1	12.52	1753	Pentonic acid	S Acid	??	DT,26,32						-5.5	1.4	1.7	
160	217.1	13.74	1923	Galacturonic acid	S acid	?	26						2.2	1.2	-1.0	
183	305	14.77	2105	myo-Inositol	S Alc	*	32						-1.4	-1.3	1.3	
190	204.1	15.07	2157	Hexose (Vidoudez)	S		32						1.2	1.8	1.5	
145	205.1	13.14	1837	Hexitol	S Alc		26,32						1.2	1.1	1.6	
150	319.2	13.46	1880	Glucose	S	*	DT,26						-1.1	-1.8	1.3	
165	333	13.98	1965	Gluconic acid	S Acid		T,32						2.7	1.4	1.7	
172	292.1	14.26	2014	Gluconic acid	S Acid		DT						-1.0	1.1	2.0	
167	217	14.04	1976	Mannono-(1-4)-lactone	S dv.		32						1.6	1.4	2.8	
169	217.1	14.10	1987	Hexonic acid (Vidoudez)	S acid	?	32						-1.5	1.6	4.1	
175	318	14.35	2031	Inositol	S Alc		32						1.1	1.0	1.4	
210	204.1	15.98	2317	EITMS_N12C_STUL_2360.7_1135EC28_G (GOLM)	S		DT						1.5	1.4	-2.9	

ID	Model ion	RT	RI	Name	Class	Ident	Analysis	Median (Co: n=3, Mono: n=5/6)								
								Day 16		Day 26		Day 32		Day 16	Day 26	Day 32
								Mono	Co	Mono	Co	Mono	Co			
281	204.1	25.08	3510	EITMS_NI2C_ATHL_3499.7_1135EC24_ (GOLM)	S		DT,32						1.7	-1.5	-1.7	
113	205.1	11.87	1666	Erythritol	S Alc	?	DT						-1.1	-1.6	-1.2	
203	204.1	15.69	2267	Galactosylglycerol	S dv.		DT,32						-1.0	2.7	-2.3	
206	239.2	15.81	2288	Galactosylglycerol	S dv.		DT						-	1.3	1.0	
245	236.1	17.82	2641	Adenosine	S dv.		DT						-2.8	-2.0	-1.6	
283	204.1	25.85	3578	Disaccharide (Vidoudez)	CS		26						1.5	4.3	-1.4	
243	361.2	17.73	2625	Sucrose	CS	*	DT,32						-3.0	-2.7	-2.1	
248	204	18.21	2710	Gentiobiose	CS		DT						-1.1	-1.4	-1.1	
251	204.1	18.39	2742	Gentiobiose	CS		DT,26,32						-1.1	-1.8	-1.2	
250	361.2	18.32	2729	Trehalose	CS	*	DT,32						-1.9	-4.7	-3.6	
252	204.1	18.47	2755	Maltose	CS	?	DT						1.4	-	-3.9	
263	204.1	19.57	2921	Galactinol	CS dv.		DT						2.1	1.1	1.2	
273	204.1	20.62	3069	Digalactosylglycerol	CS dv.		26						-7.0	-2.0	-2.0	
282	204.1	25.26	3526	Diholosite -383 (Vidoudez)	CS dv.	?	T,26						-3.0	-2.0	-1.8	
275	129.1	22.21	3258	Skel_cell_C178_sterol (Vidoudez)	St		32						1.0	-1.2	-1.9	
276	382.4	22.26	3263	Ergost-5-en-3-ol (Campesterol)	St		26						-1.0	1.3	1.1	
114	157.1	11.89	1670	Unknown	U	-	26						-	1.5	1.2	
115	195.1	11.90	1671	Unknown	U	-	26						-	1.6	1.4	
220	167	16.39	2390	Unknown	U	-	26						-	1.1	-	
107	137.1	11.66	1639	Unknown	U	-	26,32						-4.2	1.8	1.8	
129	392.2	12.49	1750	Unknown	U	-	26						-	-2.9	-1.9	
135	302.1	12.76	1786	Skel_cell_C065 (Vidoudez)	U		26						-	-1.9	-2.4	
233	103.1	17.23	2538	Skel_Cell_C145 (Vidoudez)	U	?	26						-7.0	-1.9	-2.1	

ID	Model ion	RT	RI	Name	Class	Ident	Analysis	Median (Co: n=3, Mono: n=5/6)						Fold		
								Day 16		Day 26		Day 32		Day 16	Day 26	Day 32
								Mono	Co	Mono	Co	Mono	Co			
234	103.1	17.30	2551	Skel_Cell_C146 (Vidoudez)	U	?	26						-3.1	-2.8	-2.2	
28	112.1	8.03	1150	Unknown	U	-	32						-	-	1.8	
58	167.1	9.44	1340	Unknown	U	-	32						-	-1.5	-	
61	240.1	9.54	1354	Unknown	U	-	DT						-	-	1.0	
78	234.1	10.29	1454	Unknown	U	-	T,26,32						1.4	2.6	3.8	
93	292	10.95	1543	Unknown	U	-	T,26,32						1.8	2.3	2.1	
109	215.2	11.73	1647	Unknown	U	-	DT						1.5	1.1	1.1	
142	294.2	13.01	1819	Unknown	U	-	DT						-	-1.5	1.1	
168	215.2	14.07	1981	Unknown	U	-	32						-	1.9	1.9	
181	204	14.67	2086	EITTMS_N12C_ATHR_2988.6_1135EC44_ (GOLM)	U	-	32						1.4	1.4	1.4	
193	85	15.19	2179	Unknown	U	-	DT						-	-1.5	1.5	
230	217.1	17.02	2500	Unknown	U	-	DT						-1.1	-1.5	1.1	
4	204.1	6.83	990	Unknown	U	-	32						-	-	-	
71	103.1	9.95	1409	Unknown	U	-	32						2.3	-2.1	-7.1	
82	155.1	10.47	1479	Unknown	U	-	32						-2.1	-1.1	-1.4	
246	130.1	17.99	2672	Unknown	U	-	32						-	-1.3	-2.8	
247	204.1	18.02	2676	Unknown	U	-	32						1.3	-	-6.2	
122	255.1	12.16	1705	Unknown	U	-	DT						-	1.5	-1.3	
261	309.3	19.38	2893	Unknown	U	-	DT						-	1.4	-1.4	
120	129	12.06	1692	EITTMS_N12C_ATHR_1704.6_1135EC44_ (GOLM)	U	?	DT,32						-1.0	1.0	-2.2	
224	259.1	16.71	2446	Unknown	U	-	DT						-	-1.0	-1.4	
229	217.1	16.97	2492	EITTMS_N12C_ATHR_2761.3_1135EC44_ (GOLM)	U	??	DT						1.8	-1.2	-1.1	
259	211.2	19.22	2870	Unknown	U	-	DT						-	-1.4	-1.2	

ID	Model ion	RT	RI	Name	Class	Ident	Analysis	Median (Co: n=3, Mono: n=5/6)								
								Day 16		Day 26		Day 32		Fold		
								Mono	Co	Mono	Co	Mono	Co	Day 16	Day 26	Day 32
284	383.3	26.00	3591	Unknown	U	-	DT	-	-	-	-	-	-4.0	-7.3		
35	163.1	8.27	1183	MesocosmC066 (Vidoudez)	U	?	DT,26	-	-	-	-	-	-	-8.6	-2.1	
86	155.1	10.67	1505	Unknown	U	-	DT,32	-	-	-	-	2.8	-2.6	-1.6		

In case derivatized molecules are detected, the table entry lists their putative parent compounds. Each MST is characterized by **ID**, **model ion**, retention time (**RT**), retention index (**RI**) and its underlying CAP **analysis**. CAP analyses comprised the overall analysis with a-priori grouping by treatment and day (**DT**), with a-priori grouping by treatment (**T**), as well as daywise subset analysis on day 26 (**26**) and day 32 (**32**). Metabolites were identified via libraries. If metabolites were verified with a standard, they are marked with *. “?” indicates a reversed match between 700 and 800, “??” a reversed match between 600 and 700 and “???” indicates cases where the reversed match was ≤ 600 . “1” tags metabolites with a match smaller than 600. Class abbreviations: Amine (**A**), alcohol (**Alc**), alkaloid (**Alk**), carboxylic acid (**CA**), complex sugar (**CS**), derivatives of a certain class (**dv.**), sugar (**S**), sugar alcohol (**S Alc**), sugar acid (**S Acid**), sterol (**St**), terpene (**T**), others (**O**), unknown (**U**). **Vidoudez** refers to an MST code given by the in-house library, **GOLM** refers to an MST code given by distinct libraries of the Golm Metabolome Database.

2.3 Medium experiments

The medium experiments confirmed the findings of enhanced growth of *T. weissflogii* in interaction with *S. costatum*, as documented in the interaction experiment. Maximum cell numbers of *T. weissflogii* were around 50 % higher in co-cultivation, compared to mono-cultivation. However, the initial environment of *S. costatum*, without the presence of *S. costatum* cells, did not induce this growth effect.

With respect to *S. costatum* growth, the findings were ambiguous, but replicated the findings of the interaction experiment. The chl a fluorescence exhibited interaction-induced changes, as was observed in the interaction experiment. However, although all treatment groups differed statistically significant from each other in their growth parameters, the differences in cell counts were considered biologically irrelevant, as they were $\leq 10\%$ between all treatment groups. An influence of the initial environment⁴³ of *T. weissflogii*, as visible in altered chl a fluorescence, could not be fully excluded.

I tested the influence of the initial environment of the interaction partner for each diatom species in an individual experiment and recreated by introducing the “medium group” into the experimental design (more details in chapter 2.1.3).

To investigate if diatom growth differed significantly among the treatment groups, I chose a linear mixed model approach (more details in chapter 6.7.1). Model graphs, as well as model validation graphs can be found in the appendix (**Appendix 24 - Appendix 29**).

2.3.1 *T. weissflogii* medium experiment

Performing an ANOVA on the fitted model data showed highly significant differences in the group-wise development of both chl a ($F(28,84) = 7.177, P \leq 0.0001$, **Figure 20A**) and cell counts ($F(14,42) = 5.125, P \leq 0.0001$, **Figure 20B**) over time. Subsequently, the differences confirmed by the statistical analyses are described and evaluated in detail.

The growth dynamic of the negative control (mono-cultivation of *T. weissflogii*) was similar to the observations in the interaction experiment (chapter 2.2.1). The chl a fluorescence indicated three different growth phases (**Figure 20A**): The regular growth phase lasted until day 18, followed by a rather stationary phase of growth with a slower fluorescence increase over time

⁴³ Referring to the spent medium of a diatom culture at the onset of the experiment

until day 34 and subsequent decline in fluorescence. In mono-cultivation maximum chl a fluorescence was reached on day 34 with 15836 ± 1957 RFU.

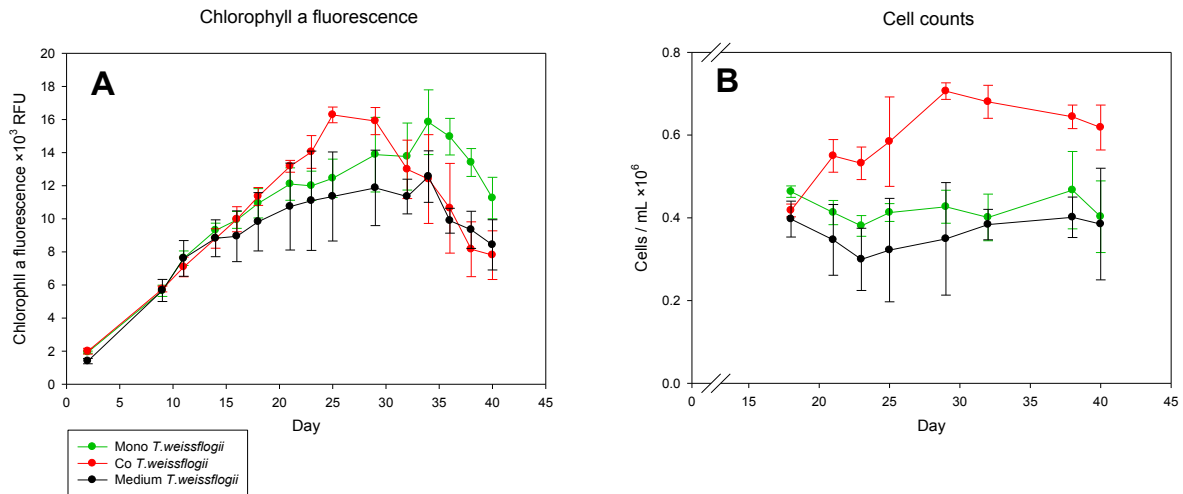


Figure 20: Diatom growth in the medium experiment of *T. weissflogii*.

The line plot **A** shows means of chl a (RFU: relative fluorescence units), plot **B** represent diatom cell counts (cells / mL) of *T. weissflogii*. The treatment groups are indicated by color: mono-cultivation of *T. weissflogii* (green, negative control), co-cultivation of each species (red, positive control) and the medium group (black, experimental group). Values are arithmetic means, error bars indicate standard deviation between biological replicates ($n = 3$).

The cell counts in *T. weissflogii* mono-cultivation were stable between day 18 and 40 with an average cell count of $4.2 \times 10^5 \pm 0.3 \times 10^5$ cells / mL (**Figure 20B**). This supported the finding that between day 18 and 40 the culture was in the stationary phase of growth. Decline in chl a fluorescence, as observed from day 34 onwards, was not reflected in cell counts and rather represented alterations of cell physiology.

In co-cultivation, both the chl a fluorescence and the cell counts developed significantly different compared to mono-cultivation. These findings were in agreement with the previously documented growth effect of *T. weissflogii* in interaction with *S. costatum* (chapter 2.2.1, **Figure 4**). On day two the chl a fluorescence was similar to the one of mono-cultivated *T. weissflogii* (mono: 1935 ± 65 RFU, co: 1995 ± 173 RFU), as was the fluorescence development until day 18. But while the mono-cultivated cultures entered into a rather stationary phase of growth from day 18 on, in co-cultivation the phase of increased growth was prolonged for seven days, until reaching maximum chl a of 16278 ± 475 RFU on day 25. Subsequently the chl a fluorescence dropped quickly, reaching a 52 % lower value on day 40 compared to day 34. On day 25, fluorescence values in co-cultivation were 31 % higher, compared to co-cultivation. However, absolute values of fluorescence that were reached in both cultivation types were similar and differed by only 3 %, but the point of maximum fluorescence was shifted by nine days (day 25 in co-cultivation, day 34 in mono-cultivation).

The phase of increased growth in co-cultivation was also reflected in diatom cell counts. While cell counts were approximately constant in mono-cultivation from day 18 on, in co-cultivation they increased by 69% (day 29 compared to day 18), to reach maximum values of $7.1 \times 10^5 \pm 0.2 \times 10^5$ cells / mL on day 29. The maximum cell numbers reached in co-cultivation (on day 29) were 51 % higher compared to maximum cell numbers in mono-cultivation (on day 38). From day 29 on, cell counts in co-cultivation showed a tendency of decrease, but remained rather stable with an average value of $6.6 \times 10^5 \pm 0.4 \times 10^5$ cells / mL between day 29 and 40.

It was the objective of this experiment to investigate, whether a positive growth effect, as observed in co-cultivation compared to mono-cultivation, could be caused by the initial spent medium of the partner. Thus the focus of this experiment was to evaluate the growth parameter of the medium exchange group and to compare the observations with the positive (co-cultivation) and negative control (mono-cultivation).

In the medium exchange group, the development of both parameters was more similar to the negative, than the positive control. In chl a fluorescence the growth phases were identical with mono-cultivation, as was the day of maximum fluorescence. Cell counts remained stable, showing values of $3.6 \times 10^5 \pm 0.4 \times 10^5$ cells / mL between day 18 and 40. Furthermore no elevated values of chl a fluorescence and cell numbers could be found in the medium exchange group, compared to the negative control. On the contrary, absolute values were even lower in the medium exchange group, compared to mono-cultivation. This might be due to the fact that initial chl a fluorescence was already 29 % lower compared to the average of the other groups.

It can be summarized that there were distinct differences in the dynamic of chl a fluorescence and cell counts between mono- and co-cultivation. Furthermore, the absolute cell numbers were significantly higher in co-cultivation, compared to mono-cultivation. These findings were in accordance with the documented growth effect in the interaction experiment (see chapter 2.2.1). However, among the growth parameters measured in the medium exchange group, there is no indication that initial conditions of *S. costatum* caused enhanced growth in *T. weissflogii*, as could be found in co-cultivation with *S. costatum*. The cell count data do not reflect any stimulatory effect on growth.

2.3.2 *S. costatum* medium experiment

After the investigation of the influence of the initial environment on *T. weissflogii*, as described above, I investigated the influence on *S. costatum* with an analog strategy. Both the chl a ($F(18,54) = 2.900$, $P = 0.0013$) and the cell counts ($F(4,12) = 3.519$, $P = 0.0403$) developed significantly different over time among the cultivation groups of *S. costatum*.

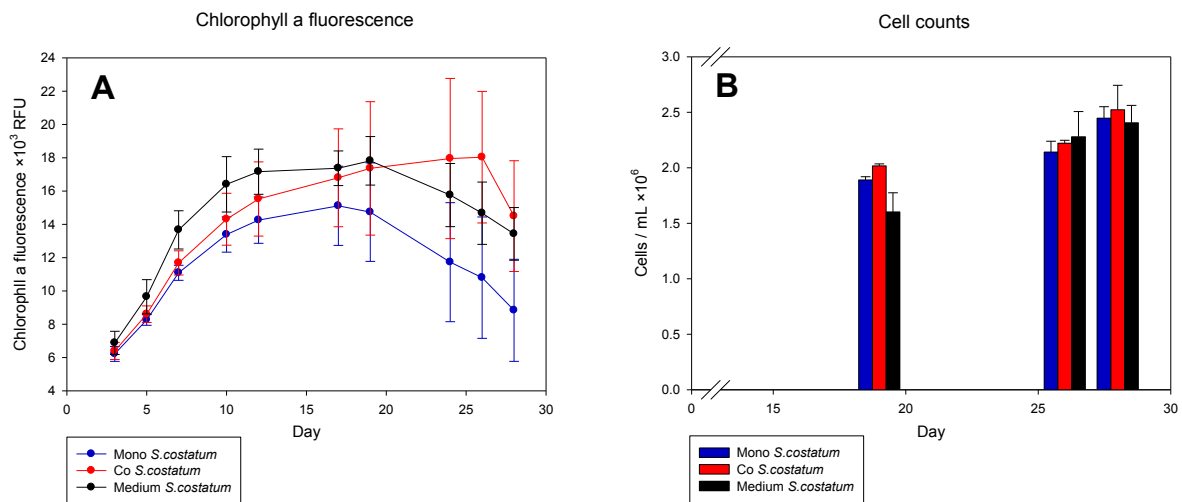


Figure 21: Diatom growth in the medium experiment of *S. costatum*.

The line plot **A** shows means of chl a (RFU: relative fluorescence units), bar plot **B** represent diatom cell counts (cells / mL) of *S. costatum*. The treatment groups are indicated by color: mono-cultivation of *S. costatum* (**blue**, negative control), co-cultivation of each species (**red**, positive control) and the medium group (**black**, experimental group). Values are arithmetic means, error bars indicate standard deviation between biological replicates ($n = 3$).

The dynamic of chl a fluorescence in mono and co-cultivated *S. costatum* was in agreement with the findings in the first investigation of the interaction between *T. weissflogii* and *S. costatum* (chapter 2.2.1). In both groups the chl a fluorescence indicated a phase of regular growth until day 12 (**Figure 21A**). The subsequent fluorescence development was group specific: in mono-cultivation this phase was followed by a phase of stationary growth until day 19 and subsequent rapid decline in fluorescence. Maximum values of 15111 ± 2376 RFU were reached on day 17. On the contrary, the chl a fluorescence in co-cultivation reached its maximum on day 26 (18034 ± 3953 RFU). The phase of fluorescence increase was prolonged and followed by a decline in fluorescence starting day 26.

The difference between mono- and co-cultivation was not only apparent in the different fluorescence dynamics over time, but also in the absolute fluorescence values, which were 19 % higher in co-cultivation (day 26), compared to mono-cultivation (day 17). Considering the chl a fluorescence per day, the difference between mono- and co-cultivation was highest on day 26, with 67 % higher values in co-cultivation. Thus, chl a fluorescence was indicative for an interaction-induced alteration.

I took cell counts at three distinct points in time (**Figure 21B**). In all cultivation groups maximum cell numbers were reached on day 28, as there was a constant increase of cell numbers between day 19 and 28 (29 % in mono-cultivation, 25 % in co-cultivation and 50 % in the medium exchange group). While the chl a fluorescence indicated a phase of rather stationary growth and subsequent decline from day 12 on, cell counts indicated further growth of the culture.

Comparing the positive and negative control, there were no distinct differences in cell numbers between mono- and co-cultivation within each sampling day. Cell numbers in co-cultivation were elevated by only 3 % (on day 28) to 7 % (on day 19), compared to mono-cultivation. These differences were negligible. Thus, cell counts were not indicative for an interaction-induced alteration.

In summary, co-cultivated *S. costatum* showed a distinctly different chl a fluorescence over time compared to mono-cultivated *S. costatum*. As previously described in chapter 2.2.1, the maximum fluorescence occurred later due to a prolonged phase of relatively stable chl a, opposite to decreasing fluorescence in mono-cultivation. Considering cell counts, there were no distinct differences between co- and mono-cultivation on the days of sampling.

To investigate the impact of the initial environment of *T. weissflogii* on the growth of *S. costatum*, I evaluated the medium exchange group. Between day 3 and 19 the chl a in the medium exchange set-ups was higher than the fluorescence in negative (mono-cultivation) and positive (co-cultivation) control (**Figure 21A**).

Cell counts in the medium exchange group were 15 % lower than those in mono-cultivation and 21 % lower than those in co-cultivation on day 19 (**Figure 21B**). On day 26 this group showed the highest cell numbers, compared to mono-cultivation (+ 6.4 %) and co-cultivation (+ 2.6 %). While on day 28 cell numbers in the medium exchange group showed the lowest values again. However, these differences were minor and significant differences in the cell count development over time, as indicated by linear mixed modeling, were probably caused by the alternating growth dynamic.

Differences in average cell counts between the groups were statistically significant over time ($F(2,6) = 7.254$, $P = 0.0250$). However, as these differences were not bigger than 4 % of the absolute cell counts (mono-cultivation vs. co-cultivation), I considered the effect not meaningful in a biological context. Furthermore, as I found cell count differences to not be indicative for an interaction-induced effect, no further comparisons are reasonable. However, as chl a fluorescence of the medium exchange group, a parameter indicative of an interaction-induced effect, showed traits of both mono- and co-cultivated cultures, an influence of the initial conditions could not be fully excluded.

2.3.3 Metadata

I used the metadata to monitor the state of the cultures in the interaction and medium experiments (see experimental designs in chapter 2.1.3 and data in appendix, chapter 7.1.4). I conducted no further statistical analyses. For the medium experiments, I measured PSII efficiency, nutrient levels, pH and bacterial abundance during the interaction. Considering that the same diatom strains (RCC75 and RCC76) were used in the interaction and medium experiments, and that the experimental approach was highly similar, the results for nutrient levels, bacterial abundance and pH can and can be generalized.

Neither PSII, nor bacterial abundance and pH seemed to be relevantly influenced by the interaction. PSII efficiency of the diatoms developed differently, depending on the diatom species and the experiment. The diatom cultures were non-axenic and bacterial abundance increased over the course of the medium experiments. The pH in the medium during the interaction was only measured in the context of the *T. weissflogii* medium experiment and seemed to decrease over time.

I took nutrient levels to monitor the abiotic environment of the cultures. I observed no striking differences between the treatment groups. Except for the decrease-increase dynamic in silicate availability, which seemed to differ between *S. costatum* und *T. weissflogii* cultures.

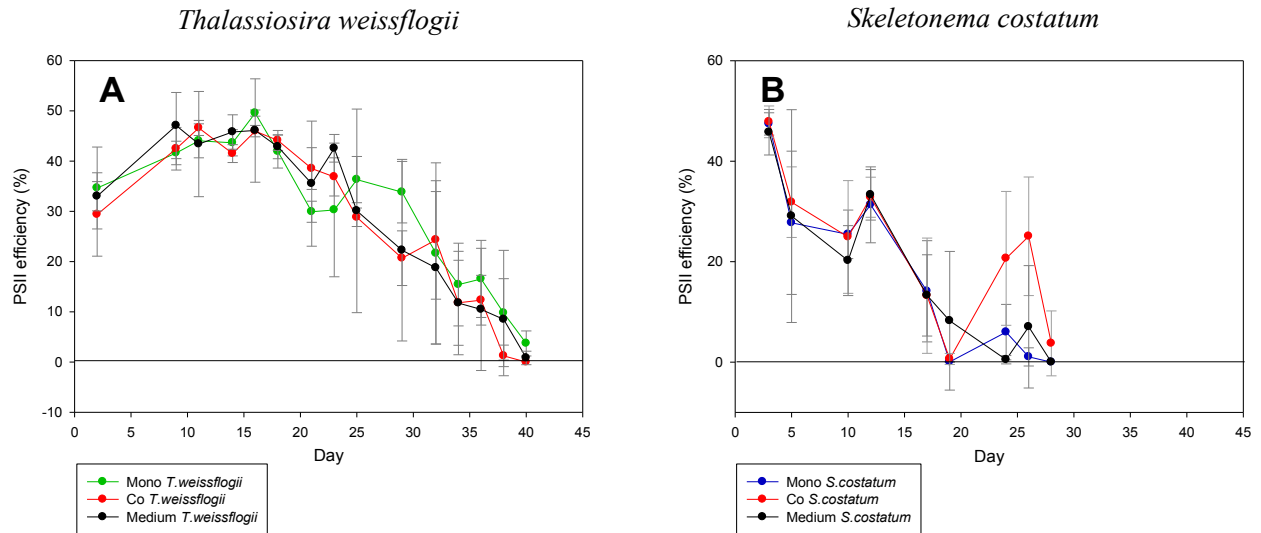
PSII efficiency

Figure 22: PSII efficiency of the diatom cultures in the medium experiment of *T. weissflogii* and *S. costatum*. The figure shows means of PSII efficiency (%) of *T. weissflogii* (graph **A**) and *S. costatum* (graph **B**) in the context of the medium experiments. Mono-cultivation of *T. weissflogii* is depicted in **green** (Mono *T. weissflogii*), mono-cultivation of *S. costatum* in **blue** (Mono *S. costatum*), both representing negative controls. Each species in co-cultivation is colored in **red** (Co *T. weissflogii* / Co *S. costatum*), representing the positive controls. The medium manipulated groups are depicted in **black** (Medium *T. weissflogii* / Medium *S. costatum*). Error bars indicate standard deviation between biological replicates ($n = 3$).

Concerning *T. weissflogii* (**Figure 22A**), the PSII efficiency was approximately stable in all cultivation groups in regular growth phase⁴⁴ (showing an average value of $41 \pm 6\%$ between day two and 23 throughout all groups), with subsequent decline towards 0% until day 40. Concerning *S. costatum* (**Figure 22B**), the initial PSII efficiency within all cultures was $47 \pm 1\%$ on day 3. From day three on, the PSII efficiency decreased until reaching an efficiency $\leq 8.2\%$ in all groups on day 19. It was striking that after reaching values of $0.6 \pm 1.1\%$ on day 19, the PSII efficiency in co-cultivated *S. costatum* showed a local maximum on day 24 ($20.7 \pm 13.3\%$) and 26 ($25.1 \pm 11.8\%$), before crashing again. However, in consideration of the standard deviations per group per day, the difference in PSII efficiency between the groups within each species seemed to be negligible.

⁴⁴ Regular phase in the *S. costatum* medium experiment lasted until day 12, regular phase in the *T. weissflogii* medium experiment lasted until day 18 (more details in chapter 2.3).

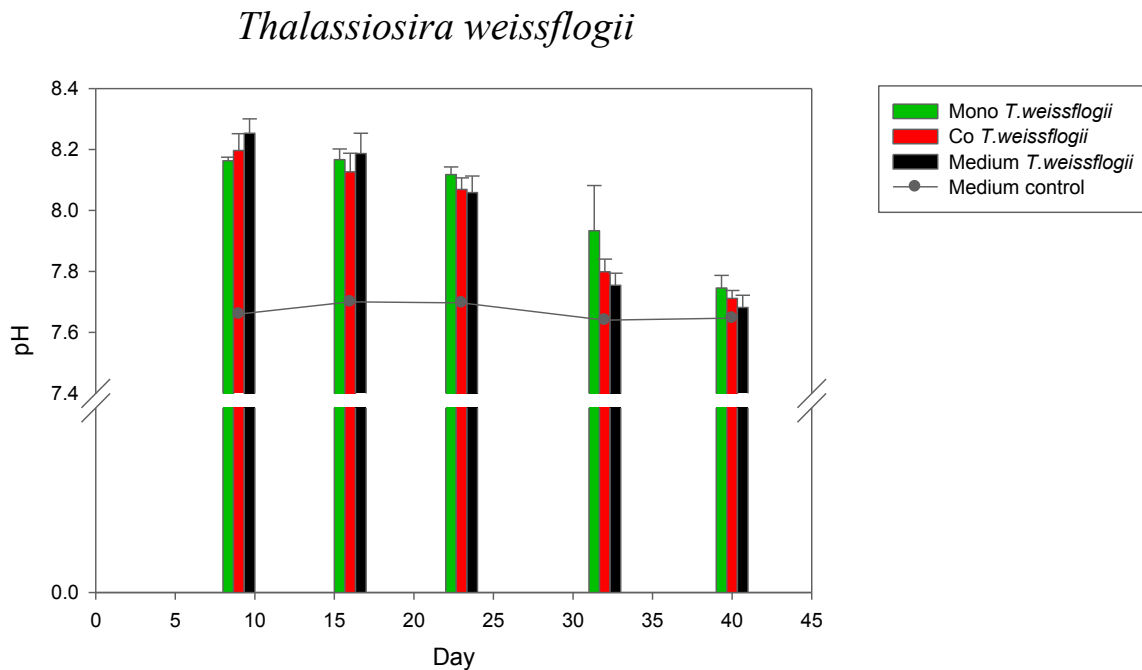
pH

Figure 23: pH of the diatom cultures in the medium experiment of *T. weissflogii*.

The figure shows means of pH in the cultures of *T. weissflogii* in the context of the medium experiments. Mono-cultivation of *T. weissflogii* is depicted in **green** (Mono *T. weissflogii*), representing negative control. Co-cultivation is colored in **red** (Co *T. weissflogii*), representing the positive control. The medium manipulated group is depicted in **black** (Medium *T. weissflogii*). Values for the seawater control are represented in **grey**. Error bars indicate standard deviation between biological replicates ($n = 3$, medium control: $n = 1$).

On day nine, the first measured pH of the *T. weissflogii* cultures was 8.20 ± 0.05 throughout all groups (**Figure 23**). Compared to the seawater control, showing a pH of 7.70 on day nine, the pH was elevated. Between day nine and day 40, the pH steadily decreased in the culture groups until reaching a pH of 7.70 ± 0.03 (average throughout all groups) on day 40. In consideration of the standard deviations per group per day, the difference in pH between the groups seemed to be negligible. The pH in the seawater control remained constant around 7.70 ± 0.03 throughout all measured points in time. No pH measurements were available for the *S. costatum* medium experiment.

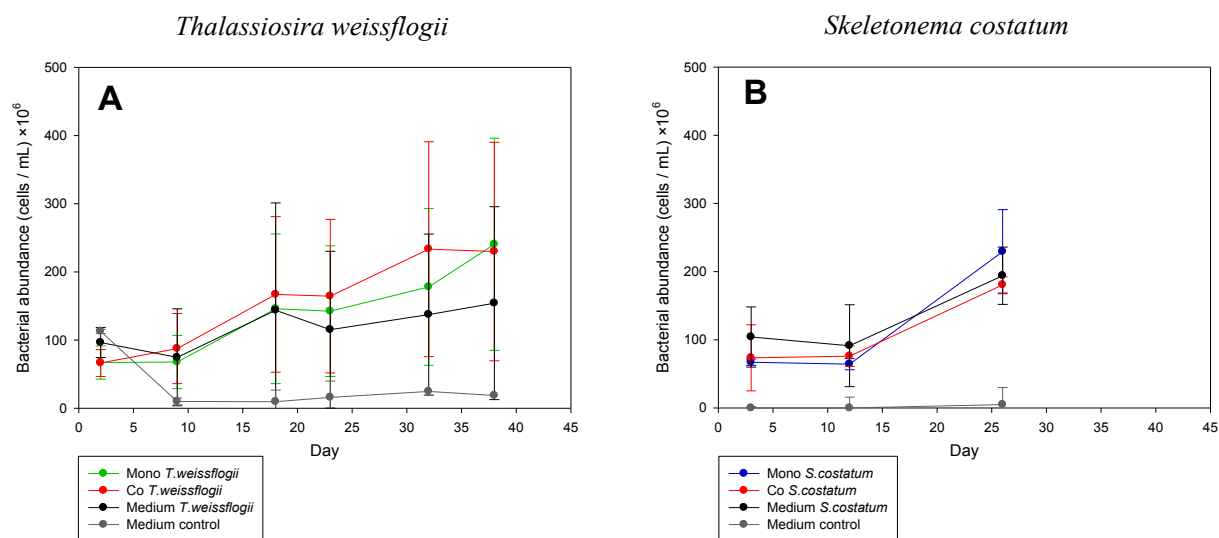
Bacterial abundance

Figure 24: Bacterial abundance in the medium experiment of *T. weissflogii* with *S. costatum*.

The figure shows means of bacterial abundance (cells/mL) in the cultures of *T. weissflogii* (graph A) and *S. costatum* (graph B) in the context of the medium experiments. Mono-cultivation of *T. weissflogii* is depicted in green (Mono *T. weissflogii*), mono-cultivation of *S. costatum* in blue (Mono *S. costatum*), both representing negative controls. Each species in co-cultivation is colored in red (Co *T. weissflogii* / Co *S. costatum*), representing the positive controls. The medium manipulated groups are depicted in black (Medium *T. weissflogii* / Medium *S. costatum*). Values for the seawater control are represented in grey. Error bars indicate standard deviation between biological replicates (n = 3, medium control: n = 1).

The diatom cultures of both species were non-axenic. Compared to diatom cells, the bacterial cell number was elevated in the order of 309 to 515 - fold in *T. weissflogii* culture medium (calculated per group per day) and in the range of 81 to 107 - fold in *S. costatum* medium (calculated per group on day 26, the only day where both diatom and bacterial cell counts were taken simultaneously).

The bacterial abundance in *T. weissflogii* cultures started from $76.6 \times 10^6 \pm 17.1 \times 10^6$ bacterial cells/mL (average throughout all groups) on day 2, to reach a maximum of $208.1 \times 10^6 \pm 47.1 \times 10^6$ bacterial cells/mL (average throughout all groups) on day 38 (**Figure 24A**). In *S. costatum* cultures, bacterial abundance started from very similar values ($81.5 \times 10^6 \pm 19.8 \times 10^6$ bacterial cells/mL, average throughout all groups on day 3) to reach a maximum of $201.2 \times 10^6 \pm 25.2 \times 10^6$ bacterial cells/mL (average throughout all groups) on day 26 (**Figure 24B**).

In both species' cultivation chambers the bacterial abundance increased constantly. The development and abundance of bacterial cell numbers was similar in both species and all treatment groups. In consideration of the standard deviations per group per day, the difference in bacterial cell counts between the groups of each species seemed to be negligible.

In the medium experiment of *T. weissflogii*, the medium control showed a substantial amount of bacteria as well. Thus, a contamination due to insufficient instrument sterilization or cross-contamination couldn't be excluded. However, absolute numbers in the medium control (with exception of day 2) were lower than in diatom cultures (only six to 14 % compared to the average bacterial abundance in all groups on the respective day). On the contrary, the medium control of *S. costatum* showed no bacterial contamination, except for day 26.

Nutrient levels

To monitor the abiotic state of the culture, I measured nitrate, nitrite, phosphate and silicate concentrations at distinct points in time of the culture growth curves. The number of sampling points was limited by the small culture volumes in the co-cultivation set-up to a maximum of four.

An investigation of different diatom species revealed that average nutrient concentrations, reducing the uptake rate of the specific nutrients by 50%, averaged 1.6 μM for nitrate, 1.2 μM for phosphate and 3.9 μM for silicate (Sarhou et al., 2005). However, these rates can vary among species. Under these conditions, diatoms can only maintain maximum growth rates over a short period of time, before the specific growth rate decreases substantially (Sarhou et al., 2005). Limitation of nutrients initiates the transition from regular growth to the stationary phase.

Diatom cultures of both species were depleted of silicate around day 18 for *T. weissflogii* and around day 12 for *S. costatum* (**Appendix 22** and **Appendix 23**). This coincides with the transition into stationary growth phase, as described in the previous chapters. A depletion of nitrate was observed between days 23-32.

The phosphate measurements were ambiguous, as in general the measured phosphate concentrations in the samples and medium blanks (with exception of the medium blank in the medium experiment of *S. costatum*) were elevated around roughly 7 - fold compared to the adjusted concentrations in the artificial seawater medium used for cultivation. Absolute concentrations must therefore be interpreted with care, and rather the general trend over time was considered.

Interestingly, the silicate availability in the medium of cultures containing only the diatom cells of the species *S. costatum* (mono-cultivated *S. costatum* and medium group in the context of the *S. costatum* medium experiment) increased again at the end of the stationary phase, after reaching a minimum at the end of regular growth phase (**Appendix 23 B2**). Silicate concentration on day 26 were 3 - fold higher in mono-cultivation ($67.02 \pm 15.43 \mu\text{mol} / \text{L}$) and 2.7 - fold higher in the

medium exchange group ($78.8 \pm 4.59 \mu\text{mol} / \text{L}$), compared to concentrations of the respective cultures on day 17.

The observation of increased silicate availability at the end of stationary phase was not found for cultures containing only *T. weissflogii* cells (mono-cultivated *T. weissflogii* and medium group in the context of the *T. weissflogii* medium experiment). However, in co-cultivation the elevated silicate availability was also observed, but less substantial. Concentrations were only around $9.08 \pm 0.62 \mu\text{mol} / \text{L}$ (*S. costatum* medium experiment, (**Appendix 23 B2**) on day 26 and thus merely 13.5 % of the silicate concentrations found in cultures containing only *S. costatum*.

Nitrite concentrations increased until reaching a maximum concentration of up to $14 \mu\text{M}$ (co-cultivation group in the *S. costatum* medium experiment on day 17, **Appendix 22 B2**) in stationary phase. Subsequently, nitrite concentrations declined to below the detection limit within ten days.

2.4 Evaluation of DMSP as growth mediator

I hypothesized that the observed growth effect of *T. weissflogii* might be caused by a DMSP release-uptake dynamic between the diatom partners. This hypothesis was based on the observation that only *S. costatum* is able to de-novo synthesize DMSP, while *T. weissflogii* seems to completely rely on the active uptake of externally available DMSP (Spielmeyer et al., 2011; Spielmeyer and Pohnert, 2012).

To investigate the effect of DMSP as semiochemical in the interaction between *T. weissflogii* and *S. costatum*, I simulated two modes of action: the availability of distinct DMSP pulses (chapter 2.4.1) and the continuous availability of DMSP (chapter 2.4.2).

DMSP was not able to enhance growth of *T. weissflogii* cultures. Both, a daily availability of DMSP (100 nM) and the addition of distinct DMSP pulses (100 nM, 1 μ M, 2.5 μ M) during stationary and declining phase were not stimulating the growth of *T. weissflogii*.

2.4.1 Influence of DMSP pulses on diatom growth

I tested if DMSP was able to enhance growth of *T. weissflogii*, as was observed in the interaction of *T. weissflogii* with *S. costatum* (see chapter 2.2.1).

I used chl a fluorescence as estimator for diatom growth. Based on this parameter, diatom growth was characterized by a regular growth phase (until approximately day 12), a stationary phase of growth and a subsequent declining phase (starting around day 27), as can be seen in **Figure 26A** and **Figure 25A**. As enhanced growth due to the interaction of *T. weissflogii* with *S. costatum* has been observed to occur after the regular growth phase, this period was the focus of the investigation.

I added pulses of different DMSP concentrations (final concentrations in the cultures: 100 nM, 1 μ M, 2.5 μ M) to *T. weissflogii* cultures at two distinct points in time during stationary phase (day 20 and 24) and one during declining phase (day 32). I statistically tested the effect on diatom growth via cell counts⁴⁵ (**Figure 26B**): A 2-way repeated measures ANOVA indicated that there is no significant interaction between cell counts and time among the treatment groups and the control.

⁴⁵ Cell count samples have been counted in two different charges. Charge one comprising day 8, 15, 20, 24, 32 and charge two comprising day 27, 30, 34, 36. Due to differences in absolute values caused by count systematics, only charge two has been depicted in **Figure 25**. However, within both charges there are no statistically significant interactions between treatment and time (tested via two-way repeated measures ANOVA).

This means that DMSP did not significantly influence the growth of *T. weissflogii* over time. I confirmed these statistical findings by a visual evaluation of the chl a fluorescence, indicating no relevant differences between the groups (**Figure 26A**).

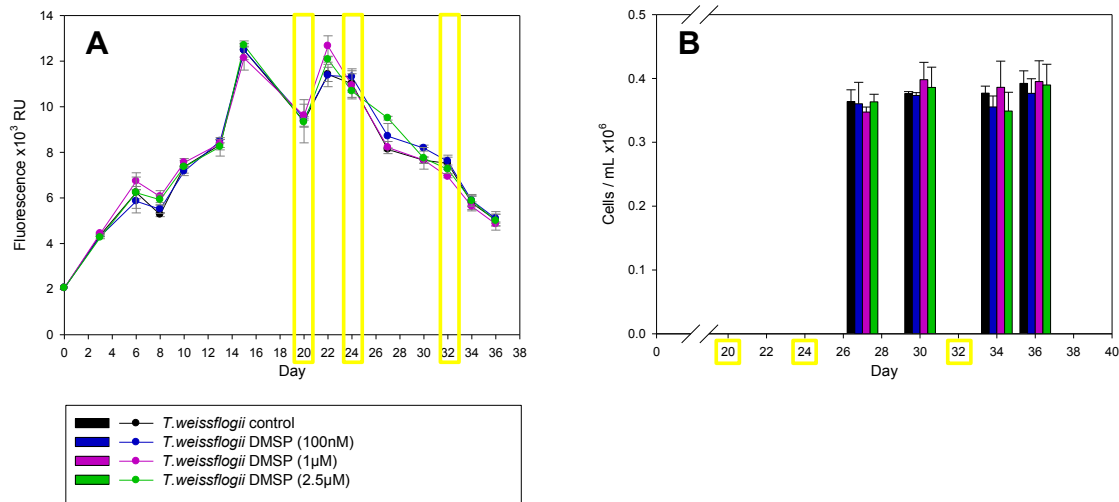


Figure 25: Influence of multiple DMSP pulses (100 nM, 1 μM, 2.5 μM) on the growth of *T. weissflogii* (RCC76). The line plot (A) shows means of chl a (RFU: relative fluorescence units), the bar charts (B) represent diatom cell counts (cells/mL) of *T. weissflogii*. At three distinct points in time during diatom growth (marked by yellow frames), DMSP was added to the cultures, reaching final concentrations in the medium of 100 nM, 1 μM, 2.5 μM DMS. The treatment groups are indicated by color: negative control (black), 100 nM DMSP (blue), 1 μM DMSP (purple), 2.5 μM DMSP (green). Values are arithmetic means, error bars indicate standard deviation between biological replicates (n = 3).

2.4.2 Influence of continuously available DMSP on diatom growth

In addition to distinct DMSP pulses, I investigated the influence of a continuously available amount of DMSP on the growth of *T. weissflogii*. Therefore, DMSP was added on a regular basis (five out of seven days per week) in concentrations of 100 nM per culture. However, I found no differences in diatom growth, as estimated via chl a fluorescence (**Figure 26A**). I confirmed these findings via cell counts. On day 24, cell counts of *T. weissflogii* (**Figure 26B**) were not significantly different due to the DMSP addition, compared to control (as tested with an unpaired Student's t-test).

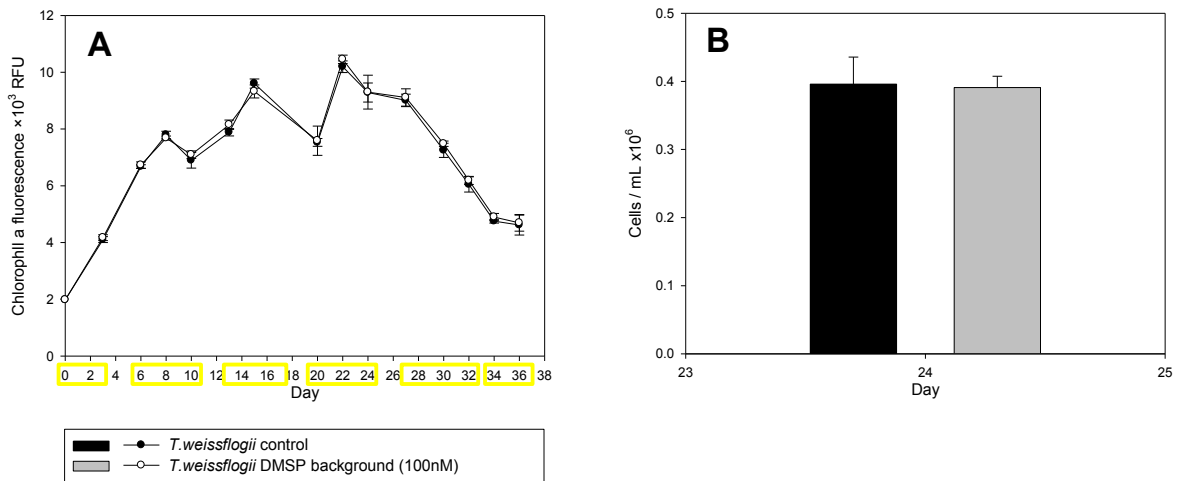


Figure 26: Influence of continuous DMSP addition on the growth of *T. weissflogii* (RCC76)

The line plot (A) shows means of chl a (RFU: relative fluorescence units), the bar charts (B) represent diatom cell counts (cells / mL) of *T. weissflogii*. In a daily manner (approximately five out of seven days per weeks, as indicated by yellow frames in graph A), DMSP was added to the diatom cultures to reach final concentrations of 100 nM per culture. Black indicates the control group, while white/grey represents the experimental group of continuous DMSP addition. Values are arithmetic means, error bars indicate standard deviation between biological replicates (n = 3).

2.5 Discussion of the metabolomic strategy

Metabolomics complement traditional ‘omics’ techniques, such as genomics - sequencing and analyzing the totality of genes via molecular genetics - , transcriptomics - investigating the collectivity of (m)RNA molecules - and proteomics - analyzing of the totality of protein molecules (Kell and Oliver, 2016). They are used to investigate mostly low-molecular weight compounds, which are intermediate products of the cell’s biochemical pathways (Fiehn, 2002). Via ‘omics’ techniques, researchers try to understand the biology of an organism or a system. However, only metabolomic techniques allow a direct functional approach, as the metabolomic profile of a cell is directly linked to the biological function (Oliver, 1996; Fiehn, 2002).

Comparative metabolomic approaches are a common and highly valuable tool in chemical ecology (Kuhlisch and Pohnert, 2015), as described in chapter 1.4 (“Metabolomic strategies in environmental science”). They have been successfully applied in the investigation of chemically-mediated interactions in phytoplanktonic organisms. For example in the elucidation of the first diatom pheromone diproline of the pennate diatom *Seminavis robusta* (Gillard et al., 2013), the characterization of the interaction between the bacterium *Dinoroseobacter shibae* and the diatom *T. pseudonana* (Paul et al., 2013) or the interaction between the diatoms *S. costatum* and *T. weissflogii* (Paul et al., 2009).

The major advantage of comparative metabolomic approaches is that physiological responses of organisms due to ‘disturbances’ are investigated under consideration of their physiological responses in an ‘undisturbed’ context. Thus, an adequate metabolomic baseline is created - as discussed by Viant - that enables the detection of relevant physiological alterations (Viant, 2007). For example in the present interaction investigation, the co-cultivation group (**Figure 2B**) is compared to the mono-cultivation groups (**Figure 2A, C**). Hereby, the former presents disturbance in form of an interaction partner and the latter constitute the metabolomic baseline of the specific species.

In this thesis, I chose a comparative metabolomic profiling analysis via GC-EI/TOF/MS, focusing on both the endometabolome and the exometabolome of the interacting organisms. It is important to point out that on the one hand, differences in the exometabolome - as defined by the collectivity of exuded metabolites in the medium - might point out potential allelochemicals. However, on the other hand, differences in the endometabolome refer to physiological changes in each species due to the presence of a partner.

2.5.1 Metabolomic sampling and extraction protocol

A suitable sampling, extraction and storage protocol and a standardized work-flow are important for the investigation (Fernie et al., 2011). Standardizing GC-MS metabolomics aims at eliminating all sources of biases and is thus essential in any investigation (Kanani, Chrysanthopoulos and Klapa, 2008). The protocol used for metabolite extraction, derivatization and analysis was developed by Vidoudez (Vidoudez, 2010; Vidoudez and Pohnert, 2011). It is optimized for the investigation of diatom metabolomes with following outcome:

1. Sampling and sample treatment minimize the introduction of artificial / serial variability and artifacts in samples (randomization, standardized workflow, adequate sample quenching, high purity chemicals / solvents / materials) (Vidoudez, 2010).
2. The chosen extraction mix or the solid phase extraction cartridge covers a maximally broad range of compound classes, shows high reproducibility and high balanced recovery rate among different classes (Vidoudez, 2010).
3. The derivatization method guarantees good recovery of compound classes with minimal variability and realizes minimal storage time before measurement under high-throughput conditions (Vidoudez, 2010). The use of the standard ribitol evaluates derivatization effects in the context of standardization (Lisec et al., 2006), furthermore it can be used for normalization (Vidoudez, 2010).
4. The GC method enables optimal transfer of liquid samples onto the column, good separation of compounds and reduction of artificially introduced variability (choosing and changing the liner, adequate temperature program, column choice and split mode). (Vidoudez, 2010)
5. The MS method guarantees high-resolution measurements with optimal performance due to regular instrument tuning, calibration and quality controls (see chapter 6.6.4).

2.5.2 Chemical analysis via GC-TOF/EI/MS

GC-MS is a widely used approach in metabolomic investigations (Allen et al., 2008; Plaza et al., 2010; Vidoudez and Pohnert, 2011; Paul et al., 2012, 2013; Bromke et al., 2013; Mausz and Pohnert, 2015). The compounds susceptible to GC analysis are low-molecular weight, medium or low polar compounds in ppb-ppm concentrations (Stashenko and Martínez, 2014). To be eligible for GC-MS analysis, a compound is required to be volatile enough and thermally stable to pass through the GC system - these properties can be modified by chemical derivatization (Stashenko and Martínez, 2014).

Chemical derivatization

Chemical derivatization increases volatility, thermal stability and chromatographic mobility of polar and unstable compounds (Halket and Zaikin, 2003). Vidoudez suggests the use of a combined silylation / methoxymation derivatization and presented a derivatization protocol optimized for the investigation of diatom metabolomes (Vidoudez, 2010), which I used in the scope of this thesis.

In the metabolomic context, silylation was used to modify compounds with OH (alcohols, phenols, carboxylic acids, oximes, sulfo-acids, phosphorus acids, enols etc.), NH (amines, amides and imines etc.) and SH groups (thioles and thiocarboxylic acids etc.) by replacing the active H (Halket and Zaikin, 2003). Methoxymation chemically altered aldehyde- and keto-groups and made them less polar.

One drawback of chemical derivatization is the potential to introduce artificial variability into metabolomic profiles. Chemical derivatization is a complex process as multiple, chemically different compound classes are addressed at once. Although the derivatization strategy used has been optimized and standardized (Vidoudez, 2010), each compound class shows slightly different susceptibility to derivatization biases. Kanani et al. described three categories of possible derivatization outcome and / or bias (Kanani and Klapa, 2007):

1. Metabolites resulting in only one derivative
2. Metabolites resulting in two oxime-TMS derivatives
3. Metabolites resulting in multiple derivatives with different silylation degrees.

The derivatization result depends on the reaction kinetics of different functional groups ((Kanani and Klapa, 2007) and references herein for more details). Accordingly, metabolites with only hydroxyl and / or carboxylic functional groups result in category (1), metabolites with additional ketone functional groups result in category (2) and those with amine groups in category (3) (Gehrke et al., 1969; Kanani and Klapa, 2007). Additionally, structural alterations due to derivatization have been reported, for example the transformation of glutamate-3 TMS into TMS-pyroglutamate due to cyclization (Gehrke et al., 1969). In the scope of this thesis, oftentimes I observed multiple peaks per compound, potentially tracing back to named derivatization artifacts. Another possible explanation for multiple peaks per substance might be an ambiguous identification via libraries. Especially, compounds with highly similar MS-spectra, like sugars or terpenoids.

Further potential bias sources like incomplete derivatization or suboptimal derivatization parameters were already counteracted by the standardized protocol used in this thesis. The

internal standard ribitol was introduced into the experimental protocol *inter alia* to test for silylation success in the workflow (see chapter 2.5.3 “Metabolomic data processing and statistics”).

Choice of method

One major challenge of metabolomics is the enormous chemical diversity of metabolites that needs to be simultaneously covered by adequate analytical techniques. In this context, the perfectly suited, ‘ideal’ analytical method is described to be (Theodoridis and Wilson, 2008): comprehensive over a wide range of metabolite classes, suitable for complex matrices, a direct method without sample preparation, capable of high throughput and unbiased analysis over all classes, robust, sensitive, repeatable, reproducible and capable of identifying all detected MSTs. However, no such ideal method exists.

In the metabolomics field, hyphenated techniques like LC-MS and GC-MS as well as NMR are the most prominent analytical tools in use (Sardans et al., 2011). Often, these techniques are used complementarily to increase the analytical power of an investigation as every analytical method by itself has a certain bias (Halket et al., 2005; Sardans et al., 2011): While GC-MS is best suited for low-molecular weight metabolites of the primary metabolism (sugars, amino acids, fatty acids etc.), LC-MS is better suited to depict a higher range of polar and high-molecular weight substances and thus cover the richness of secondary metabolites (Fernie et al., 2011; Sardans et al., 2011).

In contrast, NMR is able to investigate the whole spectrum of polar to unpolar compounds. NMR is often considered “the gold standard for structural identification” (Fernie et al., 2011), as it is highly reproducible and enables unambiguous identification of compounds based on mere physical criteria (Fernie et al., 2011). However, NMR is a rather insensitive method that struggles with complex samples and needs comparably high compound concentrations for their identification (Sardans et al., 2011). In contrary, MS techniques are known to be highly sensitive and robust methods.

In the context of this thesis, I chose a GC-MS approach for several reasons. Due to the design of the experiment, the concentration of potential infochemicals in samples was considered too low and the sample matrix too complex for NMR. The objective of this investigation was to complement the findings of Paul et al., which were conducted via LC-MS analysis (Paul et al., 2009). In addition, the GC-MS at hand was equipped with EI (electron impact ionization) and both a commercial and an in-house compound library facilitating compound identification.

Finally, GC-MS is a robust, well-documented method with optimized protocols for diatom metabolomics (Vidoudez, 2010).

Compound identification

Silylation not only changes the physico-chemical properties of substances as described above, but also enhances the specificity of characteristic compound fragments via EI mass spectrometry (Halket and Zaikin, 2003). Generally, the “hard” EI in EI/MS approaches fragments each compound into highly specific compound fragments, which can be used to establish compound libraries to facilitate compound identification. In metabolomic studies, GC is mostly coupled with EI/MS (Stashenko and Martínez, 2014).

Generally, hyphenated MS techniques like GC-MS are able to separate and identify a wide range of compounds. However, they fail to unambiguously identify highly related metabolites or exact chemical isomers (Fernie et al., 2011). For compound identification, two approaches are common: library based identification and / or standard based identification. The best way to identify a compound is based on the comparison with an authentic standard, ideally an isotopically labeled internal standard (Fernie et al., 2011). However, the availability of commercial standards (both labeled and non-labeled) is limited. In this case, the library based compound identification can be a solid alternative, which is routinely used in GC-MS (Stein et al., 2007).

In the course of this thesis, I applied both approaches, with a predominance of library based identification (see chapter 6.7.4). In terms of standard based identification, I used non-labeled standards (see chapter 6.7.4). In order to increase the reliability of compound identification via libraries, I considered three parameters, as previously done (Vidoudez, 2010; Matusz, 2014) and recommended (Wagner, Sefkow and Kopka, 2003): Match value, R-Match value and retention index (RI). Furthermore, I reported full information about the derivatization chemistry, protocols used and system metadata - forming the basis of identification - in chapter 6.6, as strongly recommended (Fernie et al., 2011).

Match and R-Match values were obtained as a validation parameter during library search via “The NIST Mass Spectral Search Program for the NIST/EPA/NIH Mass Spectral Library⁴⁶”. These parameters characterize the similarity of sample spectrum and library spectrum. While the Match value considers all peaks in the sample spectrum, the R-Match disregards all peaks that

⁴⁶ See chapter 6.7.4 for more details

are in the sample spectrum but not in the library spectrum⁴⁷. However, mass spectral matching is not sufficient for unambiguous compound identification (Wagner et al., 2003). In fact, the RI (retention index) needs to be considered. The RI is based on a series of *n*-alkanes and calculated as described in chapter 6.7.4. This index aims at improving compound identification by characterizing each compound with a standardized RI, which is calculated on the basis of the instrument-specific retention time. Thus, an instrument-independent characterization of a compound in a simple and reproducible manner is guaranteed (Vandendool and Kratz, 1963).

In this thesis, I considered structure suggestions if the Match was ≥ 600 and if the retention index (RI) provided by the libraries was close to the calculated RI. In some cases, namely when the structure suggestions were identical among the three samples with the highest peak intensity of the considered metabolite, a Match of ≤ 600 was accepted. Those metabolites were marked with “1” in the heatmaps. Structures were accepted if in addition the R-Match was ≥ 800 and / or the substance could be identified via standard (marked with “*”). In that case the RI of the standard must be highly similar and the mass spectrum of the standard must show an identical fragmentation pattern. If the R-Match is ≤ 800 , the structure was accepted with a tag “?” if the R-Match is between 700 and 800, with “??” if the R-Match is between 600 and 700 and with “???” if the R-Match is ≤ 600). The latter tagged substances were referred to as “putative”, as their identity was uncertain due to low R-Match.

However, in some cases the suggested structure of putatively identified compounds was not plausible. For example in chapter 3.2.3, metabolite #205 was putatively identified as 2-(adamantan-1-yl)ethanol by the MS libraries. As the suggested structure was clearly not a natural product, the identification was rejected. Therefore, putatively identified compounds always need an additional plausibility check and further confirmation, if they prove to be of interest for the research question.

Nevertheless, the library based structure suggestions are providing a very good evaluation of compound nature and class. Therefore, I conducted the discussion of potential infochemicals on library based structure suggestions in the scope of this thesis. Thus, a first impression of compound nature and relevance was obtained. However, in a next step, I recommend further confirmation of relevant compounds and potential infochemicals, especially of those with putative structure suggestions.

⁴⁷ As described in the “NIST 2008 User Guide” inherent in “The NIST Mass Spectral Search Program for the NIST/EPA/NIH Mass Spectral Library”

2.5.3 Metabolomic data processing and statistics

Metabolomic investigations usually produce extensive and complex data sets. Simplifying the complexity of these data sets is essential in order to gain relevant insights and to facilitate the biological interpretation, as commented by Eick et al. (Eick and Pohnert, 2015). Especially, in the context of chemically-mediated interactions, it is essential to distinguish relevant metabolomic changes from other sources of variability. The choice of a data processing strategy is therefore a crucial step in setting the scope of an interaction.

A common strategy is to use multivariate statistics on the basis of pre-processed data, for example the Canonical Analysis of Principal Coordinates (CAP). Before the CAP is discussed, the data pre-processing pipeline of this thesis will be outlined.

Data pre-processing

The objective of data pre-processing is to clean up raw data, combine raw data from different measurements, transform raw data into easy to use data formats and most importantly to extract characteristics of every observed MST (Katajamaa and Orešič, 2007), as for example m/z ratio, RT, RI and suggestion of structural identity. In this investigation, pre-processing comprised the following steps:

(1) Background-noise subtraction

In the first step, each sample spectrum was cleaned via background-noise subtraction. In such a way, any instrument-inherent background was eliminated. Furthermore, in a later phases of the pipeline, the background introduced by the analytical process (*e.g.* by heptacosyl, plasticizers or other contaminations) was subtracted from each sample with the help of blank measurements.

(2) Spectral deconvolution

Secondly, a feature detection program was used to extract all observed MSTs. With the help of AMDIS (automated mass spectral deconvolution and identification system, chapter 6.7.2), peak detection and deconvolution analysis was performed. In principle, the program performed a deconvolution of spectra by finding ions that display the same intensity profiles and consequently associating a representative ion trace with a single compound. In this way, compounds can be detected via ion trace dynamics, although they co-elute with more intense compounds or their peaks are not visible in the total ion current chromatogram (TIC). AMDIS also offers an initial identification of detected compounds by library search. However, these results were treated as

preliminary identifications, due to the fact that compound identification was performed manually at a later phase of the data processing.

In brief, AMDIS generated an ion/retention time pair list as input file for MET-IDEA (Metabolomics Ion-based Data Extraction Algorithm, V 2.08). Each ion/retention time pair, representing an MST, was characteristic of a specific compound (Broeckling et al., 2006), but a specific compound could be described by various ions for its retention time.

(3) Peak alignment, annotation and integration

I used MET-IDEA to quantify the MSTs via peak area. If AMDIS reported several “model” ions per MST, MET-IDEA selected the more abundant of the ions that met a certain set of criteria (chapter 6.7.2) for quantification (Broeckling et al., 2006). When AMDIS reported no model ion that met the criteria, a value of “1” was reported (Broeckling et al., 2006) and I decided for each case to either exclude the “-1”-ion/retention time pair from further analysis or, if available, to manually specify a new model ion. For the analysis, MET-IDEA needed a representative file, which was chosen according to the highest amount of compounds and targets. I used the retention times of the RI-mix for retention time correction, performed for each file individually, on a file-by-file basis via a calculated fixed value correction (Broeckling et al., 2006).

As stated by Lei et al., manual intervention in peak integration of complex metabolomics data is inevitable (Lei et al., 2012). Thus I manually inspected peak annotation and integration for crude mistakes and corrected if necessary. Furthermore, single chromatographic peaks can improperly be deconvoluted into two or more peaks (Broeckling et al., 2006; Lu et al., 2008). These redundancies were characterized by nearly identical retention times and could be detected with the help of a Pearson’s correlation-based redundancy analysis, as offered by MET-IDEA. If peaks showed nearly identical retention times and if r-square values were larger than 0.8, they were considered artifacts and redundant peaks were diluted.

Another challenge for deconvolution is the broad range of metabolite concentrations in samples (Koek et al., 2011). If the concentration of a metabolite is too high, the quality of mass spectral information is impeded due to the fact that some masses in the mass spectrum are out of the linear range (Koek et al., 2011). This phenomenon was mostly observed in the interaction experiment of *T. weissflogii* with *S. marinoi* and *S. dohrnii* (chapters 3 and 4). Beyond that, it is a general problem in complex biological matrices containing both very high and very low metabolite concentrations. However, the sample normalization to cell counts aimed at providing comparable metabolite concentrations between samples and to thus standardize the impact.

In the context of chemically-mediated interactions, it makes sense to deliberately discriminate against very high abundant metabolites and to focus on low abundance metabolites, as infochemicals are usually present in low concentrations. I pursued this strategy in the scope of this thesis. Nevertheless, mass spectral overload poses a problem and might result in loss of potentially relevantly regulated metabolites due to inaccurate, relative quantification. Based on the hypothesis that potential infochemicals will occur in rather low concentrations and considering the fact that it was ensured that ribitol (used for normalization) was never showing mass spectral overload, I considered the impact of mass spectral overload to be low and acceptable in view of the research focus.

Furthermore, MET-IDEA used an RT (retention time) calibration algorithm to remove retention time shifts between measurements. Thus, comparability of samples from different measurements was assured.

(4) Normalization

Intracellular metabolomic data was normalized by peak sum. Assuming an equivalent total MST signal per sample, this procedure aims at making samples more comparable to each other by compensating for variability (Chen et al., 2014). However, an equivalent total MST signal cannot be assumed between different species. Therefore, overall analyses of the endometabolomic data set need to be interpreted with care, as they manifest normalization-inflicted differences between species. However, this restriction was of minor relevance as the focus of this thesis was set on the detailed endometabolomic analysis of each species individually. Variability in samples can be caused by differences in biomass after cell-count normalization, physiological differences and variability from the analytical method itself (Chen et al., 2014).

Furthermore, the endometabolome was normalized to an experiment- and species-specific cell count. Intensity changes in endometabolites directly reflected metabolomic alterations at the cellular level.

Extracellular MST data was normalized sample-wise to the peak area of the external standard ribitol (Vidoudez, 2010; Vidoudez and Pohnert, 2011). As the hypothesis of an equivalent total MST signal per sample (Chen et al., 2014) was not fulfilled due to species heterogeneity among the samples, the normalization to the external standard ribitol was chosen over a peak sum normalization. Assuming that variation in external standard can only result from derivatization or systematic errors and that different metabolites behaved similar to the external standard, this normalization accounted for analytical errors (De Livera et al., 2012; Chen et al., 2014). However, ribitol presents some inherent limitations and disadvantages – *e.g.* it is not well suited

to represent the behaviors of non-polar compounds or to evaluate the methoxymation step (Vidoudez, 2010).

Opposite to cell-count normalization, extracellular MST data was previously normalized by volume (chapter 6.6.2), not by cell-count. Thus, extracellular MST data represent the chemical environment of the interaction set-up independent from actual diatom cell numbers.

Data analysis

As a result of data pre-processing, every sample was characterized by a table containing all MSTs, characterized via m/z ratio of the respective model ion and the retention time (RT), as well as the normalized peak area of each MST. Generally, the peak area profile of a sample's metabolites constitutes its metabolomic profile (Kanani and Klapa, 2007). The peak area hereby correlates with MST abundance.

I used principal coordinate analysis (PCoA), followed by a canonical discriminant analysis (CDA), to investigate differences in the endo- and exometabolome of the diatoms, as caused by the interaction. This combined analysis was called CAP ("Canonical Analysis of Principal Coordinates"). The CAP of metabolomics data offered the following four items (Anderson and Willis, 2003a): robust unconstrained ordination, an appropriate constrained analysis by reference to a specific hypothesis, a statistical test of the hypothesis and a characterization of metabolites responsible for multivariate patterns.

CDA used the a-priori definition of groups. The misclassification error is a measure for the fit of the defined groups and indicates the distinction of the groups in multivariate space (Anderson and Willis, 2003a). With the help of the trace statistics and obtaining a p-value by permutation, the null hypothesis of "no significant differences in multivariate location among groups" was tested (Anderson and Willis, 2003a). The squared canonical correlation (δ_1^2) and its corresponding p-value represented the proportion of shared variance between each of the canonical variates of dependent and independent variables (Sherry and Henson, 2005). In order to evaluate the separation of a priori groups, the classification and ordination success had to be considered in combination.

In general, three different kinds of plots were produced: unconstrained score plot, constrained score plot and correlation loading plot. To explore individual and group differences of the samples, an unconstrained score plot was created, based on the transformed MST intensities. The plot was produced with the help of the first two principal coordinate axes from the CAP output (Anderson and Willis, 2003a). To reveal potentially masked but ecologically important patterns

in unconstrained ordination a canonical ordination was performed. The constrained score plot of the CDA used the first two canonical axes produced by CAP (Anderson, 2004). The axes were characterized by the squared canonical correlations δ^2 .

In order to identify metabolites that are responsible for groupings observed in constrained ordination, the correlation of the metabolites with the first two canonical axes was calculated and the metabolites were plotted as vectors in a loading plot, superimposing the constrained score plot. Correlations of the MSTs with the CAP axes were considered significant if the Pearson's correlation coefficient with canonical axis 1 or canonical axis 2 exceeded a critical value (only absolute values were considered). The critical value for the correlation coefficient was calculated by performing a 2-tailed t-test with a given significance level and $(n-2)$ degrees of freedom (n being the number of samples). Only vectors with a correlation coefficient above the critical value were plotted. In cases of low critical values and a high number of significant metabolites, a predefined number of highest correlated metabolites was chosen.

As distance measure, I chose the Bray-Curtis distance. The data was transformed by standardization via $\log_{10}(x+1)$ to reduce the influence of highly abundant metabolites on the analysis (Kindt and Coe, 2005). In the context of exometabolomic data, the exometabolome of the two chamber-halves per cultivation chamber was pooled and each chamber was treated as one biological replicate.

In the context of endometabolomic data, each chamber-half of each co-cultivation chamber was sampled individually and treated as one biological replicate. Taking the co-cultivation set-up as an example, each co-cultivation chamber comprised one biological replicate of species A and one biological replicate of species B. Accordingly, each mono-cultivation set-up comprised two biological replicates of the same species. To account for this inherent dependency of the two chamber-halves in one cultivation chamber, I performed the canonical discriminant analysis according to a modified function written by Dr. Jens Schumacher⁴⁸ (function is documented in the digital appendix chapter 7.4).

The modified function follows the original description of Anderson & Willis as presented in the Ecological Archives E084-011-A1 (Anderson and Willis, 2003b). However, to obtain p-values for the trace statistic and the greatest root statistic δ_1^2 , the random permutations of group labels was restricted to reflect the dependency of the chamber-halves. Furthermore, the misclassification error was given as a result of a "leave-one-chamber-out cross validation". I

⁴⁸ Institute of Mathematics/Stochastics, Faculty of Mathematics and Computer Science, Friedrich-Schiller-University Jena

manually chose the number of principal coordinate axes (m) used in the canonical analysis in agreement with the recommended guidelines (Anderson and Willis, 2003a), resulting in the lowest misclassification error of the “leave-one-chamber-out cross validation”.

2.6 Interim conclusion

The interaction between the diatoms *S. costatum* and *T. weissflogii* resulted in unambiguously enhanced growth of *T. weissflogii* - as measured in cell counts - of up to 81 % (chapter 2.2.1). I could reproduce the stimulatory growth effect reliably in various independent experiments, e.g. in the medium experiment (chapter 2.3) and a second interaction experiment (data not shown) and could confirm previously documented effects (Paul et al., 2009). Interaction-induced growth stimulation of *T. weissflogii* manifested at the end of the regular growth phase, where stimulated cultures showed prolonged regular growth and higher maximum cell yields. In the interaction experiment, this effect was documented by cell counts at three different time points (**Figure 4**). These findings were complemented by the medium experiment, in which cell counts were taken more regularly and the stimulated growth is depicted in higher resolution (**Figure 20**). Thus, the interaction-induced growth stimulation of *T. weissflogii* was clearly recognizable.

Furthermore, I documented significant alterations in *S. costatum* chl a fluorescence at the beginning of the stationary phase due to the interaction (chapter 2.2.1 and 2.3). As these changes were not reflected in altered cell counts, they were not thought to indicate biomass alterations but rather modifications of the cells' physiological state (Kruskopf and Flynn, 2006).

I excluded the involvement of the prominent infochemical DMSP in the stimulatory growth effect on *T. weissflogii*, as hypothesized by Paul et al. (chapter 2.1.4) (Paul et al., 2009). Furthermore, among metadata, I observed no relevant interaction-induced alterations, with exception of the silicate availability. Diatom cultures were non-axenic, as measured via bacterial abundance (chapter 2.2.2 and 7.1.4). However, the medium experiment indicated that the bacterial community of the partner diatom is not capable of producing the observed stimulatory effect on diatom growth (chapter 2.3).

To link observed growth to the nutrient status of the cultures, nutrient samples were taken. However, in the course of the interaction experiment (chapter 2.2) the nutrient status was not recorded. Nevertheless, nutrient measurements were carried out in the medium experiment (chapter 2.3) and as the interaction experiment and medium experiment were both conducted under highly similar conditions, insights can be generalized for the interaction experiment as well. In summary, the transition from regular growth into the stationary phase coincided with nutrient limitation, preceding with silicate limitation. Interestingly, I observed an increase in silicate availability during the stationary phase in *S. costatum* mono-culture, but not in *T. weissflogii* mono-culture. I assumed that in the co-cultivation experiment, *T. weissflogii* is exposed to increased silicate availability as well. As no relevant increase of available silicate has

been documented in the co-cultivation medium, an increased uptake of silicate by *T. weissflogii* might be suggested (further discussion in chapter 5).

Interaction-induced metabolomic alterations strongly suggest a chemically-mediated interaction

In the present study, I advanced insights into the interaction specifics. Hereby, the experimental design of Paul et al. was improved by combining the elaborate small-scale co-cultivation set up with high-resolution GC-EI/MS/TOF analysis - an analytical approach that enabled library-based structure suggestions on top of unambiguous characterization of relevant MSTs, as already reported (Paul et al., 2009). Furthermore, the co-cultivation set up enabled identical growth conditions for all investigated treatment groups. An improvement, compared to the heterogeneity in culturing caused by the mixed use of glass vessel and dialysis tube environments (Paul et al., 2009). With the metabolomics approach, it was clearly possible to link physiological alterations - on the metabolomic level - to the presence of an interaction partner and thus confirm previous findings (Paul et al., 2009).

The endometabolomic analysis unraveled significant interaction-induced differences in the endometabolomes of *T. weissflogii* and *S. costatum*. Interestingly, these alterations only occurred from a certain point of the interaction onwards. I investigated the endometabolome on three distinct time points during the interaction. Thus, a more dynamic investigation of interaction-induced metabolomic alterations – compared to Paul et al. – was ensured, another strength of the present study. While Paul et al. investigated only one distinct time-point during the late phase of the interaction, the presented design offers the opportunity to assess the diatom's metabolomic state at multiple points before and during the observed growth effect.

The first sampling was done at the transition from regular growth to stationary phase (day 16), representing a reference point before the onset of the stimulatory effect. The later sampling points have been chosen to capture an early and late stage of the observed growth effect in *T. weissflogii*. The exometabolomic findings suggest that both diatom partners are able to adapt their phenotype and thus react to the presence of each other, as interaction-induced alterations of metabolite levels in the diatom's medium were observed. Furthermore, at both latter sampling points, I found significant endometabolomic alterations due to the presence of a partner, suggesting that both diatoms are able to notice each other. Similarly, it has been reported in the context of negative allelopathy that interactions between the microalga *K. brevis* and competing algae cause alterations in algal metabolism, even if only modest growth effects are observed (Poulson-Ellestad et al., 2014a).

The documented physiological alterations during late stages of the interaction between *T. weissflogii* and *S. costatum* are in agreement with previous observations (Paul et al., 2009). However, the findings that co-cultivated *T. weissflogii* cultures exhibit lower metabolite concentrations throughout all MSTs – compared to mono-cultivation – could not be confirmed (Paul et al., 2009). In the present study I documented both, increased and decreased metabolite concentrations in co-cultivation. One possible reason for observed differences might be the fact that different analytical methods were used and that GC-MS and LC-MS cover different ranges of the metabolite spectrum. Due to the inherent differences in the hyphenated MS-approaches and due to the fact that no RI data was reported by Paul et al., a direct comparison of MSTs between these methods was not possible and a comparison of results on a more detailed level was precluded. Nevertheless, the general conclusions are in agreement.

The endometabolomic alterations strongly suggested a compound transfer between the diatom partners, responsible for the observed alterations. Other than the endometabolomic alterations, which manifested on day 26 and 32, I found significant interaction-induced differences in diatom exometabolomes on day 16 and 26. Thus, already before any growth effect is observed, the chemical environment in diatom cultures is altered due to the presence of a partner. These interaction-induced exometabolomic alterations sustained until day 26, but were not found on day 32. The precedence of endometabolomic alterations with exometabolomic alterations strengthens the presumption of a chemically-mediated interaction. I hypothesized that the release and uptake of chemical compounds between the partners, as documented on day 16 and 26, entailed endometabolomic changes, as documented on day 26 and 32. I suggested several metabolites and MSTs as potential semiochemicals.

Metabolite flux hypotheses at the onset of the observed growth effect

I hypothesized MSTs that were correlating with the onset of the observed growth effect (day 16) to trigger the observed growth stimulatory effect. On day 16, pattern - I - metabolites strongly suggest heightened metabolite exudation as response to the presence of a partner. This effect was found for 26 MSTs, nine metabolites were identified. The fatty acids myristic acid (#111), pentadecanoic acid (#113, #117), palmitoleic acid (#122, #123), oleic acid (#132) and nonanoic acid (#48), as well as the carboxylic acids 4-hydroxybutanoic acid (#33), putative 2-hydroxypentanoic acid (#40) and putative 2-methylbenzoic acid (#50) and the putative alkaloid 2-hexylpyridine (#51). Another 15 MSTs⁴⁹ remained unidentified.

⁴⁹ #44, #49, #58, #60, #65, #71, #85, #91, #93, #101, #109, #110, #128, #133, #138

The fatty acids myristic acid (#111), palmitoleic acid (#122, #123) and oleic acid (#132) have been previously found in the cells of *T. weissflogii* and *S. costatum* (John et al., 2001), the latter being more abundant in *T. weissflogii*, than in *S. costatum* (John et al., 2001).

The metabolomic analysis shows that a substantial amount of these correlating metabolites was hypothesized to be involved in a release-uptake mechanism. Namely, putative 2-hydroxypentanoic acid (#40), putative alkaloid 2-hexylpyridine (#51), myristic acid (#111), pentadecanoic acid (#117), palmitoleic acid (#122, #123), oleic acid (#132) and nine MSTs⁵⁰. The observation of increased abundance in co-cultivation on day 16 (pattern I) and subsequent reduced abundance on day 26 (pattern II / III) suggested interaction-induced release and subsequent uptake of these compounds by the partner.

Among metabolites exhibiting pattern II / III on day 16, two were of relevance. The carboxylic acid succinic acid (#41) was present in the exometabolome of both diatoms during early stages of the interaction (day 16 and 26), but completely absent in co-cultivation on day 16. Thus, either an increased uptake, transformation or reduced exudation due to the interaction on day 16 were suggested. Interestingly, on day 26 succinic acid (#41) was most abundant in co-cultivation – exhibiting pattern I – compared to both mono-cultivations. The reverse of intensity patterns (from pattern II / III to pattern I) between day 16 and 26, might stress the relevance of succinic acid (#41) at the onset of the interaction, potentially mediating the interaction.

The terpenoid dehydroabietic acid (#135) exhibited reduced abundance in co-cultivation over all three sampling days. As dehydroabietic acid was considerably more abundant in mono-cultivated *T. weissflogii* and close to absent in the medium of mono-cultivated *S. costatum*, it was thought to originate from *T. weissflogii*. It was hypothesized to be constantly taken up by *S. costatum* in the interaction. Alternatively, the secretion of dehydroabietic acid by *T. weissflogii* might have been inhibited in the interaction with *S. marinoi*. As discussed in chapter 5, dehydroabietic acid has previously been known from the aquatic environment.

On day 26, five unidentified metabolites were potentially involved in a reduced release / uptake or transformation mechanisms and on day 32, the amine 2,2'-iminodiethanol (#37), the alkaloid 3-pyridinol (#11), a terpenoid similar to lumichrome (#45) and an unidentified MST #114. This dynamic characterized not only the onset of the growth effect, but also the effect during the late stationary phase of growth.

⁵⁰ #44, #58, #60, #65, #71, #93, #128, #133, #138

Metabolite flux hypotheses during the phase of pronounced growth effect

I hypothesized metabolites correlating with the phase of pronounced growth effect, as represented by day 26, to be responsible for sustaining the stimulatory growth (chapter 2.2.3). On day 26, five MSTs⁵¹ were characterized with pattern I. They were all hardly present on day 16 and more characteristic for later growth phases. Neither MST could be allocated to only one of the diatoms, as all MSTs were found in the medium of both mono-cultured diatoms. However, in co-cultivation the secretion of these compounds was increased.

Additionally, five MSTs⁵² were taken up or metabolized on day 26, including two compounds (#104, #107) that have previously been found in the medium of *S. marinoi* (Vidoudez, 2010; Vidoudez and Pohnert, 2011). They predominantly shaped the chemical environment of *S. costatum*, although they were present in the one of *T. weissflogii* as well. The remaining MSTs were more abundant in the medium of *T. weissflogii* on day 26, therefore it can be hypothesized that they were exuded by this diatom and taken up or metabolized by *S. costatum*.

Unfortunately, in the exometabolomic analyses, only a small subset of MSTs could be identified. Identification was impeded by the very low abundance of relevant MSTs, which affected the mass spectral quality and thus goodness of library-spectrum fit. Also, if MSTs represented novel compounds, no library-spectra would be available and MSTs would remain 'unknown'. Zamboni et al. pointed out that the structure elucidation of MSTs is the biggest challenge in metabolomics (Zamboni, Saghatelian and Patti, 2015). Nevertheless, all MSTs were unambiguously characterized via *m/z*, RT and RI.

Paul et al. hypothesized release-uptake-mechanisms based on the observation of *inter alia* nine further unidentified pattern - II / III - MSTs as well (Paul et al., 2009). Hereby, eight out of nine MSTs originated from *S. costatum*. While Paul et al. observed distinct exometabolomic alterations on day 38 – a late stage of the interaction – the present study connects distinct exometabolomic changes with early stages of the interaction. No significant interaction-induced alterations in the diatom's exometabolome were found on day 32 (representing the latest sampling point). In summary, both studies agree on interaction-induced exometabolomic alterations and suggest release-uptake or metabolization mechanisms between the diatoms. The fact that both studies differ in the temporal placement of the interaction-induced metabolomic alterations might be simply caused by slightly varying experimental specifics and is not thought to question the conclusion.

⁵¹ #62, #63, #77, #92, #96

⁵² #1, #95, #104, #107, #126

Discussion of metabolite flux between the diatom partners

The introduced abundance patterns represent a simplified mean to unravel metabolite flux between both diatom partners. Simplification is essential to generate testable hypotheses, however at the same time, over-generalization is a major pitfall in metabolomic analyses (Zamboni et al., 2015). Therefore, when interpreting exometabolomic findings, some aspects need to be taken into consideration.

The influence of increased biomass on the chemical diatom environment

Due to the fact that the exometabolome was not normalized to cell counts, cell count differences between treatments need to be taken into account in the interpretation of exometabolite patterns. I hypothesized pattern - I - metabolites to be increasingly exuded due to the interaction, while I hypothesized pattern - II / III - metabolites to be either taken up, reduced in secretion or metabolized. However, increased cell counts in co-cultivation weaken the interpretation of pattern I - metabolites and strengthen the interpretation of pattern -II / III - metabolites.

For example, increased MST abundance in co-cultivation (pattern I) is suggested to result from interaction-induced, increased exudation. This will be reasonable, if diatom biomass in all treatments is comparable. However, increased MST abundance will merely reflect increased biomass, if co-cultivation exhibits increased cell counts compared to other treatments. This scenario occurred at sampling points 26 and 32, due to stimulated growth of *T. weissflogii*.

The opposite is the case for pattern II and III. Both patterns indicate interaction-induced uptake, metabolization or reduced exudation of exometabolites. These patterns are characterized by reduced MST abundance in co-cultivation. In a context where diatom biomass increases in co-cultivation, the occurrence of pattern II and III is clearly an opposing trend. Thus, the expressiveness of the suggested interpretation for pattern II and III is further strengthened.

On day 16, cell count differences between mono- and co-cultivation were existent, but compared to later sampling points rather small (*T. weissflogii* +15 %, *S. costatum* +21 %⁵³). Therefore, the reliability of pattern I metabolites is still given. However, on day 26 the interpretation of pattern I is more error-prone, as diatom cell counts in co-cultivation were substantially increased compared to mono-cultivations. Meaning that pattern I might simply be caused by increased biomass.

⁵³ Co-cultivation relative to mono-cultivation

Limitations of abundance patterns I, II and III and their impact on hypothesized release-uptake mechanisms

Firstly, the defined patterns (I – III) reflect extreme and clear-cut examples among MST abundance patterns. They set a deliberate, artificial threshold and discriminate against less distinct marginal cases with a higher error-proneness. Thus, I reduced the complexity of the screening process and all metabolites matching the defined intensity patterns of interest were considered candidate molecules, potentially driving the interaction. However, although this approach enables a high-throughput workflow, it might miss out on potential semiochemicals.

Secondly, the pattern-based exometabolomic analysis via fingerprinting techniques is blind for exometabolomic alterations, which manifest themselves in altered metabolite flux with concurrent unaltered absolute metabolite intensities ((Chokkathukalam et al., 2014) and references herein). For example, if at the same time a metabolite is increasingly secreted by one diatom and increasingly taken up by the other diatom, this dynamic will possibly be reported to not be relevantly altered due to the interaction. This is caused by the fact that the multivariate statistical analysis as well as the pattern-based analysis of exometabolites are based on absolute metabolite levels and are unable to detect metabolite flux alterations.

Thirdly, patterns II and III should not only be interpreted as increased uptake of an exometabolite, but also as a decrease in metabolite secretion due to the interaction or potential transformation. All processes result in decreased abundance of a metabolite in the medium of the interaction set-up. As a consequence, hypothesized release-uptake mechanisms could possibly have alternative explanations as well. For simplification purposes, the possibility of metabolite transformation will implicitly be included in the release-uptake nomenclature and not specifically mentioned at every occasion.

To get more insights into the dynamics behind observed exometabolomic alterations and to address some of the mentioned limitations, I recommend the labeling of an organism's endometabolome – e.g. via ^{13}C (Chokkathukalam et al., 2014). This labeling approach is termed metabolomic flux analysis (Zamboni et al., 2015), or – in the context of exometabolomic analyses – metabolic foot printing (Weber et al., 2013) and has been suggested by Paul et al. as well (Paul et al., 2009).

Taking the interaction between *S. costatum* and *T. weissflogii* as an example, in the context of exometabolomics, this means that a labeled *S. costatum* culture is brought into interaction with an unlabeled *T. weissflogii* culture. Labeling is achieved by culturing a photosynthetic organism like *S. costatum* using stable-isotope labeled inorganic nutrients. Thus, the endometabolome of

the diatom is gradually labeled with a stable-isotope. If only one of the partners is labeled, any labeled metabolite found in the medium of the set-up can be clearly assigned to origin from *S. costatum*. Furthermore, if any labeled compounds are found in the endometabolome of *T. weissflogii*, a release-uptake dynamic between both partners is confirmed. By labeling both diatom partners subsequently, a comprehensive insight into interaction dynamics can be gained. However, considering the long duration of the interaction experiments, keeping up high labeling degrees of one diatom's endometabolome during the course of the investigation can be a challenge.

Involvement of third party organisms in the interaction

As previously stated, the used diatom cultures were non – axenic. Multiple interactions between diatoms and bacteria have been documented, involving chemical signaling ((Cole, 1982; Grossart and Simon, 2007; Amin et al., 2012, 2015; Limardo and Worden, 2015), compare chapter 2.1.3). It is therefore possible that bacteria, associated to the diatom partner, cause the observed growth effect, instead of the diatom partner itself. To test this hypothesis, I conducted two medium experiments, clearly stating that the presence of *S. costatum* is necessary to stimulate the growth of *T. weissflogii* in the interaction (chapter 2.3). Thereby, I answered one of the questions posed in the study of Paul et al. (Paul et al., 2009). However, the participation of bacteria as third party organisms, e.g. via the modification or degradation of exuded metabolites, cannot be excluded (Borowitzka, 2016).

In the context of the medium experiments (see chapter 2.3) it might be objected that during the centrifugation step, aiming at separating diatom cells from the surrounding medium, bacterial cells sedimented along with diatom cells. Thus, the modified culture in the medium exchange group would be expected to exhibit increased bacterial abundance due to the fact that the bacterial community introduced via the medium added to the bacterial community retained alongside the diatom cells. However, the comparison of bacterial cell count data between both chamber halves of the medium exchange group (data not shown) did not indicate relevant differences at the first sampling point after the onset of the experiment.

To conclude, this subchapter summarized the findings of the interaction-investigation between *T. weissflogii* and *S. costatum* and discussed several aspects, which need to be taken into account during hypotheses-generation. I will present a general conclusion to all interaction experiments in chapter 5.

3 Interaction of *T. weissflogii* with *S. marinoi*

I based the first interaction experiments on the diatom strains used by Paul et al., which were not available in an axenic state (chapter 2.2 - 2.3; (Paul et al., 2009)). However, I aspired axenic cultures to reduce the interaction system to the presence of only two diatom partners. Therefore, I obtained new axenic strains from the National Center for Marine Algae and Microbiota (NCMA). Among multiple axenic *T. weissflogii* strains – available in the NCMA – I chose the one that was reported to be identical with the non-axenic RCC76 strain. As the species concept of *S. costatum* has been revoked, I used axenic strains of *S. marinoi* and *S. dohrnii* (formerly *S. costatum* (Sarno et al., 2005)) as substitutes. Both have been collected at sites, which exhibit close proximity to the collection site of *T. weissflogii*⁵⁴.

Subsequently, I present the results of the interaction investigation between *T. weissflogii* and *S. marinoi* as well as between *T. weissflogii* and *S. dohrnii* (chapter 4). I designed these investigations in the context of an explorative approach to supplement the insights of the primarily conducted interaction experiment between *T. weissflogii* and *S. costatum*.

3.1 Experimental design

I based the interaction experiment between *T. weissflogii* (CCMP 1336) and *S. marinoi* (CCMP 1332) on the experimental design and the general strategy described for the interaction experiment with *T. weissflogii* and *S. costatum* (more details in chapters 2.1.1 and 2.1.2). Experimental specifics are documented in chapter 6.2.7.

The metabolomic samples in the interaction investigation of *T. weissflogii* and *S. marinoi* (as well as in the interaction investigation of *T. weissflogii* and *S. dohrnii*, chapter 4) were normalized to higher cell counts, compared to the previously described interaction (**Table 22**). As a consequence, I observed an overload among a subset of peaks – representing the most abundant MSTs – in the corresponding mass spectra. As these MSTs might have been integrated via masses that are not in the linear range due to overloading, the quantification might have been impaired. Nevertheless, I chose this strategy with the aim to focus on potential infochemicals, which usually occur in rather low abundances (discussion in chapter 2.5.3).

⁵⁴ *S. dohrnii* (CCMP3373) was isolated from Narragansett Bay, Rhode Island, USA, *S. marinoi* (CCMP1332) from Milford, Connecticut, USA, *T. weissflogii* from Gardiners Island, Long Island, New York. The former *S. costatum* (RCC76) was of unknown origin, but was reported to form blooms in Narragansett Bay (Borkman and Smayda, 2009)

3.2 Results

3.2.1 Diatom growth

Growth of *S. marinoi* was significantly enhanced due to the interaction with *T. weissflogii*. Compared to the negative control, cell counts in co-cultivation were increased up to 41 % and chl a fluorescence up to 31 % (day 42). Considering growth parameters of *T. weissflogii*, no consistent and distinct long-term trend of increase or decrease was observed. Statistically, significant differences in chl a fluorescence and cell counts corresponded to rather short term variations.

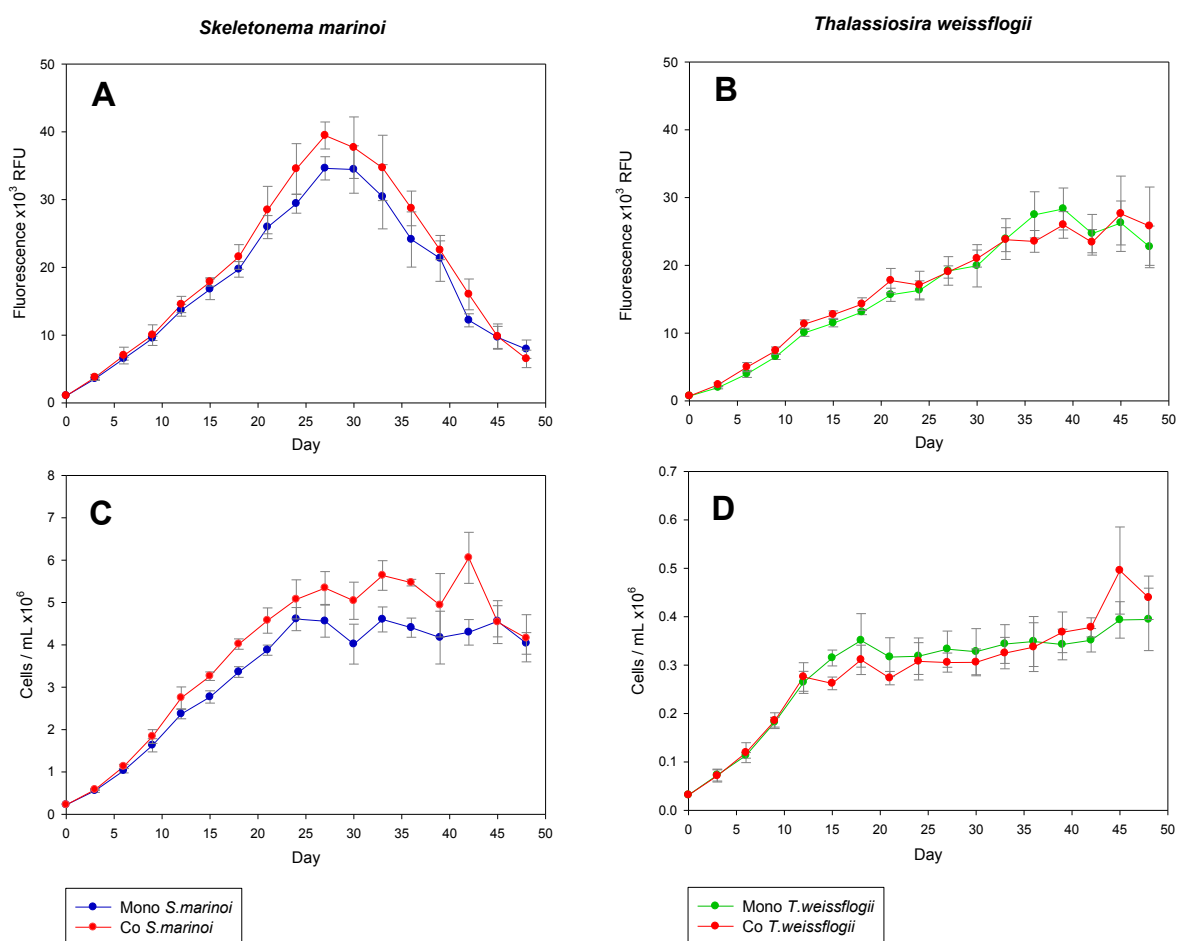


Figure 27: Diatom growth in the interaction experiment of *T. weissflogii* and *S. marinoi*.

Graphs **A** and **B** show means of chl a (RFU: relative fluorescence units), graphs **C** and **D** represent the cell counts (cells / mL). The results for *S. marinoi* are shown on the left, the results for *T. weissflogii* on the right. The treatment groups are indicated by color: mono-cultivation of *S. marinoi* (blue, control), mono-cultivation of *T. weissflogii* (green, control) and the co-cultivation of each species (red, interaction). Values are arithmetic means, error bars indicate standard deviation between biological replicates (mono-cultivation $n = 4$, co-cultivation $n = 4$). Notice different scaling.

Within each species, I used linear mixed models to test for significant differences between mono-cultivation and co-cultivation over time. More details on the chosen models, graphs and evaluation can be found in the appendix (**Appendix 30 - Appendix 35**).

S. marinoi

Linear mixed modeling showed a statistically significant difference in the development of chl a fluorescence ($F(16,96) = 4.2354, P \leq 0.0001$) and cell counts ($F(16,96) = 4.997, P \leq 0.0001$) in treatments over time.

In general, the growth curve – based on diatom cell counts (**Figure 27C**) – indicated a phase of regular growth until day 24, followed by a phase of stationary growth. While in mono-cultivation this phase lasted until the end of the experiment, in co-cultivation a declining phase was observed between day 42 and 48.

Comparing mono- and co-cultivation, I observed a clear trend of elevated cell densities in co-cultivation between day three and day 42 (**Figure 27C**). I found the largest difference between the treatments on day 42, with 41 % increased cell-counts in co-cultivation. Starting from initial cell counts of 2.2×10^5 cells / mL, maximum densities of $4.6 \times 10^6 \pm 0.3 \times 10^6$ cells / mL were reached in mono-cultivation on day 24 and $6.05 \times 10^6 \pm 0.6 \times 10^6$ cells / mL in co-cultivation on day 42. Relative to mono-cultivation, the maximum cell density in co-cultivation was elevated by 31 %. In general, the differences in cell counts were established during regular growth phase and maintained in stationary phase of growth.

Chl a fluorescence of *S. marinoi* exhibited an increase-decrease dynamic over time. Similar to the findings in cell counts, fluorescence was increased in co-cultivation, compared to mono-cultivation (**Figure 27A**). Starting with 1052 RFU, the fluorescence increased until reaching maximum values of $3.5 \times 10^4 \pm 1713$ RFU in mono-cultivation and $4 \times 10^4 \pm 1991$ RFU in co-cultivation on day 27. This corresponded to a 14 % increase in co-cultivation compared to mono-cultivation on day 27. The difference in chl a fluorescence was largest on day 42, with 31 % higher fluorescence in co-cultivation. While chl a fluorescence is hypothesized to correlate to diatom biomass until day 27, the subsequent decrease in chl a fluorescence during the stationary phase – which was not reflected in cell counts – was thought to be caused by physiological alterations in the diatom cells.

Both chl a fluorescence and cell counts indicated significantly enhanced growth in *S. marinoi* due to the interaction with *T. weissflogii*.

T. weissflogii

The linear mixed model approach showed a significantly different development of chl a fluorescence ($F(16,96) = 2.6128$, $P = 0.002$) and cell counts ($F(16,96) = 3.5408$, $P = 0.0001$) in mono- and co-cultivation over time. However, a visual evaluation of the parameter curves (**Figure 27B, D**) lacks meaningful differences between the treatments.

Figure 27D depicts the growth curve of *T. weissflogii*, starting with 3.2×10^4 cells / mL at the onset of the experiment. The cultures grew regularly until day 12, before entering a stationary phase of growth, which lasted until the end of the experiment. During stationary growth phase, average cell numbers of $3.45 \times 10^5 \pm 0.3 \times 10^5$ cells / mL were reached in mono-cultivation and $3.42 \times 10^5 \pm 0.7 \times 10^5$ cells / mL in co-cultivation.

Comparing mono- and co-cultivated *T. weissflogii*, the development of cell counts over time was very similar. In regular growth phase, the differences between mono- and co-cultivation were less than 5 % (co-cultivation relative to mono-cultivation of each day). Between day 15 and 36, cell numbers were slightly lower in co-cultivation, with a maximum reduction of 17 % on day 15 and an average difference of 8.6 ± 5 %. However, cell numbers in co-cultivation slightly increased between day 39 and 48 to reach maximum enhancement of 26 % on day 45 and an average increase of 13.1 ± 9 %. Over the course of the experiment, the average difference between the cell counts of mono- and co-cultivation was 7.9 ± 6 % (relative to mono-cultivation throughout all differences).

Chl a fluorescence started at 700 RFU and subsequently increased until reaching maximum values of 28321 ± 3093 RFU in mono-cultivation on day 39 and values of 27606 ± 5554 RFU in co-cultivation on day 45 (**Figure 27B**). The difference between mono- and co-cultivation was largest on day six with 25 % higher fluorescence in co-cultivation. However, over the course of the experiment the average difference between the treatments (relative to mono-cultivation over all differences) was 9.7 ± 7 %.

In general, I found no long-term trend of increase or decrease of chl a fluorescence and cell counts in co-cultivation, compared to mono-cultivation. I found statistically significant differences between the treatments in the development of both parameters over time. However, due to lacking persistency, comparably large standard deviations (error bars in **Figure 27B, D**) and average differences ≤ 10 %, I considered these differences biologically irrelevant.

3.2.2 Metadata

I used the metadata to describe the biotic and abiotic state of the interaction. The PSII efficiency of both diatom species showed comparable absolute values and temporal dynamics. All cultures experienced nutrient depletion between day 15 and day 24, correlating with the end of regular and beginning of stationary growth phase. The bacterial abundance in *S. marinoi* was less than the abundance of diatom cells, while bacterial numbers in *T. weissflogii* exceeded diatom cell counts. In general, I observed no distinct differences between co- and mono-cultivation in parameter dynamics over time.

PSII efficiency

S. marinoi started with a PSII efficiency of 37 %, while *T. weissflogii* started with an efficiency of 44 %. Within each species, the treatments showed a very similar temporal dynamic and no obvious differences between mono- and co-cultivation were observed (**Figure 28**). In general, the PSII efficiency remained almost stable until day 18, exhibiting average values of 34 ± 4 % in *S. marinoi* and 41 ± 4 % in *T. weissflogii*. Subsequently, the PSII efficiency declined until *T. weissflogii* reached values close to zero around day 39 and *S. marinoi* reached a local minimum on day 42 exhibiting an efficiency ≤ 4 %.

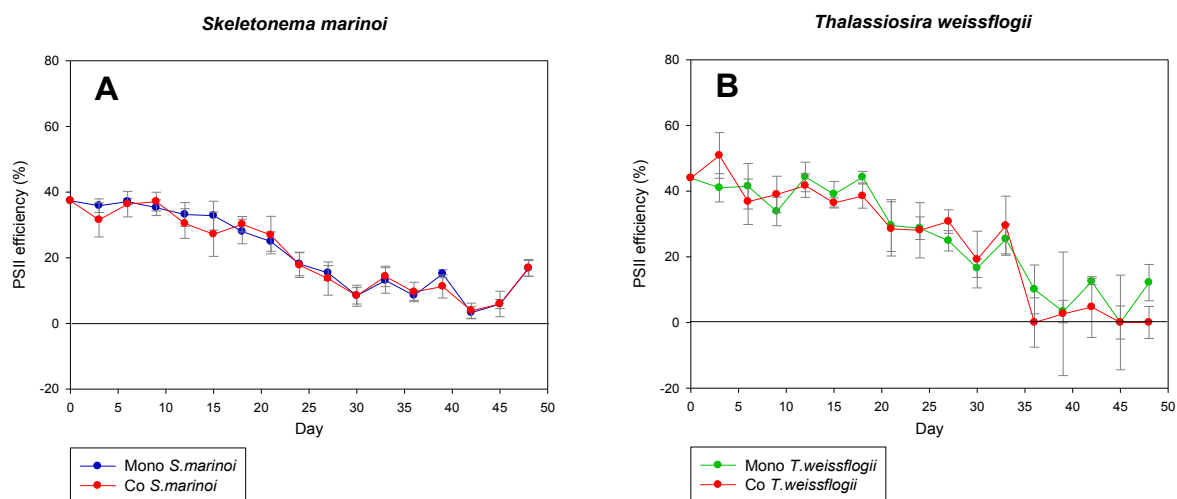


Figure 28: PSII efficiency of the diatoms in the interaction experiment of *T. weissflogii* with *S. marinoi*. The figure shows means of PSII efficiency (%) of *S. marinoi* (graph A) and *T. weissflogii* (graph B), comparing mono-cultivation in green (Mono *T. weissflogii*) and blue (Mono *S. marinoi*) to co-cultivation of the particular diatom in red. Error bars indicate standard deviation between biological replicates (mono-cultivation n = 4, co-cultivation n = 4).

Bacterial abundance

The diatom strains *T. weissflogii* (CCMP1336) and *S. marinoi* (CCMP1332) were axenic when ordered. However, it was not possible to maintain the axenic state and bacteria became present

in all diatom cultures (**Figure 29**). This problem has been reported by other researchers as well ((Vidoudez and Pohnert, 2011), (Borowitzka, 2016) and references herein). Although axenic cultures are desired in the investigation of chemically-mediated interactions, the close association between bacteria and diatoms reflects natural conditions (Borowitzka, 2016).

At the onset of the experiment, bacterial numbers were lower than diatom cell numbers (only 3 - 42 % of diatom cell counts) in all treatments. While bacterial numbers remained smaller than diatom numbers in *S. marinoi* (with exception of day nine and mono-cultivation on day 30), bacterial numbers exceeded diatom numbers up to 32 - fold (day 21) in *T. weissflogii*.

In general, bacterial numbers seemed to increase in the middle of the interaction experiment (day nine to day 30), reaching maximum numbers of up to 1×10^7 cells / mL (mono-cultivation *T. weissflogii*, day 30) with subsequent decrease towards day 48.

The medium control exhibited considerable bacterial numbers, indicating a possible contamination. However, the medium control group was only represented by one biological replicate and as the bacterial numbers sometimes exceeded the ones measured in diatom cultures, a specific contamination in the medium control group was suspected.

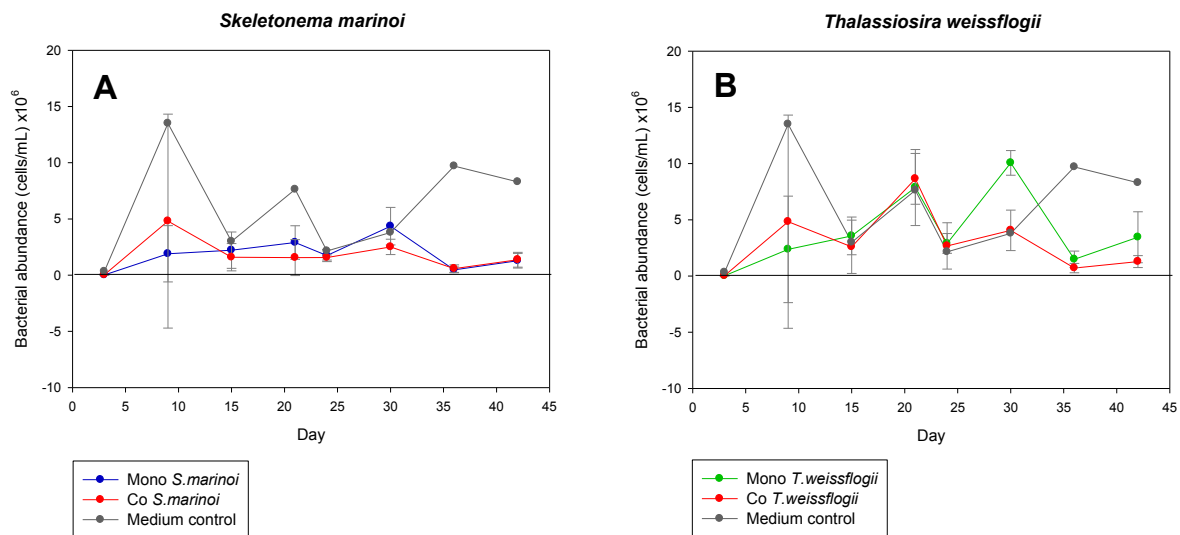


Figure 29: Bacterial abundance in the medium experiment of *T. weissflogii* with *S. marinoi*.

The figure shows means of bacterial abundance (cells / mL) in the cultures of *S. marinoi* (graph A) and *T. weissflogii* (graph B), comparing mono-cultivation in green (Mono *T. weissflogii*) and blue (Mono *S. marinoi*) to co-cultivation of the particular diatom in red. Values for the medium control are represented in grey. Error bars indicate standard deviation between biological replicates (n = 4, medium control: n = 1).

Nutrient levels

In the context of the nutrient analysis, I investigated silicate, nitrate, phosphate and nitrite levels. Diatom cultures became depleted of nitrate, phosphate and silicate between day 15 and day 24 (**Figure 30**). These points in time were correlating with the end of regular growth phase and the

early stationary phase. More specifically, nitrate and phosphate concentration was $\leq 4 \mu\text{M}$ in all treatments on day 24 and silicate concentration was $\leq 6 \mu\text{M}$. The nitrite concentrations increased until reaching maximum values on day 15, followed by a subsequent decrease towards day 24.

While I observed no distinct differences in nitrate, phosphate and silicate levels between the treatments, nitrite levels were highest in mono-cultivated *T. weissflogii* (maximum of $9 \mu\text{M}$ on day 15) and lowest in mono-cultivated *S. marinoi* (maximum of $2 \mu\text{M}$ on day 15). The nitrite concentration in co-cultivation was an average of both mono-cultivations on day 15 ($5 \mu\text{M}$).

The nutrient concentrations of the medium control matched the expected values present in the artificial seawater medium.

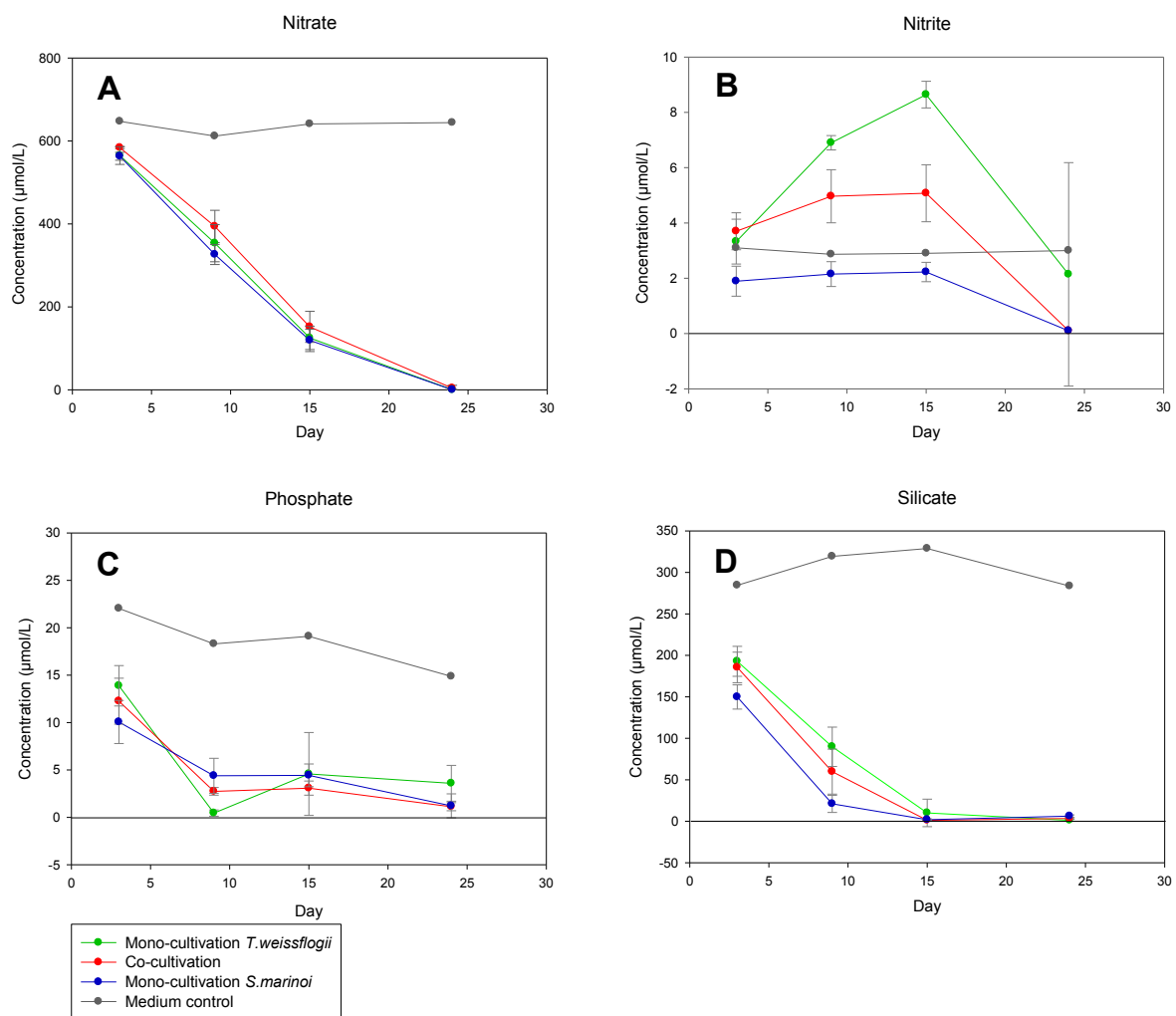


Figure 30: Nutrient levels in the medium experiment of *T. weissflogii* with *S. marinoi*.

The figure shows means of nitrate (A), nitrite (B), phosphate (C) and silicate (D) concentration (μM). Mono-cultivation of *T. weissflogii* is depicted in green, mono-cultivation of *S. marinoi* in blue and co-cultivation is colored in red. Values for the medium control are represented in grey. Error bars indicate standard deviation between biological replicates ($n = 4$, medium control: $n = 1$).

3.2.3 Exometabolomic investigation

In summary, significant differences in the exometabolomes of *S. marinoi* and *T. weissflogii* due to time, treatments and treatment per time were statistically confirmed. A daywise analysis indicated that the treatments (mono-cultivation of each species and co-cultivation) significantly differed from each other on day 18, 30 and 42. As demonstrated by the misclassification errors, exometabolomic differences between the treatments were more distinct during later stages of diatom growth. The exometabolome of the co-cultivation group exhibited similar traits as the exometabolome of mono-cultivated *S. marinoi*.

In general, 66 MSTs were potentially part of interaction-induced release mechanisms. Most of these MSTs were correlating with day 42 and thus late stages of the interaction. A multitude of metabolite classes were involved and some metabolites were characterized by distinct temporal intensity dynamics.

Among metabolites that were correlating with early stages of the interaction, the following were of special relevance: Gluconic acid (#206), gluconic acid 1,5-lactone (#180) and three unknown metabolites (#119, #132, #210) were upregulated in co-cultivation during the late regular growth phase. Additionally, putative 7-tetradecanol (#103, #104) and MST (#205) were upregulated in co-cultivation and might have been released by *S. marinoi* due to the interaction.

Metabolites that were upregulated during the stationary phase of growth (day 30) comprised *inter alia* putative 2-(4-methyl-1-piperazinyl)ethanol (#53), hydroquinone (#73), 4-hydroxybenzaldehyde (#99), putative uridine (#275), putative adenosine (#299, #300), putative maltose (#304), uridine (#270), guanosine (#311) and further unknown metabolites. The majority of all candidate metabolites with enhanced abundance in co-cultivation was correlating with day 42, a time point long after the observed interaction-induced growth effect.

In the context of interaction-induced uptake, transformation or reduced release mechanisms, six metabolites were of relevance, including two unknown metabolites (#162, #193), maltotriose (#339), 2-phenoxyethanol (#66), galactosylglycerol (#251) and the sterol putative 3,18-bis(acetyloxy)-14,15-epoxy-pregn-16-en-20-one (#306). It is hypothesized that the sterol #306 and the unknown MST #193 originated from the exometabolome of *S. marinoi*.

The discussion of metabolite flux between the diatom partners will be given in chapter 5.

Data exploration via CAP

Overall Analysis

I conducted the CAP on the basis of 342 MSTs, which I obtained after data pre-processing of 35 exometabolomic samples from the interaction of *T. weissflogii* and *S. marinoi*. The first explorative data analysis indicated a strong influence of time on diatom exometabolomes, as well as similarities between the *S. marinoi* mono-cultivation and co-cultivation group within each sampling day. The exometabolomes of *T. weissflogii* and *S. marinoi* were distinctly different from each other.

The PCoA score plot (**Appendix 36**) indicates a gradual separation of samples according to sampling days by principal coordinate axis 1 and a tendency of separation between treatments via principal coordinate axis 2. In the unconstrained analysis, mono-cultivated *S. marinoi* and mono-cultivated *T. weissflogii* were clearly separated by principal coordinate axis 2. While mono-cultivated *T. weissflogii* formed a distinct group on day 42 (quadrant III), samples from day 30 and 18 were mixed and thus very similar (quadrant II). Samples from mono-cultivated *S. marinoi* were clustered in three distinct sample groups according to the three sampling days, separated by principal coordinate axis 1. Co-cultivation samples formed distinct groups according to day 18, 30 and 42, but showed close proximity to mono-cultivated *S. marinoi* within each sampling day. While on day 18 and 30 both treatments were separable by a combination of axes 1 and 2, on day 42 they formed a homogenous sample group.

The strong influence of time on diatom exometabolomes was supported by the CDA. Not only did the trace statistic confirm significant differences between the exometabolomes on day 18, 30 and 42 (**Table 11**), but also did the misclassification error of 0 % confirm a strong classification. Considering the time-independent influence of treatment on exometabolomic dissimilarities, significant differences were found throughout all three sampling days (trace statistic: $P = 0.0001$). However, the misclassification error was highest with a-priori grouping by treatment (34.29 %, **Table 11**). This misclassification error was caused by the previously observed strong similarities between co-cultivation and *S. marinoi* mono-cultivation, as confirmed by the cross validation results (**Appendix 37**).

If I considered time in addition to treatment (a-priori grouping by treatment per day), the classification was more successful (misclassification error 8.57 %). In the cross validation process (**Appendix 38**), treatments formed very distinct groups on day 30 and 42 with a reallocation success of 100 %. On day 18, *T. weissflogii* mono-cultivation and co-cultivation were very distinct groups as well. The misclassification error of 8.57 % was caused by mono-

cultivated *S. marinoi*, as three out of four samples were wrongly reallocated to co-cultivation on day 18 and 30.

In general, the overall analysis indicated that treatments significantly influence diatom exometabolomes. However, if I considered time as a factor as well, these differences were stronger during later stages of the interaction (day 38 and 42). For the identification of relevant exometabolites, both a-priori grouping by treatment and treatment per day was considered. To annihilate the strong influence of time in the CAP analysis, I performed subset analyses within each sampling day.

Table 11: Permutation and cross-validation test results for the CAP analysis of different a-priori groups in the exometabolome analysis of the interaction between *S. marinoi* and *T. weissflogii*

A-priori grouping by	m	Groups	Trace statistic	δ_1^2	Misclassification error (%)
Day	3	3	1.808 (P = 0.0001)	0.971 (P = 0.0001)	0
Treatment	3	3	0.808 (P = 0.0001)	0.808 (P = 0.0001)	34.29
Day & treatment	4	9	3.713 (P = 0.0001)	0.990 (P = 0.0001)	8.57
<u>Subset I: day 18</u> treatment	5	3	1.396 (P = 0.035)	0.987 (P = 0.0005)	33.33
<u>Subset II: day 30</u> treatment	2	3	1.308 (P = 0.0001)	0.994 (P = 0.0001)	0
<u>Subset III: day 42</u> treatment	1	1	0.921 (P = 0.0002)	0.921 (P = 0.0002)	8.33

δ_1^2 being the first squared canonical correlation. *m* represents the number of PCoA axes included in the CAP.

Subset analysis per day

The statistical diagnostics confirm significant differences between the treatments during all three sampling days (**Table 11**). As misclassification errors were lowest on day 30 and 42, the exometabolomic differences between the treatments were more distinct on later phases of diatom growth. These findings are also visible in the PCoA score plot (**Appendix 40**) and in agreement with the results of the overall analysis.

The unconstrained analysis showed clear grouping of the treatments on day 30 and 42. On day 30, principal coordinate axis 1 separated *T. weissflogii* mono-cultivation and axis 2 separated *S. marinoi* mono-cultivation from co-cultivation (**Appendix 40B**). However, as axis 1 explained 68.72 % of the data variance and axis 2 only 12.26 %, previous findings were confirmed as the exometabolomes of mono-cultivated *S. marinoi* and co-cultivated species shared common traits and exhibited close proximity in multivariate space. On day 42, principal coordinate axis 1 was sufficient to separate the three treatments (**Appendix 40C**). Again, co-cultivation and *S. marinoi*

mono-cultivation exhibited close proximity in multivariate space. On day 18, these two treatments were inseparable by principal coordinate axis 1 and 2. However, *T. weissflogii* mono-cultivation was distinctly separated by principal coordinate axis 1 (**Appendix 40A**).

Identification of exometabolites correlating with relevant a-priori groups

Overall Analysis

In the overall analysis, I further investigated a-priori grouping by treatment and treatment per day. The constrained score plot of the CDA with a-priori grouping by treatment (**Figure 31A**) shows the separation of mono-cultivated *T. weissflogii* from the other treatments by canonical axis 1. *S. marinoi* mono-cultivation and co-cultivation samples shared close proximity and were located in quadrant III and IV. As the eigenvalue of canonical axis 2 was very low (value of 0.023), the separation of samples by this axis did not exhibit strong explanatory power compared to axis 1.

The corresponding loading plot (**Figure 31B**) indicates that the majority of highly correlated MSTs ($|r| \geq 0.6100$, $P \leq 0.0001$) were characteristic for *S. marinoi* mono-cultivation and / or co-cultivation, as they were located in quadrant III and IV. A clear affiliation of MST vectors to treatment groups was difficult, as co-cultivation and *S. marinoi* mono-cultivation samples did not form distinct groups in the score plot (**Figure 31A**). However, I speculated that 7 - tetradecanol (#103 and #104) was characteristic for co-cultivation. An evaluation of the heatmap (**Table 12**) clarified that 7 - tetradecanol was indeed most abundant in co-cultivation on day 18. MSTs #137 and #334 were characteristic for mono-cultivated *T. weissflogii*.

The constrained score plot of the CDA with a-priori grouping by treatment per day (**Figure 31C**) exhibits a pattern highly similar to the one described for the unconstrained analysis via PCoA. The majority of MST vectors in the corresponding loading plot (**Figure 31D**) was located in quadrant III and IV. Same applies to samples from co-cultivation and *S. marinoi* mono-cultivation on day 30 and 42. Thus, the majority of MST vectors was highly correlating with named samples.

Out of the remaining metabolites, MST #137 characterized mono-cultivated *T. weissflogii*, confirming the findings of the analysis with a-priori grouping by treatment. In general, only MSTs are depicted in the loading plot that exceeded a Pearson's correlation coefficient of $|r| \geq 0.6100$ and exhibited a significance $P \leq 0.0001$.

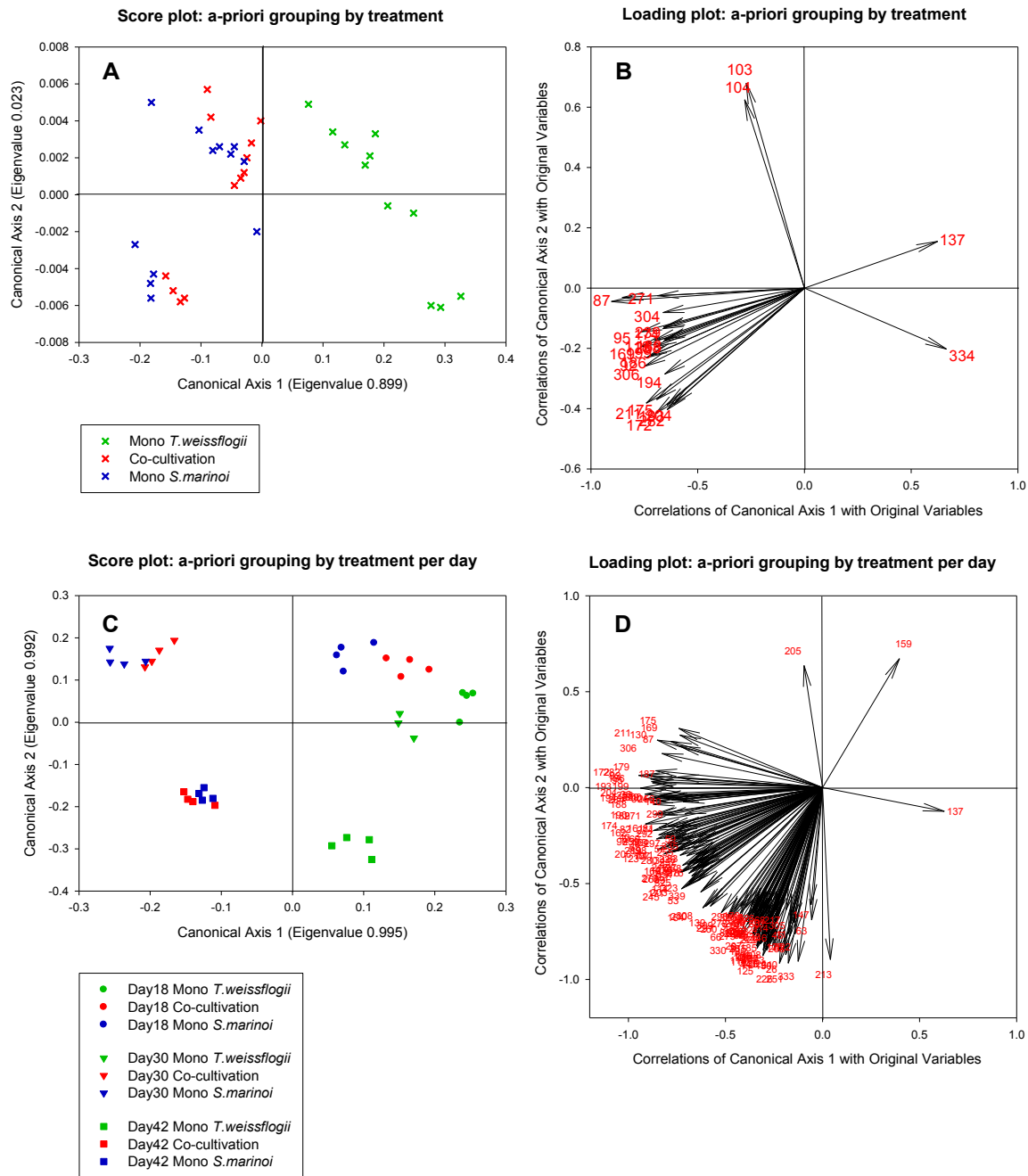


Figure 31: Constrained score and loading plots of exometabolomic samples from the overall analysis of the interaction between *T. weissflogii* and *S. marinoi*.

The constrained score plots (graph **A**, **C**) visualize significant differences between the sample groups as found via CDA with a-priori groups by treatment (trace statistic $P = 0.0001$, misclassification error of 34.29 % for $m = 3$, graph **A**) and a-priori groups by treatment per day (trace statistic $P = 0.0001$, misclassification error of 8.57 % for $m = 4$, graph **C**). Vectors in the CAP loading plots (graph **B**, **D**) represent metabolites, characterized by their ID (red numbers). Only vectors with a significant correlation coefficient above the critical value of $|r| \geq 0.6100$ ($P \leq 0.0001$) are plotted. The direction of the vectors in 2-dimensional space correlates with exometabolomic sample groupings shown in the score plots of the respective analysis.

In the corresponding heatmap (**Table 12**), Group A comprises metabolites that were most abundant in co-cultivation on day 18 (A18), day 30 (A30) or day 42 (A42). Group B summarizes metabolites that were least abundant in co-cultivation, compared to both mono-cultivations on day 18 (B18) and day 30 (B30).

In **Appendix 39**, I clustered potential biomarkers for *S. marinoi* in group Sm(1) (characteristic for day 30 and 42) and Sm(2) (characteristic for day 42), as they demonstrated highest abundance in the *S. marinoi* mono-cultivation group compared to the other treatment groups. I observed that MST intensities were more similar between *S. marinoi* mono-cultivation and co-cultivation than between each of the groups and *T. weissflogii* mono-cultivation. Thus, the similarities in the exometabolomes of *S. marinoi* mono-cultivation and co-cultivation were further strengthened. Potential biomarkers for *T. weissflogii* are represented by groups Tw(1)-(3). MST #137 in group Tw(1) was most abundant on day 18, metabolites in group Tw(2) were characteristic for day 30 and / or day 42 and those in group Tw(3) for day 42.

Table 12: Heatmap (part I) of exometabolite intensities for the overall analysis of the interaction between *T. weissflogii* and *S. marinoi*. Medians of MST intensities, normalized to the external standard ribitol (per sample) and subsequently metabolite-wise auto scaled, are represented by a color code ranging from high (yellow) to low intensities (blue). White indicates the absence of the respective MST after data pre-processing. Metabolites are sorted according to abundance patterns (separated by black lines), class and RI. Only metabolites significantly correlating with the separation of treatments and treatment per day are shown. The fold change of MST abundance in co-cultivation relative to mono-cultivations is given and coded with a second color code. Black indicates a higher abundance in co-cultivation, grey a higher abundance in mono-cultivation.

									Metabolite intensity						Fold change		Group						
									low			high			UP	DOWN							
ID	Model ion	RT	RI	Name	Class	Ident	Analysis	Median (n=3/4)										Fold (Co relative to:)					
								Day 18			Day 30			Day 42				Day 18		Day 30		Day 42	
								SM Mono	Co	TW Mono	SM Mono	Co	TW Mono	SM Mono	Co	TW Mono	SM Mono	TW Mono	SM Mono	TW Mono	SM Mono	TW Mono	
103	187.1	9.89	1522	7-Tetradecanol	Alc	1	T										2.6	8.5	-	-	-4.1	282.9	
104	189.1	9.92	1526	7-Tetradecanol	Alc	1	T										3.0	8.4	-	-	-3.5	29.9	
119	217.1	10.46	1598	Unknown	S		DT									1.9	-	-	-	-1.2	2.8		
206	321.2	13.44	2020	Gluconic acid	S acid	?1	DT									1.6	2.1	-1.1	3.1	1.0	3.2		
180	319.2	12.61	1881	Gluconic acid 1,5-lactone	S dv.		DT									2.5	-	-	-	-1.2	2.0		
205	293.2	13.41	2015	Unknown		-	DT									1.1	-	1.7	-	-	-		
210	351.2	13.63	2055	Unknown	U	-	DT									3.0	2.1	-1.4	3.5	-1.3	2.5		
73	239.1	8.85	1385	Hydroquinone	Alc		DT									-	-	1.2	2.5	-1.3	2.0		
99	223.1	9.67	1493	4-Hydroxybenzaldehyde	Alc		DT									-1.3	-1.1	1.0	1.7	-1.9	3.0		
53	113.1	8.00	1272	2-(4-Methyl-1-piperazinyl)ethanol	Alk	?	DT									-	-	1.2	-	-1.4	3.2		
304	447.3	17.19	2674	Maltose	S	??1	DT,T									-1.5	2.3	1.2	7.1	-1.0	2.5		
270	217.1	16.08	2481	Uridine	S dv.		DT									-1.4	-	1.2	-	1.1	5.9		
275	145.1	16.22	2505	Uridine	S dv.	??1	DT									-	-	1.0	-	-1.5	23.0		
299	159.1	16.98	2638	Adenosine	S dv.	?	DT									-1.8	-	1.4	5.0	2.0	2.4		
300	236.1	17.05	2649	Adenosine	S dv.		DT									-7.5	1.1	1.1	-	-1.0	937.5		
311	245.1	17.65	2755	Guanosine	S dv.		DT									-1.0	4.2	1.0	-	1.1	3.2		
59	292.1	8.22	1301	Unknown	U	-	DT									-	-	1.2	-	1.6	4.3		
241	300.1	14.88	2272	Unknown	U	-	DT									-	-	1.8	-	3.0	2.1		
260	287.2	15.59	2396	Unknown	U	-	DT									-1.2	1.2	2.3	1.9	1.1	1.1		

ID	Model ion	RT	RI	Name	Class	Ident	Analysis	Median (n=3/4)									Fold (Co relative to:)						Group
								Day 18			Day 30			Day 42			Day 18		Day 30		Day 42		
								SM Mono	Co	TW Mono	SM Mono	Co	TW Mono	SM Mono	Co	TW Mono	SM Mono	TW Mono	SM Mono	TW Mono	SM Mono	TW Mono	
108	117.1	10.01	1538	Unknown	U	-	DT	-	-	-	-	-	-	-	-	-	-	-	-	1.3	1.1		
110	274.2	10.10	1550	Unknown	U	-	DT	-	-	-	-	-	-	-	-	-	-	-	-	1.0	1.3		
138	170.1	11.20	1696	Unknown	U	-	DT	-	-	-	-	-	-	-	-	-	-	-	-	1.7	1.7		
140	387.2	11.30	1708	Unknown	U	-	DT	-	-	-	-	-	-	-	-	-	-1.2	-	-	1.7	-		
168	143.1	12.22	1830	Unknown	U	-	DT	-	-	-	-	-	-	-	-	-	-	-	-	1.6	6.6		
170	143.1	12.28	1839	Unknown	U	-	DT	-	-	-	-	-	-	-	-	-	-	-	-	1.6	12.9		
177	191.1	12.53	1872	Unknown	U	-	DT	-	-	-	-	-	-	-	-	-	-	-	-	1.6	1.6		
179	166.1	12.57	1877	Unknown	U	-	DT	-	-	-	-	-	-	-	-	-	-1.4	31.6	-	1.0	1.8		
187	387.2	12.82	1912	Unknown	U	-	DT	-	-	-	-	-	-	-	-	-	-2.2	-	-	2.1	-		
214	132	13.89	2099	Unknown	U	-	DT	-	-	-	-	-	-	-	-	-	-	-	-	1.3	2.0		
240	361.2	14.85	2267	Unknown	U	-	DT	-	-	-	-	-	-	-	-	-	-	-	-	1.5	1.2		
271	447.3	16.12	2488	Unknown	U	-	DT,T	-	-	-	-	-	-	-	-	-1.1	2.1	-1.2	2.3	1.1	1.7		
273	459.3	16.18	2499	Unknown	U	-	DT	-	-	-	-	-	-	-	-	-12.0	-4.9	-2.4	-	1.1	1.1		
283	179.1	16.51	2556	Unknown	U	-	DT	-	-	-	-	-	-	-	-	-	-	-	-	1.2	2.9		
288	277.1	16.67	2585	Unknown	U	-	DT	-	-	-	-	-	-	-	-	3.4	-	-3.5	-	1.5	2.9		
298	380.2	16.96	2634	Unknown	U	-	DT	-	-	-	-	-	-	-	-	-	-	-3.5	-	1.4	8.8		
305	399.1	17.20	2677	Unknown	U	-	DT	-	-	-	-	-	-	-	-	-	-	-	-	-	1.7		
331	558.2	19.33	3023	Unknown	U	-	DT	-	-	-	-	-	-	-	-	-	-	-1.3	-	1.1	8.8		
139	186.1	11.26	1703	4-Methyl-2,6-bis(2-methyl-2-propanyl)phenol	Alc	?? ¹	DT	-	-	-	-	-	-	-	-	-	-	-1.6	-	-1.4	2.1		
11	148.1	5.88	992	2-Oxopropanoic acid (Pyruvic acid)	CA		DT	-	-	-	-	-	-	-	-	-	-	-	-	-1.0	1.2		
339	204.1	24.29	3520	Maltotriose	CS		DT	-	-	-	-	-	-	-	-	-2.6 E+07	-5.2 E+06	-1.1	2.5	-1.2	6.4		
114	235.1	10.33	1580	Pentofuranose	S		DT	-	-	-	-	-	-	-	-	-	-	-1.2	-	-1.2	1.9		
289	230.1	16.71	2591	Inosine	S dv.		DT	-	-	-	-	-	-	-	-	-	-	-1.6	-	-1.3	5.8		

ID	Model ion	RT	RI	Name	Class	Ident	Analysis	Median (n=3/4)									Fold (Co relative to:)						Group		
								Day 18			Day 30			Day 42			Day 18		Day 30		Day 42				
								SM Mono	Co	TW Mono	SM Mono	Co	TW Mono	SM Mono	Co	TW Mono	SM Mono	TW Mono	SM Mono	TW Mono	SM Mono	TW Mono			
306	327.2	17.23	2681	Pregn-16-en-20-one, 3,18-bis(acetyloxy)-14,15-epoxy-	ST	?? ¹	DT,T																		
150	221.1	11.68	1759	Skel_MEDIA_C196 (Vidoudez)	U	-	DT																		
162	223.1	12.05	1808	Unknown	U	-	DT																		
193	327.2	13.04	1951	Unknown	U	-	DT,T																		
198	146.1	13.15	1970	Unknown	U	-	DT																		
216	470.3	13.98	2116	Unknown	U	-	DT																		
297	171.1	16.93	2630	Unknown	U	-	DT																		
66	151.1	8.54	1343	2-Phenoxyethanol	Alc	-	DT																		
251	204.1	15.29	2343	Galactosylglycerol	S dv.	-	DT																		

In case derivatized molecules are detected, the table entry lists their putative parent compounds. Each MST is characterized by **ID**, **model ion**, retention time (**RT**), retention index (**RI**) and its underlying CAP **analysis**. CAP analyses comprised the overall analysis with a-priori grouping by treatment and day (**DT**) and with a-priori grouping by treatment (**T**). Metabolites were identified via libraries. If metabolites were verified with a standard, they are marked with *. “?” indicates a reversed match between 700 and 800, “??” a reversed match between 600 and 700 and “???” indicates cases where the reversed match was ≤ 600 . “1” tags metabolites with a match smaller than 600. Class abbreviations: Amine (**A**), alcohol (**Alc**), alkaloid (**Alk**), carboxylic acid (**CA**), complex sugar (**CS**), derivatives of a certain class (**dv.**), sugar (**S**), sugar alcohol (**S Alc**), sugar acid (**S Acid**), sterol (**St**), terpene (**T**), others (**O**), unknown (**U**). **Vidoudez** refers to an MST code given by the in-house library, **GOLM** refers to an MST code given by distinct libraries of the Golm Metabolome Database.

Subset analysis per day

The constrained analysis within each sampling day resulted in a clear separation of the three treatments on day 18, 30 and 42 in the constrained score plots (**Figure 32**). The corresponding loading plots depicts metabolites that were highly correlating with the separation of treatments (day 18 and 42: $|r| \geq 0.8233$, $P \leq 0.001$; day 30: $|r| \geq 0.8470$, $P \leq 0.001$). In general, the majority of vectors was correlating with co-cultivation and *S. marinoi* mono-cultivation.

On day 18, the separation of treatments was established by canonical axis 1 (**Figure 32A**). Furthermore, canonical axis 2 established a gradual separation between co-cultivation and mono-cultivation of *S. marinoi*. Both treatments exhibited close proximity in multivariate space. The corresponding loading plot (**Figure 32B**) indicates that the clear majority of metabolites was correlating with co-cultivation and mono-cultivation of *S. marinoi*. 7-Tetradecanol (#103) characterized co-cultivation on day 18 and metabolites #39 (3-hydroxy-3-methylbutanoic acid), #136, #137 and #263 (uridine) were correlating with mono-cultivated *T. weissflogii*.

On day 30, the relationship of canonical axis 1 and 2 with the separation of treatments in the constrained score plot (**Figure 32C**) was identical with the one on day 18. Furthermore, a distinct instead of a gradual separation of mono-cultivated *S. marinoi* (quadrant IV) and co-cultivation (III) was visible. In the corresponding loading plot (**Figure 32D**), only MST #334 was correlating with *T. weissflogii* on day 30. The allocation of metabolites to *S. marinoi* mono-cultivation and co-cultivation was difficult via loading plot and was performed on the basis of a heatmap.

On day 42, canonical axis 1 was sufficient to separate the treatments (**Figure 32E**). Interestingly, all highly correlated metabolites were characteristic for co-cultivation and mono-cultivated *S. marinoi*. Both the samples of these groups, as well as all MST vectors in the corresponding loading plot were located on the right side of the origin (**Figure 32F**).

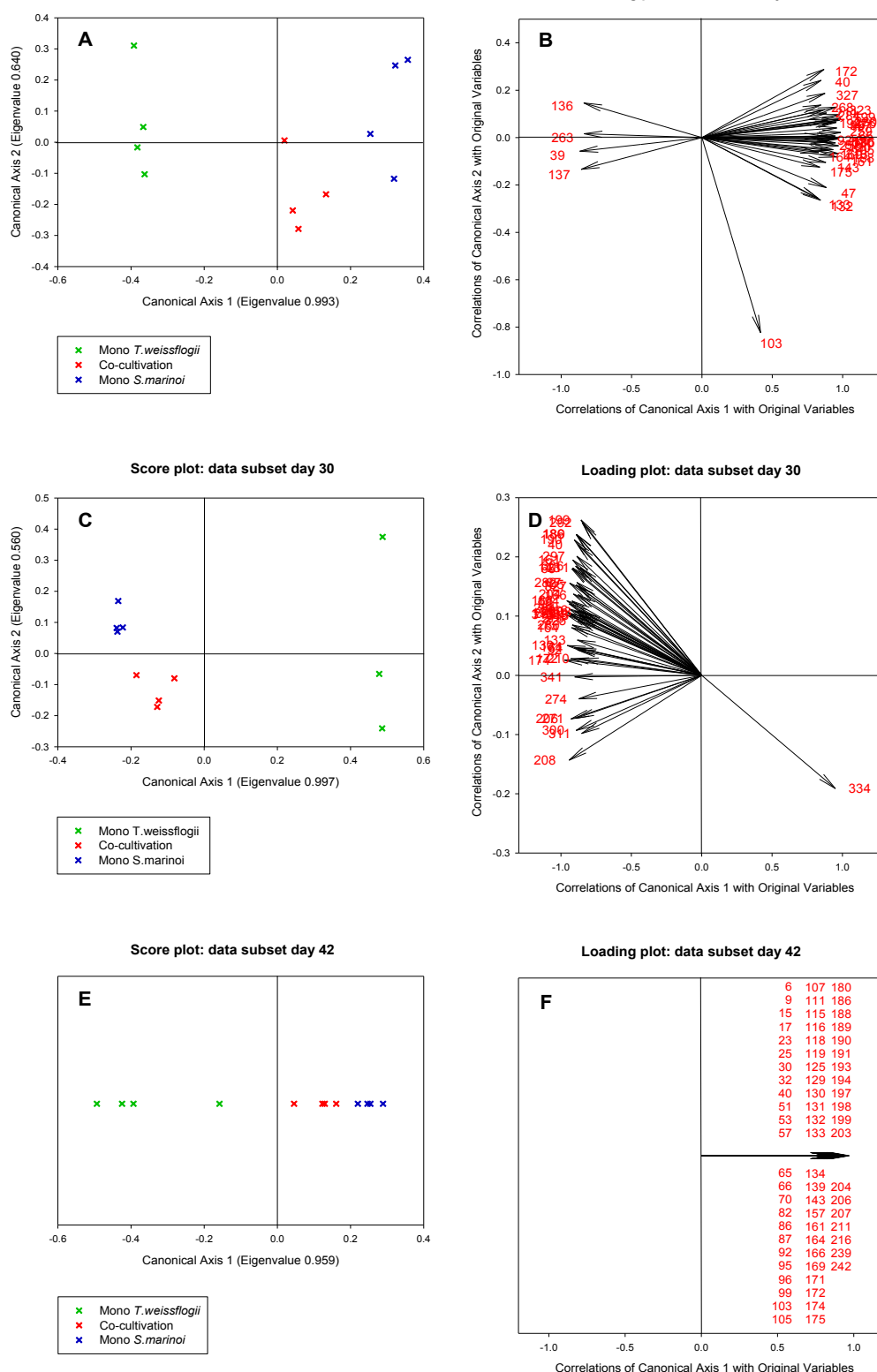


Figure 32: Constrained score and loading plots of exometabolomic samples from the daywise subset analysis of the interaction between *T. weissflogii* and *S. marinoi*.

The constrained score plots (graph **A**, **C**, **E**) visualize significant differences between the treatments, as confirmed via CDA for the subset analysis on day 18 (graph **A**, **B**), day 30 (graph **C**, **D**) and day 42 (graph **E**, **F**). These differences between treatments are highly significant (**Table 11**). Vectors in the CAP loading plots (graph **B**, **D**, **F**) represent metabolites, characterized by their ID (red numbers, pooled per group). Only vectors with a significant correlation coefficient above the critical value of $|r| \geq 0.8233$ ($P \leq 0.001$) for day 18 and 42 and $|r| \geq 0.8470$ ($P \leq 0.001$) for day 30 are plotted. The direction of the vectors in 2-dimensional space correlates with exometabolomic sample groupings shown in the score plots of the respective analysis.

To further unravel the affiliation of correlated metabolites with distinct a-priori groups, I created heatmaps for the subset analysis of each day, visualizing intensity dynamics of all highly correlated MTs over treatments and time. The complete heatmaps⁵⁵ are depicted in the appendix (day 18: **Appendix 41**, day 30: **Appendix 42** and day 42: **Appendix 43**). I conducted a classification according to the following intensity patterns: group A summarizes metabolites that exhibited highest abundance in co-cultivation on the respective day. Group Sm summarizes potential biomarkers for *S. marinoi* and group Tw comprises potential biomarkers for *T. weissflogii*. As only groups A of the daywise subset analysis were relevant in the screening for interaction specific release and / or uptake of potential infochemicals, I additionally summarized them in **Table 13**.

The daywise subset analysis indicated eight MSTs that were characteristic for the co-cultivation group, as they were highest abundant in co-cultivation compared to both mono-cultivations (**Table 13**). The co-cultivation group was characterized by 7-tetradecanol (#103) and an unknown MST (#132) on day 18, by adenosine (#300), guanosine (#311) and MST #208 on day 30, as well as by phenylalanine (#111), gluconic acid (#206) and an unknown sugar (#118) on day 42.

⁵⁵ Metabolites #30 (dodecamethylpentasiloxane), #159 (terephthalic acid) and #280 (diphenyl phthalate) were excluded, as they were considered potential contaminations

Table 13: Partial Heatmap of relative exometabolite intensities for the daywise subset analysis of the interaction between *T. weissflogii* and *S. marinoi*.

Only metabolites are depicted that contain metabolites with highest abundance in co-cultivation on the respective day. Medians of MST intensities, normalized to the external standard ribitol (per sample) and subsequently metabolite-wise auto scaled, are represented by a color code ranging from high (yellow) to low intensities (blue). White indicates the absence of the respective MST after data pre-processing. Metabolites are sorted according to abundance patterns (separated by black lines), class and RI. Only metabolites significantly correlating with the separation of treatments and treatment per day are shown. The fold change of MST abundance in co-cultivation relative to mono-cultivations is given and coded with a second color code. Black indicates a higher abundance in co-cultivation, grey a higher abundance in mono-cultivation.

ID	Model ion	RT	RI	Name	Class	Ident	Metabolite intensity			Fold change		Group
							Median (n=3/4)			Fold (Co relative to:)		
							SM Mono	Co	TW Mono	SM Mono	TW Mono	
103	187.1	9.89	1522	7-Tetradecanol	Alc	*			2.6	8.5	A (Day 18)	
132	187.1	11.03	1672	Unknown	U	-		1.2	-			
300	236.1	17.05	2649	Adenosine	S dv.	-			1.1	-	A (Day 30)	
311	245.1	17.65	2755	Guanosine	S dv.	-			1.0	-		
208	221.1	13.55	2040	Unknown	U	-			1.2	-		
111	120.1	10.14	1555	Phenylalanine	AA	-			1.4	-	A (Day 42)	
118	313.2	10.42	1592	Unknown	S	?			1.3	2.6		
206	321.2	13.44	2020	Gluconic acid	S acid	? ¹			1.0	3.2		

In case derivatized molecules are detected, the table entry lists their putative parent compounds. Each MST is characterized by **ID**, **model ion**, retention time (**RT**) and retention index (**RI**). Metabolites were identified via libraries. If metabolites were verified with a standard, they are marked with *. “?” indicates a reversed match between 700 and 800, “??” a reversed match between 600 and 700 and “???” indicates cases where the reversed match was ≤ 600 . “1” tags metabolites with a match smaller than 600. Class abbreviations: Amine (**A**), alcohol (**Alc**), alkaloid (**Alk**), carboxylic acid (**CA**), complex sugar (**CS**), derivatives of a certain class (**dv.**), sugar (**S**), sugar alcohol (**S Alc**), sugar acid (**S Acid**), sterol (**St**), terpene (**T**), others (**O**), unknown (**U**). **Vidoudez** refers to an MST code given by the in-house library, **GOLM** refers to an MST code given by distinct libraries of the Golm Metabolome Database.

Screening for interaction specific release and / or uptake of potential infochemicals

On the basis of observed exometabolomic differences between the treatments and the highly correlated metabolites (as presented in the previous subchapters), hypotheses about interaction specific release and/or uptake of potential infochemicals were drawn. The underlying principle used in the screening process is explained in chapter 2.2.3. Three prominent abundance patterns aimed at unraveling potential interaction-induced release / uptake processes.

It is important to note that the categorization of MSTs by day was not only performed on basis of visual intensity dynamics, but mainly on the significance of correlation, as given by the CAP analysis.

Enhanced abundance of exometabolites in co-cultivation - Pattern I:

During the screening process, 66 MSTs were identified in the overall and subset analyses of the exometabolomic investigation as potential candidate molecules matching pattern I. They were all characterized by enhanced abundance in co-cultivation, relative to both mono-cultivation groups. Thus, potentially indicating interaction-induced release mechanisms. While only eight of them were correlating with day 18 and 17 with day 30, the majority (41) of the identified MSTs were correlating with day 42 and thus late stages of the interaction. The MSTs originated from groups A18, A30 and A42 of the overall analysis and group A(Day18), A(Day30) and A(Day42) of the daywise subset analyses (**Table 12**, **Table 13**).

A comprehensive summary of the temporal intensity dynamic of all metabolites of pattern I is visualized via boxplots in the appendix (**Appendix 44 - Appendix 46**). Subsequently, only representative metabolites, segmented by day, will be shown to highlight prominent intensity dynamics.

Day 18

The intensity dynamics of MSTs correlating with day 18 were classified in three categories:

(1) MSTs with distinct temporal increase / decrease dynamics

Among metabolites with distinct temporal dynamics, a time dependent increase dynamic within each treatment group in combination with enhanced abundance in co-cultivation on day 18 was observed for putative gluconic acid (#206), MST #132 and #210 (**Figure 33**).

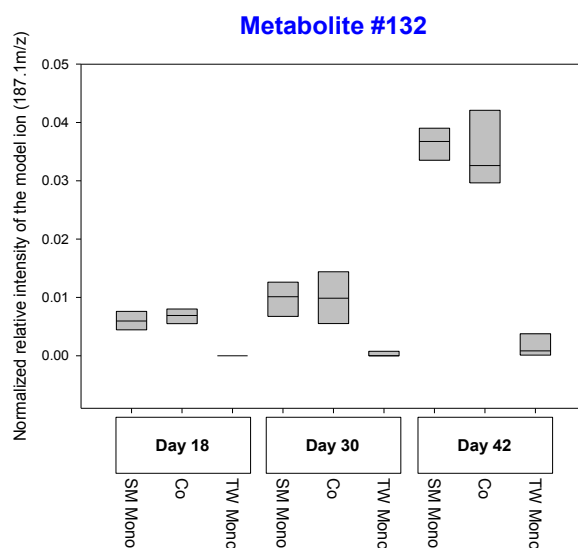


Figure 33: Exemplary metabolite #132 with interaction-induced release mechanism on day 18 and distinct temporal regulation, in the interaction between *T. weissflogii* and *S. marinoi* (intensity pattern I).

(2) MSTs correlated with day 18, but predominant on day 42

Secondly, gluconic acid 1,5-lactone (#180) and the unknown MST #119 matched pattern I on day 18, but were predominant on day 42 (**Figure 34**). Although these metabolites might play a role as potential infochemicals mediating the interaction, their relevance was estimated to be low due to their very low relative abundance on day 18.

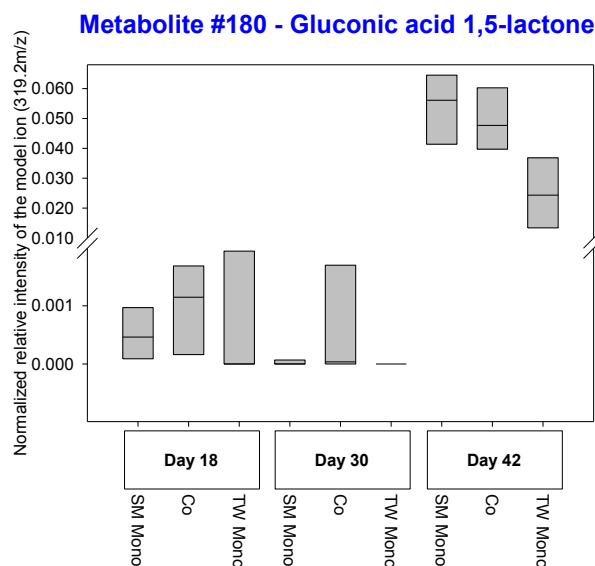


Figure 34: Exemplary MST #180 with interaction-induced release mechanism on day 18 but predominance on day 42 in the interaction between *T. weissflogii* and *S. marinoi* (intensity pattern I).

(3) MSTs with predominance in *S. marinoi*

Forming the 3rd category, putative 7-tetradecanol (#103, #104) and MST (#205) were characteristic for *S. marinoi*, as they were most abundant in *S. marinoi* mono- and co-cultivation and almost absent in *T. weissflogii* mono-cultivation (**Figure 35**). As they matched pattern I on day 18, they might be released by *S. marinoi* due to the interaction.

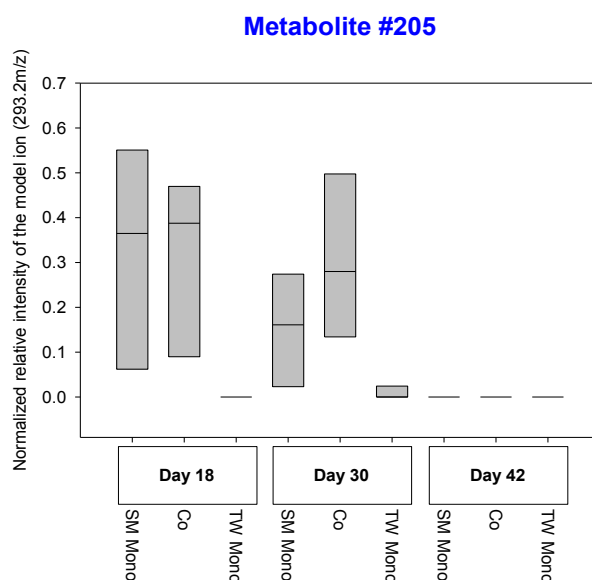


Figure 35: Exemplary MST #205 with interaction-induced release mechanism on day 18 and potential origin from *S. marinoi* in the interaction between *T. weissflogii* and *S. marinoi* (intensity pattern I).

Day 30

Most of the metabolites that exhibited pattern I on day 30 were characterized by a distinct temporal increase dynamic, as visualized with the help of MST #260 (**Figure 36**). In total, 15 exometabolites were temporally regulated. Of those metabolites, hydroquinone (#73), 4-hydroxybenzaldehyde (#99), putative uridine (#275), putative adenosine (#299, #300), putative maltose (#304) and three unknown metabolites (#265, #291, #330) exhibited pattern I on day 30 only. On the other hand, uridine (#270), guanosine (#311) and four unknown MSTs (#59, #208, #241, #260) showed pattern I on day 30 and 42.

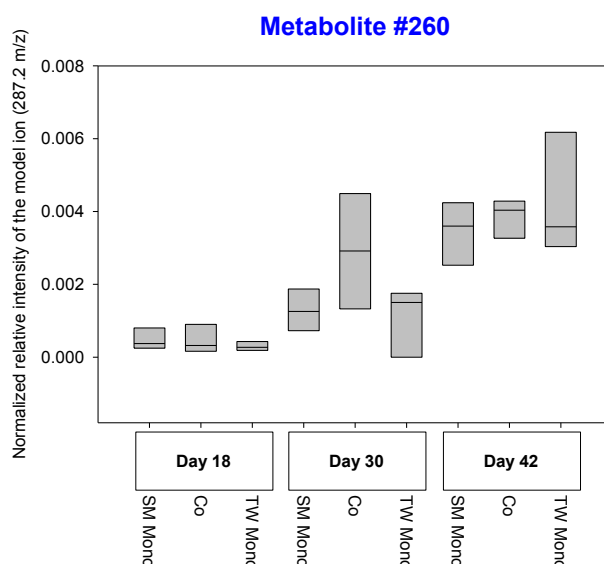


Figure 36: Exemplary MST #260 with interaction-induced release on day 30 and distinct temporal regulation mechanism, in the interaction between *T. weissflogii* and *S. marinoi* (intensity pattern I).

The remaining two metabolites, putative 2-(4-methyl-1-piperazinyl)ethanol (#53) and MST #278, were not only characterized by increased metabolite abundance in co-cultivation, relative to mono-cultivation on day 30, but also by absence on day 18 and intensity maxima on day 42 (**Figure 37**). Thus, these metabolites were characteristic for the stationary phase of growth.

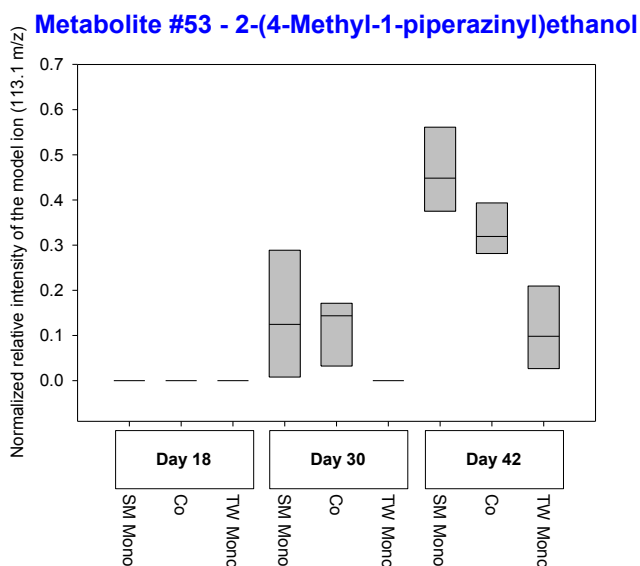


Figure 37: Exemplary MST #53 with interaction-induced release mechanism on day 30 in the interaction between *T. weissflogii* and *S. marinoi* (intensity pattern I).

Day 42

The majority of all candidate metabolites with enhanced abundance in co-cultivation was correlating with day 42. In general three characteristic intensity dynamics were observed:

- (1) Metabolites with predominance on day 42
- (2) Metabolites with distinct temporal increase / decrease dynamics
- (3) Metabolites with rather unspecific abundance on all sampling days.

A typical temporal dynamic of an MST with predominance on day 42 is visualized in **Figure 38** via putative 4-pyridinol (#27). Besides putative 2-aminoethanol (#2), 2-pyridinol (#3), putative 4-pyridinol (#27), cytosine (#69), putative 6-hydroxy-1,3-dimethyl-2,4(1H,3H)-pyrimidinedione (#141), xylitol (#145), adenosine (#301) and putative maltose (#302), another ten unknown metabolites⁵⁶ followed this trend.

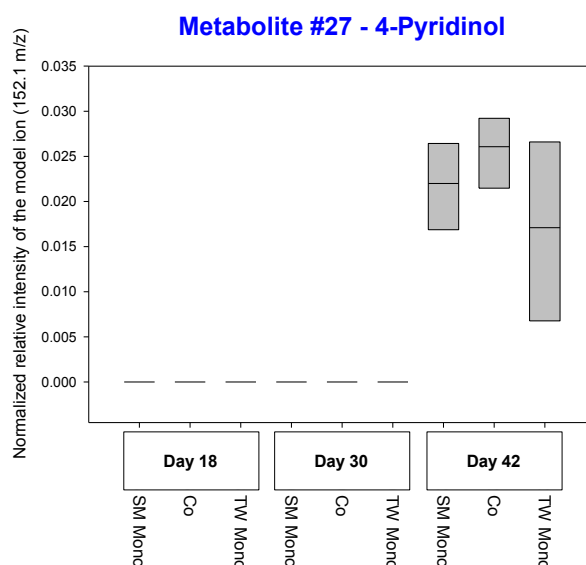


Figure 38: Exemplary MST #27 with interaction-induced release mechanism on day 42 and predominance on this day in the interaction between *T. weissflogii* and *S. marinoi* (intensity pattern I).

Among metabolites with a distinct temporal dynamic, phenylalanine (#111), galactose (#184), putative gluconic acid (#206), putative uridine (#263), maltose (#308) and five unknown metabolites⁵⁷ exhibited a distinct temporal increase dynamic, as visualized in **Figure 39**. Furthermore, MST #179 was also temporally regulated, although there was no clear trend visible.

⁵⁶ Metabolites #8, #35, #44, #49, #72, #90, #108, #110, #127, #138, #168, #170, #177, #214, #240, #283, #298, #305

⁵⁷ Metabolites #118, #271, #273, #288, #331

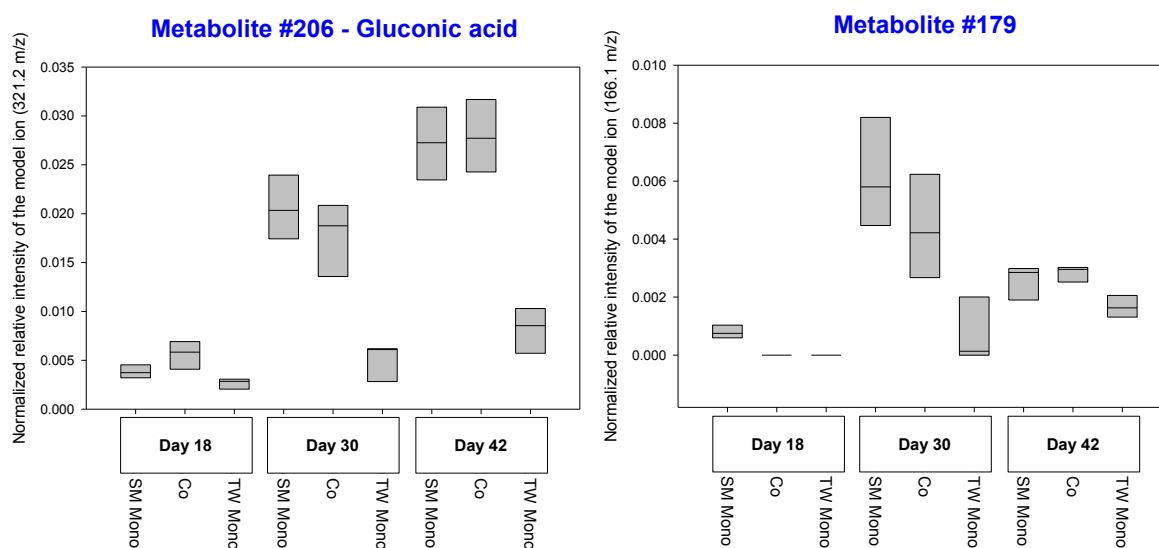


Figure 39: Exemplary MST #206 and #179 with interaction-induced release mechanism on day 42 and distinct temporal regulation in the interaction between *T. weissflogii* and *S. marinoi* (intensity pattern I).

Thirdly, metabolites #81, #88, #140 and #187 were characterized by pattern I on day 42, but exhibited rather unspecific abundance on day 30 and 42 without distinct increase / decrease dynamics (**Figure 40**).

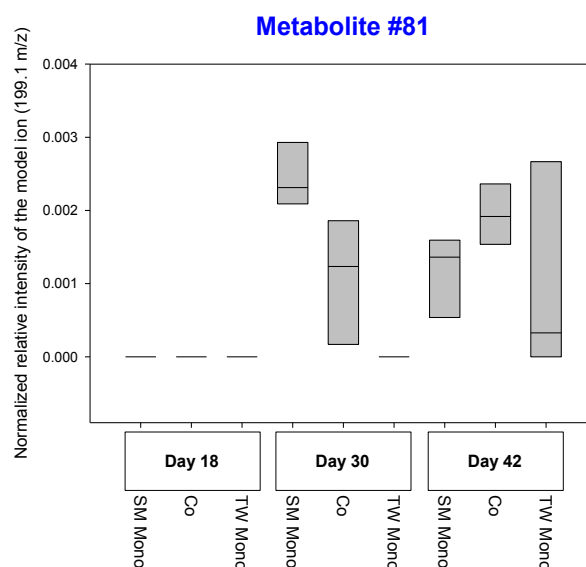


Figure 40: Exemplary MST #81 with interaction-induced release mechanism on day 42 in the interaction between *T. weissflogii* and *S. marinoi* (intensity pattern I).

Reduced abundance of exometabolites in co-cultivation - Pattern II / III:

The second major trend revealed in the screening process for potential infochemicals in the interaction between *S. marinoi* and *T. weissflogii* are MSTs with reduced abundance of exometabolites in co-cultivation. In summary, 14 exometabolites were characterized by pattern II or pattern III on at least one sampling day. They were classified as group B in the overall CAP analysis (**Table 12**).

An evaluation of the candidate metabolites matching pattern III in the heatmap via boxplots indicated that eight MSTs did indeed show abundance in co-cultivation, which was not apparent if the median was used in the heatmaps (**Appendix 47**)⁵⁸. As, strictly speaking, these metabolites did not fit pattern III, they were subsequently excluded.

Day 18

Four of the remaining six MST candidates were correlating with day 18. Maltotriose (#339) and MST #162 were present in the exometabolomes of *S. marinoi* and *T. weissflogii* and increased in intensity to reach maximum values in the stationary phase of growth (day 30 and 42). On day 18, these metabolites matched pattern II, exhibiting lowest concentrations in co-cultivation (**Figure 41**).

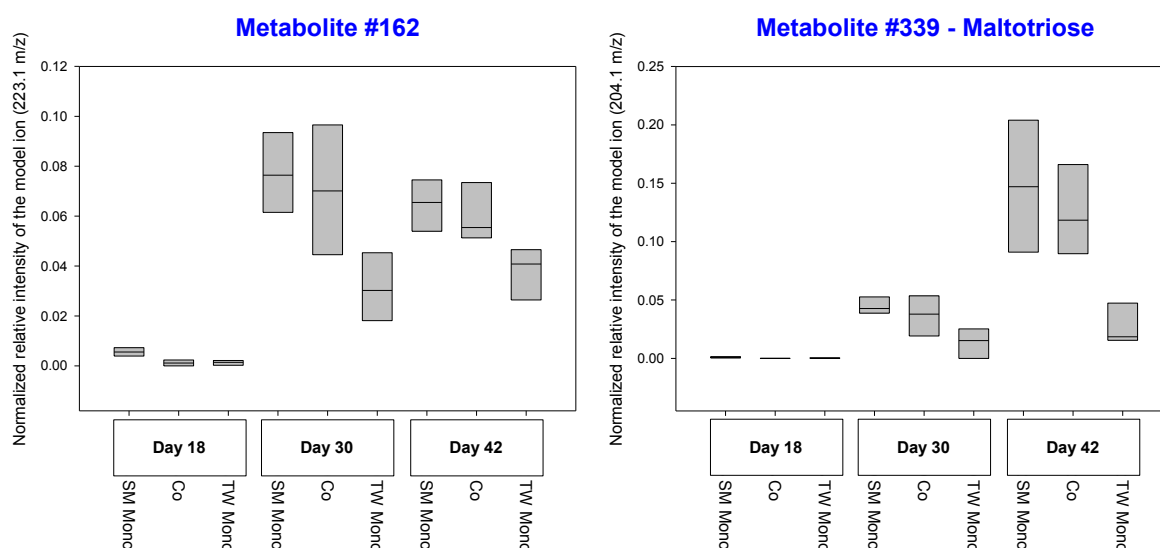


Figure 41: Potential infochemical with interaction-induced uptake, transformation or reduced release mechanisms on day 18 in the interaction between *T. weissflogii* and *S. marinoi* (intensity pattern II).

The sterol 3,18-bis(acetyloxy)-14,15-epoxy)-pregn-16-en-20-one (#306, putatively identified), as well as MST #193 presented themselves as very interesting candidate molecules, matching pattern II / III (**Figure 42**). Both were characteristic for the exometabolome of *S. marinoi*, as they were completely absent in mono-cultivated *T. weissflogii* and exhibited pattern III on day 18.

MST #193 showed highest abundance in the stationary phase of growth (day 30 and 42) and was present at comparably low concentrations on day 18. On the contrary, the sterol #306 exhibited similar intensities in *S. marinoi* mono-cultivation throughout all three sampling days. In general, both metabolites potentially originated from *S. marinoi* and were involved in an interaction-induced uptake, transformation or reduced release mechanism on day 18. The very

⁵⁸ Metabolites #11, #114, #139, #150, #198, #216, #289, #297

clear intensity pattern on day 18, as well as over treatments and time stressed the importance of both metabolites as potential infochemical, involved in mediating the interaction at the onset of the observed growth effect.

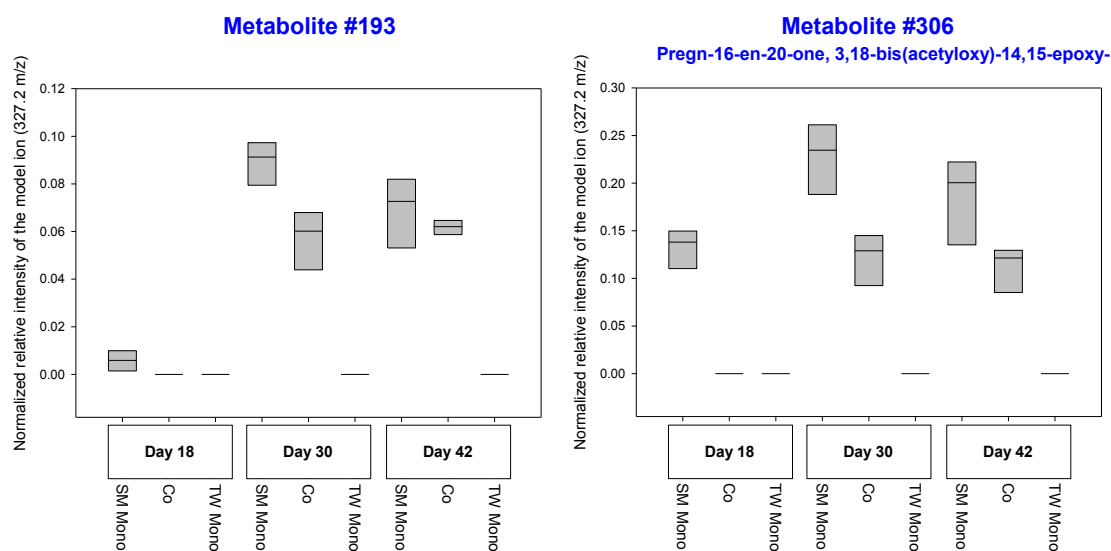


Figure 42: Exemplary metabolites #193 and #306 with interaction-induced uptake, transformation or reduced release mechanisms on day 18 in the interaction between *T. weissflogii* and *S. marinoi* (intensity pattern III).

Day 30 and 42

Galactosylglycerol (#251) matched intensity pattern II on day 30 and 42 and exhibited a temporal increase dynamic within each treatment group (**Figure 43**). Accordingly, this metabolite shaped the exometabolomes of the diatom cultures during late diatom growth stages and was potentially involved in uptake, transformation or reduced release mechanisms on day 30 and 42. Glycolipids play a fundamental role in plants, eukaryotic algae and cyanobacteria. They occur in the membrane of chloroplasts. are important signal and regulatory molecules and were found to exhibit antiviral, antifungal and antitumor properties ((Da Costa et al., 2016) and references herein, (Harwood and Guschina, 2009)).

2-Phenoxyethanol (#66) matched pattern III on day 30 and was predominant on day 42 (**Figure 43**). However, this metabolite showed rather large variance on day 30 and was only present in mono-cultivated *S. marinoi* on this day, while it was characteristic for both species on day 42. Therefore, the meaning of this metabolite as interaction-induced infochemical was rated rather low.

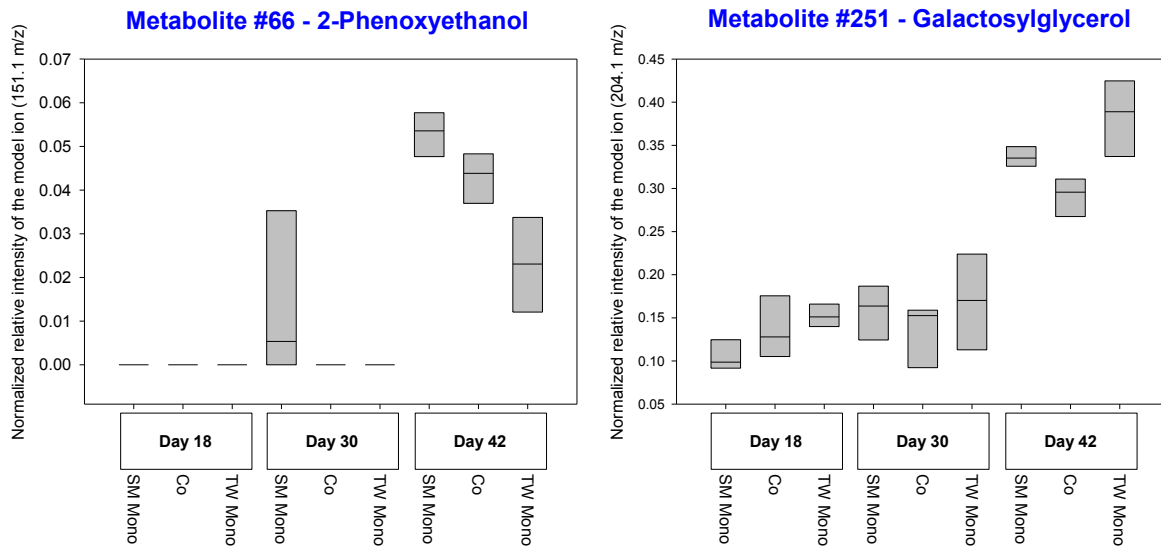


Figure 43: Exemplary MST #66 and #251 with interaction-induced uptake, transformation or reduced release mechanisms on day 30 and 42 in the interaction between *T. weissflogii* and *S. marinoi* (intensity pattern II / III).

3.2.4 Endometabolomic investigation

In the interaction between *T. weissflogii* and *S. marinoi*, the presence of the interaction partner induced significant endometabolomic changes. This concerned day 30 in *T. weissflogii* and day 18 and 42 in *S. marinoi*. Generally, 224 MSTs were highly correlating with significant differences between a-priori groups in *T. weissflogii* and 172 MSTs in *S. marinoi*.

I rated the influence of the interaction on *T. weissflogii* endometabolomes weaker than the one on *S. marinoi*, as the influence of time. Similar to the interaction of *T. weissflogii* and *S. costatum*, species affiliation was strongly shaping diatom endometabolomes.

In summary, the endometabolomic changes of *T. weissflogii*, induced by the interaction with *S. marinoi*, were mainly apparent in the downregulation of many metabolite classes on day 30. Amino acids were most abundant on day 18 and relevantly downregulated on day 18 and 30. I observed a similar pattern in complex sugars, which were generally downregulated in co-cultivation on day 18 and 30. Fatty acids and their derivatives characterized the stationary growth phase (day 30 and 42) and shared the tendency of downregulation in co-cultivation on day 30. With exception of few metabolites, the same observation holds for amines, alcohols, alkaloids, sugars, complex sugars, sterols and the hydrocarbon 14-heptacosanone (#358). Among carboxylic acids, I observed a trend of upregulation in co-cultivation on day 18 with subsequent downregulation on day 30 and 42.

Generally, the interaction-induced regulation of the endometabolome of *S. marinoi* seemed more complex than the one of *T. weissflogii*. I observed no consistent comprehensive trend, but a trend of upregulation in co-cultivation, which was not specific for a single sampling day and not observed in *T. weissflogii*. Alcohols, carboxylic acids, fatty acids, sugars, complex sugars and their derivatives did not exhibit clear trends. In the class of sugars and derivatives, the picture was rather complex. Amino acids were most abundant on day 18, fatty acids on day 30 and 42 and complex sugars characterized only day 42.

Interestingly, sterols exhibited a very distinct regulation pattern of upregulation in co-cultivation on day 18 and downregulation on day 42. Among amines and their derivatives, the regulation of putrescine (#173) was oppositional to the one observed in *T. weissflogii*, as it was upregulated on day 18 and 30. Also oppositional was the regulation of 1H-pyrrole-2-carboxylic acid (#82), which was upregulated on day 18 as well.

I performed the endometabolomic investigations in the manner of descriptive analyses. Their main purpose was to qualitatively describe metabolomic alterations within the organisms and to potentially support hypotheses drawn from the exometabolomic investigations.

In the endometabolomic investigation of the interaction between *T. weissflogii* and *S. marinoi*, I analyzed 71 samples resulting in 403 MSTs. After the onset of the interaction experiment, I took endometabolomic samples on days 18, 30 and 42. I performed the analysis as described in the interaction of *T. weissflogii* and *S. costatum* (chapter 2.1.2). The endometabolome of *T. weissflogii* was normalized to a count of 1.9×10^7 diatom cells, the endometabolome of *S. marinoi* to a count of 5×10^7 diatom cells (see chapter 6.6.2).

Data exploration via CAP

The unconstrained score plot of the PCoA visualizes clear separation of samples by species via principal coordinate axis 1 and a gradual separation of *S. marinoi* samples by time via principal coordinate axis 2 (**Appendix 48**). *T. weissflogii* samples formed a rather homogenous group, without temporal gradient. The CDA confirmed the very strong influence of species and time on diatom endometabolomes, as the trace statistic for the corresponding a-priori groups was highly significant and the misclassification error amounted to 0 % ($P \leq 0.0001$, **Table 14**).

Furthermore, the overall analysis indicated significant differences in diatom endometabolomes due to treatment, as the trace statistic for a-priori grouping by treatment and treatment per day was highly significant ($P \leq 0.0001$, **Table 14**). To further unravel these interaction-induced changes, I performed subset analyses.

Table 14: Permutation and cross-validation test results for the overall analysis of different a-priori groups in the endometabolome analysis of the interaction between *S. marinoi* and *T. weissflogii*

A-priori grouping by	m	Groups	Trace statistic	δ_1^2	Misclassification error (%)
Species	1	2	0.974 ($P \leq 0.0001$)	0.974 ($P \leq 0.0001$)	0
Day	11	3	1.721 ($P \leq 0.0001$)	0.921 ($P \leq 0.0001$)	0
Treatment	9	4	1.660 ($P \leq 0.0001$)	0.993 ($P \leq 0.0001$)	16.90
Day & treatment	11	12	5.425 ($P \leq 0.0001$)	0.995 ($P \leq 0.0001$)	12.68

δ_1^2 being the first squared canonical correlation. *m* represents the number of PCoA axes included in the CAP.

Species-specific subset analysis

The species-specific subset analyses confirmed the findings of the overall PCoA. Generally, time had a stronger influence on endometabolomic alterations in *S. marinoi*, compared to *T. weissflogii*.

The PCoA score plot of *S. marinoi* shows a clear separation of the three sampling days via principal coordinate axis 1 (**Appendix 49B**). However, within each sampling day no distinct grouping by treatment was observed. In the context of *T. weissflogii*, samples from day 18 formed a homogenous group in quadrant I without distinct demarcation according to treatments (**Appendix 49A**). Samples from day 30 and 42 were represented by a rather widespread group, which was mainly located in quadrant II and III. Interestingly, co-cultivation samples on day 30 were distinctly different, as they were located in quadrant IV.

Again, I confirmed the strong influence of time with the CDA via highly significant trace statistic and misclassification errors of 0 % in both species ($P \leq 0.0001$, **Table 15**). Considering interaction-induced endometabolomic alterations, I found significant differences due to treatment in *S. marinoi* endometabolomes. Both, a-priori grouping by treatment and treatment per day yielded significant trace statistics, as well as misclassification errors of 5.56 % ($P \leq 0.01$, **Table 15**).

On the other hand, the endometabolomes of *T. weissflogii* only exhibited significant differences due to treatment if time was regarded as factor (a-priori grouping by treatment per day, $P \leq 0.0001$, **Table 15**). In a time-independent approach, via a-priori grouping by treatment, I didn't find treatments to be significantly different in *T. weissflogii*. Thus, compared to *S. marinoi*, I graded the influence of the interaction on *T. weissflogii* endometabolomes weaker.

To get more insights into interaction-induced endometabolomic alterations and to further specify the origin of these significant differences, I analyzed daywise subsets per species.

Table 15: Permutation and cross-validation test results for the species-specific subset analysis of different a-priori groups in the endometabolome analysis of the interaction between *S. marinoi* and *T. weissflogii*

A-priori grouping by	m	Groups	Trace statistic	δ_1^2	Misclassification error (%)
<i>T. weissflogii</i> : day	4	3	1.723 ($P \leq 0.0001$)	0.910 ($P \leq 0.0001$)	0
<i>T. weissflogii</i> : treatment	13	2	0.467 ($P = 0.3808$)	0.467 ($P = 0.3808$)	8.57
<i>T. weissflogii</i> : day & treatment	13	6	3.293 ($P \leq 0.0001$)	0.983 ($P = 0.0001$)	5.71
<i>S. marinoi</i> : day	1	3	0.941 ($P \leq 0.0001$)	0.941 ($P \leq 0.0001$)	0
<i>S. marinoi</i> : treatment	9	2	0.606 ($P = 0.0073$)	0.606 ($P = 0.0073$)	5.56
<i>S. marinoi</i> : day & treatment	9	6	2.971 ($P \leq 0.0001$)	0.989 ($P \leq 0.0001$)	5.56

δ_1^2 being the first squared canonical correlation. m represents the number of PCoA axes included in the CAP.

Daywise subset analysis per species

The daywise analysis via CDA indicated that interaction-induced differences in the endometabolomes were significant on day 30 for *T. weissflogii* and on day 18 and 42 for *S. marinoi*. On those days, the trace statistic was significant ($P \leq 0.029$) and the classification according to treatments was very strong, as could be shown with a misclassification error of 0 % (Table 16). However, these differences remained hidden in the PCoA score plots (Appendix 50). I observed no clear separation of mono- and co-cultivation samples.

Table 16: Permutation and cross-validation test results for the species-specific and daywise subset analysis of different a-priori groups in the endometabolome analysis of the interaction between *S. marinoi* and *T. weissflogii*

A-priori grouping by	m	Groups	Trace statistic	δ_1^2	Misclassification error (%)
<i>T. weissflogii</i> : day 18	5	2	0.747 ($P = 0.1494$)	0.747 ($P = 0.1494$)	0
<i>T. weissflogii</i> : day 30	3	2	0.869 ($P \leq 0.0001$)	0.869 ($P \leq 0.0001$)	0
<i>T. weissflogii</i> : day 42	8	2	0.459 ($P = 0.9586$)	0.459 ($P = 0.9586$)	8.33
<i>S. marinoi</i> : day 18	5	2	0.873 ($P = 0.0294$)	0.873 ($P = 0.0294$)	0
<i>S. marinoi</i> : day 30	6	2	0.881 ($P = 0.1182$)	0.881 ($P = 0.1182$)	0
<i>S. marinoi</i> : day 42	5	2	0.929 ($P \leq 0.0001$)	0.929 ($P \leq 0.0001$)	0

δ_1^2 being the first squared canonical correlation. m represents the number of PCoA axes included in the CAP.

Identification of metabolites correlating with relevant a-priori groups

I conducted the identification of metabolites correlating with interaction-induced endometabolomic alterations on the basis of the species-specific analyses (*T. weissflogii*: a-priori grouping by treatment per day, *S. marinoi*: a-priori grouping by treatment and treatment per day) and the daywise analyses (*T. weissflogii*: day 30, *S. marinoi*: day 18 and 42), which showed significant differences.

T. weissflogii

The constrained score plot visualizes the significant differences between a-priori grouping by treatment per day in *T. weissflogii* (**Figure 44A**), as they were already described in the species-specific subset analysis (**Table 15**). All three sampling days formed distinct groups: Samples from day 18 were located in quadrant III and IV and were separated by canonical axis 1 from the other two sampling days. Samples from day 42 were located in quadrant II and samples from day 30 in quadrant I. While no separation of mono- and co-cultivation samples was visible within day 18 and 42, the treatments were clearly separated by canonical axis 2 during sampling day 30.

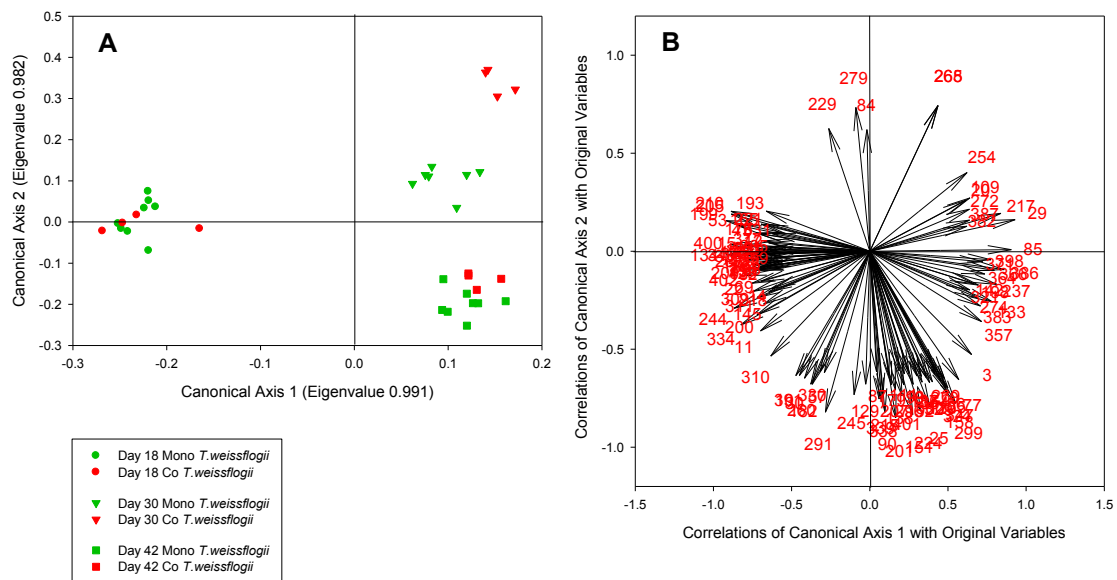


Figure 44: Constrained score and loading plot of endometabolomic samples from *T. weissflogii* in a species-specific subset analysis of the interaction between *T. weissflogii* and *S. marinoi*.

The constrained score plot visualizes significant differences between the sample groups as found via CDA with a-priori groups by treatment per day (trace statistic $P \leq 0.0001$, misclassification error of 5.71 % for $m = 13$, graph **A**). Vectors in the CAP loading plot (graph **B**) represent metabolites, characterized by their ID (red numbers). Only vectors with a significant correlation coefficient above the critical value of $|r| \geq 0.6100$ ($P \leq 0.0001$) are plotted. The direction of the vectors in 2-dimensional space correlates with endometabolomic sample groupings shown in the score plots of the respective analysis.

The loading plot depicts 122 MSTs that were highly correlating with the separation of a-priori groups ($|r| \geq 0.6100$, $P \leq 0.0001$; **Figure 44B**). I performed further categorization of the MST vectors via heatmap (**Table 17, Appendix 51**).

The constrained score plot of the daywise analysis of day 30 shows a clear separation of mono- and co-cultivated samples by canonical axis 1 (**Figure 45A**). In total, 11 metabolites were significantly correlating with the endometabolome of *T. weissflogii* in co-cultivation on day 30, comprising gulonic acid (#228, #230), galactono-1,4-lactone (#231), myo-inositol (#242, #254), an unknown endometabolite already described within *S. marinoi* cells (Skel_Cell_C128_RT14.776 (#265-268), (Vidoudez, 2010)) and two unknown metabolites. Furthermore, 135 metabolites⁵⁹ were correlating with the endometabolome in mono-cultivation on this day ($|r| \geq 0.6021$, $P \leq 0.05$; **Figure 45B**).

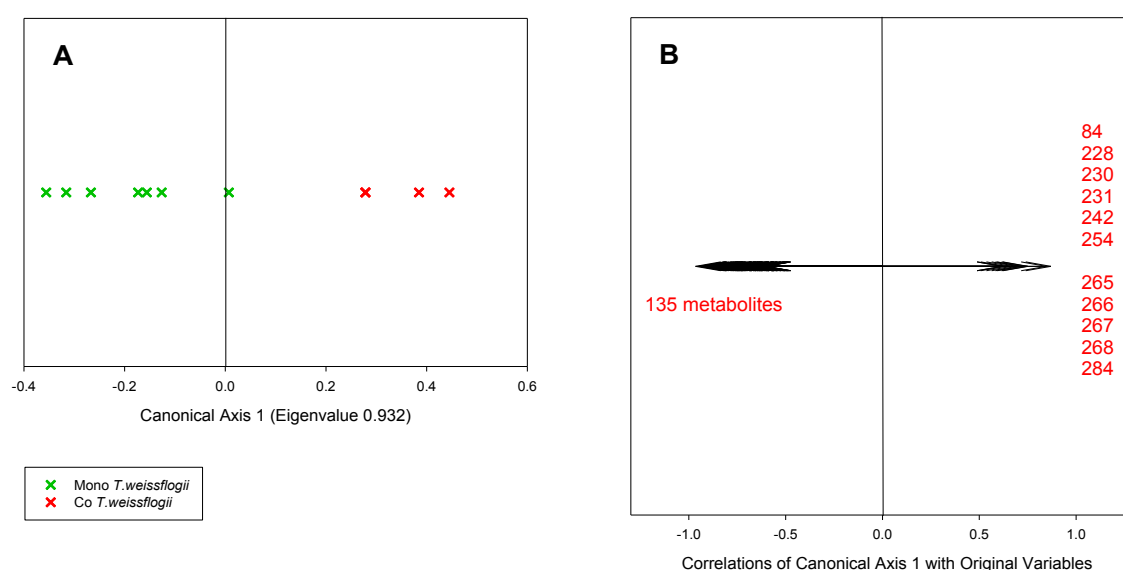


Figure 45: Constrained score and loading plots of endometabolomic samples from *T. weissflogii* in a daywise subset analysis on day 30 of the interaction between *T. weissflogii* and *S. marinoi*.

The constrained score plot (graph **A**) visualizes significant differences between the treatments, as confirmed via CDA for the subset analysis on day 30. These differences between treatments are highly significant (trace statistic $P \leq 0.0001$, misclassification error of 0 % for $m = 3$). Vectors in the CAP loading plot (graph **B**) represent metabolites, characterized by their ID (red numbers, pooled per group). Only vectors with a significant correlation coefficient above the critical value of $|r| \geq 0.6021$ ($P \leq 0.05$) are plotted. The direction of the vectors in 2-dimensional space correlates with endometabolomic sample groupings shown in the score plots of the respective analysis.

⁵⁹ #4, #12-15, #17, #18, #25, #28, #30, #31, #37-40, #43, #45, #49, #53, #54, #58, #62, #65, #66, #67, #71, #76-79, #90, #92, #101-104, #108, #112, #117, #119, #126, #128-131, #134, #138, #147, #150, #151, #159, #165, #167-169, #173, #176, #178-180, #182, #187, #195, #200, #201, #204, #215, #221, #222, #224, #232, #237, #241, #243, #245, #248, #263, #273, #276-278, #287, #288, #292, #293, #295, #296, #298-300, #302, #303, #307, #308, #310, #312, #313, #316-318, #320-323, #238, #331-333, #335-339, #343, #347, #350, #352, #354, #356, #358, #359, #363, #367, #369

To gain a better understanding of the character and association of relevant MSTs to the investigated a-priori groups, I summarized all highly correlated metabolites in a heatmap (**Table 17**). To facilitate the interpretation, the heatmap was categorized by metabolite classes and ordered by intensity patterns within each class. It is important to point out that all metabolites identified by the daywise analyses were mainly considered relevant for the separation of treatments within the respective day of the analysis. I summarized all MSTs of unknown identity in **Appendix 51**.

Interestingly, a multitude of the correlated metabolites was characterized by rather small intensity differences between mono- and co-cultivation within each sampling day. By only considering metabolites that exhibited intensity differences $\geq 30\%$ ⁶⁰, the focus was set on relevant changes in endometabolite levels. Only the metabolites complying with this criterion were considered relevantly up- or downregulated in co-cultivation. Furthermore, the overall abundance dynamic of each MST was taken into consideration and especially those points in time with high MST abundance, relative to other time points, were considered relevant and evaluated in the context of interaction-induced regulation. Subsequently, I describe only relevant up- or downregulations.

Among amines, putrescine (#173) was downregulated in co-cultivation on day 18 and 30 before reaching equal levels in both treatments on day 42. Generally, the amount of putrescine (#173) within each cell increased over time. Putative urea (#56) exhibited a similar temporal trend. However, on day 18, putative urea was 2.4 - fold upregulated in co-cultivation. Similar to putrescine, urea levels were equal in both treatments on day 42. 1H-pyrrole-2-carboxylic acid (#82) was downregulated on day 30 and exhibited approximately equal MST intensities among mono- and co-cultivation on day 18 and 42. While the three amine candidates were most abundant on either day 18 or day 42, they shared the common trait of absence in co-cultivation on day 30.

In total, seven amino acids and two amino acid derivatives were correlating with the separation of treatments in *T. weissflogii*. With the exception of threonine (#67), all metabolites of this class were most abundant on day 18 and downregulated in co-cultivation, with up to 35.6 - fold⁶¹ higher values in mono-cultivation on day 18 and 30. While valine (#12, #49), alanine (#13, #14), serine (#59), isoleucine (#66), proline (#69), glycine (#72), pyroglutamic acid (#123) and N-acetylglutamic acid (#126) followed this trend, threonine (#67) was only abundant on day 30.

⁶⁰ as identified via fold-changes $|x| \geq 1.3$

⁶¹ N-acetylglutamic acid (#126) on day 30

Furthermore, this metabolite was highly characteristic for mono-cultivated *T. weissflogii*, as it was downregulated in co-cultivation until under the detection limit of the method.

Considering the class of alcohols, I putatively identified three metabolites. On the one hand, glycerol (#20) was upregulated in co-cultivation on day 18 and 42. On the other hand, 1,2,3-butanetriol (#40) and 1,12-dodecanediol (#169) were downregulated until under the detection limit of the method on day 30 and were thus responsible for the separation of treatments on this day. While 1,12-dodecanediol (#169) exhibited a trend of significant downregulation throughout all three sampling days, 1,2,3-butanetriol (#40) was standing out on day 30 only and showed similar intensity levels among co- and mono-cultivation on the remaining days.

Interestingly, among the class of alkaloids all three candidates showed a tendency of downregulation in co-cultivation throughout all sampling days. However, the intensity deviations on day 18 and 42 were smaller than the determined 30 %. Putative 3-pyridinol (#4), putative 6-methyl-3-pyridinol (#38, #39) and lumichrome (#79) were identified in the daywise analysis on day 30 and were thus responsible for the separation of treatments on this day.

Relevant changes in the carboxylic acid class concerned glycolic acid (#11) and 3-hydroxy-3-methylbutanoic acid (#47), which were upregulated in co-cultivation on day 18, putative 3-hydroxybutanoic acid⁶² (#17), which was downregulated on all sampling days – with up to 23 - fold higher values in mono-cultivation – and benzoic acid (#57), which was downregulated on day 42. Considering the temporal dynamic of carboxylic acids, putative 3-hydroxybutanoic acid (#17) and 3-hydroxy-2-methylpropanoic acid (#29) were characteristic for the stationary growth phase, while the remaining carboxylic acids were almost absent on day 30 in both treatments and rather characterizing regular growth phase and late stationary growth phase.

Interestingly, all metabolites affiliated with the class of fatty acids and their derivatives were downregulated in co-cultivation on day 30. With exception of stearic acid (#277) and oleic acid (#273), which were 1.6 - to 2.3 - fold upregulated on day 18, all remaining fatty acids and derivatives were present at approximately equal intensities among both treatments on day 18 and 42, as indicated by intensity differences smaller than 30 %. In summary, this class comprised four saturated fatty acids – myristic acid (#200, #201), stearic acid (#277), pentadecanoic acid

⁶² The putative structure suggestions for MST #10 and MST #17 need to be interpreted with caution. The succession of both MSTs' RI is not in agreement with the succession of the RIs of their suggested structures hexanoic acid and 3-hydroxybutanoic acid. Thus, compound identification is considered preliminary, as the structure suggestions don't fit accurately. Further validation is needed. Nevertheless, both compounds appear to be carboxylic acids and suggested compound names are given as lead reference point.

(#224) and palmitic acid (#245), three unsaturated fatty acids – oleic acid (#273), putative linoleic acid (#274) and putative arachidonic acid (#278, #303) as well as ten fatty acid derivatives.

Within hydrocarbons and derivatives, only 14-heptacosanone (#358) exhibited significant downregulation in co-cultivation on day 30. In general, the abundance of this endometabolite increased over time and was characteristic for the stationary phase of growth in mono-cultivated *T. weissflogii*.

Most of the identified endometabolites belonged to the class of sugars and their derivatives, like sugar acids and sugar alcohols. With a focus on intensity differences of $\geq 30\%$ between the treatments, the following metabolites were considered relevantly regulated: erythronic acid (#132) was downregulated in co-cultivation on day 18 and 30 and glucuronic acid (#221, #244) throughout all three sampling days. Both sugar acids were characteristic for the regular growth phase, as they decreased in intensity during later growth stages. Galactinol (#254, #257, and #364) was downregulated on day 18 and 30 as well, but characteristic for the stationary phase, as its intensity increased in mono-cultivation over time.

On day 30, the majority of sugars and derivatives were downregulated (with up to 7.4 - fold higher intensities in mono-cultivation for 2-keto-gluconic acid (#180)). This applied to three sugars – a pentofuranose (#147), a hexofuranose (#195) and a putative inositol isomer (#272), the sugar derivatives putative uridine (#300) as well as three sugar acids – glyceric acid (#78), threonic acid (#128, #131) and putative gluconic acid (#241), two sugar acid derivatives – 2-keto-gluconic acid (#180) and gulono-1,4-lactone (#232) and the sugar alcohol ononitol (#237). Considering upregulation in co-cultivation on day 30, gulonic acid (#228, #230) and myo-inositol (#242, #254) were of relevance, as they were up to 2.7 - fold upregulated.

Interestingly, two MSTs were identified as galactono-1,4-lactone, exhibiting oppositional regulations: On day 30 MST #231 was upregulated on day 30 and MST #215 was downregulated in co-cultivation. As due to many isomers and very similar MS spectra sugars and their derivatives are impossible to be unambiguously identified via MS libraries, it might be possible that one of the MSTs represented an isomer of galactono-1,4-lactone.

In the class of complex sugars, five MSTs were characteristic for the regular growth phase, as they were highest abundant on day 18. However, only a putative trisaccharide (#311) was downregulated in co-cultivation with 1.5 -fold higher intensities in mono-cultivation, while all other candidates exhibited only minor intensity differences between the treatments. Another six MSTs were relevantly downregulated in co-cultivation on day 30, including two disaccharides (#394, #397), 4-O-hexopyranosylhexose (#395), melibiose (#398) and putative

digalactosylglycerol (#378, #385). Considering metabolites that were characteristic for day 42, only maltotriose (#401) was meaningfully upregulated in co-cultivation. A general trend of reduced abundance of complex sugars and their derivatives in co-cultivation became apparent.

The identified sterols were characteristic for the stationary phase of growth. While sterol abundances were approximately equal on day 18 and 42, three sterols⁶³ were meaningfully downregulated in co-cultivation on day 30: 24-Oxocholest-5-en-3-yl acetate (#371), campesterol (#383) and putative ergosta-5,24-dien-3-yl acetate (#360, #369). Among the terpenes, phytol (#263) was characteristic for early stages of the diatom growth and downregulated in co-cultivation on day 30, with 5.7 - fold higher intensities in mono-cultivation.

In total, 119 unknown MSTs could not be chemically characterized. They were sorted by prominent intensity patterns and documented in **Appendix 51**. Interestingly, MST #104 characterized day 30 of the interaction and exhibited 43 - fold higher intensities in mono-cultivation on this day. However, this unknown MST was the only one with quite a strong treatment-dependent regulation. All other unknown MSTs are not further discussed.

⁶³MS spectra were very similar. Although the strategy of MST identification via MS libraries was retained, the sterol identities must be interpreted with caution.

Table 17: Heatmap of endometabolite intensities categorized by MST classes for the species-specific and daywise analysis of *T. weissflogii* in the interaction with *S. marinoi*. Medians of MST intensities, normalized to peak sum per sample and subsequently metabolite-wise auto scaled, are represented by a color code ranging from high (yellow) to low intensities (blue). White indicates the absence of the respective MST after data pre-processing. Metabolites are sorted according to classes (separated by black lines) and abundance patterns. Only metabolites significantly correlating with the separation of treatments and treatment per day are shown. The fold change of MST abundance in co-cultivation relative to mono-cultivation is given and coded with a second color code. Black indicates a higher abundance in co-cultivation, grey a higher abundance in mono-cultivation.

ID	Model ion	RT	RI	Name	Class	Ident	Analysis	Median MST intensity						Fold change		
								low high						UP	DOWN	
								Median (Co: n=4, Mono: n=7/8)						Fold (Co relative to Mono)		
								Day 18		Day 30		Day 42		Day 18	Day 30	Day 42
TW Mono	TW Co	TW Mono	TW Co	TW Mono	TW Co											
82	240.1	8.38	1324	1H-Pyrrole-2-carboxylic acid	A		DT						1.1	-	-1.1	
56	139.1	7.38	1190	Urea	A	?	DT						2.4	-	1.0	
173	174.1	11.58	1747	1,4-Butanediamine (Putrescine)	A	*	30						-1.7	-	1.0	
12	146.1	5.93	999	Valine	AA	*	DT,30						-2.3	-	1.8	
14	116.1	6.05	1014	Alanine	AA	*	DT,30						-1.8	-	1.2	
49	144.1	7.12	1156	Valine	AA		DT,30						-1.5	-4.3	1.9	
59	116.1	7.54	1212	Serine	AA	*	DT						-10.1	-	-	
66	158.1	7.86	1254	Isoleucine	AA	*	DT,30						-1.2	-17.4	2.3	
69	142.1	7.91	1261	Proline	AA		DT						-2.0	-	1.1	
72	174.1	8.01	1274	Glycine	AA		30						-1.4	-10.9	-1.1	
123	156.1	9.88	1522	5-Hydroxy-3,4-dihydro-2H-pyrrole-2-carboxylic acid (Pyroglutamic acid)	AA dv.		DT						-1.3	-3.4	1.3	
126	174.1	9.97	1533	N-Acetylglutamic acid	AA dv.		30						1.0	-35.6	2.0	
13	116.1	5.98	1005	Alanine	AA	*	30						-1.8	-	-1.3	
67	146.1	7.88	1257	Threonine	AA	*	30						-	-	-	
20	103.1	6.31	1049	Glycerol	Alc	?	DT						2.4	-1.2	1.4	
40	210.1	6.90	1127	1,2,3-Butanetriol	Alc	?	30						1.0	-	1.3	
169	133.1	11.39	1721	1,12-Dodecanediol	Alc	??	30						-1.9	-	-3.8	
4	152.1	5.35	922	3-Pyridinol	Alk	?	30						1.2	-	-1.0	
38	166.1	6.85	1121	6-Methyl-3-pyridinol	Alk	??	30						-1.1	-3.9	-1.2	

ID	Model ion	RT	RI	Name	Class	Ident	Analysis	Median (Co: n=4, Mono: n=7/8)						Fold (Co relative to Mono)		
								Day 18		Day 30		Day 42		Day 18	Day 30	Day 42
								TW Mono	TW Co	TW Mono	TW Co	TW Mono	TW Co			
39	166.1	6.86	1121	6-Methyl-3-pyridinol	Alk	??	30							-1.1	-3.9	-1.2
79	184	8.24	1305	7,8-Dimethylbenzo[g]pteridine-2,4(1H,3H)-dione (Lumichrome)	Alk		30							1.0	-	-1.1
10	173.1	5.72	971	Hexanoic acid ⁶²	CA	?	DT							1.2	-	-1.1
11	177.1	5.77	978	2-Hydroxyethanoic acid (Glycolic acid)	CA		DT							1.3	-	-1.1
47	247.1	7.07	1149	3-Hydroxy-3-methylbutanoic acid	CA		DT							1.3	-1.4	-1.5
57	179.1	7.47	1203	Benzoic acid	CA		DT							1.0	-	-1.4
17	117	6.15	1027	3-Hydroxybutanoic acid ⁶²	CA	?	30							-1.1	-23.0	-1.3
29	233.1	6.59	1086	3-Hydroxy-2-methylpropanoic acid	CA		DT							1.7	-1.0	1.1
200	126.1	12.34	1847	Myristic acid	FA		DT,30							1.1	-	-1.1
218	143.1	12.91	1922	Methyl palmitate	FA dv.		DT							1.1	-1.3	-1.0
279	239.2	14.96	2288	2-Hydroxyethyl palmitate	FA dv.	??	DT							1.2	1.1	1.2
277	117	14.90	2277	Octadecanoic acid (Stearic acid)	FA		30							2.3	-	-1.1
273	339.3	14.76	2252	9-Octadecenoic acid (Oleic acid)	FA		30							1.6	-15.1	-1.0
274	105.1	14.78	2256	Octadecadienoic acid (Linoleic acid)	FA	??	DT							-1.3	-1.4	1.2
278	197.1	14.94	2284	5,8,11,14-Icosatetraenoic acid (Arachidonic acid)	FA	?	30							-1.2	-30.3	-1.1
287	116	15.24	2336	2,3-Dihydroxypropyl palmitate	FA dv.	??	30							1.0	-2.4	1.1
296	129.1	15.57	2394	1,3-Dihydroxy-2-propanyl myristate	FA dv.		DT,30							1.0	-4.1	-1.1
298	343.3	15.75	2425	2,3-Dihydroxypropyl myristate	FA dv.		30							1.2	-2.7	-1.2
303	108.1	15.94	2458	5,8,11,14-Icosatetraenoic acid (Arachidonic acid)	FA	?	30							-1.1	-2.7	1.1
307	105.1	16.13	2492	Methyl-4,7,10,13,16,19-docosahexaenoate	FA dv.		30							1.1	-3.0	-1.0
308	357.3	16.28	2517	2,3-Dihydroxypropyl pentadecanoate	FA dv.	?	30							1.1	-3.1	-1.1
317	218.1	16.61	2575	1,3-Dihydroxy-2-propanyl palmitate (2-Palmitoylglycerol)	FA dv.		30							-1.0	-3.7	-1.1
320	369.3	16.70	2591	C16:1-glycerol ?	FA dv.		30							1.1	-2.9	-1.0

ID	Model ion	RT	RI	Name	Class	Ident	Analysis	Median (Co: n=4, Mono: n=7/8)						Fold (Co relative to Mono)		
								Day 18		Day 30		Day 42		Day 18	Day 30	Day 42
								TW Mono	TW Co	TW Mono	TW Co	TW Mono	TW Co			
321	129.1	16.73	2596	C16:1-glycerol ?	FA dv.		DT,30					1.1	-1.8	-1.1		
322	367.3	16.73	2597	C16:1-glycerol ?	FA dv.		30					1.1	-3.7	-1.2		
224	117	13.03	1939	Pentadecanoic acid	FA		DT,30					-1.2	-	-1.1		
245	117	13.68	2025	Palmitic acid	FA	*	DT,30					1.2	-	-1.1		
201	117	12.36	1850	Myristic acid	FA	*	DT,30					1.1	-	-1.1		
158	195.1	11.05	1677	Unknown (potentially C17:1)	FA dv.	?	DT					-	-	-1.1		
199	123.1	12.31	1842	2-Methyl-7-octadecyne	HC	?	DT					1.2	1.1	-1.1		
210	123.1	12.61	1882	1,19-Icosadiene	HC	?	DT					1.1	1.3	-1.2		
358	211.2	18.35	2871	14-Heptacosanone	HC dv.		30					1.2	-5.6	1.0		
128	292.1	10.03	1541	2,3,4-Trihydroxybutanoic acid (Threonic acid)	S acid		DT,30					-1.0	-3.5	1.1		
132	140	10.20	1564	2,3,4-Trihydroxybutanoic acid (Erythronic acid)	S acid		DT					-1.4	-	2.9		
139	217	10.45	1597	Arabinofuranose	S		DT					-1.1	1.4	-1.1		
145	218	10.63	1621	Pentofuranose	S		DT					-1.1	-1.3	-1.1		
221	333.1	12.96	1929	Glucuronic acid	S acid		DT,30					-1.4	-3.9	-1.4		
244	217.1	13.63	2018	Glucuronic acid	S acid	?	DT					-1.1	-1.3	-1.2		
109	205.1	9.29	1443	Erythrose	S	?	DT					1.2	1.1	1.1		
228	103	13.17	1957	Hexonic acid (Gulonic acid)	S acid		30					-1.1	1.5	1.0		
230	345	13.20	1961	Hexonic acid (Gulonic acid)	S acid		30					-1.0	2.7	1.3		
231	217	13.22	1963	5-(1,2-Dihydroxyethyl)-3,4-dihydroxydihydro-2(3H)-furanone (Galactono-1,4-lactone)	S acid dv.		30					1.0	1.6	1.1		
242	319	13.55	2007	myo-Inositol	S alc		30					1.2	1.5	1.1		
254	191	13.98	2116	myo-Inositol	S alc	*	DT,30					1.2	2.0	1.1		
78	189.1	8.22	1302	2,3-Dihydroxypropanoic acid (Glyceric acid)	S acid		30					1.0	-5.8	1.0		
131	292.1	10.15	1558	2,3,4-Trihydroxybutanoic acid (Threonic acid)	S acid		30					1.0	-3.1	1.0		
147	212	10.66	1624	Pentofuranose	S		30					1.3	-3.6	-1.3		
180	292.1	11.78	1773	2-Keto-gluconic acid	S acid dv.		30					-1.2	-7.4	1.1		
195	117	12.20	1828	Hexofuranose	S		30					1.1	-1.5	1.2		

ID	Model ion	RT	RI	Name	Class	Ident	Analysis	Median (Co: n=4, Mono: n=7/8)						Fold (Co relative to Mono)		
								Day 18		Day 30		Day 42		Day 18	Day 30	Day 42
								TW Mono	TW Co	TW Mono	TW Co	TW Mono	TW Co			
215	217.1	12.79	1906	5-(1,2-Dihydroxyethyl)-3,4-dihydroxydihydro-2(3H)-furanone (Galactono-1,4-lactone)	S acid dv.		DT,30						-1.3	-6.1	-1.1	
217	217.1	12.88	1918	Galactofuranose	S		DT						-1.3	-1.2	-1.2	
229	432.9	13.18	1959	Hexonic acid (Gulonic acid)	S acid		DT						1.0	-1.1	-1.0	
232	114.1	13.25	1968	Gulono-1,4-lactone	S acid dv.	?	30						1.1	-	1.2	
237	217.1	13.38	1985	6-Methoxy-1,2,3,4,5-cyclohexanepentol (Ononitol)	S alc		DT,30						-1.1	-1.3	-1.1	
241	333.1	13.49	1999	Gluconic acid	S acid	?	30						-1.5	-2.4	-1.2	
272	305.1	14.72	2245	Inositol isomer	S	?	DT						1.1	-1.5	1.2	
300	217.1	15.79	2433	Uridine	S dv.	?	30						-1.1	-4.8	-1.2	
354	191.1	18.13	2836	Galactinol	S dv.	?	DT,30						-1.1	-	-1.1	
357	204.1	18.32	2867	Galactinol	S dv.		DT						-1.9	-2.1	-1.0	
364	204.1	18.99	2971	Galactinol	S dv.		DT						-2.2	-1.8	-1.0	
118	155.1	9.61	1486	Erythro-pentopyranose	S	?	DT						1.2	-	1.1	
207	307.2	12.52	1871	Galactose	S	*	DT						1.1	1.0	1.0	
311	217.1	16.33	2527	Trisaccharide (Vidoudez)	CS	?	DT						-1.5	-2.0	-1.0	
340	360.9	17.53	2736	Maltose	CS		DT						-1.0	1.1	-1.2	
393	381.3	23.57	3461	Disaccharide (Vidoudez)	CS	?	30						-1.2	-3.3	-1.0	
400	361.2	24.85	3569	Maltotriose	CS		DT						1.1	1.1	-1.0	
402	361.2	25.70	3640	Maltotriose	CS		DT						1.1	-3.0	-1.3	
394	204.1	23.66	3469	Disaccharide (Vidoudez)	CS		30						-1.7	-2.8	-1.0	
397	204.1	24.35	3527	Disaccharide (Vidoudez)	CS		30						-1.3	-4.1	1.0	
378	204.1	19.79	3097	Digalactosylglycerol ? (Vidoudez)	CS dv.		30						-3.6	-3.2	1.0	
385	204.1	21.69	3304	Digalactosylglycerol ? (Vidoudez)	CS dv.	?	30						-	-	-	
395	204.1	23.84	3484	4-O-Hexopyranosylhexose	CS		30						-1.5	-	1.2	
398	204.1	24.48	3538	6-O- α -D-Galactopyranosyl- β -D-glucopyranose (Melibiose)	CS		DT						-	-1.7	1.2	
338	204.1	17.43	2718	Maltose	CS		DT,30						-1.6	-3.8	-1.2	

ID	Model ion	RT	RI	Name	Class	Ident	Analysis	Median (Co: n=4, Mono: n=7/8)						Fold (Co relative to Mono)		
								Day 18		Day 30		Day 42		Day 18	Day 30	Day 42
								TW Mono	TW Co	TW Mono	TW Co	TW Mono	TW Co			
339	204.1	17.43	2719	Maltose	CS		DT,30						-1.6	-3.8	-1.2	
401	217.1	25.68	3638	Maltotriose	CS		DT						-	-	1.4	
330	361.2	17.04	2650	Sucrose	CS	?	DT						-1.1	-3.0	1.0	
391	361.2	22.95	3410	Melezitose	CS	?	DT						-1.1	-4.8	1.1	
382	107.1	20.99	3245	Skel_cell_C178_sterol (Vidoudez)	St		DT						1.1	1.2	1.1	
371	382.4	19.29	3018	24-Oxocholest-5-en-3-yl acetate	St		DT						1.1	-1.3	-1.0	
383	343.3	21.04	3250	Ergost-5-en-3-ol (Campesterol)	St		DT,30						-1.3	-1.8	-1.1	
386	129.1	21.84	3316	Stigmasta-5,24(28)-dien-3-ol (Fucosterol)	St		DT						1.2	-1.2	1.1	
387	386.3	22.02	3331	M000000_A337005-101-xxx_NA_3358,28_PRED_VAR5_ALK_NA	St		DT						1.1	-1.1	1.1	
360	145.1	18.44	2885	Ergosta-5,24-dien-3-yl acetate	St	?	DT						1.2	-1.8	-1.1	
369	204.1	19.14	2995	Ergosta-5,24-dien-3-yl acetate	St		30						1.5	-2.1	1.0	
263	143.1	14.48	2203	3,7,11,15-Tetramethyl-2-hexadecen-1-ol (Phytol)	T		DT,30						1.0	-5.7	1.2	

In case derivatized molecules are detected, the table entry lists their putative parent compounds. Each MST is characterized by **ID**, **model ion**, retention time (**RT**), retention index (**RI**) and its underlying CAP **analysis**. CAP analyses comprised the overall analysis with a-priori grouping by treatment and day (**DT**), with a-priori grouping by treatment (**T**), as well as daywise subset analysis on day 18 (**18**), day 30 (**30**) and day 42 (**42**). Metabolites were identified via libraries. If metabolites were verified with a standard, they are marked with *. “?” indicates a reversed match between 700 and 800, “??” a reversed match between 600 and 700 and “???” indicates cases where the reversed match was ≤ 600 . “!” tags metabolites with a match smaller than 600. Class abbreviations: Amine (**A**), alcohol (**Alc**), alkaloid (**Alk**), carboxylic acid (**CA**), complex sugar (**CS**), derivatives of a certain class (**dv.**), hydrocarbons (**HC**), sugar (**S**), sugar alcohol (**S Alc**), sugar acid (**S Acid**), sterol (**St**), terpene (**T**), others (**O**), unknown (**U**). **Vidoudez** refers to an MST code given by the in-house library, **GOLM** refers to an MST code given by distinct libraries of the Golm Metabolome Database.

S. marinoi

The constrained score plots of the species specific analysis of *S. marinoi* visualize the separation of samples with a-priori grouping by treatment (**Figure 46A**) and treatment per day (**Figure 46C**). In the analysis with a-priori grouping by treatment, canonical axis 1 separated the treatments gradually from each other. The corresponding loading plot depicts the three significantly correlated metabolites ($|r| \geq 0.6028$, $P \leq 0.0001$; **Figure 46B**). MST #85 (Skel_MEDIA_C097), which was also found in the medium of *S. marinoi* and identified via the in-house library described mono-cultivated *S. marinoi*. Metabolites #372 and #373 described co-cultivated *S. marinoi*.

In the analysis with a-priori grouping by treatment per day, the clear separation of sampling days is visualized in the CAP score plot (**Figure 46C**). Within the sampling days, only day 18 exhibited a separation of treatments, the separation of treatments within day 42, as shown in the daywise analysis, was not visible in the 2D score plot. With regard to the highly correlated metabolites, a clear assignment to the a-priori groups was difficult, as the loading plot was very crowded ($|r| \geq 0.6028$, $P \leq 0.0001$; **Figure 46D**).

The constrained score plots of the daywise analyses stressed the significant differences between the treatments on day 18 and 42, as mono- and co-cultivation samples were distinctly separated by canonical axis 1 (**Figure 47A, C**). The corresponding loading plots reveal the affiliation of the correlated metabolites to the treatment groups ($|r| \geq 0.5760$, $P \leq 0.05$; **Figure 47B, D**). I performed further classification of all highly correlated metabolites via heatmap (**Table 18, Appendix 52**).

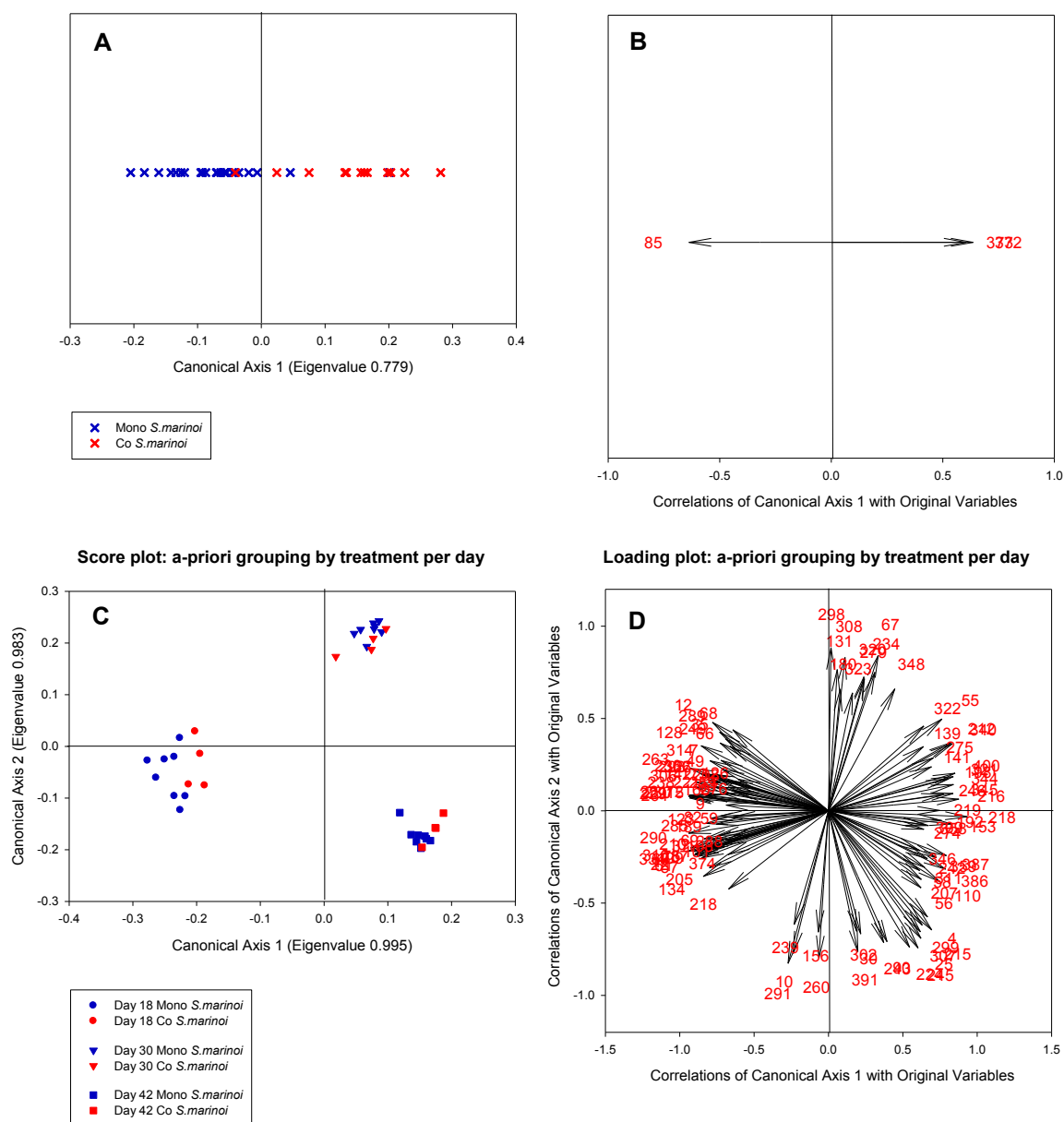


Figure 46: Constrained score and loading plots of endometabolomic samples from *S. marinoi* in a species-specific subset analysis of the interaction between *T. weissflogii* and *S. marinoi*.

The constrained score plots (graph **A**, **C**) visualize significant differences between the sample groups as found via CDA with a-priori groups by treatment (trace statistic $P = 0.0073$, misclassification error of 5.56 % for $m = 9$, graph **A**) and a-priori groups by treatment per day (trace statistic $P \leq 0.0001$, misclassification error of 5.56 % for $m = 9$, graph **C**). Vectors in the CAP loading plots (graph **B**, **D**) represent metabolites, characterized by their ID (red numbers). Only vectors with a significant correlation coefficient above the critical value of $|r| \geq 0.6028$ ($P \leq 0.0001$) are plotted. The direction of the vectors in 2-dimensional space correlates with endometabolomic sample groupings shown in the score plots of the respective analysis.

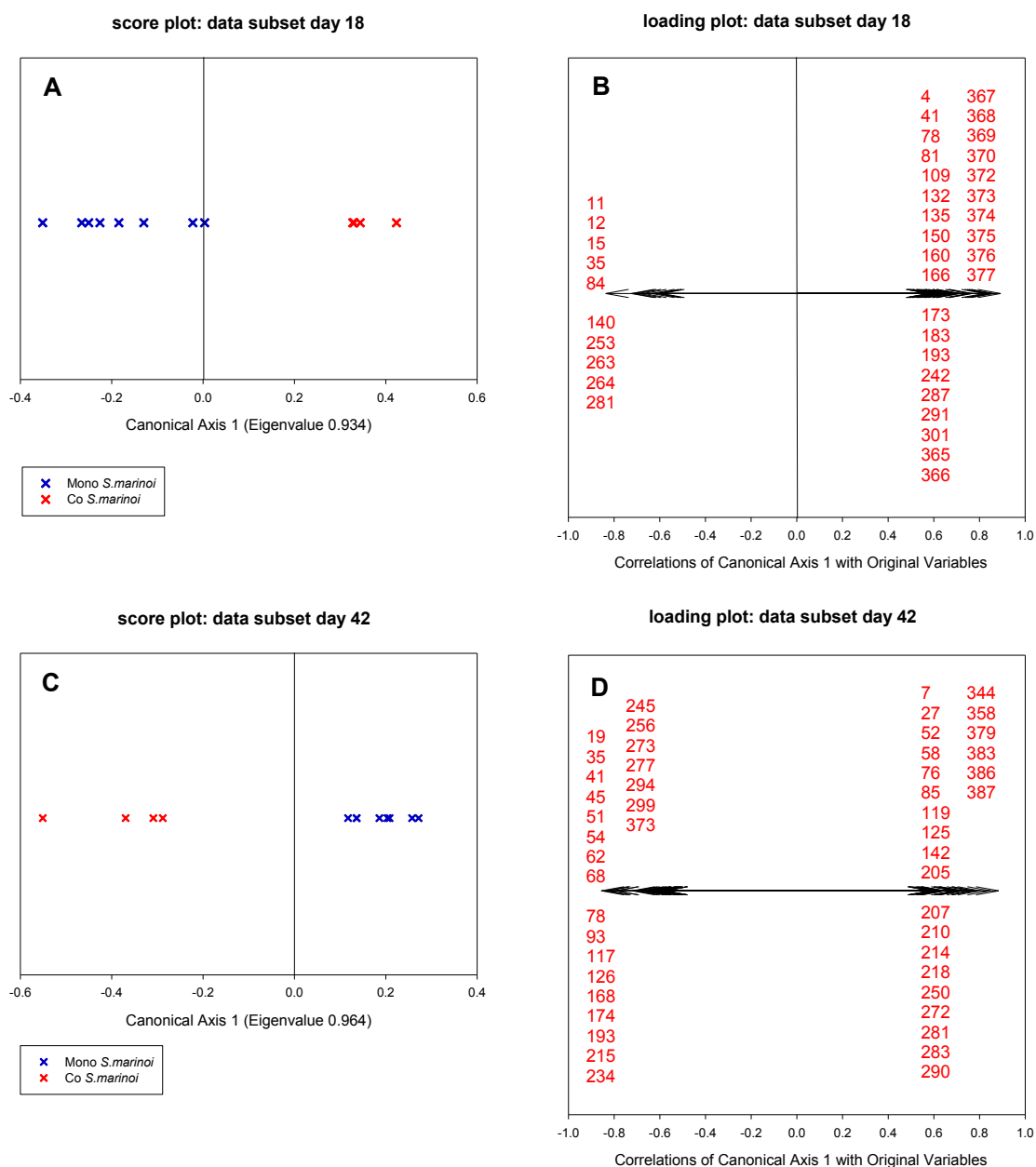


Figure 47: Constrained score and loading plots of endometabolomic samples from *S. marinoi* in a daywise subset analysis of the interaction between *T. weissflogii* and *S. marinoi*.

The constrained score plots (graph **A**, **C**) visualize significant differences between the treatments, as confirmed via CDA for the subset analysis on day 18 (graph **A**, **B**) and day 42 (graph **C**, **D**). These differences between treatments are significant (trace statistic $P = 0.0294$, misclassification error of 0 % for $m = 5$ (day 18) and $P \leq 0.0001$, misclassification error of 0 % for $m = 5$ (day 42)). Vectors in the CAP loading plots (graph **B**, **D**) represent metabolites, characterized by their ID (red numbers, pooled per group). Only vectors with a significant correlation coefficient above the critical value of $|r| \geq 0.5760$ ($P \leq 0.05$) are plotted. The direction of the vectors in 2-dimensional space correlates with endometabolomic sample groupings shown in the score plots of the respective analysis.

I conducted the evaluation of endometabolomic regulations via heatmap (**Table 18, Appendix 52**) as described for *T. weissflogii*.

Among amines, five candidates were highly correlating with the separation of treatments: 2-[(2-Chloroethyl)(ethyl)amino]ethanol (#27, #52) and urea (#55, #56) were downregulated in co-cultivation on day 30 and 42 of the stationary growth phase, as intensities were 1.3 - to 1.9 - fold higher in mono-cultivation. Similar to the findings in *T. weissflogii*, 1H-pyrrole-2-carboxylic acid (#82) was most abundant on day 18. In *T. weissflogii*, equal levels of this metabolite were documented in both treatments on day 18. However, in *S. marinoi* this MST was 1.5 - fold upregulated in co-cultivation. Furthermore, the regulation of putrescine (#173) was oppositional to the one observed in *T. weissflogii*: Instead of a downregulation as in *T. weissflogii* an upregulation of this amine in co-cultivation of *S. marinoi* was observed on day 18 and 30.

In total, six amino acids and two amino acid derivatives were significantly regulated in *S. marinoi* due to the interaction. As already described for *T. weissflogii*, all identified class members – with the exception of threonine (#67) – were most abundant on day 18 and thus characteristic for this day. Generally, serine (#59), proline (#69), pyroglutamic acid (#123) and N-acetylglutamic acid (#126) were upregulated in co-cultivation up to 2.8 - fold on all three sampling days. Furthermore, valine (#12, #49) was downregulated on day 18 and 30. However, although threonine (#68) and glycine (#72) were most abundant on day 18 as well, they were relevant for the separation of treatments on day 42, where they were clearly upregulated (threonine) or downregulated (glycine) in co-cultivation.

Among relevant alcohols, phenol (#7) and glycerol (#60, #61) were most abundant on day 18, while 1,2,3-butanetriol (#41) characterized day 30. Glycerol (#60, #61) was 1.4 - to 1.5 - fold more abundant in mono-cultivation on day 18 and 1,2,3- butanetriol (#41) was up to 8.4 - fold upregulated in co-cultivation on all three sampling days, thus characterizing *S. marinoi* in co-cultivation.

In both species, the alkaloid 3-pyridinol (#4) was correlating with the separation of treatments. However, while in *T. weissflogii* no meaningful regulation was observed, in *S. marinoi* this alkaloid was characteristic for day 42. On this day, it was downregulated in co-cultivation, with 1.5 - fold higher intensities in mono-cultivation. During earlier points of the stationary growth phase an upregulation in co-cultivation between 1.4 - and 2.2 - fold was found.

Considering carboxylic acids, putative hexanoic acid (#10), benzoic acid (#57) and glycolic acid (#11) were characteristic for day 18. However, only glycolic acid (#11) exhibited significant downregulation in co-cultivation. 3-Hydroxy-3-methylbutanoic acid (#47) and 3-hydroxy-2-

methylpropanoic acid (#29) were most abundant on day 30 and 42 and upregulated up to 38.5 - fold in co-cultivation. The abundance of citric acid (#192) increased during stationary phase. However, the abundance was only influenced by treatments on day 18, where an upregulation of 2.7 - fold in co-cultivation became apparent.

In the class of fatty acids, six fatty acids and eight fatty acid derivatives were identified. However, considering the relevance of each MST over time as indicated by temporal peaks in abundance, only nine metabolites were significantly regulated. Putative linoleic acid (#274) and putative 2-hydroxyethyl palmitate (#279) were upregulated on day 30. Considering day 42, putative 2,3-dihydroxypropyl palmitate (#287) was downregulated and putative C16:1-glycerol (#321) as well as stearic acid (#277) were up to 2.5 - fold upregulated on day 42. Note that putative C16:1-glycerol was represented by three MSTs (#320, #321, and #322). However, all of them showed the same trend in regulation. Both, 2,4-octadecadienoic acid (#239) and oleic acid (#273) were upregulated throughout all three sampling days, the latter up to 86 - fold. On the other hand, methyl-5,8,11,14,17-icosapentaenoate (#281) and methyl-4,7,10,13,16,19-docosahexaenoate (#307) were downregulated in co-cultivation on day 42, with up to 4.4 - fold higher intensities in mono-cultivation. Generally, fatty acids and their derivatives were characteristic for later stages of regular growth (day 30 and 42).

Among hydrocarbons, only 14-heptacosanone (#358) was regulated due to the interaction. Similar to the findings in *T. weissflogii*, this metabolite was downregulated in co-cultivation during stationary phase of growth (day 42).

In total, 28 identified MSTs made up the class of sugars and derivatives. The sugar acids threonic acid (#128), erythronic acid (#132), glucuronic acid (#221), the derivative gluconic acid-1,5-lactone (#208) and the sugar putative ribose (#160) were most abundant on day 18 and exhibited a clear tendency of upregulation throughout all three sampling days (up to 2.2 - fold in gluconic acid-1,5-lactone (#208) on day 42). Within this category, only sugar #140 (putative erythrose) and galactosylglycerol (#289) were downregulated in co-cultivation on day 18.

All remaining sugars and derivatives were characteristic for day 30 and 42. While on day 30 only sugar #109 (putative erythrose) was meaningfully upregulated in co-cultivation and arabinofuranose (#141) meaningfully downregulated, day 42 exhibited a significant regulation of this class. Besides the metabolites that were significantly upregulated throughout all three sampling days, arabinofuranose (#139, #141), 2-keto-gluconic acid (#180), sugar #109 (putative erythrose) and glyceric acid (#78) were upregulated and galactose (#207), myo-inositol (#242, #253) and a putative inositol isomer (#272) were downregulated on day 42.

Compared to *T. weissflogii*, more identified sugars and derivatives characterized day 18 in *S. marinoi* and were consistently upregulated in co-cultivation. While in *T. weissflogii* this metabolite class was strongly regulated on day 30 and rarely characteristic for day 42, the opposite was the case for *S. marinoi*. Here, sugars and derivatives were rather unspecific for treatments on day 30 and strongly regulated due to the interaction on day 42.

With exception of one putative disaccharide (#368), which was 128 - fold upregulated in co-cultivation on day 18, all complex saccharides were characteristic for later stages of the stationary growth phase (day 30 and 42). However, only three complex saccharides were significantly regulated: putative melezitose (#391) was upregulated throughout all three sampling days, a putative trisaccharide (#311) was downregulated on day 30, with 11.1 - fold higher intensities in mono-cultivation, and lactose (#346) was 1.4 - fold upregulated on day 42.

Interestingly, sterols exhibited a very distinct regulation pattern. Generally, sterols were most abundant on day 42, compared to the other sampling days. While most sterols were significantly upregulated in co-cultivation, relative to mono-cultivation on day 18, they were downregulated in co-cultivation on day 42. This regulation exceeded the threshold of 30 % for ergosta-5,24-dien-3-yl acetate (#365, #369 on day 18), ergosta-5,22-dien-3-yl acetate (#370), the further unidentified sterol “skel_cell_C178_sterol” (#375, (Vidoudez, 2010)), all of which were identified in the daywise analysis of day 18. Furthermore, campesterol (#383 on day 42), which was relevant for the separation of treatments on day 42, as well as fucosterol (#386 on day 18) and the sterol #387 (on day 42).

In the class of terpenes, I identified only phytol (#263). Although this metabolite was most abundant on day 18, it was meaningfully upregulated in co-cultivation on day 30 and 42. All unknown metabolites are summarized in **Appendix 52**.

Interestingly, three unknown metabolites were very strongly connected to the separation of treatments. Metabolites #372, #373 and #85 were strongly upregulated in co-cultivation on all three sampling days. The former were most abundant in the regular growth phase. MST #372 was only abundant in co-cultivation on day 18 and MST #373 was 113.2 - fold upregulated in co-cultivation on this day. MST #85, which was characterized via in-house library as Skel_MEDIA_C097 (Vidoudez, 2010) characterized all three sampling points equally. The other unknown metabolites are not further discussed.

ID	Model ion	RT	RI	Name	Class	Ident	Analysis	Median (Co: n=4, Mono: n=8)						Fold (Co relative to Mono)		
								Day 18		Day 30		Day 42		Day 18	Day 30	Day 42
								SM Mono	SM Co	SM Mono	SM Co	SM Mono	SM Co			
41	117	6.93	1130	1,2,3-Butanetriol	Alc		18,42						2.5	3.0	8.4	
4	152.1	5.35	922	3-Pyridinol	Alk	?	DT,18						2.2	1.4	-1.5	
10	173.1	5.72	971	Hexanoic acid	CA	?	DT						1.2	-	-1.7	
57	179.1	7.47	1203	Benzoic acid	CA		DT						1.0	-	-	
11	177.1	5.77	978	2-Hydroxyethanoic acid (Glycolic acid)	CA		DT,18						-1.8	-	-	
47	247.1	7.07	1149	3-Hydroxy-3-methylbutanoic acid	CA		42						-1.3	1.2	9.3	
29	233.1	6.59	1086	3-Hydroxy-2-methylpropanoic acid	CA		42						1.5	3.2	38.5	
192	273.1	12.13	1819	Citric acid	CA		DT						2.7	-1.0	-1.0	
218	143.1	12.91	1922	Methyl palmitate	FA dv.		DT,42						-1.1	-1.5	-2.4	
274	105.1	14.78	2256	Octadecadienoic acid (Linoleic acid)	FA	??	DT						-	2.0	-1.0	
279	239.2	14.96	2288	2-Hydroxyethyl palmitate	FA dv.	??	DT						1.1	1.3	-1.3	
298	343.3	15.75	2425	2,3-Dihydroxypropyl myristate	FA dv.		DT						1.0	1.0	-1.1	
308	357.3	16.28	2517	2,3-Dihydroxypropyl pentadecanoate	FA dv.	?	DT						1.3	1.0	-1.0	
320	369.3	16.70	2591	C16:1-glycerol ?	FA dv.		DT						1.1	-1.0	1.1	
287	116	15.24	2336	2,3-Dihydroxypropyl palmitate	FA dv.	??	18						-	-1.1	-1.3	
321	129.1	16.73	2596	C16:1-glycerol ?	FA dv.		DT						6.0	-1.1	1.3	
322	367.3	16.73	2597	C16:1-glycerol ?	FA dv.		DT						1.0	-1.0	1.1	
245	117	13.68	2025	Palmitic acid	FA	*	DT,42						-	-	1.2	
239	234.2	13.45	1994	2,4-Octadecadienoic acid	FA	?	DT						1.1	1.4	1.2	
273	339.3	14.76	2252	9-Octadecenoic acid (Oleic acid)	FA		42						1.2	86.0	2.1	
277	117	14.90	2277	Octadecanoic acid (Stearic acid)	FA		42						-	-	2.5	
224	117	13.03	1939	Pentadecanoic acid	FA		DT						-	-	-1.1	
281	117	15.06	2304	Methyl-5,8,11,14,17-icosapentaenoate	FA dv.		18,42						-2.4	-1.2	-4.4	
307	105.1	16.13	2492	Methyl-4,7,10,13,16,19-docosahexaenoate	FA dv.		DT						-3.4	1.4	-1.6	
199	123.1	12.31	1842	2-Methyl-7-octadecyne	HC	?	DT						-1.1	-1.5	-3.7	
210	123.1	12.61	1882	1,19-Icosadiene	HC	?	DT,42						-1.1	-1.4	-3.5	

ID	Model ion	RT	RI	Name	Class	Ident	Analysis	Median (Co: n=4, Mono: n=8)						Fold (Co relative to Mono)		
								Day 18		Day 30		Day 42		Day 18	Day 30	Day 42
								SM Mono	SM Co	SM Mono	SM Co	SM Mono	SM Co			
358	211.2	18.35	2871	14-Heptacosanone	HC dv.		DT,42						1.4	-1.1	-1.7	
128	292.1	10.03	1541	2,3,4-Trihydroxybutanoic acid (Threonic acid)	S acid		DT						1.0	1.0	1.4	
132	140	10.20	1564	2,3,4-Trihydroxybutanoic acid (Erythronic acid)	S acid		18						1.9	1.9	1.5	
160	205.1	11.10	1682	Ribose	S	?	DT,18						1.6	1.3	1.1	
208	319.2	12.55	1874	3,4,5-Trihydroxy-6-(hydroxymethyl)tetrahydro-2H-pyran-2-one (Gluconic acid-1,5-lactone)	S dv.		DT,42						1.0	2.0	2.2	
221	333.1	12.96	1929	Glucuronic acid	S acid		DT						1.3	1.3	2.0	
259	204.1	14.27	2166	Methyl-β-D-galactopyranoside	S dv.		DT						1.1	-1.2	1.3	
314	204.1	16.52	2560	Gulose	S		DT						1.0	-1.2	-1.0	
140	258.1	10.49	1602	Erythrose	S	?	18						-1.4	-1.0	-1.6	
229	432.9	13.18	1959	Hexonic acid (Gulonic acid)	S acid		DT						-1.1	1.2	1.2	
230	345	13.20	1961	Hexonic acid (Gulonic acid)	S acid		DT						-1.1	-1.0	1.3	
231	217	13.22	1963	5-(1,2-Dihydroxyethyl)-3,4-dihydroxydihydro-2(3H)-furanone (Galactono-1,4-lactone)	S		DT						-1.1	1.0	1.1	
249	205	13.86	2095	Methyl-β-D-galactopyranoside	S dv.		DT						-1.0	-1.0	-1.0	
289	204.1	15.30	2347	2,3-Dihydroxypropyl galactopyranoside (Galactosylglycerol)	S dv.		DT						-1.3	-1.1	-1.1	
131	292.1	10.15	1558	2,3,4-Trihydroxybutanoic acid (Threonic acid)	S acid		DT						1.2	-1.1	-1.0	
139	217	10.45	1597	Arabinofuranose	S		DT						1.1	-1.2	1.4	
141	217.1	10.51	1605	Arabinofuranose	S		DT						-	-1.4	1.5	
180	292.1	11.78	1773	2-Keto-gluconic acid	S acid dv.		DT						1.3	-1.1	1.4	
212	319.2	12.70	1894	Glucose	S		DT						1.0	-1.0	-1.1	
109	205.1	9.29	1443	Erythrose	S	?	18,42						1.6	1.6	2.4	
78	189.1	8.22	1302	2,3-Dihydroxypropanoic acid (Glyceric acid)	S acid		18,42						1.5	-1.1	1.8	
156	103.1	10.98	1667	Xylose	S	?	DT						-1.3	-	1.1	

ID	Model ion	RT	RI	Name	Class	Ident	Analysis	Median (Co: n=4, Mono: n=8)						Fold (Co relative to Mono)		
								Day 18		Day 30		Day 42		Day 18	Day 30	Day 42
								SM Mono	SM Co	SM Mono	SM Co	SM Mono	SM Co			
215	217.1	12.79	1906	5-(1,2-Dihydroxyethyl)-3,4-dihydroxydihydro-2(3H)-furanone (Galactono-1,4-lactone)	S acid dv.		DT,42	-	-	-	-	-	-	-	-	1.2
207	307.2	12.52	1871	Galactose	S	*	DT,42						1.1	-1.2	-1.7	
216	319.2	12.84	1913	Glucose	S	*	DT						1.0	-1.1	-1.2	
217	217.1	12.88	1918	Galactofuranose	S		DT						-1.1	-1.1	-1.2	
242	319	13.55	2007	myo-Inositol	S alc		DT,18						1.3	-1.1	-2.0	
253	107.1	13.97	2114	myo-Inositol	S alc		18						-1.3	-1.2	-2.0	
272	305.1	14.72	2245	Inositol isomer	S	?	42						1.5	-1.1	-2.0	
368	383.3	19.12	2992	Disaccharide -383 (Vidoudez)	CS	?	18						128.0	-	3.0	
340	360.9	17.53	2736	Maltose	CS		DT						1.2	-1.0	1.1	
400	361.20	24.85	3569	Maltotriose	CS		DT						1.5	-1.0	-1.2	
311	217.1	16.33	2527	Trisaccharide (Vidoudez)	CS	?	DT	-	-				-	-11.1	1.1	
346	204.1	17.79	2782	Lactose	CS	?	DT	-	-				-	1.2	1.4	
391	361.2	22.95	3410	Melezitose	CS	?	DT						1.9	-	1.3	
365	296.3	19.01	2974	Ergosta-5,24-dien-3-yl acetate	St	?	18						12.5	1.6	-1.3	
369	204.1	19.14	2995	Ergosta-5,24-dien-3-yl acetate	St		18	-					-	3.0	-1.2	
370	380.3	19.24	3011	Ergosta-5,22-dien-3-yl acetate	St		18						1.5	1.2	-2.6	
375	211.2	19.59	3066	Skel_cell_C178_sterol	St	??	18						5.2	-1.1	-2.7	
383	343.3	21.04	3250	Ergost-5-en-3-ol (Campesterol)	St		42						1.1	-1.1	-1.6	
386	129.1	21.84	3316	Stigmasta-5,24(28)-dien-3-ol (Fucosterol)	St		DT,42						1.7	1.1	-1.2	
387	386.3	22.02	3331	M000000_A337005-101-xxx_NA_3358,28_PRED_VAR5_ALK_NA (GOLM)	St		DT,42						1.2	1.1	-1.5	
263	143.1	14.48	2203	3,7,11,15-Tetramethyl-2-hexadecen-1-ol (Phytol)	T		DT,18						-1.2	1.4	1.4	

In case derivatized molecules are detected, the table entry lists their putative parent compounds. Each MST is characterized by **ID**, **model ion**, retention time (**RT**), retention index (**RI**) and its underlying CAP **analysis**. CAP analyses comprised the overall analysis with a-priori grouping by treatment and day (**DT**), with a-priori grouping by treatment (**T**), as well as daywise subset analysis on day 18 (**18**), day 30 (**30**) and day 42 (**42**). Metabolites were identified via libraries. If metabolites were verified with a standard, they are marked with *. “?” indicates a reversed match between 700 and 800, “??” a reversed match between 600 and 700 and “???” indicates cases where the reversed match was ≤ 600 . “!” tags metabolites with a match smaller than 600. Class abbreviations: Amine (**A**), alcohol (**Alc**), alkaloid (**Alk**), carboxylic acid (**CA**), complex sugar (**CS**), derivatives of a certain class (**dv.**), hydrocarbons (**HC**), sugar (**S**), sugar alcohol (**S Alc**), sugar acid (**S Acid**), sterol (**St**), terpene (**T**), others (**O**), unknown (**U**). **Vidoudez** refers to an MST code given by the in-house library, **GOLM** refers to an MST code given by distinct libraries of the Golm Metabolome Database.

3.3 Interim Conclusion

Due to the interaction with *T. weissflogii*, the growth of *S. marinoi* was significantly enhanced up to 41 % percent, as measured via cell counts. This effect manifested in the phase of regular growth due to increased growth rate of *S. marinoi* and continued to prevail in the stationary phase of growth as well. Compared to the interaction of *T. weissflogii* and *S. costatum*, the stimulatory effect was less pronounced.

Concerning the growth of *T. weissflogii*, I observed statistically significant but biologically negligible fluctuations of increased and decreased growth. As differences between mono- and co-cultivation were minor, I assumed the growth dynamic of *T. weissflogii* to lack any signs of relevant, interaction-induced alterations.

Among metadata, I documented no relevant interaction-induced alterations. Bacterial abundance data indicated the presence of bacteria, from the onset of the experiment. Meaning that the axenic state of the diatom cultures could not be maintained during the interaction. Interestingly, while in the interaction between *T. weissflogii* and *S. costatum* I documented increased silicate concentrations, in *S. costatum* cultures due to senescence no such observation was made in the present interaction.

In the context of metabolomic analyses, I based the choice of metabolomic sampling points on the same criteria described in chapter 2.6. The interaction of *T. weissflogii* and *S. marinoi* resulted in significant alterations in the metabolism of each diatom partner. These results resemble the ones for the interaction between *T. weissflogii* and *S. costatum* (chapter 2). I suggest that both diatom partners were able to sense and react to the presence of each other, as endometabolomic changes were found to be significant on day 18 and 42 within *S. marinoi* and on day 30 within *T. weissflogii*.

However, the extent of endometabolomic alterations was less distinctive compared to the interaction of *T. weissflogii* and *S. costatum*, as a multitude of the correlating metabolites was characterized by rather small intensity differences between mono- and co-cultivation. This observation might be connected to the fact that the growth stimulation was lesser in size as well. Furthermore, I graded the phenotypic response of *T. weissflogii* weaker, compared to the one of *S. marinoi*.

The exometabolomic analysis revealed significant, interaction-induced alterations on all three sampling days, suggesting an ongoing metabolite flux between the interaction partners. Interestingly, *S. marinoi* had a stronger impact on shaping the chemical environment in the

interaction, compared to *T. weissflogii*. This might be influenced by either different metabolite secretion rates (per cell) or by differences in cell counts between the species. In the present investigation, cell counts of *S. marinoi* were between 7 - to 17 - fold higher in co-cultivation, than cell counts of *T. weissflogii*. Thus, it seems reasonable that *S. marinoi* had a comparably higher impact on the chemical environment during the interaction. In comparison, cell counts of *S. costatum* were only 1.5 - to 3 - fold higher than *T. weissflogii* cell counts in co-cultivation (see interaction investigation in chapter 2.2).

I suggested eight metabolites to be regulated by reduced release, transformation or increased uptake mechanisms between *S. marinoi* and *T. weissflogii*. Hereby, the sterol 3,18-bis(acetyloxy)-14,15-epoxy-)pregn-16-en-20-one (#306, putatively identified), as well as the MST #193 presented themselves as very interesting candidate semiochemicals on day 18, as they exhibited a clear cut intensity pattern. Both were characteristic for the exometabolome of *S. marinoi*, completely absent in co-cultivation on day 18 and thus suggested to be involved in an interaction-induced uptake by *T. weissflogii*, transformation or reduced release mechanism on day 18. Furthermore, maltotriose (#339) and MST #162 are suggested to be involved in uptake mechanisms on day 18, as well as galactosylglycerol (#251) on day 30 and 42.

As discussed in chapter 2.6, the interpretation of pattern I metabolites – which potentially reflect interaction-induced increase in secretion – will become difficult and error-prone if cell count differences among treatment groups are observed. In the present investigation, I documented species-specific differences in cell-counts between the treatments over all sampling days⁶⁴. Nevertheless, a speculative interpretation of the patterns on days 18 and 30 will be given and pattern I metabolites correlating with day 40 were omitted due to differences in cell counts between treatments of approximately 40 %.

On day 18, I found the secretion of eight MSTs to be enhanced due to the interaction: putative gluconic acid (#206), gluconic acid 1,5-lactone (#180) and putative 7-tetradecanol (#103, #104), as well as the MSTs #119, #132, #205 and #210. Hereby, putative gluconic acid (#206) and the MSTs #132 and #205 were predominantly found in the medium of *S. marinoi* cultures, possibly suggesting increased secretion by *S. marinoi* due to the interaction.

On day 30, I hypothesized 17 metabolites to be secreted in higher amounts due to the interaction as they matched pattern I, including putative 2-(4-methyl-1-piperazinyl)ethanol (#53), hydroquinone (#73), 4-hydroxybenzaldehyde (#99), putative uridine (#275, #270), putative adenosine (#299, #300), guanosine (#311), putative maltose (#304) as well as the MSTs #59,

⁶⁴ ≤ 20 % on day 18, ≤ 25 % on day 30 and up to 41 % on day 42

#208, #241, #260, #265, #278, #291 and #330. Hereby, I suggested putative 2-(4-methyl-1-piperazinyl)ethanol (#53), the nucleosides putative uridine (#275, #270) and putative adenosine (#299, #300) as well as the MSTs #59, #208, #278, #29 and #241 to be excreted by *S. marinoi*, as they were hardly present in the medium of mono-cultivated *T. weissflogii* culture.

As growth stimulation occurred in *S. marinoi*, metabolite flux from *T. weissflogii* to *S. marinoi* might be expected as well. This lack of observable metabolite flux might be interpreted in several ways. For example, it might be possible that other factors than transfer of metabolites between the partners are responsible for the observed growth stimulation, e.g. nutrient effects, which cannot be depicted by the metabolomics approach. Or that the metabolomic profiling approach is simply blind towards certain metabolite flux dynamics, as discussed in chapter 2.6. Nevertheless, the present study clearly suggests a chemically-mediated interaction between both diatom partners.

In conclusion, I documented increased growth of *S. marinoi* in the presence of the diatom *T. weissflogii*. Metabolomic analyses revealed significantly altered cell physiology in both diatoms due to the interaction, as well as potential metabolite flux between the partners. Interestingly, the chemical environment of the diatoms was predominantly shaped by *S. marinoi*. Furthermore, I introduced two candidate semiochemicals, which are hypothesized to be secreted by *S. marinoi* and taken up or transformed by *T. weissflogii*.

4 Interaction of *T. weissflogii* with *S. dohrnii*

4.1 Experimental design

The experimental design of the interaction investigation of *T. weissflogii* and *S. dohrnii* resembled the one described in chapter 3. The investigation was used to further supplement previous findings. However, the cultures used for this interaction experiment were very susceptible to disturbances and were observed to repeatedly collapse during several pre-treatment attempts. Therefore, the robustness of the experiment was thought to be reduced. Nevertheless, value was created from the principal and metabolomic insights gained and the experimental conclusions will be subsequently described. The associated data is provided in the appendix (chapter 7.3).

4.2 Interim conclusion

In the interaction between *S. dohrnii* and *T. weissflogii*, I observed no meaningful interaction-induced growth effect for *S. dohrnii* (chapter 7.3.1). Considering growth parameters of *T. weissflogii*, the chl *a* fluorescence in co-cultivation was enhanced up to 17 % during the stationary phase of growth. However, I found no significant interaction-induced alterations of cell counts between the treatments. Compared to the interaction of *S. costatum* with *T. weissflogii*, the impact of the interaction between *S. dohrnii* and *T. weissflogii* on diatom growth parameters seemed weaker and more ambiguous, if present at all.

I used the metadata to monitor the interaction (chapter 7.3.2). Among PSII efficiency, no distinct differences were found between mono- and co-cultivated cultures within each species. Generally, the bacterial contamination in diatom cultures was minor, as bacterial cell counts only made up a fraction of diatom cell counts in both species. Furthermore, bacterial abundance decreased after the onset of the experiment. The diatom cultures were depleted of phosphate and silicate on day 11 or 15 and of nitrate on day 27. Interestingly, mono-cultivated cultures of *S. dohrnii* exhibited increased silicate availability on day 35. Apart from this observation, the metadata did not show distinct and meaningful differences among parameter dynamics due to the interaction.

The ambiguously observed growth effect was accompanied by minor phenotypical responses (chapter 7.3.4). A significant, interaction-induced alteration of the diatoms' endometabolomes was only observed on day 35 in *T. weissflogii* and on day 15 for *S. dohrnii*. Furthermore, it became apparent that compared to the other interactions, only a relatively small amount of

identified endometabolites exceeded the 30 % threshold. Especially in the context of the *S. dohrnii* endometabolomics, interaction-induced alterations seemed less distinct than the ones for *S. costatum* and *S. marinoi*.

Significant exometabolomic alterations due to the interaction between *T. weissflogii* and *S. dohrnii* suggested ongoing metabolite flux between the partners (chapter 7.3.3). As shown by the misclassification errors, interaction-induced exometabolomic differences were most distinct during early stages of diatom growth. Similar to the observation made in chapter 3.3, the chemical environment of the interaction was mainly shaped by *S. dohrnii*.

In total, 11 MSTs were potentially part of interaction-induced release mechanisms. Most of these MSTs were correlating with day 35 and thus late stages of the interaction. With exception of putatively identified 2-hydroxyhexanedioic acid (#94, related to day 27) and 4-(2-hydroxyethyl)phenol (#77, related to day 35), all metabolites were of unknown identity. Interestingly, MST #219 showed enhanced abundance in co-cultivation throughout all sampling days. It might be hypothesized that this MST is increasingly released by *S. dohrnii* in an ongoing manner due to the interaction with *T. weissflogii*. In the context of interaction-induced uptake, transformation or reduced release mechanisms, nine MSTs were of relevance, all of unknown identity.

To conclude, the interaction between *S. dohrnii* and *T. weissflogii* is – if at all – weakly pronounced, with slightly enhanced chl *a* fluorescence in *T. weissflogii*. As I found no meaningful differences in cell counts, the diatom interaction was categorized as a neutral interaction, causing no distinct growth stimulation or inhibition. Even though they were only marginally pronounced, endometabolomic alterations were documented at isolated sampling points, suggesting that the diatom partners were able to sense and react to the presence of each other at some points. Significant interaction-induced exometabolomic alterations suggest a metabolite flux between the diatom partners. Unfortunately, only few MSTs could be identified.

5 Concluding Discussion

In the scope of this thesis, I metabolomically investigated diatoms in three different interaction situations with the aim to advance our understanding of chemically-mediated interactions in phytoplanktonic organisms. Hereby, the metabolomic design guaranteed a direct assessment of interaction-induced phenotypical alterations (Fiehn, 2002) and the valuation of metabolite flux⁶⁵ between the partners. Generally, I set the focus on exometabolomic surveys with endometabolomic analyses supporting the investigations. The comparative nature of the approach gave room for simplification of the data sets to reduce the complexity of metabolomic investigations. Although limitations are inherent to every methodological approach (as discussed in chapter 2.5), the combination of elaborate and well-established techniques maximized the comprehensiveness of this investigation.

Experimental design

A previous study already introduced a co-culturing metabolomics approach and served as a basis for the method development presented here (Paul et al., 2009). I realized several improvements of the experimental. Firstly, I designed the interaction investigation in a dynamic way, investigating several time points before and during the observed growth effects. Secondly, the use of a GC-EI/TOF/MS analytical approach advanced the chemical identification of metabolomic alterations within the cell and in the chemical environment. Thirdly, an elaborate co-cultivation set-up replaced the simple dialysis tube-based approach to recreate chemical mediated interactions (Paul et al., 2013). Thus, I fundamentally increased the comparability of treatment groups within the experimental design (see chapter 2.1.1). Fourthly, I investigated the hypotheses of bacterial involvement and the impact of the prominent infochemical DMSP. Both factors were found to be incapable of stimulating the growth of *T. weissflogii*. Additionally, I broadened the scope of the investigation by substituting *S. costatum* in the interaction experiment with two closely related *Skeletonema* species, *S. dohrnii* and *S. marinoi*.

Although the explorative nature of the chosen metabolomic approach yielded in fertile insights, it also raised several questions, which will be subsequently discussed.

⁶⁵ As assessed via metabolite abundance patterns (chapter 2.2.3)

Ecological facilitation

One common trait of all three interactions was the observation of neutral to positive effects on diatom growth in interaction situations. Interestingly, I observed no distinct negative effects on diatom growth even though negative effects might be expected due to nutrient or interference competition (Reigosa et al., 1999; Legrand et al., 2003; Granéli and Hansen, 2006; Poulson-Ellestad et al., 2014a).

The observed growth stimulation strongly indicates ecological facilitation between the diatom partners (Stachowicz, 2001; Bruno, Stachowicz and Bertness, 2003). Facilitation is an ecological concept that comprises mutualistic interactions, where both partners benefit and commensalistic relationship, where one partner benefits and the other remains unaffected. Although positive interactions have the power to shape communities with a similar impact as negative interactions do, they are still rarely reported in current literature ((Stachowicz, 2001; Bruno et al., 2003) and references herein).

The investigated interactions are commensalistic in the case of *T. weissflogii* and *S. costatum*, as it is characterized by growth stimulation of *T. weissflogii*. As well as in the case of the interaction between *T. weissflogii* and *S. marinoi*, which results in growth stimulation of *S. marinoi*. As the interaction between *T. weissflogii* and *S. dohrnii* didn't cause any relevant alteration in diatom growth, it is considered neutral in an ecological sense. Although the outcome of the interaction experiments differed in respect to the extent of growth stimulation and the impacted species, all interactions were characterized by significantly altered chemical environments and distinct physiological alterations in the diatom partners.

In the marine environment, facilitation has previously been documented: The growth of the dinoflagellate *Alexandrium fundyense* is stimulated by the presence of native bacteria (Ferrier, Martin and Rooney-Varga, 2002) and marine cyanobacteria are known to stimulate the growth of other cyanobacteria and green algae (Lopes and Vasconcelos, 2011; Roy et al., 2013). Furthermore, mutualistic relationships between marine bacteria and phytoplankton have been reported, which are based for example on the exchange of fixed carbon and iron (Amin et al., 2009; Sieg et al., 2011) or vitamin B12 and vitamin B1 (Croft et al., 2005; Wagner-Döbler et al., 2010; Grant et al., 2014).

Ecological facilitation can have many faces ((Bruno et al., 2003) and references herein). Generally, the outcome of ecological facilitation is highly dynamic and varies with the biotic and abiotic environment (Bronstein, 1994): It is *inter alia* dependent on size, age and abundance of the participants, resource availability and the presence of 3rd party interaction partners. As a

consequence, the outcome of interactions ranges on a continuous scale from beneficial to antagonistic (Bronstein, 1994). A phenomenon also observed in the context of *Skeletonema* spp., as described in chapter 1.3 and demonstrated in the interaction experiments of this thesis.

Simply by growing, organisms alter their environment and thereby potentially create conditions favorable to other organisms (Stachowicz, 2001). However, why would naturally co-existing organisms, potentially competing for light, nutrients and light, indulge in a facilitative interaction?

By nature, co-existence comes with certain costs. Facilitation might be especially effective in face of environmental stress, when groups of organisms are better able to withstand than individual organisms do by themselves (Stachowicz, 2001). Here, the benefits of all positive or facilitative interactions need to be higher than costs (Stachowicz, 2001). In the context of marine ecology of microalgae, such stress could be for instance caused by nutrient limitation or predation. Facilitation might occur when organisms intermingle and modify the habitat in a way that makes it more favorable for another organism, e.g. by exuding compounds / nutrients that can be capitalized by another species (Stachowicz, 2001) and help them survive in otherwise unfavorable conditions.

Interestingly, the occurrence of a positive effect in the investigated diatom interactions (see chapter 2 and 3) coincides with the beginning of the stationary phase of growth, where nutrients become limited and environmental conditions more and more unfavorable. Thus, an incentive for the development of facilitative relationships is given. The phenomenon of ecological facilitation might be explained by three principles: (1) altered nutrient conditions, (2) heterotrophic interactions or (3) allelopathic interactions with their partner. All of which are caused by the presence of a partner organism and have the potential to cause the observed endometabolomic alterations in the diatoms.

Nutrient conditions

Alterations in nutrient conditions due to the presence of a partner can be discussed via two exemplary scenarios. Firstly, if a strong nutrient competitor is pooled with a weak nutrient competitor, the presence of the weaker partner might result in a surplus of available nutrients (compared to the mere presence of strong competitors), which might lead to enhanced growth and physiological alterations in the stronger partner. In order to differ between weak and strong competitors, nutrient uptake rates, which were reported to be species-specific (Harrison, Parslow and Conway, 1989; Sarthou et al., 2005) and the capability to indulge in ‘luxury’ consumption of nutrients (e.g. phosphorus) can be used. The latter means that under optimal-growth

conditions, nutrients are depleted from the medium and stored within the cells (Dyhrman, 2016). However, in this scenario the weaker partner would be expected to suffer from a lack of available nutrients and exhibit signs of decreased growth, assuming that nutrient needs will not change and nutrient availability is limited. Observations that were not in agreement with my findings.

Secondly, the liberation of nutrients by one partner and subsequent use by the other partner is possible, which results in stimulated growth. Interestingly, in two out of three interaction experiments (chapters 2.6 and 4.2), increased silicate availability in the medium of mono-cultivated *Skeletonema* sp. cells was observed (compared to the co-cultivation set-up), suggesting either a release of silicate by the diatom species or the release of silicate due to bacterial remineralization of dead diatom's frustules due to senescence (Roubeix, Becquevort and Lancelot, 2008; Diekmann et al., 2009; Vidoudez, 2010).

The described re-availability of silicate in cultures has also been documented for *T. weissflogii* in a bloom simulation experiment (Diekmann et al., 2009). Thus, it does not seem to be a species-specific phenomenon. The fact that silicate re-availability in the interaction experiment was only observed in *Skeletonema* mono-cultures, but not in *T. weissflogii* mono-cultures might have two reasons. Firstly, it might be hypothesized that senescence in both diatoms – and thus re-availability of silicate – proceeds at different rates. This might be supported by the fact that *S. costatum* cell counts decrease between day 26 and 32 while cell counts of *T. weissflogii* remain rather stable (chapter 2.2.1). Secondly, under the assumption of similar remineralization rates in both cultures, it might be hypothesized that the reuptake of silicate is faster in *T. weissflogii* cultures.

As silicate availability is known to crucially influence diatom growth rates and is an essential constituent of diatom frustules (Coombs et al., 1967; Diekmann et al., 2009), altered silicate re-availability due to the presence of a partner might be responsible for the observed growth effect. However, as only one of the two interactions exhibited a stimulatory effect, these findings suggest that underlying principles might be more complex than mere exchange of silicate, but may include the latter.

Heterotrophic interaction

Interaction-induced exometabolomic alterations strongly suggest the transfer of organic molecules between the partners. This might take place in the context of heterotrophic or allelopathic interactions. Heterotrophic interactions are mediated by primary metabolites (nutrition), which are used as an energy source in the trophic context. Allelopathic interactions

are mediated by secondary metabolites (infochemicals), which carry a message to the partner to elicit response (see chapter 1.2, (Nordlund and Lewis, 1976; Dicke and Sabelis, 1988)).

The differentiation between nutritionally and infochemically-mediated effects is one fundamental challenge in the field of allelopathy research. On the one hand, healthy cells are known to exude a multitude of organic compounds, possibly as a mechanism of extracellular storage in phytoplankton (Fogg, Nalewajko and Watt, 1965; Hellebust, 1965; Fogg, 1977; Sharp, 1977; Aaronson, 1978; Mykkestad, 1995; Barofsky, Vidoudez and Pohnert, 2009; Shniukova and Zolotareva, 2015): For example, carbohydrates, carbonic acids, amino acids, vitamins, fatty acids, sugars and other primary metabolites. Those primary metabolites present additional energy sources and can be taken up and metabolized in the context of heterotrophy (Metting and Pyne, 1986). On the other hand, several secondary metabolites, which might represent growth regulators in the context of allelopathy, rather than energy sources are produced by algae (Hay, 1996; Ianora et al., 2006).

Without knowing the identity of the substance, including potential modifications by third party organisms and the mode of action in the receiving organism, no clear distinction of mechanisms can be achieved (Borowitzka, 2016). A labeling experiment, as discussed in chapter 2.6 can be used to trace the origin and metabolomic path of substances of interest. Thus, underlying mechanisms can be unraveled.

Heterotrophic activity in algae is mostly connected to life in dark environments, as it sustains phytoplankton growth under adverse living conditions with very low irradiation, *e.g.* under ice in polar regions ((Morales-Sanchez et al., 2015) and references herein). Under those conditions, some microalgae can activate a heterotrophic metabolism instead of forming dormancy stages ((Tuchman et al., 2006) and references herein). Additionally, heterotrophic or mixotrophic⁶⁶ uptake of organic compounds is prominent in eutrophic waters with high organic compound concentrations ((Burkholder, Glibert and Skelton, 2008) and (Borowitzka, 2016) with references herein).

In the pelagic environment, heterotrophy was proposed to be less common as hydrodynamics and scaling between organisms might impair the exchange of organic compounds ((Coughlan, 1977) and references herein). However, in 1972 the concept of the phycosphere was coined (Bell, 1983). Despite relatively dominant hydrodynamics, cells are able to establish high compound concentrations within a diffusive boundary layer that surrounds each cell, which is called

⁶⁶ meaning the simultaneous utilization of heterotrophic and autotrophic mechanisms, to acquire organic compounds

phycosphere (Amin et al., 2012). Thus, cells are able to defy hydrodynamics to a certain extent and establish compound concentrations for effective exchange between partners. This is especially the case in bloom situations with close proximity and density of organisms.

Carboxylic acids, saturated fatty acids and multiple other classes of organic compounds are involved in heterotrophy among phytoplanktonic organisms ((Tuchman et al., 2006) and references herein). Furthermore, phytoplanktonic organisms are able to use dissolved organic nitrate (DON) to satisfy their N-needs, a capability that was long believed to be held by bacteria only (Bronk et al., 2006). Raven summarized that “amino acids, urea, purines, pyrimidines and glycine betaine, and, possibly, peptides and proteins” can be taken up by algae ((Raven and Giordano, 2016) and references herein). In the context of algae and bacteria, a mechanism has been documented where algae and bacteria share DON: Here, enzymatic properties at the alga’s surface clip nitrogen compounds in a way that the N-property is available for the alga and the C-backbone for bacteria (Palenik and Morel, 1990; Bronk et al., 2006). Additionally, the exchange of vitamins B1 and B12 between microalgae and bacteria (Croft et al., 2005; Wagner-Döbler et al., 2010; Grant et al., 2014) and the exchange of DMSP between microalgae (see discussion in chapter 2.1.4 and 2.4) is relevant in the context of heterotrophy as well.

Concerning the connectedness of heterotrophy and growth stimulation, Coughlan stated “if an alga can utilize an organic compound present in the medium then the growth characteristics of this alga in batch culture might be expected to be changed compared with a control with no substrate” (Coughlan, 1977). Among interaction-induced exometabolomic alterations, several primary metabolites have been found to be of relevance. Thus, the involvement of heterotrophy in the interactions between *T. weissflogii* and *Skeletonema* sp. is possible, although the involvement of DMSP as organic nutrient can be excluded.

The exometabolomic investigations yielded several identified compounds, which might establish heterotrophic relationships between the diatom partners. Especially, if nutrients become limited. In general, I set the focus of the metabolomic analysis on identifying already known chemical substances via library hits.

In the interaction of *T. weissflogii* and *S. costatum*⁶⁷, among others four fatty acids (myristic acid #111, pentadecanoic acid #117, palmitoleic acid #122/#123 and oleic acid #132), as well as a carboxylic acid (putative 2-hydroxypentanoic acid #40) were potentially involved in release-uptake mechanisms between day 16 and 26 (early phase of the interaction). Furthermore, the carboxylic acid succinic acid (#41) might be taken up, metabolized or released in a reduced way

⁶⁷ Chapter 2.2.3

due to the interaction. Interestingly, succinic acid was present in the exometabolomes of both diatoms grown in mono-cultures, but completely absent in co-cultivation on day 16, indicating uptake metabolization or reduced release. In addition, the carboxylic acids 4-hydroxybutanoic acid (#33) and putative 2-methylbenzoic acid (#50) as well as the fatty acid nonanoic acid (#48) were upregulated in co-cultivation on day 16.

As for the case of palmitoleic acid (#176, chapter 2.2.4), the endometabolomic analysis confirmed that this metabolite is found in the endometabolome of both diatoms and is characteristic for early stages of the growth phase as it is most abundant on day 16 and 26 of the interaction. Palmitoleic acid is a common fatty acid in diatoms (Volkman, 1986). Interestingly, in the endometabolome of *S. costatum* palmitoleic acid is less abundant in co-cultivation on day 16 and in the endometabolome of *T. weissflogii* it is more abundant in co-cultivation on this day, compared to mono-cultivation. As the exometabolomic availability in the interaction context is increased on day 16, it can be hypothesized that this is caused by the exudation of palmitoleic acid by *T. weissflogii*, resulting from increased endometabolomic availability.

Vice versa, on day 26 (stationary phase of growth) palmitoleic acid is more abundant in the endometabolome of *S. costatum* and less abundant in *T. weissflogii* on this day, both relative to mono-cultivation. Here, increased demand in *T. weissflogii* might be balanced out by increased uptake from the medium, which is reflected by low abundance of palmitoleic acid in the exometabolome in the interaction set-up on day 26, compared to both mono-cultivations. One reason for the fact that the hypothesized palmitoleic acid uptake is not reflected in an increased abundance in the *T. weissflogii* endometabolome might be a high turn-over rate. Generally, palmitoleic acid is a common fatty acid constituent of diatoms, which has been documented for *Skeletonema* sp. and *Thalassiosira* sp. (Pratt, 1966; Prartono, Kawaroe and Katili, 2013; Stonik and Stonik, 2015).

In the interaction of *T. weissflogii* and *S. marinoi*, maltotriose (#339, day 18) and galactosylglycerol (#251, day 30 and 42) might be taken up, metabolized or released in a reduced way due to the interaction, as their abundance was decreased in the interaction context. On the other hand, on day 18 (in the early stage of the interaction) the abundance of the sugar acid putative gluconic acid (#206), its derivative gluconic acid 1,5-lactone (#180) and the alcohol putative 7-tetradecanol (#103, #104) were enhanced in the interaction context. The latter was potentially secreted by *S. marinoi* during the interaction. On day 30, the presence of the alcohol 4-hydroxybenzaldehyde (#99), the sugar putative maltose (#304) and the nucleosides guanosine (#311), putative uridine (#275, #270) and putative adenosine (#299, #300) were enhanced due to

the interaction. The last two were potentially excreted by *S. marinoi*, as they were hardly present in the exometabolome of *T. weissflogii* cultures in mono-cultivation.

In the interaction of *T. weissflogii* and *S. dohrnii*, putative 2-hydroxhexanedioic acid (#94) showed enhanced abundance on day 27.

Generally, the abundance of the presented exometabolites in the culture medium can be used to not only draw hypotheses about release / uptake mechanisms, but also about the regulation of intracellular metabolite pathways, which account for the observed exometabolomic alterations. Those intracellular regulations can partly be assessed via the endometabolomic analysis. However, in this thesis I consciously set the focus to not investigate metabolomic pathways, as the used metabolomic technique is not optimized for intracellular flux analyses. I rather used the endometabolomic analysis as a snapshot tool to characterize the endometabolomic state. To extract more information about metabolite flux within the cell, I advise a metabolite flux analysis with ^{13}C -labeling (see discussion later on and in chapter 2.6).

Allelopathic interactions

The allelopathic potential of diatoms has been widely reported (Sharp et al., 1979; Borowitzka, 2016). In the case of *S. costatum*, both negative as well as positive allelopathic effects towards a multitude of organisms have been documented and the involvement of various allelochemicals has been assumed (compare chapter 1.3, (Yamasaki et al., 2007, 2011, 2012; Qiu et al., 2014))⁶⁸. In contrast to heterotrophic effects, allelopathic effects are mediated via secondary metabolites (Legrand et al., 2003; Borowitzka, 2016).

I presented principles of allelopathic investigations in chapter 1.3, including: the types of allelopathic interactions, factors influencing the outcome of allelopathic interactions and the allelopathic potential of *Skeletonema* spp.. Under the assumption of allelopathy and in consideration of the different interaction outcomes, possible explanations could be species-specific differences in allelopathic potential between the *Skeletonema* strains (Keating, 1977, 1978; Fistarol et al., 2004; Kubanek et al., 2005; Yamasaki et al., 2011), intrastrain variability between the used *T. weissflogii* strains (Alpermann et al., 2009, 2010), or variations in receiver and emitter population density (Sharp et al., 1979; Jonsson et al., 2009; Yamasaki et al., 2011; Qiu et al., 2014). Furthermore, the susceptibility of the receiver might be influenced by its physiological state (Fistarol et al., 2005; Ianora et al., 2006).

⁶⁸ A comprehensive description and discussion of the allelopathy concept is given in chapter 1.3.

In the context of allelopathy between *Thalassiosira* sp. and *Skeletonema* sp., the impact of different initial cell count ratios, as well as the impact of time on the allelopathic effect has previously been tested (Yamasaki et al., 2011). Interestingly, the growth of *T. rotula* cultures, as measured via maximum chl *a* fluorescence, was stimulated by *S. costatum*. However, with increased ratios of initial *S. costatum* / *T. rotula* concentrations, the extent of the stimulatory effect on *T. rotula* decreased and an initial lag phase appeared. Thus, variance in the outcome of observed stimulatory effects might result from initial cell count ratios of both diatom partners.

From an evolutionary perspective the explanation of negative allelopathy is far easier than the explanation of positive allelopathy: it is hypothesized that allelopathic potency presents a competitive advantage to the emitting organism (Legrand et al., 2003). This mechanism is referred to as interference competition and is well known from terrestrial ecosystems (Wink, 2003): by emitting allelochemicals, microalgae could reduce competition in their close vicinity and thus gain benefit for survival and / or reproductive fitness. While interference competition is a common explanation used in the context of negative allelopathic effects in the marine environment, it struggles with the explanation of positive allelopathic effects. Especially, if a targeted communication is assumed.

Generally, Lewis et al. strongly questioned the concept of targeted chemical interactions based on the nature of aqueous environments and proposed the production of allelochemicals in the context of interference competition as an evolutionary unstable concept (Lewis, 1986). This was mainly due to the fact that metabolomic costs for allelochemical production are rather high and that both spatial associations between organisms as well as organisms and their released allelochemicals is often not given in aqueous environments; furthermore transmission of compounds in water is a very inefficient process due to velocity and distance (Lewis, 1986; Martin, 2003; Arrieta, Barreira and Tuval, 2015). As a consequence, targeted communication based on allelochemicals was proposed to be an ecological unstable concept.

Nevertheless, Lewis interpreted the findings of Keating as clear evidence for allelopathy in field conditions (Keating, 1977, 1978). To explain this phenomenon, an alternative explanation was suggested - the allelochemicals-signal hypothesis (Lewis, 1986): Generally, allelochemicals might be used as environmental cues by the receiving organisms, which enable them to align their life cycles to the environmental conditions. In this hypothesis, the significance of allelochemicals is completely determined by the receiving organism, from emitter perspective they are mere exudates. This hypothesis harmonizes with the understanding that ecological facilitation often results from natural, potentially untargeted modification of the environment by growing organisms (Stachowicz, 2001).

Among interaction-induced exometabolomic alterations, in this study I identified several secondary metabolites, strongly suggesting an allelopathic interaction. The subsequent discussion is mainly based on identified metabolites. Unfortunately, I could identify only a fraction of metabolites, but numerous unknown MSTs bear the potential to mediate the interaction as well. I described and classified all MSTs in the respective chapters and interim conclusions (chapters 2.2.3 and 2.6, 3.2.3 and 3.3, 4.2 and appendix chapter 7.3.3), but they will not be further addressed at this point.

In the interaction of *T. weissflogii* and *S. costatum*, the putative alkaloid 2-hexylpyridine (#51) might be involved in release-uptake mechanisms at the onset of the interaction. 2-Hexylpyridine has previously been isolated from bacteria and in previous investigations showed inhibitory activity towards microorganisms (Salih and Çelikbıçak, 2012). However, its role in the marine environment is still to be determined and no negative effect as such was documented in the investigated diatom interaction. Furthermore, the terpenoid dehydroabietic acid (#135) exhibited reduced abundance in co-cultivation on all three sampling days with clearest characteristic during early stages of the interaction. I suggest this terpenoid to originate from *T. weissflogii* and either its exudation by *T. weissflogii* was reduced, or it was continuously taken up by *S. costatum* or transformed over the course of the interaction.

Dehydroabietic acid (#135) has been intensely studied as conifer biomarker and is known for its antibacterial and antifungal activity (Vargas et al., 1999; Savluchinske-Feio et al., 2006; González, 2015; Costa et al., 2016). Just recently, dehydroabietic acid was proposed to be an allelochemical in the aquatic environment as well, as it is produced and released by several cyanobacteria strains and exhibits antibacterial properties (Costa et al., 2016). The compound was not reported to have antialgal activity, as tested via *Chlorella vulgaris* (Costa et al., 2016).

In the interaction between *T. weissflogii* and *S. marinoi*⁶⁹, I hypothesized the sterol⁷⁰ #306 to be either taken up by *T. weissflogii*, metabolized or less exuded by *S. marinoi* due to the interaction on day 18. Sterols are part of the diatoms' cell membranes and determine its stability and permeability (Stonik and Stonik, 2015). It has been proposed that the concentrations of sterols in the cell membranes influence and signal transduction and membrane permeability (Dufourc, 2008). Thus, the reduced release of sterols, as hypothesized for *S. marinoi*, might directly result in an altered membrane permeability and thus modify the biological activity of *S. marinoi* and indirectly shape the allelochemistry between the interaction partners.

⁶⁹ Chapter 3.2.3

⁷⁰ Putative 3,18-bis(acetyloxy)-14,15-epoxy-)pregn-16-en-20-one

Furthermore, sterols are involved in cellular defense mechanisms against oxygen and are precursors for hormones and bioactive secondary metabolites ((Fabris et al., 2014) with reference to (Dufourc, 2008; Galea and Brown, 2009)). In diatoms, sterols containing C₂₇-C₂₉ backbones are most abundant (Rampen et al., 2010). In plants, steroids in general are known for their essential role as hormones. In this context, growth-promoting compounds have been reported, e.g. brassinosteroids from rape pollen, which have the potential to promote growth of other plants (Mitchell et al., 1970; Bishop and Koncz, 2002). Considering the hypothesis that the uptake of sterol #306 by *T. weissflogii* is increased, it might be possible that sterol #306 conveys a growth promoting message.

In addition, MST #205 was increasingly exuded on day 18 and putative 2-(4-methyl-1-piperazinyl)ethanol (#53) and hydroquinone (#73) on day 30. Hereby, metabolite #53 was potentially excreted by *S. marinoi*. While putative 2-(4-methyl-1-piperazinyl)ethanol (#53) is an unknown natural product, hydroquinone derivatives have been widely reported to occur in marine sponges and are known for their antitumor, antibacterial and antiviral activity (Wright, Rueth and Cross, 1991; Nguyen et al., 2016). Furthermore, the allelopathic potential of hydroquinone towards diatoms has been reported as growth, photosynthesis and the physiological state of diatoms is negatively affected (Yang et al., 2013). Thus, hydroquinone has been proposed as algaecide to control marine microalgae (Yang et al., 2013).

Interestingly however, in the interaction between *T. weissflogii* and *S. marinoi*, I documented no negative impact on diatom growth. As previously described, the allelopathic effect depends on a multitude of factors and one allelochemical may convey both positive and negative messages to its receiver, depending on the circumstances. Therefore in a next step, the impact of the potential allelochemicals in the context of the interaction between *T. weissflogii* and *S. marinoi* must be further investigated.

In the interaction of *T. weissflogii* and *S. dohrnii*⁷¹ I documented no relevant growth effect. Nevertheless, I suspected 4-(2-hydroxyethyl)phenol (#77) to be involved in interaction-induced release mechanisms on day 35. Phenolic compounds are known to be involved in stress responses, as they can protect cells from reactive oxygen species (Bentes et al., 2011; Rico et al., 2013) and various phenolic compounds have been found in diatoms like *Phaeodactylum tricorutum* (Rico et al., 2013). However, the role of this compound in the interaction is unclear.

Although further analyses are needed to understand the meaning and biological role of the proposed metabolites, I excluded the involvement of the prominent infochemical DMSP in the

⁷¹ Chapter 4.2

stimulatory growth effect on *T. weissflogii*. Also I could show that the bacterial community of the partner diatom is not capable of producing the observed stimulatory effect on diatom growth.

Summary and outlook

In the context of this thesis it was my aim to unravel underlying principles of allelopathic phytoplankton dynamics with a focus on the interactions between *Thalassiosira* sp. and *Skeletonema* sp., both dominant bloom formers in the phytoplankton (Kooistra et al., 2008; Dreux Chappell et al., 2013). Chemically-mediated interactions impact ecosystem structure and functionality on a very basic level as they are involved in a number of key life processes (Borowitzka, 2016). Among chemically-mediated interactions in the phytoplankton, allelopathy is the most studied type (Borowitzka, 2016). However, underlying mechanisms of those interactions are still to be fully clarified.

Diatoms are of essential importance for marine and terrestrial ecosystems: They impact the global carbon cycle (Keeling and Shertz, 1992; Field et al., 1998), global climate (Bates et al., 1987; Charlson et al., 1987) and form the basis of the marine food web. To understand these fundamental and global ecosystem dynamics, it is of great interest to investigate underlying principles and dynamics in phytoplankton communities.

This thesis focuses on the poorly understood positive allelopathy in phytoplankton.

The outcome of the investigated interactions indicates ecological facilitation between *Thalassiosira* sp. and *Skeletonema* sp.. Interestingly, I observed only positive to neutral effects on diatom growth, but no negative or inhibitory effects. The interaction effect hereby differed among the *Skeletonema* species: *S. costatum* or *S. marinoi* and *T. weissflogii* interacted in a commensalistic way, while I considered the interaction between *S. dohrnii* and *T. weissflogii* to be ecologically neutral.

Picking up findings of Paul et al. on the positive allelopathy in the interaction between *T. weissflogii* and *S. costatum* (Paul et al., 2009), a GC-EI/TOF/MS analytical approach advanced the identification of metabolomic alterations within the diatom cells and in their environment. I used an elaborate co-cultivation set-up to manipulate the interaction and to monitor chemically-mediated interactions in a standardized experimental design. By broadening the scope of the interaction and introducing three different *Skeletonema* species into the interaction investigation, it was possible to investigate three interactions clearly showing traits of ecological facilitation.

- In the interaction of *T. weissflogii* and *S. costatum*, *T. weissflogii* showed significantly enhanced growth in co-cultivation. Cell counts were elevated by up to 81 % (day 26)

and chlorophyll a up to 39 % (day 23) due to the interaction. The effects on the growth of *S. costatum* were ambiguous.

- In the interaction between *T. weissflogii* and *S. marinoi*, growth of *S. marinoi* was significantly enhanced due to the interaction with *T. weissflogii*. Compared to the negative control, cell counts in co-cultivation were increased up to 41 % and chlorophyll a fluorescence up to 31 % (day 42). Considering growth parameters of *T. weissflogii*, I observed no consistent and distinct long-term trend of increase or decrease.
- In the interaction between *T. weissflogii* and *S. dohrnii*, no meaningful interaction-induced growth effect was observed for *S. dohrnii*. Considering growth parameters of *T. weissflogii*, the chlorophyll a fluorescence in co-cultivation was enhanced up to 17 % during the stationary phase of growth. However, I found no significant interaction-induced alterations of cell counts between the treatments.

Each interaction was characterized by significant endometabolomic alterations within the interaction partners. Independent of the type of interaction, diatom partners are able to sense the presence of each other, as indicated by a significantly altered intracellular metabolome.

In all three interactions, the exometabolomic analyses strongly suggest a metabolite transfer between the interaction partners. As both primary and secondary metabolites were involved, I discussed allelopathy and heterotrophy as underlying principles and broadened the initial hypothesis of allelopathy. In the context of both theories, I introduced a set of highly interesting metabolites and potential allelochemicals. Furthermore, in this thesis I proposed hypotheses about release / uptake mechanisms and interaction-induced alterations of the chemical environment described (compare chapter 5).

In the context of allelopathy

In the interaction of *T. weissflogii* and *S. costatum*⁷², the putative alkaloid 2-hexylpyridine (#51) might be involved in release-uptake mechanism at the onset of the interaction. Release-uptake mechanisms refer to dynamics where one interaction partner releases metabolites, which are subsequently taken up by the other partner. Furthermore, the terpenoid dehydroabietic acid (#135) exhibited reduced abundance in co-cultivation on all three sampling days with clearest characteristics during early stages of the interaction. I thought this terpenoid to originate from

⁷² Chapter 2.2.3

T. weissflogii and either its exudation by *T. weissflogii* was reduced, or it was continuously taken up by *S. costatum* or transformed over the course of the interaction.

In early stages of the interaction between *T. weissflogii* and *S. marinoi*⁷³, I hypothesized a sterol⁷⁴ #306 to be either taken up by *T. weissflogii*, metabolized or less exuded by *S. marinoi* due to the interaction. In addition, MST #205 was increasingly exuded during early stages as well and putative 2-(4-methyl-1-piperazinyl)ethanol (#53) and hydroquinone (#73) during later stages. Hereby, metabolite #53 was potentially excreted by *S. marinoi*.

In the interaction of *T. weissflogii* and *S. dohrnii*⁷⁵ I suspect 4-(2-hydroxyethyl)phenol (#77) to be involved in interaction-induced release mechanisms during later stages of the interaction.

In the context of heterotrophic interactions

In the interaction of *T. weissflogii* and *S. costatum*, among others four fatty acids (myristic acid #111, pentadecanoic acid #117, palmitoleic acid #122/#123 and oleic acid #132) as well as a carboxylic acid (putative 2-hydroxypentanoic acid #40) were potentially involved in release-uptake mechanisms during early stages of the interaction. Furthermore, the carboxylic acid succinic acid (#41) might be taken up, metabolized or its release might be reduced due to the interaction. In addition, the carboxylic acids 4-hydroxybutanoic acid (#33) and putative 2-methylbenzoic acid (#50), as well as the fatty acid nonanoic acid (#48) were upregulated in co-cultivation during early stages of the interaction.

In the interaction of *T. weissflogii* and *S. marinoi*, maltotriose (#339) and galactosylglycerol (#251) might be taken up, metabolized or their release might be reduced due to the interaction, as their abundance was decreased in the interaction context. On the other hand, the abundance of the sugar acid putative gluconic acid (#206), its derivative gluconic acid 1,5-lactone (#180) and the alcohol putative 7-tetradecanol (#103, #104) were enhanced in the interaction context. The latter was potentially secreted by *S. marinoi* during the interaction. In the stationary phase, the presence of the alcohol 4-hydroxybenzaldehyde (#99), the sugar putative maltose (#304) as well as the nucleosides guanosine (#311), putative uridine (#275, #270) and putative adenosine (#299, #300) were enhanced due to the interaction. The last two were potentially excreted by *S. marinoi* as they were hardly present in the exometabolome of *T. weissflogii* cultures in mono-cultivation.

⁷³ Chapter 3.2.3

⁷⁴ Putative 3,18-bis(acetyloxy)-14,15-epoxy-)pregn-16-en-20-one, numbers refer to entries in respective data tables (here **Table 12**)

⁷⁵ Chapter 4.2

In the interaction of *T. weissflogii* and *S. dohrnii*, putative 2-hydroxhexanedioic acid (#94) showed enhanced abundance in co-cultivation during the stationary phase of growth. Significant exometabolomic alterations due to the interaction between *T. weissflogii* and *S. dohrnii* suggested ongoing metabolite flux between the partners. Interaction-induced exometabolomic differences were most distinct during early stages of diatom growth. Unfortunately, only few MSTs could be identified.

Although further analyses are needed to understand the meaning and biological role of the proposed metabolites, I could present a clear picture of interaction-induced regulation of metabolites and proposed potential transfer dynamics between the interaction partners. Furthermore, I excluded the involvement of the prominent infochemical DMSP in the stimulatory growth effect on *T. weissflogii*. Also I showed that the associated bacterial community of the partner diatom is not capable of producing the observed stimulatory effect on diatom growth.

While the results of this thesis help to better understand and characterize interactions between *Thalassiosira* sp. and *Skeletonema* sp., I advise further supplementary investigations:

First of all, the preliminary identified metabolites need to be verified via co-injection of standard substances. Secondly, to test the hypotheses of heterotrophy and allelopathy, the biological activity of the identified allelochemicals needs to be tested, as well as the heterotrophic potential of the identified primary metabolites. As a starting point, I recommend small-scale growth experiments, *e.g.* in well-plates or small culture flasks. By adding the identified fatty acids, carboxylic acids, sugars and their derivatives, alcohols and nucleosides in the context of a feeding experiment as well as the secondary metabolites in the context of an allelochemical experiment, their impact on diatom growth can be assessed. Using the insights of these experiments, candidate molecules should be submitted to further analyses for unambiguous identification.

To get more clarity on underlying principles and to further pursue the proposed hypotheses of uptake and release mechanisms, a ^{13}C labeling approach via metabolite flux analyses is strongly advised (see discussion in chapter 2.6). The subsequent labeling of both interaction partners allows to gain comprehensive insights into the interaction dynamic and the metabolite flux in the interaction. With the help of this method it is possible to trace the metabolite origin, uptake and even metabolization by the interaction partner. Another advantage is that this approach also allows the assessment of synergies between several metabolites and is open to both hypotheses: allelopathy and heterotrophic interactions.

In a next step, these insights need to be introduced into more complex experimental set-ups, which allow the verification in an ecological context. Not only considering larger scale

experiments like micro- or mesocosms, but also ecologically more complex scenarios like tripartite communities. Thus, after elucidating the chemical mediators between organisms, their relevance can be evaluated under different ecological scenarios.

Zusammenfassung und Ausblick

Im Kontext der vorliegenden Dissertation war es mein Ziel, die zu Grunde liegenden Prinzipien allelopathischer Dynamiken in phytoplanktonischen Lebensgemeinschaften aufzuklären. Der Fokus lag hierbei auf den Interaktionen zwischen *Thalassiosira* und *Skeletonema* Spezies, welche dominante Phytoplankton-Blüten bilden können (Kooistra et al., 2008; Dreux Chappell et al., 2013). Chemisch mediierte Interaktionen beeinflussen die Struktur und Funktionalität von Ökosystemen auf einer basalen Ebene, da sie einer Vielzahl von essentiellen biologischen Prozessen zu Grunde liegen (Borowitzka, 2016). Unter den chemisch mediierten Interaktionen wurde Allelopathie am meisten untersucht (Borowitzka, 2016), jedoch sind die zu Grunde liegenden Mechanismen noch immer nicht vollständig aufgeklärt.

Diatomeen sind für marine und terrestrische Ökosysteme von essentieller Bedeutung. Sie beeinflussen den globalen Kohlenstoffzyklus (Keeling and Shertz, 1992; Field et al., 1998), das globale Klima (Bates et al., 1987; Charlson et al., 1987) und stellen weiterhin die Basis des marinen Nahrungsnetzes dar. Um diese fundamentalen und globalen Dynamiken innerhalb des Ökosystems zu verstehen, ist es wichtig, die Dynamiken und Prinzipien innerhalb von phytoplanktonischen Lebensgemeinschaften zu untersuchen. Die vorliegende Arbeit fokussierte sich auf die bisher noch wenig untersuchte positive Allelopathie im Phytoplankton.

Zwischen *Thalassiosira* und *Skeletonema* Spezies zeichnet sich das Bild ökologischer Erleichterung⁷⁶. Interessanterweise habe ich entlang der untersuchten Interaktionen keine negativen oder inhibitorischen Effekte beobachtet, sondern ausschließlich stimulierende bis neutrale Einflüsse. Die Ausprägung des Interaktionseffekts variierte unter den *Skeletonema* Spezies: *S. costatum*, *S. marinoi* und *T. weissflogii* interagierten kommensalistisch, während die Interaktion zwischen *S. dohrnii* und *T. weissflogii* ökologisch neutral verlief.

Aufbauend auf den Ergebnissen von Paul et al. zur positiven Allelopathie in der Interaktion zwischen *T. weissflogii* und *S. costatum* (Paul et al., 2009), habe ich einen GC-EI/TOF/MS-basierten analytischen Ansatz gewählt, um die Identifizierung von metabolomischen Änderungen innerhalb der Diatomeenzellen und innerhalb ihrer Umwelt voranzutreiben. Ein innovatives Co-Kultivierungssystem ermöglichte die Manipulation der Interaktion und die Untersuchung von chemisch mediierten Interaktionen mit Hilfe eines standardisierten experimentellen Designs. Da ich den Umfang der Untersuchung auf drei verschiedene

⁷⁶ Übersetzung von „ecological facilitation“

Skeletonema Arten erweitert habe, konnte ich drei Interaktionen dokumentieren, die alle klare Anzeichen ökologischer Erleichterung aufwiesen.

- In der Interaktion zwischen *T. weissflogii* und *S. costatum* zeigte *T. weissflogii* signifikant gesteigertes Wachstum in Co-Kultivierung. Auf Grund der Interaktion waren die Zellzahlen bis zu 81 % (Tag 26) und die Chlorophyll a Fluoreszenz bis zu 39 % (Tag 23) erhöht. Der Einfluss auf das Wachstum von *S. costatum* war nicht eindeutig.
- In der Interaktion zwischen *T. weissflogii* und *S. marinoi* war das Wachstum von *S. marinoi* durch die Anwesenheit von *T. weissflogii* signifikant gesteigert. Im Vergleich zur Negativkontrolle waren die Zellzahlen in Co-Kultivierung bis zu 41 % und die Chlorophyll a Fluoreszenz um bis zu 31 % (Tag 42) erhöht. Entlang der Wachstumsparameter von *T. weissflogii* konnte ich keinen beständigen und eindeutigen Langzeittrend feststellen, der auf Zunahme oder Abnahme des Wachstums hindeutete.
- In der Interaktion zwischen *T. weissflogii* und *S. dohrnii* habe ich bei *S. dohrnii* keinen aussagekräftigen und durch die Interaktion verursachten Wachstumseffekt beobachtet. Unter Betrachtung der Wachstumsparameter von *T. weissflogii*, habe ich eine Steigerung der Chlorophyll a Fluoreszenz während der stationären Wachstumsphase um bis zu 17 % dokumentiert. Jedoch habe ich keine signifikanten Unterschiede in den Zellzahlen festgestellt.

Jede Interaktion wurde durch signifikante endometabolomische Änderungen innerhalb beider Interaktionspartner charakterisiert. Unabhängig vom Interaktionstyp sind beide Diatomeen Partner in der Lage, die Präsenz des anderen zu fühlen, wie durch die signifikanten Änderungen des intrazellulären Metaboloms belegt wurde.

In allen drei Interaktionen wiesen die exometabolomischen Analysen stark auf einen Metabolitentransfer zwischen den Interaktionspartnern hin. Da sowohl Primär-, als auch Sekundärmetabolite involviert waren, habe ich Allelopathie und Heterotrophie als zu Grunde liegende Mechanismen diskutiert und so die initiale Hypothese der Allelopathy erweitert. Im Kontext beider Theorien, stelle ich eine Auswahl sehr interessanter Metabolite und potentieller Allelochemikalien vor. Weiterhin schlage ich Hypothesen zu Freisetzungs- / Aufnahme-Mechanismen vor und beschreibe interaktionsbedingte Veränderungen der chemischen Umwelt (vergleiche Kapitel 5).

Im Kontext der Allelopathie

In der Interaktion zwischen *T. weissflogii* und *S. costatum*⁷⁷ war der putativ identifizierte Alkaloid 2-Hexylpyridin (#51) zu Beginn der Interaktion möglicherweise in Freisetzungs- / Aufnahme-Mechanismen involviert. Freisetzungs- / Aufnahme-Mechanismen beschreiben Dynamiken, in denen ein Interaktionspartner Metabolite freisetzt, welche im Anschluss daran vom entsprechenden Partner aufgenommen werden. Die terpenoide Verbindung Abieta-8(14),9(11),12-trien-18-säure (#135) kam in Co-Kultivierung an allen drei Beprobungstagen in reduzierter Häufigkeit vor. Die Reduktion war hierbei in frühen Stadien der Interaktion am prägnantesten. Ich vermute, dass dieser Metabolit von *T. weissflogii* stammt und entweder die Freisetzung des Metabolites reduziert wird, die Aufnahme durch *S. costatum* gesteigert ist oder eine Transformation stattfindet.

Für die frühen Phasen der Interaktion zwischen *T. weissflogii* und *S. marinoi*⁷⁸ stelle ich die Hypothese auf, dass der Sterol Metabolit⁷⁹ #306 entweder von *T. weissflogii* aufgenommen, metabolisiert oder in reduzierter Menge von *S. marinoi* freigesetzt wurde. Darüber hinaus wird der Metabolit #205 ebenfalls zu Beginn der Interaktion vermehrt freigesetzt und 2-(4-Methyl-1-piperazinyl)ethanol (#53, putativ identifiziert) und Hydrochinon (#73) zu späteren Zeitpunkten. Dabei stammt der Metabolit #53 potentiell von *S. marinoi*.

In späten Phasen der Interaktion zwischen *T. weissflogii* und *S. dohrnii*⁸⁰ vermute ich, dass 4-(2-Hydroxyethyl)phenol (#77) in einen interaktionsinduzierten Freisetzungs-Mechanismus involviert war.

Im Kontext der Heterotrophie

In frühen Phasen der Interaktion zwischen *T. weissflogii* und *S. costatum* waren unter anderem vier Fettsäuren (Myristinsäure #111, Pentadecansäure #117, 9-Hexadecensäure #122/#123 und 9-Octadecensäure #132), sowie eine Carbonsäure (2-Hydroxypentansäure #40 putativ identifiziert) potentiell in Freisetzungs- / Aufnahme-Mechanismen involviert. Außerdem ist es möglich, dass die Carbonsäure Bernsteinsäure (#41) im Kontext der Interaktion aufgenommen, metabolisiert oder in verminderter Menge freigesetzt wurde. Darüber hinaus waren die Carbonsäuren 4-Hydroxybutansäure (#33) und putativ identifizierte 2-Methylbenzoesäure (#50)

⁷⁷ Kapitel 2.2.3

⁷⁸ Kapitel 3.2.3

⁷⁹ Putativ 3,18-bis(acetyloxy)-14,15-epoxy-)pregn-16-en-20-one, die Zahlen verweisen auf die entsprechenden Datentabellen (hier **Table 12**)

⁸⁰ Kapitel 4.2

wie auch die Fettsäure Nonansäure (#48) während frühen Phasen der Interaktion in Co-Kultivierung hochreguliert.

In der Interaktion zwischen *T. weissflogii* und *S. marinoi* ist es möglich, dass Maltotriose (#339) und Galactosylglycerol (#251) im Kontext der Interaktion aufgenommen, metabolisiert oder in verminderter Menge freigesetzt wurden, da ihr Vorkommen im Interaktionskontext vermindert war. Auf der anderen Seite war die Abundanz der Zuckersäure Gluconsäure (#206), des Derivates Glucono-1,5-lactone (#180) und des putativ identifizierten Alkohols 7-Tetradecanol (#103, #104) im Interaktionskontext gesteigert. Letzt-genannter Metabolit wird während der Interaktion potenziell von *S. marinoi* freigesetzt. In der stationären Wachstumsphase war das Vorkommen des Alkohols 4-Hydroxybenzaldehyd (#99), des putativ identifizierten Zuckers Maltose (#304) sowie der Nukleoside Guanosin (#311), Uridin (#275, #270, putativ identifiziert) und Adenosin (#299, #300, putativ identifiziert) während der Interaktion gesteigert. Die beiden Letztgenannten wurden potenziell von *S. marinoi* freigesetzt, da sie im Exometabolom von *T. weissflogii* Kulturen kaum präsent waren.

In der Interaktion zwischen *T. weissflogii* und *S. dohrnii* war die Abundanz von putativ identifizierter 2-Hydroxyhexandisäure (#94) in Co-Kultivierung in der stationären Wachstumsphase gesteigert. Signifikante exometabolomische Änderungen, welche durch die Interaktion zwischen *T. weissflogii* und *S. dohrnii* verursacht wurden, legen einen kontinuierlichen Metabolitenaustausch zwischen den Interaktionspartnern nahe. Interaktionsinduzierte Unterschiede im Exometabolom traten am stärksten ausgeprägt während frühen Wachstumsphasen auf. Leider konnten nur wenige Metabolite identifiziert werden.

Auch wenn weitere Analysen notwendig sind, um die Bedeutung und biologische Relevanz der vorgestellten Metabolite vollständig aufzuklären, konnte ich doch ein klares Bild der interaktions-induziert regulierten Substanzen zeichnen und potenzielle Transferdynamiken zwischen den Interaktionspartnern vorschlagen. Weiterhin konnte ich die Beteiligung der prominenten Infochemikalie DMSP an dem stimulierenden Wachstumseffekt von *T. weissflogii* ausschließen. Außerdem habe ich gezeigt, dass die assoziierte bakterielle Lebensgemeinschaft der jeweiligen Partner-Diatomee nicht fähig ist, den beobachteten stimulierenden Wachstumseffekt bei Diatomeen zu reproduzieren.

Die Ergebnisse dieser Arbeit tragen dazu bei, die Interaktionen zwischen *Thalassiosira* und *Skeletonema* Spezies besser zu verstehen und zu charakterisieren. Ich empfehle darüber hinaus folgende weiterführende Untersuchungen:

In einem ersten Schritt müssen die vorläufig identifizierten Metabolite via Co-Injektion von Standardsubstanzen final identifiziert werden. Im Anschluss daran soll die biologische Aktivität der identifizierten Allelochemikalien, sowie das heterotrophische Potenzial der identifizierten Primärmetabolite getestet werden. Hierbei empfehle ich, mit Modellversuchen im kleinen Maßstab anzufangen, z.B. in Well-Platten oder kleinvolumigen Kulturflaschen. Der Einfluss der Substanzen auf das Wachstum von Diatomeen kann im Kontext von verschiedenen Experimenten getestet werden: die identifizierten Fettsäuren, Carbonsäuren, Zucker und entsprechenden Derivate, Alkohole und Nukleoside können im Kontext eines Heterotrophieexperimentes getestet werden und der Einfluss der Sekundärmetabolite in einem Allelopathieexperiment. Aufbauend auf den Ergebnissen dieser Experimente, sollten Kandidatenmetabolite weiteren Analysen unterzogen werden, um die Struktur final aufzuklären.

Um Klarheit über die zu Grunde liegenden Prinzipien zu erlangen und um die vorgestellten Hypothesen von Freisetzung und Aufnahme der Metaboliten weiter zu verfolgen, schlage ich ein ^{13}C basiertes Labeling-Experiment im Kontext einer Flux-Analyse vor (weitere Informationen in der Diskussion in Kapitel 2.6). Die nacheinander folgende Markierung beider Interaktionspartner erlaubt es hierbei, umfassende Einblicke in die Interaktionsdynamik und den Metabolitenfluss während der Interaktion zu gewinnen. Mit Hilfe dieser Methode ist es möglich, den Ursprung, die Aufnahme und sogar die Metabolisierung von Metaboliten durch die Interaktionspartner nachzuverfolgen. Ein weiterer Vorteil dieses Verfahrens ist, dass Synergieeffekte zwischen verschiedenen Metaboliten untersucht werden können und dass die Untersuchung beider Hypothesen möglich ist: Allelopathie und Heterotrophie.

In einem nächsten Schritt, müssen alle gewonnenen Erkenntnisse in ein komplexeres experimentelles Design überführt werden, welches eine Verifizierung im ökologischen Kontext gewährleistet. Dabei sollte nicht nur die Skalierung vergrößert werden, z.B. in Mikro- oder Mesokosmos Experimenten, sondern auch ökologisch komplexere Szenarios untersucht werden, z.B. Interaktionen in Lebensgemeinschaften mit mehr als zwei Organismen. Auf diese Weise kann die Relevanz der zuvor final identifizierten chemischen Substanzen in verschiedenen ökologischen Szenarien evaluiert werden.

6 Material and methods

6.1 Algae

6.1.1 Strains

Non-axenic strains of *Skeletonema costatum* (RCC75) and *Thalassiosira weissflogii* (RCC76, strain synonym CCMP1336) were obtained from Roscoff Culture Collection, Roscoff, France. *T. weissflogii* (CCMP1336) was isolated from Gardiners Island, Long Island, New York USA.

Axenic strains of *Skeletonema marinoi* (CCMP1332), *Skeletonema dohrnii* (CCMP 3373) and *Thalassiosira weissflogii* (CCMP1336) were obtained from The National Center for Marine Algae and Microbiota, East Boothbay, Maine, USA. *S. marinoi* (CCMP1332) was isolated from Milford, Connecticut USA. *S. dohrnii* (CCMP3373) was isolated from Narragansett Bay, Station 2, Rhode Island USA.

Axenic state of the purchased algae has been tested by The National Center for Marine Algae and Microbiota before shipment.

6.1.2 Medium

All strains have been cultured in artificial seawater medium, prepared similarly to the descriptions by Maier and Calenberg (Maier and Calenberg, 1994). Nutrient concentrations were 246 $\mu\text{mol/L}$ silicate, 11 $\mu\text{mol/L}$ phosphate and 621 $\mu\text{mol/L}$ nitrate. The artificial seawater medium was HEPES buffered with a pH of 7.8. It was stored in Nalgene® Polypropylene 1 L bottles and autoclaved at a sterilization temperature of 121 °C with a sterilization time of 15 min (end temperature 80 °C) before use.

Seawater medium for axenic cultures (up to a culture volume of max. 400 mL) has additionally been 0.20 μm sterile filtered (Filtropur S 0.2; Sarstedt, Nümbrecht, Germany) before addition.

6.1.3 Cultivation Parameters of Algal Stock

Stock cultures of all strains were grown in 40 mL sterile cell culture flasks (Sarstedt, Nümbrecht, Germany). They were cultivated with five replicates per species. Cultures were stored on an orbital shaker (75 rpm) under a 14/10 hours light/dark cycle in a climate chamber at 15 °C. The light intensity was approximately 55 $\mu\text{mol photons s}^{-1}\text{m}^{-2}$ provided from the top by Osram Lumilux® Cool White 15 W lamps.

For maintenance, cultures were inoculated into sterile filtered fresh medium (v/v_{sw} 1/1) once a month. All cultures were constantly held under sterile conditions. Culture vessels were only opened under a vertical flow sterile bench (BDK, Germany). Handling of cultures followed standard sterile techniques.

6.2 Co-cultivation

6.2.1 Chamber parts

The co-cultivation set-up as subsequently presented was developed and previously described by Carsten Paul (Paul, 2012; Paul et al., 2013).

A co-cultivation set-up consists of two chamber-halves, separated by a 0.22 μm hydrophilic PVDF membrane filter (Durapore®, Merck Millipore, Cork, Ireland). Each chamber-half was built from commercially available Duran flasks (VWR, Dresden, Germany), modified by a glass blower to possess a 100 mm flat edge opening and an additional opening with a 29 mm neck. When assembled, both chamber-halves frame the semi-permeable membrane, where in one of the halves an O-ring made out of silicone (201-0159, VWR, Dresden, Germany) guarantees the proper fit and alignment with the second half. A metal holding clamp (201-0192, VWR, Dresden, Germany) upon a layer of parafilm are used to fit both chamber-halves together and to prevent leaking. Upright storage of the assembled co-cultivation set-up on a cork ring ensures stability even on an orbital shaker. The openings for sampling are covered with cellulose stoppers and aluminum foil (both sterilized).

6.2.2 Chamber preparation and maintenance

While handling any parts of the co-cultivation system (details in 4.2.1), it is mandatory to wear clean gloves to avoid contamination of the parts. Before assembly, co-cultivation glass chambers and O-rings were cleaned in a laboratory dish washer twice without the presence of rinsing agents or any other contaminated glass ware. Metal holding clamps were cleaned with deionized water and dried before use. To ensure sterility, all parts necessary for the co-cultivation chamber assembly (with exception of parafilm) were autoclaved individually at a sterilization temperature of 121 °C with a sterilization time of 20 minutes and a dry time of ten minutes (end temperature 120 °C) before use under a vertical flow sterile bench.

6.2.3 Culture preparation

Before the onset of an experiment, stock cultures were inoculated into fresh artificial seawater medium (v/v_{SW} 1/3). To increase the culture volume and to keep the cultures in regular growth phase, cultures were repeatedly diluted (at least four times). Depending on culture viability, dilution steps were performed every four to ten days with dilution ratios of 1/1 to 1/3 (v/v_{SW}) to final culture volumes of up to 2 L in sterile cell culture flasks (Sarstedt, Nümbrecht, Germany). Volumes bigger than 400 mL were grown in sterilized Erlenmeyer flasks (500 mL, 1 L and 2 L) and sealed with autoclaved cellulose stoppers (VWR, Dresden, Germany) and sterilized aluminum foil. All solids were autoclaved at 121 °C for 15 min and cooled down to 80 °C before opening of the autoclave.

Investigation of the interaction between T. weissflogii and Skeletonema sp.

At the onset of the experiment (day 0), each chamber-half was filled with 400 mL freshly inoculated culture under sterile conditions. In the interaction of *T. weissflogii* with *S. costatum* (chapter 2.2) and *S. marinoi* (chapter 3) inoculation cultures were diluted 1/3 (v/v_{SW}), in the interaction with *S. dohrnii* (chapter 4) 1.5/2.5 (v/v_{SW}).

Investigation of initial co-cultivation conditions on T. weissflogii and S. costatum (medium experiment)

In the investigation of initial co-cultivation conditions (see medium experiment chapter 2.3) on *T. weissflogii* and *S. costatum*, a new experimental group was introduced: the medium exchange group (see experimental design in chapter 2.1.3). This group needed a medium manipulation of the species under investigation, before the inoculation of the co-cultivation chambers at day 0. Subsequently the medium manipulation is exemplarily explained for the investigation of *T. weissflogii*:

All cultures in use, originated from a pooled culture stock for *S. costatum* and *T. weissflogii*. The manipulated *T. weissflogii* culture was obtained, by combining the cell equivalent of 200 mL of *T. weissflogii* stock culture with the medium equivalent of 200 mL of *S. costatum* stock culture per chamber half. The medium equivalent was received by filtrating 200 mL of undiluted *S. costatum* stock-culture a GF/C filter (Whatman, Kent, UK) under reduced vacuum (≈ 700 mBar). For the cell equivalent, 200 mL of undiluted *T. weissflogii* stock culture were centrifuged at 15000 rcf for ten minutes. After decanting the supernatant medium, the retained *T. weissflogii* cells were immediately washed with fresh artificial seawater medium and the centrifugation-washing step was repeated (this procedure was performed twice). The last

centrifugation of the *T. weissflogii* cells was followed by resuspension of the cells in 200 mL *S. costatum* medium equivalent, resulting in a manipulated *T. weissflogii* culture. All steps were performed under sterile conditions.

At the onset of the experiments (day 0), both the medium manipulated and unaltered cultures were diluted with artificial seawater medium in a ratio 1/1 (v/v_{sw}). Each chamber-half was then filled with 400 mL freshly inoculated culture under sterile conditions.

6.2.4 Co-cultivation parameters

Cultures were stored on an orbital shaker (75 rpm) under a 14/10 hours light/dark cycle in a climate chamber at 15 °C. The light intensity was approximately 35 $\mu\text{mol photons s}^{-1}\text{m}^{-2}$ provided from the top by Osram Lumilux® Cool White 15 W lamps.

6.2.5 Sampling procedure

Before sampling, co-cultivation set-ups were gently, manually shaken to ensure thorough mixing of the cultures. Subsequently, regular sampling was performed under a vertical sterile bench and with standard sterile technique. The total sample volume was collected in sterile Falcon tubes or sterile Erlenmeyer bottles (depending on total sample volume and nature of the samples), before subsamples were taken for metabolomic and metadata analysis. To ensure maximum comparability, the sampling procedure was standardized and performed at the same time of the day within each experiment.

6.2.6 Biological replication in co-cultivation

The experimental designs for each conducted experiment are described in chapter 2.1, 3.1 and 4.1. Within each experimental group, three co-cultivation chambers were used as interaction replicates (4 co-cultivation chambers in the investigation of *T. weissflogii* and *S. marinoi*, chapter 3). The seawater control group was represented by one replicate, with exception of the investigation of *T. weissflogii* and *S. costatum*, in which no seawater control group was introduced.

The definition of one biological replicate differed among the investigated parameters. In general, each chamber half of each co-cultivation set-up was sampled and measured individually. With exception of nutrient analysis, pH and exometabolomic samples, for which volumes were pooled before measurement.

In the investigation of cell-based parameters (chl a, PSII efficiency, cell counts, bacterial abundance, endometabolome etc.), which were specific for each chamber half, one chamber of

the mono-cultivation groups was equivalent to one biological replicate ($n = 3/4$): Both chamber halves were sampled and measured individually, but for the analysis average values were used. In the co-cultivation group one chamber contained one biological replicate of *S. costatum* and one biological replicate of *T. weissflogii*. Thus, per species, one chamber half was considered one biological replicate with a total of three biological replicates for each species in co-cultivation ($n = 3/4$).

In the investigation of medium-based parameters (pH, nutrients, exometabolome etc.), the samples of both chamber halves were pooled and considered one biological replicate in both mono- and co-cultivation. Thus each experimental group contained three (4) biological replicates.

6.2.7 Experimental specifics

Interaction experiment between T. weissflogii and S. costatum

See chapter 2.1.2 for details.

In the endometabolome analysis of the interaction between *T. weissflogii* and *S. costatum* (chapter 2), two replicates of the mono-cultivation treatment of *T. weissflogii* were missing on day 16 and one mono-cultivation replicate of *S. costatum* was missing on day 32. There were just two exometabolomic replicates of the co-cultivation treatment available on day 26 due to the loss of a sample in the work-up process.

Medium experiment within the context of the interaction between T. weissflogii with S. costatum (chapter 2.3)

The investigation of *T. weissflogii* was conducted over 40 days, with three chamber replicates per treatment group. To monitor the growth and state of diatom cultures, chl a and PSII efficiency samples were taken every 2nd/3rd day (no sampling has been conducted between day two and 9), as well as cell counts starting from day 18. To measure bacterial abundance in the cultures, flow cytometry samples were taken once a week. Samples for nutrient analysis and pH measurements were taken at distinct time points of the growth curve.

The investigation of *S. costatum* was conducted over 28 days. Chl a and PSII efficiency were measured approximately every 2nd to 3rd day. Flow cytometry samples, to measure bacterial abundance, were taken on day 3, day 12 and day 26 after the onset of the experiment. Nutrient samples were collected weekly. On three distinct time points of the growth curve (days 19, 26 and 28) cell counts were taken.

The definition of biological replicates within the measured parameters was performed as described for the interaction experiment (see chapter 2.1.2 “Metadata”). In the context of the medium exchange group, only the not manipulated chamber half was considered for all cell-based parameters (resulting in $n = 3$), as this group was designed to recreate the co-cultivation group, sampling was performed accordingly.

Interaction experiment between *T. weissflogii* with *S. marinoi* (chapter 3)

In addition to the primary set of treatment groups described in chapter 2.1.1, a medium control was introduced, containing one co-cultivation chamber filled with artificial seawater medium. Thus, the experimental design consisted of four treatment groups: *T. weissflogii* mono-cultivation, *S. marinoi* mono-cultivation, co-cultivation and medium control. Except for the medium control group ($n = 1$), all treatment groups contained four chambers, replicating the respective set-up.

The experiment was conducted over 48 days. Chl *a* fluorescence, PSII efficiency and cell count samples were taken every 3rd day to monitor the growth and physiological state of the cultures. Approximately once a week, the bacterial abundance in the culture medium was determined. Furthermore, nutritional analyses were conducted weekly for the first four weeks of the experiment and metabolomic samples were taken on three distinct points during the diatom growth, on day 18, day 30 and day 42.

Due to sample loss during filtration, the *T. weissflogii* mono-cultivation group on day 30 comprised only seven biological replicates (instead of 8) in the endometabolomic analysis and three biological replicates (instead of 4) in the exometabolomic analysis. The medium control group was represented by one sample. As a consequence, the data analysis workflow differed in one step: to get rid of potential contaminations, within each sampling day the integrated data of the medium control group were trifold subtracted from each sample (see chapter 6.7.3).

Interaction experiment between *T. weissflogii* with *S. dohrnii* (chapter 4)

The approach was similar to the one described for the interaction between *T. weissflogii* and *S. marinoi* (see above), with the difference that all treatment groups, except the medium control group, contained three chamber replicates.

The experiment was conducted over 35 days. Chl *a* fluorescence, PSII efficiency and cell count samples were taken approximately every 2nd - 3rd day to monitor the growth and physiological state of the cultures. Approximately once a week, the bacterial abundance in the culture medium

was determined. Furthermore, nutritional analyses⁸¹ were conducted and metabolomic samples were taken at three distinct points of the diatom growth curve, on day 15, day 27 and day 35.

Due to sample loss during filtration, the *S. dohrnii* mono-cultivation group on day 35 comprised only five biological replicates (instead of 6) in the endometabolomic. The medium control group was represented by one sample. The integrated data of the medium control group were trifold subtracted from each sample.

6.3 Evaluation of DMSP as growth mediator

6.3.1 Cultivation parameters

Before the onset of an experiment, stock cultures of *T. weissflogii* (RCC76) were inoculated into fresh artificial seawater medium. To increase the culture volume and to keep the cultures in regular growth phase, cultures were repeatedly diluted (v/v_{SW} 1/1). At the onset of the experiment (day 0), cultures were inoculated into sterile cell culture flasks (v/v_{SW} 1/1), resulting in a total culture volume of 80 mL for the investigation of the influence of a continuous DMSP availability and 40 mL for the investigation of the influence of DMSP pulses.

Cultures were stored on an orbital shaker (75 rpm) under a 14/10 hours light/dark cycle in a climate chamber at 15 °C. The light intensity was approximately 35 $\mu\text{mol photons s}^{-1}\text{m}^{-2}$ provided from the top by Osram Lumilux® Cool White 15 W lamps.

6.3.2 Chemicals

DMSP * HCl, synthesized by Kathleen Thume, was diluted in artificial seawater medium, to create DMSP stock solutions of 100 μM , 0.5 mM, 1.25 mM. The stock solutions were subsequently 0.20 μm sterile filtered and stored at -80 °C until further use. To reach final concentrations of 100 nM, 0.5 μM and 1.25 μM in the culture medium, 40 μL (80 μL) of the respective DMSP stock solution were added to 40 mL (80 mL) of diatom culture under sterile conditions.

6.3.3 DMSP addition to *T. weissflogii* culture

Investigation of the influence of continuous DMSP availability: Sterile DMSP solution was added to each culture in a daily manner (five out of seven days per week).

⁸¹ No nutrient levels were available for the co-cultivation group on day 4

Investigation of the influence of DMSP pulses of different concentrations: Sterile DMSP solution was added to every culture on day 20, 24 and 32 after inoculation, to reach final concentrations of 200 nM, 1 μ M and 2.5 μ M in the diatom cultures.

Control groups were established by adding sterile artificial seawater medium in a volume analog to the addition of respective DMSP solutions.

6.3.4 Experimental specifics

Both experiments in the context of the interaction between *T. weissflogii* with *S. costatum* (chapter 2.4) have been conducted over 36 days, starting with freshly diluted cultures (v/v_{sw} 1/1). Chl a and PSII efficiency were measured every 2nd to 3rd day to estimate diatom growth and fitness. Additionally cell counts were taken at distinct points in time during the experiment.

For the continuous DMSP availability experiment, two experimental groups were established: a control group and a DMSP group. Each comprised triplicates of 80 mL cultures. In a daily manner (five out of seven days per week), sterile DMSP solution was added to each culture of the DMSP group to reach final concentrations of 100 nM per culture. In the control group, an equivalent volume of artificial seawater was added instead of DMSP.

For the investigation of DMSP pulses, four treatment groups were established. One control group, analog to the one described above and three groups to which different DMSP concentrations were added on day 20, 24 and 32 after inoculation, to reach final concentrations in the cultures of 100 nM, 1 μ M and 2.5 μ M. Each group comprised triplicates of 80 mL cultures.

6.4 Sampling

Depending on the design of the experiment, samples were taken in regular intervals (for more details see chapter 2.1 and 6.2.7). Samples for cell counts, chl a and photosystem II activity were taken every 2nd to 4th day, bacterial count samples for flow cytometry measurements were taken approximately once a week and nutrient analysis as well as metabolomics samples (comprising endo- and exometabolomic samples) were taken at distinct points of the growth curve.

Table 19: Sampling strategy per chamber-half for co-cultivation experiments

	Volume	Vessel	Storage	Protocol
<u>Chl a/PSII efficiency</u>	1 mL	Eppendorf Tube (1.5 mL)	Immediate measurement	Chapter 6.5.1, 6.5.2
<u>Cell count</u>	1 mL	Eppendorf Tube (1.5 mL)	Storage in the dark at room temperature	Chapter 6.5.3
<u>Flow cytometry</u>	1 mL	Eppendorf Tube (1.5 mL)	Storage at -80 °C	Chapter 6.5.4
<u>pH</u>	10 mL	Falcon Tube (15 mL)	Immediate measurement	
<u>Nutritional analysis</u>	20 mL	Falcon Tube (50 mL)	Storage at -20 °C	Chapter 6.5.4
<u>Metabolomic samples</u>	80 ⁸² mL	Sterile Erlenmeyer flask (100 mL)	Storage at -80 °C	Chapter 6.6

6.5 Metadata acquisition

6.5.1 Chlorophyll a fluorescence

Chl a was measured using a Mithras LB 940 plate reader. 96-multiwell plates were prepared by adding 200 µL of each well-mixed culture per well. Plates were then measured row by row with an excitation filter of 430 nm (lamp energy 15000 mcd) and an emission filter of 665 nm. To ensure comparability and validity, measurements were performed directly after sampling, at the same time of day with three to five technical replicates and two analytical replicates. If a seawater control was available in the experimental design, chl a values were corrected by subtraction of the seawater control values. If no seawater control was available, fluorescence was corrected by subtracting blank values of the plate. Chl a was measured per chamber half, average values per chamber were used in the mono-cultivation groups.

6.5.2 Photosystem II activity measurements

Photosystem II activity can be calculated according to the formula $\frac{(F_m - F_0)}{F_m}$ as described in (Roy and Legendre, 1979). Both the initial fluorescence (F_0) and the maximum fluorescence (F_m) were obtained using the same plates as prepared for chl a. Measurements of both parameters were conducted as described for chl a in chapter 6.5.1. However, the following steps were modified:

⁸² 75 mL in the interaction of *T. weissflogii* and *S. costatum*

Before F_0 measurements the prepared plates were stored in the dark at 15 °C for 30 minutes and shaken in the instruments for 60 seconds. Subsequently, F_m measurements were conducted after adding 15 μ L of aqueous 3'-(3,4-dichlorophenyl)-1',1'-dimethylurea (71.7 μ M; Sigma-Aldrich, Munich, Germany) per well and shaking the plate in the instrument for 180 seconds. PSII efficiency were considered zero if they showed negative values. If a seawater control was available in the experimental design, F_0 and F_m values were corrected by subtraction of the seawater control values. If no seawater control was available, values were corrected by subtracting blank values of the plate. PSII efficiency was measured per chamber half, average values per chamber were used in the mono-cultivation groups.

6.5.3 Cell counts

Samples were immediately fixed by addition of one drop of acidic lugol solution per Eppendorf tube. Lugol solution is prepared by dissolving 20 g of KI (Sigma-Aldrich, Steinheim, Germany) in 200 mL deionized water and adding 10 g of crystalline I_2 (VWR, Leuven, Belgium). Afterwards, 20 mL of glacial acetic acid (Sigma-Aldrich, Steinheim, Germany) were added. Before storage in the dark, the solution was filtered and routinely checked for precipitation ((Thronsen, 1978) as stated in (Guillard and Sieracki, 2005)). Samples can then be stored in the dark until counting.

Cell counts were obtained with an upright microscope (DM2000, Leica, Heerbrugg, Switzerland) using a Fuchs-Rosenthal haemocytometer. At least 400 cells were counted for each sample. Cell counting was performed by two undergraduate students, which were employed as student assistants in this context.

6.5.4 pH

For each chamber half 5 mL of the culture was taken and pooled in a 15 mL FALCON Tube under sterile conditions. Directly after sampling, the pH was measured in three analytical replicates with a HI 1131 electrode (Roth) attached to a C830 pH meter (Consort, Turnhout, Belgium). The pH meter was calibrated with standard solutions of pH 7.0 and pH 4.00 (Roth), each time before use.

6.5.5 Flow cytometry measurements

Sample workup and storage

Samples were immediately fixed by addition of 20 μ L per 1 mL sample of a 25 % glutaraldehyde solution (electron microscopy grade, Sigma Aldrich, Munich, Germany) to reach

a final concentration of 0.5 % per sample. The samples were then thoroughly vortexed and stored in the dark at 4 °C for 30 minutes before being cryopreserved with liquid nitrogen and stored at 80 °C until further analysis.

Sample preparation

The sample preparation was performed according to a protocol used by Michaela Mauß (Mausz, 2014), which was adapted from (Marie et al., 1999; Brussaard, 2004). To thaw, samples were put in a water bath at 35 °C for five minutes. If necessary (especially with non-axenic cultures or in later growth phases), samples were subsequently diluted up to 50 - fold in sterile (0.20 µm) filtered TE buffer (10 mM Tris-HCl and 1 mM EDTA, pH 8.0). For staining, a SYBR® Gold Nucleic Acid Gel Stain (10000 - fold concentrated in DMSO; life technology, Eugene, OR, USA) was diluted 1:100 (v/v) in sterile filtered TE buffer (storage of the diluted dye in the dark at 20 °C possible). For sample staining, 5 µL of the diluted SYBR® Gold stock solution were added to 500 µL sample volume resulting in a final dilution of 1:10000 (v/v) of the commercial SYBR® Gold stain. Subsequently, the samples were stored for ten minutes at 80 °C in the dark (drying oven) to intensify staining. In between the steps, samples were thoroughly vortexed. Samples were measured immediately after staining.

Sample measurement

For measurements, 100 µL of stained and diluted samples together with 100 µL calibration standard and 300 µL sterile filtered TE buffer were carefully mixed in flow cytometry tubes (Rotilabo®; Carl Roth, Karlsruhe, Germany). Samples were prepared in duplicates. To eliminate unwanted signals from the bacterial count measurements, blanks consisting of stained, sterile filtered TE buffer were measured in duplicates within each batch (consisting of max. 32 samples) and subtracted from the samples.

Samples were measured with a medium flow rate of 30 µL/min over 60 seconds. The calibration standard beads were identified at 575 nm and calibrated at 525 nm. The bacterial population was identified and quantified at 525 nm, as 525 nm was also used as discriminator. Detector voltages were set according to **Table 20**.

Table 20: Detector settings for flow cytometry sample measurements (parameters modified from protocols of Michaela Mausz)

Sensor	Type	Wavelength (nm)	Sample measurement		Calibration standard	
			Volts	Gain	Volts	Gain
FS	Photodiode		550	1	1000	2
SS			1000	7.5	850	5
FL1	Photo- multiplier tubes (PMTs)	525	370	1	350	1
FL2		575	500	1	337	1
FL3		620	390	1	300	1
FL4		675	400	1	450	1
FL5		755	500	1	577	1
AUX (auxiliary parameter)			300	1	300	1

Calibration standard

For calibration, diluted Fluoresbrite™ Plain YG 1.0 µm Mikron Microspheres (latex; Polysciences, Warrington, PA, USA) with final concentration of approximately 1000 beads/µL in sterile filtered ultrapure water were used. This so called calibration standard was considered stable for up to two weeks, when stored at 4 °C in the dark. To determine absolute bead counts of the calibration standard, the diluted Fluoresbrite™ Plain YG bead solution itself was calibrated with the help of CountBright™ absolute counting beads (7 µm diameter; life technologies, Eugene, OR, USA). This absolute count calibration of the calibration standard was performed after every 2nd to 4th sample batch, by thoroughly mixing 100 µL Fluoresbrite™ Plain YG calibration beads together with 100 µL CountBright™ absolute counting beads and 300 µL sterile filtered TE buffer in flow cytometry tubes. Calibration measurements were performed at least in triplicates immediately after mixing.

The calibration samples were measured with a low flow rate of 10 µL/min over 60 seconds. Both the calibration standard beads and absolute counting beads were identified and calibrated at 575 nm. 525 nm were used as discriminator. Detector voltages were set according to **Table 20**.

Quality Control

Quality control measurements were performed daily with the help of Flow-Check™ Fluorespheres (Beckman Coulter, Galway, Ireland).

6.5.6 Nutritional analysis

For each chamber half 20 mL of the culture was taken and sterile-filtered. For each chamber; the aliquots of the two chamber halves were pooled in a 50 mL FALCON Tube under sterile conditions. Subsequently samples were stored in the dark at 20 °C until shipment. The GEOMAR (Frank Malien, Chemical Oceanography, Kiel, Germany) was commissioned to do nutritional analyses. Samples were sent in a frozen state and cooled with cool-packs during delivery. Measurements were performed in analytical triplicates.

Methods for the analysis of nitrite, nitrate and dissolved inorganic silicate can be found in (Hansen and Koroleff, 2007). Determination of nitrite was conducted as described in chapter 10.2.8, p.177-178). The method is based on the proposal of (Shinn, 1941) and adapted for seawater by (Bendschneider and Robinson, 1952). Nitrate concentrations are determined as described in chapter 10.2.9, p.180-182 and silicate concentrations as described in chapter 10.2.11, p-193-194. Ortho-phosphate is measured according to a method of the firm BRAN + LUEBBE (now SEAL Analytical, Norderstedt, Germany) (SEAL-Analytical, 2002). In principle this method follows the method of (Murphy and Riley, 1958) and is based on the spectrophotometrical quantification of a blue phosphor-molybdenum complex.

Instrument

Samples were measured with two instruments, depending on instrument availability. The first instrument is a 5-channel continuous flow analyzer for shipboard use self-designed by the GEOMAR and described in chapter 10.3.1 of (Hansen and Koroleff, 2007). The other instrument is a QuAAtro continuous segmented flow analyzer (Seal Analytical, Norderstedt, Germany). Within one experiment the same instrument was used and samples were shipped together to maintain maximum comparability.

6.6 Metabolomic analysis

The metabolomics analysis (as described in this chapter) was conducted based on the protocols and methods developed by Charles Vidoudez (Vidoudez, 2010; Vidoudez and Pohnert, 2011).

6.6.1 Chemicals and consumables

Solvents

If not otherwise stated, the following solvents were used in the context of metabolomics:

- acetone (analytical reagent grade; Fisher Chemical, Leicestershire, UK),
- chloroform (HiPerSolv CHROMANORM for HPLC; VWR, Leuven, Belgium),
- ethanol (LiChrosolv® gradient grade for liquid chromatography; Merck, Darmstadt, Germany),
- methanol (CHROMASOLV® Plus, for HPLC; Sigma-Aldrich, Steinheim, Germany),
- *n*-hexane (SupraSolv® for gas chromatography; Merck, Darmstadt, Germany),
- pyridine (CHROMASOLV® Plus for HPLC, $\geq 99.9\%$; Sigma-Aldrich, Steinheim, Germany),
- tetrahydrofuran (HiPerSolv CHROMANORM for HPLC; VWR, Leuven, Belgium),
- water (CHROMASOLV® Plus for HPLC; Sigma-Aldrich, Steinheim, Germany).

N-hexane and pyridine were stored with a molecular sieve (4 Å, 0.4 nm, type 514; Carl Roth, Karlsruhe, Germany).

Materials

In the context of metabolomics, all pipettes, tips and centrifuge tubes (1.5 mL) used were from Eppendorf (Eppendorf, Hamburg, Germany). For sample processing and analysis, two kinds of 1.5 mL glass vials were used. On the one hand 1.5 mL glass vials (N9, flat) sealable with screw caps containing silicone-PTFE septa (N9, 1 mm thickness) and combinable with glass inserts (wide opening, 0.2 mL, 6×31 mm) and metal springs were used (all from Macherey-Nagel, Düren, Germany). On the other hand 1.5 mL glass vials (Wicom, Heppenheim, Germany) sealable with screw caps containing PTFE-butyl-PTFE septa (1.3 mm thickness; VWR, Dresden, Germany) and combinable with glass inserts (tight opening; Wicom, Heppenheim, Germany) and metal springs were used. Extracellular metabolite samples were stored in 4 mL glass vials (N13, flat; Macherey-Nagel, Düren, Germany) sealable with screw caps containing butyl-PTFE Septa (VWR, Dresden, Germany). In order to avoid contaminations all materials and chemicals were only handled with gloves and used in a very clean environment. Within one experiment, the same kinds of materials were used for all samples to obtain maximum comparability.

Retention Index Mix

The retention index (RI) mix contained six *n*-alkanes dissolved in hexane in concentrations of 1 mM and 0.5 mM (**Table 21**). A stock of each *n*-alkane dissolved in hexane (10 mM and 5 mM) was stored in 4 mL glass vials at 20 °C. To obtain the RI-mix 100 μ L of each *n*-alkane stock solution were mixed in a 4 mL glass vial and filled up with hexane to reach a final volume of 1 mL. The RI-mix was stored at 20 °C. Within each experiment, the same RI-Mix aliquot was used for all samples to ensure maximum comparability.

Table 21: Chemical compounds of the RI-mix

<i>n</i> -alkane	Stock concentration	RI-mix concentration
decane (≥ 99 %; Sigma-Aldrich, Steinheim, Germany)	10 mM	1 mM
dotriacontane (97 %; Sigma-Aldrich, Steinheim, Germany)	10 mM	1 mM
hexatriacontane (98 %; Sigma-Aldrich, Steinheim, Germany)	5 mM	0.5 mM
nonadecane (purum ≥ 99 %; Fluka, Steinheim, Germany)	10 mM	1 mM
octacosane (purum ≥ 98 %; Fluka, Steinheim, Germany)	10 mM	1 mM
pentadecane (purum ≥ 98 %; Fluka, Steinheim, Germany)	10 mM	1 mM

External standard:

A stock of ribitol (> 99 %; Sigma-Aldrich, Steinheim, Germany) dissolved in water (40 mM) was stored in 4 mL glass vials at 20 °C. Before use, the stock solution was diluted 1:10 (v/v) in 1.5 mL glass vials to reach a final concentration of 4 mM ribitol in water. Within each experiment the same ribitol aliquot was used.

Extraction mix:

The extraction mix was freshly prepared before each extraction of intracellular metabolites. It contained a mix of methanol:ethanol:chloroform in a ratio of 2:6:2 (v/v/v).

Agilent Test

For quality assessment and as analytical reference material, the Agilent Test (DB-5ms; Agilent Technologies, Santa Clara, CA, USA) was injected into the GC-EI/TOF/MS system before and after each sample batch. The Agilent Test stock contains the following substances: *n*-tetradecane, *n*-tridecane, 1-undecanol, 1,6-hexanediol, 2-ethylhexanoic acid, 4-chlorophenol, dicyclohexylamine, 1-methylnaphtalene solved in hexane/acetone (1:1, v/v) in mass

concentrations of 0.001 mg/mL. Before use, the Agilent test stock was diluted 1:10 (v/v) in hexane/acetone (1:1, v/v).

6.6.2 Protocol for metabolomic sample preparation and storage

The protocol for metabolomic sample extraction and preparation is based on the standard operating procedure (SOP) of Charles Vidoudez (Vidoudez, 2010; Vidoudez and Pohnert, 2011) and contains minor changes. The procedures were performed as follows:

Intracellular metabolite sample preparation

Extraction protocol

After randomized sampling of 80 mL culture volume (75 mL in the analysis of the interaction between *S. costatum* and *T. weissflogii*, chapter 2) per chamber-half, the samples were extracted by concentrating diatom cells on a GF/C filter (Whatman, Kent, UK) under vacuum (≈ 700 mBar). The filter was not allowed to run completely dry, thus avoiding stress reactions of the cell before extraction. The flow-through was collected by pooling the volumes of each two halves of the same co-cultivation chamber for further analysis of extracellular metabolites. The extracellular metabolite samples were temporarily stored in 500 mL glass vessels (Schott, Mainz, Germany) until further preparation.

Immediately after cell concentration, the filter was transferred to a 25 mL glass beaker, in which the cells on the GF/C filter were re-suspended in 1 mL of ice-cold extraction mix and transferred in an Eppendorf centrifuge tube. After vortexing (≥ 10 sec) 5 μ L of ribitol solution (4 mM) were added to each sample. Samples were temporarily stored on ice until the extraction was completed for all samples, before storage at 80 °C until further analysis.

Sample preparation protocol

Sample randomization was carried out within each sampling day. Samples were unfrozen at room temperature and thoroughly vortexed. In order to ensure maximum comparability of the metabolomic profiles, all extraction volumes were normalized to a certain diatom cell count. The cell count was uniform within each species within each experiment (see **Table 22** for more details). The equivalent amount of cells was transferred from the unfrozen samples in a new Eppendorf tube. Subsequently, 100 μ L of extraction mix were added, samples were placed in an ultrasound bath for ten minutes and centrifuged at 29000 rcf at 4 °C for 15 minutes. The supernatant was then transferred into 1.5 mL glass vials (sealable with PTFE-butyl-PTFE septa) and evaporated to dryness under vacuum. The evaporation was conducted by lowering the

pressure (starting at 500 mBar) by 100 mBar per hour to avoid boiling of the samples. Pressure reduction steps were adjusted if needed, depending on the used solvent's boiling point. The exsiccator was vented with argon.

Table 22: Overview over cell counts used for the endometabolomic normalization of *T. weissflogii* and *Skeletonema* sp. in the interaction experiments.

Interaction experiment	Chapter	Cell counts used for the endometabolomic normalization within	
		<i>T. weissflogii</i>	<i>Skeletonema</i> sp.
<i>T. weissflogii</i> (RCC76) - <i>S. costatum</i> (RCC75)	2	18.7×10^6 cells	18.7×10^6 cells
<i>T. weissflogii</i> (CCMP 1336) - <i>S. marinoi</i> (CCMP 1332)	3	1.9×10^7 cells	5×10^7 cells
<i>T. weissflogii</i> (CCMP 1336) - <i>S. dohrnii</i> (CCMP 3373)	4	3×10^7 cells	5×10^7 cells

Extracellular metabolite sample preparation

Extraction protocol

Extracellular metabolite samples were collected as previously described (see chapter 6.6.2 “Intracellular metabolite sample preparation”). In the interaction between *T. weissflogii* and *S. marinoi* (chapter 3), as well as *T. weissflogii* and *S. dohrnii* (chapter 4), the samples were 0.20 µm sterile filtered before solid phase extraction. Subsequently, EASY cartridges (3 mL / 200 mg, CHROMABOND®; Macherey-Nagel, Düren, Germany) were prepared by washing each cartridge successively with 4 mL methanol and 4 mL water. Cartridges were then connected with a Teflon® tubing on the input side of the cartridge to build a Teflon®-tubing-EASY-cartridge filtration unit. The Teflon® tubing end of the unit was put into the extracellular metabolite sample whereas the output end of the cartridge was connected to a vacuum pump. Samples were passed through the cartridge drop by drop at a vacuum of approximately 800 mBar. Subsequently, cartridges were washed with 4 mL of water and air dried while being connected to the vacuum pump under maximum vacuum. Gravity-based elution of metabolites into a 4 mL glass vials was performed by adding 2 mL of methanol followed by 2 mL of methanol:THF 1:1 (v/v). For the exometabolomic investigation of the interaction between *S. costatum* and *T. weissflogii* (chapter 2), 2 mL of ethanol:THF 1:1 (v/v) were used instead, during the last elution step. After addition of 5 µL ribitol external standard, the glass vials were closed and stored at 80 °C until further use.

Sample preparation protocol

Sample preparation was randomized. Samples were unfrozen at room temperature. 1.5 mL of the sample was transferred into a 1.5 mL glass vial and evaporated to dryness under vacuum. The evaporation was conducted by lowering the pressure (starting at 500 mBar) by 100 mBar per hour to avoid boiling of the samples. Vacuum was held at ≈ 0 mBar for at least 2 hours. Pressure reduction steps were adjusted if needed. The exsikkator was vented with argon.

6.6.3 Derivatization

Derivatization comprised a methoxymation and a silylation step with sample batches of maximum 20 samples. The derivatization was conducted according to protocols developed by Charles Vidoudez (Vidoudez, 2010; Vidoudez and Pohnert, 2011).

Methoxymation

The dryness of methoxyamine hydrochloride (Sigma Aldrich, Steinheim, Germany) was ensured by storage under vacuum for at least six hours and subsequent venting with argon before derivatization. Afterwards, 20 mg of methoxyamine hydrochloride were dissolved in 1 mL of pyridine in a 4 mL glass vial and sonicated for five minutes until complete dissolution. For each sample, 50 μ L of this methoxymation solution were added to a maximum of 20 dry samples. Samples were vortexed for 2 minutes before they were incubated at 60 °C in a heat block for one hour. This was followed by another incubation period of nine to 14 hours at room temperature. Within one experiment the time of the incubation period at room temperature was the same to ensure maximum comparability.

Silylation

40 μ L of RI mix were injected into a new 1 mL vial of MSTFA (N-Methyl-N-trimethylsilyltrifluoro acetamide; Macherey-Nagel, Düren, Germany) with a glass syringe (50 μ L; Hamilton, Bonaduz, Switzerland). The glass syringe was cleaned with hexane after each sample batch. After thoroughly vortexing the MSTFA vial, 50 μ L of silylation solution per sample were added with a glass syringe (500 μ L, Hamilton, Bonaduz, Switzerland). The glass syringe was carefully cleaned with acetone after each sample batch. Samples were incubated at 40 °C for one hour before they were transferred into glass inserts and analyzed immediately.

Remark

In the endometabolomic investigation of the interaction between *S. costatum* and *T. weissflogii* (chapter 2), the derivatization process of the samples varied. The samples were measured in three batches. Batch one comprised all samples from day 16 in randomized order, whereas batch two and three contained all samples from day 26 and 32. Due to instrument issues, sample set two was frozen for 24 hours after the methoxylation step, before continuing the derivatization. Furthermore sample set three was exposed to elevated temperatures (60 °C for 12 h) in the silylation step.

6.6.4 GC-MS measurements

Hardware and software specifications

GC-EI/TOF/MS measurements were conducted based on methods developed by Vidoudez (Vidoudez, 2010). Sample batches of maximum 20 samples, randomized within each sampling day per experiment, were measured with a Micromass® GCT Premier™ (Waters, Manchester, UK) orthogonal acceleration time-of-flight mass spectrometer (MS) coupled to an Agilent 6890 (Agilent Technologies, Santa Clara, CA, USA) gas chromatograph (GC) with autosampler (7683 series, Agilent Technologies, Santa Clara, CA, USA).

GCT settings were typically applied according to **Table 23**.

Table 23: General GCT settings

GC Inlet Settings	
GC re-entrant	280 °C
Reference reservoir	50 °C
Reference re-entrant	150 °C
MS Source Settings	
Source temperature	250 °C
Electron energy	70 eV
Trap current	196 µA
Ion repeller	1.2
MS DRE Settings	
High sensitivity	Activated
z-focus	40 V
z-lens steering	0 V
Gain drop monitoring	Activated

MS TDC Settings	
Trigger threshold	300 mV
Signal threshold	20 mV
Threshold	1 to 50
Inhibit Push	Activated
Inhibit value	4
Centroiding parameters	Centroid threshold 1, Min points 5, Np multiplier 0.7
Low mass cut-off	45 Da

The column used was a DB-5MS+DG Durabond column (Agilent Technologies, Santa Clara, CA, USA), with a length of 30 m (plus up to 10 m Duroguard precolumn), a diameter of 0.25 mm and a film of 0.25 μm . The column was non-polar, containing a phenyl arylene polymer equivalent to a (5 %-phenyl)-methylpolysiloxane.

Before each batch of 20 samples a new glass liner (4×6.3×78.5 mm inner \varnothing × outer \varnothing × length; Agilent, Waldbronn, Germany) was inserted. Liners were deactivated, equipped with glasswool (INNO-Sil) and conditioned by CS Chromatographie Service, Langerwehe, Germany.

Automatic injections were conducted with a 10 μL syringe (Agilent Technologies, Santa Clara, CA, USA). Chromatograms and spectra were visualized and analyzed in MassLynx (V4.1; Waters, Milford, MA, USA).

Tuning and calibration of instrument

The GCT is capable of exact mass measurements due to an internal lock mass correction with heptacosyl (Heptacosylfluorotributylamine, analytical standard for mass spectrometry; Fluka, Steinheim, Germany). For optimal performance the instrument was tuned before the measurement of each experiment to reach highest possible resolution at 501.97 m/z (**Table 24**).

Table 24: GCT Tuning settings

Tuning Settings	
Scan Time	0.9 s
Inter scan delay	0.1 s
Mass range	50-615 m/z

To obtain exact mass measurements, the GCT was calibrated with heptacosane as reference before each sample batch to reach mean residual values of $\text{RMS} \leq 10^4$ amu over the mass range 45-700 m/z .

Quality Control:

Solvent controls (for each experiment) were measured to identify potential contaminations. By injecting air into the GCT, blank measurements were conducted to identify system-related contaminations. Agilent test measurements were performed to evaluate the quality and state of liner and column.

GC method parameters

The carrier gas helium was delivered with a constant flow of 1 mL/min. The injection volume of the syringe was 1 μL . The parameters of the methods used are described in the following:

Metabolomic method:

Unless stated otherwise, the following method was used to measure intracellular and extracellular metabolite samples.

The injector temperature was set to 300 °C with a split ratio of 10. Oven temperature ramps started with an initial temperature of 60 °C for one minute, then temperature increased with a rate of 15 °C/min to a final temperature of 310 °C that was then held for ten minutes.

Before injection, the syringe was washed with both ethyl acetate (or acetone) and heptane three times and once with the sample itself. Before injection the sample was pumped up and down six times (sampling offset of 6 mm). After injection the six washing steps with both ethyl acetate and heptane followed.

Agilent method:

The Agilent method was used to measure the Agilent test reference material for quality control purposes.

The injector temperature was 250 °C with a split ratio of 1. Oven temperature ramps started with an initial temperature of 80 °C, then temperature increased first with a rate of 8 °C/min to a temperature of 119 °C and in a second step with a rate of 40 °C/min to a final temperature of 320 °C which was then held for 2.5 minutes

Before injection, the syringe was washed with both ethyl acetate and heptane three times and once with the sample itself. Before injection the sample was pumped up and down three times (sampling offset of 2 mm). After injection, the three washing steps with both ethyl acetate and heptane followed.

MS Method

Mass spectra were acquired in positive ion mode with electron impact ionization. Data were acquired in centroid mode.

Metabolomic method:

Data was acquired with a scan rate of 5 scans/second (scan time of 0.19 s and inter scan delay of 0.01 s) over 28 minutes within a mass range of 35 to 1000 m/z .

Agilent method:

Data was acquired with a scan rate of 2 scans/sec (scan time of 0.49 s and inter scan delay of 0.01 s) over 20 minutes within a mass range of 50 to 600 m/z .

6.7 Data analysis

6.7.1 Metadata analysis

To test for significance among the visible differences in chl a fluorescence and cell counts between mono- and co-cultivation of both species over time, a linear mixed modeling approach was chosen. R (R Development Core Team, 2008) was utilized through the graphical user interface RStudio. Here, linear mixed effect modeling was performed using the package nlme (Pinheiro et al., 2015). The following packages: AICcmodavg (Mazerolle, 2015), car (Fox and Weisberg, 2011), ggplot2 (Wickham, 2009) and plyr (Wickham, 2011) were also used for the analysis.

Four different models were proposed using the lme function (package nlme). All models proposed were random intercept models. Each model was built with a fixed term, treating day as factor, and a random term. The fixed term reflected the influence of day, group and the interaction of day and group on the response variable. The random term accounted for the repeated measures design, by treating the chambers (each repeatedly sampled) as random factor. This basic model was represented by model 1. Furthermore, to account for heterogeneity, different weighing

functions were additionally introduced in model 1 (see models 2-4), using the constant variance function structure (`VarIdent`) in the weights argument.

Model 1: representing the standard random intercept model used as basis for all further models.

```
Model 1 <- lme(variable ~ Group*Day, random=~1|fChamber, data=data, method="REML")83
```

Model 2: additionally accounts for heterogeneity among days by introducing a `varIdent` variance structure

```
Model 2 <- lme(variable ~ Group*Day, random=~1|fChamber, data=data,
weights=varIdent(form=~1|Day), method="REML")83
```

Model 3: additionally accounts for heterogeneity among groups by introducing a `varIdent` variance structure

```
Model 3 <- lme(variable ~ Group*Day, random=~1|fChamber, data= data,
weights=varIdent(form=~1|Group), method="REML")83
```

Model 4: additionally accounts for heterogeneity among groups and days by introducing a `varIdent` variance structure

```
Model 4 <- lme(variable ~ Group*Day, random=~1|fChamber, data=data,
weights=varComb(varIdent(form=~1|Group), varIdent(form=~1|Day)), method="REML")
```

Model 4b: identical with model 4, but the number of iterations was specified for model convergence

```
Model 4b <- lme(variable ~ Group*Day, random=~1|fChamber, data=data, control=ctrl,
weights=varComb(varIdent(form=~1|Group), varIdent(form=~1|Day)), method="REML")
ctrl <- lmeControl(maxIter=100, msMaxIter = 100, msMaxEval = 400)
```

Data analysis specifics

In the interaction experiment of *T. weissflogii* with *S. costatum* (chapter 2.2.1), model 4 showed the best fit for modeling chl a fluorescence of both species and cell counts of *T. weissflogii*, while model 1 was best suited to model cell counts of *S. costatum*.

In the medium experiments (chapter 2.3) chl a fluorescence was modeled via linear mixed model 4 and cell counts via linear mixed model 3 in the *T. weissflogii* medium experiment and model 2 in the *S. costatum* medium experiment

⁸³ R code used

Linear mixed model 2 was best fitted to model chl a fluorescence in the interaction of *T. weissflogii* and *S. marinoi* (chapter 3), while cell counts were modeled with model 3.

In the interaction between *T. weissflogii* and *S. dohrnii* (chapter 4) linear mixed model 4 was used to test for significant differences between mono-cultivation and co-cultivation over time, with regard to cell counts in both diatom species. Chl a fluorescence in *S. dohrnii* was modeled with linear mixed model 4 as well and chl a fluorescence in *T. weissflogii* with model 4b.

6.7.2 Metabolomic data processing

Data processing as described in this chapter was based on protocols used by Charles Vidoudez and Michaela Mausz (Vidoudez, 2010; Vidoudez and Pohnert, 2011; Mausz, 2014). It comprised the following steps:

(1) Background-noise subtraction

In a first step background-noise correction was performed on all samples with the CODA algorithm (MCQ Index = 0.8; smoothing window = 3 points) in MassLynx V4.1. Subtracted chromatograms were then converted into NetCDF files with DataBridge.

(2) Spectral deconvolution

With the help of AMDIS (automated mass spectral deconvolution and identification system, V 2.71) peak detection and deconvolution analysis was performed using the simple analysis mode (Table 25).

Table 25: Analysis settings of AMDIS

Identification of Compounds	
Minimum match factor	30
Multiple identifications per compound	activated
Instrument Settings	
Low m/z and high m/z	Auto
Threshold	Off
Scan direction	None
Instrument type	Quadrupole
Deconvolution	
Component width	12
Omitted ions (m/z)	147, 176, 193, 207, 219
Adjacent peak subtraction	Two
Resolution	Low
Sensitivity	Medium
Shape requirement	Low
Library	
Target compounds library	GOLMWITHRI
QA/QC	
Column bleed	Activated (207 m/z)

(3) Peak alignment, annotation and integration

MET-IDEA (Metabolomics Ion-based Data Extraction Algorithm, V 2.08) was used to quantify the ion/retention time pairs and thus specific compounds via peak area by using a certain set of criteria (Table 26).

Table 26: Analysis settings of MET-IDEA

Chromatography	
Chromatography	GC
Average peak width	0.08
Minimum peak width	$0.5 \times$ average peak width
Maximum peak width	$2 \times$ average peak width
Peak start/stop slope	1.5
Adjusted retention time accuracy	$0.25 \times$ average peak width
Peak overload factor	0.9
Mass spec	
Mass spectrometers	TOF
Mass accuracy	0.1
Mass range (+/-)	0.3
AMDIS	
Exclude ion list	71,97,147,193,281,341,415
Lower mass limit	100
Ions per component	1

To align the spectra, the option “Calibrate RT” was chosen, when setting up the MET-IDEA job. Data output contained the peak areas of each MST per sample in form of a tab-delimited text file.

6.7.3 Metabolomic data analysis

Data analysis as described in this chapter was conducted and arranged as needed. It was comprised of the following parts:

(1) General data pre-treatment

The MET-IDEA data output was further processed in Excel 2013 (Microsoft, Redmont, WA, USA). In a first step, all originally detected and manually corrected metabolites were given a substance number (A1, A2, A3,...). Secondly, all peaks were deleted that are (a) identified as redundant peaks, via redundancy analysis (Chapter 6.7.2), (b) part of the RI-mix, (c) ribitol, (d) contain the value “1”, or (e) were abundant in less than three samples. The remaining metabolites were given a new coherent substance ID (1,2,3,...). This ID was also used for characterization of the metabolites in all subsequent analyses.

To eliminate contaminants from the data set, the blank average (specific for each sampling day) was subtracted three times from each sample⁸⁴. Resulting negative peak areas were substituted by zero. For the analysis in chapter 2 solvent blanks were used, for the analysis in chapter 3 and 4 the seawater control was considered as the blank.

Intracellular metabolite data was normalized by peak sum. Within one sample each metabolite's peak-area was divided by the overall peak sum of that sample. Extracellular metabolite data was normalized sample-wise to the peak area of the external standard ribitol.

(2) Canonical Analysis of Principal Coordinates

Principal coordinate analysis (PCoA), followed by a canonical discriminant analysis (CDA) was used to investigate differences in the endo- and exometabolome of the diatoms, as caused by the interaction. This combined analysis is termed CAP ("Canonical Analysis of Principal Coordinates") (Anderson and Robinson, 2003; Anderson and Willis, 2003a; Anderson, 2004). Compare chapter 2.5.3 for a detailed discussion.

Analysis of exometabolomic data

Exometabolomic data was analyzed with the program CAP12.exe⁸⁵ (Anderson and Robinson, 2003; Anderson and Willis, 2003a; Anderson, 2004), using the parameters listed in **Table 27**.

Table 27: Analysis parameters for CAP12.exe

CAP12	
Transformation	Log ₁₀ (x+1)
Standardization	None
Distance measure	Bray-Curtis dissimilarity
Type of analysis	Discriminant analysis
Let the computer program choose m	
<i>Note: m is the number of principal coordinate axes to be used in the canonical analysis</i>	Yes
Do you wish to output the principal coordinate axes?	Yes
How many axes do you want in the output?	999 (meaning all)
Do you wish to test by permutation?	Yes
Type the number of random permutations for the test	9999
Type an integer to be used as the seed for the random permutations	12

⁸⁴ The peak area corresponding to ribitol was excluded from any subtraction, as ribitol was also added to medium blanks

⁸⁵ <http://www.esapubs.org/archive/ecol/E084/011/suppl-1.htm>

As the exometabolome of the two chamber-halves per cultivation chamber was pooled, each chamber was treated as one biological replicate in the context of exometabolomic data. Results of the CAP were visualized with the help of Sigma Plot (Version 11.0, Systat Software, San Jose, CA, USA).

Analysis of endometabolomic data

The analysis of endometabolomic data was performed combining the software CAP12.exe with R run in RStudio, using the packages lattice (Sarkar, 2008), MASS (Venables and Ripley, 2002), permute (Simpson, 2015) and vegan (Oksanen et al., 2015). The data was transformed by applying $\log_{10}(x+1)$ to reduce the influence of highly abundant metabolites on the analysis (Kindt and Coe, 2005). The number of principal coordinate axes (m) used in the canonical analysis, was chosen manually in agreement with the recommended guidelines (Anderson and Willis, 2003a), resulting in the lowest misclassification error of the “leave-one-chamber-out cross validation”.

In the analysis, each chamber-half of each co-cultivation chamber was sampled individually and treated as one biological replicate. To account for this inherent dependency of the two chamber-halves in one cultivation chamber, the canonical discriminant analysis was performed according to a modified function written by Dr. Jens Schumacher⁸⁶ (function is documented in the digital appendix chapter 7.4). For plotting, the results calculated by CAP12.exe concerning the principal coordinate axes, canonical axes and the correlations of the canonical axes with original variables were used. The permutation test, as well as the “leave-one-chamber-out cross validation” was performed in R. The integer used as the seed for the random permutations in R was “13”.

(3) Creation of heatmaps

Heatmaps of certain data subsets were created from the autoscaled median of normalized MST intensities. Metabolites with a median of zero in all considered samples were deleted. To highlight abundance patterns of metabolites, a color code of blue (low abundance) to yellow (high abundance) was applied.

The fold change of MSTs was given on the basis of MST medians⁸⁷ and coded with a second color code. Black indicates an upregulation of MST intensity in co-cultivation relative to mono-cultivation. If a metabolite was 10 - fold upregulated, it was 10 – times more abundant in co-cultivation (MST intensity = 10) compared to mono-cultivation (MST intensity = 1). Grey

⁸⁶ Institute of Mathematics/Stochastics, Faculty of Mathematics and Computer Science, Friedrich-Schiller-University Jena

⁸⁷ Not autoscaled

indicated a downregulation of exometabolites in co-cultivation relative to mono-cultivation of both diatoms. If a metabolite was -10 - fold downregulated, it was 10 – times more abundant in mono-cultivation (MST intensity = 10) compared to co-cultivation (MST intensity = 1).

Each MST was characterized by ID (being unique for each exo- and endometabolomic analysis within each interaction), model ion, retention time (RT) and retention index (RI). MSTs were identified via libraries (for more information see chapter 6.7.4) and marked accordingly (chapter 6.7.4).

The following class abbreviations were used: amino acid (AA), amine (A), alcohol (Alc), alkaloid (Alk), carboxylic acid (CA), derivatives of a certain class (dv.), fatty acid (FA), sugar (S), sugar acid (S acid), sugar alcohol (S alc), sterol (St), terpene (T), others (O). Addition of “Vidoudez” in the metabolite name refers to an MST code from the in-house library, “GOLM” refers to an MST code given by distinct libraries of the Golm Metabolome Database (for more information see chapter 6.7.4). The cultivation types, referred to as treatments, were abbreviated as Mono (mono-cultivation) and Co (co-cultivation). Concerning fold-changes, “-“ indicates the absence of the MST in mono-cultivation, “0” indicated the absence in co-cultivation.

6.7.4 Metabolite identification

Relevant metabolites were identified via “The Mass Spectral Search Program for the NIST/EPA/NIH Mass Spectral Library” (Version 2.0 d)⁸⁸. The following libraries were implemented for structure identification, as suggested in (Vidoudez, 2010; Mausz, 2014):

⁸⁸ Software by S. Stein, Y. Mirokhin, D. Tchekhovskoi, and G. Mallard. Built 26.04.2005

Table 28: MS libraries

Name	Version	Specifics	URL / Reference
NIST Mass Spectral and Retention Index Libraries	2005	Main EI MS library, Replicate EI MS Library, Retention Index Library	http://www.nist.gov/srd/nist1a.cfm
The Golm Metabolome Database	2004-03-01	t_msri_id (GOLM) q_msri_id (MPI)	http://csbdb.mpimp-golm.mpg.de/csbdb/gmd/msri/gmd_msri.html , (Wagner et al., 2003)
	2011-11-21	GMD_20111121_VAR5 _Alk_MSP (GMD)	http://gmd.mpimp-golm.mpg.de/download/
Metabo	In-house library	(Vidoudez)	(Vidoudez, 2010)

Structure suggestions were considered if the Match was ≥ 600 and if the retention index (RI) provided by the libraries was close to the substance's RI. In some cases, a Match of ≤ 600 was accepted, when the structure suggestions were identical among the three samples with the highest peak intensity of the considered metabolite. Those metabolites were marked with “1” in the heatmaps.

Structures were accepted if additionally the R-Match was ≥ 800 and / or the substance could be identified via standard (marked with “*”). In that case the RI of the standard must be highly similar and the mass spectrum of the standard must show an identical fragmentation pattern. If the R-Match is ≤ 800 , the structure was accepted with a tag “?” if the R-Match is between 700 and 800, with “??” if the R-Match is between 600 and 700 and with “???” if the R-Match is ≤ 600). Those tagged substances were referred to as “putative”.

Retention Index

The retention index for programmed temperature gas chromatography was calculated via Excel 2013 (Microsoft, Redmont, USA) according to the following equation (Vandendool and Kratz, 1963).

$$RI = 100 i \frac{X - M_{(n)}}{M_{(n+i)} - M_{(n)}} + 100 n$$

The alkanes framing the unknown substance were characterized by the retention time $M_{(n)}$, for the first eluting alkane, and $M_{(n+1)}$ for the later eluting alkane. n being the number of C-atoms of

the shorter alkane chain, and i being the C-atom difference to the longer alkane chain. X represents the retention time of the unknown substance. For substances eluting at a retention time before the first eluting alkane and after the last eluting alkane, the two alkanes with the closest retention times to the respective substances were defined as the framing alkanes.

Standards

To identify substances with the help of chemical standards, measurements of Michaela Mauß, as documented in (Mausz, 2014) and Carsten Paul (Paul et al., 2013) were used for structure verification. Furthermore standards, dissolved, dried and derivatized by Matthias Hirth, were used for measurements at the GC-EI/TOF/MS.

Carsten Paul measured 17 amino acids at the GC-EI/TOF/MS with the standard temperature program of the metabolomics method. He used 25 μL of 4 mM standard solution, evaporated them to dryness and derivatized them as described in chapter 6.6.3. All samples, except for valine, measured in split 10 mode, were measured in split 5 mode.

The standards of Matthias Hirth were dissolved in water, methanol, water/methanol (3:1 v/v) or chloroform. 100 nM dissolved substance were evaporated to dryness and derivatized. He used protocols as described in chapter 6.6.3. I then performed measurements at the GC-EI/TOF/MS using the metabolomics method.

References

- Aaronson, S. (1978) Excretion of organic matter by phytoplankton in vitro. *Limnology and Oceanography*, **23**, 838.
- Allen, A.E., Laroche, J., Maheswari, U., Lommer, M., Schauer, N., Lopez, P.J., et al. (2008) Whole-cell response of the pennate diatom *Phaeodactylum tricorutum* to iron starvation. *Proceedings of the National Academy of Sciences of the United States of America*, **105**, 10438–10443.
- Allen, A.E., Vardi, A. and Bowler, C. (2006) An ecological and evolutionary context for integrated nitrogen metabolism and related signaling pathways in marine diatoms. *Current Opinion in Plant Biology*, **9**, 264–273.
- Alpermann, T.J., Beszteri, B., John, U., Tillmann, U. and Cembella, A.D. (2009) Implications of life-history transitions on the population genetic structure of the toxigenic marine dinoflagellate *Alexandrium tamarense*. *Molecular Ecology*, **18**, 2122–2133.
- Alpermann, T.J., Tillmann, U., Beszteri, B., Cembella, A.D. and John, U. (2010) Phenotypic variation and genotypic diversity in a planktonic population of the toxigenic marine dinoflagellate *Alexandrium tamarense* (Dinophyceae). *Journal of Phycology*, **46**, 18–32.
- Amin, S.A., Green, D.H., Hart, M.C., Küpper, F.C., Sunda, W.G. and Carrano, C.J. (2009) Photolysis of iron-siderophore chelates promotes bacterial-algal mutualism. *Proceedings of the National Academy of Sciences of the United States of America*, **106**, 17071–6.
- Amin, S.A., Hmelo, L.R., VanTol, H.M., Durham, B.P., Carlson, L.T., Heal, K.R., et al. (2015) Interaction and signalling between a cosmopolitan phytoplankton and associated bacteria. *Nature*, **522**, 98–101.
- Amin, S.A., Parker, M.S. and Armbrust, E.V. (2012) Interactions between diatoms and bacteria. *Microbiology and Molecular Biology Reviews: MMBR*, **76**, 667–684.
- Anderson, M.J. (2004) *CAP: A FORTRAN Computer Program for Canonical Analysis of Principal Coordinates*. Department of Statistics University of Auckland, Auckland, New Zealand.
- Anderson, D.M., Kulis, D.M., J.J., S., Hall, S. and Lee, C. (1990) Dynamics and physiology of saxitoxin production by the dinoflagellates *Alexandrium* spp. *Marine Biology*, **104**, 511–524.
- Anderson, M.J. and Robinson, J. (2003) Generalized discriminant analysis based on distances. *Australian and New Zealand Journal of Statistics*, **45**, 301–318.
- Anderson, M.J. and Willis, T.J. (2003a) Canonical analysis of principal coordinates: a useful method of constrained ordination for ecology. *Ecology*, **84**, 511–525.
- Anderson, M.J. and Willis, T.J. (2003b) Appendix A. Statistical details of the canonical analysis of principal coordinates (CAP). *Ecology*, **84**, 1–5.
- Andreae, M.O. (1990) Ocean-atmosphere interactions in the global biogeochemical sulfur cycle. *Marine Chemistry*, **30**, 1–29.
- Armbrust, E.V., Berges, J., Bowler, C., Green, B., Martinez, D. and Putnam, N. (2004) The genome of the diatom *Thalassiosira pseudonana*: ecology, evolution and metabolism. *Science*, **306**, 79–86.
- Arrieta, J., Barreira, A. and Tuval, I. (2015) Microscale patches of nonmotile phytoplankton. *Physical Review Letters*, **114**, 1–5.
- Arzul, G., Seguel, M., Guzman, L. and Erard-le Denn, E. (1999) Comparison of allelopathic

- properties in three toxic *Alexandrium* species. *Journal of Experimental Marine Biology and Ecology*, **232**, 285–295.
- Barofsky, A., Vidoudez, C. and Pohnert, G. (2009) Metabolic profiling reveals growth stage variability in diatom exudates. *Limnology and Oceanography: Methods*, **7**, 382–390.
- Bates, T.S., Charlson, R.J. and Gammon, R.H. (1987) Evidence for the climatic role of marine biogenic sulphur. *Nature*, **329**, 319–321.
- Bekker, A., Holland, H.D., Wang, P.-L., Rumble, D., Stein, H.J., Hannah, J.L., et al. (2004) Dating the rise of atmospheric oxygen. *Nature*, **427**, 117–120.
- Bell, W.H. (1983) Bacterial utilization of algal extracellular products. 3. The specificity of algal-bacterial interaction. *Limnology and Oceanography*, **28**, 1131–1143.
- Bendschneider, K. and Robinson, R.J. (1952) A new spectrophotometric method for the determination of nitrite in sea water. *Journal of Marine Research*, **11**, 87–96.
- Bentes, A.L.A., Borges, R.S., Monteiro, W.R., De Macedo, L.G.M. and Alves, C.N. (2011) Structure of dihydrochalcones and related derivatives and their scavenging and antioxidant activity against oxygen and nitrogen radical species. *Molecules*, **16**, 1749–1760.
- Van Den Berg, R.A., Hoefsloot, H.C.J., Westerhuis, J.A., Smilde, A.K. and Van Der Werf, M.J. (2006) Centering, scaling, and transformations: improving the biological information content of metabolomics data. *BMC genomics*, **7**, 1–15.
- Bidle, K.D. (2016) Programmed cell death in unicellular phytoplankton. *Current Biology*, **26**, 594–607.
- Bishop, G.J. and Koncz, C. (2002) Brassinosteroids and plant steroid hormone signaling. *The Plant Cell*, **Supplement**, 97–110.
- Borkman, D.G. and Smayda, T. (2009) Multidecadal (1959–1997) changes in *Skeletonema* abundance and seasonal bloom patterns in Narragansett Bay, Rhode Island, USA. *Journal of Sea Research*, **61**, 84–94.
- Borowitzka, M.A. (2016) Chemically-mediated interactions in microalgae. *The Physiology of Microalgae* (eds MA Borowitzka, JA Raven and J Beardall), pp. 321–359. Springer.
- Bowler, C., Vardi, A. and Allen, A.E. (2010) Oceanographic and biogeochemical insights from diatom genomes. *Annual Review of Marine Science*, **2**, 333–365.
- Brand, L.E., Campbell, L. and Bresnan, E. (2012) *Karenia*: The biology and ecology of a toxic genus. *Harmful Algae*, **14**, 156–178.
- Broeckling, C.D., Reddy, I.R., Duran, A.L., Zhao, X. and Sumner, L.W. (2006) MET-IDEA: data extraction tool for mass spectrometry-based metabolomics. *Analytical Chemistry*, **78**, 4334–4341.
- Bromke, M.A., Giavalisco, P., Willmitzer, L. and Hesse, H. (2013) Metabolic analysis of adaptation to short-term changes in culture conditions of the marine diatom *Thalassiosira pseudonana*. *PLOS ONE*, **8**, 1–11.
- Bronk, D.A., See, J.H., Bradley, P. and Killberg, L. (2006) DON as a source of bioavailable nitrogen for phytoplankton. *Biogeosciences*, **4**, 283–296.
- Bronstein, J.L. (1994) Conditional outcomes in mutualistic interactions. *Trends in Ecology and Evolution*, **9**, 214–217.
- Bruno, J.F., Stachowicz, J.J. and Bertness, M.D. (2003) Inclusion of facilitation into ecological theory. *Trends in Ecology and Evolution*, **18**, 119–125.
- Brussaard, C.P.D. (2004) Viral control of phytoplankton populations - a review. *Journal of Eukaryotic Microbiology*, **51**, 125–138.

- Buchanan, R.E. (1918) Life phases in a bacterial culture. *Oxford Journals*, **23**, 109–125.
- Burkholder, J.A.M., Glibert, P.M. and Skelton, H.M. (2008) Mixotrophy, a major mode of nutrition for harmful algal species in eutrophic waters. *Harmful Algae*, **8**, 77–93.
- Caldwell, G.S. (2009) The influence of bioactive oxylipins from marine diatoms on invertebrate reproduction and development. *Marine Drugs*, **7**, 367–400.
- Cembella, A.D. (2003) Chemical ecology of eukaryotic microalgae in marine ecosystems. *Phycologia*, **42**, 420–447.
- Chambers, S.T., Kunin, C.M., Miller, D. and Hamada, A. (1987) Dimethylthetin can substitute for glycine betaine as an osmoprotectant molecule for *Escherichia coli*. *Journal of Bacteriology*, **169**, 4845–4847.
- Charlson, R.J., Lovelock, J.E., Andreae, M.O. and Warren, S.G. (1987) Oceanic phytoplankton, atmospheric sulphur, cloud albedo and climate. *Nature*, **326**, 655–661.
- Chen, M., Rao, R.S.P., Zhang, Y., Zhong, C.X. and Thelen, J.J. (2014) A modified data normalization method for GC-MS-based metabolomics to minimize batch variation. *SpringerPlus*, **3**, 439.
- Chen, G. and Rynearson, T.A. (2016) Genetically distinct populations of a diatom co-exist during the North Atlantic spring bloom. *Limnology and Oceanography*, **61**, 2165–2179.
- Chokkathukalam, A., Kim, D.-H., Barrett, M.P., Breitling, R. and Creek, D.J. (2014) Stable isotope-labeling studies in metabolomics: new insights into structure and dynamics of metabolic networks. *Bioanalysis*, **6**, 511–524.
- Cole, J.J. (1982) Interactions between bacteria and algae in aquatic ecosystems. *Annual Review of Ecology and Systematics*, **13**, 291–314.
- Coombs, J., Halicki, P.J., Holm-Hansen, O. and Volcani, B.E. (1967) Studies on the biochemistry and fine structure of silica shell formation in diatoms: II. Changes in concentration of nucleoside triphosphates in silicon-starvation synchrony of *Navicula pelliculosa* (Bréb.) Hilse. *Experimental Cell Research*, **47**, 315–328.
- Cosquer, A., Pichereau, V., Pocard, J.A., Minet, J., Cormier, M. and Bernard, T. (1999) Nanomolar levels of dimethylsulfoniopropionate, dimethylsulfonioacetate, and glycine betaine are sufficient to confer osmoprotection to *Escherichia coli*. *Applied and Environmental Microbiology*, **65**, 3304–3311.
- Da Costa, E., Silva, J., Mendonca, S.H., Abreu, M.H. and Domingues, M.R. (2016) Lipidomic approaches towards deciphering glycolipids from microalgae as a reservoir of bioactive lipids. *Marine Drugs*, **14**, 101–128.
- Costa, M.S., Rego, A., Ramos, V., Afonso, T.B., Freitas, S., Preto, M., et al. (2016) The conifer biomarkers dehydroabietic and abietic acids are widespread in cyanobacteria. *Scientific Reports*, **6**, 1–11.
- Coughlan, S. (1977) The effect of organic substrates on the growth, photosynthesis and dark survival of marine algae. *British Phycological Journal*, **12**, 155–162.
- Croft, M.T., Lawrence, A.D., Raux-Deery, E., Warren, M.J. and Smith, A.G. (2005) Algae acquire vitamin B12 through a symbiotic relationship with bacteria. *Nature*, **438**, 90–93.
- Dicke, M. and Sabelis, M.W. (1988) Infochemical terminology: based on cost-benefit analysis rather than origin of compounds? *Functional Ecology*, **2**, 131–139.
- Diekmann, A.B.S., Peck, M.A., Holste, L., St John, M.A. and Campbell, R.W. (2009) Variation in diatom biochemical composition during a simulated bloom and its effect on copepod production. *Journal of Plankton Research*, **31**, 1391–1405.
- Dreux Chappell, P., Whitney, L.P., Haddock, T.L., Menden-Deuer, S., Roy, E.G., Wells, M.L.,

- et al. (2013) *Thalassiosira* spp. community composition shifts in response to chemical and physical forcing in the northeast Pacific Ocean. *Frontiers in Microbiology*, **4**, 1–14.
- Dufourc, E.J. (2008) Sterols and membrane dynamics. *Journal of Chemical Biology*, **1**, 63–77.
- Dunker, S., Althammer, J., Pohnert, G. and Wilhelm, C. (2017) A fateful meeting of two phytoplankton species - chemical vs. cell-cell-interactions in co-cultures of the green algae *Oocystis marsonii* and the cyanobacterium *Microcystis aeruginosa*. *Microbial Ecology*, **74**, 22–32.
- Dyrhman, S.T. (2016) Nutrients and their acquisition: phosphorus physiology in microalgae. *The physiology of microalgae* (eds MA Borowitzka, J Beardall and JA Raven), pp. 155–185. Springer.
- Eick, K. and Pohnert, G. (2015) Simplifying complexity in metabolomics. *Chemistry & Biology*, **22**, 567–568.
- Ellis, D.I., Dunn, W.B., Griffin, J.L., Allwood, J.W. and Goodacre, R. (2007) Metabolic fingerprinting as a diagnostic tool. *Pharmacogenomics*, **8**, 1243–1266.
- Ellis, D.I. and Goodacre, R. (2006) Metabolic fingerprinting in disease diagnosis: biomedical applications of infrared and Raman spectroscopy. *The Analyst*, **131**, 875–878.
- Fabris, M., Matthijs, M., Carbonelle, S., Moses, T., Pollier, J., Dasseville, R., et al. (2014) Tracking the sterol biosynthesis pathway of the diatom *Phaeodactylum tricornutum*. *The New Phytologist*, **204**, 521–535.
- Falkowski, P.G. (1994) The role of phytoplankton photosynthesis in global biogeochemical cycles. *Photosynthesis Research*, **39**, 235–258.
- Falkowski, P. (2012) The power of plankton. *Science*, **483**, 7–10.
- Falkowski, P.G., Barber, R.T. and Smetacek, V. (1998) Biogeochemical controls and feedbacks on ocean primary production. *Science*, **281**, 200–206.
- Falkowski, P.G., Katz, M.E., Knoll, A.H., Quigg, A., Raven, J.A., Schofield, O., et al. (2004) The evolution of modern eukaryotic. *Science*, **305**, 354–360.
- Fernie, A.R., Aharoni, A., Willmitzer, L., Stitt, M., Tohge, T., Kopka, J., et al. (2011) Recommendations for reporting metabolite data. *The Plant Cell*, **23**, 2477–2482.
- Ferrier, M., Martin, J.L. and Rooney-Varga, J.N. (2002) Stimulation of *Alexandrium fundyense* growth by bacterial assemblages from the Bay of Fundy. *Journal of Applied Microbiology*, **92**, 706–716.
- Fiehn, O. (2002) Metabolomics - the link between genotypes and phenotypes. *Plant Molecular Biology*, **48**, 155–171.
- Fiehn, O., Robertson, D., Griffin, J., Van Der Werf, M., Nikolau, B., Morrison, N., et al. (2007) The metabolomics standards initiative (MSI). *Metabolomics*, **3**, 175–178.
- Field, C.B., Behrenfeld, M.J., Randerson, J.T. and Falkowski, P.G. (1998) Primary production of the biosphere: integrating terrestrial and oceanic components. *Science*, **281**, 237–240.
- Fistarol, G.O., Legrand, C. and Granéli, E. (2005) Allelopathic effect on a nutrient-limited phytoplankton species. *Aquatic Microbial Ecology*, **41**, 153–161.
- Fistarol, G.O., Legrand, C., Selander, E., Hummert, C., Stolte, W. and Granéli, E. (2004) Allelopathy in *Alexandrium* spp.: effect on a natural plankton community and on algal monocultures. *Aquatic Microbial Ecology*, **35**, 45–56.
- Fleming, R.H. (1940) The composition of plankton and units for reporting populations and production. *Proceedings of the Sixth Pacific Science Congress of the Pacific Science Association* pp. 535–540. University of California Press, Berkeley.

- Flewelling, L.J., Naar, J.P., Abbott, J.P., Baden, D.G., Barros, N.B., Bossart, G.D., et al. (2005) Brevetoxicosis: red tides and marine mammal mortalities. *Nature*, **435**, 755–756.
- Fogg, G.E. (1977) Excretion of organic matter by phytoplankton. *Limnology and Oceanography*, **22**, 576–577.
- Fogg, G.E., Nalewajko, C. and Watt, W.D. (1965) Extracellular products of phytoplankton photosynthesis. *Proceedings of the Royal Society B: Biological Sciences*, **162**, 517–534.
- Fogg, G.E. and Thake, B. (1987) *Algal Cultures and Phytoplankton Ecology*, 3rd ed (eds GE Fogg and B Thake). University of Wisconsin Press, Madison.
- Fox, J. and Weisberg, S. (2011) *An R Companion to Applied Regression*, 2nd ed (eds V Knight and L Habib). Sage Publications, Thousand Oaks, USA.
- Freeberg, L.R., Marshall, A. and Heyl, M. (1979) Interrelationships of *Gymnodinium breve* (Florida red tide) within the phytoplankton community. *Toxic Dinoflagellate Blooms* (eds D.L. Taylor, & H.H. Seliger), pp. 139–144. Elsevier, Amsterdam.
- Galea, A.M. and Brown, A.J. (2009) Special relationship between sterols and oxygen: were sterols an adaptation to aerobic life? *Free Radical Biology and Medicine*, **47**, 880–889.
- Gehrke, C.W., Nakamoto, H. and Zumwalt, R.W. (1969) Gas-liquid chromatography of protein amino acid trimethylsilyl derivatives. *Journal of Chromatography A*, **45**, 24–51.
- Gillard, J., Frenkel, J., Devos, V., Sabbe, K., Paul, C., Rempt, M., et al. (2013) Metabolomics enables the structure elucidation of a diatom sex pheromone. *Angewandte Chemie - International Edition*, **52**, 854–857.
- González, M. (2015) Aromatic abietane diterpenoids: their biological activity and synthesis. *Natural Product Reports*, **32**, 684–704.
- Gran, H.H. (1931) On the conditions for the production of plankton in the sea. *Rapports et procès-verbaux des réunions / Conseil permanent international pour l'exploration de la mer*, **75**, 37–46.
- Granéli, E. and Hansen, P.J. (2006) Allelopathy in harmful algae: a mechanism to compete for resources? *Ecology of Harmful Algae*, **189**, 189–201.
- Granéli, E. and Johansson, N. (2003) Increase in the production of allelopathic substances by *Prymnesium parvum* cells grown under N- or P-deficient conditions. *Harmful Algae*, **2**, 135–145.
- Granéli, E. and Pavia, H. (2006) Allelopathy in marine ecosystems. *Allelopathy: A Physiological Process with Ecological Implications* (eds MJ Reigosa, N Pedrol and L González), pp. 415–431. Springer, Dodrecht.
- Granéli, E. and Salomon, P.S. (2010) Factors influencing allelopathy and toxicity in *Prymnesium parvum*. *Journal of the American Water Resources Association*, **46**, 108–120.
- Grant, M.A., Kazamia, E., Cicuta, P. and Smith, A.G. (2014) Direct exchange of vitamin B12 is demonstrated by modelling the growth dynamics of algal-bacterial cocultures. *The ISME Journal*, **8**, 1418–1427.
- Grattan, L.M., Holobaugh, S. and Morris, J.G. (2016) Harmful algal blooms and public health. *Harmful Algae*, **57**, 2–8.
- Gross, E.M. (2003) Allelopathy of aquatic autotrophs. *Critical Reviews in Plant Sciences*, **22**, 313–339.
- Gross, E.M., Meyer, H. and Schilling, G. (1996) Release and ecological impact of algicidal hydrolysable polyphenols in *Myriophyllum spicatum*. *Phytochemistry*, **41**, 133–138.
- Grossart, H.-P., Levold, F., Allgaier, M., Simon, M. and Brinkhoff, T. (2005) Marine diatom

- species harbour distinct bacterial communities. *Environmental Microbiology*, **7**, 860–873.
- Grossart, H.-P. and Simon, M. (2007) Interactions of planktonic algae and bacteria: effects on algal growth and organic matter dynamics. *Aquatic Microbial Ecology*, **47**, 163–176.
- Gross, E.M., Wolk, P.C. and Jüttner, F. (1991) Fischerellin, a new allelochemical from the freshwater cyanobacterium *Fischerella muscicola*. *Journal of Phycology*, **27**, 686–692.
- Guillard, R.R.K. and Kilham, P. (1977) The ecology of marine planktonic diatoms. *The Biology of Diatoms*, 1st ed (ed D. Werner), pp. 372–496. Blackwell Scientific Publications, London.
- Guillard, R. and Sieracki, M. (2005) Counting cells in cultures with the light microscope. *Algal Culturing Techniques*, 1st ed (ed R.A. Andersen), pp. 239–252. Phycological Society of America, Burlington, USA.
- Halket, J.M., Waterman, D., Przyborowska, A.M., Patel, R.K.P., Fraser, P.D. and Bramley, P.M. (2005) Chemical derivatization and mass spectral libraries in metabolic profiling by GC/MS and LC/MS/MS. *Journal of Experimental Botany*, **56**, 219–243.
- Halket, J.M. and Zaikin, V.G. (2003) Derivatization in mass spectrometry - 1. silylation. *European Journal of Mass Spectrometry*, **9**, 1–21.
- Hamm, C.E., Merkel, R., Springer, O., Jurkojc, P., Maier, C., Prectel, K., et al. (2003) Architecture and material properties of diatom shells provide effective mechanical protection. *Nature*, **421**, 841–843.
- Hansen, E. and Eilertsen, H.C. (2007) Do the polyunsaturated aldehydes produced by *Phaeocystis pouchetii* (Hariot) Lagerheim influence diatom growth during the spring bloom in Northern Norway? *Journal of Plankton Research*, **29**, 87–96.
- Hansen, H.P. and Koroleff, F. (2007) Determination of nutrients. *Methods of Seawater Analysis*, 3rd ed (eds K Grasshoff, K Kremling and M Ehrhardt), pp. 159–228. WILEY-VCH Verlag GmbH, Weinheim.
- Harrison, P., Parslow, J. and Conway, H. (1989) Determination of nutrient uptake kinetic parameters: a comparison of methods. *Marine Ecology Progress Series*, **52**, 301–312.
- Harwood, J.L. and Guschina, I.A. (2009) The versatility of algae and their lipid metabolism. *Biochimie*, **91**, 679–684.
- Hay, M.E. (1996) Marine chemical ecology: what's known and what's next? *Journal of Experimental Marine Biology and Ecology*, **200**, 103–134.
- Hay, M.E. (2009) Marine chemical ecology: chemical signals and cues structure marine populations, communities, and ecosystems. *Annual Review of Marine Science*, **1**, 193–212.
- Hay, M.E. and Kubanek, J. (2002) Community and ecosystem level consequences of chemical cues in the plankton. *Journal of Chemical Ecology*, **28**, 2001–2016.
- Hellebust, J.A. (1965) Excretion of some organic compounds by marine phytoplankton. *Limnology and Oceanography*, **10**, 192–206.
- Honjo, T., Shimouse, T. and Hanaoka, T. (1978) A red tide occurred at the Hakozaki Fishing Port, Hakata Bay [Japan], in 1973: the growth process and the chlorophyll content. *Bulletin of Plankton Society of Japan*, **25**, 7–12.
- Huseby, S., Degerlund, M., Zingone, A. and Hansen, E. (2012) Metabolic fingerprinting reveals differences between northern and southern strains of the cryptic diatom *Chaetoceros socialis*. *European Journal of Phycology*, **47**, 480–489.
- Ianora, A., Bentley, M.G., Caldwell, G.S., Casotti, R., Cembella, A.D., Engström-Öst, J., et al. (2011) The relevance of marine chemical ecology to plankton and ecosystem function: an emerging field. *Marine Drugs*, **9**, 1625–1648.

- Ianora, A., Boersma, M., Casotti, R., Fontana, A., Harder, J., Hoffmann, F., et al. (2006) New trends in marine chemical ecology. *Estuaries and Coasts*, **29**, 531–551.
- Ianora, A. and Miralto, A. (2010) Toxicogenic effects of diatoms on grazers, phytoplankton and other microbes: a review. *Ecotoxicology*, **19**, 493–511.
- Inderjit and Duke, S.O. (2003) Ecophysiological aspects of allelopathy. *Planta*, **217**, 529–539.
- John, M.A. St., Clemmesen, C., Lund, T. and T., K. (2001) Diatom production in the marine environment: implications for larval fish growth and condition. *ICES Journal of Marine Science*, **58**, 1106–1113.
- Jonsson, P.R., Pavia, H. and Toth, G. (2009) Formation of harmful algal blooms cannot be explained by allelopathic interactions. *Proceedings of the National Academy of Sciences of the United States of America*, **106**, 11177–11182.
- Kanani, H., Chrysanthopoulos, P.K. and Klapa, M.I. (2008) Standardizing GC-MS metabolomics. *Journal of Chromatography B*, **871**, 191–201.
- Kanani, H.H. and Klapa, M.I. (2007) Data correction strategy for metabolomics analysis using gas chromatography-mass spectrometry. *Metabolic Engineering*, **9**, 39–51.
- Karsten, U., Wiencke, C. and Kirst, G. (1991) The effect of salinity changes upon the physiology of eulittoral green macroalgae from Antarctica and southern Chile. *Journal of Experimental Botany*, **42**, 1533–1539.
- Katajamaa, M. and Orešič, M. (2007) Data processing for mass spectrometry-based metabolomics. *Journal of Chromatography A*, **1158**, 318–328.
- Keating, K.I. (1977) Allelopathic influence on blue-green bloom sequence in a eutrophic lake. *Science*, **196**, 885–887.
- Keating, K.I. (1978) Blue-green algal inhibition of diatom growth: transition from mesotrophic to eutrophic community structure. *Science*, **199**, 971–973.
- Keeling, R.F. and Shertz, S.R. (1992) Seasonal and interannual variations in atmospheric oxygen and implications for the global carbon cycle. *Nature*, **358**, 723–727.
- Kell, D.B. and Oliver, S.G. (2016) The metabolome 18 years on: a concept comes of age. *Metabolomics*, **12**, 148.
- Kiene, R.P., Linn, L.J. and Bruton, J.A. (2000) New and important roles for DMSP in marine microbial communities. *Journal of Sea Research*, **43**, 209–224.
- Kiene, R.P. and Slezak, D. (2006) Low dissolved DMSP concentrations in seawater revealed by small volume gravity filtration and dialysis sampling. *Limnology and Oceanography: Methods*, **4**, 80–95.
- Kindt, R. and Coe, R. (2005) Analysis of differences in species composition. *Tree diversity analysis: A Manual and Software for Common Statistical Methods for Ecological and Biodiversity Studies*, 1st ed pp. 123–138. World Agroforestry Centre, Nairobi.
- Kirst, G.O., Thiel, C., Wolff, H., Nothnagel, J., Wanzek, M. and Ulmke, R. (1991) Dimethylsulfoniopropionate (DMSP) in icealgae and its possible biological role. *Marine Chemistry*, **35**, 381–388.
- Koek, M.M., Jellema, R.H., Van Der Greef, J., Tas, A.C. and Hankemeier, T. (2011) Quantitative metabolomics based on gas chromatography mass spectrometry: status and perspectives. *Metabolomics*, **7**, 307–328.
- Kooistra, W.H.C.F., Gersonde, R., Medlin, L.K. and Mann, D.G. (2007) The origin and evolution of the diatoms: their adaptation to a planktonic existence. *Evolution of Primary Producers in the Sea*, 1st ed (eds P.G. Falkowski, & A.H. Knoll), pp. 207–249. Elsevier, Amsterdam.

- Kooistra, W.H.C.F., Sarno, D., Balzano, S., Gu, H., Andersen, R.A. and Zingone, A. (2008) Global diversity and biogeography of *Skeletonema* species (Bacillariophyta). *Protist*, **159**, 177–193.
- Kopka, J. (2006) Current challenges and developments in GC–MS based metabolite profiling technology. *Journal of Biotechnology*, **124**, 312–322.
- Kruskopf, M. and Flynn, K.J. (2006) Chlorophyll content and fluorescence responses cannot be used to gauge reliably phytoplankton biomass, nutrient status or growth rate. *New Phytologist*, **169**, 525–536.
- Kubanek, J., Hicks, M.K., Naar, J. and Villareal, T.A. (2005) Does the red tide dinoflagellate *Karenia brevis* use allelopathy to outcompete other phytoplankton? *Limnology and Oceanography*, **50**, 883–895.
- Kuhlisch, C. and Pohnert, G. (2015) Metabolomics in chemical ecology. *Natural Product Reports*, **32**, 879–1156.
- Landsberg, J.H., Flewelling, L.J. and Naar, J. (2009) *Karenia brevis* red tides, brevetoxins in the food web, and impacts on natural resources: decadal advancements. *Harmful Algae*, **8**, 598–607.
- Leflaive, J. and Ten-Hage, L. (2009) Chemical interactions in diatoms: role of polyunsaturated aldehydes and precursors. *New Phytologist*, **184**, 794–805.
- Legrand, C., Rengefors, K., Fistarol, G.O. and Granéli, E. (2003) Allelopathy in phytoplankton - biochemical, ecological and evolutionary aspects. *Phycologia*, **42**, 406–419.
- Lei, Z., Li, H., Chang, J., Zhao, P.X. and Sumner, L.W. (2012) MET-IDEA version 2.06; improved efficiency and additional functions for mass spectrometry-based metabolomics data processing. *Metabolomics*, **8**, S105–S110.
- Lewis, W.M. (1986) Evolutionary interpretations of allelochemical interactions in phytoplankton algae. *The American Naturalist*, **127**, 184–194.
- Limardo, A.J. and Worden, A.Z. (2015) Exclusive networks in the sea. *Nature*, 6–7.
- Lisec, J., Schauer, N., Kopka, J., Willmitzer, L. and Fernie, A.R. (2006) Gas chromatography mass spectrometry–based metabolite profiling in plants. *Nature Protocols*, **1**, 387–396.
- De Livera, A.M., Dias, D.A., De Souza, D., Rupasinghe, T., Pyke, J., Tull, D., et al. (2012) Normalizing and integrating metabolomics data. *Analytical Chemistry*, **84**, 10768–10776.
- Lochte, K., Ducklow, H.W., Fasham, M.J.R. and Stienen, C. (1993) Plankton succession and carbon cycling at 47-degrees-N-20-degrees-W during the JGOFS North-Atlantic Bloom Experiment. *Deep Sea Research Part II: Topical Studies in Oceanography*, **40**, 91–114.
- Lopes, V.R. and Vasconcelos, V.M. (2011) Bioactivity of benthic and picoplanktonic estuarine cyanobacteria on growth of photoautotrophs: inhibition versus stimulation. *Marine Drugs*, **9**, 790–802.
- Lu, H., Liang, Y., Dunn, W.B., Shen, H. and Kell, D.B. (2008) Comparative evaluation of software for deconvolution of metabolomics data based on GC-TOF-MS. *Trends in Analytical Chemistry*, **27**, 215–227.
- Ma, H., Krock, B., Tillmann, U. and Cembella, A. (2009) Preliminary characterization of extracellular allelochemicals of the toxic marine dinoflagellate *Alexandrium tamarense* using a *Rhodomonas salina* bioassay. *Marine Drugs*, **7**, 497–522.
- Maier, I. and Calenberg, M. (1994) Effect of extracellular Ca²⁺ and Ca²⁺ -antagonists on the movement and chemoorientation of male gametes of *Ectocarpus siliculosus* (Phaeophyceae). *Botanica Acta*, **107**, 451–460.
- Mann, D.G. and Droop, S.J.M. (1996) Biodiversity, biogeography and conservation of diatoms.

- Hydrobiologia*, **336**, 19–32.
- Marie, D., Brussaard, C.P.D., Thyraug, R., Bratbak, G. and Vaultot, D. (1999) Enumeration of marine viruses in culture and natural samples by flow cytometry. *Applied and Environmental Microbiology*, **65**, 45–52.
- Martin, A.P. (2003) Phytoplankton patchiness: the role of lateral stirring and mixing. *Progress In Oceanography*, **57**, 125–174.
- Matrai, P.A. and Keller, M.D. (1993) Dimethylsulfide in a large-scale coccolithophore bloom in the Gulf of Maine. *Continental Shelf Research*, **13**, 831–843.
- Mausz, M.A. (2014) *PhD Thesis: Metabolic Investigation of the Microalga Emiliania Huxleyi in Laboratory and Mesocosm Experiments with Focus on Viral Infection*. Friedrich-Schiller-University Jena.
- Mausz, M.A. and Pohnert, G. (2015) Phenotypic diversity of diploid and haploid *Emiliania huxleyi* cells and of cells in different growth phases revealed by comparative metabolomics. *Journal of Plant Physiology*, **172**, 137–148.
- Maxwell, K. and Johnson, G.N. (2000) Chlorophyll fluorescence - a practical guide. *Journal of Experimental Botany*, **51**, 659–668.
- Mazerolle, M.J. (2015) *AICcmodavg: Model Selection and Multimodel Inference Based on (Q)AIC(c)*. <http://CRAN.R-project.org/package=AICcmodavg>, R package version 2.0-3.
- Medeiros, P.M. and Simoneit, B.R.T. (2007) Analysis of sugars in environmental samples by gas chromatography-mass spectrometry. *Journal of Chromatography A*, **1141**, 271–278.
- Medlin, L.K., Elwood, H.J., Stickel, S. and Sogin, M.L. (1991) Morphological and genetic variation within the diatom *Skeletonema costatum* (Bacillariophyta): evidence for a new species, *Skeletonema pseudocostatum*. *Journal of Phycology*, **27**, 514–524.
- Metting, B. and Pyne, J.W. (1986) Biologically active compounds from microalgae. *Enzyme and Microbial Technology*, **8**, 386–394.
- Miller, M.G. (2007) Environmental metabolomics: a SWOT analysis (strengths, weaknesses, opportunities, and threats). *Journal of Proteome Research*, **6**, 540–545.
- Miralto, A., Barone, G., Romano, G., Poulet, S.A., Ianora, A., Russo, G.L., et al. (1999) The insidious effect of diatoms on copepod reproduction. *Nature*, **402**, 173–176.
- Mitchell, J.W., Mandava, N., Worley, J.F., Plimmer, J.R. and Smith, M.V. (1970) Brassins - a new family of plant hormones from rape pollen. *Nature*, **225**, 1065–1066.
- Molisch, H. (1937) *Der Einfluss Einer Pflanze Auf Die Andere: Allelopathie*. Gustav Fisher, Jena.
- Morales-Sanchez, D., Martinez-Rodriguez, O.A., Kyndt, J. and Martinez, A. (2015) Heterotrophic growth of microalgae: metabolic aspects. *World Journal of Microbiology and Biotechnology*, **31**, 1–9.
- Murphy, J. and Riley, J.P. (1958) A single-solution method for the determination of soluble phosphate in sea water. *Journal of the Marine Biological Association of the United Kingdom*, **37**, 9–14.
- Myklestad, S.M. (1995) Release of extracellular products by phytoplankton with special emphasis on polysaccharides. *Science of the Total Environment*, **165**, 155–164.
- Nevitt, G. a. (2008) Sensory ecology on the high seas: the odor world of the procellariiform seabirds. *The Journal of Experimental Biology*, **211**, 1706–1713.
- Nguyen, H.M., Ito, T., Win, N.N., Kodama, T., Hung, V.Q., Nguyen, H.T., et al. (2016) New antibacterial sesquiterpene aminoquinones from a Vietnamese marine sponge of *Spongia*

- sp. *Phytochemistry Letters*, **17**, 288–292.
- Nordlund, D.A. and Lewis, W.J. (1976) Terminology of chemical releasing stimuli in intraspecific and interspecific interactions. *Journal of Chemical Ecology*, **2**, 211–220.
- Oksanen, J., Blanchet, F.G., Kindt, R., Legendre, P., Minchin, P.R., O'Hara, R.B., et al. (2015) *Vegan: Community Ecology Package*. <http://CRAN.R-project.org/package=vegan>, R package version 2.3-2.
- Oliver, S.G. (1996) From DNA sequence to biological function. *Nature*, **379**, 597–600.
- Palenik, B. and Morel, F.M.M. (1990) Amino acid utilization by marine phytoplankton: a novel mechanism. *Limnology and Oceanography*, **35**, 260–269.
- Parkhill, J., Maillet, G. and Cullen, J.J. (2001) Fluorescence-based maximal quantum yield for PSII as a diagnostic of nutrient stress. *Journal of Phycology*, **37**, 517–529.
- Paul, C. (2012) *PhD Thesis: Allelopathic Interactions of Marine Diatoms*. Friedrich-Schiller-University Jena.
- Paul, C., Barofsky, A., Vidoudez, C. and Pohnert, G. (2009) Diatom exudates influence metabolism and cell growth of co-cultured diatom species. *Marine Ecology Progress Series*, **389**, 61–70.
- Paul, C., Mausz, M. a. and Pohnert, G. (2013) A co-culturing/metabolomics approach to investigate chemically mediated interactions of planktonic organisms reveals influence of bacteria on diatom metabolism. *Metabolomics*, **9**, 349–359.
- Paul, C., Reunamo, A., Lindehoff, E., Bergkvist, J., Mausz, M. a, Larsson, H., et al. (2012) Diatom derived polyunsaturated aldehydes do not structure the planktonic microbial community in a mesocosm study. *Marine drugs*, **10**, 775–92.
- Pinheiro, J., Bates, D., DebRoy, S., Sarkar, D. and R Core Team. (2015) *Nlme: Linear and Nonlinear Mixed Effects Models*. <http://cran.r-project.org/package=nlme>, R package version 3.1-122.
- Plaza, M., Santoyo, S., Jaime, L., García-Blairsy Reina, G., Herrero, M., Señoránsb, F.J., et al. (2010) Screening for bioactive compounds from algae. *Journal of Pharmaceutical and Biomedical Analysis*, **51**, 450–455.
- Pohnert, G. (2009) Chemical noise in the silent ocean. *Journal of Plankton Research*, **32**, 141–144.
- Pohnert, G., Steinke, M. and Tollrian, R. (2007) Chemical cues, defence metabolites and the shaping of pelagic interspecific interactions. *Trends in Ecology & Evolution*, **22**, 198–204.
- Poulson-Ellestad, K.L., Jones, C.M., Roy, J., Viant, M.R., Fernández, F.M., Kubanek, J., et al. (2014a) Metabolomics and proteomics reveal impacts of chemically mediated competition on marine plankton. *Proceedings of the National Academy of Sciences of the United States of America*, **111**, 9009–9014.
- Poulson-Ellestad, K., Mcmillan, E., Montoya, J.P. and Kubanek, J. (2014b) Are offshore phytoplankton susceptible to *Karenia brevis* allelopathy? *Journal of Plankton Research*, **36**, 1344–1356.
- Poulson, K.L., Sieg, R.D. and Kubanek, J. (2009) Chemical ecology of the marine plankton. *Natural Product Reports*, **26**, 729–745.
- Prariono, T., Kawaroe, M. and Katili, V. (2013) Fatty acid composition of three diatom species *Skeletonema costatum*, *Thalassiosira* sp. and *Chaetoceros gracilis*. *International Journal of Environment and Bioenergy*, **6**, 28–43.
- Pratt, D.M. (1966) Competition between *Skeletonema costatum* and *Olisthodiscus luteus* in Narragansett Bay and in culture. *Limnology and Oceanography*, **6**, 447–455.

- Prince, E.K., Myers, T.L. and Kubanek, J. (2008a) Effects of harmful algal blooms on competitors: allelopathic mechanisms of the red tide dinoflagellate *Karenia brevis*. *Limnology and Oceanography*, **53**, 531–541.
- Prince, E.K., Myers, T.L., Naar, J. and Kubanek, J. (2008b) Competing phytoplankton undermines allelopathy of a bloom-forming dinoflagellate. *Proceedings of the Royal Society B: Biological Sciences*, **275**, 2733–2741.
- Prince, E.K. and Pohnert, G. (2010) Searching for signals in the noise: metabolomics in chemical ecology. *Analytical and Bioanalytical Chemistry*, **396**, 193–197.
- Prince, E.K., Poulson, K.L., Myers, T.L., Sieg, R.D. and Kubanek, J. (2010) Characterization of allelopathic compounds from the red tide dinoflagellate *Karenia brevis*. *Harmful Algae*, **10**, 39–48.
- Qiu, X., Shimasaki, Y., Yoshida, Y., Matsubara, T., Yamasaki, Y., Kawaguchi, M., et al. (2014) Allelopathic effects of *Skeletonema* spp. may influence interspecific competition and bloom formation of co-occurring harmful flagellates. *Journal of the Faculty of Agriculture, Kyushu University*, **59**, 373–382.
- Qiu, X., Yamasaki, Y., Shimasaki, Y., Gunjikake, H., Gunjikake, H., Shikata, T., et al. (2011) Growth interactions between raphidophytes *Chattonella antiqua* and *Heterosigma akashiwo*. *Thalassas*, **27**, 33–45.
- Rad-Menéndez, C., Stanley, M., Green, D.H., Cox, E.J. and Day, J.G. (2015) Exploring cryptic diversity in publicly available strains of the model diatom *Thalassiosira pseudonana* (Bacillariophyceae). *Journal of the Marine Biological Association of the United Kingdom*, **95**, 1081–1090.
- R Development Core Team. (2008) *R: A Language and Environment for Statistical Computing. Version 3.2.2*. R Foundation for Statistical Computing, Vienna, Austria.
- Ragueneau, O., Tréguer, P., Leynaert, A., Anderson, R.F., Brzezinski, M.A., DeMaster, D.J., et al. (2000) A review of the Si cycle in the modern ocean: recent progress and missing gaps in the application of biogenic opal as a paleoproductivity proxy. *Global and Planetary Change*, **26**, 317–365.
- Rampen, S.W., Abbas, B.A., Schouten, S. and Damsté, J.S.S. (2010) A comprehensive study of sterols in marine diatoms (Bacillariophyta): implications for their use as tracers for diatom productivity. *Limnology and Oceanography*, **55**, 91–105.
- Raven, J.A. and Giordano, M. (2016) Combined nitrogen. *The Physiology of Microalgae*, 1st ed (eds M.A. Borowitzka, J. Beardall, & J.A. Raven), pp. 143–155. Springer.
- Redfield, A.C. (1958) The biological control of chemical factors in the environment. *American Scientist*, **46**, 205–221.
- Reigosa, M.J., Sánchez-Moreiras, A. and González, L. (1999) Ecophysiological approach in allelopathy. *Critical Reviews in Plant Sciences*, **18**, 577–608.
- Ribalet, F., Berges, J. a, Ianora, A. and Casotti, R. (2007) Growth inhibition of cultured marine phytoplankton by toxic algal-derived polyunsaturated aldehydes. *Aquatic toxicology*, **85**, 219–227.
- Ribalet, F., Intertaglia, L., Lebaron, P. and Casotti, R. (2008) Differential effect of three polyunsaturated aldehydes on marine bacterial isolates. *Aquatic Toxicology*, **86**, 249–55.
- Rico, M., López, A., Santana-Casiano, J.M., González, A.G. and González-Dávila, M. (2013) Variability of the phenolic profile in the diatom *Phaeodactylum tricorutum* growing under copper and iron stress. *Limnology and Oceanography*, **58**, 144–152.
- Romero, O.E., Fischer, G., Karstensen, J. and Cermeno, P. (2016) Eddies as trigger for diatom

- productivity in the open-ocean Northeast Atlantic. *Progress in Oceanography*, **147**, 38–48.
- Roubeix, V., Becquevort, S. and Lancelot, C. (2008) Influence of bacteria and salinity on diatom biogenic silica dissolution in estuarine systems. *Biogeochemistry*, **88**, 47–62.
- Round, F., Crawford, R. and Mann, D. (1990) *The Diatoms. Biology and Morphology of the Genera*, 4th ed. Cambridge University Press, Cambridge.
- Roy, S. and Legendre, L. (1979) DCMU-enhanced fluorescence as an index of photosynthetic activity in phytoplankton. *Marine Biology*, **55**, 93–101.
- Roy, J.S., Poulson-Ellestad, K.L., Drew Sieg, R., Poulin, R.X. and Kubanek, J. (2013) Chemical ecology of the marine plankton. *Natural Product Reports*, **30**, 1364–1379.
- Ruiz-Matute, A.I., Hernández-Hernández, O., Rodríguez-Sánchez, S., Sanz, M.L. and Martínez-Castro, I. (2011) Derivatization of carbohydrates for GC and GC-MS analyses. *Journal of Chromatography B: Analytical Technologies in the Biomedical and Life Sciences*, **879**, 1226–1240.
- Ryther, J.H. (1969) Photosynthesis and fish production in the sea. *Science*, **166**, 72–76.
- Salih, B. and Çelikbiçak, Ö. (2012) *Gas Chromatography - Biochemicals, Narcotics and Essential Oils*, 1. (eds Ö Çelikbiçak and S Bekir). InTech, Rijeka.
- Sardans, J., Penuelas, J. and Rivas-Ubach, A. (2011) Ecological metabolomics: overview of current developments and future challenges. *Chemoecology*, **21**, 191–225.
- Sarkar, D. (2008) *Lattice: Multivariate Data Visualization with R* (eds R Gentleman, K Hornik, and G Parmigiani). Springer, New York.
- Sarno, D., Kooistra, W.H.C.F., Balzano, S., Hargraves, P.E. and Zingone, A. (2007) Diversity in the genus *Skeletonema* (bacillariophyceae): III. Phylogenetic position and morphological variability of *Skeletonema costatum* and *Skeletonema grevillei*, with the description of *Skeletonema ardens* sp. nov. *Journal of Phycology*, **43**, 156–170.
- Sarno, D., Kooistra, W.H.C.F., Medlin, L.K., Percopo, I. and Zingone, A. (2005) Diversity in the genus *Skeletonema* (Bacillariophyceae). II. an assessment of the taxonomy of *S. costatum* - like species with the description of four new species. *Journal of Phycology*, **41**, 151–176.
- Sarthou, G., Timmermans, K.R., Blain, S. and Tréguer, P. (2005) Growth physiology and fate of diatoms in the ocean: a review. *Journal of Sea Research*, **53**, 25–42.
- Savluchinske-Feio, S., Curto, M.J.M., Gigante, B. and Roseiro, J.C. (2006) Antimicrobial activity of resin acid derivatives. *Applied Microbiology and Biotechnology*, **72**, 430–436.
- Schäfer, H. and Abbas, B. (2002) Genetic diversity of “satellite” bacteria present in cultures of marine diatoms. *FEMS Microbiology Ecology*, **42**, 25–35.
- Schmidt, L.E. and Hansen, P.J. (2001) Allelopathy in the prymnesiophyte *Chrysochromulina polylepis* effect of cell concentration, growth phase and pH. *Marine Ecology Progress Series*, **216**, 67–81.
- Schwartz, E.R., Poulin, R.X., Mojib, N. and Kubanek, J. (2016) Chemical ecology of marine plankton. *Natural Product Reports*, **33**, 843–860.
- SEAL-Analytical. (2002) AutoAnalyzer Multi-test Methods. URL <http://www.seal-analytical.com/Methods/AutoAnalyzerMethods/AutoAnalyzerMulti-testMethods/tabid/80/language/en-US/Default.aspx> [accessed 15 July 2014]
- Selander, E., Thor, P., Toth, G. and Pavia, H. (2006) Copepods induce paralytic shellfish toxin production in marine dinoflagellates. *Proceedings of the Royal Society B: Biological Sciences*, **273**, 1673–1680.
- Seymour, J.R., Simo, R., Tanvir, A. and Stocker, R. (2010) Chemoattraction to

- dimethylsulfoniopropionate throughout the marine microbial food web. *Science*, **329**, 342–346.
- Sharp, J.H. (1977) Excretion of organic matter by marine phytoplankton: do healthy cells do it? *Limnology and Oceanography*, **22**, 381–399.
- Sharp, J.H., Underhill, P.A. and Hughes, D.J. (1979) Interaction (allelopathy) between marine diatoms *Thalassiosira pseudonana* and *Phaedoactylum tricorutum*. *Journal of Phycology*, **15**, 353–362.
- Sherry, A. and Henson, R.K. (2005) Conducting and interpreting canonical correlation analysis in personality research: a user-friendly primer. *Journal of Personality Assessment*, **84**, 37–48.
- Shikata, T., Nagasoe, S., Matsubara, T., Yoshikawa, S., Yamasaki, Y., Shimasaki, Y., et al. (2008) Factors influencing the initiation of blooms of the raphidophyte *Heterosigma akashiwo* and the diatom *Skeletonema costatum* in a port in Japan. *Limnology and Oceanography*, **53**, 2503–2518.
- Shilo, M. (1967) Formation and mode of action of algal toxins. *Bacteriological Reviews*, **31**, 180–193.
- Shinn, M.B. (1941) Colorimetric method for determination of nitrate. *Industrial & Engineering Chemistry Analytical Edition*, **13**, 33–35.
- Shniukova, E.I. and Zolotareva, E.K. (2015) Diatom exopolysaccharides: a review. *International Journal on Algae*, **17**, 50–67.
- Shulaev, V. (2006) Metabolomics technology and bioinformatics. *Briefings in Bioinformatics*, **7**, 128–139.
- Sieg, R.D., Poulson-Ellestad, K.L. and Kubanek, J. (2011) Chemical ecology of the marine plankton. *Natural Product Reports*, **28**, 388–399.
- Sieracki, M.E., Verity, P.G. and Stoecker, D.K. (1993) Plankton community response to sequential silicate and nitrate depletion during the 1989 North Atlantic spring bloom. *Deep-Sea Research Part II*, **40**, 213–225.
- Simpson, G.L. (2015) *Permute: Functions for Generating Restricted Permutations of Data*. <http://CRAN.R-project.org/package=permute>, R package version 0.8-4.
- Smayda, T.J. (1997a) Harmful algal blooms: their ecophysiology and general relevance to phytoplankton blooms in the sea. *Limnology and Oceanography*, **42**, 1137–1153.
- Smayda, T.J. (1997b) What is a bloom? A commentary. *Limnology and Oceanography*, **42**, 1132–1136.
- Smetacek, V. and Cloern, J.E. (2008) On phytoplankton trends. *Science*, **319**, 1346–1348.
- Snyder, M., Mias, G., Stanberry, L. and Kolker, E. (2014) Metadata checklist for the integrated personal OMICS study: proteomics and metabolomics experiments. *OMICS A Journal of Integrative Biology*, **18**, 81–85.
- Sournia, A. (1995) Red tide and toxic marine phytoplankton of the world ocean an inquiry into biodiversity. *Proceedings of the 6th International Conference on Toxic Marine Phytoplankton* pp. 103–112. Paris Lavoisier Publishing, Nantes.
- Spielmeier, A., Gebser, B. and Pohnert, G. (2011) Investigations of the uptake of dimethylsulfoniopropionate by phytoplankton. *Chembiochem: A European Journal of Chemical Biology*, **12**, 2276–9.
- Spielmeier, A. and Pohnert, G. (2012) Daytime, growth phase and nitrate availability dependent variations of dimethylsulfoniopropionate in batch cultures of the diatom *Skeletonema marinoi*. *Journal of Experimental Marine Biology and Ecology*, **413**, 121–130.

- Stachowicz, J.J. (2001) Mutualism, facilitation, and the structure of ecological communities. *BioScience*, **51**, 235–246.
- Stashenko, E. and Martínez, J.R. (2014) Gas chromatography-mass spectrometry. *Advances in Gas Chromatography* (ed X. Guo), pp. 1–38. InTech.
- Stefels, J. (2000) Physiological aspects of the production and conversion of DMSP in marine algae and higher plants. *Journal of Sea Research*, **43**, 183–197.
- Stein, S.E., Babushok, V.I., Brown, R.L. and Linstrom, P.J. (2007) Estimation of Kováts retention indices using group contributions. *Journal of Chemical Information and Modeling*, **47**, 975–980.
- Steinke, M., Stefels, J. and Stamhuis, E. (2006) Dimethyl silfide triggers search behavior in copepods. *Limnology and Oceanography*, **51**, 1925–1930.
- Stonik, V. and Stonik, I. (2015) Low-molecular-weight metabolites from diatoms: structures, biological roles and biosynthesis. *Marine Drugs*, **13**, 3672–3709.
- Strom, S.L. (2008) Microbial ecology of ocean biogeochemistry: a community perspective. *Science*, **320**, 1043–1045.
- Sunda, W., Kieber, D.J., Kiene, R.P. and Huntsman, S. (2002) An antioxidant function for DMSP and DMS in marine algae. *Nature*, **418**, 317–20.
- Tameishi, M., Yamasaki, Y., Nagasoe, S., Shimasaki, Y., Oshima, Y. and Honjo, T. (2009) Allelopathic effects of the dinophyte *Prorocentrum minimum* on the growth of the bacillariophyte *Skeletonema costatum*. *Harmful Algae*, **8**, 421–429.
- Theodoridis, G. and Wilson, I.D. (2008) Hyphenated techniques for global metabolite profiling. *Journal of Chromatography B*, **871**, 141–142.
- Thronsen, J. (1978) Preservation and storage. *Phytoplankton Manual: Monographs on Oceanographic Methodology*, **6**, 69–74.
- Tillmann, U., John, U. and Cembella, A. (2007) On the allelochemical potency of the marine dinoflagellate *Alexandrium ostenfeldii* against heterotrophic and autotrophic protists. *Journal of Plankton Research*, **29**, 527–543.
- Tuchman, N.C., Schollett, M.A., Rier, S.T. and Geddes, P. (2006) Differential heterotrophic utilization of organic compounds by diatoms and bacteria under light and dark conditions. *Hydrobiologia*, **561**, 167–177.
- Vandendool, H. and Kratz, P.D. (1963) A generalization of the retention index system including linear temperature programmed gas - liquid partition chromatography. *Journal of Chromatography*, **11**, 463–471.
- Vardi, A. (2008) Cell signaling in marine diatoms. *Communicative & Integrative Biology*, **1**, 134–136.
- Vardi, A., Eisenstadt, D., Murik, O., Berman-Frank, I., Zohary, T., Levine, A., et al. (2007) Synchronization of cell death in a dinoflagellate population is mediated by an excreted thiol protease. *Environmental Microbiology*, **9**, 360–369.
- Vardi, A., Formiggini, F., Casotti, R., De Martino, A., Ribalet, F., Miralto, A., et al. (2006) A stress surveillance system based on calcium and nitric oxide in marine diatoms. *PLOS Biology*, **4**, 0411–0419.
- Vargas, I., Sanz, I., Moya, P. and Prima-Yuferá, E. (1999) Antimicrobial and antioxidant compounds in the nonvolatile fraction of expressed orange essential oil. *Journal of Food Protection*, **62**, 929–932.
- Vargo, G.A. (2009) A brief summary of the physiology and ecology of *Karenia brevis* Davis (G. Hansen and Moestrup comb. nov.) red tides on the West Florida Shelf and of hypotheses

- posed for their initiation, growth, maintenance, and termination. *Harmful Algae*, **8**, 573–584.
- Venables, W.N. and Ripley, B.D. (2002) *Modern Applied Statistics with S*, 4th ed. Springer, New York.
- Viant, M.R. (2007) Metabolomics of aquatic organisms: the new “omics” on the block. *Marine Ecology Progress Series*, **332**, 301–306.
- Vidoudez, C. (2010) *PhD Thesis: Diatom Metabolomics*. Friedrich-Schiller-University Jena.
- Vidoudez, C. and Pohnert, G. (2008) Growth phase-specific release of polyunsaturated aldehydes by the diatom *Skeletonema marinoi*. *Journal of Plankton Research*, **30**, 1305–1313.
- Vidoudez, C. and Pohnert, G. (2011) Comparative metabolomics of the diatom *Skeletonema marinoi* in different growth phases. *Metabolomics*, **8**, 654–669.
- Vila-Costa, M., Simó, R., Harada, H., Gasol, J.M., Slezak, D. and Kiene, R.P. (2006) Dimethylsulfoniopropionate uptake by marine phytoplankton. *Science*, **314**, 652–654.
- Volk, T. and Hoffert, M.I. (1985) Ocean carbon pumps: analysis of relative strengths and efficiencies in ocean-driven atmospheric CO₂ changes. *The carbon cycle and atmospheric CO₂: natural variations archean to present* (eds ET Sundquist and WS Broecker), pp. 99–110. American Geophysical Union, Washington.
- Volkman, J.K. (1986) A review of sterol markers for marine and terrigenous organic matter. *Organic Geochemistry*, **9**, 83–99.
- Wagner-Döbler, I., Ballhausen, B., Berger, M., Brinkhoff, T., Buchholz, I., Bunk, B., et al. (2010) The complete genome sequence of the algal symbiont *Dinoroseobacter shibae*: a hitchhiker’s guide to life in the sea. *The ISME Journal*, **4**, 61–77.
- Wagner, C., Sefkow, M. and Kopka, J. (2003) Construction and application of a mass spectral and retention time index database generated from plant GC/EI-TOF-MS metabolite profiles. *Phytochemistry*, **62**, 887–900.
- Watkins, S.M. (2008) Neurotoxic shellfish poisoning. *Marine Drugs*, **6**, 431–455.
- Weber, R.J.M., Selander, E., Sommer, U. and Viant, M.R. (2013) A stable-isotope mass spectrometry-based metabolic footprinting approach to analyze exudates from phytoplankton. *Marine Drugs*, **11**, 4158–4175.
- Wickham, H. (2009) *ggplot2: Elegant Graphics for Data Analysis*, 1st ed. Springer, New York.
- Wickham, H. (2011) The split-apply-combine strategy for data analysis. *Journal of Statistical Software*, **40**, 1–20.
- Willis, R.J. (1985) The historical bases of the concept of allelopathy. *Journal of the History of Biology*, **18**, 71–102.
- Wink, M. (2003) Evolution of secondary metabolites from an ecological and molecular phylogenetic perspective. *Phytochemistry*, **64**, 3–19.
- Wright, A.E., Rueth, S.A. and Cross, S.S. (1991) An antiviral sesquiterpene hydroquinone from the marine sponge *Strongylophora hartmani*. *Journal of Natural Products*, **54**, 1108–1111.
- Yamasaki, Y., Nagasoe, S., Matsubara, T., Shikata, T., Shimasaki, Y., Oshima, Y., et al. (2007) Allelopathic interactions between the bacillariophyte *Skeletonema costatum* and the raphidophyte *Heterosigma akashiwo*. *Marine Ecology Progress Series*, **339**, 83–92.
- Yamasaki, Y., Nagasoe, S., Tameishi, M., Shikata, T., Zou, Y., Jiang, Z., et al. (2010) The role of interactions between *Prorocentrum minimum* and *Heterosigma akashiwo* in bloom formation. *Hydrobiologia*, **641**, 33–44.
- Yamasaki, Y., Ohmichi, Y., Hirose, M., Shikata, T., Shimasaki, Y., Oshima, Y., et al. (2012)

- Low molecular weight allelochemicals produced by the diatom, *Skeletonema costatum*. *Thalassas*, **28**, 9–17.
- Yamasaki, Y., Ohmichi, Y., Shikata, T., Hirose, M., Shimasaki, Y., Oshima, Y., et al. (2011) Species-specific allelopathic effects of the diatom *Skeletonema costatum*. *Thalassas*, **27**, 21–32.
- Yamasaki, Y., Shikata, T., Nukata, A., Ichiki, S., Nagasoe, S., Matsubara, T., et al. (2009) Extracellular polysaccharide-protein complexes of a harmful alga mediate the allelopathic control it exerts within the phytoplankton community. *The ISME Journal*, **3**, 808–817.
- Yang, C., Zhou, J., Liu, S., Fan, P., Wang, W. and Xia, C. (2013) Allelochemical induces growth and photosynthesis inhibition, oxidative damage in marine diatom *Phaeodactylum tricornutum*. *Journal of Experimental Marine Biology and Ecology*, **444**, 16–23.
- Yentsch, C.S., Yentsch, C.M., Phinney, D.A., Lapointe, B.E. and Yentsch, S.F.W. (2004) The odyssey of new production. *Journal of Experimental Marine Biology and Ecology*, **300**, 15–30.
- Zabaglo, K., Chrapusta, E., Bober, B., Kaminski, A., Adamski, M. and Bialczyk, J. (2016) Environmental roles and biological activity of domoic acid: a review. *Algal Research*, **13**, 94–101.
- Zamboni, N., Saghatelian, A. and Patti, G.J. (2015) Defining the metabolome: size, flux, and regulation. *Molecular Cell*, **58**, 699–706.
- Zimmer, R.K. and Zimmer, C.A. (2008) Dynamic scaling in chemical ecology. *Journal of Chemical Ecology*, **34**, 822–836.
- Zingone, A., Percopo, I., Sims, P.A. and Sarno, D. (2005) Diversity in the genus *Skeletonema* (Bacillariophyceae). I. A reexamination of the type material of *S. costatum* with the description of *S. grevillei* sp. nov. *Journal of Phycology*, **41**, 140–150.
- Zuur, A.F., Leno, E.N., Walker, N.J., Saveliev, A.A. and Smith, G.M. (2009) *Mixed Effects Models and Extensions in Ecology with R*, 1st ed (eds M Gail, K Krickeberg, JM Samet, A Tsiatis and W Wong). Springer-Verlag New York.

Curriculum Vitae

Selbstständigkeitserklärung

Ich erkläre, dass ich die vorliegende Arbeit selbstständig und unter Verwendung der angegebenen Hilfsmittel, persönlichen Mitteilungen und Quellen angefertigt habe.

München, 6. Januar 2018

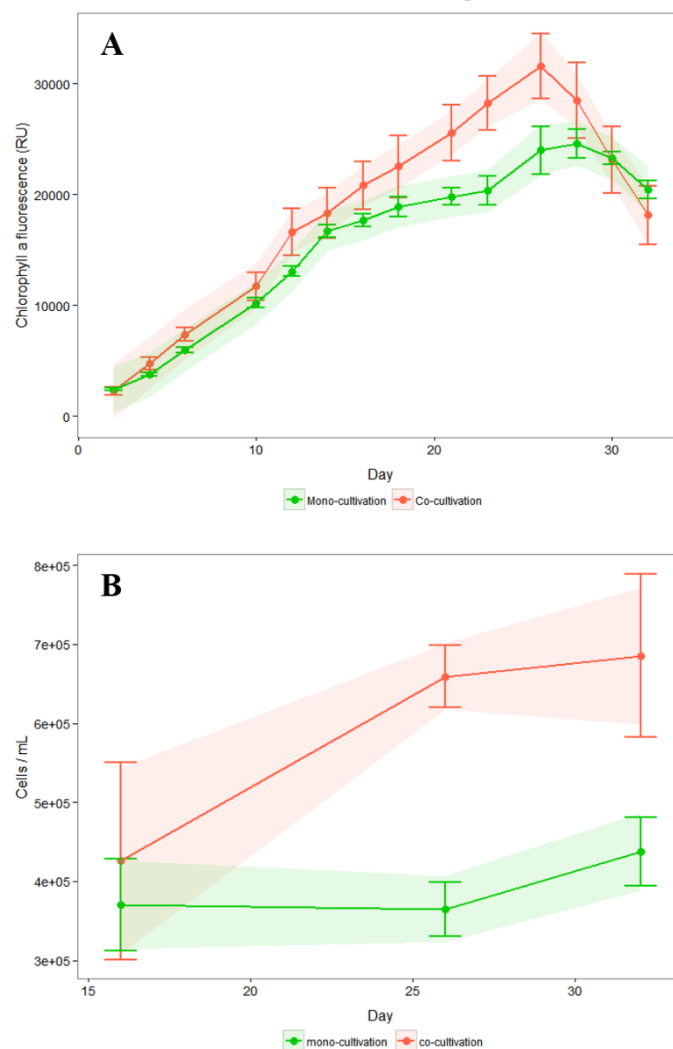
Katharina Christine Eick

7 Digital Appendix

7.1 Appendix: Interaction of *T. weissflogii* with *S. costatum*

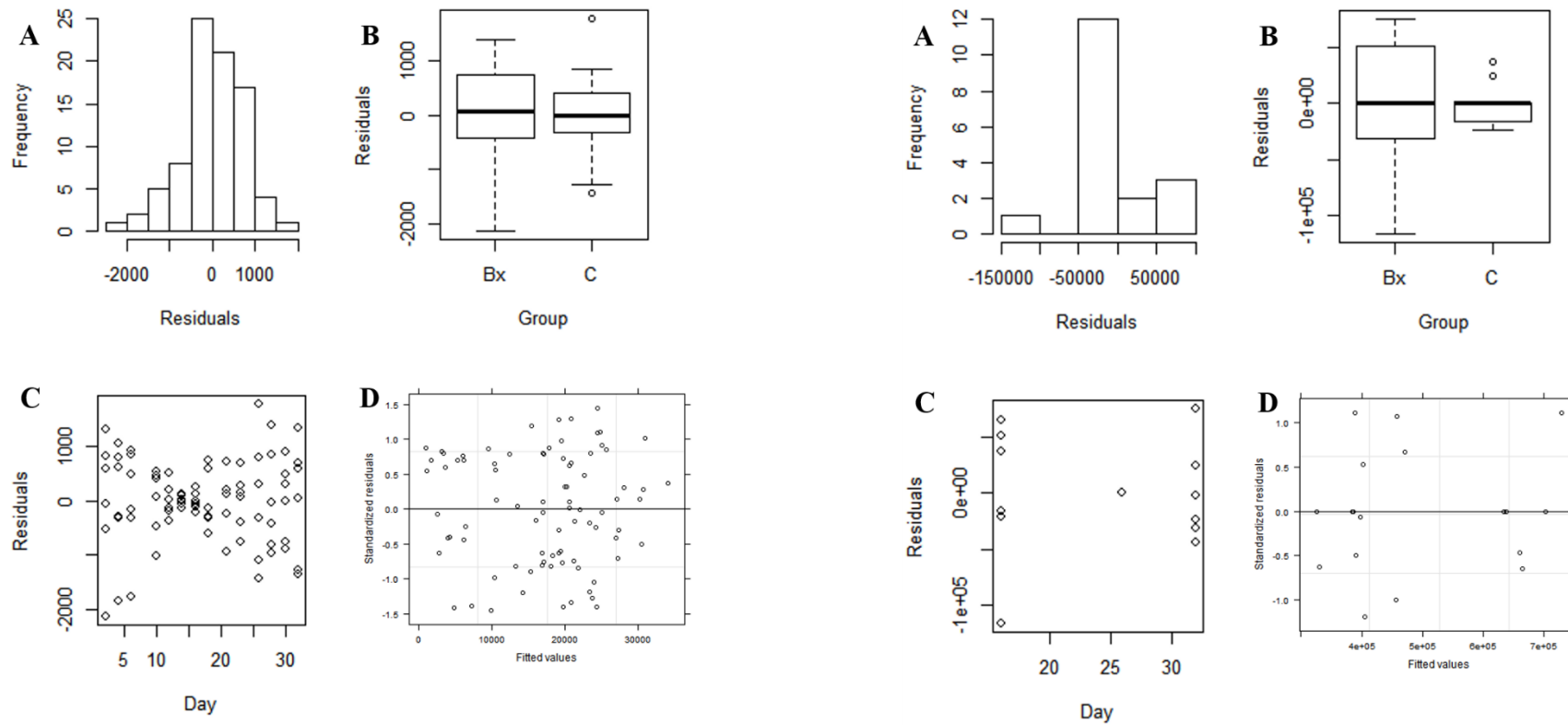
7.1.1 Diatom growth

T. weissflogii



Appendix 1: Linear mixed model of chl a (A, RU: relative units) and cell counts (B, cells / mL) of *T. weissflogii* in interaction with *S. costatum*

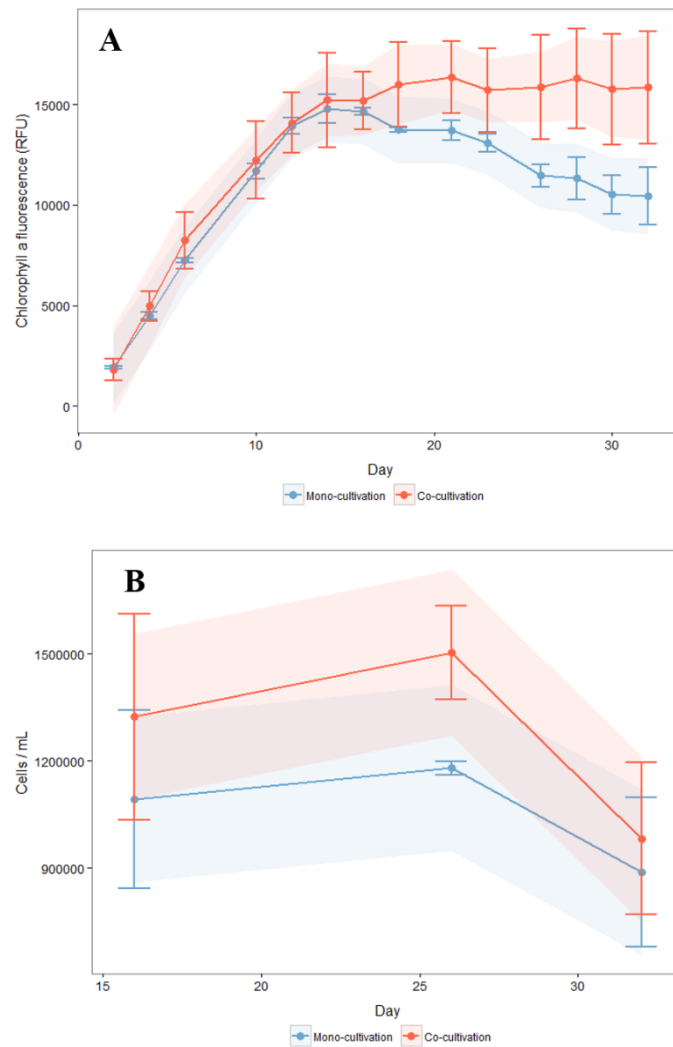
The graph shows the linear mixed model 4. Mean values ($n = 3$) are shown as dot plot, error bars represent the standard deviation. The line chart shows the model fit, with colored areas representing the confidence interval (95%). Mono-cultivation of *T. weissflogii* is depicted in **green**, co-cultivation is shown in **red**.



Appendix 2: Model validation graphs for the linear mixed model of the chl a for *T. weissflogii* in the interaction with *S. costatum*

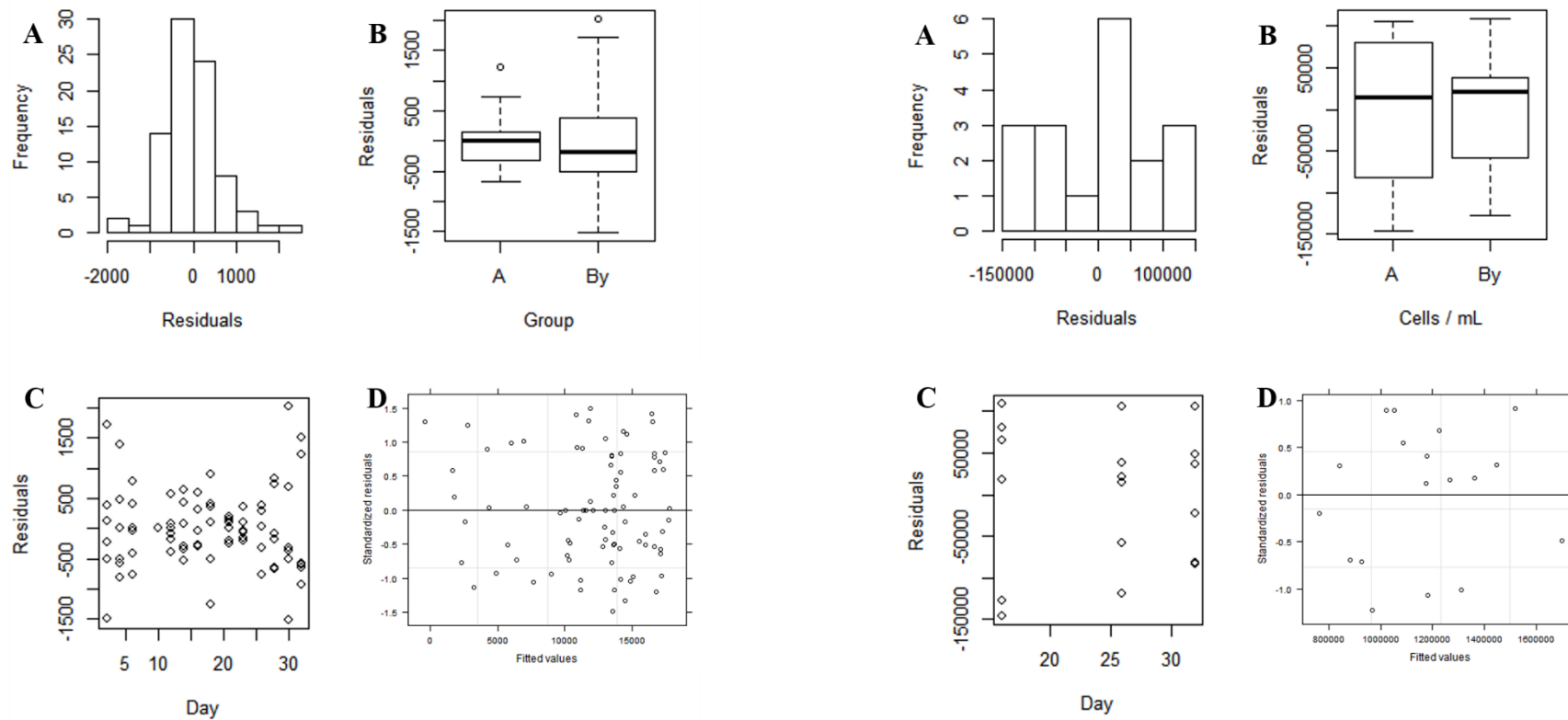
Appendix 3: Model validation graphs for the linear mixed model of the cell counts for *T. weissflogii* in the interaction with *S. costatum*

(A) Histogram of residuals for check of normality, (B) residuals versus group (C: mono-cultivation, Bx: co-cultivation) as explanatory variable, (C) residuals versus day as explanatory variable, (D) standardized residuals versus fitted values of the model to verify homogeneity of variances among residuals.

S. costatum

Appendix 4: Linear mixed model of chl a (**A**, RU: relative units) and cell counts (**B**, cells / mL) of *S. costatum* in interaction with *T. weissflogii*

The graph shows the linear mixed model 4 (chl a) and model 1 (cell counts). Mean values (n = 3) are shown as dot plot, error bars represent the standard deviation. The line chart shows the model fit, with colored areas representing the confidence interval (95%). Mono-cultivation of *S. costatum* is depicted in **blue**, co-cultivation is shown in **red**.

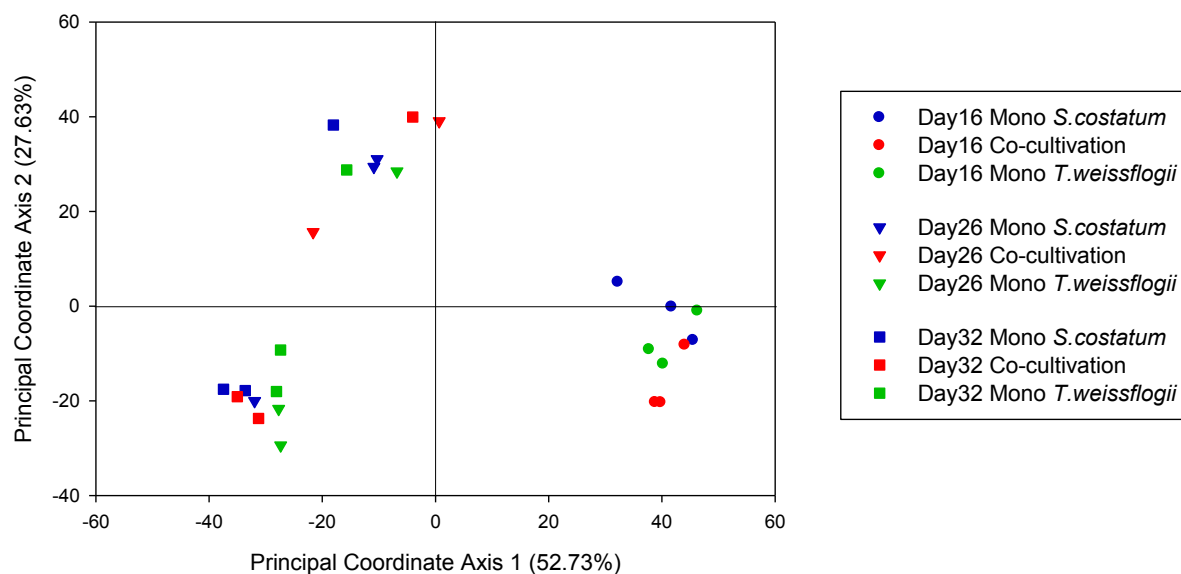


Appendix 5: Model validation graphs for the linear mixed model of the chl a for *S. costatum* in interaction with *T. weissflogii*

Appendix 6: Model validation graphs for the linear mixed model of the cell counts for *S. costatum* in interaction with *T. weissflogii*

(A) Histogram of residuals for check of normality, (B) residuals versus group (A: mono-cultivation, By: co-cultivation) as explanatory variable, (C) residuals versus day as explanatory variable, (D) standardized residuals versus fitted values of the model to verify homogeneity of variances among residuals.

7.1.2 Exometabolomic investigation

Overall analysis via CAP

Appendix 7: PCoA score plot of exometabolomic samples from an overall analysis of the interaction between *T. weissflogii* and *S. costatum*.

The plot is based on metabolites obtained from mono-cultivated *S. costatum* (blue), mono-cultivated *T. weissflogii* (green) and co-cultivation of both diatoms (red) on day 16 (●), day 26 (▼) and day 32 (■).

Appendix 8: Cross validation results (leave-one-out allocation of observations to groups) for the analysis of the exometabolomic data of the interaction between *S. costatum* and *T. weissflogii* with a-priori grouping by day.

	Day16	Day26	Day32	Total	%correct
Day16	9	0	0	9	100
Day26	0	7	1	8	87.5
Day32	0	2	7	9	77.78
Misclassification error: 11.54 %					

Mono SC: mono-cultivated *S. costatum*, **Mono TW:** mono-cultivated *T. weissflogii*, **Co:** co-cultivated diatoms, **Total:** total number of samples, **%correct:** percentage of correctly allocated samples to their respective group. Number of samples correctly allocated to their group are highlighted in green, wrong allocations are highlighted in grey.

Appendix 9: Cross validation results (leave-one-out allocation of observations to groups) for the analysis of the exometabolomic data of the interaction between *S. costatum* and *T. weissflogii* with a-priori grouping by treatment

	Mono SC	Co	Mono TW	Total	%correct
Mono SC	7	2	0	9	77.78
Co	3	3	2	8	37.5
Mono TW	0	4	5	9	55.56
Misclassification error: 42.31 %					

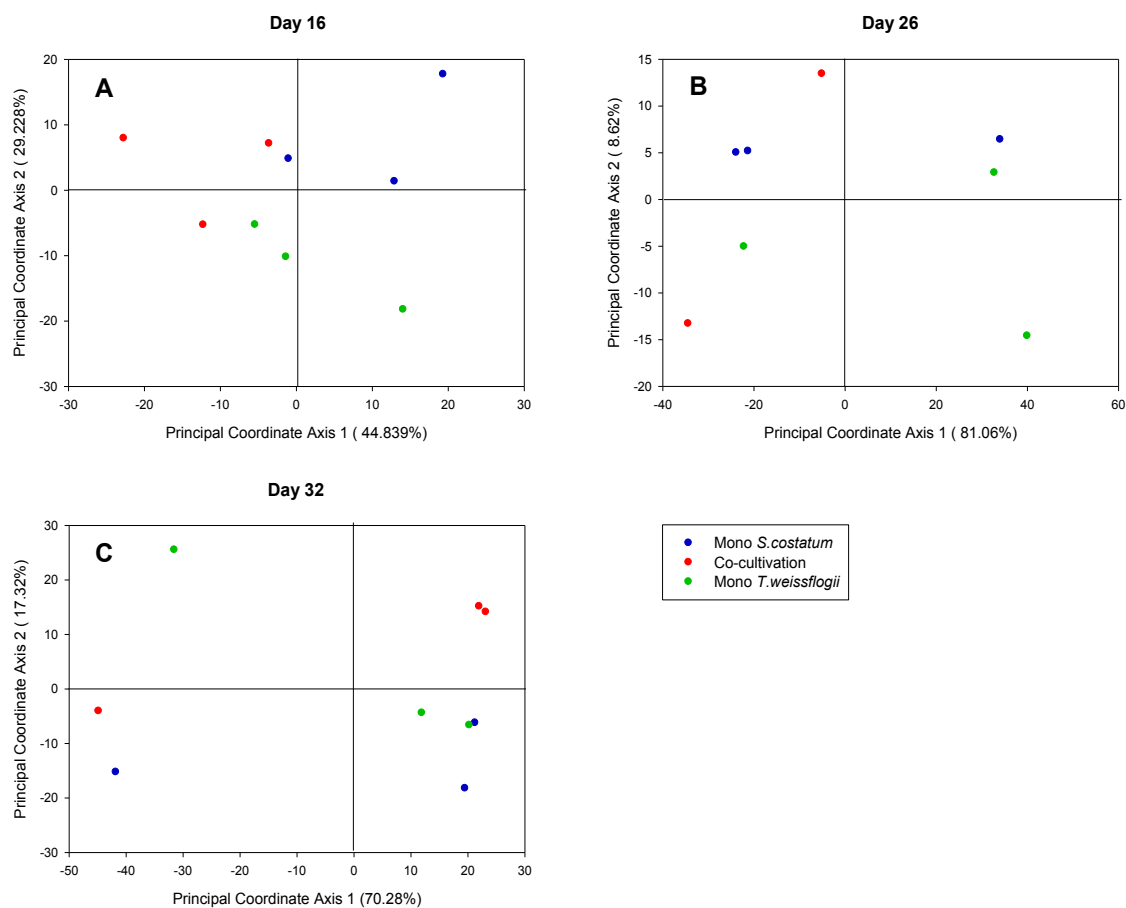
Mono SC: mono-cultivated *S. costatum*, **Mono TW:** mono-cultivated *T. weissflogii*, **Co:** co-cultivated diatoms, **Total:** total number of samples, **%correct:** percentage of correctly allocated samples to their respective group. Number of samples correctly allocated to their group are highlighted in green, wrong allocations are highlighted in grey.

Appendix 10: Cross validation results (leave-one-out allocation of observations to groups) for the analysis of the exometabolomic data of the interaction between *S. costatum* and *T. weissflogii* with a-priori grouping by day and treatment

	Day16			Day26			Day32			Total	%correct
	Mono SC	Co	Mono TW	Mono SC	Co	Mono TW	Mono SC	Co	Mono TW		
Day16 Mono SC	3	0	0	0	0	0	0	0	0	3	100
Day16 Co	1	2	0	0	0	0	0	0	0	3	66.67
Day16 Mono TW	0	0	3	0	0	0	0	0	0	3	100
Day26 Mono SC	0	0	0	2	1	0	0	0	0	3	66.67
Day26 Co	0	0	0	1	1	0	0	0	0	2	50
Day26 Mono TW	0	0	0	0	2	0	0	1	0	3	0
Day32 Mono SC	0	0	0	1	0	0	2	0	0	3	66.67
Day32 Co	0	0	0	0	0	0	1	2	0	3	66.67
Day32 Mono TW	0	0	0	0	0	2	0	1	0	3	0
Misclassification error: 42.31 %											

Mono SC: mono-cultivated *S. costatum*, **Mono TW:** mono-cultivated *T. weissflogii*, **Co:** co-cultivated diatoms, **Total:** total number of samples, **%correct:** percentage of correctly allocated samples to their respective group. Number of samples correctly allocated to their group are highlighted in green, wrong allocations are highlighted in grey.

Daywise analysis via CAP



Appendix 11: PCoA score plot of exometabolomic samples from a daywise subset analysis of the interaction between *T. weissflogii* and *S. costatum* on day 16, 26 and 32.

The plots are based on metabolites obtained from mono-cultivated *S. costatum* (blue), mono-cultivated *T. weissflogii* (green) and co-cultivation of both diatoms (red) on day 16 (graph A), day 26 (graph B) and day 32 (graph C).

Appendix 12: Cross validation results (leave-one-out allocation of observations to groups) for the analysis of the daily subsets of exometabolomic data characterizing the interaction between *S. costatum* and *T. weissflogii* on day 16 with a-priori grouping by treatment.

	Mono SC	Co	Mono TW	Total	%correct
Mono SC	2	1	0	3	66.67
Co	1	2	0	3	66.67
Mono TW	0	1	2	3	66.67
Misclassification error: 33.33 %					

Mono SC: mono-cultivated *S. costatum*, **Mono TW:** mono-cultivated *T. weissflogii*, **Co:** co-cultivated diatoms, **Total:** total number of samples, **%correct:** percentage of correctly allocated samples to their respective group. Number of samples correctly allocated to their group are highlighted in green, wrong allocations are highlighted in grey.

Appendix 13: Cross validation results (leave-one-out allocation of observations to groups) for the analysis of the daily subsets of exometabolomic data characterizing the interaction between *S. costatum* and *T. weissflogii* on day 26 with a-priori grouping by treatment.

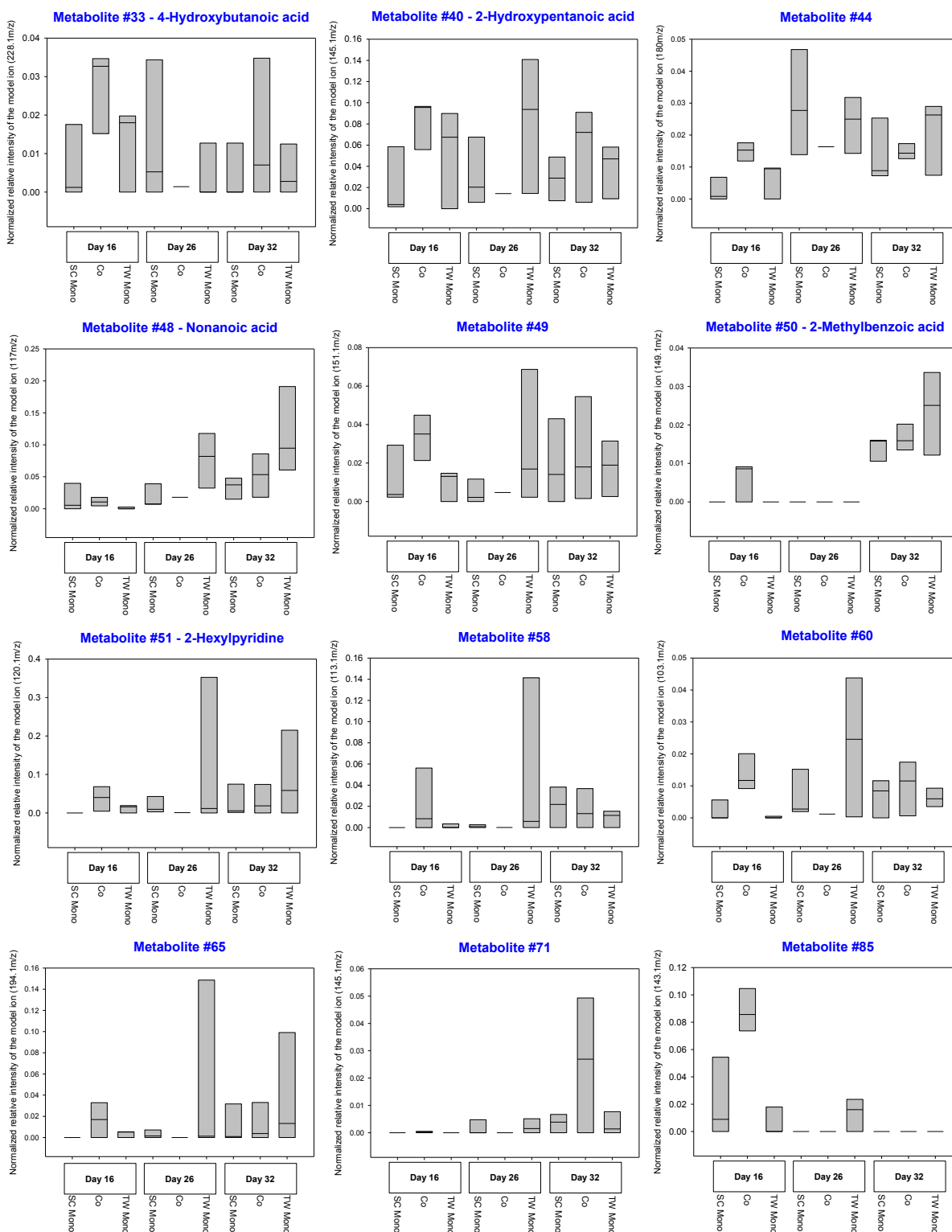
	Mono SC	Co	Mono TW	Total	%correct
Mono SC	3	0	0	3	100
Co	2	0	0	2	0
Mono TW	0	0	3	3	100
Misclassification error: 25 %					

Mono SC: mono-cultivated *S. costatum*, **Mono TW:** mono-cultivated *T. weissflogii*, **Co:** co-cultivated diatoms, **Total:** total number of samples, **%correct:** percentage of correctly allocated samples to their respective group. Number of samples correctly allocated to their group are highlighted in **green**, wrong allocations are highlighted in **grey**.

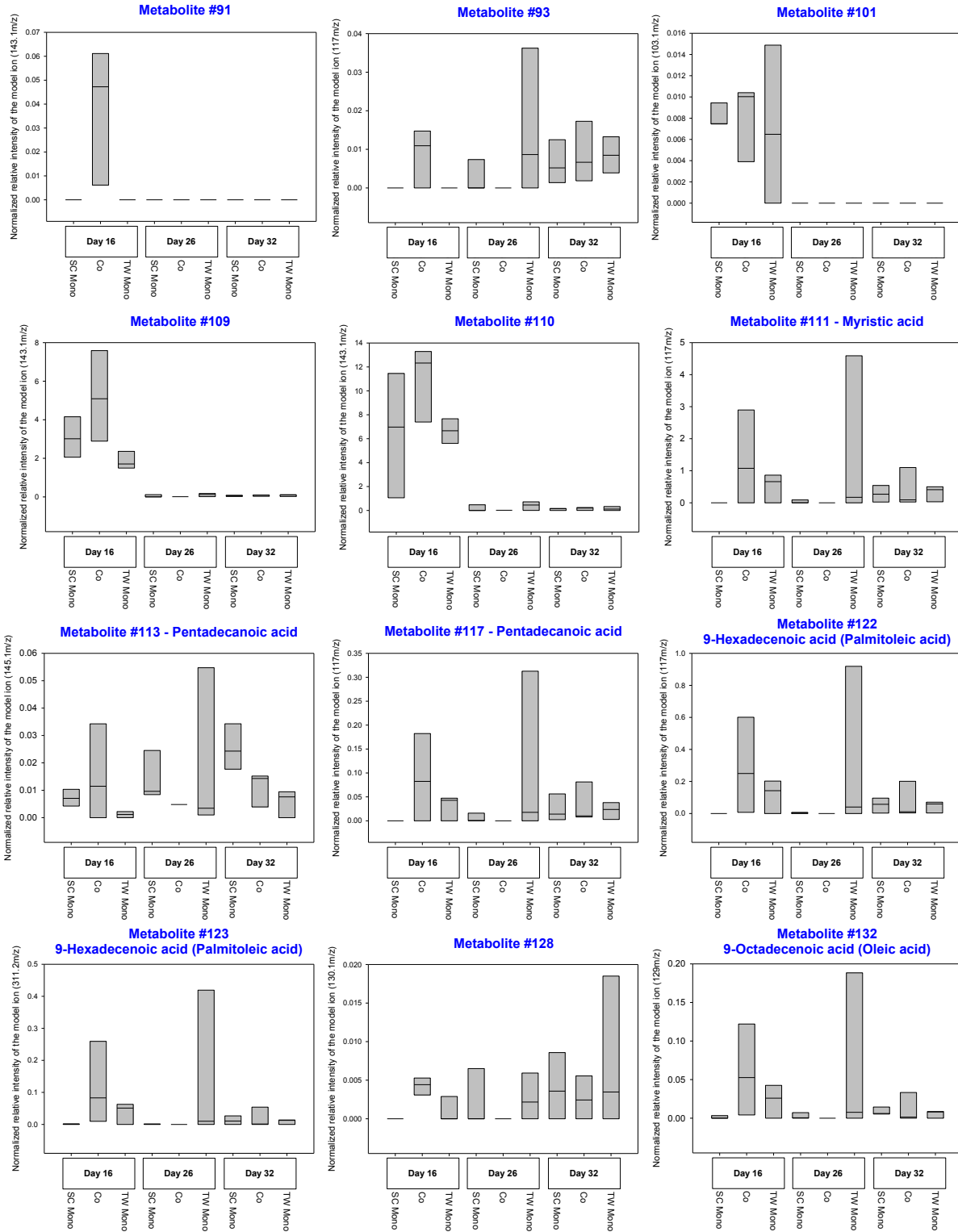
Screening for interaction specific release and/or uptake of potential infochemicals

Appendix 14: Intensity dynamic of exometabolites, enhanced in co-cultivation on day 16 in the interaction between *T. weissflogii* and *S. costatum*.

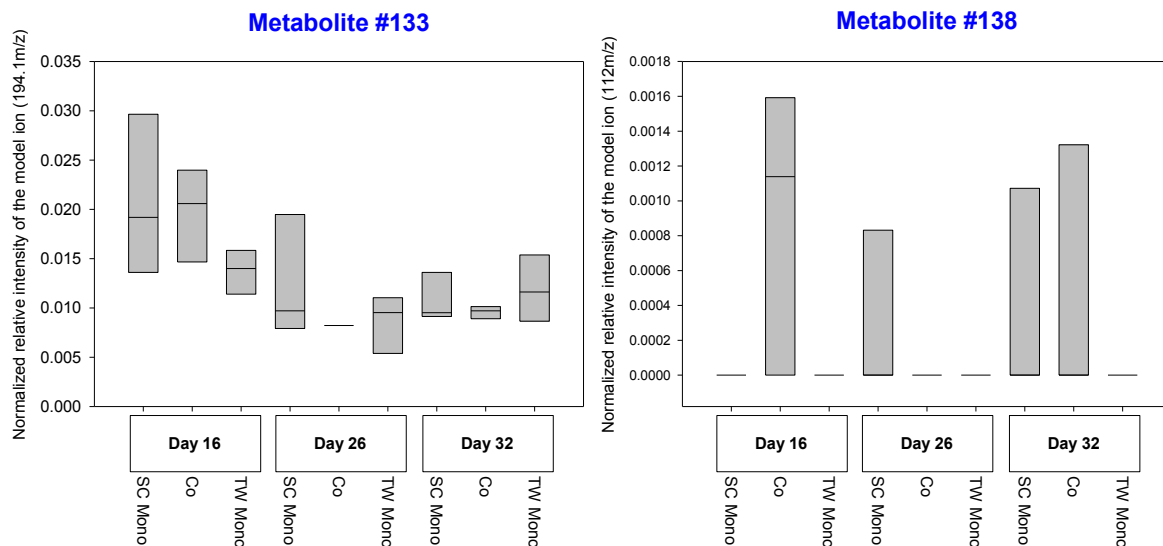
Boxplots visualized intensity dynamics over time and treatments via relative MST intensities (ribitol normalized) of the respective model ion.



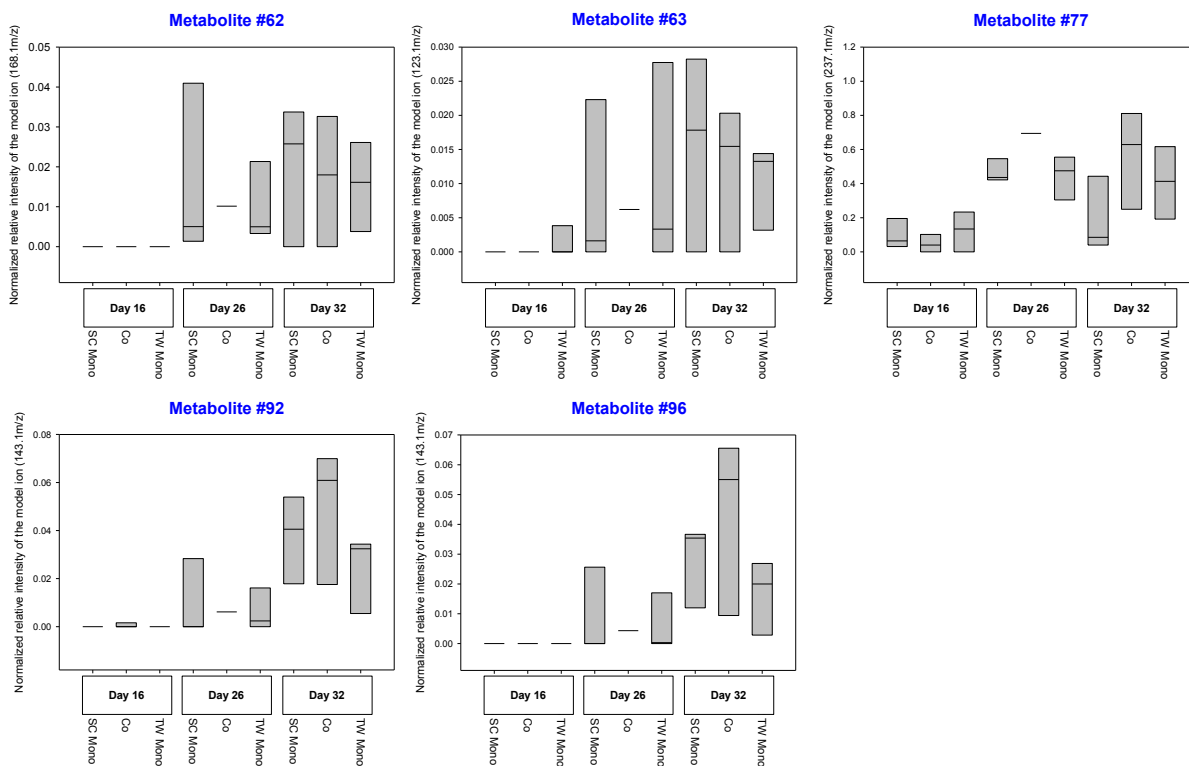
Appendix 14 continued



Appendix 14 continued

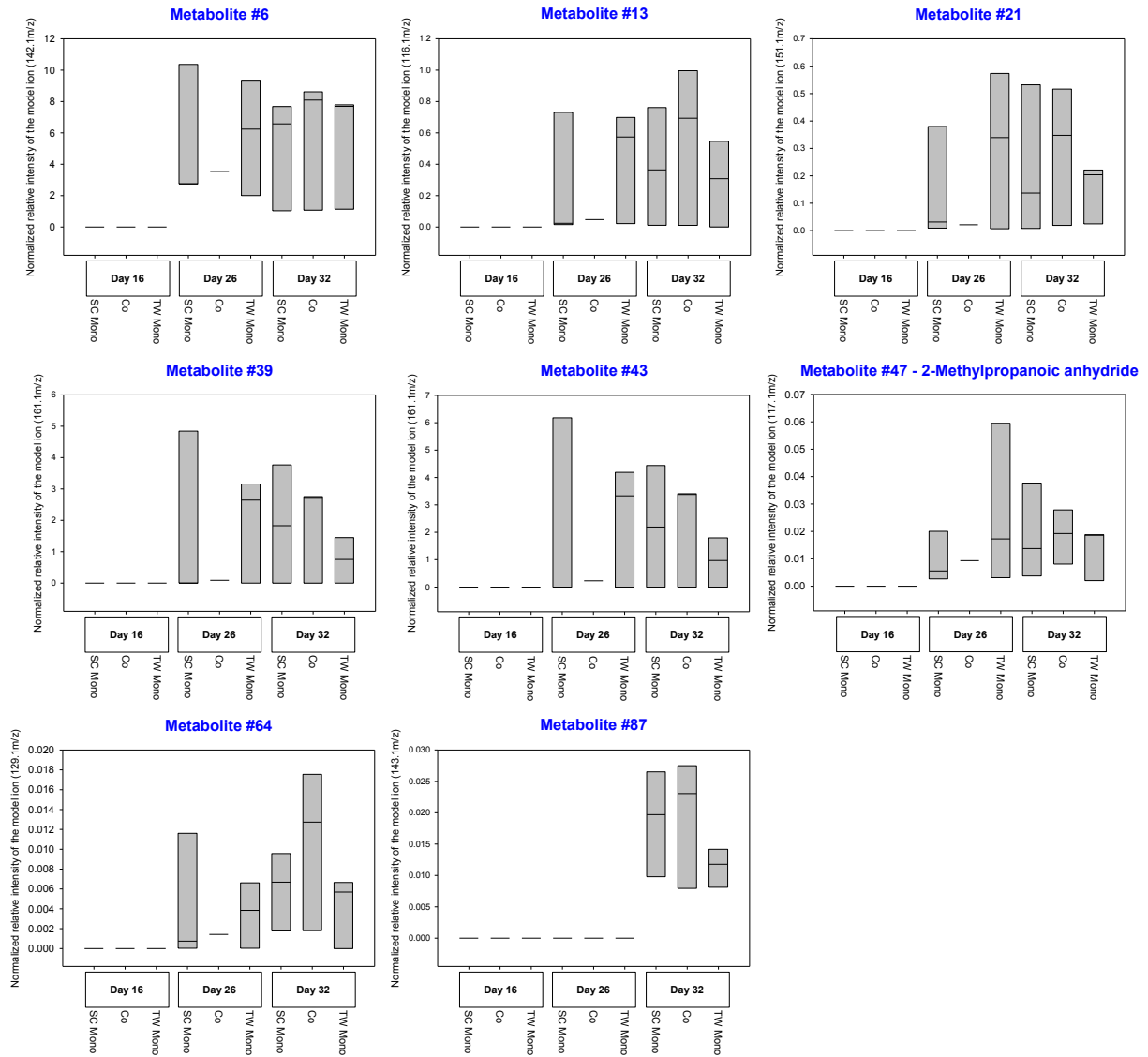


Appendix 15: Intensity dynamic of exometabolites, enhanced in co-cultivation on day 26 in the interaction between *T. weissflogii* and *S. costatum*. Boxplots visualized intensity dynamics over time and treatments via relative MST intensities (ribitol normalized) of the respective model ion.



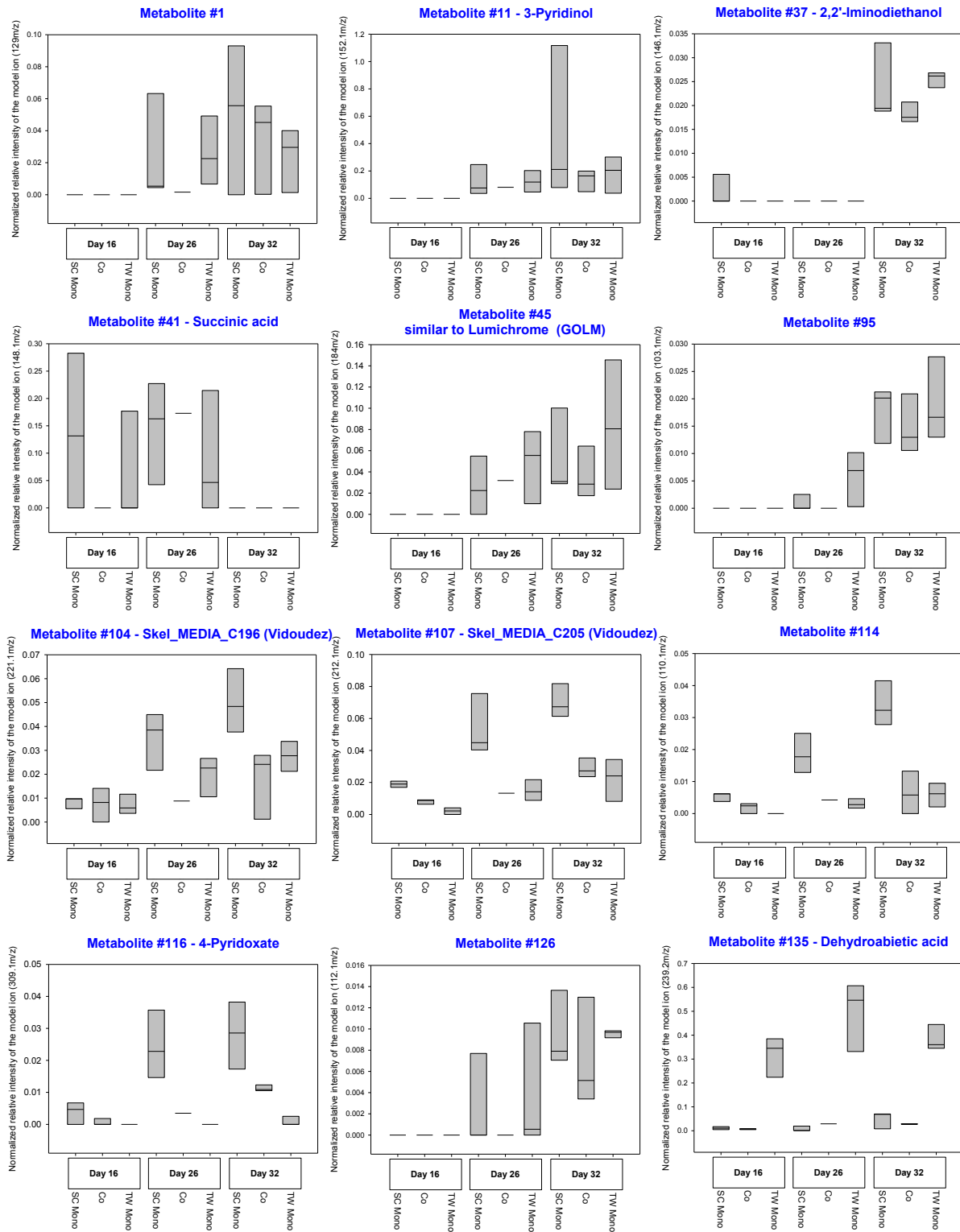
Appendix 16: Intensity dynamic of exometabolites, enhanced in co-cultivation on day 32 in the interaction between *T. weissflogii* and *S. costatum*.

Boxplots visualized intensity dynamics over time and treatments via relative MST intensities (ribitol normalized) of the respective model ion.



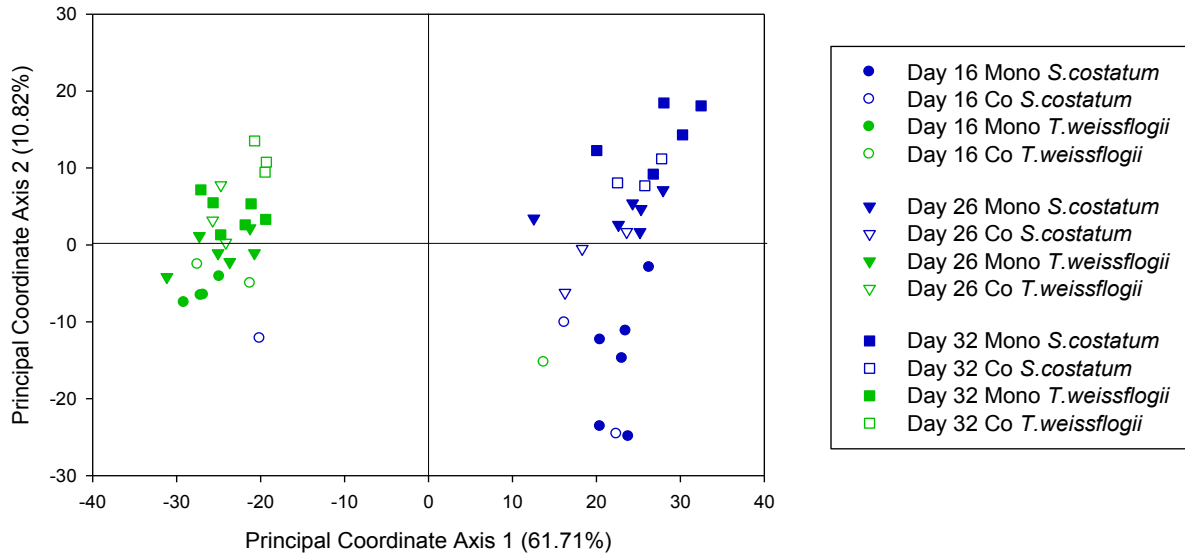
Appendix 17: Intensity dynamic of exometabolites, reduced in co-cultivation in the interaction between *T. weissflogii* and *S. costatum*.

Boxplots visualized intensity dynamics over time and treatments via relative MST intensities (ribitol normalized) of the respective model ion.



7.1.3 Endometabolomic investigation

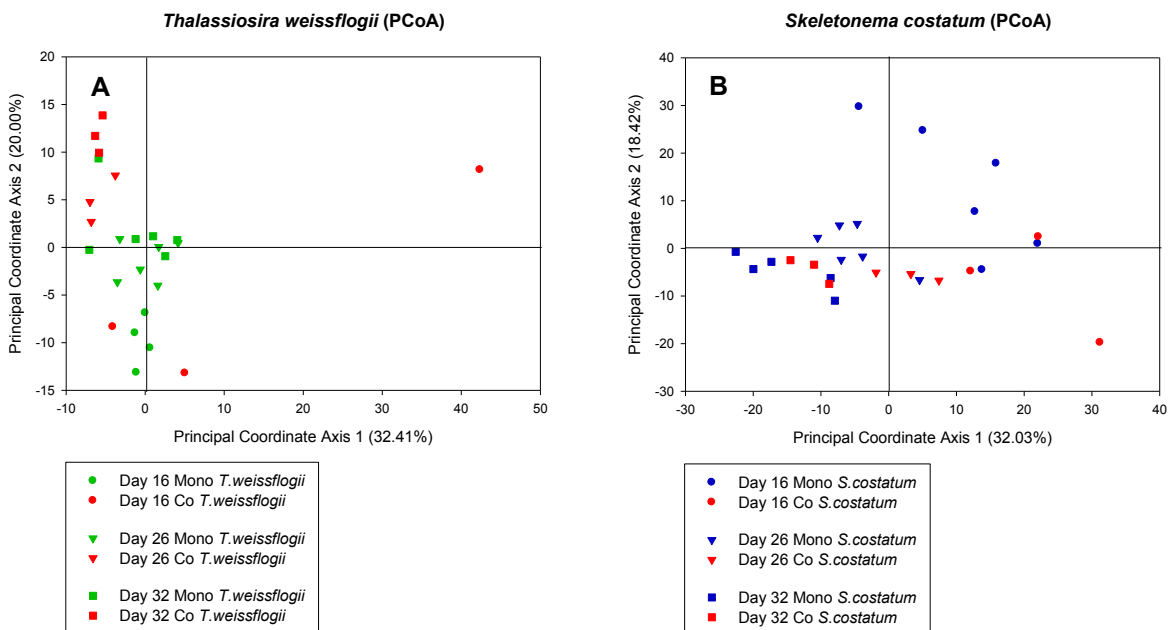
Overall analysis via CAP



Appendix 18: PCoA score plot of endometabolomic samples from an overall analysis of the interaction between *T. weissflogii* and *S. costatum*.

The plot is based on metabolites obtained from *S. costatum* (blue) and *T. weissflogii* (green) on day 16 (●), day 26 (▼) and day 32 (■). Samples from mono-cultivation are represented by filled symbols, samples from co-cultivation by empty symbols.

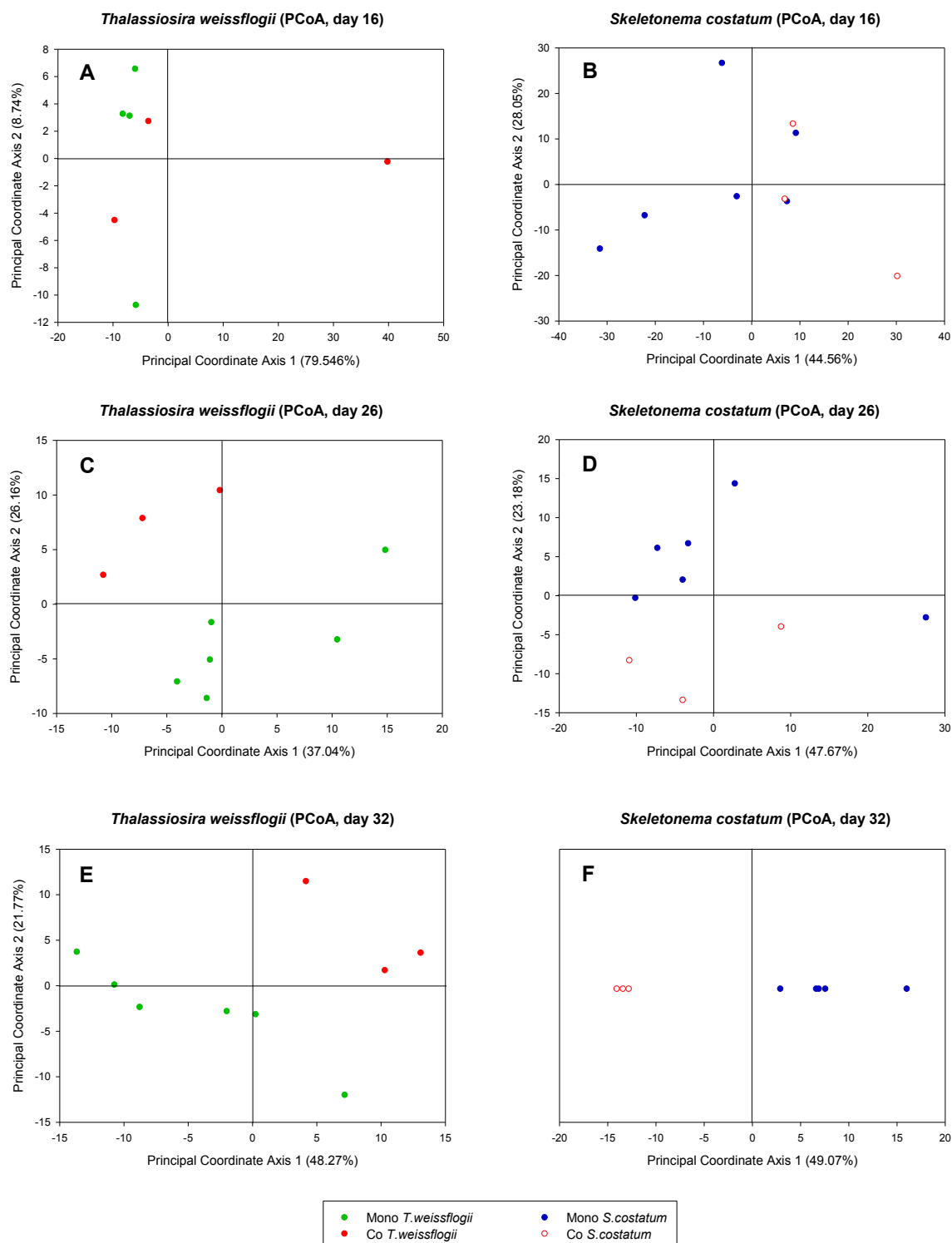
Species-specific analysis via CAP



Appendix 19: PCoA score plot of endometabolomic samples from a species-specific subset analysis of the interaction between *T. weissflogii* and *S. costatum*.

The plots are based on metabolites obtained from mono-cultivated (**green**) and co-cultivated (**red**) *T. weissflogii* (graph **A**) and mono-cultivated (**blue**) and co-cultivated (**red**) *S. costatum* (graph **B**) on day 16 (●), day 26 (▼) and day 32 (■). The analysis was performed for each species individually.

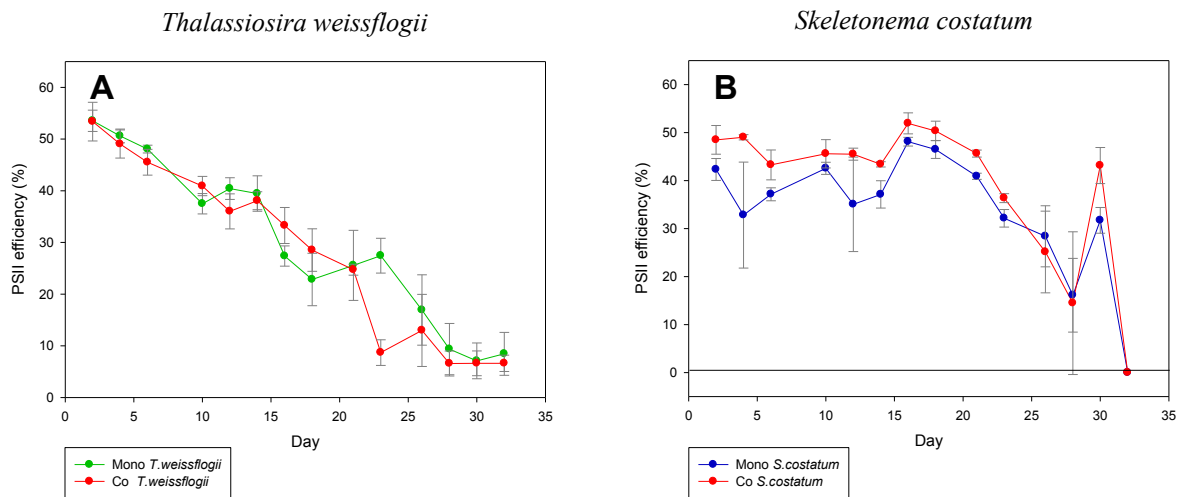
Daywise and species-specific analysis via CAP



Appendix 20: PCoA score plot of endometabolomic samples from a species-specific subset analysis of the interaction between *T. weissflogii* and *S. costatum* on day 16, 26 and 32.

The plots are based on metabolites obtained from mono-cultivated (**green**) and co-cultivated (**red**) *T. weissflogii* (graph **A**, **C**, **E**) and mono-cultivated (**blue**) and co-cultivated (**red**) *S. costatum* (graph **B**, **D**, **F**) on day 16 (●, graph **A**, **B**), day 26 (●, graph **C**, **D**) and day 32 (●, graph **E**, **F**). The analysis was performed for each species and day individually.

7.1.4 Metadata

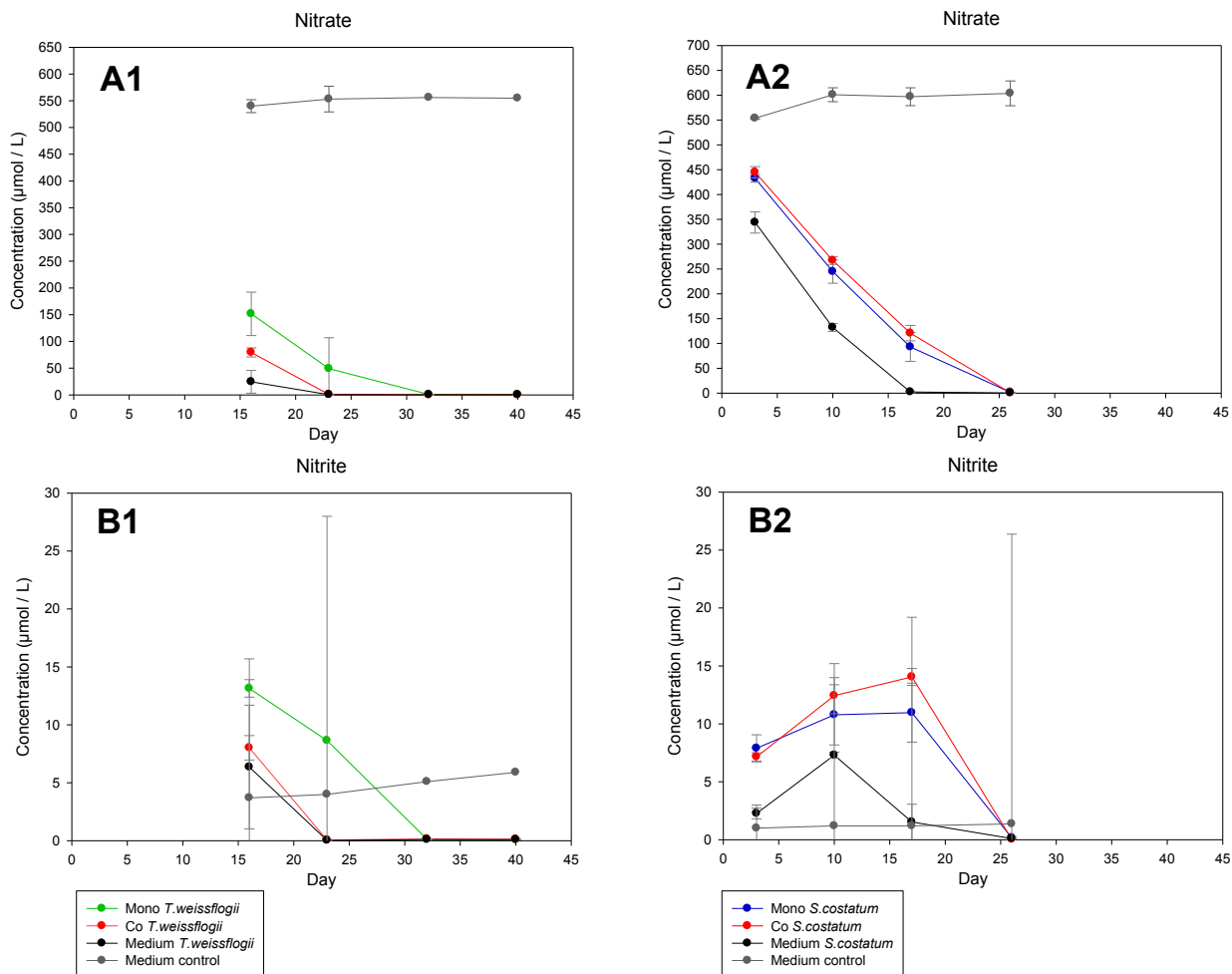
Metadata interaction experiment**Appendix 21:** PSII efficiency of the diatoms in the interaction experiment of *T. weissflogii* with *S. costatum*.

The graph shows means of PSII efficiency (%) of *T. weissflogii* (graph **A**) and *S. costatum* (graph **B**), comparing mono-cultivation in **green** (Mono *T. weissflogii*) and **blue** (Mono *S. costatum*) to co-cultivation of the particular diatom in **red**. Values show as means + SD (n = 3).

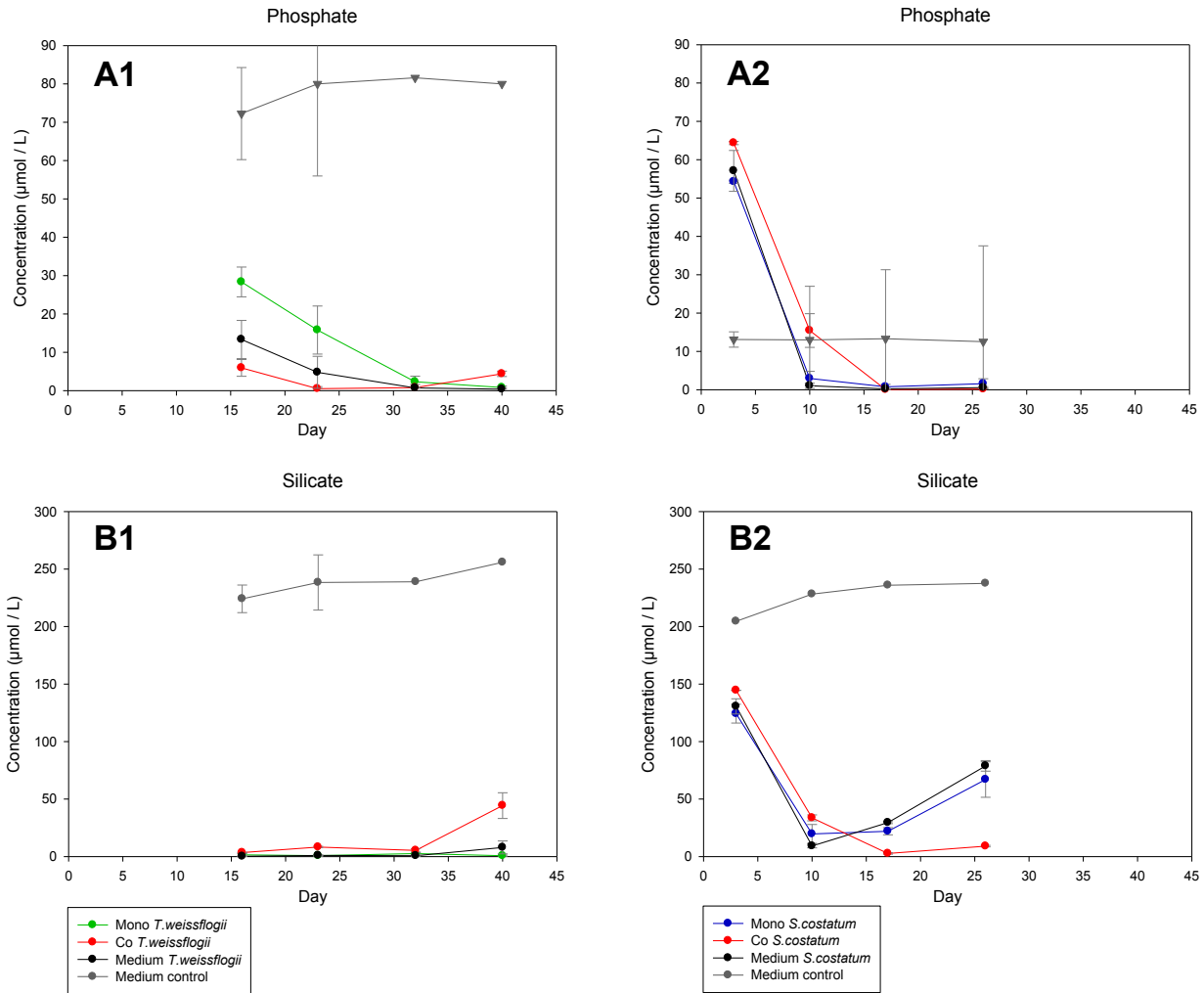
I estimated the physiological state and nutrient status of the cultures via PSII efficiency. All treatment groups in both species started with an average PSII efficiency of $49 \pm 5\%$ on day 2. While the PSII efficiency of both cultivation types in *T. weissflogii* decreased constantly until reaching a value of 7 to 8% on day 32 (**Appendix 21A**), the PSII efficiency of *S. costatum* remained almost stable during the regular growth phase⁸⁹ (with an average value of $43 \pm 6\%$ between day two and 16), before subsequent decrease (**Appendix 21B**).

The different development of PSII efficiency over time seemed to be more prominent between the species, than between the treatments within each species. The species-specific nature of PSII efficiency has been documented (Roy and Legendre, 1979; Kruskopf and Flynn, 2006). No further statistical tests were performed, PSII efficiency was used for general monitoring of the culture states (see discussion in chapter 2.1.2).

⁸⁹ Regular growth until day 12 in *S. costatum* cultures (more details in chapter 2.2.1).

Metadata medium experiment**Appendix 22:** Nitrate and nitrite levels in the medium experiment of *T. weissflogii* with *S. costatum*.

The figure shows means of nitrate (graphs A) and nitrite (graphs B) concentration (µM) in the cultures of *T. weissflogii* (graphs 1) and *S. costatum* (graphs 2) in the context of the medium experiments. Mono-cultivation of *T. weissflogii* is depicted in green (Mono *T. weissflogii*), mono-cultivation of *S. costatum* in blue (Mono *S. costatum*), both representing negative controls. Each species in co-cultivation is colored in red (Co *T. weissflogii* / Co *S. costatum*), representing the positive controls. The medium manipulated groups are depicted in black (Medium *T. weissflogii* / Medium *S. costatum*). Values for the medium control are represented in grey. Error bars indicate standard deviation between biological replicates (n = 3, medium control: n = 1).

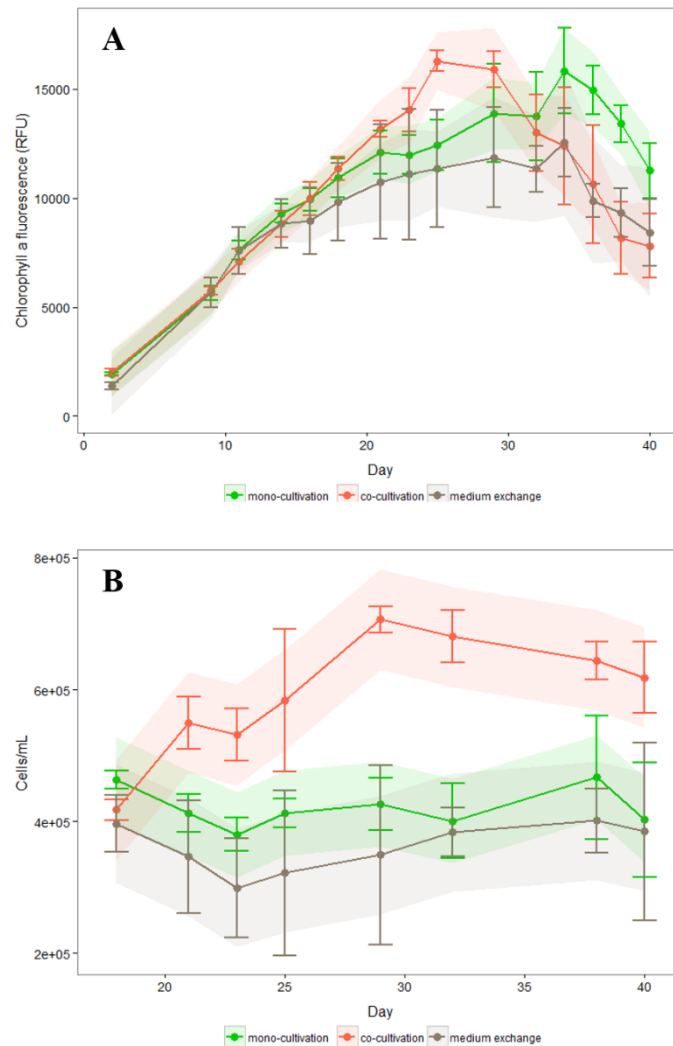


Appendix 23: Phosphate and silicate levels in the medium experiment of *T. weissflogii* with *S. costatum*.

The figure shows means of nitrate (graphs A) and nitrite (graphs B) concentration (μM) in the cultures of *T. weissflogii* (graphs 1) and *S. costatum* (graphs 2) in the context of the medium experiments. Mono-cultivation of *T. weissflogii* is depicted in **green** (Mono *T. weissflogii*), mono-cultivation of *S. costatum* in **blue** (Mono *S. costatum*), both representing negative controls. Each species in co-cultivation is colored in **red** (Co *T. weissflogii* / Co *S. costatum*), representing the positive controls. The medium manipulated groups are depicted in **black** (Medium *T. weissflogii* / Medium *S. costatum*). Values for the medium control are represented in **grey**. Error bars indicate standard deviation between biological replicates ($n = 3$, medium control: $n = 1$).

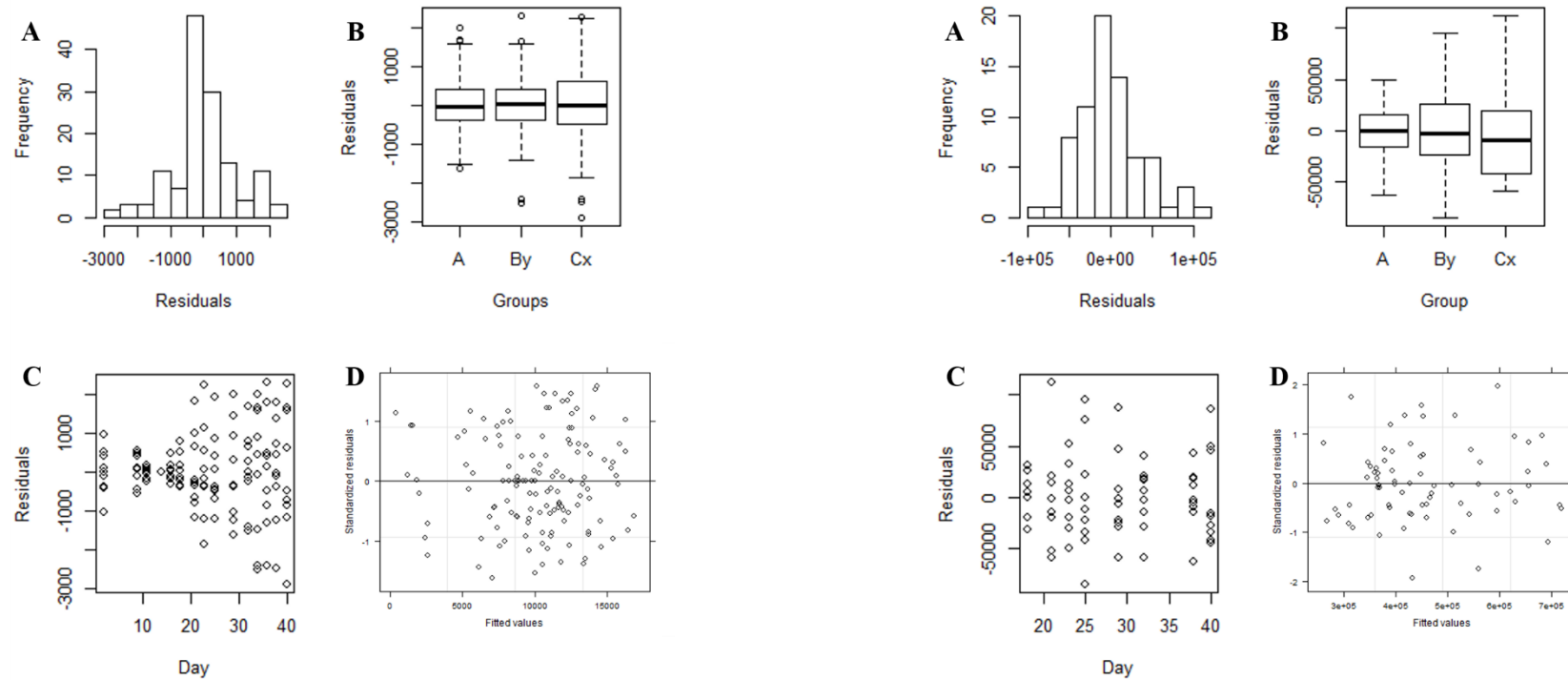
7.1.5 Influence of the initial environment of the interaction partner on diatom growth parameters

T. weissflogii medium experiment



Appendix 24: Linear mixed model of chl a (**A**, RU: relative units) and cell counts (**B**, cells / mL) of *T. weissflogii* in the medium experiment.

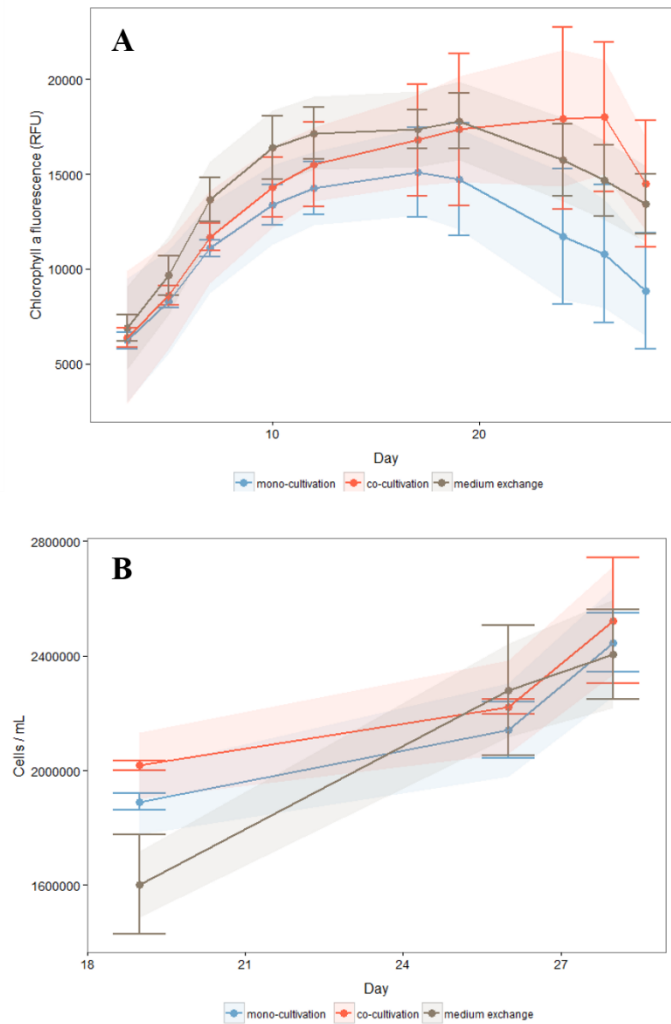
The graph shows the linear mixed model 4 for chl a fluorescence and model 3 for cell counts. Mean values ($n = 3$) are shown as dot plot, error bars represent the standard deviation. The line chart shows the model fit, with colored areas representing the confidence interval (95%). Mono-cultivation of *T. weissflogii* is depicted in **green**, co-cultivation is shown in **red** and the medium group is represented in **black**.



Appendix 25: Model validation graphs for the linear mixed model of the chl a for *T. weissflogii* in the medium experiment

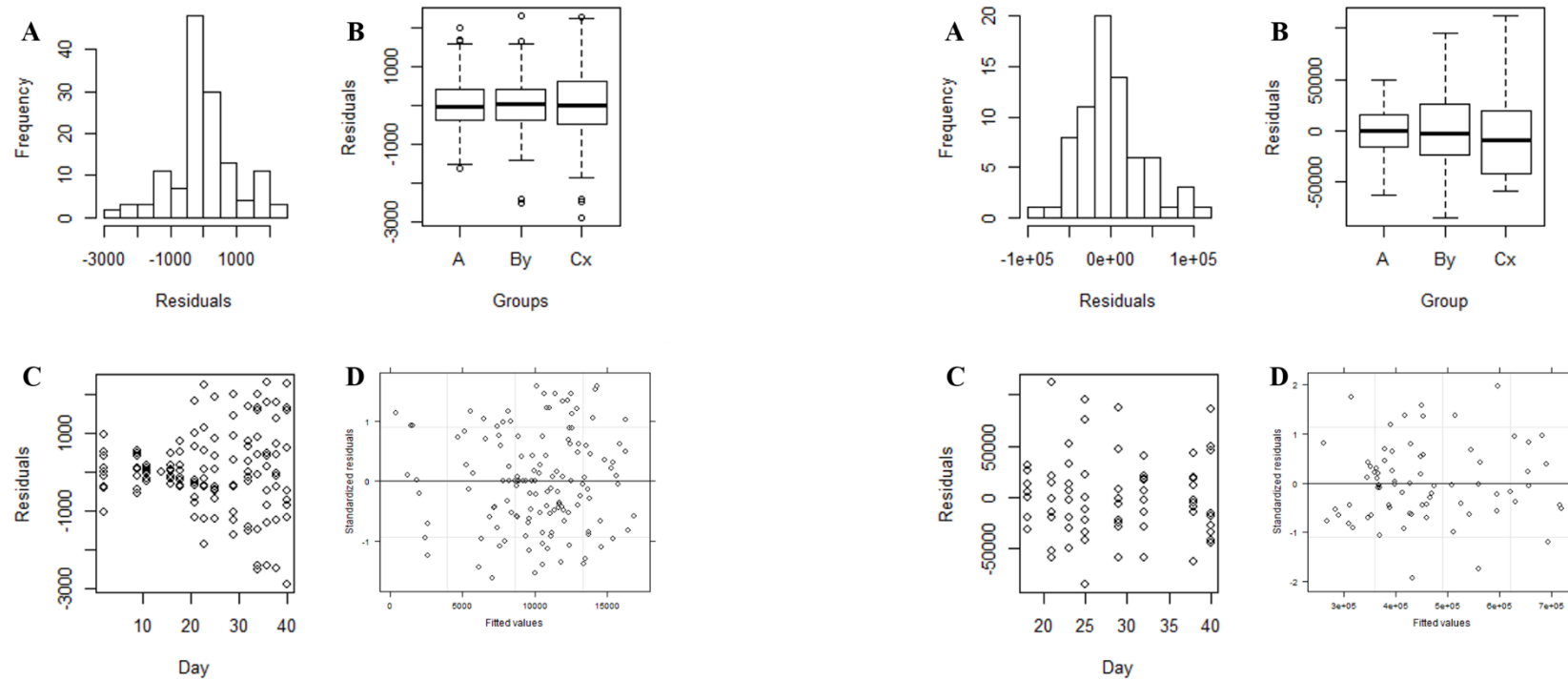
Appendix 26: Model validation graphs for the linear mixed model of the cell counts for *T. weissflogii* in the medium experiment

(A) Histogram of residuals for check of normality, (B) residuals versus group (A: mono-cultivation, By: co-cultivation, Cx: medium group) as explanatory variable, (C) residuals versus day as explanatory variable, (D) standardized residuals versus fitted values of the model to verify homogeneity of variances among residuals.

S. costatum medium experiment

Appendix 27: Linear mixed model of chl a (**A**, RU: relative units) and cell counts (**B**, cells / mL) of *S. costatum* in the medium experiment.

The graph shows the linear mixed model 4 (chl a) and model 2 (cell counts). Mean values ($n = 3$) are shown as dot plot, error bars represent the standard deviation. The line chart shows the model fit, with colored areas representing the confidence interval (95%). Mono-cultivation of *S. costatum* is depicted in **blue**, co-cultivation is shown in **red** and the medium group is represented in **black**.



Appendix 28: Model validation graphs for the linear mixed model of the chl a for *S. costatum* in the medium experiment

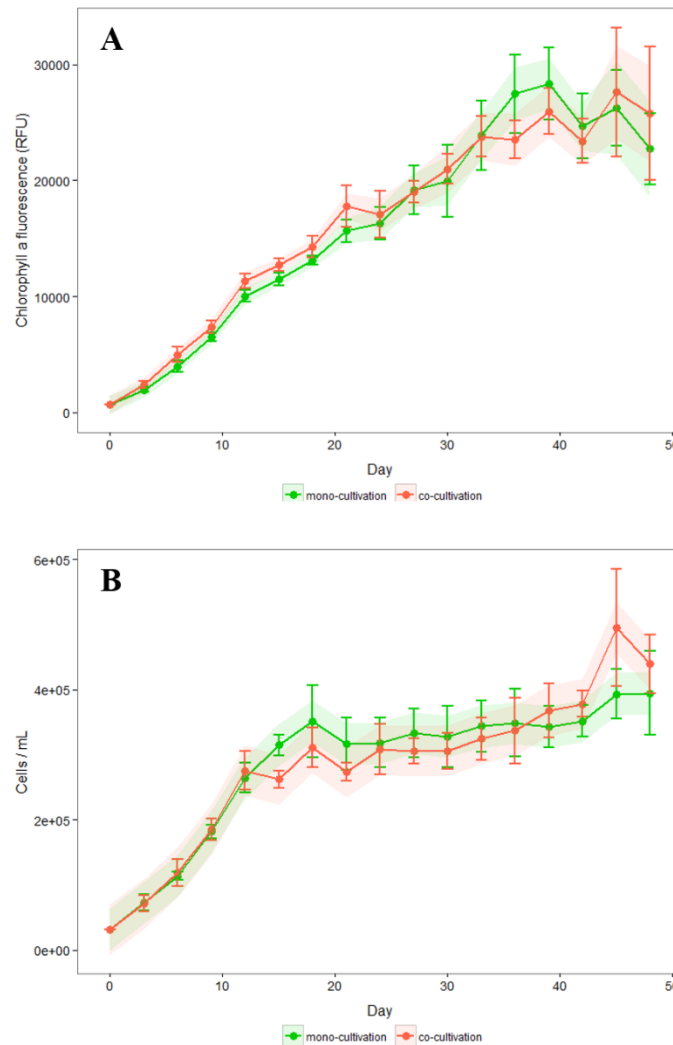
Appendix 29: Model validation graphs for the linear mixed model of the cell counts for *S. costatum* in the medium experiment

(A) Histogram of residuals for check of normality, (B) residuals versus group (A: mono-cultivation, By: co-cultivation, Cx: medium group) as explanatory variable, (C) residuals versus day as explanatory variable, (D) standardized residuals versus fitted values of the model to verify homogeneity of variances among residuals.

7.2 Appendix: Interaction of *T. weissflogii* with *S. marinoi*

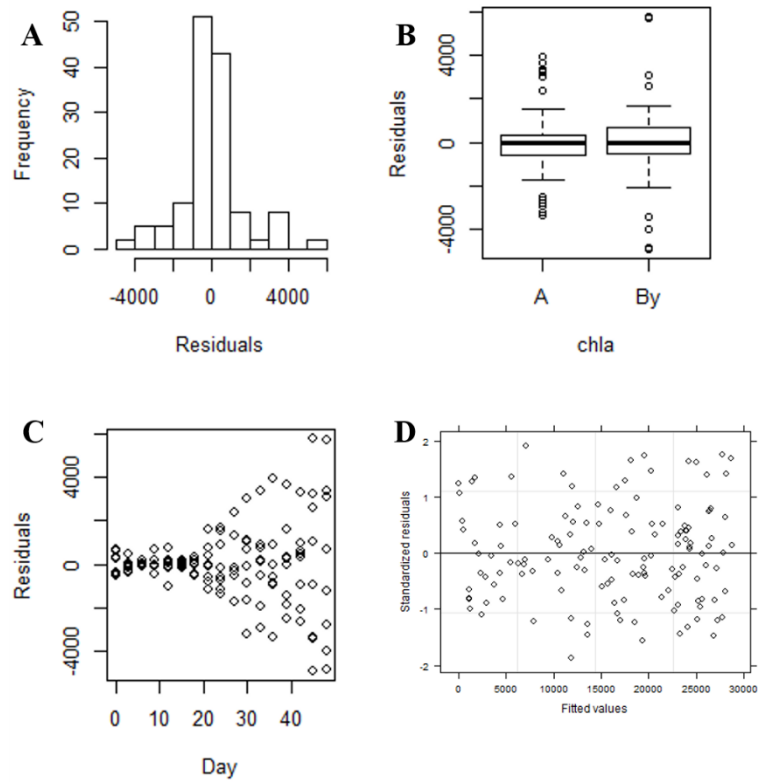
7.2.1 Diatom growth

T. weissflogii

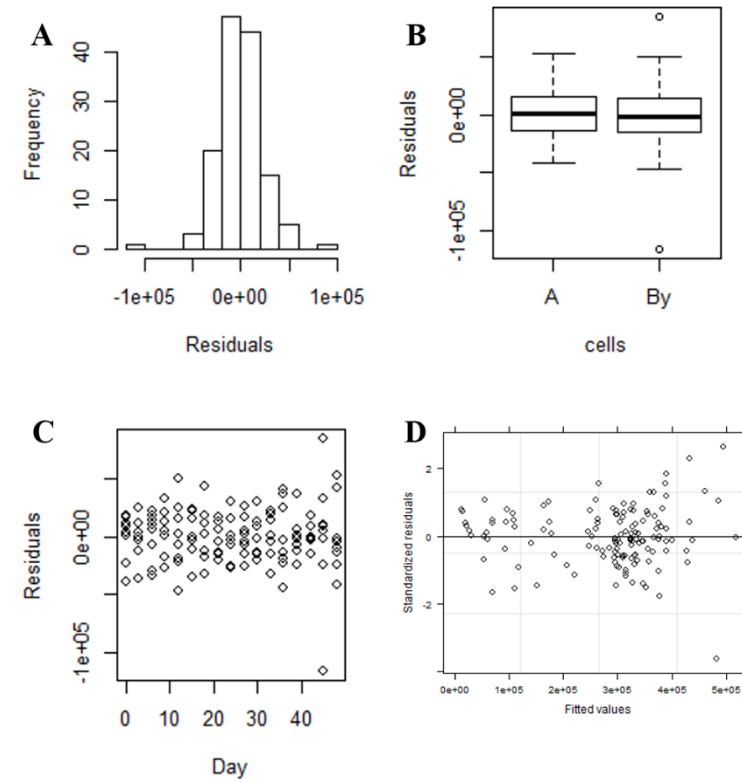


Appendix 30: Linear mixed model of chl a (**A**, RFU: relative fluorescence units) and cell counts (**B**, cells / mL) of *T. weissflogii* in interaction with *S. marinoi*.

The graph shows the linear mixed model 2 (chl a) and 3 (cell counts). Mean values (n = 4) are shown as dot plot, error bars represent the standard deviation. The line chart shows the model fit, with colored areas representing the confidence interval (95%). Mono-cultivation of *T. weissflogii* is depicted in **green**, co-cultivation is shown in **red**.

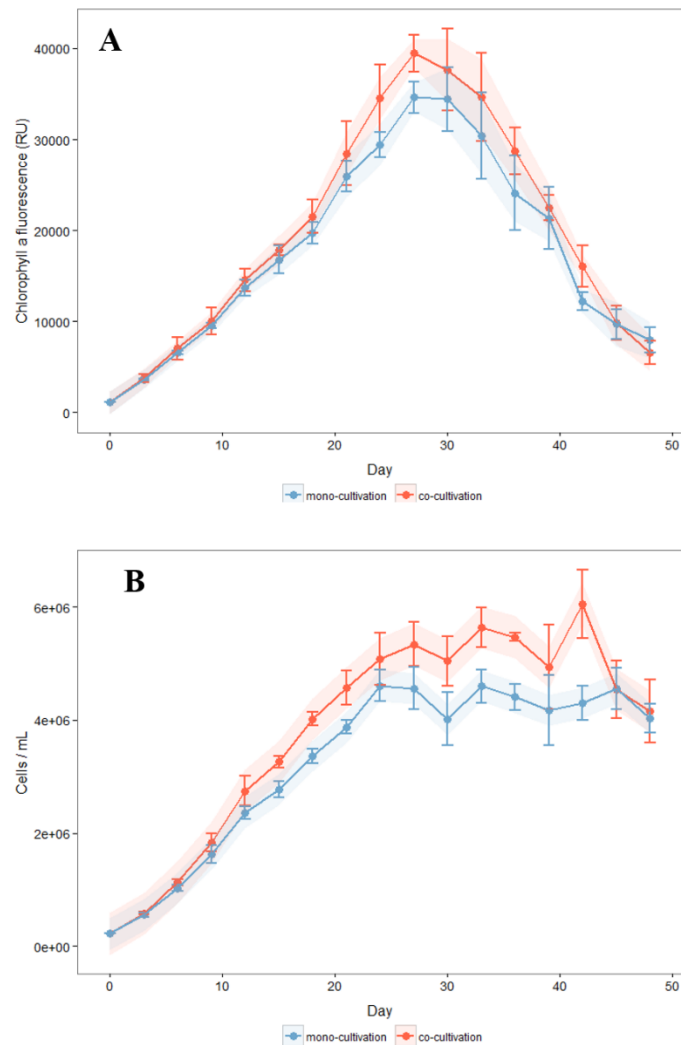


Appendix 31: Model validation graphs for the linear mixed model of the chl a for *T. weissflogii* in interaction with *S. marinoi*.



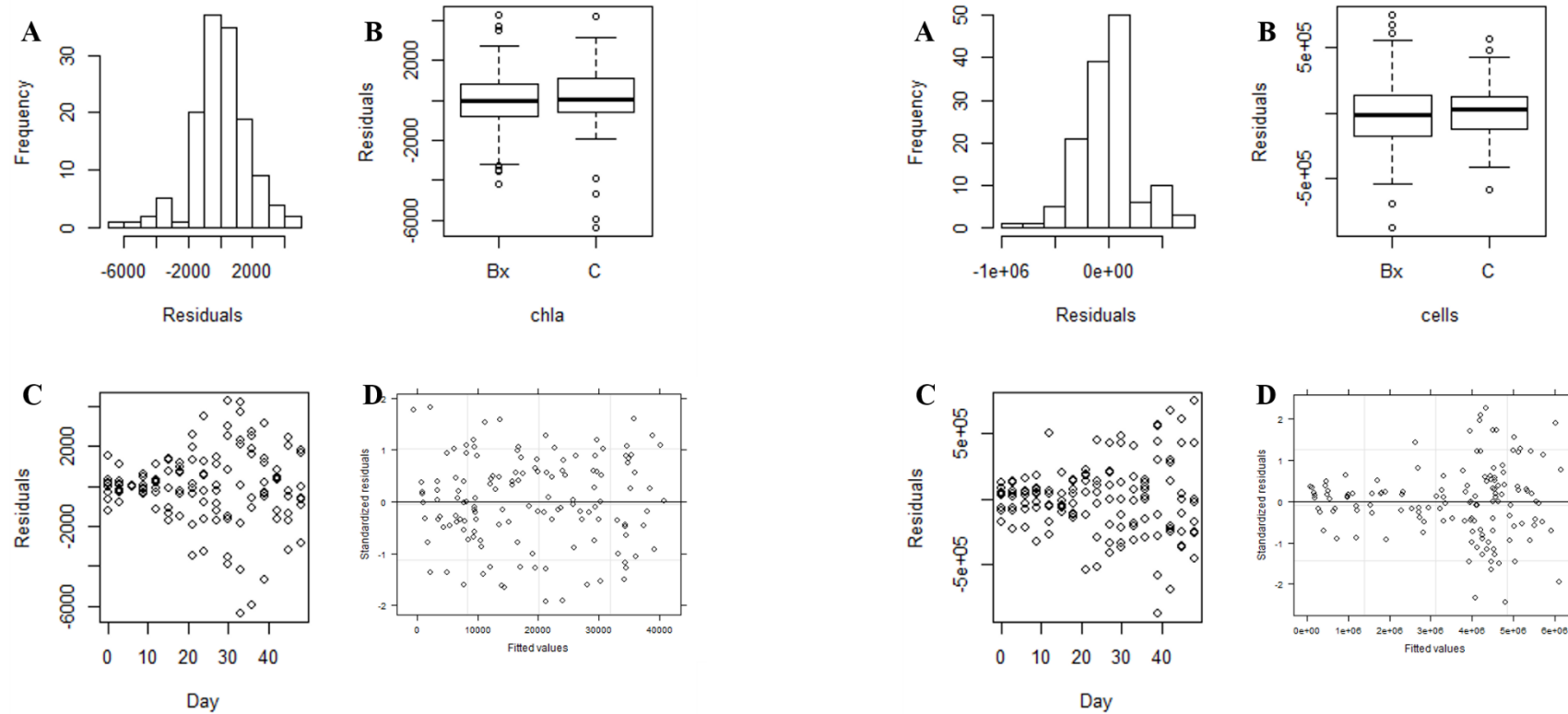
Appendix 32: Model validation graphs for the linear mixed model of the cell counts for *T. weissflogii* in interaction with *S. marinoi*.

(A) Histogram of residuals for check of normality, (B) residuals versus group (A: mono-cultivation, By: co-cultivation) as explanatory variable, (C) residuals versus day as explanatory variable, (D) standardized residuals versus fitted values of the model to verify homogeneity of variances among residuals.

S. marinoi

Appendix 33: Linear mixed model of chl a (**A**, RU: relative units) and cell counts (**B**, cells / mL) of *S. marinoi* in interaction with *T. weissflogii*.

The graph shows the linear mixed model 2 (chl a) and 3 (cell counts). Mean values ($n = 4$) are shown as dot plot, error bars represent the standard deviation. The line chart shows the model fit, with colored areas representing the confidence interval (95%). Mono-cultivation of *S. marinoi* is depicted in **blue**, co-cultivation is shown in **red**.



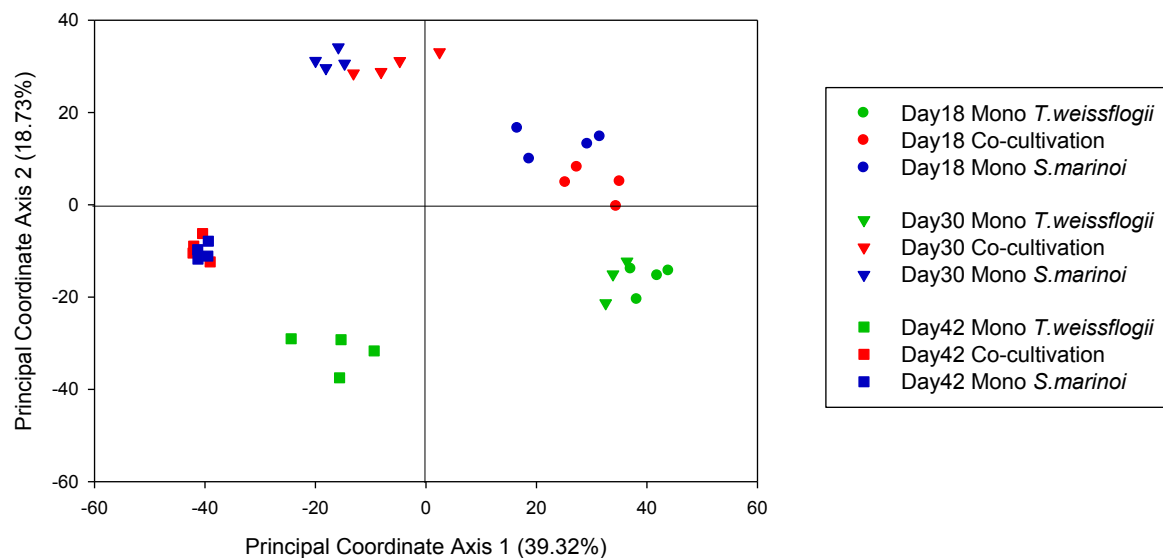
Appendix 34: Model validation graphs for the linear mixed model of the chl a for *S. marinoi* in interaction with *T. weissflogii*.

Appendix 35: Model validation graphs for the linear mixed model of the cell counts for *S. marinoi* in interaction with *T. weissflogii*.

(A) Histogram of residuals for check of normality, (B) residuals versus group (C: mono-cultivation, Bx: co-cultivation) as explanatory variable, (C) residuals versus day as explanatory variable, (D) standardized residuals versus fitted values of the model to verify homogeneity of variances among residuals.

7.2.2 Exometabolomic investigation

Overall analysis via CAP



Appendix 36: PCoA score plot of exometabolomic samples from an overall analysis of the interaction between *T. weissflogii* and *S. marinoi*.

The plot is based on metabolites obtained from mono-cultivated *S. marinoi* (blue), mono-cultivated *T. weissflogii* (green) and co-cultivation of both diatoms (red) on day 18 (●), day 30 (▼) and day 42 (■).

Appendix 37: Cross validation results (leave-one-out allocation of observations to groups) for the analysis of the exometabolomic data of the interaction between *S. marinoi* and *T. weissflogii* with a-priori grouping by treatment

	Mono TW	Co	Mono SM	Total	%correct
Mono TW	10	1	0	11	90.909
Co	0	8	4	12	66.667
Mono SM	0	6	5	11	45.455
Misclassification error: 34.29 %					

Mono SM: mono-cultivated *S. marinoi*, **Mono TW:** mono-cultivated *T. weissflogii*, **Co:** co-cultivated diatoms, **Total:** total number of samples, **%correct:** percentage of correctly allocated samples to their respective group. Number of samples correctly allocated to their group are highlighted in green, wrong allocations are highlighted in grey.

Appendix 38: Cross validation results (leave-one-out allocation of observations to groups) for the analysis of the exometabolomic data of the interaction between *S. marinoi* and *T. weissflogii* with a-priori grouping by day and treatment

		Day18			Day30			Day42			Total	%correct
		Mono TW	Co	Mono SM	Mono TW	Co	Mono SM	Mono TW	Co	Mono SM		
Day18	Mono TW	4	0	0	0	0	0	0	0	0	4	100
	Co	0	4	0	0	0	0	0	0	0	4	100
	Mono SM	0	2	1	0	1	0	0	0	0	4	25
Day30	Mono TW	0	0	0	3	0	0	0	0	0	3	100
	Co	0	0	0	0	4	0	0	0	0	4	100
	Mono SM	0	0	0	0	0	4	0	0	0	4	100
Day42	Mono TW	0	0	0	0	0	0	4	0	0	4	100
	Co	0	0	0	0	0	0	0	4	0	4	100
	Mono SM	0	0	0	0	0	0	0	0	4	4	100
Misclassification error: 8.57 %												

Mono SM: mono-cultivated *S. marinoi*, **Mono TW:** mono-cultivated *T. weissflogii*, **Co:** co-cultivated diatoms, **Total:** total number of samples, **%correct:** percentage of correctly allocated samples to their respective group. Number of samples correctly allocated to their group are highlighted in **green**, wrong allocations are highlighted in **grey**.

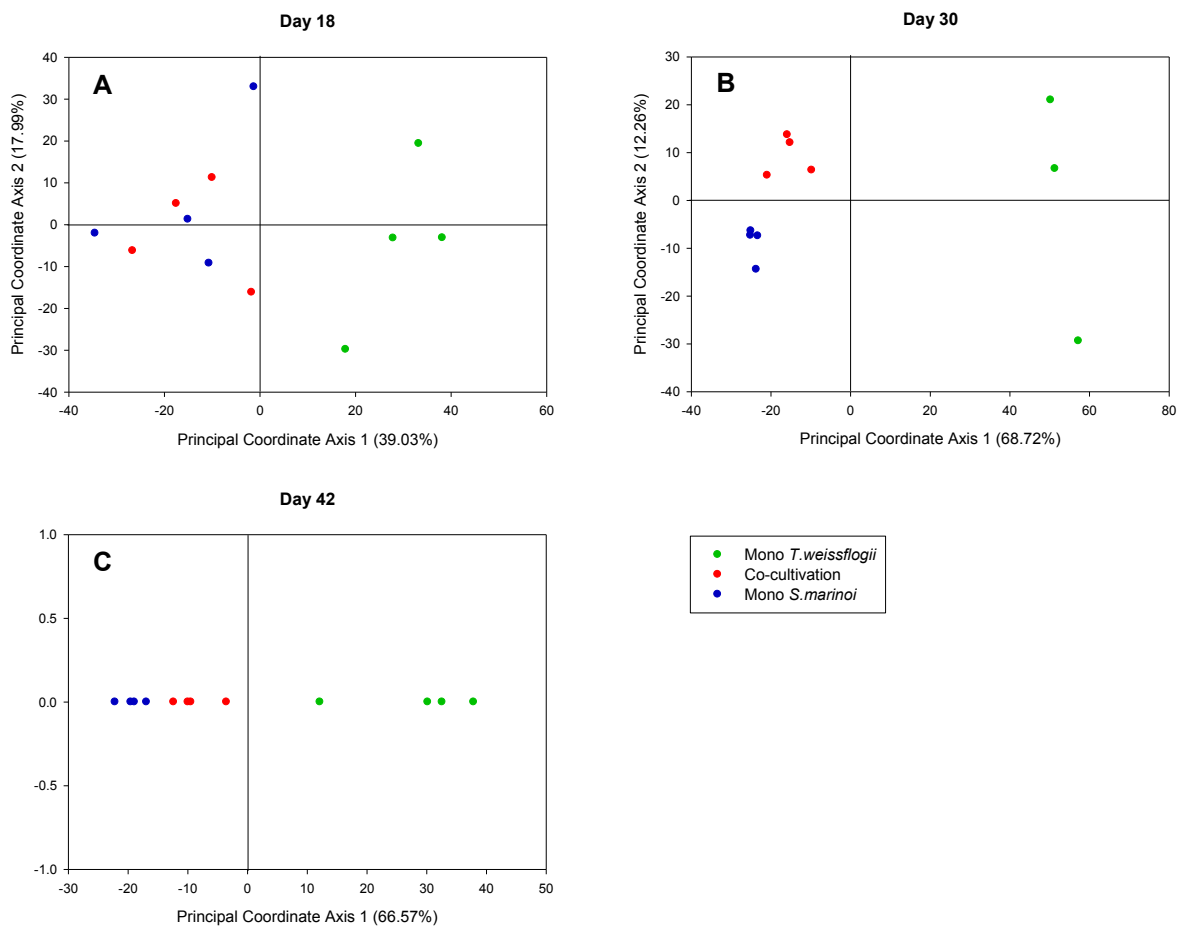
Appendix 39: Heatmap (part II) of exometabolite intensities for the overall analysis of the interaction between *T. weissflogii* and *S. marinoi*. Medians of MST intensities, normalized to the external standard ribitol (per sample) and subsequently metabolite-wise auto scaled, are represented by a color code ranging from high (yellow) to low intensities (blue). White indicates the absence of the respective MST after data pre-processing. Metabolites are sorted according to abundance patterns (separated by black lines), class and RI. Only metabolites significantly correlating with the separation of treatments and treatment per day are shown. The fold change of MST abundance in co-cultivation relative to mono-cultivations is given and coded with a second color code. Black indicates a higher abundance in co-cultivation, grey a higher abundance in mono-cultivation.

ID	Model ion	RT	RI	Name	Class	Ident	Analysis	Metabolite intensity									Fold change		Group								
								Median (n=3/4)			Fold (Co relative to:)						UP	DOWN									
								Day 18			Day 30			Day 42			Day 18			Day 30		Day 42					
								SM Mono	Co	TW Mono	SM Mono	Co	TW Mono	SM Mono	Co	TW Mono	SM Mono	TW Mono		SM Mono	TW Mono	SM Mono	TW Mono				
68	103.1	8.60	1352	2-(4-Methyl-1,3-thiazol-5-yl)ethanol (Sulfurol)	Alk		DT	-	-	-	-	-	-	-	-	-	-	-	-3.5	1.1	Sm (1)						
284	334.2	16.53	2560	5-Ethyl-5-phenyl-2,5-pyrimidinediol (Liskantin)	Alk	?? ¹	DT	-	-	-	-	-	-	-	-	-	-	-	-3.8	-		-1.5	-	-1.6	18.3		
143	303.2	11.37	1718	Suberic acid	CA	?	DT	-	-	-	-	-	-	-	-	-	-	-	-1.8	-		-1.6	-	-1.8	5.3		
280	225.1	16.38	2533	Diphenyl phthalate	CA dv.		DT	-	-	-	-	-	-	-	-	-	-	-	-1.9	8.5		-1.7	18.8	-1.7	18.1		
336	259.2	22.95	3409	Melezitose	CS	?	DT	-	-	-	-	-	-	-	-	-	-	-	-2.2	17.8		-1.6	-	-1.7	101.6		
134	103.1	11.11	1683	Ribose	S		DT	-	-	-	-	-	-	-	-	-	-	-	-	-		-	-1.9	-	-1.1	538.4	
335	368.4	20.18	3157	Cholesterol	S	?? ¹	DT	-	-	-	-	-	-	-	-	-	-	-	-	-1.4		-	-	12.2	-	-1.6	19.7
130	250.1	10.95	1662	2-Deoxypentonic acid	S acid	?	DT,T	-	-	-	-	-	-	-	-	-	-	-	-1.3	4.5		-1.3	4.0	-1.0	2.5		
309	204.1	17.57	2740	Galactosylglycerol	S dv.		DT	-	-	-	-	-	-	-	-	-	-	-	-1.0	2.5		-1.4	-	-1.1	5.6		
40	186.1	7.14	1158	Unknown	U	-	DT	-	-	-	-	-	-	-	-	-	-	-	-4.4	-		-1.8	13.3	-1.6	3.3		
57	196.1	8.16	1294	Skel_MEDIA_C086 (Vidoudez)	U	?	DT	-	-	-	-	-	-	-	-	-	-	-	-1.2	1.7		-1.8	2.4	-1.7	3.2		
65	199.1	8.49	1337	Skel_MEDIA_C097 (Vidoudez)	U		DT	-	-	-	-	-	-	-	-	-	-	-	-1.4	2.8		-1.9	3.9	-1.6	3.2		
82	127.1	9.14	1422	Unknown	U	-	DT	-	-	-	-	-	-	-	-	-	-	-	-	-		-	-2.2	-	-1.6	3.5	
83	174.1	9.15	1425	Unknown	U	-	DT	-	-	-	-	-	-	-	-	-	-	-	-	-		-	-2.1	-	-1.6	4.0	
87	187.2	9.26	1439	Unknown	U	-	DT,T	-	-	-	-	-	-	-	-	-	-	-	-1.8	3.8		-1.7	6.5	-1.2	2.8		

ID	Model ion	RT	RI	Name	Class	Ident	Analysis	Median (n=3/4)									Fold (Co relative to:)						Group
								Day 18			Day 30			Day 42			Day 18		Day 30		Day 42		
								SM Mono	Co	TW Mono	SM Mono	Co	TW Mono	SM Mono	Co	TW Mono	SM Mono	TW Mono	SM Mono	TW Mono	SM Mono	TW Mono	
92	188.1	9.44	1463	Unknown	U	-	DT,T			-			-				-3.1	-	-1.4	-	-1.1	3.0	
95	231.1	9.50	1471	Skel_MEDIA_C127 (Vidoudez)	U	-	DT,T										-1.6	3.3	-1.5	-	-1.4	2.4	
96	157.1	9.53	1474	Unknown	U	-	DT			-							-10.9	-	-1.5	3.9	-1.1	3.9	
105	184.1	9.95	1530	Skel_MEDIA_C141 (Vidoudez)	U	-	DT										-1.6	3.4	-1.7	4.8	-1.7	4.6	
107	122.1	9.99	1536	Unknown	U	-	DT										-1.7	2.1	-2.0	2.9	-1.6	2.2	
123	284.1	10.60	1616	Unknown	U	-	DT										-1.1	6.1	-1.4	1.4	-1.3	1.7	
157	277.1	11.88	1786	Unknown	U	-	DT			-							-5.8	-	-3.3	-	-1.8	2.3	
161	253.1	12.02	1804	Skel_MEDIA_C205 (Vidoudez)	U	-	DT										-1.4	4.1	-1.8	5.4	-1.8	4.9	
164	211.1	12.10	1814	Unknown	U	-	DT										-1.6	3.5	-1.6	4.4	-1.7	2.8	
166	157.1	12.15	1820	Skel_MEDIA_C215 (Vidoudez)	U	?	DT										-1.4	1.6	-1.5	48.9	-1.4	2.6	
169	263.2	12.25	1834	Unknown	U	-	DT,T			-							-2.1	-	-2.7	-	-1.7	13.6	
171	353.2	12.34	1845	Unknown	U	-	DT			-							-2.3	-	-1.2	17.0	-1.3	3.0	
172	197.1	12.41	1856	Unknown	U	-	DT,T										-1.6	3.9	-1.4	19.7	-1.2	3.2	
174	197.1	12.46	1862	Unknown	U	-	DT,T										-1.3	3.9	-1.3	4.4	-1.2	2.6	
175	241.1	12.49	1866	Unknown	U	-	DT,T										-2.2	89.3	-2.6	101.9	-1.3	3.2	
186	153.1	12.79	1908	Unknown	U	-	DT,T										-1.8	11.1	-2.0	9.6	-1.6	6.2	
188	324.2	12.86	1919	Unknown	U	-	DT,T										-1.7	52.8	-1.5	-	-1.4	-	
189	382.2	12.88	1923	Unknown	U	-	DT										-1.9	3.3	-2.5	25.6	-1.9	25.0	
190	382.2	12.96	1936	Unknown	U	-	DT										-1.7	3.1	-2.6	24.4	-1.9	23.6	
194	199.1	13.08	1957	Unknown	U	-	DT,T										-2.2	3.0	-1.6	6.3	-1.3	5.0	
197	382.2	13.13	1966	Unknown	U	-	DT										-1.7	3.5	-2.6	8.3	-2.1	18.2	
199	197.1	13.18	1975	Unknown	U	-	DT,T										-1.9	7.1	-2.1	5.1	-1.8	3.5	
203	351.2	13.34	2003	Unknown	U	-	DT										-1.3	1.1	-1.5	1.8	-1.4	2.2	
204	156.1	13.36	2007	Unknown	U	-	DT,T			-							-	-	-1.7	-	-1.3	3.1	
211	238.1	13.80	2084	Unknown	U	-	DT,T			-							-4.6	-	-1.8	-	-1.6	30.8	
239	146.1	14.81	2260	Unknown	U	-	DT,T										-2.0	3.2	-2.0	-	-1.3	4.7	

ID	Model ion	RT	RI	Name	Class	Ident	Analysis	Median (n=3/4)									Fold (Co relative to:)						Group
								Day 18			Day 30			Day 42			Day 18		Day 30		Day 42		
								SM Mono	Co	TW Mono	SM Mono	Co	TW Mono	SM Mono	Co	TW Mono	SM Mono	TW Mono	SM Mono	TW Mono	SM Mono	TW Mono	
183	204.1	12.69	1892	Mannose	S		DT	-	-	-	-	-	-	-	-	-	-	-1.1	1.9				
200	204.1	13.20	1978	Glucose	S		DT	-	-	-	-	-	-	-	-	-	-	-1.1	1.8				
307	204.1	17.48	2725	Maltose	S	??	DT	-	-	-	-	-	-	-1.9	4.2	-	-	-1.1	3.3				
129	217.1	10.92	1659	2-Deoxypentonic acid	S acid		DT	-	-	-	-	-	-	-	-	-	-	-1.3	3.0				
41	230.2	7.18	1164	Unknown	U	-	DT	-	-	-	-	-	-	-	-	-	-	-1.5	2.2				
45	183.1	7.55	1213	Unknown	U	-	DT	-	-	-	-	-	-	-	-	-	-	-1.2	1.3				
76	217.1	9.00	1404	Unknown	U	-	DT	-	-	-	-	-	-	-	-	-	-	-1.2	4.3				
98	155.1	9.61	1485	Unknown	U	-	DT	-	-	-	-	-	-	-	-	-	-	-1.1	2.0				
102	155.1	9.80	1510	Unknown	U	-	DT	-	-	-	-	-	-	-	-	-	-	-1.0	11.7				
135	127.1	11.15	1688	Unknown	U	-	DT	-	-	-	-	-	-	-	-	-	-	-1.2	2.6				
146	141.1	11.57	1744	Unknown	U	-	DT	-	-	-	-	-	-	-	-	-	-	-1.4	2.8				
147	273.1	11.59	1747	Unknown	U	-	DT	-	-	-	-	-	-	-	-	-	-	-1.3	1.4				
185	204.1	12.77	1904	Unknown	U	-	DT	-	-	-	-	-	-	-	-	-	-	-1.2	2.0				
207	231	13.50	2032	Unknown	U	-	DT	-	-	-	-	-	-	-	-	-	-	-1.1	2.2				
279	217.1	16.33	2524	Unknown	U	-	DT	-	-	-	-	-	-	-3.4	5.5	-	-	-1.3	3.1				
315	204.1	17.79	2779	Unknown	U	-	DT	-	-	-	-	-	-	-	-	-	-	-1.1	2.2				
322	295.1	18.31	2862	Unknown	U	-	DT	-	-	-	-	-	-	-	-	-	-	-1.3	1.3				
324	133	18.39	2875	Unknown	U	-	DT	-	-	-	-	-	-	-	-	-	-	-1.1	1.1				
326	132	18.62	2912	Unknown	U	-	DT	-	-	-	-	-	-	-	-	-	-	-2.1	1.8				
329	221.1	19.07	2983	Unknown	U	-	DT	-	-	-	-	-	-	-	-	-	-	-1.3	2.6				
137	143.1	11.19	1694	Unknown	U	-	DT,T	-	-	-	-	-	-	13.4	-2.2	-	-2.0	4.6	-1.1	Tw (1)			
333	204.1	19.83	3101	Digalactosylglycerol	CS dv.		DT	-	-	-	-	-	-	4.3	-2.6	2.2	-2.4	1.2	-1.3				
213	204.1	13.88	2097	Unknown	U	-	DT	-	-	-	-	-	-	-	-3.1	1.8	-4.8	1.0	-1.7				
217	293.2	14.00	2119	Unknown	U	-	DT	-	-	-	-	-	-	1.7	-1.5	2.4	-1.0	3.3	-1.2	Tw (2)			
226	377.2	14.33	2176	Unknown	U	-	DT	-	-	-	-	-	-	-	-	1.2	-2.7	1.1	-1.2				
334	124.1	19.93	3117	Unknown	U	-	T	-	-	-	-	-	-	-	-23.6	-	-2.4	-	-1.9				

Daywise analysis via CAP



Appendix 40: PCoA score plot of exometabolomic samples from a daywise subset analysis of the interaction between *T. weissflogii* and *S. marinoi* on day 18, 30 and 42.

The plots are based on metabolites obtained from mono-cultivated *S. marinoi* (blue), mono-cultivated *T. weissflogii* (green) and co-cultivation of both diatoms (red) on day 18 (graph A), day 30 (graph B) and day 42 (graph C).

Appendix 41: Heatmap of exometabolite intensities for the subset analysis of the interaction between *T. weissflogii* and *S. marinoi* on day 18. Medians of MST intensities, normalized to the external standard ribitol (per sample) and subsequently metabolite-wise auto scaled, are represented by a color code ranging from high (yellow) to low intensities (blue). White indicates the absence of the respective MST after data pre-processing. Metabolites are sorted according to abundance patterns (separated by black lines), class and RI. Only metabolites significantly correlating with the separation of treatments and treatment per day are shown. The fold change of MST abundance in co-cultivation relative to mono-cultivations is given and coded with a second color code. Black indicates a higher abundance in co-cultivation, grey a higher abundance in mono-cultivation.

ID	Model ion	RT	RI	Name	Class	Ident	Metabolite intensity			Fold change		Group
							low		high	UP	DOWN	
							Median (n=4)			Fold (Co relative to:)		
Day 18			Day 18									
SM Mono	Co	TW Mono	SM Mono	TW Mono								
103	187.1	9.89	1522	7-Tetradecanol	Alc	1				2.6	8.5	A
132	187.1	11.03	1672	Unknown	U	-			1.2	-		
47	155.1	7.70	1232	Glycerol	Alc					-1.0	-	Sm
284	334.2	16.53	2560	5-Ethyl-5-phenyl-2,5-dihydro-4,6-pyrimidinediol (Liskantin)	Alk	??1				-3.8	-	
133	261.1	11.06	1677	2-Hydroxyhexanedioic acid	CA	?1				-1.0	5.7	
143	303.2	11.37	1718	Suberic acid	CA	?				-1.8	-	
130	250.1	10.95	1662	2-Deoxypentonic acid	S acid	?				-1.3	4.5	
40	186.1	7.14	1158	Unknown	U	-				-4.4	-	
57	196.1	8.16	1294	Skel_MEDIA_C086 (Vidoudez)	U	?				-1.2	1.7	
65	199.1	8.49	1337	Skel_MEDIA_C097 (Vidoudez)	U					-1.4	2.8	
87	187.2	9.26	1439	Unknown	U	-				-1.8	3.8	
92	188.1	9.44	1463	Unknown	U	-				-3.1	-	
95	231.1	9.50	1471	Skel_MEDIA_C127 (Vidoudez)	U					-1.6	3.3	
105	184.1	9.95	1530	Skel_MEDIA_C141 (Vidoudez)	U					-1.6	3.4	
161	253.1	12.02	1804	Skel_MEDIA_C205 (Vidoudez)	U					-1.4	4.1	
164	211.1	12.10	1814	Unknown	U	-				-1.6	3.5	
169	263.2	12.25	1834	Unknown	U	-				-2.1	-	
172	197.1	12.41	1856	Unknown	U	-				-1.6	3.9	
175	241.1	12.49	1866	Unknown	U	-				-2.2	89.3	

ID	Model ion	RT	RI	Name	Class	Ident	Median (n=4)			Fold (Co relative to:)		Group
							Day 18			Day 18		
							SM Mono	Co	TW Mono	SM Mono	TW Mono	
186	153.1	12.79	1908	Unknown	U	-				-1.8	11.1	
188	324.2	12.86	1919	Unknown	U	-				-1.7	52.8	
189	382.2	12.88	1923	Unknown	U	-				-1.9	3.3	
190	382.2	12.96	1936	Unknown	U	-				-1.7	3.1	
194	199.1	13.08	1957	Unknown	U	-				-2.2	3.0	
197	382.2	13.13	1966	Unknown	U	-				-1.7	3.5	
199	197.1	13.18	1975	Unknown	U	-				-1.9	7.1	
211	238.1	13.80	2084	Unknown	U	-				-4.6	-	
258	174.1	15.53	2385	Unknown	U	-				-2.1	16.0	
259	199.1	15.55	2388	Unknown	U	-				-2.3	7.9	
268	185.1	15.98	2463	Unknown	U	-				-6.4	-	
276	411.2	16.24	2509	M000000_A275005-101-xxx_NA_2736,09_PRED_VAR5_ALK_NA (GOLM)	U	-				-2.0	159.1	
313	171.1	17.75	2773	Unknown	U	-				-1.7	-	
323	204.1	18.35	2868	Unknown	U	-				-2.7	-	
327	171.1	18.64	2915	Unknown	U	-				-2.3	9.5	
39	247.1	7.06	1148	3-Hydroxy-3-methylbutanoic acid	CA					-	-2.1	
263	217.1	15.79	2431	Uridine	S dv.	?				-	-2.7	
136	279.2	11.15	1689	M000000_A170005-101-xxx_NA_1682,68_PRED_VAR5_ALK_NA (GOLM)	U	?				-	-2.5	
137	143.1	11.19	1694	Unknown	U	-				13.4	-2.2	Tw

In case derivatized molecules are detected, the table entry lists their putative parent compounds. Each MST is characterized by **ID**, **model ion**, retention time (**RT**) and retention index (**RI**). Metabolites were identified via libraries. If metabolites were verified with a standard, they are marked with *. “?” indicates a reversed match between 700 and 800, “??” a reversed match between 600 and 700 and “???” indicates cases where the reversed match was ≤ 600 . “?” tags metabolites with a match smaller than 600. Class abbreviations: Amine (**A**), alcohol (**Alc**), alkaloid (**Alk**), carboxylic acid (**CA**), complex sugar (**CS**), derivatives of a certain class (**dv.**), sugar (**S**), sugar alcohol (**S Alc**), sugar acid (**S Acid**), sterol (**St**), terpene (**T**), others (**O**), unknown (**U**). **Vidoudez** refers to an MST code given by the inhouse library, **GOLM** refers to an MST code given by distinct libraries of the Golm Metabolome Database.

Appendix 42: Heatmap of exometabolite intensities for the subset analysis of the interaction between *T. weissflogii* and *S. marinoi* on day 30.

Medians of MST intensities, normalized to the external standard ribitol (per sample) and subsequently metabolite-wise auto scaled, are represented by a color code ranging from high (yellow) to low intensities (blue). White indicates the absence of the respective MST after data pre-processing. Metabolites are sorted according to abundance patterns (separated by black lines), class and RI. Only metabolites significantly correlating with the separation of treatments and treatment per day are shown. The fold change of MST abundance in co-cultivation relative to mono-cultivations is given and coded with a second color code. Black indicates a higher abundance in co-cultivation, grey a higher abundance in mono-cultivation.

ID	Model ion	RT	RI	Name	Class	Ident	Metabolite intensity			Fold change		Group
							low		high	UP	DOWN	
							Median (n=3/4)			Fold (Co relative to:)		
Day 30			Day 30									
SM Mono	Co	TW Mono	SM Mono	TW Mono								
300	236.1	17.05	2649	Adenosine	S dv.				1.1	-	A	
311	245.1	17.65	2755	Guanosine	S dv.				1.0	-		
208	221.1	13.55	2040	Unknown	U				1.2	-		
284	334.2	16.53	2560	5-Ethyl-5-phenyl-2,5-dihydro-4,6-pyrimidinediol (Liskantin)	Alk	?? ¹			-1.5	-	Sm	
133	261.1	11.06	1677	2-Hydroxyhexanedioic acid	CA	? ¹			-1.2	-		
143	303.2	11.37	1718	Suberic acid	CA	?			-1.6	-		
341	361.2	24.90	3571	Maltotriose	CS				-1.3	3.7		
130	250.1	10.95	1662	2-Deoxypentonic acid	S acid	?			-1.3	4.0		
206	321.2	13.44	2020	Gluconic acid	S acid	? ¹			-1.1	3.1		
289	230.1	16.71	2591	Inosine	S dv.				-1.6	-		
306	327.2	17.23	2681	Pregn-16-en-20-one, 3,18-bis(acetyloxy)-14,15-epoxy-,	ST	?? ¹			-1.8	-		
40	186.1	7.14	1158	Unknown	U	-			-1.8	13.3		
64	196.1	8.45	1331	Unknown	U	-			-1.4	-		
65	199.1	8.49	1337	Skel_MEDIA_C097 (Vidoudez)	U	-			-1.9	3.9		
87	187.2	9.26	1439	Unknown	U	-			-1.7	6.5		
92	188.1	9.44	1463	Unknown	U	-			-1.4	-		
95	231.1	9.50	1471	Skel_MEDIA_C127 (Vidoudez)	U	-			-1.5	-		




ID	Model ion	RT	RI	Name	Class	Ident	Median (n=3/4)			Fold (Co relative to:)		Group
							Day 30			Day 30		
							SM Mono	Co	TW Mono	SM Mono	TW Mono	
105	184.1	9.95	1530	Skel_MEDIA_C141 (Vidoudez)	U				-1.7	4.8		
161	253.1	12.02	1804	Skel_MEDIA_C205 (Vidoudez)	U				-1.8	5.4		
164	211.1	12.10	1814	Unknown	U	-			-1.6	4.4		
166	157.1	12.15	1820	Skel_MEDIA_C215 (Vidoudez)	U	?			-1.5	48.9		
171	353.2	12.34	1845	Unknown	U	-			-1.2	17.0		
172	197.1	12.41	1856	Unknown	U	-			-1.4	19.7		
174	197.1	12.46	1862	Unknown	U	-			-1.3	4.4		
186	153.1	12.79	1908	Unknown	U	-			-2.0	9.6		
188	324.2	12.86	1919	Unknown	U	-			-1.5	-		
189	382.2	12.88	1923	Unknown	U	-			-2.5	25.6		
190	382.2	12.96	1936	Unknown	U	-			-2.6	24.4		
193	327.2	13.04	1951	Unknown	U	-			-1.5	-		
194	199.1	13.08	1957	Unknown	U	-			-1.6	6.3		
199	197.1	13.18	1975	Unknown	U	-			-2.1	5.1		
203	351.2	13.34	2003	Unknown	U	-			-1.5	1.8		
204	156.1	13.36	2007	Unknown	U	-			-1.7	-		
210	351.2	13.63	2055	Unknown	U	-			-1.4	3.5		
211	238.1	13.80	2084	Unknown	U	-			-1.8	-		
216	470.3	13.98	2116	Unknown	U	-			-1.5	-		
259	199.1	15.55	2388	Unknown	U	-			-1.8	21.0		
271	447.3	16.12	2488	Unknown	U	-			-1.2	2.3		
274	254.2	16.20	2502	Unknown	U	-			-1.6	6.1		
276	411.2	16.24	2509	M000000_A275005-101- xxx_NA_2736,09_PRED_VAR5_ALK_NA (GOLM)	U	-			-1.7	24.1		
282	148.1	16.47	2550	Unknown	U	-			-1.7	-		
292	202.1	16.81	2609	Unknown	U	-			-2.8	-		
297	171.1	16.93	2630	Unknown	U	-			-2.1	-		

ID	Model ion	RT	RI	Name	Class	Ident	Median (n=3/4)			Fold (Co relative to:)		Group
							Day 30			Day 30		
							SM Mono	Co	TW Mono	SM Mono	TW Mono	
313	171.1	17.75	2773	Unknown	U	-				-1.4	-	
318	261.1	18.01	2816	Unknown	U	-				-1.6	23.4	
323	204.1	18.35	2868	Unknown	U	-				-1.3	-	
325	204.1	18.50	2892	Unknown	U	-				-1.4	-	
327	171.1	18.64	2915	Unknown	U	-				-2.0	-	
334	124.1	19.93	3117	Unknown	U	-				-	-2.4	Tw

In case derivatized molecules are detected, the table entry lists their putative parent compounds. Each MST is characterized by **ID**, **model ion**, retention time (**RT**) and retention index (**RI**). Metabolites were identified via libraries. If metabolites were verified with a standard, they are marked with *. “?” indicates a reversed match between 700 and 800, “??” a reversed match between 600 and 700 and “???” indicates cases where the reversed match was ≤ 600 . “1” tags metabolites with a match smaller than 600. Class abbreviations: Amine (**A**), alcohol (**Alc**), alkaloid (**Alk**), carboxylic acid (**CA**), complex sugar (**CS**), derivatives of a certain class (**dv.**), sugar (**S**), sugar alcohol (**S Alc**), sugar acid (**S Acid**), sterol (**St**), terpene (**T**), others (**O**), unknown (**U**). **Vidoudez** refers to an MST code given by the inhouse library, **GOLM** refers to an MST code given by distinct libraries of the Golm Metabolome Database.

Appendix 43: Heatmap of exometabolite intensities for the subset analysis of the interaction between *T. weissflogii* and *S. marinoi* on day 42.

Medians of MST intensities, normalized to the external standard ribitol (per sample) and subsequently metabolite-wise auto scaled, are represented by a color code ranging from high (yellow) to low intensities (blue). White indicates the absence of the respective MST after data pre-processing. Metabolites are sorted according to abundance patterns (separated by black lines), class and RI. Only metabolites significantly correlating with the separation of treatments and treatment per day are shown. The fold change of MST abundance in co-cultivation relative to mono-cultivations is given and coded with a second color code. Black indicates a higher abundance in co-cultivation, grey a higher abundance in mono-cultivations.

Metabolite intensity
low  high
Fold change
UP  DOWN 

ID	Model ion	RT	RI	Name	Class	Ident	Median (n=4)			Fold (Co relative to:)		Group
							Day 42			Day 42		
							SM Mono	Co	TW Mono	SM Mono	TW Mono	
111	120.1	10.14	1555	Phenylalanine	AA				1.4	-	A	
118	313.2	10.42	1592	Unknown	S			1.3	2.6			
206	321.2	13.44	2020	Gluconic acid	S acid			1.0	3.2			
23	117.1	6.50	1073	Leucine	AA	? ¹			-1.5	5.3	Sm	
25	170.1	6.57	1083	Norleucine	AA	? ¹			-1.2	2.3		
6	151.1	5.55	948	Phenol	Alc				-1.4	2.4		
51	160.1	7.85	1253	Glycerol	Alc	? ¹			-1.1	6.5		
66	151.1	8.54	1343	2-Phenoxyethanol	Alc				-1.2	1.9		
86	103.1	9.24	1436	1,3,5-Pentanetriol	Alc	?? ¹			-1.5	11.1		
99	223.1	9.67	1493	4-Hydroxybenzaldehyde	Alc				-1.9	3.0		
103	187.1	9.89	1522	7-Tetradecanol	Alc	¹			-4.1	282.9		
139	186.1	11.26	1703	4-Methyl-2,6-bis(2-methyl-2-propanyl)phenol	Alc	?? ¹			-1.4	2.1		
53	113.1	8.00	1272	2-(4-Methyl-1-piperazinyl)ethanol	Alk	?			-1.4	3.2		
17	165.1	6.31	1049	Oxalic acid	CA	? ¹			-1.2	1.5		
32	113.1	6.80	1114	Succinic acid	CA	?? ¹			-1.0	19.2		
133	261.1	11.06	1677	2-Hydroxyhexanedioic acid	CA	? ¹			-1.5	9.9		
143	303.2	11.37	1718	Suberic acid	CA	?			-1.8	5.3		
30	282.1	6.73	1105	Dodecamethylpentasiloxane	O				-1.3	-		
115	217.1	10.35	1583	Arabinofuranose	S				-1.2	3.0		

ID	Model ion	RT	RI	Name	Class	Ident	Median (n=4)			Fold (Co relative to:)		Group
							Day 42			Day 42		
							SM Mono	Co	TW Mono	SM Mono	TW Mono	
116	284.1	10.37	1586	Arabinofuranose	S				-1.6	4.9		
119	217.1	10.46	1598	Unknown	S				-1.2	2.8		
125	217	10.66	1624	Ribofuranose	S	?			-1.1	2.3		
134	103.1	11.11	1683	Ribose	S				-1.1	538.4		
129	217.1	10.92	1659	2-Deoxypentonic acid	S acid				-1.3	3.0		
130	250.1	10.95	1662	2-Deoxypentonic acid	S acid	?			-1.0	2.5		
180	319.2	12.61	1881	Gluconic acid 1,5-lactone	S dv.				-1.2	2.0		
9	143.1	5.67	965	Unknown	U	-			-1.3	8.9		
15	240	6.12	1023	Unknown	U	-			-1.7	12.7		
40	186.1	7.14	1158	Unknown	U	-			-1.6	3.3		
57	196.1	8.16	1294	Skel_MEDIA_C086 (Vidoudez)	U	?			-1.7	3.2		
65	199.1	8.49	1337	Skel_MEDIA_C097 (Vidoudez)	U				-1.6	3.2		
70	142.1	8.69	1364	Unknown	U	-			-1.6	-		
82	127.1	9.14	1422	Unknown	U	-			-1.6	3.5		
87	187.2	9.26	1439	Unknown	U	-			-1.2	2.8		
92	188.1	9.44	1463	Unknown	U	-			-1.1	3.0		
95	231.1	9.50	1471	Skel_MEDIA_C127 (Vidoudez)	U				-1.4	2.4		
96	157.1	9.53	1474	Unknown	U	-			-1.1	3.9		
105	184.1	9.95	1530	Skel_MEDIA_C141 (Vidoudez)	U				-1.7	4.6		
107	122.1	9.99	1536	Unknown	U	-			-1.6	2.2		
131	247.1	11.00	1668	Unknown	U	-			-1.4	4.9		
132	187.1	11.03	1672	Unknown	U	-			-1.1	39.0		
157	277.1	11.88	1786	Unknown	U	-			-1.8	2.3		
161	253.1	12.02	1804	Skel_MEDIA_C205 (Vidoudez)	U				-1.8	4.9		
164	211.1	12.10	1814	Unknown	U	-			-1.7	2.8		
166	157.1	12.15	1820	Skel_MEDIA_C215 (Vidoudez)	U	?			-1.4	2.6		
169	263.2	12.25	1834	Unknown	U	-			-1.7	13.6		

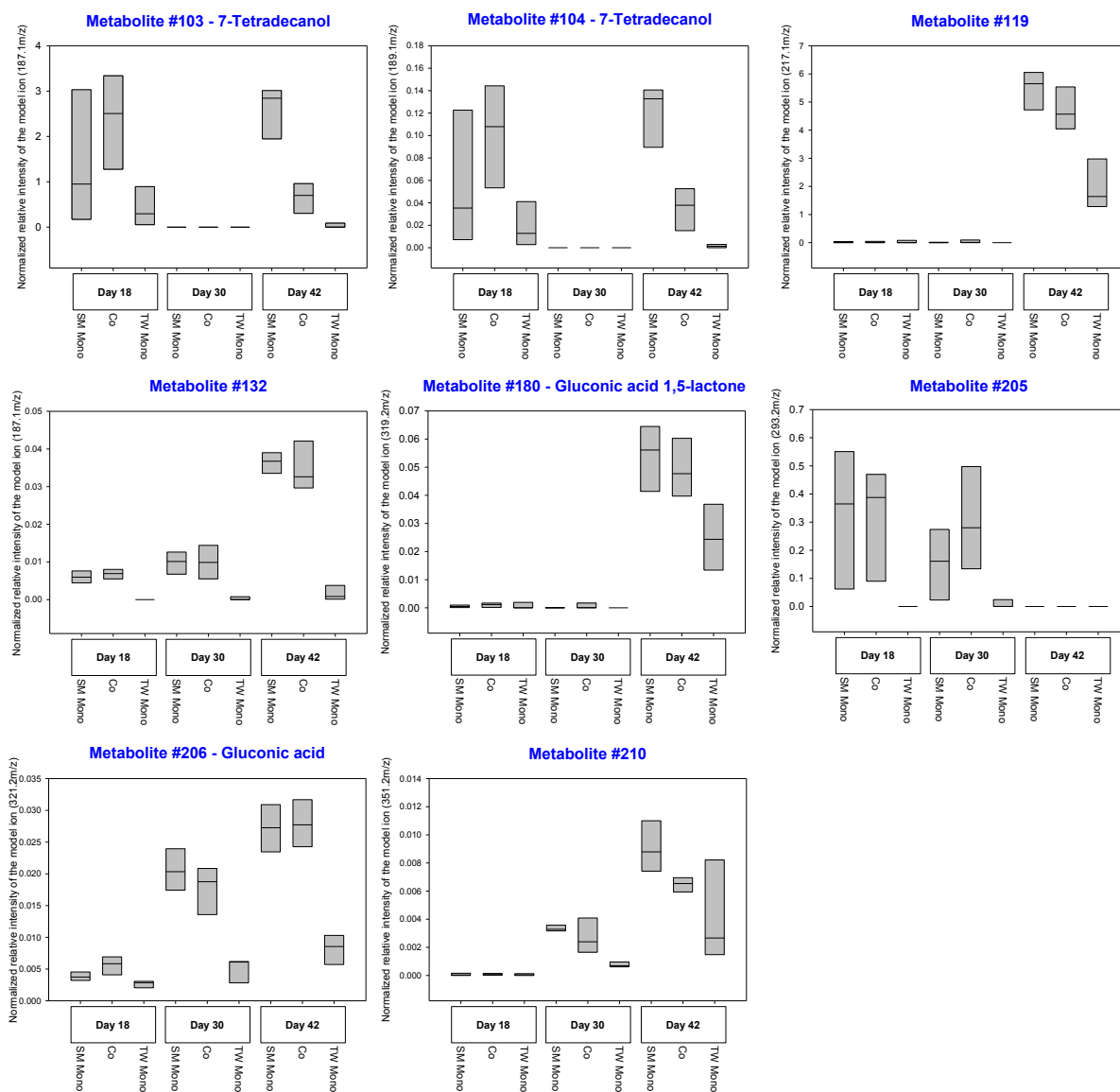
ID	Model ion	RT	RI	Name	Class	Ident	Median (n=4)			Fold (Co relative to:)		Group
							Day 42			Day 42		
							SM Mono	Co	TW Mono	SM Mono	TW Mono	
171	353.2	12.34	1845	Unknown	U	-				-1.3	3.0	
172	197.1	12.41	1856	Unknown	U	-				-1.2	3.2	
174	197.1	12.46	1862	Unknown	U	-				-1.2	2.6	
175	241.1	12.49	1866	Unknown	U	-				-1.3	3.2	
186	153.1	12.79	1908	Unknown	U	-				-1.6	6.2	
188	324.2	12.86	1919	Unknown	U	-				-1.4	-	
189	382.2	12.88	1923	Unknown	U	-				-1.9	25.0	
190	382.2	12.96	1936	Unknown	U	-				-1.9	23.6	
191	323.2	12.98	1941	Unknown	U	-				-1.2	5.1	
193	327.2	13.04	1951	Unknown	U	-				-1.2	-	
194	199.1	13.08	1957	Unknown	U	-				-1.3	5.0	
197	382.2	13.13	1966	Unknown	U	-				-2.1	18.2	
198	146.1	13.15	1970	Unknown	U	-				-1.5	16.2	
199	197.1	13.18	1975	Unknown	U	-				-1.8	3.5	
203	351.2	13.34	2003	Unknown	U	-				-1.4	2.2	
204	156.1	13.36	2007	Unknown	U	-				-1.3	3.1	
207	231	13.50	2032	Unknown	U	-				-1.1	2.2	
211	238.1	13.80	2084	Unknown	U	-				-1.6	30.8	
216	470.3	13.98	2116	Unknown	U	-				-1.3	40.9	
239	146.1	14.81	2260	Unknown	U	-				-1.3	4.7	
242	171.1	14.96	2285	Unknown	U	-				-1.7	-	

In case derivatized molecules are detected, the table entry lists their putative parent compounds. Each MST is characterized by **ID**, **model ion**, retention time (**RT**) and retention index (**RI**). Metabolites were identified via libraries. If metabolites were verified with a standard, they are marked with *. “?” indicates a reversed match between 700 and 800, “??” a reversed match between 600 and 700 and “???” indicates cases where the reversed match was ≤ 600 . “1” tags metabolites with a match smaller than 600. Class abbreviations: Amine (**A**), alcohol (**Alc**), alkaloid (**Alk**), carboxylic acid (**CA**), complex sugar (**CS**), derivatives of a certain class (**dv.**), sugar (**S**), sugar alcohol (**S Alc**), sugar acid (**S Acid**), sterol (**St**), terpene (**T**), others (**O**), unknown (**U**). **Vidoudez** refers to an MST code given by the inhouse library, **GOLM** refers to an MST code given by distinct libraries of the Golm Metabolome Database

Screening for interaction specific release and/or uptake of potential infochemicals

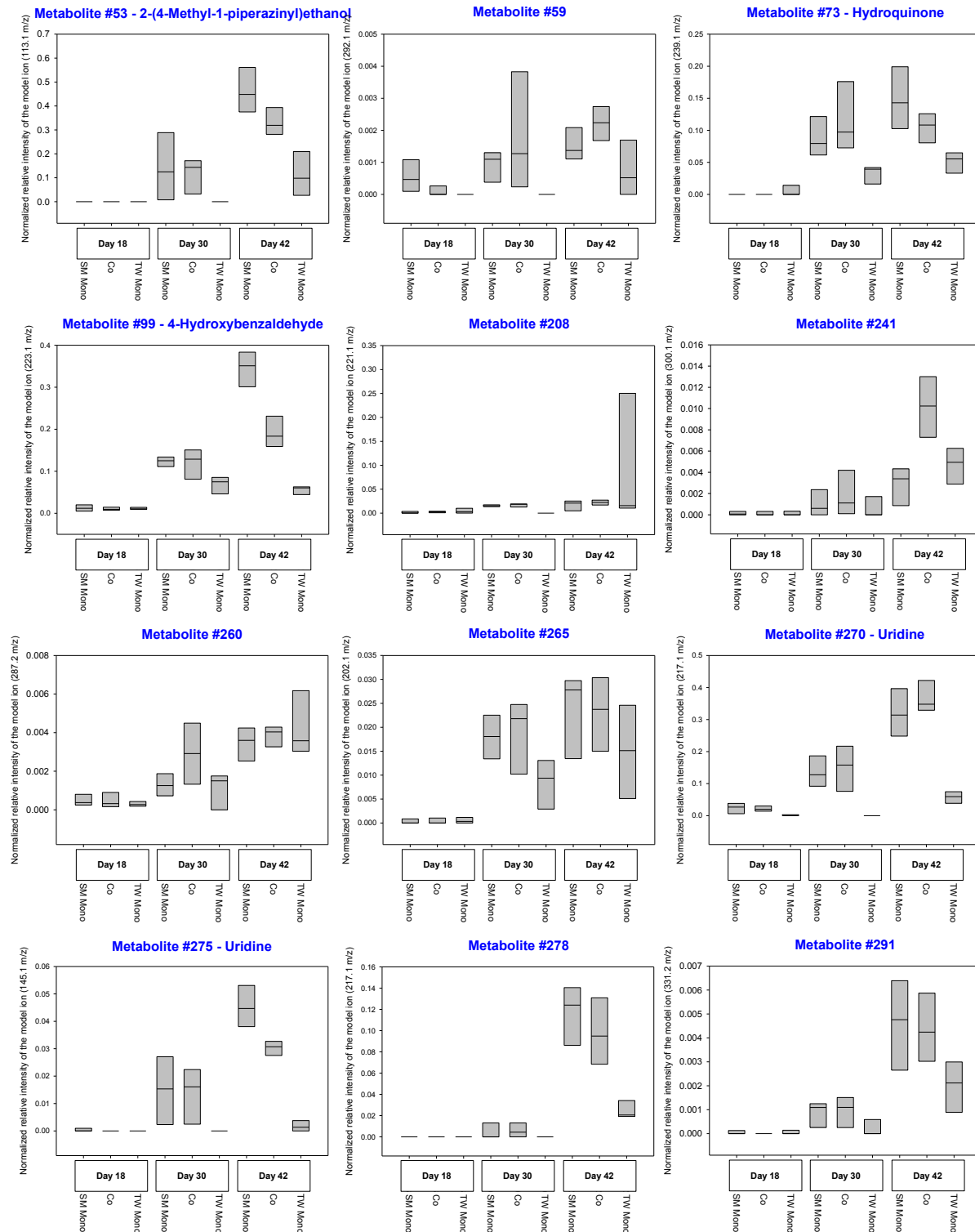
Appendix 44: Intensity dynamic of exometabolites, enhanced in co-cultivation on day 18 in the interaction between *T. weissflogii* and *S. marinoi*.

Boxplots visualized intensity dynamics over time and treatments via relative MST intensities (ribitol normalized) of the respective model ion.

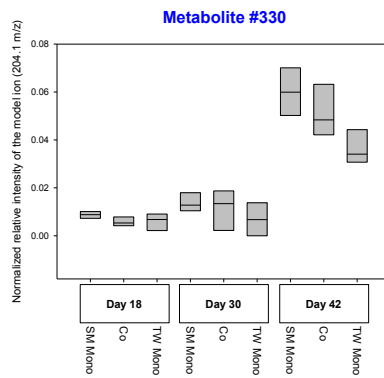
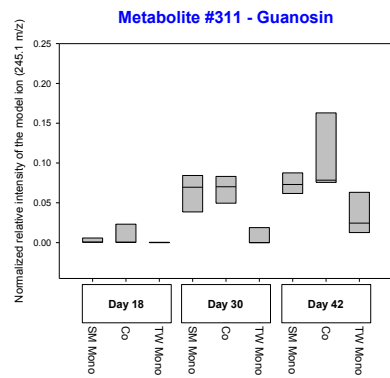
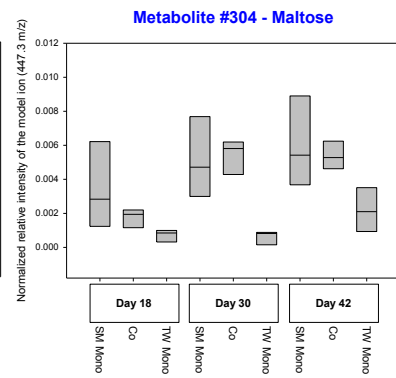
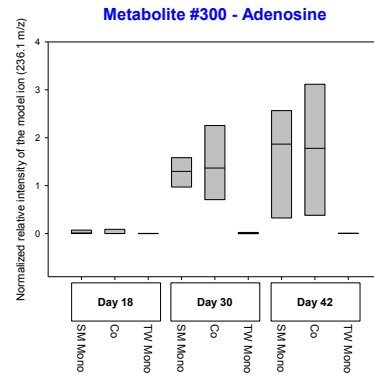
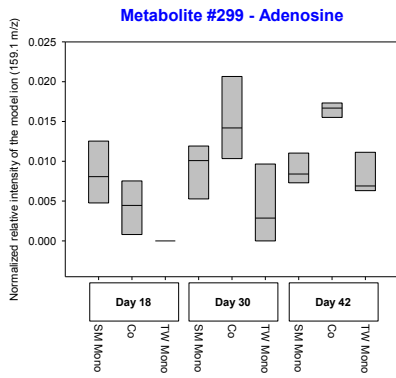


Appendix 45: Intensity dynamic of exometabolites, enhanced in co-cultivation on day 30 in the interaction between *T. weissflogii* and *S. marinoi*.

Boxplots visualized intensity dynamics over time and treatments via relative MST intensities (ribitol normalized) of the respective model ion.

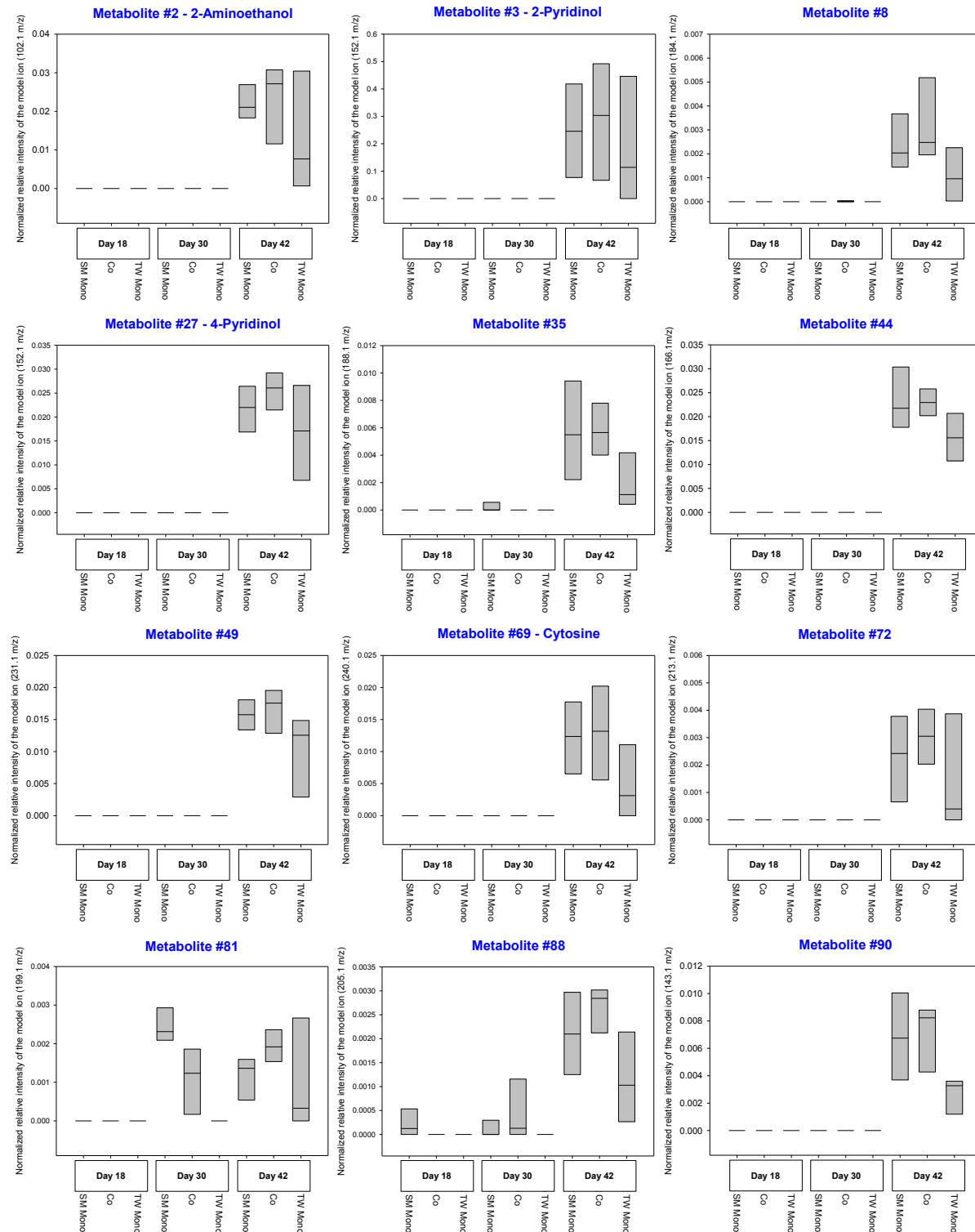


Appendix 45 continued

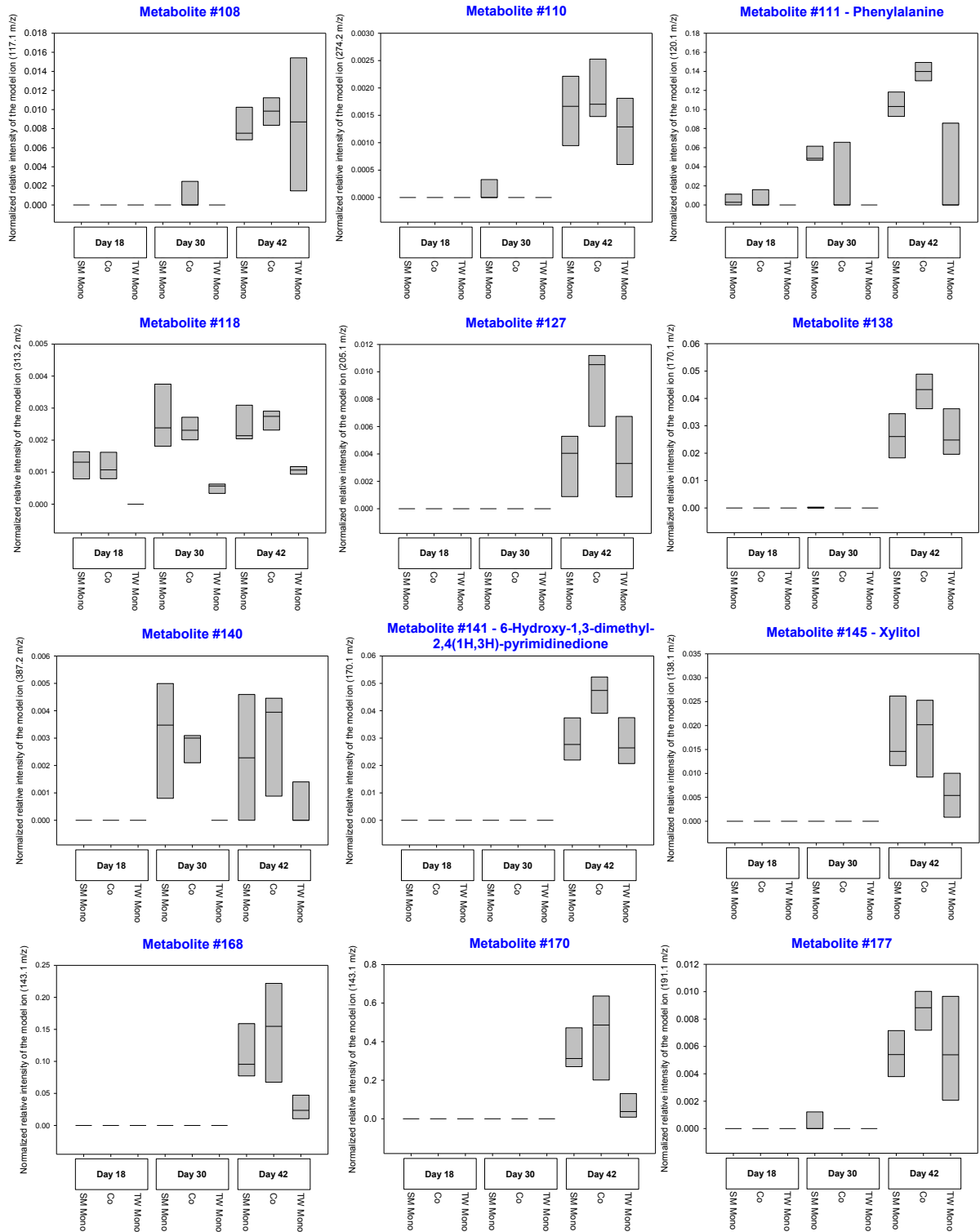


Appendix 46: Intensity dynamic of exometabolites, enhanced in co-cultivation on day 42 in the interaction between *T. weissflogii* and *S. marinoi*.

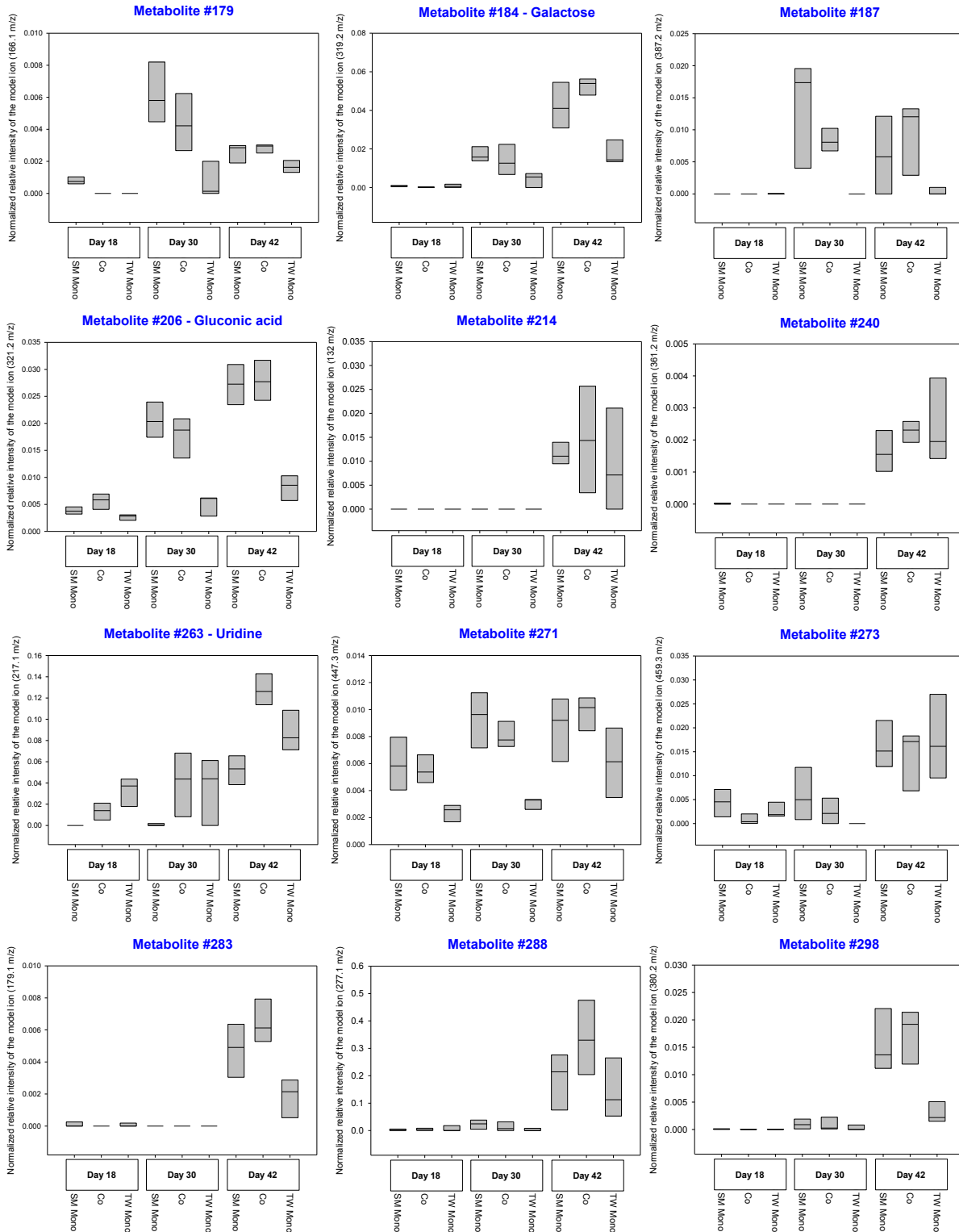
Boxplots visualized intensity dynamics over time and treatments via relative MST intensities (ribitol normalized) of the respective model ion.



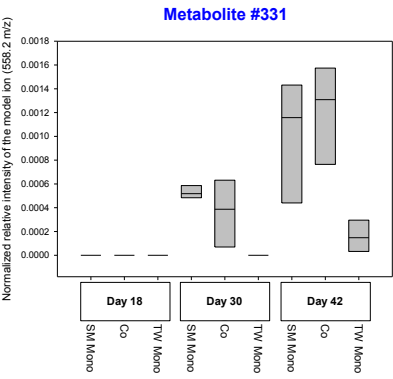
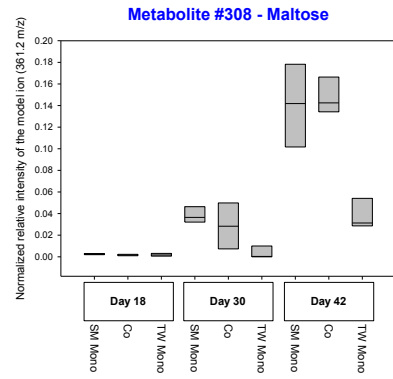
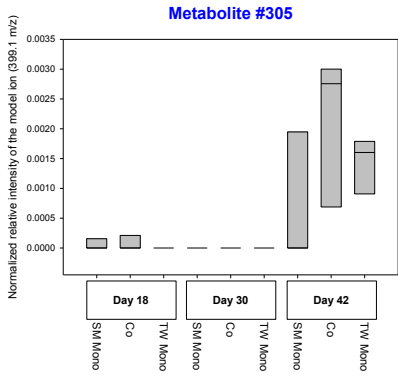
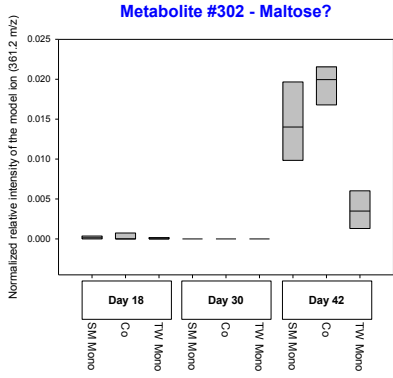
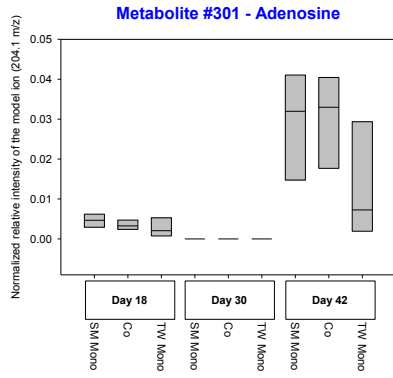
Appendix 46 continued



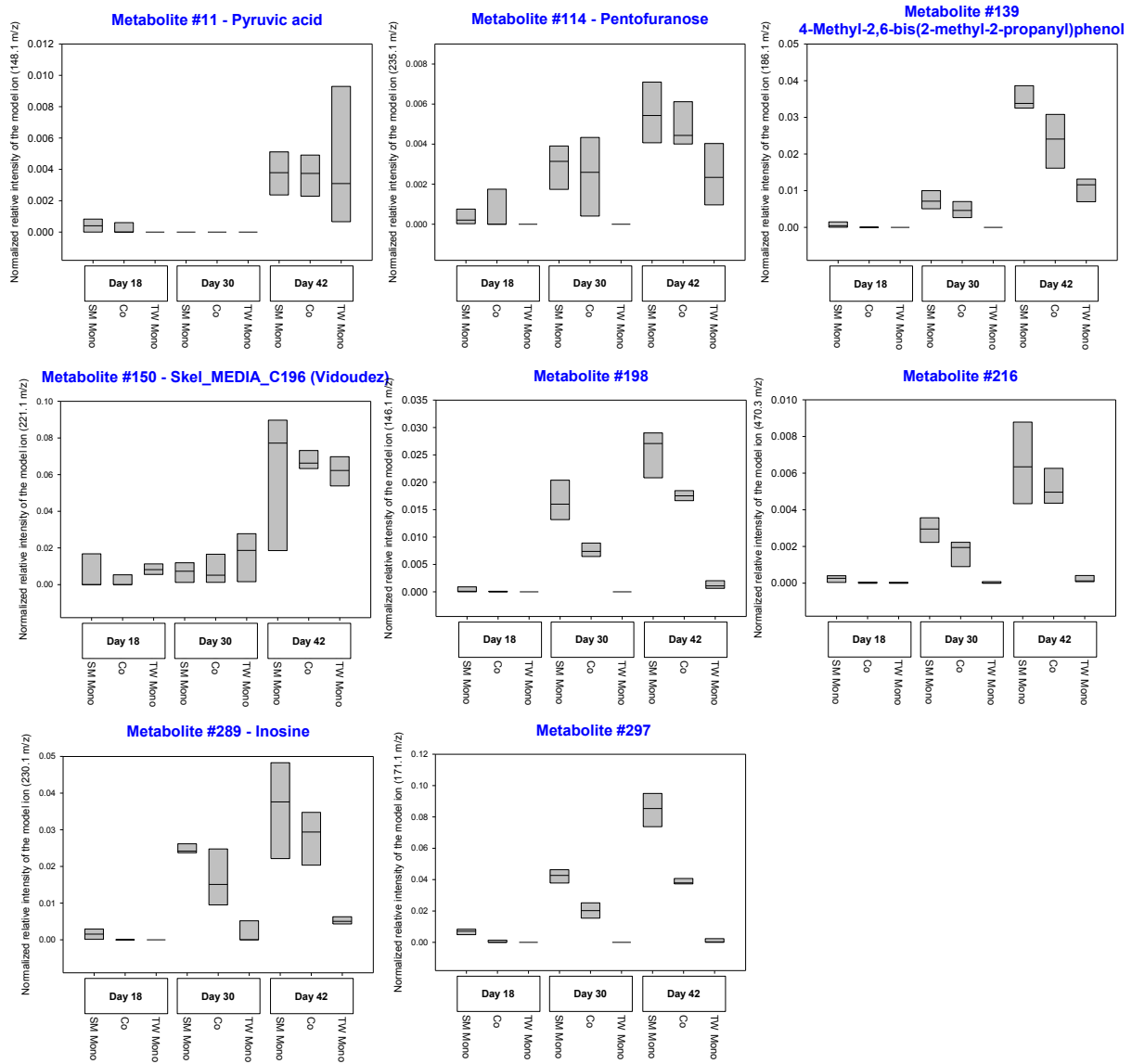
Appendix 46 continued



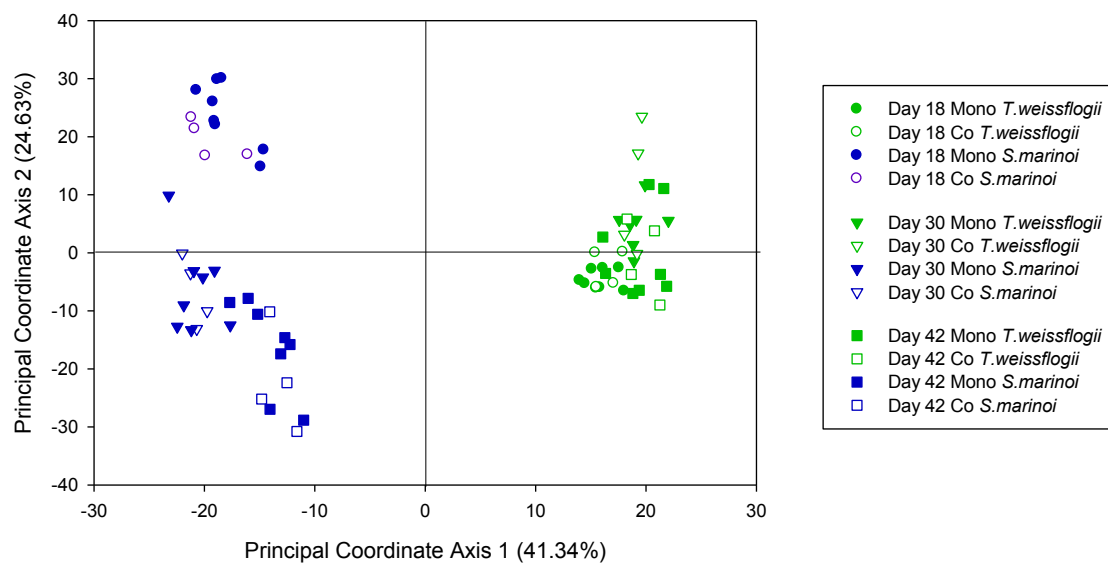
Appendix 46 continued



Appendix 47: Intensity dynamic of exometabolites excluded in the screening process for exometabolites, which were reduced in co-cultivation in the interaction between *T. weissflogii* and *S. marinoi* and matched pattern III. Boxplots visualized intensity dynamics over time and treatments via relative MST intensities (ribitol normalized) of the respective model ion.

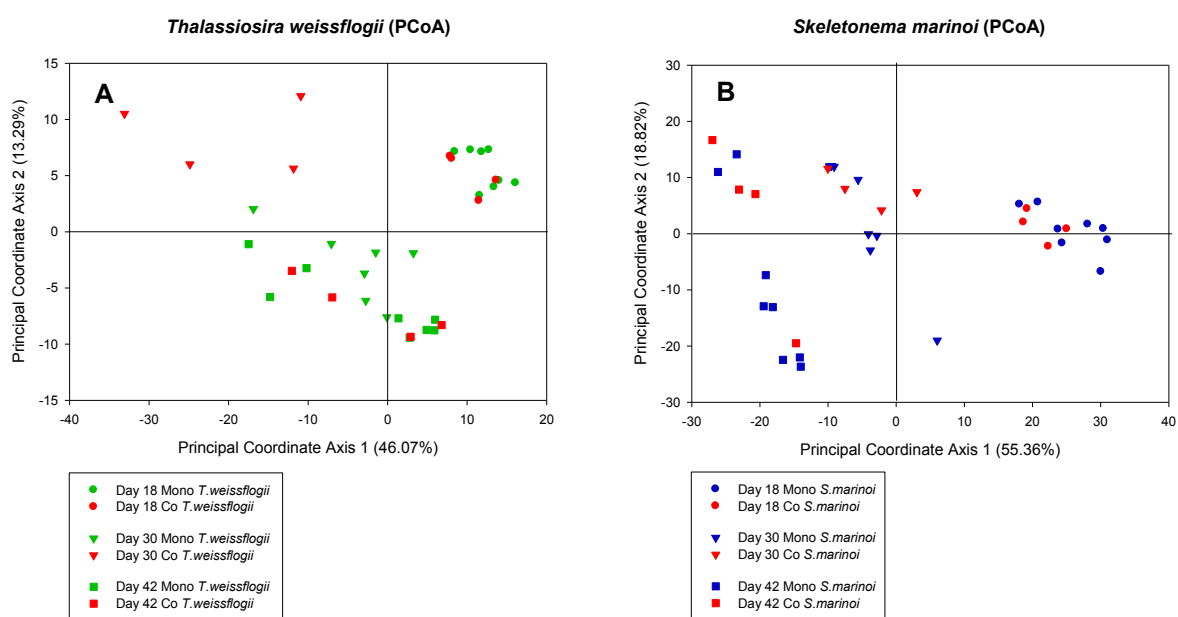


7.2.3 Endometabolomic investigation

Overall analysis via CAP

Appendix 48: PCoA score plot of endometabolomic samples from an overall analysis of the interaction between *T. weissflogii* and *S. marinoi*.

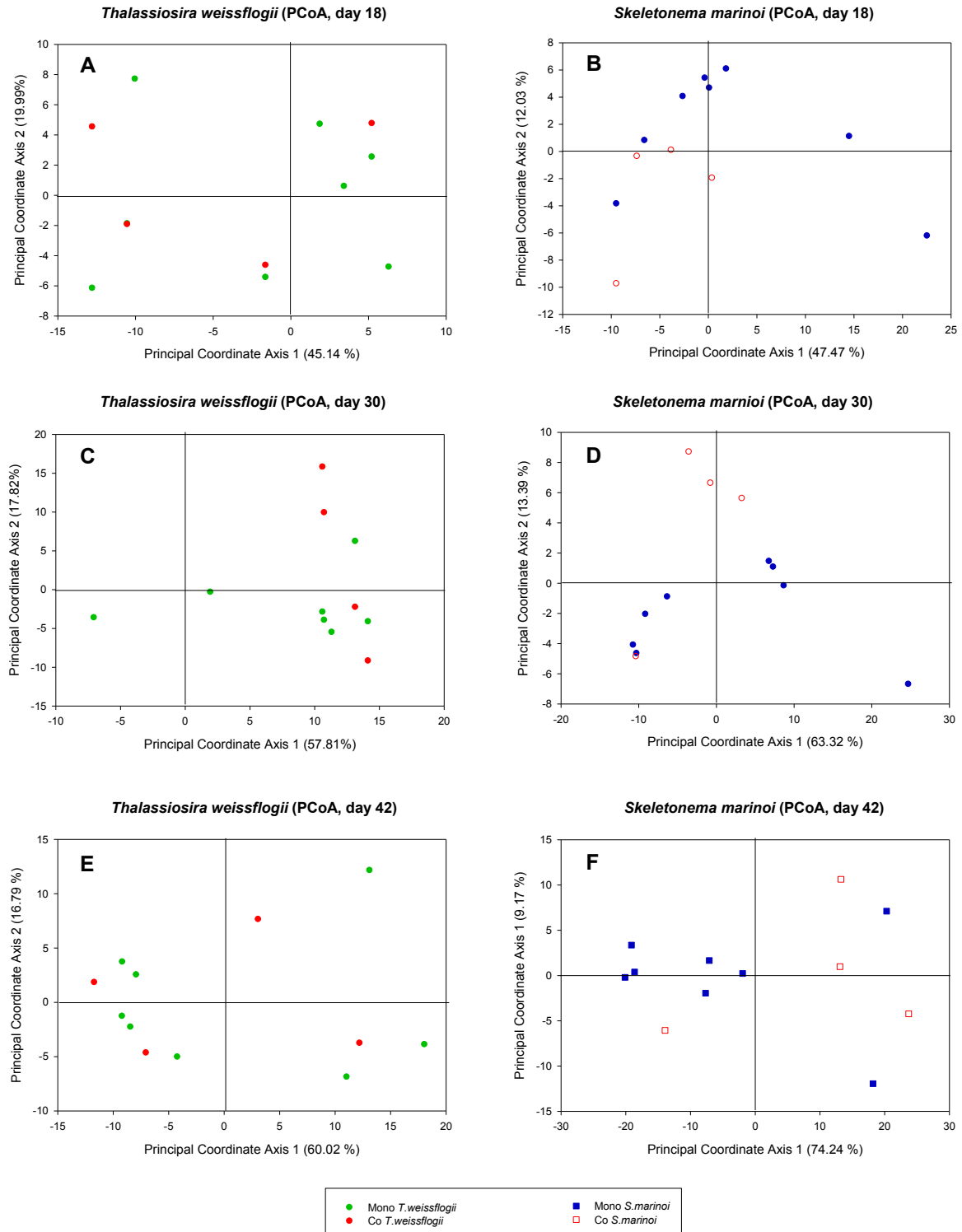
The plot is based on metabolites obtained from *S. marinoi* (blue) and *T. weissflogii* (green) on day 18 (●), day 30 (▼) and day 42 (■). Samples from mono-cultivation are represented by filled symbols, samples from co-cultivation by empty symbols.

Species-specific analysis via CAP

Appendix 49: PCoA score plot of endometabolomic samples from a species-specific subset analysis of the interaction between *T. weissflogii* and *S. marinoi*.

The plots are based on metabolites obtained from mono-cultivated (green) and co-cultivated (red) *T. weissflogii* (graph A) and mono-cultivated (blue) and co-cultivated (red) *S. marinoi* (graph B) on day 18 (●), day 30 (▼) and day 42 (■). The analysis was performed for each species individually.

Daywise and species-specific analysis via CAP



Appendix 50: PCoA score plot of endometabolomic samples from a species-specific subset analysis of the interaction between *T. weissflogii* and *S. marinoi* on day 18, 30 and 42.

The plots are based on metabolites obtained from mono-cultivated (green) and co-cultivated (red) *T. weissflogii* (graph A, C, E) and mono-cultivated (blue) and co-cultivated (red) *S. marinoi* (graph B, D, F) on day 18 (●, graph A, B), day 30 (●, graph C, D) and day 42 (●, graph E, F). The analysis was performed for each species and day individually.

Identification of metabolites correlating with relevant a-priori groups

T. weissflogii

Appendix 51: Heatmap of unknown endometabolite intensities for the species-specific and daywise analysis of *T. weissflogii* in interaction with *S. marinoi*. Medians of MST intensities, normalized to peak sum per sample and subsequently metabolite-wise auto scaled, are represented by a color code ranging from high (yellow) to low intensities (blue). White indicates the absence of the respective MST after data pre-processing. Metabolites are sorted according to classes (separated by black lines) and abundance patterns. Only metabolites significantly correlating with the separation of treatments and treatment per day are shown. The fold change of MST abundance in co-cultivation relative to mono-cultivation is given and coded with a second color code. Black indicates a higher abundance in co-cultivation, grey a higher abundance in mono-cultivation.



ID	Model ion	RT	RI	Name	Class	Ident	Analysis	Median (Co: n=4, Mono: n=7/8)						Fold (Co relative to Mono)		
								Day 18		Day 30		Day 42		Day 18	Day 30	Day 42
								TW Mono	TW Co	TW Mono	TW Co	TW Mono	TW Co			
18	228.1	6.20	1034	Unknown	U	-	30						1.4	-	1.2	
30	152.1	6.62	1090	Unknown	U	-	DT,30						1.1	-	-1.2	
31	113.1	6.67	1096	Unknown	U	-	30						2.1	-	-1.4	
33	169	6.76	1109	Unknown	U	-	DT						1.1	-	-	
43	126.1	6.96	1135	Unknown	U	-	30						2.9	-	-1.2	
46	169.1	7.02	1143	Unknown	U	-	DT						1.8	-	-	
62	299.1	7.73	1236	Unknown	U	-	30						1.2	-	-1.1	
71	113.9	7.99	1272	Skel_Cell_C021 (Vidoudez)	U	?	30						1.2	-	-1.0	
75	221.1	8.12	1288	Unknown	U	-	DT						1.7	-	-	
76	196.1	8.16	1294	Unknown	U	-	DT,30						1.1	-1.8	-1.1	
103	156.1	9.12	1421	Unknown	U	-	30						1.4	-1.4	-1.1	
108	123.1	9.26	1440	Unknown	U	-	30						1.1	-	-1.4	
134	206.2	10.28	1574	Unknown	U	-	DT,30						1.1	-9.5	1.1	
165	198.1	11.27	1706	Unknown	U	-	DT,30						1.1	-17.6	1.1	
182	175.1	11.85	1782	Unknown	U	-	DT,30						1.2	-	-1.1	

ID	Model ion	RT	RI	Name	Class	Ident	Analysis	Median (Co: n=4, Mono: n=7/8)						Fold (Co relative to Mono)		
								Day 18		Day 30		Day 42		Day 18	Day 30	Day 42
								TW Mono	TW Co	TW Mono	TW Co	TW Mono	TW Co			
183	372.2	11.88	1785	Unknown	U	-	DT						1.0	-1.6	-1.1	
193	386.2	12.15	1822	Unknown	U	-	DT						1.0	-1.4	-1.2	
205	123.1	12.48	1865	Skel_cell_C074 (Vidoudez)	U	-	DT						1.2	1.3	-1.1	
285	180.1	15.16	2323	Unknown	U	-	DT						1.1	-1.5	1.3	
293	384.2	15.47	2376	Unknown	U	-	30						1.3	-2.5	-1.2	
331	397.4	17.07	2656	Unknown	U	-	DT,30						1.1	-3.8	-1.2	
333	159.1	17.18	2674	Unknown	U	-	30						1.2	-1.9	-1.2	
334	221.1	17.19	2677	Unknown	U	-	DT						1.0	-	-1.1	
361	309.3	18.49	2893	Unknown	U	-	DT						1.7	-4.2	1.0	
367	323.3	19.11	2990	Unknown	U	-	30						1.8	-2.7	-1.0	
377	333.3	19.74	3089	Unknown	U	-	DT						1.5	-6.7	1.1	
15	186.1	6.11	1023	Unknown	U	-	DT,30						-1.9	-	-2.3	
22	156	6.37	1057	Unknown	U	-	DT						-1.0	-	-2.2	
35	146.1	6.80	1113	Unknown	U	-	DT						-1.7	-	108.4	
37	172.1	6.82	1117	Unknown	U	-	DT,30						-2.5	-117.8	-1.5	
53	112.1	7.25	1173	Unknown	U	-	DT,30						-1.1	-	-	
88	159.1	8.60	1352	Unknown	U	-	DT						-1.4	-	-	
175	169	11.64	1754	Unknown	U	-	DT						-1.4	-	-	
176	302.2	11.66	1757	Unknown	U	-	DT,30						-1.1	-7.8	-1.0	
178	133.1	11.73	1766	Unknown	U	-	30						-1.2	-36.3	-1.2	
209	307.2	12.57	1878	Unknown	U	-	DT						-1.3	-1.1	1.1	
260	221.1	14.32	2175	Unknown	U	-	DT						-1.2	-	1.3	
290	180.1	15.35	2355	Unknown	U	-	DT						-1.0	-6.8	1.1	
309	217.1	16.29	2520	Unknown	U	-	DT						-1.4	-1.3	1.0	
310	221.1	16.31	2522	Unknown	U	-	DT,30						-1.1	-	-1.2	
84	127	8.44	1330	Unknown	U	-	DT,30						1.2	5.1	1.9	
85	199.1	8.48	1337	Skel_MEDIA_C097 (Vidoudez)	U	-	DT						1.1	1.1	1.0	
265	265.1	14.52	2211	Skel_Cell_C128_RT14.776 (Vidoudez)	U	?	DT,30						-1.3	1.3	1.1	

ID	Model ion	RT	RI	Name	Class	Ident	Analysis	Median (Co: n=4, Mono: n=7/8)						Fold (Co relative to Mono)		
								Day 18		Day 30		Day 42		Day 18	Day 30	Day 42
								TW Mono	TW Co	TW Mono	TW Co	TW Mono	TW Co			
266	304.9	14.54	2214	Skel_Cell_C128_RT14.776 (Vidoudez)	U	??	30						1.1	1.6	1.2	
267	319.9	14.54	2214	Skel_Cell_C128_RT14.776 (Vidoudez)	U	?	30						1.0	1.3	1.1	
268	265	14.56	2217	Skel_Cell_C128_RT14.776 (Vidoudez)	U	?	DT,30						-1.4	1.3	1.1	
284	170.1	15.14	2319	Unknown	U	-	30						1.3	1.4	1.0	
54	234.1	7.27	1176	EITMS_N12C_ATHR_1480.5_1135EC44_ (GOLM)	U	?	30						-1.3	-5.2	-1.0	
65	248.1	7.81	1248	Unknown	U	-	30						-1.5	-6.4	-1.0	
92	228.1	8.76	1373	Unknown	U	-	30						1.8	-	-1.3	
102	201.1	9.10	1419	EITMS_N12C_ATHR_1442.5_1135EC44_ (GOLM)	U	?	30						-1.2	-1.7	-1.0	
104	228.1	9.14	1424	Unknown	U	-	30						1.4	-43.0	-1.5	
119	228.1	9.67	1494	Unknown	U	-	30						1.1	-4.1	1.0	
222	210.1	12.99	1933	Unknown	U	-	30						-1.3	-	-1.7	
288	146.1	15.26	2340	Unknown	U	-	30						1.2	-1.4	-1.0	
292	204.1	15.44	2372	Unknown	U	-	30						1.2	-2.0	1.3	
295	141.1	15.54	2388	Unknown	U	-	30						1.1	-2.0	-1.1	
316	113.1	16.59	2571	Unknown	U	-	30						1.2	-2.2	-1.1	
318	365.2	16.63	2579	Skel_Cell_C145 (Vidoudez)	U	?	30						-1.1	-3.1	-1.1	
323	371.3	16.78	2605	Unknown	U	-	30						1.1	-7.0	-1.1	
328	159.1	16.99	2641	Unknown	U	-	30						1.3	-3.7	-1.1	
335	186.1	17.22	2681	Unknown	U	-	30						1.1	-1.5	1.0	
343	113.1	17.65	2757	Unknown	U	-	30						1.2	-2.7	-1.0	
384	309.2	21.18	3261	M000000_A329005-101-xxx_NA_3284,76_PRED_VAR5_ALK_NA (GOLM)	U		30						-1.4	-3.6	-1.2	
392	145.1	23.52	3457	Unknown	U	-	30						-1.0	-	-1.1	
403	129.1	26.49	3706	Unknown	U	-	30						-1.1	-8.6	-1.1	
142	224.1	10.55	1610	Unknown	U	-	DT						1.0	-1.1	-1.0	
198	157.1	12.28	1839	Unknown	U	-	DT						1.4	-1.3	-1.1	

ID	Model ion	RT	RI	Name	Class	Ident	Analysis	Median (Co: n=4, Mono: n=7/8)						Fold (Co relative to Mono)		
								Day 18		Day 30		Day 42		Day 18	Day 30	Day 42
								TW Mono	TW Co	TW Mono	TW Co	TW Mono	TW Co			
366	382.4	19.05	2981	Unknown	U	-	DT							-1.0	-1.3	-1.0
3	110	5.33	919	Unknown	U	-	DT							1.3	-3.2	1.4
25	152.1	6.44	1066	Unknown	U	-	DT,30							2.9	-	1.1
90	240.1	8.67	1362	Unknown	U	-	DT,30							-1.0	-	1.0
129	103.1	10.05	1543	Unknown	U	-	DT,30							1.2	-9.9	1.2
133	157	10.23	1568	Unknown	U	-	DT							1.4	-1.0	1.1
138	255.1	10.41	1592	Unknown	U	-	DT,30							1.9	-	1.1
151	157.1	10.80	1643	Unknown	U	-	DT,30							1.2	-	1.1
152	257.1	10.81	1645	Unknown	U	-	DT							1.8	-	1.2
291	167	15.41	2366	Unknown	U	-	DT							1.1	-	1.1
299	255.2	15.77	2429	Unknown	U	-	DT,30							1.1	-	1.2
324	283.3	16.83	2614	M000000_A260006-101- xxx_NA_2604,01_TRUE_VAR5_ALK_D26048 2 (GOLM)	U	?	DT							-	-	1.0
16	225.1	6.13	1025	Unknown	U	-	DT							-	-	-1.4
77	215.1	8.20	1299	Unknown	U	-	DT,30							1.4	-	-1.2
87	258.1	8.58	1349	Unknown	U	-	DT							1.0	-1.4	-1.2
99	217.1	9.00	1405	Unknown	U	-	DT							1.0	-	-1.2
111	217.1	9.35	1452	Unknown	U	-	DT							1.1	-	-1.1
120	245.1	9.69	1496	Unknown	U	-	DT							-	-	-1.5
155	271.1	10.94	1662	Unknown	U	-	DT							-	-	-1.0
179	217.1	11.75	1769	EITTMS_N12C_ATHR_1770.9_1135EC25_ (GOLM)	U	-	DT,30							-1.2	-4.8	-1.1
187	342.1	11.99	1801	Unknown	U	-	DT,30							-1.1	-8.9	-1.7
269	167	14.60	2225	Unknown	U	-	DT							-	-	-1.1
270	148.1	14.62	2228	Unknown	U	-	DT							-	-	-1.6




ID	Model ion	RT	RI	Name	Class	Ident	Analysis	Median (Co: n=4, Mono: n=7/8)						Fold (Co relative to Mono)		
								Day 18		Day 30		Day 42		Day 18	Day 30	Day 42
								TW Mono	TW Co	TW Mono	TW Co	TW Mono	TW Co			
329	204.1	17.02	2647	M000000_A266012-101-xxx_NA_2659,18_PRED_VAR5_ALK_Unkno wn#sst-cgl-122 (GOLM)	U		DT							-1.7	-2.5	-1.2
347	311.3	17.82	2787	M000000_A278013-101-xxx_NA_2788,69_TRUE_VAR5_ALK_D27893 1 (GOLM)	U	?	DT,30							-	-	-1.0
150	333.1	10.76	1638	Unknown	U	-	30							1.0	-9.0	1.1
167	204.1	11.33	1713	Unknown	U	-	30							1.1	-7.4	1.2
168	303.2	11.37	1719	Unknown	U	-	30							1.3	-	-1.0
243	309.2	13.58	2011	Unknown	U	-	30							1.2	-22.6	-1.1
336	195.1	17.23	2684	Unknown	U	-	30							1.1	-	-1.1
359	129.1	18.41	2881	Unknown	U	-	30							1.0	-8.8	-1.4
45	228.1	7.01	1141	Unknown	U	-	30							-1.0	-4.2	-1.1
117	174.1	9.59	1483	Unknown	U	-	30							-1.7	-	-1.1
130	227.1	10.11	1551	Unknown	U	-	30							-1.3	-	-1.0
159	217.1	11.06	1678	Unknown	U	-	30							-2.0	-2.7	1.1
204	205.1	12.45	1861	Unknown	U	-	30							-1.2	-3.6	-1.1
312	221.1	16.37	2534	Unknown	U	-	30							-1.1	-3.3	1.0
350	423.4	17.98	2813	Unknown	U	-	30							-1.3	-4.1	-1.3
352	425.4	18.07	2827	Unknown	U	-	30							-1.2	-6.0	-1.1
356	103.1	18.20	2848	Unknown	U	-	30							-1.1	-5.9	-1.2
28	116.1	6.55	1081	Unknown	U	-	30							1.1	-1.9	1.0
112	185.1	9.40	1457	Unknown	U	-	30							1.3	-	1.1
58	166.1	7.52	1209	Unknown	U	-	30							-1.0	-5.0	-1.2
101	188.1	9.08	1416	Unknown	U	-	30							-1.1	-10.8	-1.4
248	197.1	13.82	2089	Unknown	U	-	30							-1.0	-8.7	-1.2
276	141.1	14.88	2273	Unknown	U	-	30							1.2	-1.9	-1.2
302	239.2	15.84	2441	Unknown	U	-	30							1.1	-1.8	-1.2

ID	Model ion	RT	RI	Name	Class	Ident	Analysis	Median (Co: n=4, Mono: n=7/8)						Fold (Co relative to Mono)		
								Day 18		Day 30		Day 42		Day 18	Day 30	Day 42
								TW Mono	TW Co	TW Mono	TW Co	TW Mono	TW Co			
313	103.1	16.44	2546	Skel_Cell_C145 (Vidoudez)	U	?	30						-1.6	-27.3	-1.2	
332	204.1	17.13	2666	Unknown	U	-	30						-1.0	-2.2	-1.1	
337	204.1	17.34	2702	Unknown	U	-	30						-1.1	-4.5	-1.1	
363	211.2	18.93	2962	Unknown	U	-	30						1.1	-4.6	-1.0	

In case derivatized molecules are detected, the table entry lists their putative parent compounds. Each MST is characterized by **ID**, **model ion**, retention time (**RT**), retention index (**RI**) and its underlying CAP **analysis**. CAP analyses comprised the overall analysis with a-priori grouping by treatment and day (**DT**), with a-priori grouping by treatment (**T**), as well as daywise subset analysis on day 18 (**18**), day 30 (**30**) and day 42 (**42**). Metabolites were identified via libraries. If metabolites were verified with a standard, they are marked with *. “?” indicates a reversed match between 700 and 800, “??” a reversed match between 600 and 700 and “???” indicates cases where the reversed match was ≤ 600 . “” tags metabolites with a match smaller than 600. Class abbreviations: Amine (**A**), alcohol (**Alc**), alkaloid (**Alk**), carboxylic acid (**CA**), complex sugar (**CS**), derivatives of a certain class (**dv.**), hydrocarbons (**HC**), sugar (**S**), sugar alcohol (**S Alc**), sugar acid (**S Acid**), sterol (**St**), terpene (**T**), others (**O**), unknown (**U**). **Vidoudez** refers to an MST code given by the inhouse library, **GOLM** refers to an MST code given by distinct libraries of the Golm Metabolome Database.

S. marinoi

Appendix 52: Heatmap of unknown endometabolite intensities for the species-specific and daywise analysis of *S. marinoi* in interaction with *T. weissflogii*. Medians of MST intensities, normalized to peak sum per sample and subsequently metabolite-wise auto scaled, are represented by a color code ranging from high (yellow) to low intensities (blue). White indicates the absence of the respective MST after data pre-processing. Metabolites are sorted according to classes (separated by black lines) and abundance patterns. Only metabolites significantly correlating with the separation of treatments and treatment per day are shown. The fold change of MST abundance in co-cultivation relative to mono-cultivation is given and coded with a second color code. Black indicates a higher abundance in co-cultivation, grey a higher abundance in mono-cultivation.

ID	Model ion	RT	RI	Name	Class	Ident	Analysis	Median MST intensity						Fold change		
								low  high						UP  DOWN 		
								Median (Co: n=4, Mono: n=8)						Fold (Co relative to Mono)		
								Day 18		Day 30		Day 42		Day 18	Day 30	Day 42
SM Mono	SM Co	SM Mono	SM Co	SM Mono	SM Co	Day 18	Day 30	Day 42								
9	221.1	5.60	955	Unknown	U	-	DT							1.3	-1.5	6.9
22	156	6.37	1057	Unknown	U	-	DT							1.0	-	-
37	172.1	6.82	1117	Unknown	U	-	DT							1.2	1.0	-1.3
45	228.1	7.01	1141	Unknown	U	-	42							1.2	1.2	2.2
63	121.1	7.76	1241	Unknown	U	-	DT							1.1	-1.1	-1.4
75	221.1	8.12	1288	Unknown	U	-	DT							1.0	-	-
103	156.1	9.12	1421	Unknown	U	-	DT							1.1	1.5	-2.4
125	183.1	9.93	1528	Unknown	U	-	42							1.2	-1.1	-1.8
134	206.2	10.28	1574	Unknown	U	-	DT							1.1	1.3	1.0
168	303.2	11.37	1719	Unknown	U	-	42							1.4	3.4	2.1
183	372.2	11.88	1785	Unknown	U	-	18							1.7	1.4	1.0
187	342.1	11.99	1801	Unknown	U	-	DT							1.7	-	-
189	174.1	12.04	1807	Unknown	U	-	DT							1.0	1.6	1.5
276	141.1	14.88	2273	Unknown	U	-	DT							1.1	1.1	1.3
283	204.1	15.12	2315	Unknown	U	-	42							1.1	1.0	-1.5
285	180.1	15.16	2323	Unknown	U	-	DT							1.1	-4.0	-
291	167	15.41	2366	Unknown	U	-	DT,18							1.2	-	1.4
293	384.2	15.47	2376	Unknown	U	-	DT							1.3	-1.3	1.0

ID	Model ion	RT	RI	Name	Class	Ident	Analysis	Median (Co: n=4, Mono: n=8)						Fold (Co relative to Mono)		
								Day 18		Day 30		Day 42		Day 18	Day 30	Day 42
								SM Mono	SM Co	SM Mono	SM Co	SM Mono	SM Co			
301	361.2	15.82	2438	Unknown	U	-	18						3.1	-1.7	3.8	
310	221.1	16.31	2522	Unknown	U	-	DT						1.2	-	-	
334	221.1	17.19	2677	Unknown	U	-	DT						1.0	-	-	
366	382.4	19.05	2981	Unknown	U	-	18						2.8	1.1	-1.9	
367	323.3	19.11	2990	Unknown	U	-	18						7.2	1.6	-	
372	129.1	19.43	3040	Unknown	U	-	T,18						-	-	2.3	
373	382.3	19.44	3042	Unknown	U	-	T,18,42						113.2	5.5	5.4	
374	331.3	19.56	3061	Unknown	U	-	DT,18						1.6	-	2.1	
376	335.3	19.69	3080	Unknown	U	-	18						3.3	1.2	1.7	
377	333.3	19.74	3089	Unknown	U	-	18						-	3.1	1.9	
15	186.1	6.11	1023	Unknown	U	-	DT,18,42						-1.7	-1.4	4.7	
35	146.1	6.80	1113	Unknown	U	-	DT,18,42						-1.3	1.0	2.4	
101	188.1	9.08	1416	Unknown	U	-	DT						-1.0	-	-	
142	224.1	10.55	1610	Unknown	U	-	DT,42						-1.2	-1.2	-1.4	
205	123.1	12.48	1865	Skel_cell_C074 (Vidoudez)	U	-	DT,42						-1.1	-1.4	-3.7	
236	156.1	13.36	1981	Unknown	U	-	DT						-1.2	-1.0	-1.0	
238	156.1	13.43	1991	Unknown	U	-	DT						-1.2	-1.1	1.2	
250	217	13.86	2095	Unknown	U	-	42						-1.0	-1.3	-1.7	
264	156.1	14.50	2206	Unknown	U	-	DT,18						-1.3	1.2	2.1	
288	146.1	15.26	2340	Unknown	U	-	DT						-1.1	1.1	-1.4	
290	180.1	15.35	2355	Unknown	U	-	DT,42						-1.0	-1.3	-2.8	
306	370.2	16.06	2480	Unknown	U	-	DT						-1.3	-1.2	-1.0	
336	195.1	17.23	2684	Unknown	U	-	DT						-1.0	1.3	-	
19	102.1	6.22	1037	Unknown	U	-	42						-	1.5	-	
51	117	7.17	1163	Unknown	U	-	42						1.1	1.5	2.7	
135	220.1	10.29	1576	Unknown	U	-	18						-	1.1	-	
150	333.1	10.76	1638	Unknown	U	-	18						2.8	1.6	1.8	
234	288.1	13.32	1976	Unknown	U	-	DT,42						-	1.0	-	

ID	Model ion	RT	RI	Name	Class	Ident	Analysis	Median (Co: n=4, Mono: n=8)						Fold (Co relative to Mono)		
								Day 18		Day 30		Day 42		Day 18	Day 30	Day 42
								SM Mono	SM Co	SM Mono	SM Co	SM Mono	SM Co			
275	236.2	14.85	2269	Unknown	U	-	DT							1.3	1.6	-1.3
348	236.1	17.84	2791	Unknown	U	-	DT							-	1.1	1.4
54	234.1	7.27	1176	EITTMS_N12C_ATHR_1480.5_1135EC44_(GOLM)	U	?	42							-2.3	-1.4	4.0
65	248.1	7.81	1248	Unknown	U	-	42							1.0	-1.4	6.0
117	174.1	9.59	1483	Unknown	U	-	42							1.1	-1.1	5.1
323	371.3	16.78	2605	Unknown	U	-	DT							-2.4	-1.3	8.6
379	237.1	20.00	3130	Unknown	U	-	42							1.2	-1.0	-1.3
21	158.1	6.33	1052	Unknown	U	-	42							-	-	-
62	299.1	7.73	1236	Unknown	U	-	42							-	-	-
81	217.1	8.36	1320	Unknown	U	-	18							-	4.0	1.5
90	240.1	8.67	1362	Unknown	U	-	DT							5.8	-	1.4
93	160.1	8.78	1376	Unknown	U	-	42							-	-	-
110	172.1	9.32	1447	Unknown	U	-	DT							-	-4.0	1.6
153	204.1	10.90	1657	Unknown	U	-	DT							1.5	-1.1	1.4
166	345.1	11.31	1711	Unknown	U	-	18							1.5	1.0	1.7
174	375.1	11.61	1750	Unknown	U	-	42							1.1	1.1	-
193	386.2	12.15	1822	Unknown	U	-	18,42							1.9	1.2	4.3
243	309.2	13.58	2011	Unknown	U	-	DT							15.5	-	1.1
256	992.9	14.11	2140	Unknown	U	-	42							-1.1	-1.3	-
294	167	15.52	2384	Unknown	U	-	42							-	-	-
299	255.2	15.77	2429	Unknown	U	-	DT,42							-	-	1.5
302	239.2	15.84	2441	Unknown	U	-	DT							1.2	6.4	1.5
309	217.1	16.29	2520	Unknown	U	-	DT							-	1.4	1.2
345	319.2	17.76	2777	Unknown	U	-	DT							-	-1.0	1.1
25	152.1	6.44	1066	Unknown	U	-	DT							-	-	-1.6
30	152.1	6.62	1090	Unknown	U	-	DT							1.4	2.4	-1.0
58	166.1	7.52	1209	Unknown	U	-	42							-	-1.3	-1.5
76	196.1	8.16	1294	Unknown	U	-	42							-1.0	-1.0	-2.2

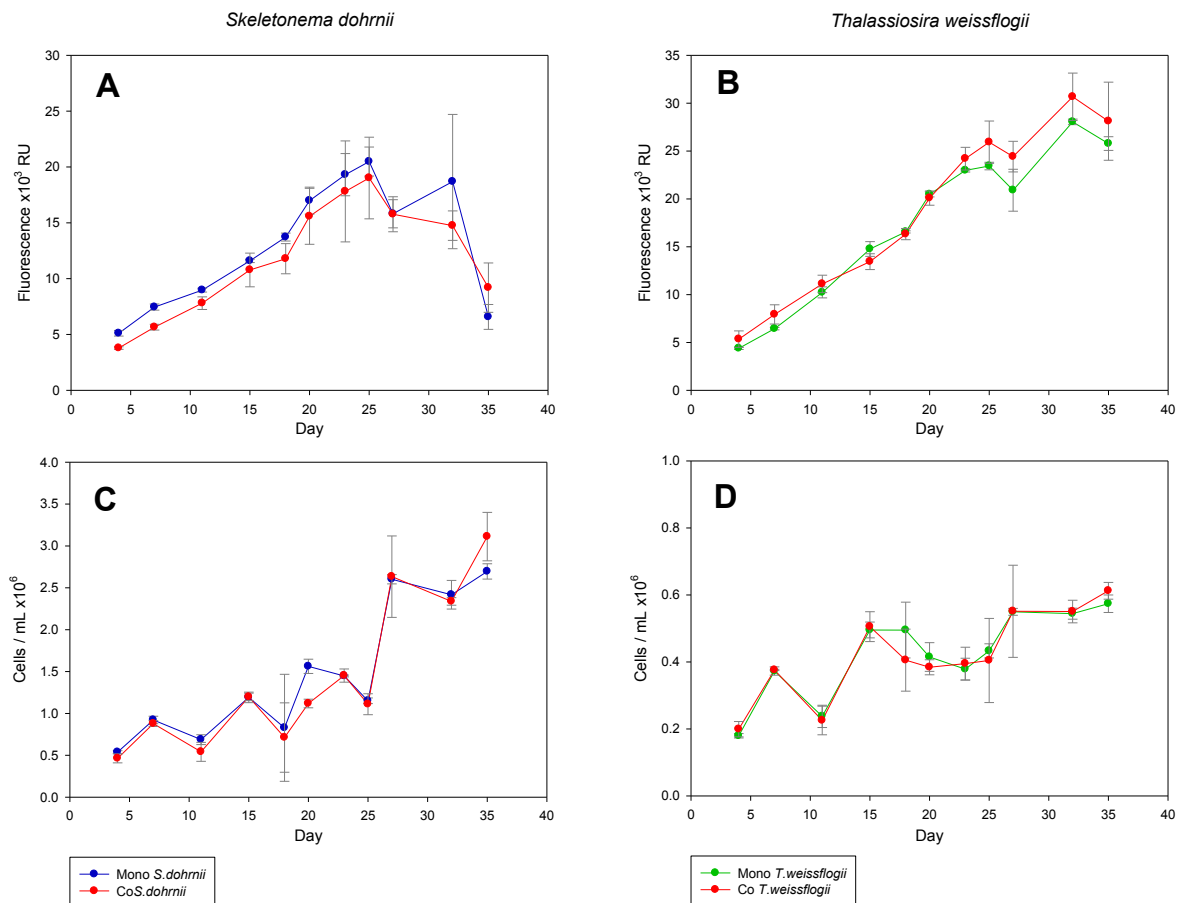
ID	Model ion	RT	RI	Name	Class	Ident	Analysis	Median (Co: n=4, Mono: n=8)						Fold (Co relative to Mono)		
								Day 18		Day 30		Day 42		Day 18	Day 30	Day 42
								SM Mono	SM Co	SM Mono	SM Co	SM Mono	SM Co			
84	127	8.44	1330	Unknown	U	-	18							-1.3	-1.3	-2.3
85	199.1	8.48	1337	Skel_MEDIA_C097 (Vidoudez)	U	-	T,42							-1.2	-1.1	-1.9
119	228.1	9.67	1494	Unknown	U	-	42							1.7	1.1	-3.5
198	157.1	12.28	1839	Unknown	U	-	DT							-1.6	-1.0	-1.2
214	236.2	12.78	1904	Unknown	U	-	42							-1.2	-1.2	-2.9
219	205.1	12.92	1924	Unknown	U	-	DT							1.0	-1.1	-1.2
246	211.2	13.72	2029	Unknown	U	-	DT							1.4	1.2	-1.5
260	221.1	14.32	2175	Unknown	U	-	DT							-1.1	-	-1.1
344	204.1	17.76	2776	Unknown	U	-	DT,42							2.7	-1.0	-2.1
359	129.1	18.41	2881	Unknown	U	-	DT							2.1	-1.0	-1.0

In case derivatized molecules are detected, the table entry lists their putative parent compounds. Each MST is characterized by **ID**, **model ion**, retention time (**RT**), retention index (**RI**) and its underlying CAP **analysis**. CAP analyses comprised the overall analysis with a-priori grouping by treatment and day (**DT**), with a-priori grouping by treatment (**T**), as well as daywise subset analysis on day 18 (**18**), day 30 (**30**) and day 42 (**42**). Metabolites were identified via libraries. If metabolites were verified with a standard, they are marked with *. “?” indicates a reversed match between 700 and 800, “??” a reversed match between 600 and 700 and “???” indicates cases where the reversed match was ≤ 600 . “!” tags metabolites with a match smaller than 600. Class abbreviations: Amine (**A**), alcohol (**Alc**), alkaloid (**Alk**), carboxylic acid (**CA**), complex sugar (**CS**), derivatives of a certain class (**dv.**), hydrocarbons (**HC**), sugar (**S**), sugar alcohol (**S Alc**), sugar acid (**S Acid**), sterol (**St**), terpene (**T**), others (**O**), unknown (**U**). **Vidoudez** refers to an MST code given by the inhouse library, **GOLM** refers to an MST code given by distinct libraries of the Golm Metabolome Database.

7.3 Appendix: Interaction of *T. weissflogii* with *S. dohrnii*

Variations and distinctive features of the current investigation that differed from the previously described design are described in chapter 6.2.7.

7.3.1 Diatom growth



Appendix 53: Diatom growth in the interaction experiment of *T. weissflogii* and *S. dohrnii*.

Graphs A and B show means of chl a (RFU: relative fluorescence units), graphs C and D represent the cell counts (cells / mL). The results for *S. dohrnii* are shown on the left, the results for *T. weissflogii* on the right. The treatment groups are indicated by color: mono-cultivation of *S. dohrnii* (blue, control), mono-cultivation of *T. weissflogii* (green, control) and the co-cultivation of each species (red, interaction). Values are arithmetic means, error bars indicate standard deviation between biological replicates (n=3). Notice different scaling.

To test for significance among the visible differences in chl a fluorescence and cell counts between mono- and co-cultivation of both species over time, a linear mixed modeling approach was chosen (see chapter 6.7.1 for more details). More details for the chosen models, graphs and evaluation can be found in chapter 7.3.5 (Appendix 74 - Appendix 79).

Skeletonema dohrnii

Linear mixed modeling showed a statistically significant difference in the development of cell counts in treatments over time ($F(10,40) = 4.475$, $P = 0.0003$), but no significant differences in chl a fluorescence ($F(10,40) = 1.7792$, $P = 0.0965$).

The growth curves based on chl a fluorescence and cell counts indicated a phase of regular growth between day 4 and 25 (**Appendix 53A, C**), starting with average cell counts of $5.1 \times 10^5 \pm 0.6 \times 10^5$ in *S. dohrnii* cultures. While subsequently the chl a fluorescence declined, the cell counts remained relatively stable around absolute cell counts of $2.6 \times 10^6 \pm 0.3 \times 10^6$ between day 27 and 35. Thus, the experimental time frame only depicted the regular as well as part of the stationary phase of growth. However, as chl a fluorescence declined drastically after day 32, a transition into the declining phase around day 35 was assumed.

In general, the growth curve – based on cell counts – had an unsteady progression with local fluctuations (**Appendix 53C**). This was probably caused by counting inaccuracies among different batches that were counted with temporal delay. However, as the treatments within each sampling day were always counted in the same batch, those fluctuations only concerned the absolute trend over time and not the cell count differences between the treatments within each sampling point. Thus, the general trend of the curve might be impaired, but the investigation of relative difference between the treatments over time was still valid.

Comparing mono- and co-cultivated *S. dohrnii*, the development of both growth parameters over time was very similar. However, linear mixed modeling indicated significant different development of cell counts in both treatments. It was observed that between day 4 and 32, cell counts in co-cultivation showed a trend of decrease up to 28 % (day 20) compared to mono-cultivation (**Appendix 53C**). However, already on day 4, cell counts in co-cultivation were reduced by 14 % compared to mono-cultivation and on eight out of 11 sampling days, these differences were smaller than 15 % relative to mono-cultivation. Thus, cell count differences were considered minor over the course of the experiment and rather characteristic for isolated sampling days than for a temporal trend. The only increase of cell counts in co-cultivation was observed on day 35, with maximum cell counts of $2.7 \times 10^6 \pm 0.9 \times 10^5$ in mono-cultivation and $3.1 \times 10^6 \pm 2.9 \times 10^5$ in co-cultivation. On this day, cell counts were heightened by 15 % in co-cultivation relative to mono-cultivation.

Chl a fluorescence in co-cultivation (**Appendix 53**) also showed a very similar trend of reduced values compared to mono-cultivation. On day 4, chl a fluorescence was already reduced in co-cultivation with values of 3783 ± 114 RFU and 5108 ± 250 RFU in mono-cultivation. Similar to

cell counts, the chl a fluorescence in co-cultivation only exhibited higher values on day 35. This observation was caused by a stronger decline of fluorescence in mono-cultivation between day 32 and 35, compared to co-cultivation, not by an increase of fluorescence relative to previous sampling points.

As both, lower chl a fluorescence and cell counts, already became manifested on day 4 the observation of reduced growth parameter values in co-cultivation was not interpreted as an interaction-induced effect, but rather as the result of slightly different culture states at the onset of the experiment. In general, no meaningful differences between the treatments were found in both growth parameters. The growth of *S. dohrnii* appeared to not be influenced by the presence of *T. weissflogii*.

Thalassiosira weissflogii

Findings for statistical significance in *T. weissflogii* were *vice versa*. While cell counts did not show statistically significant differences ($F(10,40) = 0.648$, $P = 0.7636$), the chl a fluorescence indicated highly significant differences between mono- and co-cultivation ($F(10,40) = 8.269$, $P \leq 0.0001$).

Considering growth dynamics, both chl a fluorescence and cell counts indicated a regular growth phase until day 15. Subsequently, cell counts indicated the stationary phase of growth, while chl a fluorescence further inclined until day 32. The declining phase was not depicted in this experiment, but was assumed to be initiated by declining chl a fluorescence after day 32. At the onset of the experiment, cell numbers and chl a fluorescence were very similar in both treatments with $1.8 \times 10^5 \pm 0.7 \times 10^4$ (4382 ± 118 RFU) in mono-cultivation and $2.0 \times 10^5 \pm 0.2 \times 10^5$ (5349 ± 859 RFU) in co-cultivation. Maximum chl a fluorescence was reached on day 32 and maximum cell counts on day 35 with values of $5.7 \times 10^5 \pm 0.3 \times 10^5$ (28044 ± 291 RFU) in mono-cultivation and $6.1 \times 10^5 \pm 0.2 \times 10^5$ (30667 ± 2482 RFU) co-cultivation. Generally, the growth curve based on *T. weissflogii* cell counts showed similar local fluctuations as described for *S. dohrnii*.

Comparing the treatments, the statistically significant differences in chl a fluorescence between the treatments could be explained by enhanced fluorescence in co-cultivation relative to mono-cultivation between day 23 and 35 (**Appendix 53B**). On average, chl a fluorescence in co-cultivation was enhanced around 11 % during this time, with maximum increase in co-cultivation by 17 % on day 27. No statistically significant differences were found among cell counts.

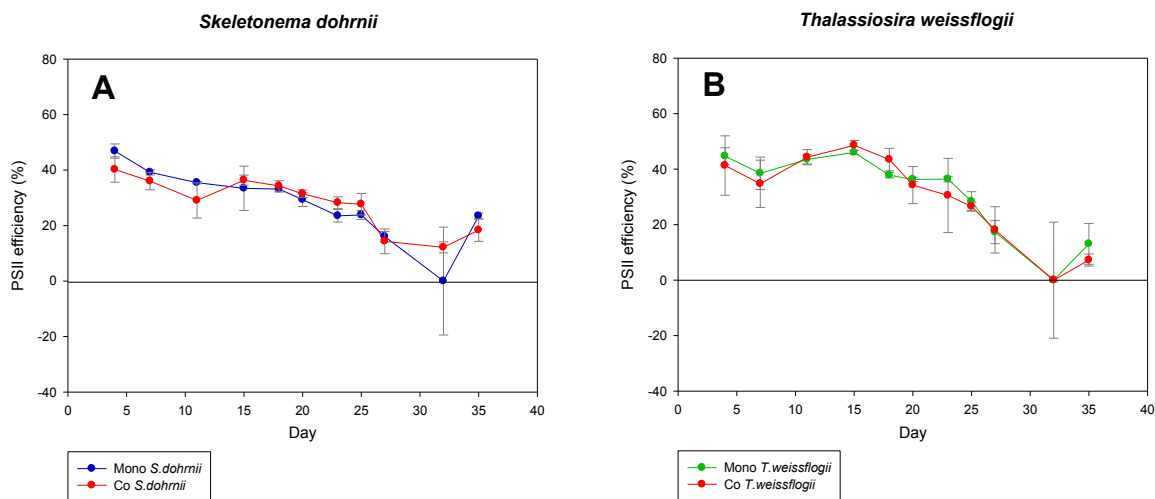
In summary, the chl *a* fluorescence in co-cultivated *T. weissflogii* cultures was enhanced up to 17 % during the stationary phase of growth. These findings were statistically significant. However, no significant differences between the treatments were found among the cell numbers.

7.3.2 Metadata

PSII efficiency

The PSII efficiency of both species was around 45 % in mono-cultivated cultures and around 41 % in co-cultivated cultures on day 5. In case of *S. dohrnii* cultures, PSII efficiency decreased slowly until reaching minimum values of 0 % (in mono-cultivation) and 12 % (in co-cultivation) on day 32 (**Appendix 54**). The PSII efficiency of *T. weissflogii* cultures remained almost constant until day 15, with subsequent drastic decline until values of 0 on day 32. In both species, a minor increase of PSII efficiency was observed between day 32 and 35 of the experiment.

In general, the PSII efficiency dynamic over time was very similar between mono- and co-cultivation within each species. No distinct differences were observed.



Appendix 54: PSII efficiency of the diatoms in the interaction experiment of *T. weissflogii* with *S. dohrnii*.

The figure shows means of PSII efficiency (%) of *S. dohrnii* (graph **A**) and *T. weissflogii* (graph **B**), comparing mono-cultivation in **green** (Mono *T. weissflogii*) and **blue** (Mono *S. dohrnii*) to co-cultivation of the particular diatom in **red**. Error bars indicate standard deviation between biological replicates (mono-cultivation n = 3, co-cultivation n = 3).

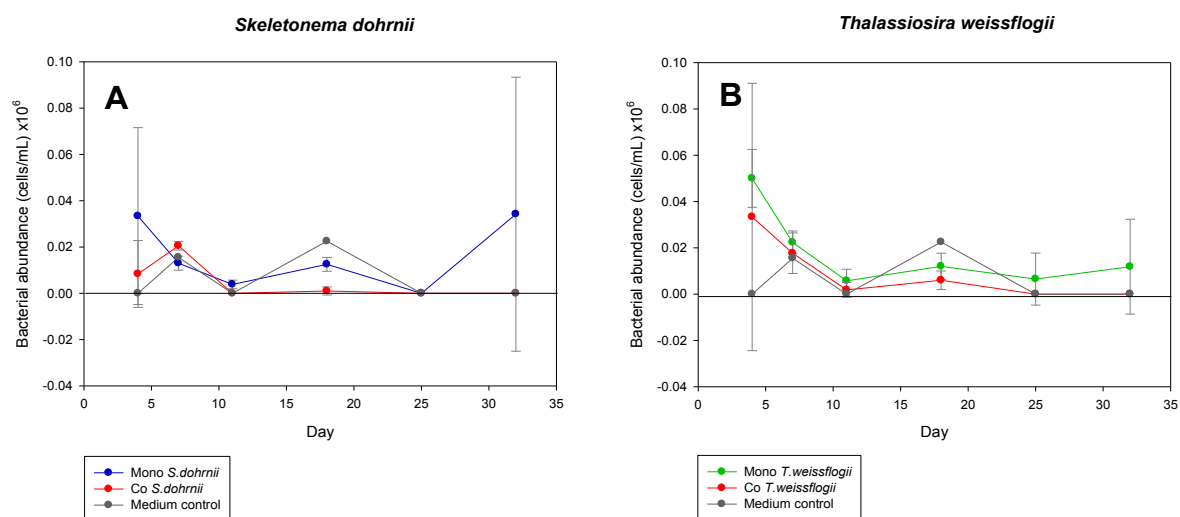
Bacterial abundance

The cultures of both *T. weissflogii* and *S. dohrnii* were ordered axenically, but could not be maintained in the axenic state. A similar problem was described for the investigation of *T. weissflogii* and *S. marinoi* (chapter 3.2.2). Generally, bacterial numbers were highest on the beginning of the interaction experiment and subsequently declined until reaching values of 0 on

day 25 (**Appendix 55**). Interestingly, the bacterial abundance in mono-cultivations of both species showed increased bacterial abundance on day 35, relative to day 25.

For *T. weissflogii* cultures, bacterial numbers were highest on day four of the interaction experiment with average values of 4.4×10^4 bacterial cells / mL. Relative to diatom cell numbers, bacterial abundance made up around 28 % in mono-cultivation and 17 % in co-cultivation. From day 11 on, bacterial abundance reached relative values of ≤ 2.5 % compared to diatom cells.

The bacterial abundance in *S. dohrnii* cultures was highest on day 32 in *S. dohrnii* mono-cultivation with 3.4×10^4 bacterial cells / mL and 2.1×10^4 bacterial cells / mL in co-cultivation on day 7. These absolute values made up 2 % – relative to diatom cells in co-cultivation – and 1 % – relative to diatom cells in mono-cultivation. The medium control exhibited bacterial contaminations on day seven and day 18, indicating possible contaminations on these days.



Appendix 55: Bacterial abundance in the medium experiment of *T. weissflogii* with *S. dohrnii*.

The figure shows means of bacterial abundance (cells / mL) in the cultures of *S. dohrnii* (graph A) and *T. weissflogii* (graph B), comparing mono-cultivation in green (Mono *T. weissflogii*) and blue (Mono *S. dohrnii*) to co-cultivation of the particular diatom in red. Values for the medium control are represented in grey. Error bars indicate standard deviation between biological replicates (n = 3, medium control: n = 1).

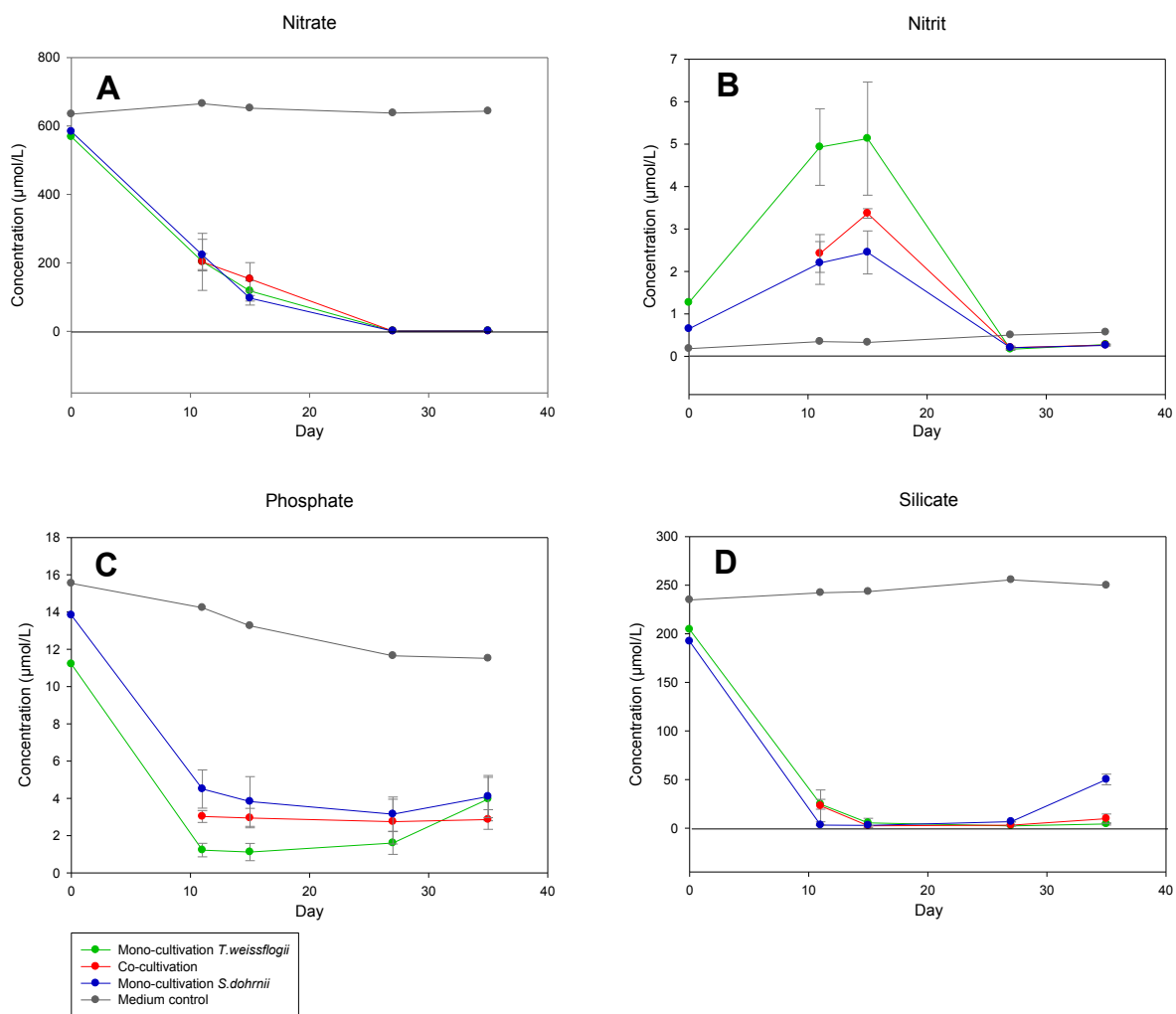
Nutrient levels

The temporal dynamic of nutrient levels showed a very similar trend as the one observed in the interaction experiment of *T. weissflogii* and *S. marinoi* (chapter 3.2.2). Diatom cultures were depleted of nitrate on day 27 and of phosphate and silicate on day 11 after the onset of the experiment (**Appendix 56**). This corresponded to nitrate concentrations of $\leq 1.5 \mu\text{M}$ on day 27, phosphate concentrations of $\leq 4.5 \mu\text{M}$ on day 11 and silicate concentrations of $\leq 7 \mu\text{M}$ on day 15. No distinct differences between the treatments were found in nitrate and silicate levels. Phosphate levels of the co-cultivation group were approximately average values of both mono-cultivation groups. Interestingly, mono-cultivated *S. dohrnii* cultures were characterized by an

increase of available silicate in the medium on day 35 (50 μM). This increase was not found in the other treatment groups.

The nitrite concentrations increased until reaching maximum values on day 15 (2-5 μM) and subsequently declined. Nitrite levels differed between the treatments. They were highest in mono-cultivated *T. weissflogii* cultures (5 μM on day 15) and lowest in mono-cultivated *S. dohrnii* cultures (2 μM on day 15). The nitrite concentration in co-cultivation cultures was in the middle of both mono-cultivation cultures (3 μM on day 15).

Considering the medium control, nutrient levels matched the expected values present in the artificial seawater. However, phosphate levels were slightly elevated up to 15 $\mu\text{mol/L}$ compared to the expected 11 $\mu\text{mol/L}$ present in artificial seawater medium.



Appendix 56: Nutrient levels in the medium experiment of *T. weissflogii* with *S. dohrnii*.

The figure shows means of nitrate (A), nitrite (B), phosphate (C) and silicate (D) concentration (μM). Mono-cultivation of *T. weissflogii* is depicted in green, mono-cultivation of *S. dohrnii* in blue and co-cultivation is colored in red. Values for the medium control are represented in grey. Error bars indicate standard deviation between biological replicates ($n = 3$, medium control: $n = 1$).

7.3.3 Exometabolomic investigation

Data exploration via CAP

Overall Analysis

The investigation of the interaction between *T. weissflogii* and *S. dohrnii* was based on a CAP with 286 MSTs, determined after pre-processing of 27 exometabolomic samples. Similar to the results found for the interaction of *T. weissflogii* and *S. marinoi* (chapter 3.2.3), the first explorative data analysis indicated distinct differences between the exometabolomes of *T. weissflogii* and *S. marinoi*, as well as exometabolomic similarities between samples of mono-cultivated *S. dohrnii* and samples from co-cultivation and an influence of time on treatment-specific exometabolomes.

The PCoA score plot (**Appendix 80**) visualizes a clear separation of exometabolomic samples from mono-cultivated *T. weissflogii* and *S. dohrnii* by principal coordinate axis 1. Samples from co-cultivation were located in close proximity to samples from mono-cultivated *S. dohrnii*, but generally in between samples from both mono-cultivations, indicating shared characteristics with both mono-cultivations.

Additionally, within each treatment a gradual separation of exometabolomic samples by time was realized by both principal coordinate axes. Interestingly, within co-cultivation all three sampling points were forming distinct groups. In both mono-cultivations on the other hand, samples from day 15 seemed distinctly different from samples from day 35, whereas samples from day 27 didn't seem to be distinctly different from the other sampling days. In mono-cultivated *S. dohrnii*, samples from day 27 resembled samples from day 35 and in mono-cultivated *T. weissflogii* samples from day 27 seemed to share traits of both, day 15 and 35.

If each sampling point was considered by itself, within day 15 and day 27 respectively, a clear separation of all three treatments was observed by principal coordinate axis 1. Whereas within day 35, co-cultivation samples and samples from mono-cultivated *S. dohrnii* cultures could not be distinctly separated from each other. Generally, the PCoA indicated strongest separation of treatments on day 15.

These tendencies found in the unconstrained analysis were further investigated via CDA, which confirmed significant influence of time, treatment and a combination of both parameters on exometabolomic samples (trace statistic $P = 0.0001$, **Appendix 57**). According to the misclassification error of 7.41 %, treatment represented the strongest classification, compared to

time (11.11 %) and treatment per day (18.52 %). The cross validation results revealed that the misclassification relating to treatment was caused by time-comprehensive similarities between mono-cultivated *S. dohrnii* and co-cultivation, as investigated by a-priori grouping by treatment (**Appendix 81**), and a rather unspecific character of exometabolomic samples from day 27, as investigated by a-priori grouping by treatment per day (**Appendix 82**).

In summary, the classification according to treatments was more successful than the classification including time. Thus, in this interaction experiment the influence of treatment was bigger than the influence of time. Nevertheless, for the identification of relevant exometabolites, both a-priori grouping by treatment and treatment per day were considered.

Appendix 57: Permutation and cross-validation test results for the CAP analysis of different a-priori groups in the exometabolome analysis of the interaction between *S. dohrnii* and *T. weissflogii*

A-priori grouping by	m	Groups	Trace statistic	δ_1^2	Misclassification error (%)
Day	8	3	1.743 (P = 0.0001)	0.942 (P = 0.0001)	11.11
Treatment	8	3	1.503 (P = 0.0001)	0.951 (P = 0.0001)	7.41
Day & treatment	9	9	5.370 (P = 0.0001)	0.996 (P = 0.0001)	18.52
<u>Subset I: day 15</u> treatment	2	3	1.782 (P = 0.002)	0.999 (P = 0.0006)	0
<u>Subset II: day 27</u> treatment	3	3	1.187 (P = 0.0307)	0.953 (P = 0.0088)	22.22
<u>Subset III: day 35</u> treatment	3	3	1.382 (P = 0.0207)	0.987 (P = 0.0029)	22.22

δ_1^2 being the first squared canonical correlation. *m* represents the number of PCoA axes included in the CAP.

Subset analysis per day

The classification success by treatment is also represented in the score plots of the unconstrained principal coordinate analysis per day (**Appendix 83**). Although on day 27 samples from co-cultivation and *S. dohrnii* mono-cultivation shared close proximity, treatments were clearly separable on day 15 and 35. The daywise CDA confirmed significant differences between the treatments within all three sampling days. The misclassification error was lowest on day 15 (0 %), indicating the best classification (**Appendix 57**). On day 27 and 35, differences between the treatments were also significant, but misclassification errors were 22.22 % (**Appendix 57**). Thus, the findings of the overall analysis were supported.

Identification of exometabolites correlating with relevant a-priori groups

Overall Analysis

For the identification of relevant exometabolites, both analyses a-priori grouping by treatment and treatment per day were considered. The constrained score plot of the CAP with a-priori grouping by treatment showed a clear separation of mono-cultivated *T. weissflogii* samples (located in quadrant I and II) from the other treatments by canonical axis 1 (**Appendix 58A**). Co-cultivation samples (mainly quadrant III) and samples from mono-cultivated *S. dohrnii* (quadrant IV) are separated from each other by canonical axis 2.

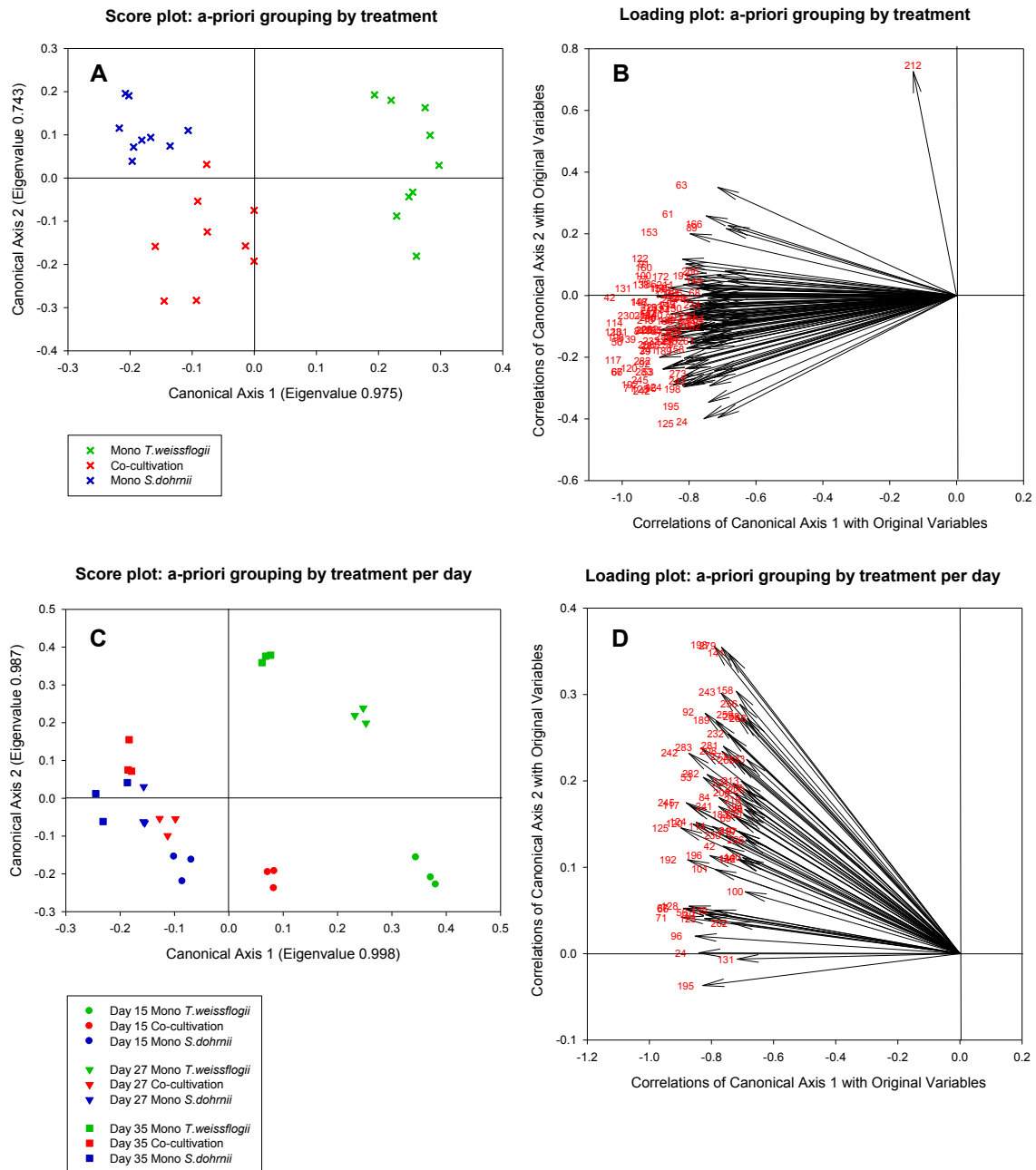
The corresponding loading plot pictures highly correlated metabolites ($|r| \geq 0.6786$, $P \leq 0.0001$), which were all located in quadrant III and IV (**Appendix 58B**). Thus, these metabolites characterized mono-cultivated *S. dohrnii* and samples from co-cultivation. The heatmap (**Appendix 59**) confirms that all those metabolites were most abundant in samples of co-cultivation and mono-cultivated *S. dohrnii*, and least abundant in mono-cultivated *T. weissflogii*.

The score plot of a-priori grouping by treatment per day (**Appendix 58C**) supports the findings of the unconstrained score plot of the PCoA (**Appendix 80** and **Appendix 83**). While canonical axis 1 separated the treatments from each other, canonical axis 2 separated samples by sampling day. Overall, samples from mono-cultivated *T. weissflogii* were distinctly different from samples of mono-cultivated *S. dohrnii*. Again, the exometabolome in co-cultivation seemed similar to the exometabolome of mono-cultivated *S. dohrnii*, as samples share close proximity. Furthermore, the CDA revealed distinct differences between the treatments within each sampling day.

The time-wise separation of samples was strongest for mono-cultivated *T. weissflogii*, followed by the co-cultivation group. Samples from mono-cultivated *S. dohrnii* shared close proximity on all three sampling days. Nevertheless, although samples from day 27 and 35 were hardly distinguishable from each other, samples from day 15 formed a distinct group. According to the constrained score plot, the separation of treatments was strongest on day 15, supporting the implications of the trace statistics and misclassification errors (**Appendix 57**).

The corresponding loading plot shows that all of the highly correlated metabolites ($|r| \geq 0.6786$, $P \leq 0.0001$) characterized the exometabolome in co-cultivation and the exometabolome of mono-cultivated *S. dohrnii* (**Appendix 58D**). Furthermore, it became evident that these metabolites mostly characterized day 27 and 35 of these treatments, as MST vectors were mainly located in quadrant IV. This finding was further supported by the heatmap, which indicates highest

abundance of highly correlated metabolites in said treatments on later stages of the interaction (**Appendix 59**).



Appendix 58: Constrained score and loading plots of exometabolomic samples from the overall analysis of the interaction between *T. weissflogii* and *S. dohrnii*.

The constrained score plots (graph **A**, **C**) visualize significant differences between the sample groups as found via CDA with a-priori groups by treatment (trace statistic $P = 0.0001$, misclassification error of 7.41 % for $m = 8$, graph **A**) and a-priori groups by treatment per day (trace statistic $P = 0.0001$, misclassification error of 18.52 % for $m = 9$, graph **C**). Vectors in the CAP loading plots (graph **B**, **D**) represent metabolites, characterized by their ID (red numbers). Only vectors with a significant correlation coefficient above the critical value of $|r| \geq 0.8983$ ($P \leq 0.001$) are plotted. The direction of the vectors in 2-dimensional space correlates with exometabolomic sample groupings shown in the score plots of the respective analysis.

All highly correlated metabolites of the overall analysis are summarized in a heatmap⁹⁰ (**Appendix 59**). Group A comprises metabolites that were most abundant in co-cultivation on day 15 (A15), day 27 (A27) or day 35 (A35). Group B summarizes metabolites that were least abundant in co-cultivation, compared to both mono-cultivations on day 15 (B15). And potential biomarkers for *S. dohrnii* are clustered in group Sd.

⁹⁰ MST #218 (diphenyl phthalate) was excluded, as it was considered potential contaminations

Appendix 59: Heatmap of exometabolite intensities for the overall analysis of the interaction between *T. weissflogii* and *S. dohrnii*.

Medians of MST intensities, normalized to the external standard ribitol (per sample) and subsequently metabolite-wise auto scaled, are represented by a color code ranging from high (yellow) to low intensities (blue). White indicates the absence of the respective MST after data pre-processing. Metabolites are sorted according to abundance patterns (separated by black lines), class and RI. Only metabolites significantly correlating with the separation of treatments and treatment per day are shown. The fold change of MST abundance in co-cultivation relative to mono-cultivations is given and coded with a second color code. Black indicates a higher abundance in co-cultivation, grey a higher abundance in mono-cultivations.

ID	Model Ion	RT	RI	Name	Class	Ident	Analysis	Metabolite intensity									Fold change				Group			
								Median (n=3)									Fold (Co relative to:)							
								Day 15			Day 27			Day 35			Day 15		Day 27			Day 35		
								SD Mono	Co	TW Mono	SD Mono	Co	TW Mono	SD Mono	Co	TW Mono	SD Mono	TW Mono	SD Mono	TW Mono		SD Mono	TW Mono	
144	122.1	13.04	1951	Unknown	U	-	DT											1.4	-	-1.5	319.1	1.1	3.4	A
219	145.1	16.43	2540	Unknown	U	-	DT											1.7	-	1.4	-	1.2	-	15
94	129.1	11.06	1677	2-Hydroxyhexanedioic acid	CA	?	DT,T											-3.4	-	1.5	-	-1.1	-	A
212	459.3	16.19	2499	Unknown	U	-	DT											-	-	1.5	1.2	-	1.1	27
77	179.1	10.29	1576	4-(2-Hydroxyethyl) phenol	Alc	?	DT											-1.4	2.3	-1.4	3.4	1.1	3.7	A
89	202.1	10.87	1652	Unknown	U	-	DT											-	-	-1.3	17.2	1.2	4.4	
91	250.1	10.95	1662	Unknown	U	-	DT											-1.7	2.3	-1.0	1.9	1.1	1.8	
123	250.2	12.19	1826	Unknown	U	-	DT,T											-1.7	8.7	-1.5	6.6	1.0	4.8	
131	197.1	12.46	1861	Unknown	U	-	DT,T											-1.9	18.1	-1.3	7.4	1.1	5.2	
166	171.1	13.98	2115	Unknown	U	-	DT											-2.9	1.4	-1.3	2.1	1.6	2.5	
68	199.1	9.97	1534	Unknown	U	-	DT											-	-	-3.2	-	-2.7	-	B
104	171.1	11.53	1739	Unknown	U	-	DT											-	-	-8.5	-	-3.0	-	
115	129.1	11.90	1788	Unknown	U	-	DT											-	-	-1.8	-	-1.2	17.4	
151	215.2	13.25	1987	Unknown	U	-	DT											-	-	-2.1	-	-1.7	4.5	
160	170.1	13.63	2054	Unknown	U	-	DT											-	-	-1.4	4.2	-1.4	3.4	
172	260.2	14.29	2169	Unknown	U	-	DT											-	-	-1.4	7.2	-1.5	6.4	
203	159.1	15.78	2427	Unknown	U	-	DT											-	-	-2.0	-	-2.9	-	
234	317.2	16.99	2638	Unknown	U	-	DT											-	-	-3.5	-	-2.6	-	

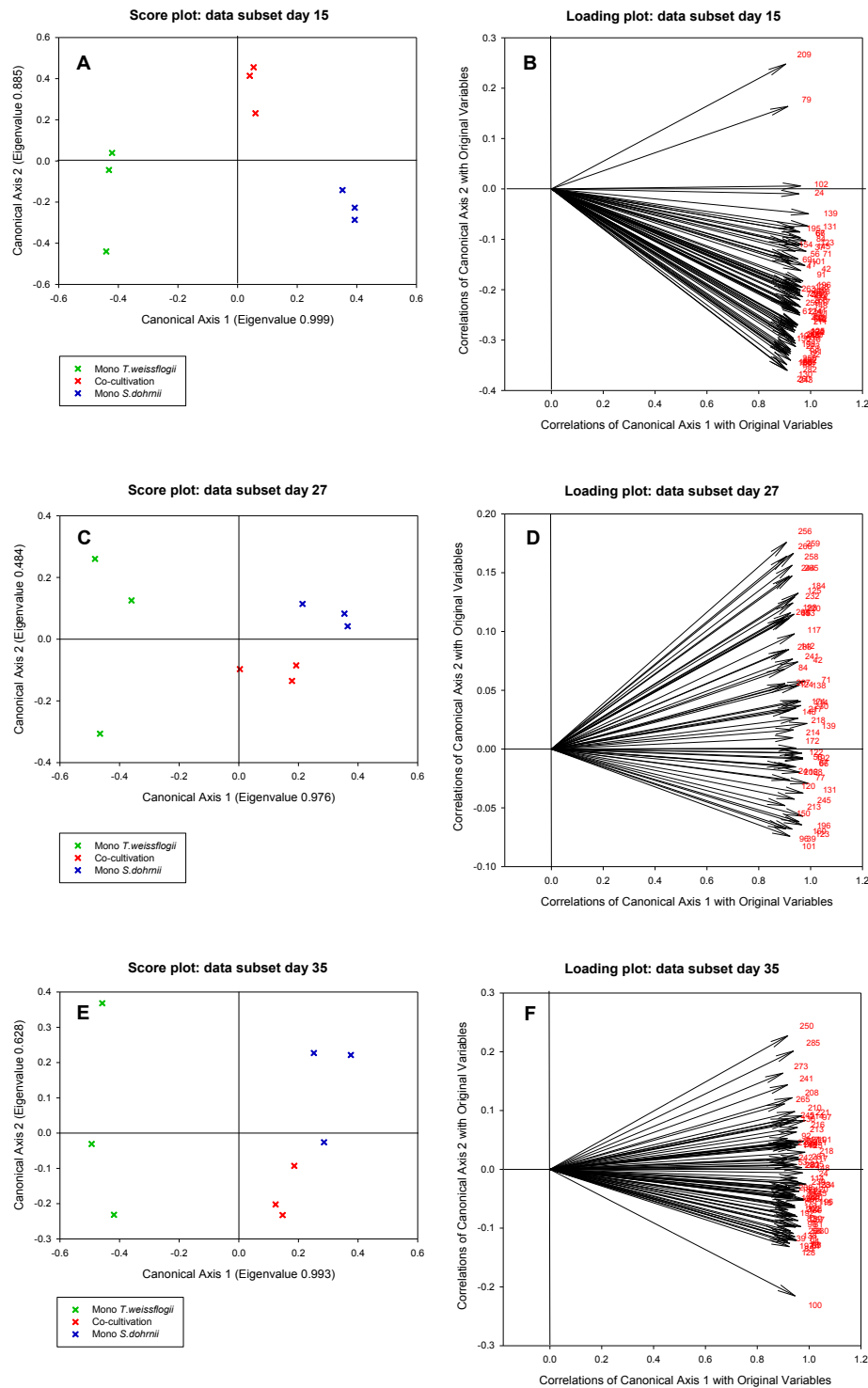
ID	Model Ion	RT	RI	Name	Class	Ident	Analysis	Median (n=3)									Fold (Co relative to:)						Group				
								Day 15			Day 27			Day 35			Day 15		Day 27		Day 35						
								SD Mono	Co	TW Mono	SD Mono	Co	TW Mono	SD Mono	Co	TW Mono	SD Mono	TW Mono	SD Mono	TW Mono	SD Mono	TW Mono					
142	382.2	13.37	2007	Unknown	U	-	DT														-1.8	2.9	-2.3	22.8	-1.7	2.8	
145	199.1	13.44	2020	Unknown	U	-	DT															-3.2	-	-2.1	9.8	-1.8	4.5
148	382.2	13.54	2037	Unknown	U	-	DT,T															-6.0	-	-3.1	-	-2.8	-
150	323.2	14.48	2201	Unknown	U	-	DT															-3.4	-	-1.9	61.5	-2.1	9.9
154	156.1	14.96	2284	Unknown	U	-	DT,T															-3.7	-	-1.7	-	-1.6	8.9
156	156.1	15.07	2303	Unknown	U	-	DT															-3.4	2.2	-2.0	-	-1.5	2.7
158	167.1	15.24	2333	Unknown	U	-	DT,T															-4.7	1.3	-1.9	3.2	-1.4	2.7
174	467.2	15.33	2349	Unknown	U	-	DT															-	-	-1.3	-	-1.1	20.8
180	146.1	7.44	1200	Unknown	U	-	DT,T															-1.7	8.1	-1.7	19.7	-1.3	-
183	171.1	15.37	2355	Unknown	U	-	DT,T															-3.2	-	-1.7	-	-1.5	-
186	171.1	15.53	2384	Unknown	U	-	DT,T															-1.9	-	-1.3	41.8	-1.1	8.6
189	287.2	15.56	2389	Unknown	U	-	DT,T															-2.5	11.8	-1.4	83.7	-1.6	14.0
191	188.1	15.59	2395	Unknown	U	-	DT,T															-3.0	-	-1.8	20.2	-1.2	4.7
192	159.1	15.61	2397	Unknown	U	-	DT,T															-3.3	14.4	-2.2	13.5	-2.7	8.2
195	173.1	15.75	2423	Unknown	U	-	DT,T															-8.0	-	-1.7	-	-1.1	-
196	199.1	15.90	2448	Unknown	U	-	DT,T															-2.5	-	-1.7	327.1	-1.4	19.4
197	467.3	15.98	2462	Unknown	U	-	DT,T															-3.3	-	-2.4	-	-2.1	150.5
202	225.2	16.15	2492	Unknown	U	-	DT															-2.5	23.7	-1.8	7.0	-1.5	11.4
206	211.1	16.21	2502	Unknown	U	-	DT,T															-2.2	-	-1.5	34.5	-1.8	10.0
208	185.1	16.25	2510	Unknown	U	-	DT															-2.9	15.2	-1.8	160.3	-2.0	27.7
210	217.1	9.77	1507	Unknown	U	-	DT															-42.3	-	-1.6	1.3	-1.1	2.7
211	317.2	16.35	2526	Unknown	U	-	DT,T															-6.3	-	-1.9	-	-1.8	25.3
213	254.2	16.45	2544	Unknown	U	-	DT,T															-6.8	-	-2.1	-	-1.3	74.7
214	411.2	16.49	2551	Unknown	U	-	DT,T															-2.5	-	-2.0	-	-1.3	-
217	145.1	16.74	2595	Unknown	U	-	T															-4.8	-	-2.2	83.3	-1.7	11.3
221	148.1	16.92	2626	Unknown	U	-	DT															-24.6	-	-6.7	-	-1.9	-
226	230.1	16.94	2630	Unknown	U	-	DT,T															-3.1	-	-2.3	-	-2.3	50.5

Subset analysis per day

The constrained score plots of the daywise analyses visualize the significant differences between the treatments within each sampling day (**Appendix 60A, C, E**). As previously described, similarities between exometabolomic samples of co-cultivated diatoms and mono-cultivated *S. dohrnii* were obvious, as samples share proximity in multivariate space on all three sampling days. Supporting the findings of the overall analysis, treatments were best separated on day 15, with increasing similarities of co-cultivation and mono-cultivation of *S. dohrnii* towards day 35. The corresponding loading plots visualize highly correlated metabolites ($|r| \geq 0.8983$, $P \leq 0.001$) that mainly characterize the co-cultivation group and mono-cultivated *S. dohrnii* (**Appendix 60B, D, F**).

I summarized all highly correlated metabolites of the daywise analyses in heatmaps⁹¹, depicted in the supplements in chapter 7.3.6 (day 15: **Appendix 84**, day 27: **Appendix 85** and day 35: **Appendix 86**). Metabolites were classified by characteristic intensity patterns, as described in the previous interactions (chapter 2.2.3 and 3.2.3). However, except for MST #85, which was part of group A of the analysis on day 35, as it was most abundant in co-cultivation, all highly correlated metabolites were classified as potential biomarkers for *S. dohrnii*. In comparison with mono-cultivation of *T. weissflogii*, they were much more abundant in mono-cultivated *S. dohrnii* and thus characteristic for the exometabolome of *S. dohrnii*. Accordingly, only one MST of the daywise subset analysis was considered relevant for the interaction.

⁹¹ MST #218 (diphenyl phthalate), #249 and #263 (siloxanes) were excluded, as they were considered potential contaminations



Appendix 60: Constrained score and loading plots of exometabolomic samples from the daywise subset analysis of the interaction between *T. weissflogii* and *S. dohrnii*.

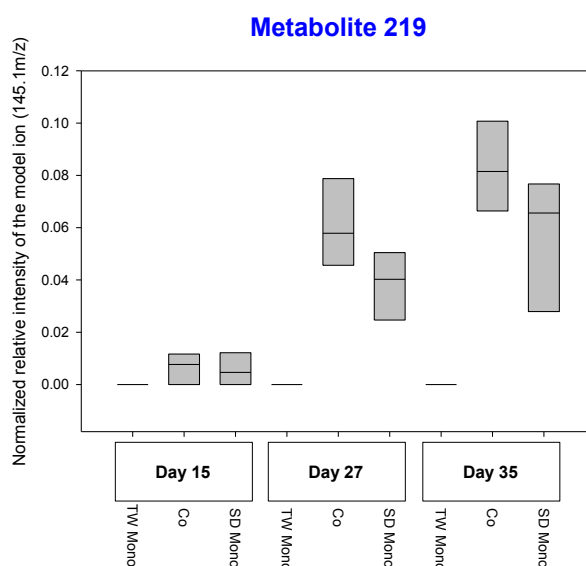
The constrained score plots (graph A, C, E) visualize significant differences between the treatments, as confirmed via CDA for the subset analysis on day 15 (graph A, B), day 27 (graph C, D) and day 35 (graph E, F). These differences between treatments are highly significant (Appendix 57). Vectors in the CAP loading plots (graph B, D, F) represent metabolites, characterized by their ID (red numbers, pooled per group). Only vectors with a significant correlation coefficient above the critical value of $|r| \geq 0.8983$ ($P \leq 0.001$) are plotted. The direction of the vectors in 2-dimensional space correlates with exometabolomic sample groupings shown in the score plots of the respective analysis.

Screening for interaction specific release and/or uptake of potential infochemicals

Along the lines of the screening process explained in chapter 2.2.3, I used only prominent abundance patterns (pattern I, II and III) in the screening process.

Enhanced abundance of exometabolites in co-cultivation - Pattern I:

In total, 11 MSTs matched pattern I, with ten being identified in the overall analysis and one in the subset analyses (day 35) of the exometabolomic investigation. All of them shared the trait of enhanced abundance in co-cultivation, compared to both mono-cultivations. Interestingly, only one MST exhibited pattern I throughout all three sampling days. MST #219 showed 1.7 - fold higher abundance in co-cultivation on day 15, 1.4 - fold on day 27 and 1.2 - fold on day 35. As MST #219 was only present in *S. dohrnii* mono-cultivation but not in mono-cultivation of *T. weissflogii*, it was assumed characteristic for the exometabolome of *S. dohrnii* (**Appendix 61**). I hypothesized that the increased release of this MST by *S. dohrnii* is interaction-induced.



Appendix 61: Potential infochemical with interaction-induced release mechanism throughout all sampling days in the interaction between *T. weissflogii* and *S. dohrnii* (intensity pattern I).

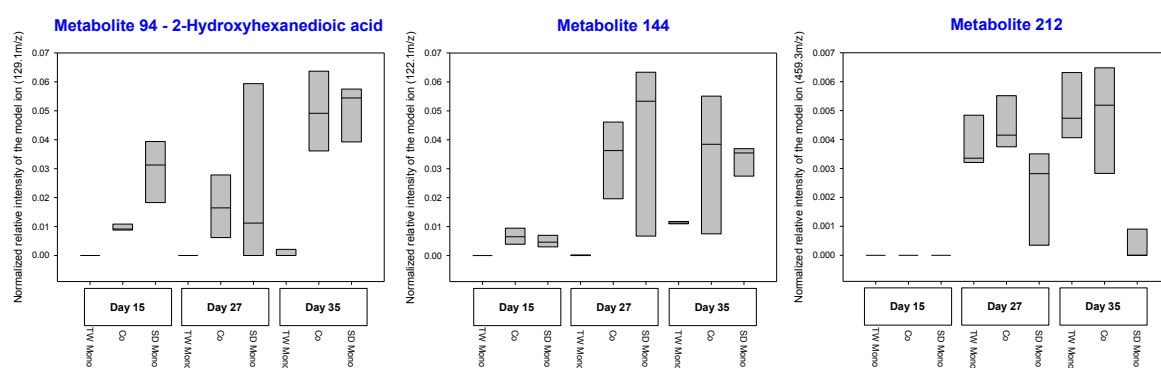
Day 15

The remaining ten metabolites showed enhanced abundance in co-cultivation on specific sampling days. MST #144 exhibited relevance for day 15 and 35. It showed enhanced abundance in co-cultivation on both days. However, pattern I was more dominant on day 15 as the MST abundance in co-cultivation was 1.4 - fold higher on day 15 compared to 1.1 - fold higher abundance on day 35 (relative to *S. dohrnii* mono-cultivation, **Appendix 62**). Furthermore, it seemed more characteristic for the exometabolome of *S. dohrnii* than the exometabolome of *T. weissflogii*, as it was more abundant in the former.

Day 27

Putative 2-hydroxyhexanedioic acid (#94) showed pattern I on day 27 and thus suggested an interaction-induced release on this day. On day 27, it was 1.5 - fold higher abundant in co-cultivation, compared to *S. dohrnii* mono-cultivation (**Appendix 62**). However, as the variance of intensities in mono-cultivation of *S. dohrnii* was comparably high on this day, interpretation of this metabolite as potential biomarker for co-cultivation must be made with care.

The unknown MST #212 was characteristic for later stages of the interaction, as it was only present on day 27 and 35. On both sampling days it exhibited pattern I with between 1.1 – 1.5 - fold enhanced abundance in co-cultivation (**Appendix 62**). Thus, it might indicate late, interaction-induced release mechanisms.



Appendix 62: Exemplary metabolites #94, #144 and #212 with interaction-induced release mechanism on specific sampling days in the interaction between *T. weissflogii* and *S. dohrnii* (intensity pattern I).

Day 35

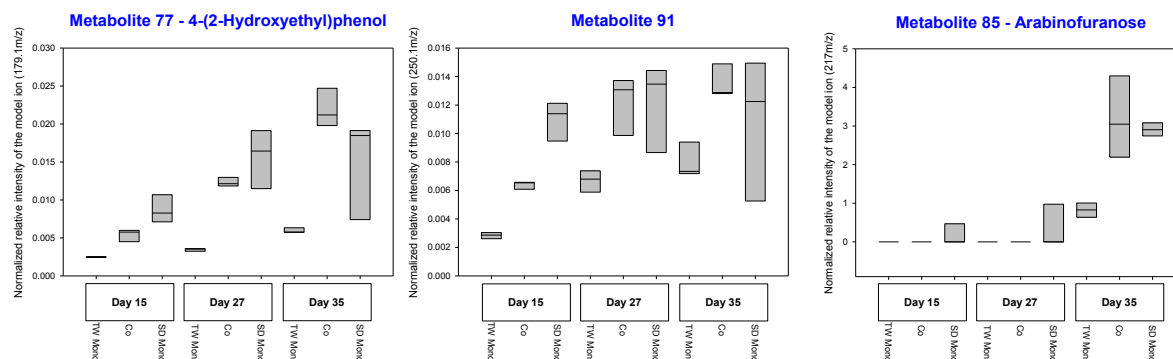
The metabolites #77, #85, #89, #91, #123, #131 and #166 were all correlating with sample differences on day 35. They shared the trait of highest abundance in co-cultivation on this respective day. Except for putative 4-(2-hydroxyethyl)phenol (#77), the identity of the remaining metabolites remained unclear. The intensity dynamics of these metabolites were classified by two categories:

- (1) Metabolites with temporal increase dynamic
- (2) Metabolites characteristic for distinct sampling days

Considering the first category, putative 4-(2-hydroxyethyl)phenol (#77, **Appendix 63**) as well as the metabolites #123 and #131 (**Appendix 87**) showed a temporal increase of abundance in all three treatments respectively. Furthermore, on day 35 the abundance in co-cultivation exceeded the reference value (**Equation 1**), resulting in pattern I. As these metabolites were only remotely abundant in mono-cultivated *T. weissflogii*, they were considered characteristic for the

exometabolome of *S. dohrnii*. Furthermore, metabolite #91 (**Appendix 63**) and #166 (**Appendix 87**) showed the same temporal increase dynamic as previously described.

Within category (2), arabinofuranose #85 (**Appendix 63**) and MST #89 (**Appendix 87**) were found to be mainly abundant on day 35, exhibiting enhanced abundance in co-cultivation on this day.



Appendix 63: Exemplary metabolites #77, #91 and #85 with interaction-induced release mechanism on day 35 and distinct temporal regulation in the interaction between *T. weissflogii* and *S. dohrnii* (intensity pattern I).

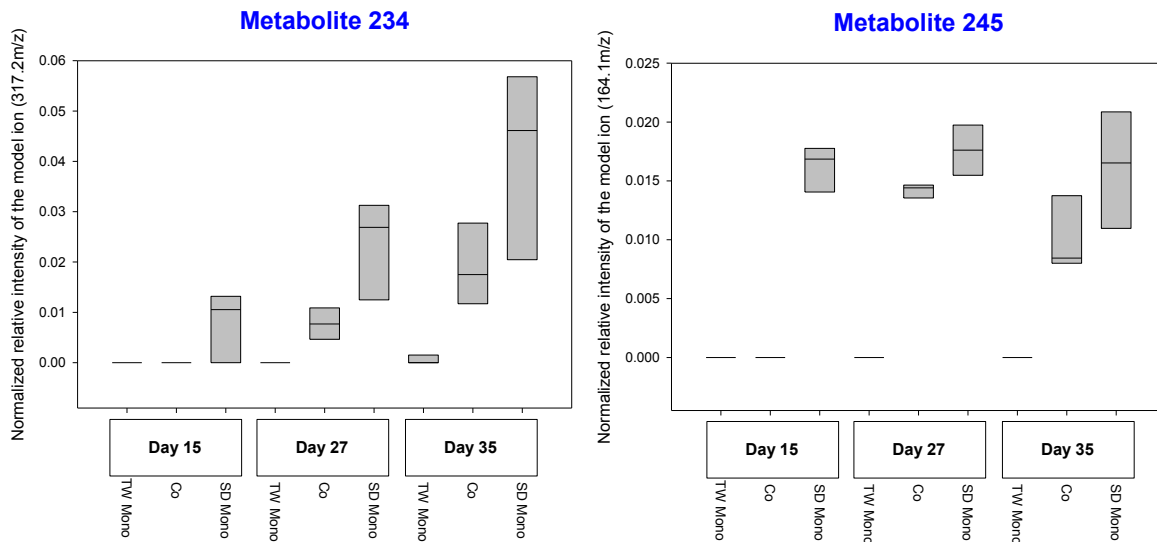
Reduced abundance of exometabolites in co-cultivation - Pattern II / III:

In the context of pattern II / III, I identified 12 metabolites in the overall CAP analysis of the interaction and summarized them in group B15 of the heatmap (**Appendix 59**). An evaluation of the candidate metabolites matching pattern III in the heatmap via boxplots indicated that three MSTs⁹² did indeed show abundance in co-cultivation on the respective day of relevance, which was only masked by the median in the heatmap (**Appendix 59**). As, strictly speaking, these metabolites did not fit pattern III, they were subsequently excluded and visualized in **Appendix 88**. The intensity dynamics across treatments and sampling days of the remaining metabolites are summarized in **Appendix 89** and are exemplarily visualized below.

Among the remaining nine metabolites, all matched pattern II or pattern III on day 15, indicating potential uptake, transformation or reduced release mechanisms at the onset of the interaction. Generally, all of them seemed to characterize the exometabolome of *S. dohrnii*, as they were more abundant in *S. dohrnii* mono-cultivation than in *T. weissflogii* mono-cultivation. Metabolites #68, #104, #151, #203, #234, #244, #246 and #266 shared a temporal increase dynamic. I exemplarily depicted MST #234, representing this group of metabolites (**Appendix 64**).

⁹² Metabolites #115, #160, #172

On the other hand, MST #245 exhibited a different temporal dynamic. Again, this MST was characteristic for the exometabolome of *S. dohrnii*. But between day 15 and 35 the abundance remained relatively stable in *S. dohrnii* mono-cultivation and no distinct temporal increase was visible. Interestingly, this MST was present in the exometabolome of co-cultivated cultures only from day 27 on (**Appendix 64**), exhibiting pattern III on day 15. The identity of all nine metabolites remained unclear.



Appendix 64: Exemplary metabolites #234 and #245 with interaction-induced uptake, transformation or reduced release mechanisms on day 15 in the interaction between *T. weissflogii* and *S. dohrnii* (intensity pattern II / III).

7.3.4 Endometabolomic investigation

After data pre-processing of 53 samples, I obtained 426 metabolites characterizing the endometabolomes on day 15, day 27 and day 35. I performed the analysis strategy as described in the interaction of *T. weissflogii* and *S. costatum* (chapter 2.1.2). The endometabolome of *T. weissflogii* was normalized to a count of 3×10^7 diatom cells, the endometabolome of *S. dohrnii* to a count of 5×10^7 diatom cells.

The metabolomic samples in the interaction investigation of *T. weissflogii* and *S. dohrnii* were normalized to higher cell counts, compared to the investigation of *T. weissflogii* and *S. costatum* (**Table 22**). I discussed possible impacts in chapter 2.5.3.

Data exploration via CAP

A PCoA indicated that time and species affiliation were strong factors influencing the diatom endometabolomes. The unconstrained PCoA score plot (**Appendix 90**) visualizes the separation of species via principal coordinate axis 1 and a gradual separation by time via principal coordinate axis 2. Within each species, samples from day 15 seemed distinctly different from samples of day 27 and 35 as they were forming clear groups in quadrant I (*T. weissflogii*) and IV (*S. dohrnii*). A constrained analysis via CDA confirmed that species and day were the strongest factors influencing sample dissimilarities. The trace statistic indicated that endometabolomes were significantly different between diatom species and sampling days ($P \leq 0.0001$, **Appendix 65**) and the misclassification errors of 0 % for a-priori grouping by species and day indicated a perfect classification of samples.

The investigation of interaction-induced endometabolomic alterations was conducted via a-priori grouping by treatment and treatment per day in a CAP. The trace statistic indicated highly significant differences between treatments and treatments per day. The classification of samples was better, if time was additionally considered besides treatment (misclassification error of 16.98 %) instead of treatment alone (28.30 %, **Appendix 65**).

Appendix 65: Permutation and cross-validation test results for the overall analysis of different a-priori groups in the endometabolome analysis of the interaction between *S. dohrnii* and *T. weissflogii*

A-priori grouping by	m	Groups	Trace statistic	δ_1^2	Misclassification error (%)
Species	1	2	0.921 ($P \leq 0.0001$)	0.921 ($P \leq 0.0001$)	0
Day	6	3	1.840 ($P \leq 0.0001$)	0.967 ($P \leq 0.0001$)	0
Treatment	10	4	1.217 ($P = 0.0003$)	0.989 ($P \leq 0.0001$)	28.30
Day & treatment	10	12	5.300 ($P \leq 0.0001$)	0.998 ($P \leq 0.0001$)	16.98

δ_1^2 being the first squared canonical correlation. m represents the number of PCoA axes included in the CAP.

To eliminate the strong influence of species and day in the CAP, I performed subset analyses within each species and additionally within each species and each sampling day.

Species-specific subset analysis

The unconstrained PCoA score plot of the subset analysis of *T. weissflogii* indicates a strong influence of time on sample similarities as a clear separation of sampling days by both principal coordinate axis 1 and 2 was apparent (**Appendix 91A**). Samples of day 15 were located in quadrant I and II, samples from day 27 mainly in quadrant IV and from day 35 mainly in quadrant III. No clear separation of treatments, neither within each sampling day nor throughout all days, was visible in the 2D score plot.

The constrained analysis via CDA confirmed both, highly significant differences in diatom endometabolomes due to time and among treatments per day ($P \leq 0.0001$, **Appendix 66**). However, the classification success by sampling day was higher (misclassification error 0 %, **Appendix 66**), compared to treatment per day (misclassification error 3.70 %, **Appendix 66**). There were no significant differences between treatments independent of time (**Appendix 66**).

In the subset analysis of *S. dohrnii*, I found similar results. The unconstrained score plot of the PCoA indicated a separation of samples via principal coordinate axis 1, although samples on day 27 and 35 shared close proximity. The strong influence of time on sample similarities was confirmed via CDA, indicating significant differences between sampling days ($P \leq 0.0001$) and a misclassification error of 0 % (**Appendix 66**). Although no clear separation of treatments was visible in the PCoA score plot (**Appendix 91**), the CDA indicated significant differences between treatments per day ($P = 0.0001$, misclassification error 7.69 %, **Appendix 66**). As with the subset analysis of *T. weissflogii*, no significant differences were found among time-independent treatments.

Generally, the species-specific subset analysis revealed time and treatment per day as strong grouping factors, significantly influencing sample dissimilarities.

Appendix 66: Permutation and cross-validation test results for the species-specific subset analysis of different a-priori groups in the endometabolome analysis of the interaction between *S. dohrnii* and *T. weissflogii*

A-priori grouping by	m	Groups	Trace statistic	δ_1^2	Misclassification error (%)
<i>T. weissflogii</i> : day	3	3	1.826 (P ≤ 0.0001)	0.976 (P ≤ 0.0001)	0
<i>T. weissflogii</i> : treatment	11	2	0.623 (P = 0.0903)	0.623 (P = 0.0903)	3.70
<i>T. weissflogii</i> : day & treatment	12	6	3.499 (P ≤ 0.0001)	0.995 (P ≤ 0.0001)	3.70
<i>S. dohrnii</i> : day	3	3	1.891 (P ≤ 0.0001)	0.992 (P ≤ 0.0001)	0
<i>S. dohrnii</i> : treatment	8	2	0.300 (P = 0.6002)	0.300 (P = 0.6002)	15.39
<i>S. dohrnii</i> : day & treatment	6	6	3.004 (P = 0.0001)	0.998 (P = 0.0002)	7.69

δ_1^2 being the first squared canonical correlation. *m* represents the number of PCoA axes included in the CAP.

Daywise subset analysis per species

The daywise subset analysis per species revealed that treatments were significantly different on day 35 in *T. weissflogii* and on day 15 in *S. dohrnii* (**Appendix 67**). Although no distinct sample grouping by treatment was observed in the unconstrained PCoA score plots (**Appendix 92**), the separation of treatments by canonical axis 1 becomes apparent in the constrained score plots (**Appendix 69**, **Appendix 72**). Within the remaining sampling days per species, no significant endometabolomic differences between the treatments were obtained.

Appendix 67: Permutation and cross-validation test results for the species-specific and daywise subset analysis of different a-priori groups in the endometabolome analysis of the interaction between *S. dohrnii* and *T. weissflogii*

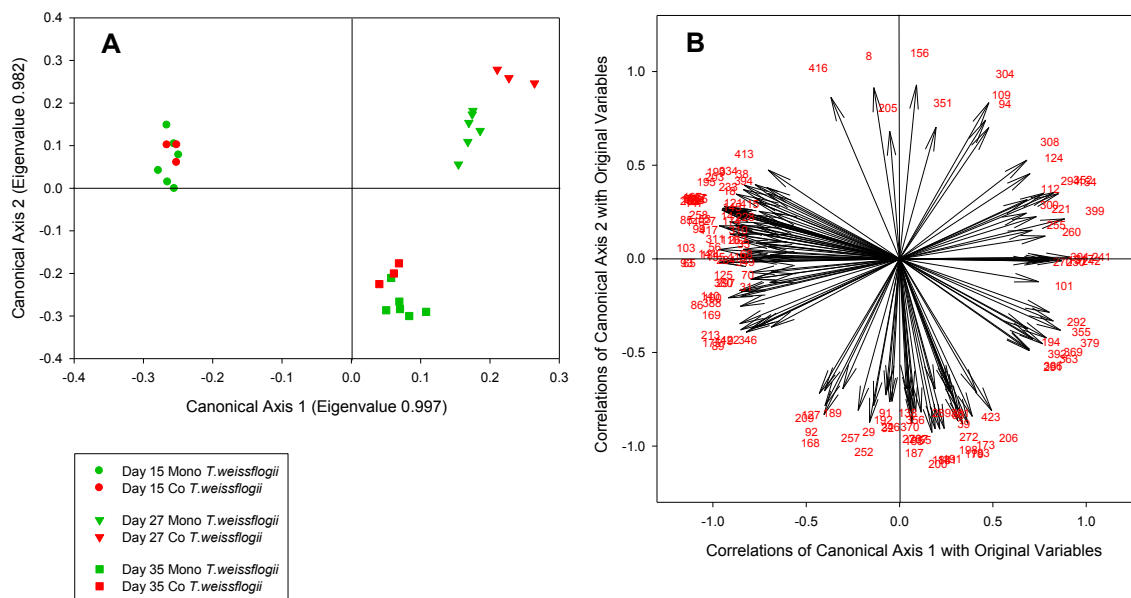
A-priori grouping by	m	Groups	Trace statistic	δ_1^2	Misclassification error (%)
<i>T. weissflogii</i> : day 15	7	2	0.978 (P = 0.3983)	0.978 (P = 0.3983)	0
<i>T. weissflogii</i> : day 27	4	2	0.703 (P = 0.4045)	0.703 (P = 0.4045)	0
<i>T. weissflogii</i> : day 35	6	2	0.980 (P ≤ 0.0001)	0.980 (P ≤ 0.0001)	0
<i>S. dohrnii</i> : day 15	5	2	0.976 (P ≤ 0.0001)	0.976 (P ≤ 0.0001)	11.11
<i>S. dohrnii</i> : day 27	3	2	0.783 (P = 0.1022)	0.783 (P = 0.1022)	11.11
<i>S. dohrnii</i> : day 35	4	2	0.841 (P = 0.0982)	0.841 (P = 0.0982)	0

δ_1^2 being the first squared canonical correlation. *m* represents the number of PCoA axes included in the CAP.

Identification of metabolites correlating with relevant a-priori groups

T. weissflogii

The score and loading plot of the constrained analysis (**Appendix 68**) summarize the results of the species-specific CDA analysis for *T. weissflogii*. As already indicated by the trace statistic (**Appendix 66**), sample separation in the constrained score plot (**Appendix 68A**) was influenced by time and treatment, as shown by a-priori grouping by treatment per day. All samples of day 15 are located in quadrant IV, those of day 27 in quadrant I and of day 35 in quadrant II. Within day 35, canonical axis 2 separates the treatments from each other, forming gradual sample groups with overlap of samples from mono- and co-cultivation. Within day 27 a distinct separation by canonical axis 2 is visible. And within day 15 no clear separation of samples is apparent. According to findings of the CAP trace statistic, only the differences between treatments on day 35 were statistically significant (as shown in the daywise analysis).



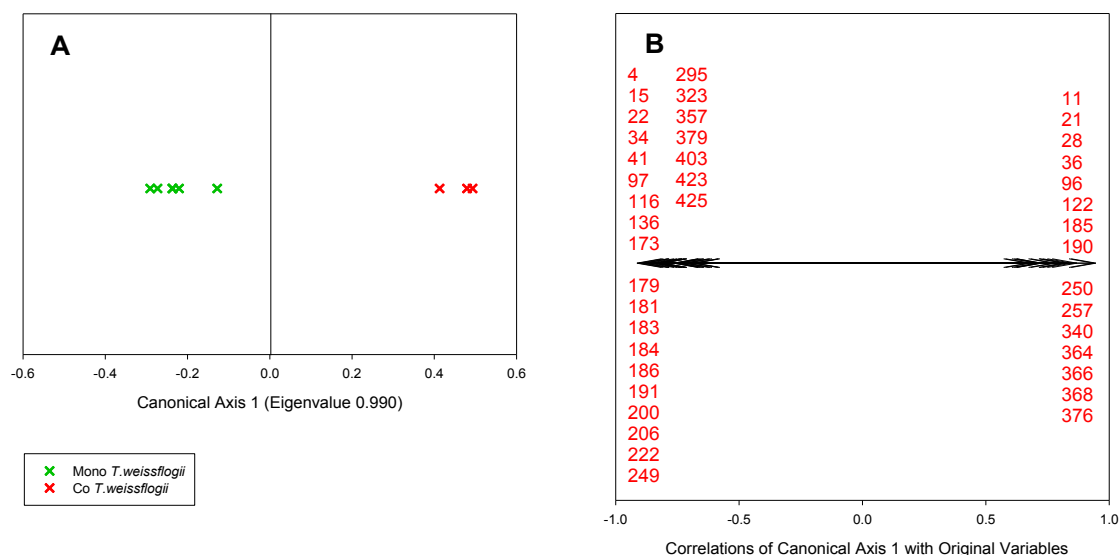
Appendix 68: Constrained score and loading plots of endometabolomic samples from *T. weissflogii* in a species-specific subset analysis of the interaction between *T. weissflogii* and *S. dohrnii*.

The constrained score plot visualizes significant differences between the sample groups as found via CDA with a-priori groups by treatment per day (trace statistic $P \leq 0.0001$, misclassification error of 3.70 % for $m = 12$, graph A). Vectors in the CAP loading plot (graph B) represent metabolites, characterized by their ID (red numbers). Only vectors with a significant correlation coefficient above the critical value of $|r| \geq 0.6786$ ($P \leq 0.0001$) are plotted. The direction of the vectors in 2-dimensional space correlates with endometabolomic sample groupings shown in the score plot.

The corresponding loading plot visualizes 135 highly correlated MSTs ($|r| \geq 0.6786$, $P \leq 0.0001$, **Appendix 68B**). A multitude of those metabolites were correlating with sampling day 15 and 35, as they point towards the location of respective sample groups in the corresponding score plot

(**Appendix 68 A**). While less metabolites were characteristic for day 27, some indicate shared relevance for day 27 and 35 as well as day 15 and 27.

The results of the daywise subset analysis per species are summarized in **Appendix 67**. The score plot (**Appendix 69A**) visualizes distinct differences between the treatments on day 35, as already indicated via significant trace statistic (**Appendix 67**). The corresponding loading plot shows all highly correlated metabolites (of $|r| \geq 0.6664$, $P \leq 0.05$, **Appendix 69B**), with the majority of vectors characterizing mono-cultivated *T. weissflogii*.



Appendix 69: Constrained score and loading plots of endometabolomic samples from *T. weissflogii* in a daywise subset analysis on day 35 of the interaction between *T. weissflogii* and *S. dohrnii*.

The constrained score plot (graph **A**) visualizes significant differences between the treatments, as confirmed via CDA for the subset analysis on day 35. These differences between treatments are highly significant (trace statistic $P \leq 0.0001$, misclassification error of 0 % for $m = 6$). Vectors in the CAP loading plot (graph **B**) represent metabolites, characterized by their ID (red numbers, pooled per group). Only vectors with a significant correlation coefficient above the critical value of $|r| \geq 0.6664$ ($P \leq 0.05$) are plotted. The direction of the vectors in 2-dimensional space correlates with endometabolomic sample groupings shown in the score plot.

In total, I summarized 162 highly correlated metabolites⁹³ of the CAP analysis of *T. weissflogii* endometabolomes (as previously described) in a heatmap (**Appendix 70**). To facilitate the interpretation, I categorized the heatmap by metabolite classes and within each class by MST ID. It is important to know that I considered all metabolites identified by the daywise analyses relevant for the separation of treatments within the respective day of the analysis. I summarized all metabolites of unknown identity in **Appendix 93**.

⁹³ Excluding dodecamethylpentasiloxane (#34 and #38) and n – dotriacontane (#380), as they represent potential contaminations and relicts of the RI-mix.

As described in the analysis of the interaction between *T. weissflogii* and *S. marinoi* (chapter 3.2.4), I only considered metabolites relevantly up- or downregulated in co-cultivation, if intensity differences exceeded 30 %⁹⁴. Thus, I set the focus on relevant changes in endometabolite levels. Subsequently, I discuss the highly correlated metabolites by compound class.

Amines seemed to characterize day 35 of the interaction, as they showed highest abundance on this sampling day. On this day, urea (#55) and putrescine (#91) were up to 1.6 - fold more abundant in co-cultivation. Furthermore, putrescine was 1.3 - fold upregulated on day 15 as well. On the other hand, putative hypotaurine (#138) was 2.2 - fold more abundant in co-cultivation on day 15, but downregulated on day 35 with 2.2 - fold higher intensities in mono-cultivation. Interestingly, on day 27, all identified amines were between 1.6 - and 7.2 - fold more abundant in mono-cultivation.

I identified three amino acids, all of them characterizing day 15 as they were most abundant on this day. While on day 15 no relevant differences in MST levels were detected, day 27 was shaped by strong downregulation of amino acids. Valine (#14) was 5 - fold, isoleucine (#33) 10.7 - fold more abundant in mono-cultivation and proline (#68) was completely absent in co-cultivation. On day 35, valine and isoleucine (#33, #36) were up to 7.1 - fold upregulated in co-cultivation. Note that isoleucine is also represented by MST #36, which shows a different regulation than tag #33 on day 27, being 1.6 - fold upregulated compared to mono-cultivation.

Among alcohols, the picture was more diverse. While 1,3 - propanediol (#8) and 3 - methylphenol (#31) were more present in early stages of the interaction, putative glycerol (#22) and putative cycloheptadecanol (#270) were most abundant on day 27. The class of alcohols is characterized by an upregulation of putative cycloheptadecanol and 1,3 - propanediol in co-cultivation on day 27 and the absence of 3 - methylphenol on day 35, otherwise MST levels were indifferent among treatments.

I identified two carboxylic acids. 3 - Hydroxypropanoic acid (#27, #28) was abundant on all three sampling days, with a tendency of upregulation in co-cultivation on day 15 and 35 (up to 1.6 - fold) and downregulation on day 27 (4.7 - fold higher abundance in mono-cultivation), whereas citric acid (#187) was most abundant on day 35 of the interaction. However, citric acid was only relevantly regulated on day 15, with lower abundance in co-cultivation, compared to 1.6 - fold higher values in mono-cultivation. Interestingly, citric acid was absent in the endometabolome of *S. dohrnii* on day 27. The carboxylic acid derivative 2,3-dihydroxypropyl

⁹⁴ as identified via fold changes $|x| \geq 1.3$

myristate (#295) shows increasing abundance over time, with reduced abundance in co-cultivation on day 27 and 35.

The majority of MSTs within the class of complex sugars and their derivatives were most abundant on day 15. On this day, only two putative trisaccharides (#310, #384) were 1.3 - fold upregulated. Melibiose (#351), melezitose (#399) and the derivative galactinol (#355, #363) were most abundant on day 27 and up to 1.8 - fold upregulated in co-cultivation on this day. Furthermore, one disaccharide (#413) was among the relevantly regulated complex sugars, as it was most abundant on day 15, with similar MST levels in both treatments, but showed reduced abundance in co-cultivation on day 27 and 35. All other intensity differences between treatments did not exceed the 30 % threshold.

Fatty acids and derivatives seemed to be only negligibly affected by treatment. Metabolite levels were very similar in mono- and co-cultivation. However, putative stearic acid (#272) and the derivative putative ethyl icosapentaenoate (#317) were downregulated in co-cultivation on day 35. Furthermore, linolenic acid (#228) was 1.5 - fold more abundant in mono-cultivation on day 27. While linoleic acid was characteristic for day 15, the other two metabolites characterized day 27 and 35 of the interaction.

Most identified sugars were characteristic for early stages of the interaction (day 15 and 27), as they showed highest abundance on these days. The only exceptions were myo-inositol (#230, #241, and #242) and erythrose (#136), which were most abundant during later growth phases (day 27 and 35). Among sugars, only five metabolites were relevantly regulated: pentafuranose #140 was downregulated in co-cultivation on day 15, putative pentofuranose #135 on day 27, putative ribofuranose (#141) was downregulated on day 27 with 18.5 - fold higher abundance in mono-cultivation, galactofuranose (#222) was downregulated on day 27 and 35, erythrose (#136) was downregulated in co-cultivation throughout all three sampling points and the MST #241, representing myo-inositol, was 1.5 - fold upregulated on day 27.

Sugar acids exhibited a trend of downregulation in co-cultivation on day 27 and 35 and did not show any relevant intensity differences between the treatments on day 15. All of them were either characteristic for day 15 or day 35. The only relevantly upregulated sugar acid was gluconic acid (#221), which was 1.5 - fold upregulated on day 27. Among the three identified sugar alcohols, only (1r,2r,3r,4r,5r,6r)-1,2,3,4,5,6-cyclohexanehexol (#260) was relevantly upregulated, as it was 1.4 - fold more abundant in co-cultivation on day 27. Interestingly, the derivative putative uridine (#297) was most abundant on day 15 and 1.5 - fold upregulated in co-cultivation.

The sterols were generally characterizing later stages of the interaction, as they were most abundant on day 27 and 35. It is striking that on day 27 all identified sterols, ergosta-5,24-dien-3-yl acetate (#366), putative (3 β ,20R,24R)-stigmast-5-en-3-yl acetate (#376), campesterol (#386) and fucosterol (#392), were relevantly upregulated in co-cultivation. Furthermore, ergosta-5,24-dien-3-yl acetate (#366) was upregulated on day 15. Ergosta-5,24-dien-3-yl acetate (#366) was identified in the daywise subset analysis on day 35 but did not show any altered metabolite levels due to the treatments on this day.

Among terpenes, only phytol was identified. It was most abundant on day 15, with a 1.3 - fold upregulation in co-cultivation). However, on day 27 phytol was downregulated in co-cultivation with 1.7 - fold higher abundance in mono-cultivation. One hydrocarbon 3-octadecyne (#203) was identified, but did not exhibit any relevant treatment-dependent regulation. The alkaloid 2-pyridinol (#4), which characterized later stages of diatom growth, was 1.3 - fold upregulated in co-cultivation on day 27, compared to mono-cultivation, but did not show relevant regulation otherwise.

In the class of “others”, 14-heptacosanone (#356) characterized late stages of the interaction and was downregulated in co-cultivation on day 27 and 35 with up to 1.9 - fold higher abundance in mono-cultivation. Tocopherol (#379) was 1.5 - fold more abundant in mono-cultivation on day 35 and also characteristic for this day. Tocopherol quinone (#388) on the other hand was most abundant on day 15, but not relevantly regulated on this day. However, on day 27 and 35 it was more abundant in co-cultivation (2.1 - fold on day 35). 2-Hexadecyloxirane (#195) and hexadecanal (#199) were characteristic for day 15, but only relevantly downregulated in co-cultivation on day 27.

In total, 98 of the 162 metabolites could not be identified and remained unknown. However, seven MSTs were documented in the GOLM and six in the in-house library (Vidoudez). No overall trend of these metabolites was observed.

ID	Model ion	RT	RI	Name	Class	Ident	Analysis	Median (Co: n=3, Mono: n=6)						Fold (Co relative to Mono)		
								Day 15		Day 27		Day 35		Day 15	Day 27	Day 35
								Mono	Co	Mono	Co	Mono	Co			
295	343.3	15.75	2424	2,3-Dihydroxypropyl myristate	CA dv.		35							-1.1	-1.7	-1.4
310	217.1	16.27	2516	Trisaccharide (Vidoudez)	CS	?	DT							1.3	1.2	1.1
311	217.1	16.31	2522	Trisaccharide (Vidoudez)	CS	?	DT							1.1	-	1.1
346	361.2	17.69	2763	Maltose	CS	*	DT							1.1	1.1	-1.2
351	204.1	18.07	2827	Melibiose	CS		DT							1.1	1.3	1.0
384	217.1	20.80	3230	Trisaccharide (Vidoudez)	CS	?	DT							1.3	-	-
399	361.2	22.61	3382	Melezitose	CS	??	DT							-	1.8	1.3
413	217.1	24.34	3527	Disaccharide (Vidoudez)	CS		DT							1.1	-1.3	-
416	173.1	24.72	3559	Maltotriose	CS		DT							1.1	1.2	1.9
417	361.2	24.75	3561	Maltotriose	CS		DT							1.1	1.2	1.1
422	273.1	25.59	3632	Maltotriose	CS		DT							1.1	-	1.1
355	204.1	18.29	2862	Galactinol	CS dv.		DT							1.0	1.8	1.0
363	204.1	18.95	2965	Galactinol	CS dv.		DT							1.1	1.7	1.1
272	199.1	14.92	2280	Octadecanoic acid (Stearic acid)	FA	?	DT							1.0	-1.1	-1.3
228	107.1	13.47	2027	Linolenic acid	FA	*	DT							-1.1	-1.5	-1.1
168	143.1	11.49	1734	Methyl myristate	FA dv.		DT							-1.1	-	-1.1
207	236.2	12.78	1906	Methyl (11E)-11-hexadecenoate	FA dv.		DT							-1.0	-1.2	-1.0
262	180.1	14.59	2222	Methyl-5,8,11,14,17-icosapentaenoate	FA dv.	?	DT							-1.2	1.2	-1.2
317	113.1	16.59	2572	Ethyl icosapentaenoate	FA dv.	??	DT							-1.2	1.1	-1.3
203	123.1	12.61	1882	3-Octadecyne	HC	?	DT							1.1	-1.2	1.1
195	123.1	12.31	1842	2-Hexadecyloxirane	O		DT							1.1	-1.5	-1.0
199	123.1	12.47	1865	Hexadecanal	O	?	DT							1.0	-1.3	1.1
356	211.2	18.35	2871	14-Heptacosanone	O		DT							1.0	-1.9	-1.3

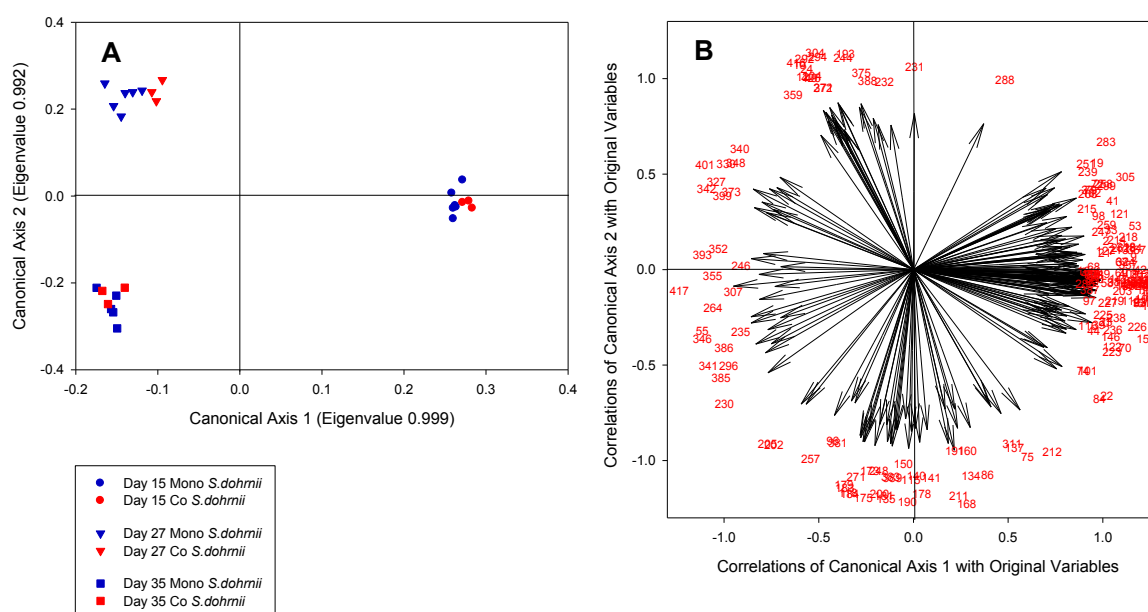
ID	Model ion	RT	RI	Name	Class	Ident	Analysis	Median (Co: n=3, Mono: n=6)								
								Day 15		Day 27		Day 35		Fold (Co relative to Mono)		
								Mono	Co	Mono	Co	Mono	Co	Day 15	Day 27	Day 35
379	237.1	20.00	3129	Tocopherol	O	*	DT,35							-1.0	-1.2	-1.5
388	574.5	21.18	3261	2-(3-Hydroxy-3,7,11,15-tetramethylhexadecyl)-3,5,6-trimethyl-1,4-benzenediol (Tocopherol quinone)	O	?	DT							1.2	1.4	2.1
101	205.1	9.25	1439	Threose	S	?	DT							1.1	1.2	-1.1
103	217.1	9.32	1448	Pentofuranose (Vidoudez)	S	?	DT			-	-			-1.1	-	-1.0
119	217.1	9.79	1510	Arabinofuranose	S		DT			-	-			1.1	-	1.0
134	218	10.32	1580	Pentofuranose (Vidoudez)	S		DT				-			-1.1	-	1.2
135	218	10.42	1593	Pentofuranose (Vidoudez)	S	?	DT							-1.1	-1.3	1.2
136	258.1	10.47	1600	Erythrose	S	?	35							-1.4	-1.5	-1.3
140	243.1	10.61	1618	Pentofuranose (Vidoudez)	S		DT			-	-			-1.3	-	1.1
141	218	10.62	1620	Ribofuranose	S	?	DT							-1.0	-18.5	1.1
156	157.1	11.05	1676	Arabinopyranose	S	?	DT							-1.0	1.0	1.2
205	204.1	12.70	1895	Glucose	S		DT							-1.2	-1.1	1.0
209	319.2	12.82	1913	Galactose	S		DT							1.0	1.1	-1.2
222	215.2	13.24	1987	Galactofuranose	S		35							1.0	-2.3	-1.3
230	204	13.54	2039	myo-Inositol	S		DT							-1.2	-1.0	1.1
241	144.1	13.94	2109	myo-Inositol	S	*	DT							-1.2	1.5	1.0
242	191	13.97	2114	myo-Inositol	S	*	DT							-1.1	1.1	1.1
125	103.1	10.02	1541	3-Deoxypentonic acid	S Acid	??	DT							-1.0	-1.3	-1.0
127	249.1	10.11	1552	Eryhronic acid	S Acid		DT							1.1	-2.6	-1.4
181	276.1	11.88	1786	Fructosonic acid	S Acid	??	DT,35							1.1	-1.5	-1.4
213	333.1	12.94	1936	Glucuronic acid	S Acid		DT							1.1	-2.9	-1.1
221	217	13.21	1981	Gluconic acid	S Acid		DT							-1.1	1.5	1.0

ID	Model ion	RT	RI	Name	Class	Ident	Analysis	Median (Co: n=3, Mono: n=6)						Fold (Co relative to Mono)		
								Day 15		Day 27		Day 35		Day 15	Day 27	Day 35
								Mono	Co	Mono	Co	Mono	Co			
121	248.1	9.88	1522	Threitol	S Alc	?	DT					1.0	-1.1	1.1		
167	217	11.44	1729	Xylitol	S Alc		DT			-	-	1.1	-	-		
260	318.9	14.53	2211	(1r,2r,3r,4r,5r,6r)-1,2,3,4,5,6-Cyclohexanehexol	S Alc	?	DT					-1.1	1.4	1.0		
297	217.1	15.80	2433	Uridine	S dv.	?	DT			-	-	1.5	-	-1.2		
366	380.4	19.25	3012	Ergosta-5,24-dien-3-yl acetate	St		35					1.3	1.4	1.2		
376	396.4	19.88	3112	(3 β ,20R,24R)-Stigmast-5-en-3-yl acetate	St	?	35					1.2	1.5	1.3		
386	382.4	21.04	3250	Ergost-5-en-3-ol (Campesterol)	St		DT					-1.1	1.3	-1.0		
392	129.1	21.83	3316	Stigmasta-5,24(28)-dien-3-ol (Fucosterol)	St		DT					1.0	1.4	-1.0		
258	143.1	14.48	2203	Phytol	T		DT					1.3	-1.7	-1.2		

In case derivatized molecules are detected, the table entry lists their putative parent compounds. Each MST is characterized by **ID**, **model ion**, retention time (**RT**), retention index (**RI**) and its underlying CAP **analysis**. CAP analyses comprised the overall analysis with a-priori grouping by treatment and day (**DT**), with a-priori grouping by treatment (**T**), as well as daywise subset analysis on day 27 (**27**) and day 35 (**35**). Metabolites were identified via libraries. If metabolites were verified with a standard, they are marked with *. “?” indicates a reversed match between 700 and 800, “??” a reversed match between 600 and 700 and “???” indicates cases where the reversed match was ≤ 600 . “1” tags metabolites with a match smaller than 600. Class abbreviations: Amine (**A**), alcohol (**Alc**), alkaloid (**Alk**), carboxylic acid (**CA**), complex sugar (**CS**), derivatives of a certain class (**dv.**), hydrocarbons (**HC**), sugar (**S**), sugar alcohol (**S Alc**), sugar acid (**S Acid**), sterol (**St**), terpene (**T**), others (**O**), unknown (**U**). **Vidoudez** refers to an MST code given by the inhouse library, **GOLM** refers to an MST code given by distinct libraries of the Golm Metabolome Database.

S. dohrnii

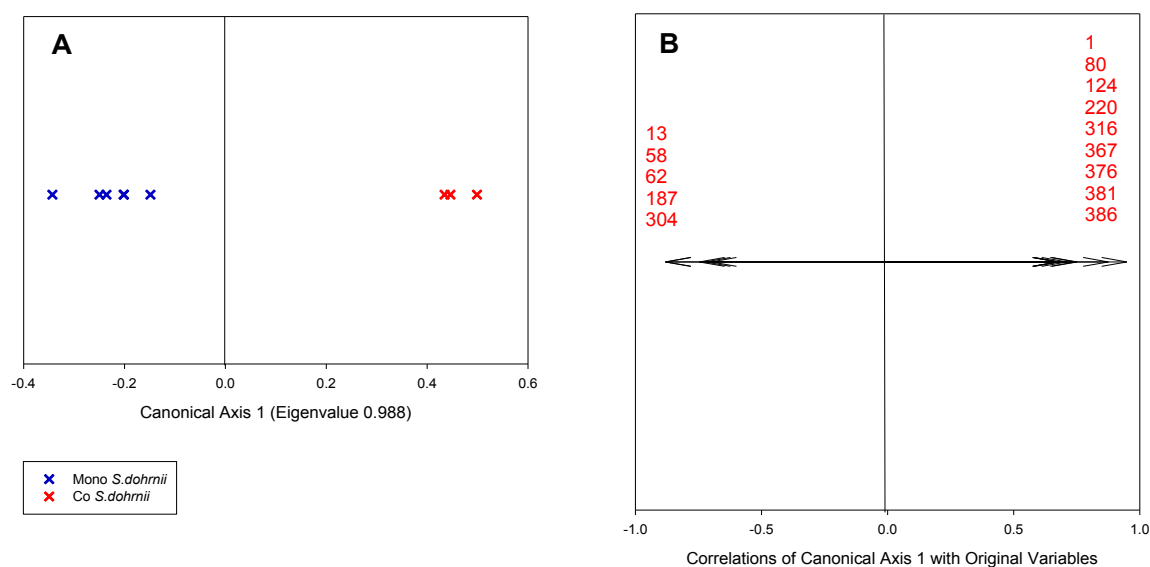
The trace statistic revealed significant endometabolomic differences in *S. dohrnii* among sampling days and treatments per day. The constrained score plot visualizes a clear separation of sampling days, as samples from day 15 were located in quadrant I and II, samples from day 27 in quadrant IV and from day 35 in quadrant III (**Appendix 71A**). Within each sampling day, treatments shared close proximity in multivariate space. Only within day 27 a gradual separation of treatments by canonical axis 1 is visible. The corresponding loading plot depicts 195 highly correlated metabolites ($|r| \geq 0.6888$, $P \leq 0.0001$, **Appendix 71B**). The majority of these metabolites characterized day 15 of the interaction. Similarly as described for *T. weissflogii*, the direction of the vectors indicates a correlation with sample groups visible in the corresponding score plot. To further evaluate characteristic metabolites, I created a heatmap (**Appendix 73**).



Appendix 71: Constrained score and loading plots of endometabolomic samples from *S. dohrnii* in a species-specific subset analysis of the interaction between *T. weissflogii* and *S. dohrnii*.

The constrained score plot (graph **A**) visualizes significant differences between the sample groups as found via CDA with a-priori groups by treatment per day (trace statistic $P \leq 0.0001$, misclassification error of 7.69 % for $m = 9$, graph **A**). Vectors in the CAP loading plot (graph **B**) represent metabolites, characterized by their ID (red numbers). Only vectors with a significant correlation coefficient above the critical value of $|r| \geq 0.6888$ ($P \leq 0.0001$) are plotted. The direction of the vectors in 2-dimensional space correlates with endometabolomic sample groupings shown in the score plots of the respective analysis.

As indicated by the permutation test of the daywise analysis of *S. dohrnii*, treatments were significantly different on day 15. The constrained score plot shows a clear separation of treatments by canonical axis 1 (**Appendix 72A**). In total, 14 metabolites were highly correlating with this separation ($|r| \geq 0.6664$, $P \leq 0.05$, **Appendix 72B**). While nine characterized the endometabolome of *S. dohrnii* in co-cultivation, five characterized the mono-cultivation state.



Appendix 72: Constrained score and loading plots of endometabolomic samples from *S. dohrnii* in a daywise subset analysis (day 15) of the interaction between *T. weissflogii* and *S. dohrnii*.

The constrained score plot (graph **A**) visualizes significant differences between the treatments, as confirmed via CDA for the subset analysis on day 15. These differences between treatments are significant (trace statistic $P \leq 0.0001$, misclassification error of 11.11 % for $m = 5$). Vectors in the CAP loading plot (graph **B**) represent metabolites, characterized by their ID (red numbers, pooled per group). Only vectors with a significant correlation coefficient above the critical value of $|r| \geq 0.6664$ ($P \leq 0.05$) are plotted. The direction of the vectors in 2-dimensional space correlates with endometabolomic sample groupings shown in the score plots of the respective analysis.

Generally, 201 metabolites⁹⁵ were identified by the CAP with a-priori grouping by treatment per day in the species-specific analysis and with a-priori grouping by treatment in the daywise analysis on day 15. Those metabolites were correlating with the significant differences between sample groups and characterized endometabolomic alterations among the a-priori groups in the respective analysis. Subsequently, the trends of different metabolite classes and interesting metabolites as apparent in the heatmap (**Appendix 73**) will be introduced. All metabolites of unknown identity are summarized in **Appendix 94**. Similarly as described for *T. weissflogii*, metabolites were only considered relevantly up- or downregulated in co-cultivation, if intensity differences exceeded 30 %.

In the class of amines, only urea (#55) showed relevant differences in metabolite levels among treatments. As described for *S. dohrnii*, the metabolite abundance increased between day 15 and day 35. While on day 27 urea was less abundant in co-cultivation, on day 35 I observed a 1.6 - fold upregulation in co-cultivation, relative to mono-cultivation.

Within identified amino acids, alanine (#16), isoleucine (#33) and proline (#68) characterized day 15, as they showed highest abundance here. This is in agreement with the observations in

⁹⁵ Excluding dodecamethylpentasiloxane (#34 and #38), as it represents potential contaminations

T. weissflogii. On this day, no relevant interaction-induced regulation was observed. However, on later days, differences in metabolite levels due to treatments exceeded 30 %: Isoleucine was up to 2.6 - fold upregulated in co-cultivation on day 27 and 35. Alanine was 1.8 - fold upregulated in co-cultivation on day 27 and downregulated on day 35 with 1.4 - fold higher abundance in mono-cultivation. Proline was downregulated to the point of absence in co-cultivation on day 27. Nevertheless, these differences in metabolite levels concerned days that were not characterized by highest abundance of the respective metabolites (compared to other points in time). Interestingly, putative norleucine (#24) was only present on day 27 and was 1.4 - fold more abundant in co-cultivation, compared to mono-cultivation.

In total nine MSTs were identified as alcohols. However, only five different metabolites were obtained after library search. Most of the alcoholic MSTs were most abundant on day 15, characterizing early stages of the interaction. On this day, only glycerol (#62) was relevantly downregulated in co-cultivation. Interestingly, putative glycerol was also represented by MSTs #22, #23 and #42, all of which were not relevantly altered by the interaction. Furthermore, 3-chloro-1,2-propanediol (#37) exhibited 1.3 - fold upregulation in co-cultivation on day 27 and downregulation on day 35 of the interaction. Please note that the intensity of this MST decreased from day 15 on.

The alkaloid 1H-pyrrole-2-carboxylic acid (#72, #77) was most abundant on day 15 and decreased in abundance during later stages of the interaction. However, on day 35 this alkaloid was downregulated in co-cultivation with up to 2.3 - fold higher abundance in mono-cultivation. The putative alkaloid derivative 2,6-diphenyl-1,7-dihydrodipyrrolo[2,3-b:3',2'-e]pyridine (#359) characterized day 27 of the interaction, but showed no interaction-induced regulation on this day. On day 35, this metabolite was downregulated in co-cultivation.

Among carboxylic acids, acetic acid (#13) was strongly downregulated in co-cultivation throughout all three sampling days. Benzoic acid (#58) was only present in mono-cultivation on day 15 and characterized this treatment on day 15, as it was absent in co-cultivation. The abundance of citric acid (#187) increased over time, as also observed in *T. weissflogii*. While at the onset of the interaction it was less abundant in co-cultivation, on day 35 citric acid was 1.9 - fold upregulated in co-cultivation. Threonic acid-1,4-lactone (#83, #84) and putative 3 - hydroxybutanoic acid (#19) were most abundant on day 15 but did not show interaction-induced alterations in abundance on this day. Subsequently both metabolites decreased in intensity.

With complex sugars and their derivatives I observed a trend of increased abundance in the diatom endometabolomes during later stages of the interaction. Most identified MSTs showed highest abundance on day 27 and 35, with exception of two putative trisaccharides (#311, #384), and a disaccharide (#413), which were most abundant on day 15. However, only few MSTs showed relevant differences in intensities among treatments: Gentobiose (#341) and maltotriose (#416, #417) were downregulated in co-cultivation on day 27. Putative melezitose (#399) was 1.4 - fold upregulated on day 27 and downregulated on day 35. Furthermore, a putative trisaccharide (#384) was characteristic for day 15, as it was only present on this day and 1.4 - fold upregulated in co-cultivation. Galactinol (#355) was 1.6 - fold higher abundant in co-cultivation on day 15, but showed lowest abundance on this sampling day, if compared to day 27 and 35. Furthermore, galactinol was also represented by MST #342, which did not show relevant differences of MST levels between treatments.

The biggest class of identified metabolites was the one of sugars and their derivatives. This class was characterized by two general trends: on the one hand most MSTs characterized the onset of the interaction, as they were most abundant in the endometabolomes on day 15 and on the other hand, if a relevant regulation was observed, in the majority of cases, this regulation became manifested in an upregulation of the respective MST in co-cultivation. Interestingly, putative threose (#101), glucose (#205) as well as the sugar acids glucuronic acid (#213) and putative gulonic acid (#220) were upregulated in co-cultivation on all three sampling days. Considering metabolites that characterized day 15: putative pentofuranose (#103) and arabinofuranose (#119) were 1.3 - fold upregulated on this day. Interestingly, only the sugar derivative ononitol (#226) was downregulated in co-cultivation on day 15 and characteristic for this sampling day. Among metabolites that characterized day 35, putative pentofuranoses (#134, #135), as well as glucose (#205) and putative galactofuranose (#211) were upregulated in co-cultivation.

Looking at fatty acids and their derivatives, a diverse picture was observed. No general time dependent trend in abundance of fatty acids was visible, but each sampling day was characterized by some of the highly correlated and identified metabolites. Most fatty acids (and derivatives) that characterized day 15 did not show relevant differences in MST intensity levels among treatments on this day. However, 2,3-dihydroxypropyl palmitate (#324) was downregulated in co-cultivation on day 15 with 1.4 - fold higher values in mono-cultivation. Although this metabolite was less abundant on day 27 and 35, an upregulation in co-cultivation of up to 2.6 - fold became apparent on both days. Putative stearic acid (#272) and octadecadienoic acid (#232) characterized day 27 of the interaction. Both were 1.4 - fold upregulated on this day. Stearic acid was also represented by MST #271, which did not exhibit any relevant interaction-




induced regulation. Considering metabolites that characterized day 35, only putative N - hydroxytetradecanamide (#235) was relevantly downregulated (1.8 - fold) in co-cultivation. All other MSTs within this metabolite class did not exhibit relevant interaction-induced regulations on the sampling day they characterized.

The regulation of highly correlated terpenes seemed unaffected by the interaction and more characterized by time than by treatment. A similar trend was observed for sterols. However, putative 24-oxocholest-5-en-3-yl acetate (#367) was 1.5 - fold upregulated in co-cultivation on day 15 and only abundant on this day. Furthermore, putative (3 β ,20R,24R)-stigmast-5-en-3-yl acetate (#376) was 1.3 - fold upregulated in co-cultivation on day 15 and downregulated on day 27. Opposite to sterol #367, this sterol characterized later stages of the interaction, as it was most abundant on day 27 and 35. While in *T. weissflogii* sterols exhibited a trend of upregulation in co-cultivation during later stages of the interaction, in *S. dohrnii* sterols characterized day 15 but were subsequently downregulated in co-cultivation (by trend).

The potential hydrocarbon 3-octadecyne (#203) was most abundant on day 15 but showed relevant interaction-induced differences in abundance only on day 27 (upregulation) and day 35 (downregulation in co-cultivation). Furthermore, five MSTs were listed in the class of 'others'. Putative 3-phenyl-1-cyclohexen-1-ol (#160) was most abundant on day 35 and 1.8 - fold upregulated in co-cultivation on this day. All other metabolites in the class 'others' did not show interaction-induced alterations in MST levels on the days of their highest abundance.

Among the unknowns, MST #268 was of interest, as it was 7 - fold upregulated on day 27 of the interaction and characteristic for the early stages of the interaction. Furthermore, MST #360 was only abundant on day 15, characterizing the onset of the interaction and downregulated in co-cultivation with 15.5 - fold higher abundance in mono-cultivation. Unfortunately, the identity of both metabolites remained unclear.

Appendix 73: Heatmap of endometabolite intensities categorized by MST classes for the species-specific and daywise analysis of *S. dohrnii* in interaction with *T. weissflogii*. Medians of MST intensities, normalized to peak sum per sample and subsequently metabolite-wise auto scaled, are represented by a color code ranging from high (yellow) to low intensities (blue). White indicates the absence of the respective MST after data pre-processing. Metabolites are sorted according to classes (separated by black lines) and abundance patterns. Only metabolites significantly correlating with the separation of treatments and treatment per day are shown. The fold change of MST abundance in co-cultivation relative to mono-cultivation is given and coded with a second color code. Black indicates a higher abundance in co-cultivation, grey a higher abundance in mono-cultivation.

ID	Model ion	RT	RI	Name	Class	Ident	Analysis	Median MST intensity						Fold change		
								low  high						UP  DOWN 		
								Median (Co: n=3, Mono: n=5/6)			Fold (Co relative to Mono)					
								Day 15		Day 27		Day 35		Day 15	Day 27	Day 35
Mono	Co	Mono	Co	Mono	Co	Day 15	Day 27	Day 35								
44	103.1	6.98	1138	(E,2S)-N-methoxy-2,3-bis(hydroxy)propan-1-imine	A		DT	-	-	-	-	1.0	-	-		
48	103.1	7.12	1157	(E,2S)-N-methoxy-2,3-bis(hydroxy)propan-1-imine	A		DT	-	-	-	-	1.2	-	-		
55	189.1	7.34	1187	Urea	A		DT	-	-	-	-	-1.1	-1.3	1.6		
16	116.1	5.97	1005	Alanine	AA	*	DT	-	-	-	-	1.1	1.8	-1.4		
24	158.1	6.33	1052	Norleucine	AA	??	DT	-	-	-	-	-	1.4	-		
33	188.1	6.56	1084	Isoleucine	AA		DT	-	-	-	-	1.1	2.0	2.6		
68	142.1	7.90	1260	Proline	AA	*	DT	-	-	-	-	-1.0	-	-		
9	151.1	5.53	947	Phenol	Alc		DT	-	-	-	-	1.0	1.2	-1.0		
10	199.1	5.56	950	Phenol	Alc		DT	-	-	-	-	-	-1.1	-		
22	103.1	6.28	1046	Glycerol	Alc	?	DT	-	-	-	-	1.1	-	1.1		
23	165.1	6.30	1048	Glycerol	Alc	?	DT	-	-	-	-	1.2	-	-		
31	165.1	6.50	1075	3-Methylphenol	Alc		DT	-	-	-	-	1.1	-	-		
37	116.1	6.81	1116	3-Chloro-1,2-propanediol	Alc		DT	-	-	-	-	1.1	1.3	-1.5		
42	103.1	6.91	1129	Glycerol	Alc	?	DT	-	-	-	-	1.0	-	-		
62	117	7.64	1226	Glycerol	Alc		15	-	-	-	-	-1.5	1.1	1.1		

ID	Model ion	RT	RI	Name	Class	Ident	Analysis	Median (Co: n=3, Mono: n=5/6)						Fold (Co relative to Mono)		
								Day 15		Day 27		Day 35		Day 15	Day 27	Day 35
								Mono	Co	Mono	Co	Mono	Co			
137	342.2	10.53	1608	1,2,3-Benzenetriol	Alc		DT	-	-	-	-	-	1.1	-	-1.1	
72	240.1	8.04	1278	1H-Pyrrole-2-carboxylic acid	Alk		DT	-	-	-	-	-	-1.0	-1.2	1.7	
77	240.1	8.37	1322	1H-Pyrrole-2-carboxylic acid	Alk		DT	-	-	-	-	-	-1.1	-1.8	2.3	
359	309.3	18.49	2892	2,6-Diphenyl-1,7-dihydrodipyrrolo[2,3-b:3',2'-e]pyridine	Alk dv.	?	DT	-	-	-	-	-	-1.2	1.1	-1.4	
12	173.1	5.71	970	Hexanoic acid	CA	?	DT	-	-	-	-	-	-	-1.2	-	
13	177.1	5.74	975	Acetic acid	CA		15	-	-	-	-	-	-1.9	-	-4.0	
19	117	6.12	1025	3-Hydroxybutanoic acid	CA	?	DT	-	-	-	-	-	1.0	-1.0	2.2	
58	179.1	7.47	1203	Benzoic acid	CA		DT,15	-	-	-	-	-	-	-	-	
83	148.1	8.60	1353	Threonic acid-1,4-lactone	CA		DT	-	-	-	-	-	-1.2	-	-	
84	103.1	8.63	1357	Threonic acid-1,4-lactone	CA		DT	-	-	-	-	-	1.2	-	1.2	
187	273.1	12.11	1817	Citric acid	CA		15	-	-	-	-	-	-1.7	-	1.9	
311	217.1	16.31	2522	Trisaccharide (Vidoudez)	CS	?	DT	-	-	-	-	-	1.1	-	1.0	
330	361.2	17.02	2647	Maltose	CS		DT	-	-	-	-	-	2.5	1.0	1.1	
341	361.1	17.50	2731	Gentobiose	CS		DT	-	-	-	-	-	-1.1	-1.3	1.2	
346	361.2	17.69	2763	Maltose	CS	*	DT	-	-	-	-	-	-1.1	-1.1	1.2	
373	204.1	19.76	3092	Melibiose	CS		DT	-	-	-	-	-	1.0	-1.0	-1.0	
384	217.1	20.80	3230	Trisaccharide (Vidoudez)	CS	?	DT	-	-	-	-	-	1.4	-	-	
399	361.2	22.61	3382	Melezitose	CS	??	DT	-	-	-	-	-	-	1.4	-1.3	
401	361.2	22.88	3404	Melezitose	CS		DT	-	-	-	-	-	-	-1.1	-1.3	
413	217.1	24.34	3527	Disaccharide (Vidoudez)	CS		DT	-	-	-	-	-	1.2	-	-	
416	173.1	24.72	3559	Maltotriose	CS		DT	-	-	-	-	-	-	-1.3	-	
417	361.2	24.75	3561	Maltotriose	CS		DT	-	-	-	-	-	-1.2	-1.6	-1.0	
342	204.1	17.54	2738	Galactinol	CS dv.		DT	-	-	-	-	-	1.2	-1.1	-1.1	

ID	Model ion	RT	RI	Name	Class	Ident	Analysis	Median (Co: n=3, Mono: n=5/6)						Fold (Co relative to Mono)		
								Day 15		Day 27		Day 35		Day 15	Day 27	Day 35
								Mono	Co	Mono	Co	Mono	Co			
355	204.1	18.29	2862	Galactinol	CS dv.		DT	-	-	-	-	-	-	1.6	1.2	1.1
232	309.2	13.58	2047	Octadecadienoic acid	FA		DT	-	-	-	-	-	-	1.4	1.4	2.6
264	108.1	14.66	2234	(9Z,12Z,15Z)-9,12,15-Octadecatrienoic acid (Linolenic acid)	FA	*	DT	-	-	-	-	-	-	-1.2	1.1	-1.2
271	117	14.90	2277	Octadecanoic acid (Stearic acid)	FA		DT	-	-	-	-	-	-	1.2	-	-1.0
272	199.1	14.92	2280	Octadecanoic acid (Stearic acid)	FA	?	DT	-	-	-	-	-	-	1.2	1.4	1.2
168	143.1	11.49	1734	Methyl myristate	FA dv.		DT	-	-	-	-	-	-	1.1	-	-1.2
212	143.1	12.91	1929	Methyl palmitate	FA dv.		DT	-	-	-	-	-	-	1.1	-	-1.3
235	211.2	13.72	2071	N-Hydroxytetradecanamide	FA dv.	??	DT	-	-	-	-	-	-	-1.1	1.1	-1.8
261	212.2	14.59	2222	Palmitamide	FA dv.		DT	-	-	-	-	-	-	-1.2	-	2.3
262	180.1	14.59	2222	Methyl-5,8,11,14,17-icosapentaenoate	FA dv.	?	DT	-	-	-	-	-	-	1.1	2.0	-1.3
307	105.1	16.14	2493	Methyl-4,7,10,13,16,19-docosahexaenoate	FA dv.		DT	-	-	-	-	-	-	1.1	-1.0	-1.1
318	129.1	16.61	2574	1,3-Dihydroxy-2-propanyl palmitate	FA dv.	?	DT	-	-	-	-	-	-	-1.0	-	-
324	371.3	16.78	2605	2,3-Dihydroxypropyl palmitate	FA dv.		DT	-	-	-	-	-	-	-1.4	2.6	1.3
426	129.1	27.23	3770	2-[(Trimethylsilyloxy)-1,3-propanediyl ditetradecanoate (Glycerine-1,3-dimyristate, 2-O-trimethylsilyl-)]	FA dv.	?? ¹	DT	-	-	-	-	-	-	-	1.2	-
203	123.1	12.61	1882	3-Octadecyne	HC	?	DT	-	-	-	-	-	-	1.0	1.3	-1.4
98	156.1	9.13	1422	Naphthalene, 1,6-dimethyl-	O	¹	DT	-	-	-	-	-	-	-1.1	-1.0	-1.9
160	246.1	11.19	1695	3-Phenyl-1-cyclohexen-1-ol	O	?	DT	-	-	-	-	-	-	1.0	-	1.8
195	123.1	12.31	1842	2-Hexadecyloxirane	O		DT	-	-	-	-	-	-	-1.1	1.3	-1.2
199	123.1	12.47	1865	Hexadecanal	O	?	DT	-	-	-	-	-	-	-1.0	1.3	-1.3

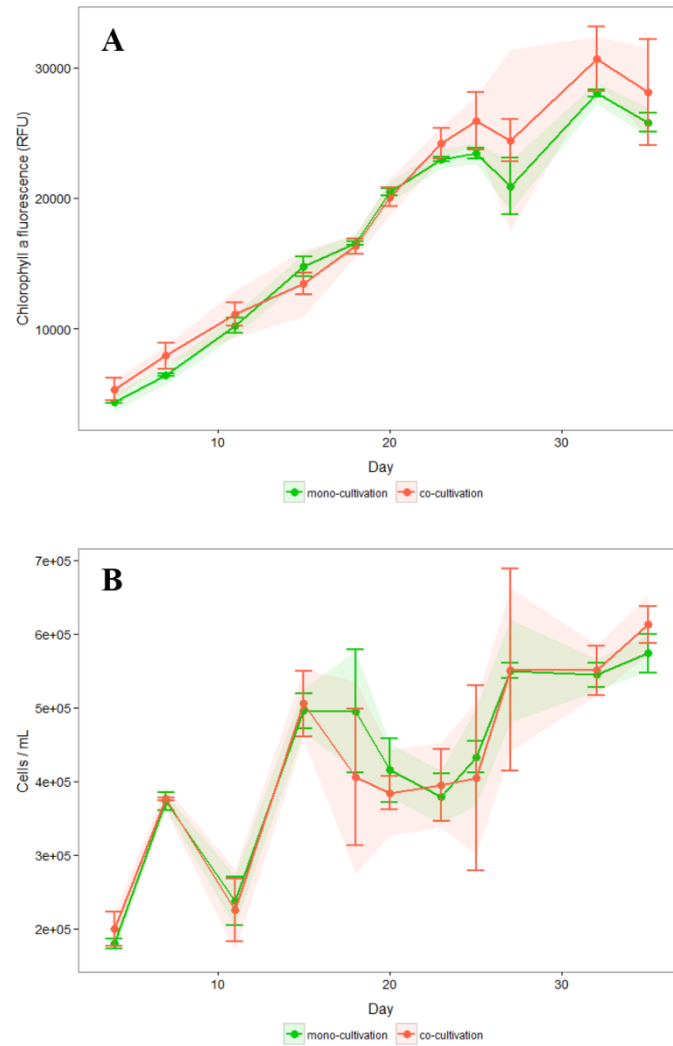
ID	Model ion	RT	RI	Name	Class	Ident	Analysis	Median (Co: n=3, Mono: n=5/6)						Fold (Co relative to Mono)		
								Day 15		Day 27		Day 35		Day 15	Day 27	Day 35
								Mono	Co	Mono	Co	Mono	Co			
388	574.5	21.18	3261	2-(3-Hydroxy-3,7,11,15-tetramethylhexadecyl)-3,5,6-trimethyl-1,4-benzenediol (Tocopherol quinone)	O	?	DT	-	-	-	-	-	-	-1.2	-1.1	-1.3
101	205.1	9.25	1439	Threose	S	?	DT	-	-	-	-	-	-	1.3	15.6	2.6
103	217.1	9.32	1448	Pentofuranose (Vidoudez)	S	?	DT	-	-	-	-	-	-	1.3	-	-
119	217.1	9.79	1510	Arabinofuranose	S		DT	-	-	-	-	-	-	1.3	-	-
134	218	10.32	1580	Pentofuranose (Vidoudez)	S		DT	-	-	-	-	-	-	1.1	-	1.3
135	218	10.42	1593	Pentofuranose (Vidoudez)	S	?	DT	-	-	-	-	-	-	1.0	-	1.1
140	243.1	10.61	1618	Pentofuranose (Vidoudez)	S		DT	-	-	-	-	-	-	1.1	-	-1.2
141	218	10.62	1620	Ribofuranose	S	?	DT	-	-	-	-	-	-	-1.1	-	-1.0
157	217.1	11.05	1677	Ribose	S		DT	-	-	-	-	-	-	1.1	-	1.4
205	204.1	12.70	1895	Glucose	S		DT	-	-	-	-	-	-	1.0	1.0	1.3
211	217.1	12.86	1920	Galactofuranose	S	?	DT	-	-	-	-	-	-	1.0	-	1.3
215	204.1	13.01	1946	Gulose	S		DT	-	-	-	-	-	-	1.1	-1.2	-1.0
230	204	13.54	2039	myo-Inositol	S		DT	-	-	-	-	-	-	-1.0	-1.1	-1.2
231	117	13.56	2043	Inositol	S		DT	-	-	-	-	-	-	1.2	1.2	-
239	204	13.85	2094	Glucopyranose	S		DT	-	-	-	-	-	-	1.1	-1.0	1.2
248	319.2	14.19	2153	myo-Inositol	S		DT	-	-	-	-	-	-	-1.2	-1.1	-1.2
125	103.1	10.02	1541	3-Deoxypentonic acid	S Acid	??	DT	-	-	-	-	-	-	1.2	-	-
127	249.1	10.11	1552	Erythronic acid	S Acid		DT	-	-	-	-	-	-	-1.2	-	-
128	217.1	10.13	1554	Threonic acid	S Acid		DT	-	-	-	-	-	-	-1.0	-	-
181	276.1	11.88	1786	Fructosonic acid	S Acid	??	DT	-	-	-	-	-	-	-1.1	1.2	1.1
213	333.1	12.94	1936	Glucuronic acid	S Acid		DT	-	-	-	-	-	-	1.3	1.6	2.4
219	157.1	13.15	1971	Gulonic acid	S Acid		DT	-	-	-	-	-	-	1.2	-	1.5

ID	Model ion	RT	RI	Name	Class	Ident	Analysis	Median (Co: n=3, Mono: n=5/6)						Fold (Co relative to Mono)		
								Day 15		Day 27		Day 35		Day 15	Day 27	Day 35
								Mono	Co	Mono	Co	Mono	Co			
220	432.9	13.17	1975	Gulonic acid	S Acid	?	15	-	-	-	-	-	-	1.3	1.3	1.4
223	217.1	13.28	1993	Hexonic acid	S Acid		DT	-	-	-	-	-	-	-1.1	-	2.0
218	319.2	13.09	1961	Gluconic acid-1,5-lactone	S Acid dv.		DT	-	-	-	-	-	-	1.1	-1.3	1.9
121	248.1	9.88	1522	Threitol	S Alc	?	DT	-	-	-	-	-	-	-1.1	1.1	1.5
167	217	11.44	1729	Xylitol	S Alc		DT	-	-	-	-	-	-	1.1	-	-
226	217.1	13.39	2013	4-O-Methyl-myo-inositol (Ononitol)	S dv.		DT	-	-	-	-	-	-	-1.4	-	-
251	204.1	14.26	2165	1-Methyl-β-D-galactopyranoside	S dv.		DT	-	-	-	-	-	-	1.2	1.0	1.1
297	217.1	15.80	2433	Uridine	S dv.	?	DT	-	-	-	-	-	-	1.3	-	-
327	204.1	16.86	2619	Adenosine	S dv.	?	DT	-	-	-	-	-	-	-1.0	-1.2	-1.0
367	382.4	19.29	3018	24-Oxocholest-5-en-3-yl acetate	St	?	DT,15	-	-	-	-	-	-	1.5	-	-
376	396.4	19.88	3112	(3β,20R,24R)-Stigmast-5-en-3-yl acetate	St	?	15	-	-	-	-	-	-	1.3	-1.3	-1.1
385	129.1	20.99	3246	(3β)-Stigmast-5-en-3-ol	St		DT	-	-	-	-	-	-	1.1	-1.1	-1.1
386	382.4	21.04	3250	Ergost-5-en-3-ol (Campesterol)	St		DT,15	-	-	-	-	-	-	1.4	-1.0	-1.1
393	386.3	22.02	3332	Stigmasta-5,24(28)-dien-3-ol (Fucosterol)	St		DT	-	-	-	-	-	-	1.1	-1.2	-1.2
193	111.1	12.26	1836	(2E)-3,7,11,15-Tetramethyl-2-hexadecene	T		DT	-	-	-	-	-	-	-	-1.2	-
238	108.1	13.79	2083	(1E,3Z,6E,10E)-14-Isopropyl-3,7,11-trimethyl-1,3,6,10-cyclotetradecatetraene (Cembrene)	T	?	DT	-	-	-	-	-	-	1.0	1.1	-1.0
247	126.1	14.15	2145	3,7,11,15-Tetramethyl-2-hexadecen-1-ol (Phytol)	T		DT	-	-	-	-	-	-	1.1	1.5	-
258	143.1	14.48	2203	Phytol	T		DT	-	-	-	-	-	-	1.0	1.3	1.4
259	111	14.49	2206	Phytol	T		DT	-	-	-	-	-	-	-1.2	1.2	1.2

In case derivatized molecules are detected, the table entry lists their putative parent compounds. Each MST is characterized by **ID**, **model ion**, retention time (**RT**), retention index (**RI**) and its underlying CAP **analysis**. CAP analyses comprised the overall analysis with a-priori grouping by treatment and day (**DT**), with a-priori grouping by treatment (**T**), as well as daywise subset analysis on day 15 (**15**), 27 (**27**) and day 35 (**35**). Metabolites were identified via libraries. If metabolites were verified with a standard, they are marked with *. “?” indicates a reversed match between 700 and 800, “??” a reversed match between 600 and 700 and “???” indicates cases where the reversed match was ≤ 600. “?” tags metabolites with

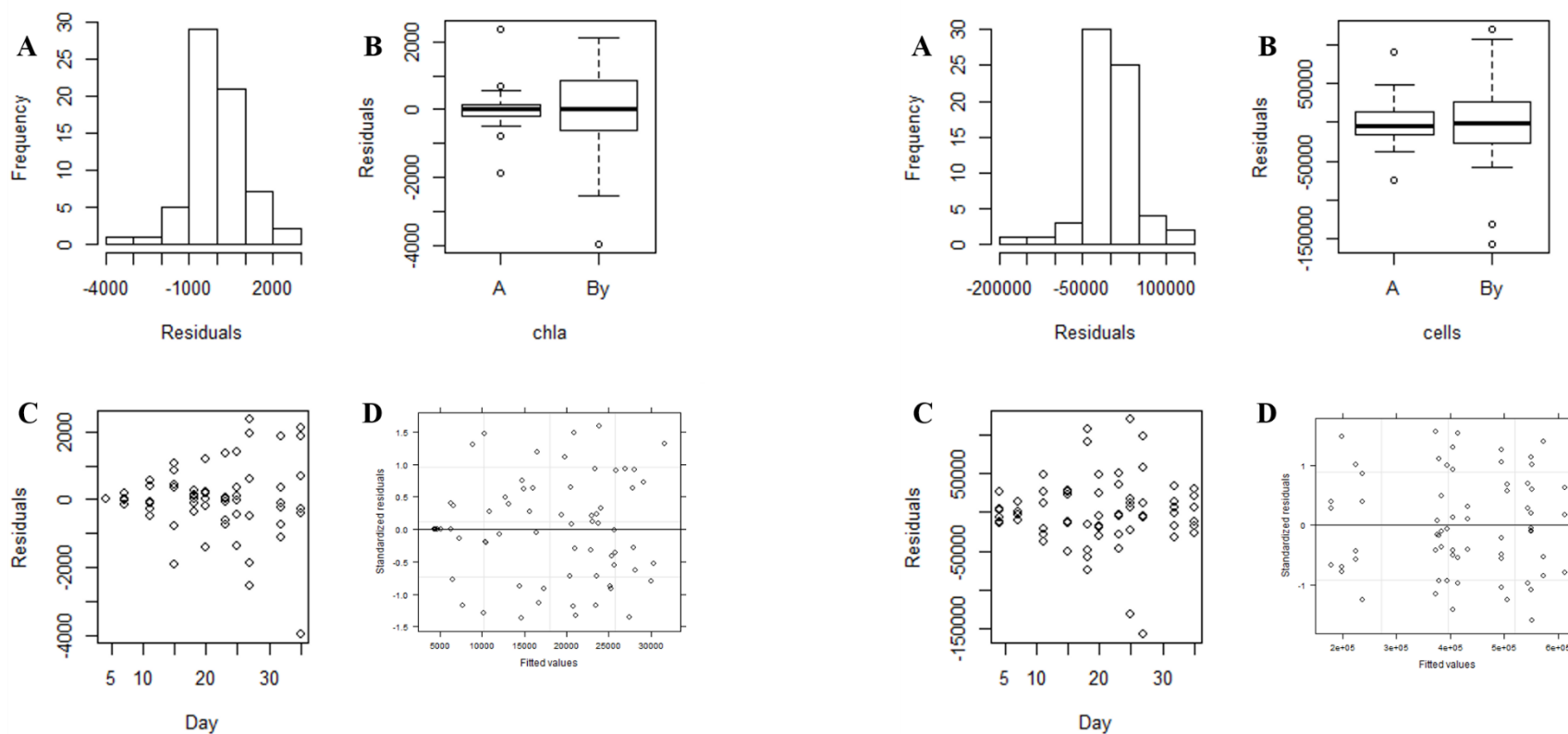
a match smaller than 600. Class abbreviations: Amine (**A**), alcohol (**Alc**), alkaloid (**Alk**), carboxylic acid (**CA**), complex sugar (**CS**), derivatives of a certain class (**dv.**), hydrocarbons (**HC**), sugar (**S**), sugar alcohol (**S Alc**), sugar acid (**S Acid**), sterol (**St**), terpene (**T**), others (**O**), unknown (**U**). **Vidoudez** refers to an MST code given by the inhouse library, **GOLM** refers to an MST code given by distinct libraries of the Golm Metabolome Database.

7.3.5 Supplements: Diatom growth

T. weissflogii

Appendix 74: Linear mixed model of chl a (**A**, RFU: relative fluorescence units) and cell counts (**B**, cells / mL) of *T. weissflogii* in interaction with *S. dohrnii*.

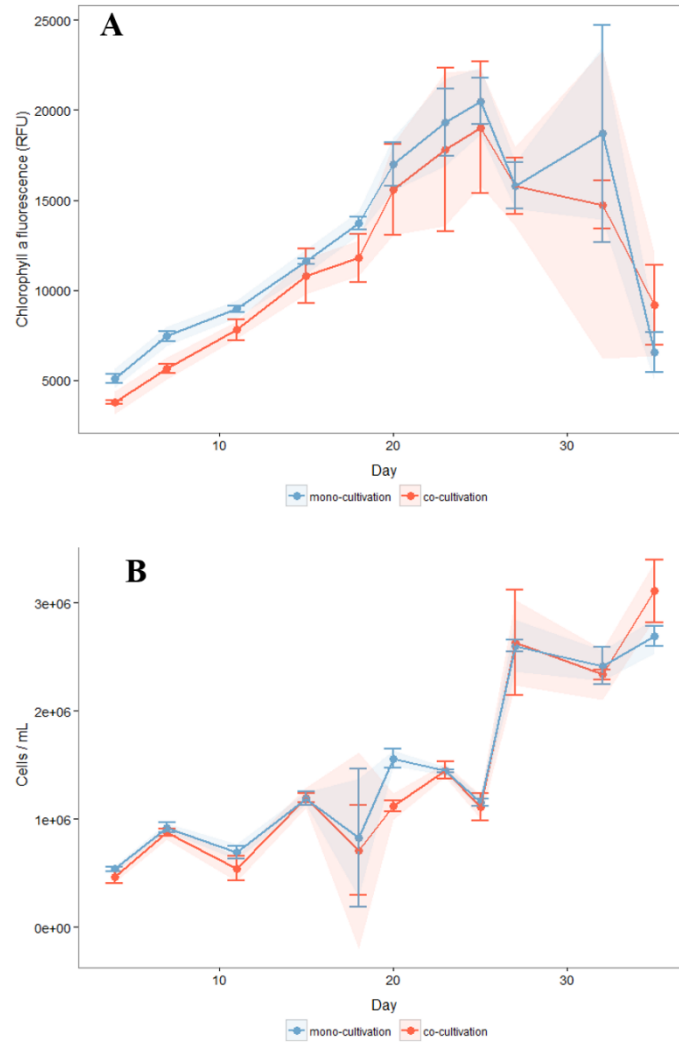
The graph shows the linear mixed model 4 (cell counts) and model 4b (chl a). Mean values ($n = 3$) are shown as dot plot, error bars represent the standard deviation. The line chart shows the model fit, with colored areas representing the confidence interval (95%). Mono-cultivation of *T. weissflogii* is depicted in **green**, co-cultivation is shown in **red**.



Appendix 75: Model validation graphs for the linear mixed model of the chl a for *T. weissflogii* in interaction with *S. dohrnii*.

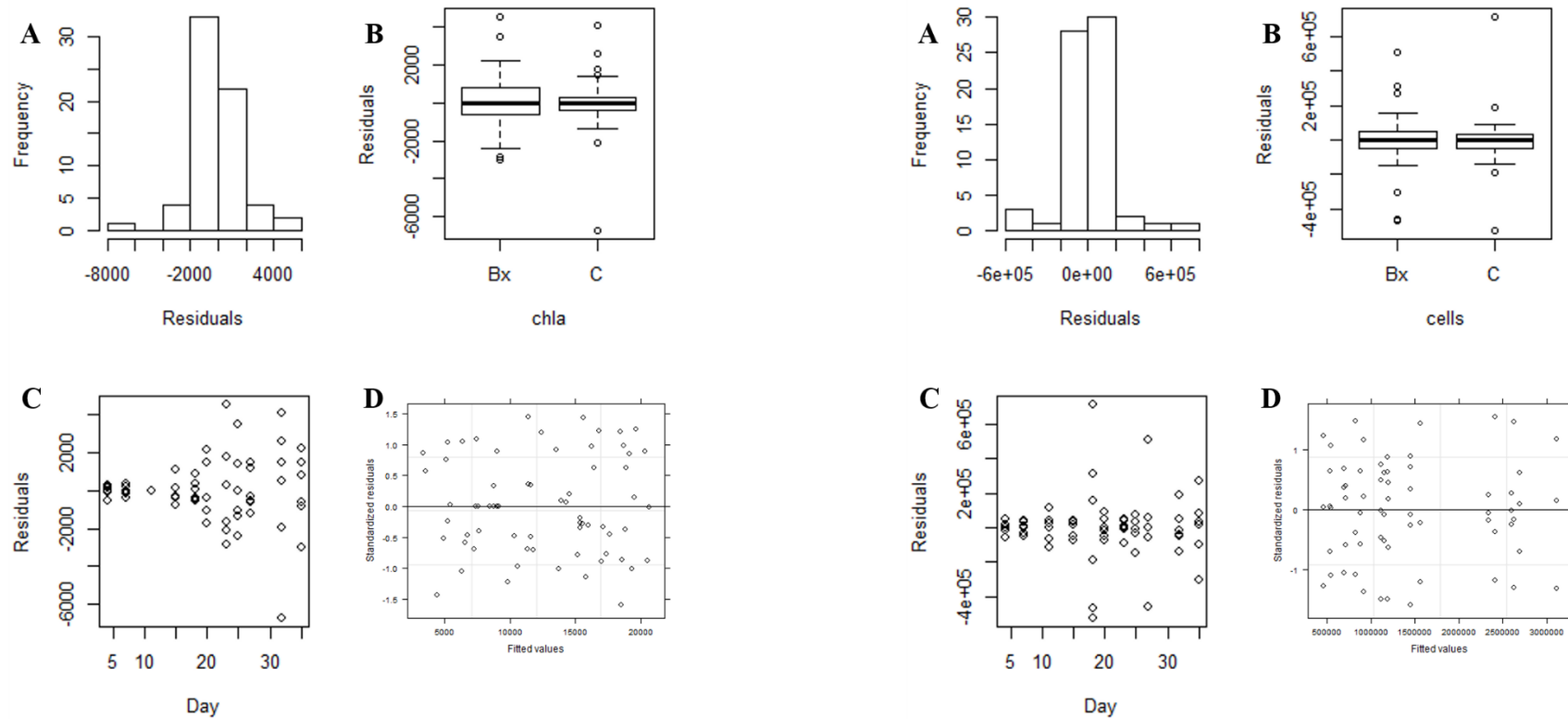
Appendix 76: Model validation graphs for the linear mixed model of the cell counts for *T. weissflogii* in interaction with *S. dohrnii*.

(A) Histogram of residuals for check of normality, (B) residuals versus group (A: mono-cultivation, By: co-cultivation) as explanatory variable, (C) residuals versus day as explanatory variable, (D) standardized residuals versus fitted values of the model to verify homogeneity of variances among residuals.

S. dohrnii

Appendix 77: Linear mixed model of chl a (**A**, RU: relative units) and cell counts (**B**, cells / mL) of *S. dohrnii* in interaction with *T. weissflogii*.

The graph shows the linear mixed model 4. Mean values ($n = 3$) are shown as dot plot, error bars represent the standard deviation. The line chart shows the model fit, with colored areas representing the confidence interval (95%). Mono-cultivation of *S. dohrnii* is depicted in **blue**, co-cultivation is shown in **red**.

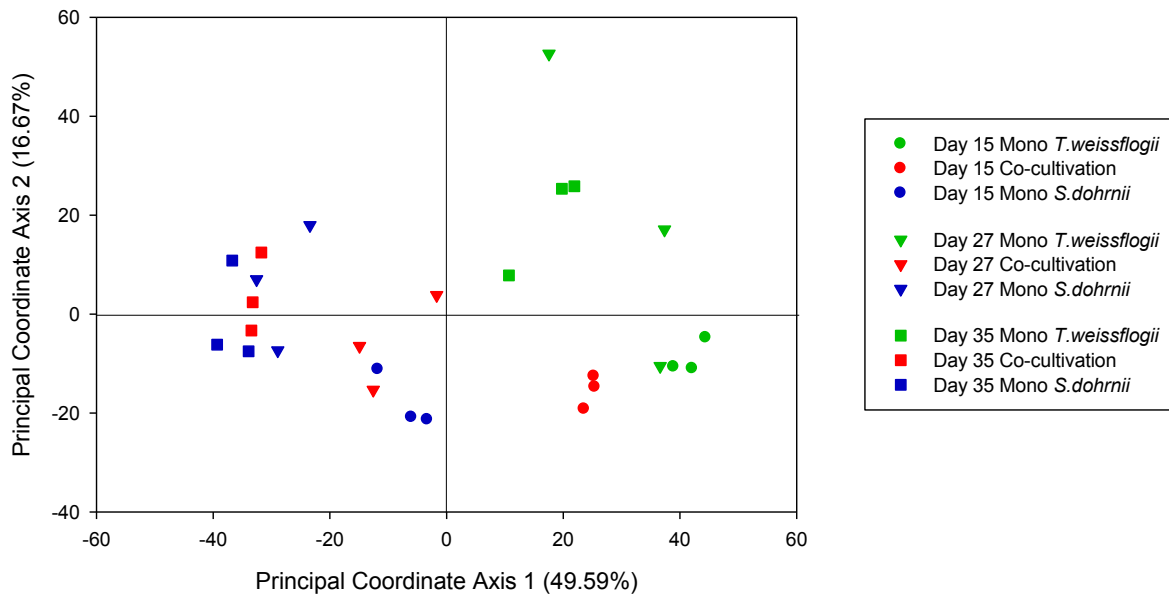


Appendix 78: Model validation graphs for the linear mixed model of the chl a for *S. dohrnii* in interaction with *T. weissflogii*.

Appendix 79: Model validation graphs for the linear mixed model of the cell counts for *S. dohrnii* in interaction with *T. weissflogii*.

(A) Histogram of residuals for check of normality, (B) residuals versus group (C: mono-cultivation, Bx: co-cultivation) as explanatory variable, (C) residuals versus day as explanatory variable, (D) standardized residuals versus fitted values of the model to verify homogeneity of variances among residuals.

7.3.6 Supplements: Exometabolomic investigation

Overall analysis via CAP

Appendix 80: PCoA score plot of exometabolomic samples from an overall analysis of the interaction between *T. weissflogii* and *S. dohrnii*.

The plot is based on metabolites obtained from mono-cultivated *S. dohrnii* (blue), mono-cultivated *T. weissflogii* (green) and co-cultivation of both diatoms (red) on day 15 (●), day 27 (▼) and day 35 (■).

Appendix 81: Cross validation results (leave-one-out allocation of observations to groups) for the analysis of the exometabolomic data of the interaction between *S. dohrnii* and *T. weissflogii* with a-priori grouping by treatment

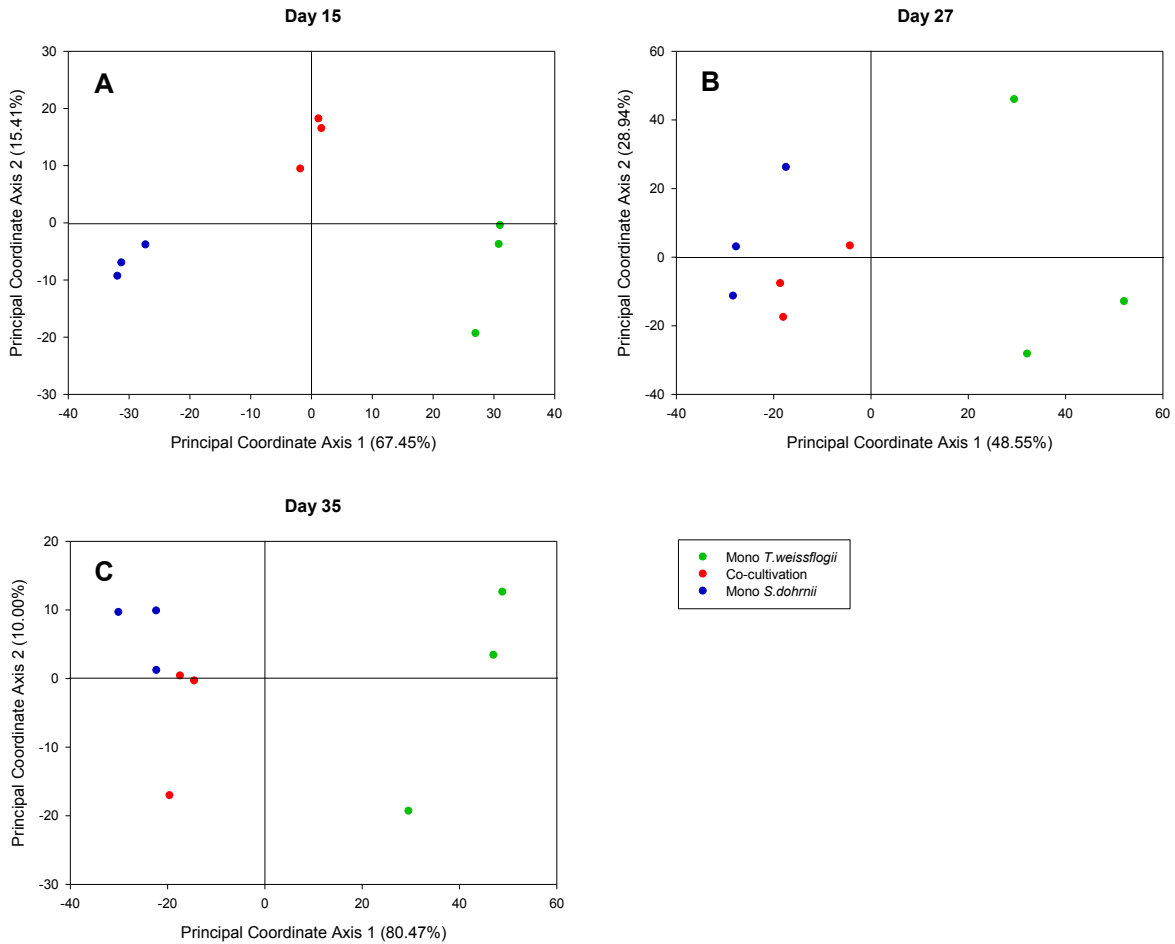
	Mono TW	Co	Mono SD	Total	%correct
Mono TW	9	0	0	9	100
Co	0	7	2	9	77.778
Mono SD	0	0	9	9	100
Misclassification error: 7.41 %					

Mono SD: mono-cultivated *S. dohrnii*, **Mono TW:** mono-cultivated *T. weissflogii*, **Co:** co-cultivated diatoms, **Total:** total number of samples, **%correct:** percentage of correctly allocated samples to their respective group. Number of samples correctly allocated to their group are highlighted in green, wrong allocations are highlighted in grey.

Appendix 82: Cross validation results (leave-one-out allocation of observations to groups) for the analysis of the exometabolomic data of the interaction between *S. dohrnii* and *T. weissflogii* with a-priori grouping by day and treatment

		Day15			Day27			Day35			Total	%correct
		Mono TW	Co	Mono SD	Mono TW	Co	Mono SD	Mono TW	Co	Mono SD		
Day15	Mono TW	3	0	0	0	0	0	0	0	0	3	100
	Co	0	3	0	0	0	0	0	0	0	3	100
	Mono SD	0	0	3	0	1	0	0	0	0	3	100
Day27	Mono TW	2	0	0	0	0	1	0	0	0	3	0
	Co	0	0	0	0	3	0	0	0	0	3	100
	Mono SD	0	0	0	0	1	1	0	1	0	3	33.333
Day35	Mono TW	0	0	0	0	0	0	3	0	0	3	100
	Co	0	0	0	0	0	0	0	3	0	3	100
	Mono SD	0	0	0	0	0	0	0	0	3	3	100
Misclassification error: 18.52 %												

Mono SD: mono-cultivated *S. dohrnii*, **Mono TW:** mono-cultivated *T. weissflogii*, **Co:** co-cultivated diatoms, **Total:** total number of samples, **%correct:** percentage of correctly allocated samples to their respective group. Number of samples correctly allocated to their group are highlighted in **green**, wrong allocations are highlighted in **grey**.

Daywise analysis via CAP

Appendix 83: PCoA score plot of exometabolomic samples from a daywise subset analysis of the interaction between *T. weissflogii* and *S. dohrnii* on day 15, 27 and 35.

The plots are based on metabolites obtained from mono-cultivated *S. dohrnii* (blue), mono-cultivated *T. weissflogii* (green) and co-cultivation of both diatoms (red) on day 15 (graph A), day 27 (graph B) and day 35 (graph C).

Appendix 84: Heatmap of exometabolite intensities for the subset analysis of the interaction between *T. weissflogii* and *S. dohrnii* on day 15. Medians of MST intensities, normalized to the external standard ribitol (per sample) and subsequently metabolite-wise auto scaled, are represented by a color code ranging from high (yellow) to low intensities (blue). White indicates the absence of the respective MST after data pre-processing. Metabolites are sorted according to abundance patterns (separated by black lines), class and RI. Only metabolites significantly correlating with the separation of treatments and treatment per day are shown. The fold change of MST abundance in co-cultivation relative to mono-cultivations is given and coded with a second color code. Black indicates a higher abundance in co-cultivation, grey a higher abundance in mono-cultivation.

ID	Model ion	RT	RI	Name	Class	Ident	Metabolite intensity			Fold change		Group
							low		high	UP	DOWN	
							Median (n=3)			Fold (Co relative to:)		
Day 15			Day 15									
SD Mono	Co	TW Mono	SD Mono	TW Mono								
77	179.1	10.29	1576	4-(2-Hydroxyethyl)phenol	Alc	?				-1.4	2.3	Sd
101	303.2	11.37	1718	1,12-Dodecanedio	Alc	??				-2.1	5.0	
4	175	5.65	964	Methyl 3-hydroxybutanoate	CA	?		-		-2.9	-	
53	187.2	9.24	1438	2-Hydroxy-3-methylbutanoic acid	CA	??				-3.1	4.9	
92	247.1	10.99	1668	2-Hydroxypentanedioic acid	CA	?!		-		-3.5	-	
180	146.1	14.82	2260	Octadecanoic acid	CA	*				-3.5	2.4	
71	179.1	10.06	1546	4-Hydroxybenzoic acid methylester	CA dv.					-2.1	38.7	
241	174.1	17.21	2677	Maltose	CS	??		-		-2.7	-	
273	204.1	19.20	2998	Galactinol	CS dv.	?				-2.3	13.3	
61	223.1	9.66	1493	4-Hydroxybenzaldehyde	O					-1.8	1.5	
96	226.1	11.10	1682	Ribose	S	?		-		-2.6	-	
102	357.2	11.48	1732	Xylitol	S					-1.7	3.3	
209	221.1	16.07	2478	Uridine	S dv.					-1.0	1.6	
210	217.1	16.09	2482	Uridine	S dv.			-		-3.5	-	
114	253.1	11.85	1781	3-(2-Hydroxyethyl)-2,2,4-trimethyl-3-cyclohexene-1-carbaldehyde	T	?				-2.2	4.8	
24	183.1	7.44	1200	Unknown	U	-				-1.7	8.1	

ID	Model ion	RT	RI	Name	Class	Ident	Median (n=3)			Fold (Co relative to:)		Group
							Day 15			Day 15		
							SD Mono	Co	TW Mono	SD Mono	TW Mono	
37	196.1	8.16	1295	Skel_MEDIA_C086 (Vidoudez)	U	?				-1.6	4.0	
39	197.1	8.29	1312	Unknown	U	-				-2.7	-	
42	199.1	8.47	1336	Skel_MEDIA_C097 (Vidoudez)	U	-				-1.9	3.3	
56	231.1	9.48	1469	Skel_MEDIA_C127 (Vidoudez)	U	-				-2.6	-	
66	184.1	9.91	1526	Skel_MEDIA_C141 (Vidoudez)	U	-				-1.7	9.5	
67	184.1	9.96	1532	Skel_MEDIA_C141 (Vidoudez)	U	-				-1.7	9.4	
69	122.1	9.99	1536	Unknown	U	-				-1.9	7.2	
72	171.1	10.11	1552	Unknown	U	-				-2.0	-	
79	226.1	10.38	1587	Unknown	U	-				-1.4	-	
84	284.1	10.59	1615	Unknown	U	-				-1.6	3.3	
91	250.1	10.95	1662	Unknown	U	-				-1.7	2.3	
117	253.1	12.02	1803	Skel_MEDIA_C205 (Vidoudez)	U	-				-2.5	9.1	
120	211.1	12.09	1813	Unknown	U	-				-2.7	13.6	
123	250.2	12.19	1826	Unknown	U	-				-1.7	8.7	
124	155.1	12.21	1829	Unknown	U	-				-3.0	-	
125	263.2	12.24	1833	Unknown	U	-				-3.1	732.3	
128	167.1	12.40	1854	Unknown	U	-				-2.5	21.9	
130	161.1	12.44	1859	Unknown	U	-				-3.8	-	
131	197.1	12.46	1861	Unknown	U	-				-1.9	18.1	
136	156.1	12.70	1894	Unknown	U	-				-3.7	-	
139	324.2	12.85	1917	Unknown	U	-				-1.8	43.2	
140	382.2	12.88	1923	Unknown	U	-				-2.4	5.3	
141	248.1	12.93	1931	Unknown	U	-				-3.1	-	

ID	Model ion	RT	RI	Name	Class	Ident	Median (n=3)			Fold (Co relative to:)		Group
							Day 15			Day 15		
							SD Mono	Co	TW Mono	SD Mono	TW Mono	
142	382.2	12.96	1936	Unknown	U	-				-2.3	5.1	
145	199.1	13.08	1957	Unknown	U	-				-1.5	2.2	
148	382.2	13.13	1966	Unknown	U	-				-2.2	6.0	
150	323.2	13.21	1979	Unknown	U	-				-3.3	13.4	
154	156.1	13.37	2007	Unknown	U	-				-1.8	2.9	
156	156.1	13.44	2020	Unknown	U	-			-	-3.2	-	
192	159.1	15.37	2355	Unknown	U	-			-	-3.2	-	
195	173.1	15.53	2384	Unknown	U	-			-	-1.9	-	
196	199.1	15.56	2389	Unknown	U	-				-2.5	11.8	
197	467.3	15.59	2395	Unknown	U	-			-	-3.0	-	
198	317.2	15.61	2397	Unknown	U	-				-3.3	14.4	
208	185.1	15.98	2462	Unknown	U	-			-	-3.3	-	
211	317.2	16.15	2492	Unknown	U	-				-2.5	23.7	
213	254.2	16.21	2502	Unknown	U	-			-	-2.2	-	
214	411.2	16.25	2510	Unknown	U	-				-2.9	15.2	
221	148.1	16.49	2551	Unknown	U	-			-	-2.5	-	
232	171.1	16.94	2630	Unknown	U	-			-	-3.1	-	
242	357.2	17.24	2681	Unknown	U	-				-3.1	42.8	
243	311.2	17.26	2686	Unknown	U	-			-	-4.5	-	
256	171.1	17.77	2773	Unknown	U	-			-	-4.0	-	
258	273.2	17.82	2782	Unknown	U	-			-	-2.6	-	
259	273.2	17.87	2792	Unknown	U	-			-	-2.7	-	
260	357.2	17.90	2795	Unknown	U	-			-	-5.6	-	

ID	Model ion	RT	RI	Name	Class	Ident	Median (n=3)			Fold (Co relative to:)		Group
							Day 15			Day 15		
							SD Mono	Co	TW Mono	SD Mono	TW Mono	
262	261.1	18.14	2834	Unknown	U	-				-3.3	8.3	
265	273.1	18.44	2880	Unknown	U	-				-2.9	-	
268	273.2	18.73	2926	Unknown	U	-				-2.6	-	
282	259.2	22.40	3360	Unknown	U	-				-4.0	-	
283	259.2	22.98	3408	Unknown	U	-				-3.9	-	

In case derivatized molecules are detected, the table entry lists their putative parent compounds. Each MST is characterized by **ID**, **model ion**, retention time (**RT**) and retention index (**RI**). Metabolites were identified via libraries. If metabolites were verified with a standard, they are marked with *. “?” indicates a reversed match between 700 and 800, “??” a reversed match between 600 and 700 and “???” indicates cases where the reversed match was ≤ 600 . “1” tags metabolites with a match smaller than 600. Class abbreviations: Amine (**A**), alcohol (**Alc**), alkaloid (**Alk**), carboxylic acid (**CA**), complex sugar (**CS**), derivatives of a certain class (**dv.**), sugar (**S**), sugar alcohol (**S Alc**), sugar acid (**S Acid**), sterol (**St**), terpene (**T**), others (**O**), unknown (**U**). **Vidoudez** refers to an MST code given by the inhouse library, **GOLM** refers to an MST code given by distinct libraries of the Golm Metabolome Database.

Appendix 85: Heatmap of exometabolite intensities for the subset analysis of the interaction between *T. weissflogii* and *S. dohrnii* on day 27. Medians of MST intensities, normalized to the external standard ribitol (per sample) and subsequently metabolite-wise auto scaled, are represented by a color code ranging from high (yellow) to low intensities (blue). White indicates the absence of the respective MST after data pre-processing. Metabolites are sorted according to abundance patterns (separated by black lines), class and RI. Only metabolites significantly correlating with the separation of treatments and treatment per day are shown. The fold change of MST abundance in co-cultivation relative to mono-cultivations is given and coded with a second color code. Black indicates a higher abundance in co-cultivation, grey a higher abundance in mono-cultivation.

ID	Model ion	RT	RI	Name	Class	Ident	Metabolite intensity			Fold change		Group
							Day 27			Day 27		
							SD Mono	Co	TW Mono	SD Mono	TW Mono	
							low	high	low	UP	DOWN	
77	179.1	10.29	1576	4-(2-Hydroxyethyl)phenol	Alc	?			-1.4	3.4	Sd	
101	303.2	11.37	1718	1,12-Dodecanediol	Alc	??			-1.7	6.2		
71	179.1	10.06	1546	4-Hydroxybenzoic acid methylester	CA dv.		-		-1.5	-		
241	174.1	17.21	2677	Maltose	CS	??		-	-1.9	-		
96	226.1	11.10	1682	Ribose	S	?		-	-1.8	-		
230	230	16.87	2617	Adenosine	S dv.				-2.2	54.9		
114	253.1	11.85	1781	3-(2-Hydroxyethyl)-2,2,4-trimethyl-3-cyclohexene-1-carbaldehyde	T	?			-1.6	5.1		
24	183.1	7.44	1200	Unknown	U	-			-1.7	19.7		
39	197.1	8.29	1312	Unknown	U	-			-1.7	5.6		
42	199.1	8.47	1336	Skel_MEDIA_C097 (Vidoudez)	U				-1.7	3.7		
56	231.1	9.48	1469	Skel_MEDIA_C127 (Vidoudez)	U				-1.7	6.4		
66	184.1	9.91	1526	Skel_MEDIA_C141 (Vidoudez)	U				-1.8	12.9		
67	184.1	9.96	1532	Skel_MEDIA_C141 (Vidoudez)	U				-1.8	12.9		
69	122.1	9.99	1536	Unknown	U	-			-2.0	4.1		
84	284.1	10.59	1615	Unknown	U	-			-1.3	1.9		
117	253.1	12.02	1803	Skel_MEDIA_C205 (Vidoudez)	U				-1.9	16.6		

120	211.1	12.09	1813	Unknown	U	-			-	-1.7	-
122	157.1	12.14	1820	Skel_MEDIA_C215 (Vidoudez)	U	?				-1.5	5.4
123	250.2	12.19	1826	Unknown	U	-				-1.5	6.6
124	155.1	12.21	1829	Unknown	U	-				-2.4	-
125	263.2	12.24	1833	Unknown	U	-				-1.8	110.2
128	167.1	12.40	1854	Unknown	U	-				-1.7	-
131	197.1	12.46	1861	Unknown	U	-				-1.3	7.4
138	153.1	12.79	1906	Unknown	U	-				-1.6	11.0
139	324.2	12.85	1917	Unknown	U	-				-1.5	-
142	382.2	12.96	1936	Unknown	U	-				-2.9	23.0
148	382.2	13.13	1966	Unknown	U	-				-1.8	9.8
150	323.2	13.21	1979	Unknown	U	-				-1.3	17.2
153	351.2	13.33	2001	Unknown	U	-				-1.7	2.5
160	170.1	13.63	2054	Unknown	U	-				-1.4	4.2
172	260.2	14.29	2169	Unknown	U	-				-1.4	7.2
174	467.2	14.48	2201	Unknown	U	-				-1.9	61.5
184	221.1	15.02	2295	Unknown	U	-				-1.6	4.3
192	159.1	15.37	2355	Unknown	U	-				-1.7	-
196	199.1	15.56	2389	Unknown	U	-				-1.4	83.7
198	317.2	15.61	2397	Unknown	U	-				-2.2	13.5
206	211.1	15.90	2448	Unknown	U	-				-1.7	327.1
207	117.1	15.95	2457	Unknown	U	-				-1.6	-
208	185.1	15.98	2462	Unknown	U	-				-2.4	-
213	254.2	16.21	2502	Unknown	U	-				-1.5	34.5
214	411.2	16.25	2510	Unknown	U	-				-1.8	160.3
217	145.1	16.35	2526	Unknown	U	-				-1.9	-
220	247.2	16.45	2544	Unknown	U	-				-2.1	-
232	171.1	16.94	2630	Unknown	U	-				-2.3	-
244	173.1	17.31	2694	Unknown	U	-				-2.1	-
245	164.1	17.35	2701	Unknown	U	-				-1.2	-

256	171.1	17.77	2773	Unknown	U	-				-2.3	88.4
258	273.2	17.82	2782	Unknown	U	-				-2.1	-
259	273.2	17.87	2792	Unknown	U	-				-2.1	-
265	273.1	18.44	2880	Unknown	U	-				-2.3	-
268	273.2	18.73	2926	Unknown	U	-				-2.2	-
283	259.2	22.98	3408	Unknown	U	-				-1.9	-

In case derivatized molecules are detected, the table entry lists their putative parent compounds. Each MST is characterized by **ID**, **model ion**, retention time (**RT**) and retention index (**RI**). Metabolites were identified via libraries. If metabolites were verified with a standard, they are marked with *. “?” indicates a reversed match between 700 and 800, “??” a reversed match between 600 and 700 and “???” indicates cases where the reversed match was ≤ 600 . “s” tags metabolites with a match smaller than 600. Class abbreviations: Amine (**A**), alcohol (**Alc**), alkaloid (**Alk**), carboxylic acid (**CA**), complex sugar (**CS**), derivatives of a certain class (**dv.**), sugar (**S**), sugar alcohol (**S Alc**), sugar acid (**S Acid**), sterol (**St**), terpene (**T**), others (**O**), unknown (**U**). **Vidoudez** refers to an MST code given by the inhouse library, **GOLM** refers to an MST code given by distinct libraries of the Golm Metabolome Database.

Appendix 86: Heatmap of exometabolite intensities for the subset analysis of the interaction between *T. weissflogii* and *S. dohrnii* on day 35.

Medians of MST intensities, normalized to the external standard ribitol (per sample) and subsequently metabolite-wise auto scaled, are represented by a color code ranging from high (yellow) to low intensities (blue). White indicates the absence of the respective MST after data pre-processing. Metabolites are sorted according to abundance patterns (separated by black lines), class and RI. Only metabolites significantly correlating with the separation of treatments and treatment per day are shown. The fold change of MST abundance in co-cultivation relative to mono-cultivations is given and coded with a second color code. Black indicates a higher abundance in co-cultivation, grey a higher abundance in mono-cultivation.

ID	Model ion	RT	RI	Name	Class	Ident	Metabolite intensity			Fold change		Group
							low		high	UP	DOWN	
							Median (n=3)			Fold (Co relative to:)		
							Day 35			Day 35		
SD Mono	Co	TW Mono	SD Mono	TW Mono								
85	217	10.63	1621	Arabinofuranose	S				1.0	3.7	A	
101	303.2	11.37	1718	1,12-Dodecanediol	Alc	??			-1.5	5.2	Sd	
53	187.2	9.24	1438	2-Hydroxy-3-methylbutanoic acid	CA	??			-1.5	3.2		
92	247.1	10.99	1668	2-Hydroxypentanedioic acid	CA	? ¹			-1.6	8.8		
94	129.1	11.06	1677	2-Hydroxyhexanedioic acid	CA	?		-	-1.1	-		
71	179.1	10.06	1546	4-Hydroxybenzoic acid methylester	CA dv.				-1.3	150.2		
218	225.1	16.39	2534	Diphenyl phthalate	CA dv.				-2.0	31.4		
215	217.1	16.28	2515	Maltose	CS	??			-1.7	18.3		
239	217.1	17.09	2655	Sucrose	CS				-1.3	220.2		
241	174.1	17.21	2677	Maltose	CS	??		-	-1.4	-		
250	361.2	17.54	2733	Maltose	CS				-1.9	6.7		
251	204.1	17.57	2739	Lactose	CS				-1.4	9.3		
257	204.1	17.79	2777	Maltose	CS	??		-	-1.2	-		
284	204.1	24.27	3516	Maltotriose	CS				-1.3	6.0		
285	217.1	24.84	3564	Maltotriose	CS				-2.4	11.3		
273	204.1	19.20	2998	Galactinol	CS dv.	?			-2.1	6.1		
78	217	10.33	1581	Arabinofuranose	S				-1.0	4.1		
81	217	10.43	1595	Arabinofuranose	S				-1.2	4.1		
83	217.1	10.49	1602	Arabinofuranose	S				-1.2	6.6		
96	226.1	11.10	1682	Ribose	S	?		-	-1.1	-		

ID	Model ion	RT	RI	Name	Class	Ident	Median (n=3)			Fold (Co relative to:)		Group
							Day 35			Day 35		
							SD Mono	Co	TW Mono	SD Mono	TW Mono	
135	319.2	12.59	1879	Gluconic acid-1,5-lactone	S acid dv.				-1.3	4.5		
210	217.1	16.09	2482	Uridine	S dv.				-1.8	7.7		
230	230	16.87	2617	Adenosine	S dv.				-1.5	15.0		
114	253.1	11.85	1781	3-(2-Hydroxyethyl)-2,2,4-trimethyl-3-cyclohexene-1-carbaldehyde	T	?			-1.4	5.2		
24	183.1	7.44	1200	Unknown	U	-			-1.3	-		
39	197.1	8.29	1312	Unknown	U	-			-1.3	3.1		
42	199.1	8.47	1336	Skel_MEDIA_C097 (Vidoudez)	U	-			-1.6	3.2		
56	231.1	9.48	1469	Skel_MEDIA_C127 (Vidoudez)	U	-			-1.3	7.2		
66	184.1	9.91	1526	Skel_MEDIA_C141 (Vidoudez)	U	-			-1.1	9.5		
67	184.1	9.96	1532	Skel_MEDIA_C141 (Vidoudez)	U	-			-1.1	9.5		
97	129.1	11.15	1689	Unknown	U	-			-1.7	-		
100	285.2	11.28	1706	Unknown	U	-			-1.0	4.3		
115	129.1	11.90	1788	Unknown	U	-			-1.2	17.4		
117	253.1	12.02	1803	Skel_MEDIA_C205 (Vidoudez)	U	-			-1.6	10.5		
120	211.1	12.09	1813	Unknown	U	-			-1.4	11.4		
122	157.1	12.14	1820	Skel_MEDIA_C215 (Vidoudez)	U	?			-1.4	3.9		
124	155.1	12.21	1829	Unknown	U	-			-1.4	-		
125	263.2	12.24	1833	Unknown	U	-			-1.7	-		
128	167.1	12.40	1854	Unknown	U	-			-1.2	62.3		
130	161.1	12.44	1859	Unknown	U	-			-1.8	11.8		
133	271.1	12.50	1867	Unknown	U	-			-1.4	11.9		
138	153.1	12.79	1906	Unknown	U	-			-1.5	4.9		
139	324.2	12.85	1917	Unknown	U	-			-1.3	105.8		
140	382.2	12.88	1923	Unknown	U	-			-1.3	11.8		
142	382.2	12.96	1936	Unknown	U	-			-1.3	11.8		
146	129.1	13.10	1961	Unknown	U	-			-2.0	-		
148	382.2	13.13	1966	Unknown	U	-			-1.5	8.7		
160	170.1	13.63	2054	Unknown	U	-			-1.4	3.4		

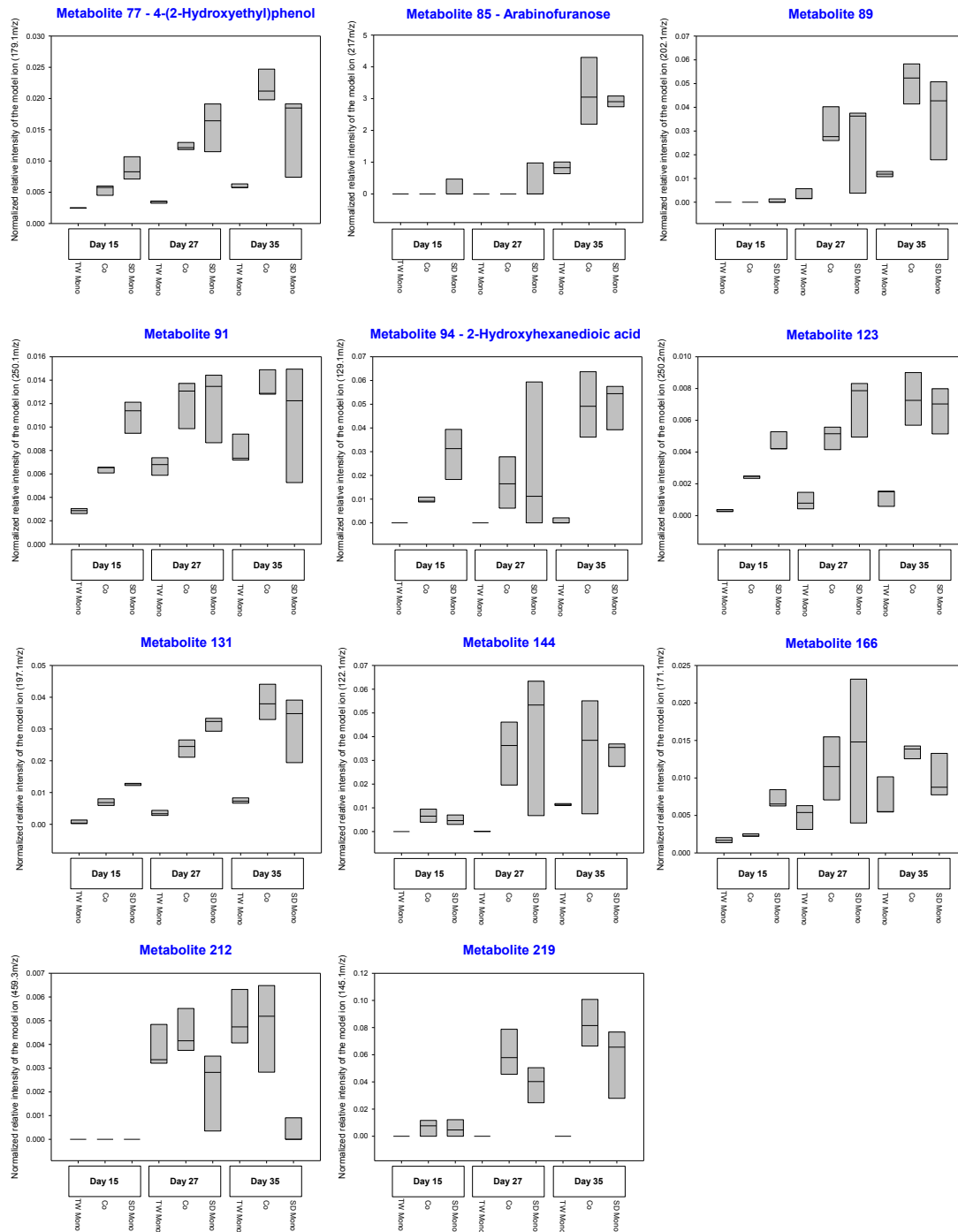
ID	Model ion	RT	RI	Name	Class	Ident	Median (n=3)			Fold (Co relative to:)		Group
							Day 35			Day 35		
							SD Mono	Co	TW Mono	SD Mono	TW Mono	
183	171.1	14.96	2284	Unknown	U	-				-1.6	8.9	
191	188.1	15.33	2349	Unknown	U	-				-1.1	20.8	
192	159.1	15.37	2355	Unknown	U	-				-1.5	-	
196	199.1	15.56	2389	Unknown	U	-				-1.6	14.0	
197	467.3	15.59	2395	Unknown	U	-				-1.2	4.7	
202	225.2	15.75	2423	Unknown	U	-				-1.1	-	
206	211.1	15.90	2448	Unknown	U	-				-1.4	19.4	
208	185.1	15.98	2462	Unknown	U	-				-2.1	150.5	
211	317.2	16.15	2492	Unknown	U	-				-1.5	11.4	
213	254.2	16.21	2502	Unknown	U	-				-1.8	10.0	
214	411.2	16.25	2510	Unknown	U	-				-2.0	27.7	
216	217.1	16.33	2522	Unknown	U	-				-1.8	-	
217	145.1	16.35	2526	Unknown	U	-				-1.8	25.3	
220	247.2	16.45	2544	Unknown	U	-				-1.3	74.7	
221	148.1	16.49	2551	Unknown	U	-				-1.3	-	
238	371.2	17.07	2652	Unknown	U	-				-1.3	6.2	
242	357.2	17.24	2681	Unknown	U	-				-1.4	23.8	
245	164.1	17.35	2701	Unknown	U	-				-2.0	-	
246	171.1	17.41	2712	Unknown	U	-				-1.5	90.9	
264	204.1	18.35	2867	Unknown	U	-				-1.3	5.7	
265	273.1	18.44	2880	Unknown	U	-				-2.2	27.7	
266	204.1	18.51	2892	Unknown	U	-				-1.6	5.3	
270	204.1	18.94	2958	Unknown	U	-				-1.3	51.7	
280	217.1	21.13	3253	Unknown	U	-				-1.1	16.0	
281	259.2	21.18	3257	Unknown	U	-				-1.6	13.9	
282	259.2	22.40	3360	Unknown	U	-				-1.6	562.0	
283	259.2	22.98	3408	Unknown	U	-				-1.8	-	

In case derivatized molecules are detected, the table entry lists their putative parent compounds. Each MST is characterized by **ID**, **model ion**, retention time (**RT**) and retention index (**RI**). Metabolites were identified via libraries. If metabolites were verified with a standard, they are marked with *. “?” indicates a reversed match between 700 and 800, “??” a reversed match between 600 and 700 and “???” indicates cases where the reversed match was ≤ 600 . “1” tags metabolites with a match smaller than 600. Class abbreviations: Amine (**A**), alcohol (**Alc**), alkaloid (**Alk**), carboxylic acid (**CA**), complex sugar (**CS**), derivatives of a certain class (**dv.**), sugar (**S**), sugar alcohol (**S Alc**), sugar acid (**S Acid**), sterol (**St**), terpene (**T**), others (**O**), unknown (**U**). **Vidoudez** refers to an MST code given by the inhouse library, **GOLM** refers to an MST code given by distinct libraries of the Golm Metabolome Database.

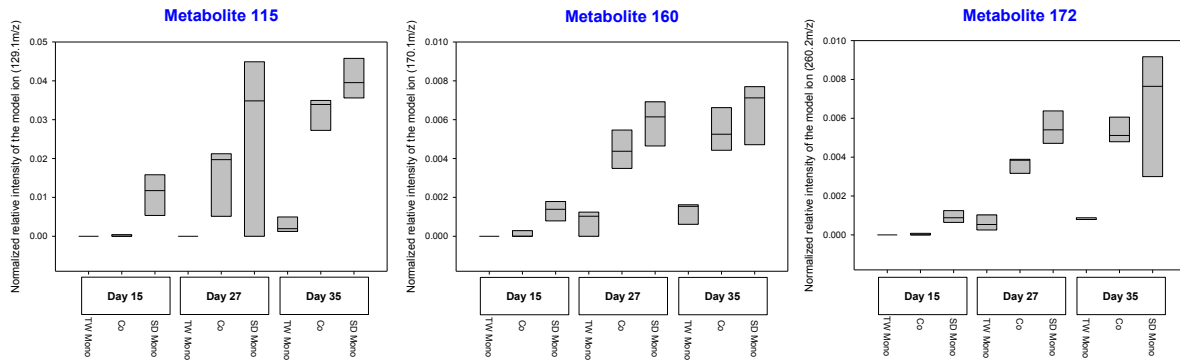
Screening for interaction specific release and/or uptake of potential infochemicals

Appendix 87: Intensity dynamic of exometabolites, enhanced (pattern I) in co-cultivation in the interaction between *T. weissflogii* and *S. dohrnii*.

Boxplots visualized intensity dynamics over time and treatments via relative MST intensities (ribitol normalized) of the respective model ion.

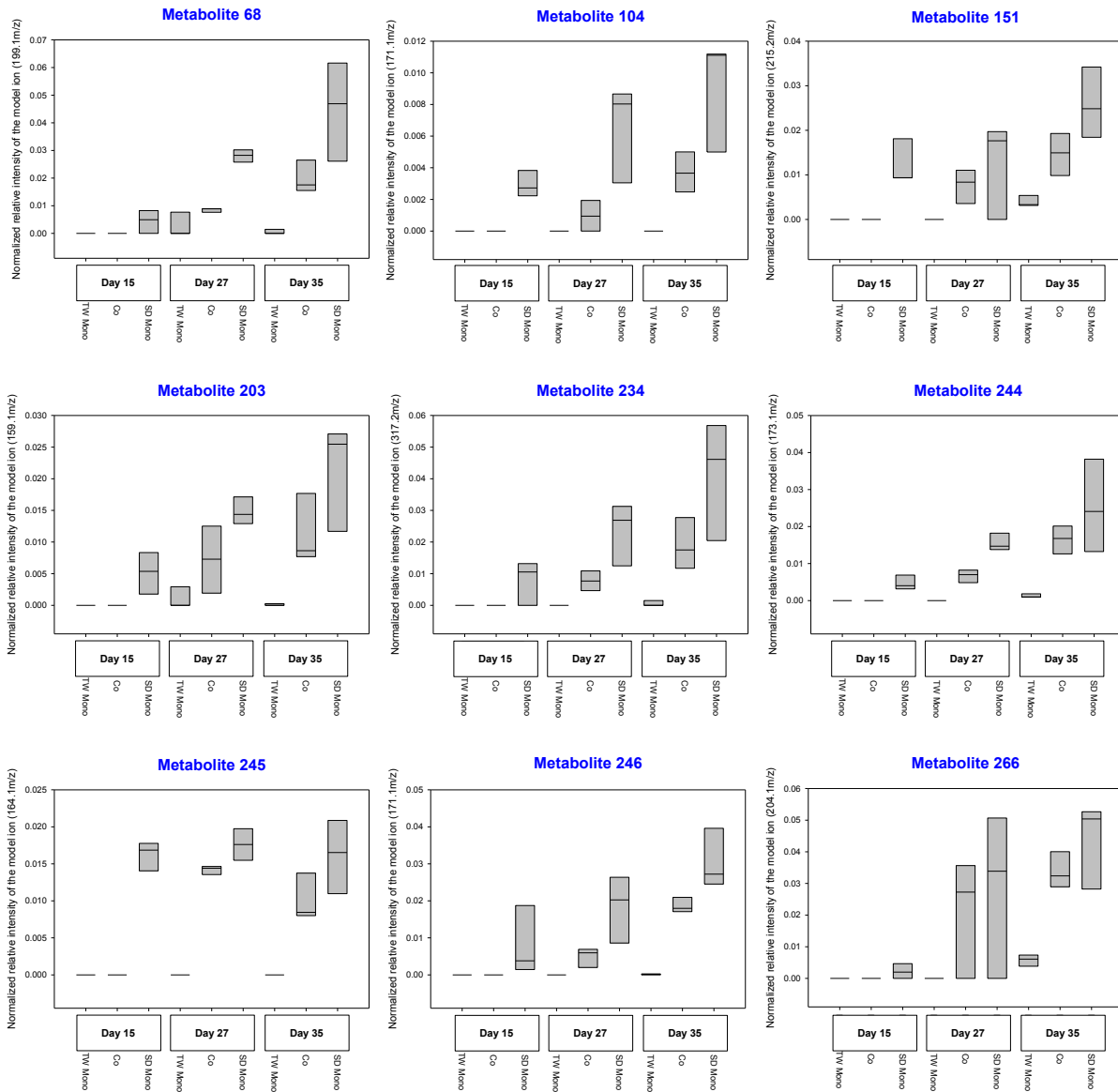


Appendix 88: Intensity dynamic of exometabolites excluded in the screening process for exometabolites, which were reduced in co-cultivation in the interaction between *T. weissflogii* and *S. dohrnii* and matched pattern III. Boxplots visualized intensity dynamics over time and treatments via relative MST intensities (ribitol normalized) of the respective model ion.



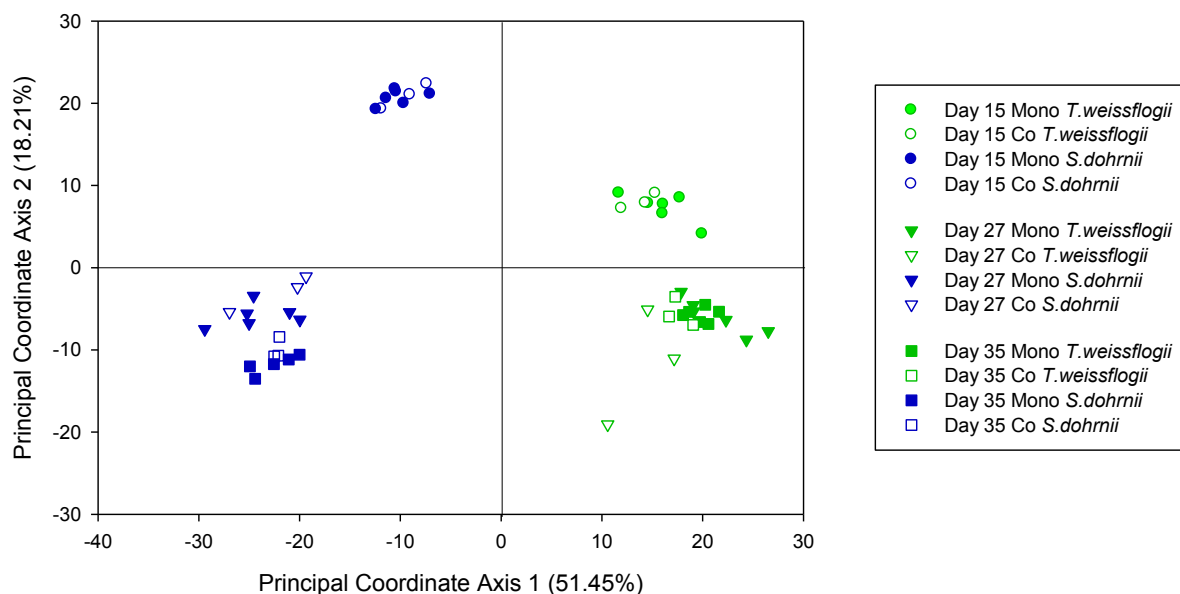
Appendix 89: Intensity dynamic of exometabolites, reduced (pattern II / III) in co-cultivation in the interaction between *T. weissflogii* and *S. dohrnii*.

Boxplots visualized intensity dynamics over time and treatments via relative MST intensities (ribitol normalized) of the respective model ion.



7.3.7 Supplements: Endometabolomic investigation

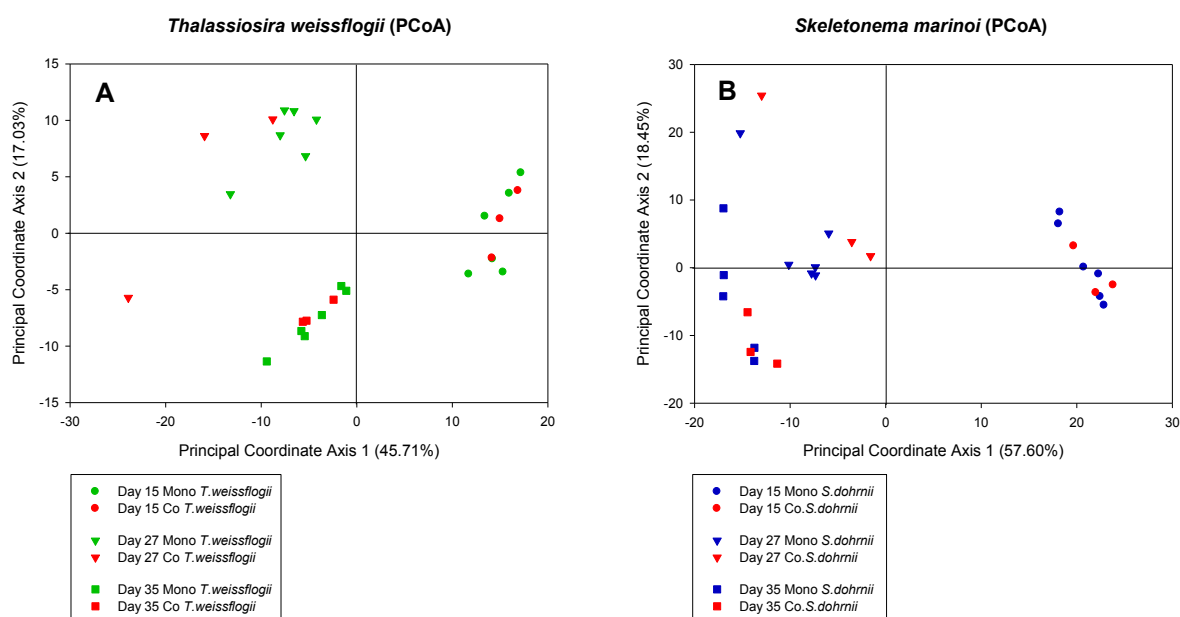
Overall analysis via CAP



Appendix 90: PCoA score plot of endometabolomic samples from an overall analysis of the interaction between *T. weissflogii* and *S. dohrnii*.

The plot is based on metabolites obtained from *S. dohrnii* (blue) and *T. weissflogii* (green) on day 15 (●), day 27 (▼) and day 35 (■). Samples from mono-cultivation are represented by filled symbols, samples from co-cultivation by empty symbols.

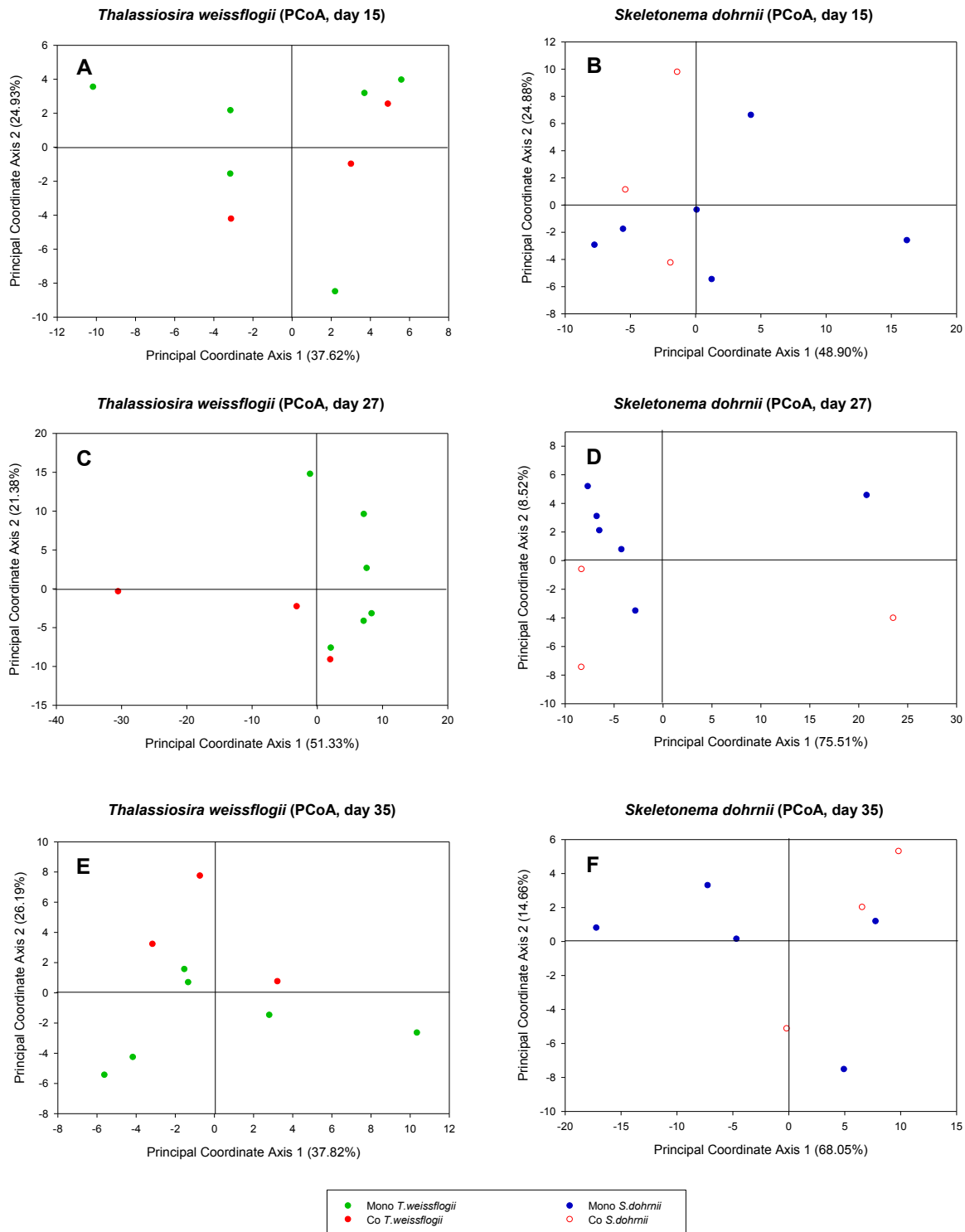
Species-specific analysis via CAP



Appendix 91: PCoA score plot of endometabolomic samples from a species-specific subset analysis of the interaction between *T. weissflogii* and *S. dohrnii*.

The plots are based on metabolites obtained from mono-cultivated (**green**) and co-cultivated (**red**) *T. weissflogii* (graph **A**) and mono-cultivated (**blue**) and co-cultivated (**red**) *S. dohrnii* (graph **B**) on day 15 (●), day 27 (▼) and day 35 (■). The analysis was performed for each species individually.

Daywise and species-specific analysis via CAP



Appendix 92: PCoA score plot of endometabolomic samples from a species-specific subset analysis of the interaction between *T. weissflogii* and *S. dohrnii* on day 15, 27 and 35.

The plots are based on metabolites obtained from mono-cultivated (**green**) and co-cultivated (**red**) *T. weissflogii* (graph **A**, **C**, **E**) and mono-cultivated (**blue**) and co-cultivated (**red**) *S. dohrnii* (graph **B**, **D**, **F**) on day 15 (●, graph **A**, **B**), day 27 (●, graph **C**, **D**) and day 35 (●, graph **E**, **F**). The analysis was performed for each species and day individually.

Identification of metabolites correlating with relevant a-priori groups

T. weissflogii

Appendix 93: Heatmap of unknown endometabolite intensities for the species-specific and daywise analysis of *T. weissflogii* in interaction with *S. dohrnii*. Medians of MST intensities, normalized to peak sum per sample and subsequently metabolite-wise auto scaled, are represented by a color code ranging from high (yellow) to low intensities (blue). White indicates the absence of the respective MST after data pre-processing. Metabolites are sorted according to classes (separated by black lines) and abundance patterns. Only metabolites significantly correlating with the separation of treatments and treatment per day are shown. The fold change of MST abundance in co-cultivation relative to mono-cultivation is given and coded with a second color code. Black indicates a higher abundance in co-cultivation, grey a higher abundance in mono-cultivation.

ID	Model ion	RT	RI	Name	Class	Ident	Analysis	Median MST intensity						Fold change				
								low high						UP	DOWN			
								Median (Co: n=3, Mono: n=6)						Fold (Co relative to Mono)				
Day 15		Day 27		Day 35		Day 15	Day 27	Day 35										
Mono	Co	Mono	Co	Mono	Co	Day 15	Day 27	Day 35										
11	221.1	5.59	955	M000000_A107001-101-xxx_NA_1060,6_PRED_VAR5_ALK_Unknown#bth-pae-059 (GOLM)	U	-	35									1.5	2.4	1.7
15	173.1	5.93	999	Unknown	U	-	35									1.0	-1.1	-1.5
18	186.1	6.09	1021	Unknown	U	-	DT									-1.4	-	-2.4
21	102.1	6.20	1035	Unknown	U	-	35									-1.7	-1.1	3.4
29	234.1	6.45	1068	Unknown	U	-	DT									1.3	-4.8	1.3
39	166.1	6.85	1121	Unknown	U	-	DT									-1.1	-1.0	-1.3
41	174.1	6.89	1127	Unknown	U	-	35									-1.2	-1.6	-1.3
53	234.1	7.25	1174	Unknown	U	-	DT									-1.0	-1.1	1.5
56	217.1	7.41	1195	Unknown	U	-	DT									1.1	-	-1.1
57	103.1	7.43	1198	MesocosmC066 (Vidoudez)	U	?	DT									1.1	-	-

ID	Model ion	RT	RI	Name	Class	Ident	Analysis	Median (Co: n=3, Mono: n=6)						Fold (Co relative to Mono)		
								Day 15		Day 27		Day 35		Day 15	Day 27	Day 35
								Mono	Co	Mono	Co	Mono	Co			
60	166.1	7.53	1211	Unknown	U	-	DT							-1.1	-1.1	-1.6
65	117	7.79	1246	Unknown	U	-	DT							1.1	-	1.7
70	217.1	7.95	1267	Unknown	U	-	DT							-1.0	-	-2.6
85	217.1	8.68	1363	EITTMS_N12C_ATHR_1770.9_1135EC25_(GOLM)	U	?	DT							-1.2	-	-1.3
86	218.1	8.71	1367	Unknown	U	-	DT							1.1	-	1.1
89	243.1	8.81	1380	EITTMS_N12C_ATHR_1456.1_1135EC44_(GOLM)	U	?	DT							1.0	-4.9	1.1
92	148.1	8.90	1392	Unknown	U	-	DT							1.4	-	-1.2
93	217.1	8.96	1400	Unknown	U	-	DT							-1.1	-	1.3
94	259.1	8.98	1403	Unknown	U	-	DT							-1.0	1.8	1.2
95	129.1	9.00	1405	Unknown	U	-	DT							1.1	-	-
96	240.1	9.03	1409	Unknown	U	-	35							1.2	1.5	1.3
97	201.1	9.07	1415	EITTMS_N12C_ATHR_1442.5_1135EC44_(GOLM)	U	?	35							-1.1	-1.3	-1.4
99	103.1	9.21	1433	Unknown	U	-	DT							-1.2	-	1.0
100	217.1	9.23	1436	Unknown	U	-	DT							1.1	-	1.5
102	318.2	9.30	1445	Unknown	U	-	DT							-1.1	-	-
109	157.1	9.49	1470	EITTMS_N12C_ATHR_1480.5_1135EC44_(GOLM)	U	-	DT							1.0	1.2	1.2
110	123.1	9.51	1473	Unknown	U	-	DT							1.2	-1.0	-1.6
112	231.1	9.57	1481	Unknown	U	-	DT							-1.1	1.1	1.1
116	228.1	9.68	1496	Unknown	U	-	35							1.4	-1.6	-1.8
122	198.1	9.92	1527	Unknown	U	-	35							1.3	1.7	1.6
124	157	9.99	1536	Unknown	U	-	DT							-1.1	1.2	1.3

ID	Model ion	RT	RI	Name	Class	Ident	Analysis	Median (Co: n=3, Mono: n=6)						Fold (Co relative to Mono)		
								Day 15		Day 27		Day 35		Day 15	Day 27	Day 35
								Mono	Co	Mono	Co	Mono	Co			
131	157	10.22	1566	Unknown	U	-	DT						1.0	1.1	1.0	
132	243.2	10.25	1571	Unknown	U	-	DT						1.2	-	-	
145	235.1	10.75	1637	Unknown	U	-	DT						1.5	-	-	
146	129.1	10.78	1640	Unknown	U	-	DT						1.1	-	-2.9	
147	257.1	10.80	1644	Unknown	U	-	DT						-1.1	-	-	
154	159.1	11.01	1671	Unknown	U	-	DT						-1.1	1.1	1.2	
166	318.2	11.41	1724	Unknown	U	-	DT						-1.0	-	-	
169	217.1	11.53	1740	Unknown	U	-	DT						-1.0	-	-1.5	
173	392.2	11.68	1759	Skel_cell_C065 (Vidoudez)	U	-	DT,35						-1.2	-1.7	-1.4	
174	238.1	11.69	1761	Unknown	U	-	DT						1.7	-	-	
175	331.2	11.72	1765	Unknown	U	-	DT						-1.2	-	1.1	
179	392.2	11.81	1777	Skel_cell_C065 (Vidoudez)	U	-	DT,35						-1.1	-1.8	-1.4	
183	392.2	11.95	1795	Skel_cell_C065 (Vidoudez)	U	-	DT,35						-1.1	-1.5	-1.5	
184	276.1	11.99	1801	Unknown	U	-	DT,35						-1.0	-1.8	-1.5	
185	253.1	12.02	1804	Skel_MEDIA_C205 (Vidoudez)	U	-	DT,35						1.2	1.1	1.2	
186	276.1	12.05	1808	Unknown	U	-	35						-1.2	1.1	-1.8	
189	342.2	12.17	1824	Unknown	U	-	DT						1.4	-	1.3	
190	218.1	12.19	1828	EITTMS_N12C_STUR_1832.7_1135EC29_ (GOLM)	U	-	35						1.2	1.5	1.3	
191	347.2	12.23	1832	Unknown	U	-	DT,35						-1.0	-1.0	-1.7	
192	372.2	12.25	1835	Unknown	U	-	DT						1.3	2.1	-1.3	
194	157.1	12.27	1838	Skel_MEDIA_C215 (Vidoudez)	U	-	DT						1.2	1.6	1.0	
198	205.1	12.44	1860	Unknown	U	-	DT						-1.2	1.1	-1.2	
200	205.1	12.49	1867	Unknown	U	-	DT,35						-1.1	-1.4	-1.6	

ID	Model ion	RT	RI	Name	Class	Ident	Analysis	Median (Co: n=3, Mono: n=6)						Fold (Co relative to Mono)		
								Day 15		Day 27		Day 35		Day 15	Day 27	Day 35
								Mono	Co	Mono	Co	Mono	Co			
206	205.1	12.75	1902	Unknown	U	-	DT,35						-1.4	-1.1	-1.5	
233	217.1	13.63	2054	Unknown	U	-	DT						-1.2	-1.7	-1.0	
246	173.1	14.12	2142	Unknown	U	-	DT						1.2	-1.4	1.2	
249	255.2	14.22	2157	Unknown	U	-	35						1.1	-1.1	-1.4	
250	221.1	14.23	2160	Unknown	U	-	35						-1.1	1.3	1.2	
252	967	14.29	2170	Unknown	U	-	DT						-1.2	-	1.2	
255	225.2	14.36	2182	Unknown	U	-	DT						-1.3	2.3	-1.0	
257	669	14.42	2193	Unknown	U	-	DT,35						-1.2	-	1.5	
263	167	14.61	2226	Unknown	U	-	DT						-1.0	-	-	
276	155.1	15.06	2304	Unknown	U	-	DT						-1.0	-	-1.2	
284	180.1	15.36	2357	Unknown	U	-	DT						-1.1	-5.1	-1.1	
289	167	15.52	2386	Unknown	U	-	DT						-	-	-	
291	342.2	15.60	2399	Unknown	U	-	DT						-1.0	1.2	-1.1	
292	111	15.63	2403	Unknown	U	-	DT						1.2	1.1	-1.1	
294	111	15.73	2421	Unknown	U	-	DT						1.2	1.2	1.0	
300	105.1	15.90	2451	Unknown	U	-	DT						-1.1	1.6	-1.2	
301	259.1	15.94	2459	Unknown	U	-	DT						1.1	1.4	1.1	
304	187.2	16.04	2475	Unknown	U	-	DT						2.0	1.2	-	
308	353.3	16.17	2498	Unknown	U	-	DT						-1.3	1.5	-1.4	
323	369.3	16.75	2600	Unknown	U	-	35						1.1	-1.7	-1.5	
334	159.1	17.18	2674	Unknown	U	-	DT						1.3	-1.2	-1.1	
340	204.1	17.40	2714	Unknown	U	-	35						1.2	1.6	1.3	

ID	Model ion	RT	RI	Name	Class	Ident	Analysis	Median (Co: n=3, Mono: n=6)						Fold (Co relative to Mono)		
								Day 15		Day 27		Day 35		Day 15	Day 27	Day 35
								Mono	Co	Mono	Co	Mono	Co			
349	311.3	17.82	2787	M000000_A278013-101-xxx_NA_2788,69_TRUE_VAR5_ALK_D278931 (GOLM)	U	?	DT							1.5	-	-
352	191.1	18.11	2834	M000000_A294006-101-xxx_NA_2939,93_PRED_VAR5_ALK_NA (GOLM)	U	?	DT							1.0	1.6	1.0
357	129.1	18.41	2881	Unknown	U	-	35							1.2	-2.6	-2.4
364	296.3	19.01	2975	Unknown	U	-	35							1.2	1.4	1.2
368	625.5	19.40	3036	Unknown	U	-	35							20.8	-7.8	-
369	275.2	19.47	3047	Unknown	U	-	DT							1.0	1.1	-1.2
370	293.3	19.50	3051	Unknown	U	-	DT							1.2	-2.1	1.4
381	468.4	20.52	3206	Unknown	U	-	DT							1.4	1.6	-1.1
387	217.1	21.05	3250	Unknown	U	-	DT							1.3	-	-
394	237.1	22.07	3336	Unknown	U	-	DT							-1.4	3.0	2.3
403	145.1	23.57	3462	Unknown	U	-	35							-1.0	1.0	-2.0
415	217.1	24.60	3549	Unknown	U	-	DT							-4.1	-	-
419	588.4	24.99	3582	Unknown	U	-	DT							1.3	-	-1.2
423	129.1	26.48	3707	Unknown	U	-	DT,35							-1.4	-1.2	-1.5
424	145.1	26.68	3724	Unknown	U	-	35							1.3	-	-
425	595.5	27.20	3767	Unknown	U	-	35							-1.2	1.1	-1.6

In case derivatized molecules are detected, the table entry lists their putative parent compounds. Each MST is characterized by **ID**, **model ion**, retention time (**RT**), retention index (**RI**) and its underlying CAP **analysis**. CAP analyses comprised the overall analysis with a-priori grouping by treatment and day (**DT**), with a-priori grouping by treatment (**T**), as well as daywise subset analysis on day 15 (**15**), 27 (**27**) and day 35 (**35**). Metabolites were identified via libraries. If metabolites were verified with a standard, they are marked with *. “?” indicates a reversed match between 700 and 800, “??” a reversed match between 600 and 700 and “???” indicates cases where the reversed match was ≤ 600 . “!” tags metabolites with a match smaller than 600. Class abbreviations: Amine (**A**), alcohol (**Alc**), alkaloid (**Alk**), carboxylic acid (**CA**), complex sugar (**CS**), derivatives of a certain class (**dv.**), hydrocarbons

(HC), sugar **(S)**, sugar alcohol **(S Alc)**, sugar acid **(S Acid)**, sterol **(St)**, terpene **(T)**, others **(O)**, unknown **(U)**. **Vidoudez** refers to an MST code given by the inhouse library, **GOLM** refers to an MST code given by distinct libraries of the Golm Metabolome Database.

S.dohrnii

Appendix 94: Heatmap of unknown endometabolite intensities for the species-specific and daywise analysis of *S. dohrnii* in interaction with *T. weissflogii*. Medians of MST intensities, normalized to peak sum per sample and subsequently metabolite-wise auto scaled, are represented by a color code ranging from high (yellow) to low intensities (blue). White indicates the absence of the respective MST after data pre-processing. Metabolites are sorted according to classes (separated by black lines) and abundance patterns. Only metabolites significantly correlating with the separation of treatments and treatment per day are shown. The fold change of MST abundance in co-cultivation relative to mono-cultivation is given and coded with a second color code. Black indicates a higher abundance in co-cultivation, grey a higher abundance in mono-cultivation.

ID	Model ion	RT	RI	Name	Class	Ident	Analysis	Median MST intensity						Fold change		
								low high						UP DOWN		
								Median (Co: n=3, Mono: n=5/6)			Fold (Co relative to Mono)					
								Day 15		Day 27		Day 35		Day 15	Day 27	Day 35
Mono	Co	Mono	Co	Mono	Co	Day 15	Day 27	Day 35								
1	148.1	5.20	904	Unknown	U	-	DT,15			-	-	-	-	1.6	-	-
2	102.1	5.25	910	Unknown	U	-	DT						1.1	1.1	-1.7	
21	102.1	6.20	1035	Unknown	U	-	DT						-1.2	1.9	1.1	
39	166.1	6.85	1121	Unknown	U	-	DT						-1.2	-	14.9	
41	174.1	6.89	1127	Unknown	U	-	DT					-	1.2	1.3	-	
43	126.1	6.95	1135	Unknown	U	-	DT			-	-	-	1.2	-	-	
49	227.1	7.15	1161	Unknown	U	-	DT	-	-			-	-	1.1	-	
53	234.1	7.25	1174	Unknown	U	-	DT						-1.2	1.1	1.6	
56	217.1	7.41	1195	Unknown	U	-	DT			-	-	-	1.1	-	-	
57	103.1	7.43	1198	MesocosmC066 (Vidoudez)	U	?	DT			-	-	-	1.1	-	-	
60	166.1	7.53	1211	Unknown	U	-	DT			-	-	-	-1.2	-	-	
67	117.1	7.87	1256	Unknown	U	-	DT			-		-	1.2	-	-	
69	180.1	7.94	1265	Unknown	U	-	DT			-	-	-	-1.9	-	-	
70	217.1	7.95	1267	Unknown	U	-	DT			-		-	-1.2	-	-	

ID	Model ion	RT	RI	Name	Class	Ident	Analysis	Median (Co: n=3, Mono: n=5/6)						Fold (Co relative to Mono)		
								Day 15		Day 27		Day 35		Day 15	Day 27	Day 35
								Mono	Co	Mono	Co	Mono	Co			
73	126.1	8.06	1281	Unknown	U	-	DT	-	-	-	-	-1.1	-	-		
74	306.2	8.07	1282	Skel_Cell_C021 (Vidoudez)	U	?	DT	-	-	-	-	1.2	-	1.5		
75	196.1	8.16	1294	Unknown	U	-	DT	-	-	-	-	1.1	-	-1.4		
79	199.1	8.48	1336	Skel_MEDIA_C097 (Vidoudez)	U	-	DT	-	-	-	-	-1.0	-1.0	1.6		
80	111.1	8.50	1339	Skel_MEDIA_C097 (Vidoudez)	U	-	15	-	-	-	-	1.6	1.1	1.3		
85	217.1	8.68	1363	EITTMS_N12C_ATHR_1770.9_1135EC25_ (GOLM)	U	?	DT	-	-	-	-	1.1	-	-		
86	218.1	8.71	1367	Unknown	U	-	DT	-	-	-	-	-1.3	-	1.4		
89	243.1	8.81	1380	EITTMS_N12C_ATHR_1456.1_1135EC44_ (GOLM)	U	?	DT	-	-	-	-	1.2	-	-		
92	148.1	8.90	1392	Unknown	U	-	DT	-	-	-	-	-1.1	-	-		
93	217.1	8.96	1400	Unknown	U	-	DT	-	-	-	-	1.3	-	-		
95	129.1	9.00	1405	Unknown	U	-	DT	-	-	-	-	3.2	-	-		
96	240.1	9.03	1409	Unknown	U	-	DT	-	-	-	-	-1.2	-1.2	1.1		
97	201.1	9.07	1415	EITTMS_N12C_ATHR_1442.5_1135EC44_ (GOLM)	U	?	DT	-	-	-	-	-1.0	-1.0	1.5		
99	103.1	9.21	1433	Unknown	U	-	DT	-	-	-	-	1.6	-	-		
100	217.1	9.23	1436	Unknown	U	-	DT	-	-	-	-	1.2	-	-		
102	318.2	9.30	1445	Unknown	U	-	DT	-	-	-	-	-1.2	4.3	-		
104	253.1	9.35	1452	Unknown	U	-	DT	-	-	-	-	-	1.2	-		
105	103.1	9.38	1455	EITTMS_N12C_ATHR_1479.3_1135EC44_ (GOLM)	U	-	DT	-	-	-	-	1.1	-	-		
106	318.2	9.43	1463	Unknown	U	-	DT	-	-	-	-	1.0	-	-		
110	123.1	9.51	1473	Unknown	U	-	DT	-	-	-	-	1.0	-1.1	1.2		
114	228.1	9.64	1490	Unknown	U	-	DT	-	-	-	-	-1.4	-1.3	-1.3		

ID	Model ion	RT	RI	Name	Class	Ident	Analysis	Median (Co: n=3, Mono: n=5/6)						Fold (Co relative to Mono)		
								Day 15		Day 27		Day 35		Day 15	Day 27	Day 35
								Mono	Co	Mono	Co	Mono	Co			
115	245.1	9.67	1494	Unknown	U	-	DT	-	-	-	-	-1.0	-	1.0		
116	228.1	9.68	1496	Unknown	U	-	DT	-	-	-	-	-1.1	1.1	1.1		
117	197.1	9.74	1504	Unknown	U	-	DT	-	-	-	-	1.1	-1.8	1.0		
118	335.2	9.77	1507	Unknown	U	-	DT	-	-	-	-	1.3	-	1.0		
122	198.1	9.92	1527	Unknown	U	-	DT	-	-	-	-	-1.1	-	1.1		
124	157	9.99	1536	Unknown	U	-	15	-	-	-	-	1.4	-	-1.5		
130	166.1	10.19	1563	Unknown	U	-	DT	-	-	-	-	-1.2	-	-		
132	243.2	10.25	1571	Unknown	U	-	DT	-	-	-	-	1.0	-	-		
145	235.1	10.75	1637	Unknown	U	-	DT	-	-	-	-	-1.1	-	-		
146	129.1	10.78	1640	Unknown	U	-	DT	-	-	-	-	1.2	-	-		
147	257.1	10.80	1644	Unknown	U	-	DT	-	-	-	-	1.7	-	-		
150	226.1	10.89	1655	Unknown	U	-	DT	-	-	-	-	-1.1	-	1.0		
151	217.1	10.90	1657	Unknown	U	-	DT	-	-	-	-	1.1	-	-		
153	217.1	10.95	1664	Unknown	U	-	DT	-	-	-	-	-1.1	-	-1.3		
166	318.2	11.41	1724	Unknown	U	-	DT	-	-	-	-	1.2	-	-		
169	217.1	11.53	1740	Unknown	U	-	DT	-	-	-	-	1.2	-	-		
171	318.2	11.61	1750	Unknown	U	-	DT	-	-	-	-	1.4	-	-		
173	392.2	11.68	1759	Skel_cell_C065 (Vidoudez)	U	-	DT	-	-	-	-	1.0	1.2	1.8		
175	331.2	11.72	1765	Unknown	U	-	DT	-	-	-	-	1.6	-	1.1		
178	143.1	11.78	1772	Unknown	U	-	DT	-	-	-	-	1.2	-	-1.2		
179	392.2	11.81	1777	Skel_cell_C065 (Vidoudez)	U	-	DT	-	-	-	-	1.2	1.3	1.3		
183	392.2	11.95	1795	Skel_cell_C065 (Vidoudez)	U	-	DT	-	-	-	-	1.2	1.3	1.2		
184	276.1	11.99	1801	Unknown	U	-	DT	-	-	-	-	-1.3	1.1	1.1		

ID	Model ion	RT	RI	Name	Class	Ident	Analysis	Median (Co: n=3, Mono: n=5/6)						Fold (Co relative to Mono)		
								Day 15		Day 27		Day 35		Day 15	Day 27	Day 35
								Mono	Co	Mono	Co	Mono	Co			
305	370.2	16.06	2480	Unknown	U	-	DT	-	-	-	-	1.0	1.5	8.2		
316	149	16.57	2567	Unknown	U	-	15	-	-	-	-	2.2	-	-		
333	195.1	17.13	2666	Unknown	U	-	DT	-	-	-	-	1.2	-	-		
336	195.1	17.23	2684	Unknown	U	-	DT	-	-	-	-	-1.3	-	-		
340	204.1	17.40	2714	Unknown	U	-	DT	-	-	-	-	1.4	-1.2	1.0		
344	175.1	17.62	2752	Unknown	U	-	DT	-	-	-	-	-1.1	-	-		
348	361.2	17.77	2777	Unknown	U	-	DT	-	-	-	-	-2.6	1.0	1.1		
349	311.3	17.82	2787	M000000_A278013-101- xxx_NA_2788,69_TRUE_VAR5_ALK_D278931 (GOLM)	U	?	DT	-	-	-	-	-1.4	-	-		
352	191.1	18.11	2834	M000000_A294006-101- xxx_NA_2939,93_PRED_VAR5_ALK_NA (GOLM)	U	?	DT	-	-	-	-	1.0	1.1	-1.3		
354	103.1	18.20	2848	Skel_Cell_C145 (Vidoudez)	U	?	DT	-	-	-	-	1.2	-	-		
357	129.1	18.41	2881	Unknown	U	-	DT	-	-	-	-	1.1	-	-		
360	113.1	18.63	2915	Unknown	U	-	DT	-	-	-	-	-15.5	-	-		
371	227.2	19.58	3064	Unknown	U	-	DT	-	-	-	-	-1.2	1.0	1.7		
372	126.1	19.70	3082	Unknown	U	-	DT	-	-	-	-	1.1	-	-		
375	337.3	19.81	3099	Unknown	U	-	DT	-	-	-	-	-1.4	1.4	-1.6		
381	468.4	20.52	3206	Unknown	U	-	DT,15	-	-	-	-	2.2	1.0	-1.8		
383	143.1	20.78	3228	Unknown	U	-	DT	-	-	-	-	1.1	-	-1.5		
387	217.1	21.05	3250	Unknown	U	-	DT	-	-	-	-	2.0	-	-		
389	143.1	21.44	3284	Unknown	U	-	DT	-	-	-	-	2.0	-	-1.2		
409	217.1	23.95	3494	Unknown	U	-	DT	-	-	-	-	1.7	-	-		
415	217.1	24.60	3549	Unknown	U	-	DT	-	-	-	-	1.5	-	-		

ID	Model ion	RT	RI	Name	Class	Ident	Analysis	Median (Co: n=3, Mono: n=5/6)						Fold (Co relative to Mono)			
								Day 15		Day 27		Day 35		Day 15	Day 27	Day 35	
								Mono	Co	Mono	Co	Mono	Co				
419	588.4	24.99	3582	Unknown	U	-	DT	-	-	-	-	-	-	-	-	-	-

In case derivatized molecules are detected, the table entry lists their putative parent compounds. Each MST is characterized by **ID**, **model ion**, retention time (**RT**), retention index (**RI**) and its underlying CAP **analysis**. CAP analyses comprised the overall analysis with a-priori grouping by treatment and day (**DT**), with a-priori grouping by treatment (**T**), as well as daywise subset analysis on day 15 (**15**), 27 (**27**) and day 35 (**35**). Metabolites were identified via libraries. If metabolites were verified with a standard, they are marked with *. “?” indicates a reversed match between 700 and 800, “??” a reversed match between 600 and 700 and “???” indicates cases where the reversed match was ≤ 600 . “” tags metabolites with a match smaller than 600. Class abbreviations: Amine (**A**), alcohol (**Alc**), alkaloid (**Alk**), carboxylic acid (**CA**), complex sugar (**CS**), derivatives of a certain class (**dv.**), hydrocarbons (**HC**), sugar (**S**), sugar alcohol (**S Alc**), sugar acid (**S Acid**), sterol (**St**), terpene (**T**), others (**O**), unknown (**U**). **Vidoudez** refers to an MST code given by the inhouse library, **GOLM** refers to an MST code given by distinct libraries of the Golm Metabolome Database.

7.4 Appendix: Modified CAP function for R

```

my.CAP <- function(y,group, m=2, trace=T)
### Canonical analysis of principal coordinates
### author: Jens Schumacher
### date: 11.11.2015
### following the original description from
### Anderson&Willis: Ecological archives E084-011-A1

{
### number of observations
  N <- nrow(y)
### principal coordinate analysis
  if (!is.factor(group)) {group <- as.factor(group)}

### distance matrix
  require(vegan)
  D <- as.matrix(vegdist(y))
### modified distance matrix
  A <- as.matrix(-D^2/2)
### centering according to formula (A.1)
  rowmeans <- matrix(rowMeans(A), nrow(A), ncol(A))
  colmeans <- matrix(colMeans(A), nrow(A), ncol(A), byrow=T)
  G <- A-rowmeans-colmeans+mean(A)
### eigenanalysis
  temp <- eigen(G)
  Q <- temp$vectors
  lambda <- temp$values
  if (trace==T)
  {
    cat("Principal Coordinate Axes (unconstrained)\n")
    cat("  Axes\n")
    cat("Sample  ")
    for (i in 1:m) cat(i,"  ")
    cat("\n")
    for (i in 1:N)
    {
      cat(format(i,width=3)," ")
      for (j in 1:m) cat(format(Q[i,j]*sqrt(lambda[j]),width=13,nsml=10)," ")
      cat("\n")
    }
  }
}

```

canonical analysis

```

X <- model.matrix(~group-1)
require(MASS)
H <- X %*% ginv(t(X)%*% X) %*% t(X)
Qm <-]
temp <- eigen(t(Qm) %*% H %*% Qm)
delta2 <- temp$values
U <- temp$vectors
Q.star <- Qm %*% U
Q[,1:m]
Q.star.rescaled <- Q.star* matrix(sqrt(delta2),byrow=T,N,m)
if (trace==T)
{
cat("-----\n")
cat("Results: CANONICAL ANALYSIS\n")
cat("-----\n\n")
cat(" Eigenvalues (Correlations)\n")
for (i in 1:m) cat(sqrt(delta2[i]), " ")
cat("\n\n")

cat(" Squared correlations)\n")
for (i in 1:m) cat(delta2[i], " ")
cat("\n\n")

cat("Canonical Axes (constrained)\n")
cat("  Axes\n")
cat("Sample ")
for (i in 1:m) cat(i," ")
cat("\n")
for (i in 1:N)
{
cat(format(i,width=3), " ")
for (j in 1:m) cat(format(Q.star.rescaled[i,j],width=13,nsml=10), " ")
cat("\n")
}
}
}

### what results should be kept?
list(trace.stat=sum(delta2), delta2.stat=delta2[1])
}

```

```
my.CAP.perm <- function(y,group,m=2, chamber,chamberlabels, perm.anz=9999, seed=13)
{
  ### function for constrained permutation
  permute.labels <- function(chamberlabels)
  {
    index <- sample(1:nrow(chamberlabels))
    t(apply(chamberlabels[index,],1,sample))
  }

  ### CAP for original data
  # y <- y[order(chamber)]
  # group <- group[order(chamber)]

  temp <- my.CAP(y,group,m, trace=F)
  trace.stat.obs <- temp$trace.stat
  delta2.stat.obs <- temp$delta2.stat

  ### CAP for permuted data sets
  set.seed(seed)
  trace.stat <- rep(0, perm.anz)
  delta2.stat <- rep(0, perm.anz)
  for (i in 1:perm.anz)
  {
    if (i %% 100 ==0) print(i)

    ### randomly shuffle group labels
    chamberlabels <- permute.labels(chamberlabels)
    group.perm <-vector(length = length(group))

    freq <- table(chamber)
    for (j in 1:length(unique(chamber)))
    {
      group.perm[chamber==unique(chamber)[j]] <- sample(chamberlabels[j,],freq[j])
    }
    group.perm <- factor(group.perm)
    temp <- my.CAP(y,group.perm,m, trace=F)
    trace.stat[i]<- temp$trace.stat
    delta2.stat[i] <- temp$delta2.stat
  }
}
```

```

cat("-----\n")
cat(" Results: PERMUTATION TEST\n")
cat("-----\n\n")

cat(" tr(Q_m'HQ_m) = ", trace.stat.obs, " P = ",sum(trace.stat>trace.stat.obs)/(perm.anz+1)," \n")
cat(" delta_1^2 = ", delta2.stat.obs, " P = ",sum(delta2.stat>delta2.stat.obs)/(perm.anz+1)," \n")
cat("-----\n\n")

cat(" No. of permutations used = ",perm.anz, "\n")
cat(" Integer for the random seed = ", seed," \n")

list(trace.stat, delta2.stat)
}

```

function to classify new observation

```

classify <- function(ynew, y, group, m)
{
  N <- nrow(y)
  D <- as.matrix(vegdist(y))
  A <- as.matrix(-D^2/2)
  rowmeans <- matrix(rowMeans(A), nrow(A), ncol(A))
  colmeans <- matrix(colMeans(A), nrow(A), ncol(A), byrow=T)
  G <- A-rowmeans-colmeans+mean(A)
  Q <- eigen(G)$vectors
  lambda <- eigen(G)$values

  X <- model.matrix(~as.factor(group))
  require(MASS)
  H <- X %*% ginv(t(X)%*% X) %*% t(X)
  Qm <- Q[,1:m]
  test2 <- eigen(t(Qm) %*% H %*% Qm)
  delta2 <- test2$values
  U <- test2$vectors
  Q.star <- Qm %*% U
  Q.star.rescaled <- Q.star* matrix(sqrt(delta2),byrow=T,N,m)

### centroids for groups
  centroids <- matrix(0,length(unique(group)),m)
  for (i in 1:m)
  {
    centroids[,i] <- tapply(Q.star.rescaled[,i], group, mean)
  }
}

```

```

Dnew <- as.matrix(vegdist(rbind(y,ynew)))
gnew <- rep(0,N)

for (i in 1:N)
{
  gnew[i] <- -1/2*(Dnew[N+1,i]^2-mean(D[i,]^2)-mean(Dnew[N+1,-(N+1)]^2)+mean(D^2))
}
qnew <- rep(0,m)
for (i in 1:m)
  qnew[i] <- sum(gnew * Q[,i])/lambda[i]

qnew.star <- t(qnew) %*% U
qnew.star.rescaled <- qnew.star * sqrt(delta2)

dist.to.centroids <- as.matrix(dist(rbind(qnew.star.rescaled,centroids)))[1,-1])
levels(group)[as.numeric(which.min(dist.to.centroids))]
} ### end classify

my.CAP.cv <- function(y,group,m=2, chamber)
{

### leave-one-chamber-out cross validation
group <- factor(group)
group.cv <- group
for (i in 1:length(unique(chamber)))
{
  y.minus <- y[-(chamber==unique(chamber)[i]),]
  group.minus <- group[-(chamber==unique(chamber)[i])]
  ynew <- y[(chamber==unique(chamber)[i]),]
  index <- (chamber==unique(chamber)[i])*(1:nrow(y))
  index <- index[index>0]
  for (j in 1:nrow(ynew))
  {
    group.cv[index[j]] <- classify(ynew = ynew[j,],y=y.minus.group.minus, m=m)
  }
}
cat("-----\n")
cat("Results cross validation (leave one chamber out)\n")
cat("-----\n\n")

```

```

cat("    Classified into\n")
cat("    Group    %correct\n")
cat("Original\n")
result <- table(group,group.cv)
row.names(result) <- paste("Group",levels(group))
print(cbind(result,diag(result)/rowSums(result)*100))

cat("-----\n")
cat("Total correct = ", sum(diag(result)),"/",sum(result), " = ",sum(diag(result))/sum(result)*100, "%\n")
cat("Misclassification error = ", 100-sum(diag(result))/sum(result)*100, "%\n")
}

```

```

my.CAP.loo <- function(y,group,m=2, chamber)
{
### leave-one-out cross validation
group <- factor(group)
group.cv <- group
for (i in 1:nrow(y))
{
y.minus <- y[-i,]
group.minus <- group[-i]
ynew <- y[i,]
group.cv[i] <- classify(ynew = ynew,y=y.minus,group.minus, m=m)

}
cat("-----\n")
cat("Results cross validation (leave one out)\n")
cat("-----\n\n")

cat("    Classified into\n")
cat("    Group    %correct\n")
cat("Original\n")
result <- table(group,group.cv)
row.names(result) <- paste("Group",levels(group))
print(cbind(result,diag(result)/rowSums(result)*100))

cat("-----\n")
cat("Total correct = ", sum(diag(result)),"/",sum(result), " = ",sum(diag(result))/sum(result)*100, "%\n")
cat("Misclassification error = ", 100-sum(diag(result))/sum(result)*100, "%\n")
}

```